Dissertation zur Erlangung des Doktorgrades

der Fakultät für Chemie und Pharmazie

der Ludwig-Maximilians-Universität München

Medizinalchemische Entwicklung von allosterischen Modulatoren für den nikotinischen Acetylcholinrezeptor zur Behandlung von Nervenkampfstoffvergiftungen

Tamara Maria Bernauer

aus

Ebersberg, Deutschland

2024

Erklärung

Diese Dissertation wurde im Sinne von § 7 der Promotionsordnung vom 28. November 2011 von Herrn Professor Dr. Klaus T. Wanner und Herrn Professor Dr. Franz F. Paintner betreut.

Eidesstattliche Versicherung

Diese Dissertation wurde eigenständig und ohne unerlaubte Hilfsmittel erarbeitet.

München, den 18. September 2024

Tamara Bernauer

Dissertation eingereicht am	18. September 2024
1. Gutachter:	Prof. Dr. Klaus T. Wanner
2. Gutachter:	Prof. Dr. Franz F. Paintner
Mündliche Prüfung am	07. November 2024

Für Mama

Die vorliegende Arbeit entstand in der Zeit von

Oktober 2019 bis September 2024

am Department für Pharmazie – Zentrum für Pharmaforschung –

der Ludwig-Maximilians-Universität München

auf Anregung und unter Leitung von

Herrn Prof. Dr. Klaus T. Wanner

Für die hervorragende und sehr engagierte Betreuung und Förderung meiner Arbeit

danke ich Herrn Prof. Dr. Klaus T. Wanner sehr herzlich.

Herrn Prof. Dr. Franz F. Paintner danke ich sehr herzlich für die ausgezeichneten Forschungsbedingungen und für die Übernahme des Koreferats

Danksagung

Ich möchte mich von ganzem Herzen bei Herrn Prof. Dr. Klaus T. Wanner bedanken, der mir die Möglichkeit gab, meine Dissertation am Department für Pharmazie an der Ludwig-Maximilians-Universität München zu verfassen. Sein Vertrauen in meine Arbeit und seine durchgehende Unterstützung haben mir nicht nur den Weg geebnet, sondern auch die nötige Inspiration geliefert, um dieses anspruchsvolle Projekt erfolgreich zu bewältigen.

Ein besonderer Dank gilt auch Herrn Prof. Dr. Franz F. Paintner, der nicht nur das Amt des zweiten Gutachters der Prüfungskommission innehatte, sondern meine Promotion in herausragender Weise begleitete und sich stets uneingeschränkt für mein Anliegen einsetzte. Seine zahlreichen Anregungen, kreativen Ideen und exzellente Betreuung waren von unschätzbarem Wert und trugen maßgeblich zur Entstehung dieser Arbeit bei.

Die fruchtbare Zusammenarbeit mit der Arbeitsgruppe von Dr. Karin V. Niessen und Dr. Thomas Seeger am Institut für Pharmakologie und Toxikologie der Sanitätsakademie der Bundeswehr in München sowie mit der Arbeitsgruppe von Prof. Dr. Holger Gohlke an der Heinrich-Heine-Universität Düsseldorf, einschließlich seiner engagierten Mitarbeiter Dr. Christoph C. W. Gertzen und Jesko Kaiser, hat mich kontinuierlich inspiriert. Diese Kooperation bildete die solide Grundlage für das Gelingen dieser Forschungsarbeit.

Einen aufrichtigen Dank richte ich an die Mitarbeitenden der analytischen Abteilung am Department der Pharmazie, die sich durch ihre effiziente und hochqualitative Aufnahme verschiedener NMR- und Massenspektren ausgezeichnet haben.

Besonderer Dank gebührt Lars Allmendinger, Georg Höfner und Jörg Pabel, die sich nicht nur bei fachlichen Fragestellungen stets hilfsbereit zeigten, sondern mich auch persönlich unermüdlich unterstützten.

Für die herzliche Aufnahme in den Arbeitskreis und die angenehmen Stunden während und nach der Arbeitszeit möchte ich meinen tiefen Dank an all meine geschätzten Kolleginnen und Kollegen richten, die ich während meiner Zeit an der LMU kennenlernen durfte. In diesem Zusammenhang spreche ich besonders Valentin Nitsche, Heinrich Rudy, Mark Währa und Hannah Kipka meinen aufrichtigen Dank aus.

Unterhaltsame und abwechslungsreiche Mittags- und Kaffeepausen mit kulinarischen Highlights durfte ich stets in Begleitung von Valentin Nitsche, Claudia Glas und Lars Allmendinger genießen. Mein herzlicher Dank gilt ihnen nicht nur für diese genussvollen Momente, sondern auch für ihre freundschaftliche Unterstützung sowie die gemeinsamen sportlichen Herausforderungen.

Auch möchte ich meinen Studienkolleginnen und engen Freundinnen Laura Tebcharani und Anna Kirchberger danken. Eure unzähligen warmen Worte und Ratschläge kamen immer zur rechten Zeit. Mit euch an meiner Seite konnte ich nicht nur Tiefpunkte überwinden, sondern auch die kleinen und großen Erfolge feiern.

Ein besonderer Dank gilt meinem Mitstreiter und Freund Valentin Nitsche. Deine Kollegialität, fachliche Expertise und Freundschaft haben meine Forschungszeit in besonderem Maße bereichert. Ich bin zutiefst dankbar für die wertvolle persönliche Erfahrung, die ich mit dir teilen durfte.

Mein größter Dank geht an meine Familie: Papa und Yvi, ich bin unendlich dankbar für eure grenzenlose Unterstützung - ohne eure ermutigenden Worte und euren Rückhalt wäre diese Arbeit nicht möglich gewesen. Der Zusammenhalt, den ihr mit mir teilt, ist das größte Geschenk. Mama, du hast mit deiner tiefen Liebe und dem ständigen Glauben in mich und meine Fähigkeiten den Grundstein für all das gelegt. Ich kann nicht in Worte fassen, wie sehr ich dich vermisse.

Ganz besonders möchte ich mich zum Abschluss bei Berni bedanken, der mir jederzeit den Rücken freihielt, mich motivierte und mich nach jedem Rückschlag unermüdlich wieder aufbaute. Deine Liebe und dein Glauben an mich gaben mir die Kraft, nicht aufzugeben und mein Ziel zu erreichen. Dafür bin ich dir von Herzen dankbar.

Die vorliegende kumulative Dissertation basiert auf folgenden Publikationen:

Erste Publikation:

Jesko Kaiser, Christoph G. W. Gertzen, **Tamara Bernauer**, Georg Höfner, Karin V. Niessen, Thomas Seeger, Franz F. Paintner, Klaus T. Wanner, Franz Worek, Horst Thiermann, Holger Gohlke, A novel binding site in the nicotinic acetylcholine receptor for MB327 can explain its allosteric modulation relevant for organophosphorus-poisoning treatment, *Toxicology Letters* **2023**, *373*, 160-171. DOI: 10.1016/j.toxlet.2022.11.018.

Zweite Publikation:

Tamara Bernauer, Valentin Nitsche, Jesko Kaiser, Christoph G. W. Gertzen, Georg Höfner, Karin V. Niessen, Thomas Seeger, Dirk Steinritz, Franz Worek, Holger Gohlke, Klaus T. Wanner, Franz F. Paintner, Synthesis and biological evaluation of novel MB327 analogs as resensitizers for desensitized nicotinic acetylcholine receptors after intoxication with nerve agents, *Toxicology Letters* **2024**, 397, 151-162. DOI: 10.1016/j.toxlet.2024.05.011.

Dritte Publikation:

Jesko Kaiser, Christoph G. W. Gertzen, **Tamara Bernauer**, Valentin Nitsche, Georg Höfner, Karin V. Niessen, Thomas Seeger, Franz F. Paintner, Klaus T. Wanner, Dirk Steinritz, Franz Worek, Holger Gohlke, Identification of ligands binding to MB327-PAM-1, a binding pocket relevant for resensitization of nAChRs, *Toxicology Letters* **2024**, 398, 91-104. DOI: 10.1016/j.toxlet.2024.05.013.

Viertes Manuskript (unveröffentlicht):

Tamara Bernauer, Valentin Nitsche, Georg Höfner, Karin V. Niessen, Thomas Seeger, Dirk Steinritz, Franz Worek, Holger Gohlke, Klaus T. Wanner, Franz F. Paintner, Structure-Affinity Relationship of Quinazoline Derivatives as Potential Resensitizers of Desensitized nAChRs After Nerve Agent Intoxication, *unpublished.*

Inhaltsverzeichnis

1 Einleitung

Der Einsatz von chemischen Kampfstoffen als Massenvernichtungswaffen begann mit der Schlacht im belgischen Ypern im ersten Weltkrieg (1914-1918). Am 22. April 1915 wurde durch deutsche Streitkräfte mit 150 Tonnen Chlorgas erstmalig ein chemischer Kampfstoff eingesetzt, wobei mehrere hundert alliierte Soldaten getötet und mehr als 2500 verwundet wurden (Joy, 1997). Gefolgt von zahlreichen weiteren Giftgasangriffen (u.a. mit Chlor-, Phosgen- oder Senfgas) auf beiden Seiten der Front bezeichnen Historiker den ersten Weltkrieg auch heute noch als Chemikerkrieg, in dem es durch chemische Kampfstoffe bis zum Waffenstillstand am 11. November 1918 mehr als 1,3 Millionen Verletzte und etwa 90.000 Tote gab (Fitzgerald, 2008). Die Verwendung von Giftgasen verstieß jedoch schon damals gegen die Haager Landkriegsordnung von 1899 (Segesser and Segesser, 2007). Zukünftige Einsätze von Chemiewaffen in zwischenstaatlichen Konflikten sollten durch das am 17. Juni 1925 unterzeichnete Genfer Protokoll „über das Verbot der Verwendung von erstickenden, giftigen oder ähnlichen Gasen […] im Kriege“ reguliert werden (Eidgenössisches Departement für Verteidigung, 1925). Doch die fehlende Berücksichtigung von Forschung zu Kampfstoffen sowie deren Produktion und Lagerung in diesem Abkommen führte zu einem Wettrüsten. Als eine No-First-Use-Vereinbarung gesehen, wurde formell das Recht vorbehalten, Vergeltungsmaßnahmen zu ergreifen, falls ein Gegner widerrechtliche Schritte einlegen würde (Meselson and Robinson, 1980). So kam es in den folgenden Jahren zu regelmäßigen Einsätzen chemischer Kampfstoffe. Italienische Streitkräfte setzten Senfgas im Krieg gegen Abessinien (1935-1936) im Vorfeld des zweiten Weltkriegs ein (Grip and Hart, 2009). Auch Japan setzte vor und während des zweiten Weltkriegs (1939-1945) im Krieg gegen China (1937-1945) bei über 2000 Gelegenheiten chemische Waffen, unter anderem Senfgas, ein (Friedrich et al., 2017). Aus Angst vor Vergeltung wurde auf den übrigen Schlachtfeldern des zweiten Weltkriegs jedoch weitgehend auf Chemiewaffen verzichtet (van Courtland Moon, 1984). Der letzte große Einsatz von chemischen Kampfstoffen in einem zwischenstaatlichen Konflikt erfolgte während des Iran-Irak-Krieges in den 1980er Jahren. Beide Seiten setzten zwischen 1980 und 1988 unter anderem Sarin, Tabun und Soman bei verschiedenen Angriffen ein (Ali, 2001). Im Jahr 1993, nach dem Zerfall der Sowjetunion und dem Ende des kalten Krieges, konnte dann schließlich ein umfassenderes UN-Chemiewaffenabkommen beschlossen werden, welches am 29. April 1997 völkerrechtlich verbindlich in Kraft trat (Thakur and Haru, 2007). Aktuell haben 193 Staaten das Abkommen der unabhängigen internationalen OPCW (Organisation for the Prohibition of Chemical Weapons) zur Vernichtung der aktuellen Chemiewaffenbestände sowie des Verbots von Entwicklung, Produktion, Ein- bzw. Verkauf, Lagerung und Einsatz von Chemiewaffen unterzeichnet (Pitschmann, 2014). Doch auch dieses Abkommen konnte den Einsatz von Chemiewaffen nicht gänzlich verhindern. Besonders hochtoxische phosphororganische Nervenkampfstoffe

werden weiterhin in Kriegssituationen eingesetzt. So zum Beispiel kostete der Sarin-Anschlag des syrischen Regimes auf die Hauptstadt Damaskus im August 2013 mehr als 1000 Menschen, darunter zahlreiche Kinder, das Leben (Meier, 2016; Pita and Domingo, 2014). Zunehmend kommt es auch in terroristischen Zusammenhängen zu einem Einsatz von Nervenkampfstoffen (Höfer, 2002; Vale et al., 2016). Mitte der 1990er Jahre verübte die Aum-Sekte in der U-Bahn von Tokio einen Anschlag mit Sarin, in dessen Folge über 5000 Menschen medizinisch behandelt werden mussten und zwölf von ihnen starben (Sidell et al., 1997). In den Jahren 2017 bis 2018 fanden mehrere gezielte, politisch motivierte Angriffe mit phosphororganischen Nervengiften statt. So erlag der Halbbruder des nordkoreanischen Diktators Kim Jong-Un, Kim Jong-Nam, einer VX-Vergiftung und Sergei Skripal, ein ehemaliger russischer Geheimdienstoffizier, und seine Tochter Yulia überlebten 2018 nur knapp einen Angriff mit dem Nervengift Novichok (Nakagawa and Tu, 2018; Vale et al., 2018). Zuletzt kam es im Jahr 2020 zu einer Vergiftung des russischen Regierungskritikers Alexei Nawalny. Dieser wurde bei einem Inlandsflug in Russland mit einem Novichok-Nervengift vergiftet und überlebte ebenfalls nur knapp (Steindl et al., 2021).

Vergiftungen mit phosphororganischen Nervengiften treten jedoch nicht nur in kriegerischen Auseinandersetzungen und im Zusammenhang mit terroristischen Anschlägen auf. Ein großes Problem stellen insbesondere in Ländern des globalen Südens umweltbedingte, aber auch in suizidaler Absicht unternommene Vergiftungen mit Pflanzenschutzmitteln auf Organophosphatbasis dar. Schätzungen zufolge sind Selbstvergiftungen mit Pestiziden weltweit für etwa ein Drittel aller Suizide verantwortlich (Freire and Koifman, 2013).

1.1 Nervengifte als chemische Kampfstoffe

Die Einteilung chemischer Kampfstoffe erfolgt über ihre Wirkungsweise in Lungen-, Blut-, Haut-, Nerven- und Psychokampfstoffe. Während Lungen-, Blut- und Hautkampfstoffe zur ersten Generation der Chemiewaffen zählen, welche vor allem im ersten Weltkrieg zum Einsatz kamen, zählen Nervenkampfstoffe, in der Regel Organophosphat- bzw. phosphonat-Verbindungen, je nach Entwicklungsstadium, zur zweiten bis vierten Generation der Chemiewaffen (Pitschmann, 2014). Zur zweiten Generation gehören dabei G- (German-) und V- (Venomous-) Kampfstoffe, während binäre GV- und Novichok-Kampstoffe zur dritten bzw. vierten Generation Chemiewaffen gezählt werden (Chauhan et al., 2008).

Die erste Synthese eines Nervenkampfstoffes erfolgte per Zufall, als Gerhard Schrader 1936 im Rahmen eines Forschungsprojekts der Firma I. G. Farben zu Organophosphat-basierten Insektiziden forschte, und nach versehentlicher Freisetzung einer Substanz für Nervengifte typische Vergiftungssymptome bei den Forschenden auftraten. Die dabei entdeckte Verbindung Dimethylphosphoramidocyanidsäureethylester, auch bekannt als Tabun (**1**), wirkt stark toxisch und wurde deshalb schnell als potenzielle Chemiewaffe erkannt (López-Muñoz et al., 2009). Diese Entdeckung legte den Grundstein für weitere phosphororganische Verbindungen, woraufhin in den folgenden Jahren Sarin (**2**), Soman (**3**) und Cyclosarin (**4**), die wie Tabun (**1**) zur G-Reihe der zweiten Generation gehören, entwickelt wurden (siehe Abbildung 1) (Pitschmann, 2014).

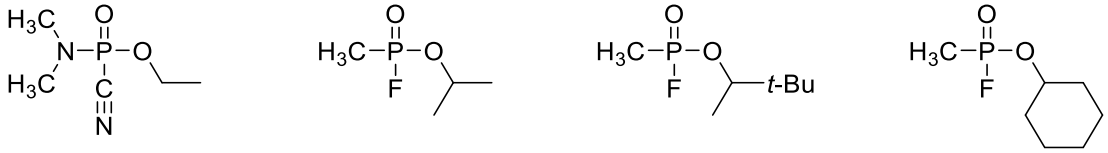

Abbildung 1: Nervengifte der G-Reihe mit zwei-Buchstaben-NATO-Code: Tabun (**1**), Sarin (**2**), Soman (**3**), Cyclosarin (**4**).

Alle Nervengifte der G-Reihe sind bei Raumtemperatur klare Flüssigkeiten mit einem Dampfdruck von 0.037 mmHg (Tabun) bis 2.1 mmHg (Sarin), sodass sie bei Raumtemperatur leicht verdampfen und somit auch über die Atmung aufgenommen werden können. Durch die relativ hohe Wasserlöslichkeit sind G-Nervengifte allerdings nicht sehr persistent (Newmark, 2007).

Die Weiterentwicklung der Substanzen führte zur V-Reihe, die wie die G-Reihe der zweiten Generation der Chemiewaffen zugeordnet wird. Das VX (**5**), zehnfach toxischer als die bisher genannten Vertreter der G-Reihe, wurde 1954 erstmals von Wissenschaftlern im Auftrag des britischen Militärs synthetisiert. Die ölige Substanz wirkt durch den deutlich geringeren Dampfdruck von 0.0007 mmHg nicht primär als Inhalations-, sondern als Dermaltoxin. Zusätzlich ist

es durch seine höhere Hydrolysebeständigkeit, verglichen mit den G-Verbindungen, weitaus persistenter (Newmark, 2007; Spradling and Dillman, 2011). Zeitgleich wurden in der ehemaligen Sowjetunion und in China die strukturverwandten Toxine VR (**6**) (sowjetisch) und CVX (**7**) (chinesisch) entwickelt (siehe Abbildung 2) (Antonijevic and Stojiljkovic, 2007; Black, 2016).

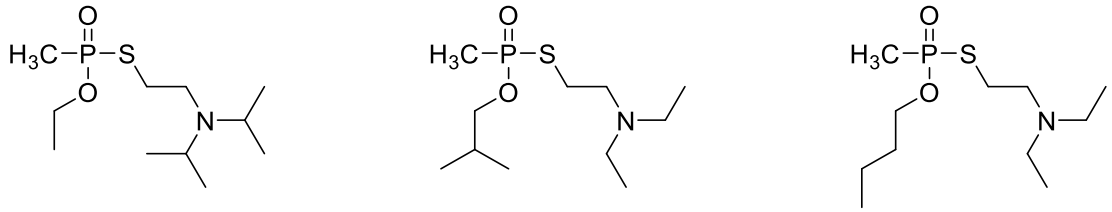

5 VX **6** VR **7** CVX

Abbildung 2: Nervengifte der V-Reihe: VX (**5**), VR (**6**) und CVX (**7**).

Unter den andauernden Spannungen des kalten Krieges wurde die Forschung an Nervengiften vorangetrieben. Dabei wurde der Fokus zunehmend auf weiterentwickelte phosphororganische Verbindungen gelegt, welche durch Kombinationen bestimmter Strukturelemente von G- und V-Agenzien hochtoxisch und gleichzeitig persistenter als Sarin und flüchtiger als VX (**5**) sein sollten (Wiener and Hoffman, 2004). Militärlabore der USA führten solche GV-Verbindungen der dritten Generation der Chemiewaffen unter der Bezeichnung IVA (Intermediate Volatility Agents) ein. Die Instabilität dieser Verbindungen erforderte jedoch die Anwendung einer neuen, besonderen Technik: Als binäre Munition werden dabei zwei ungiftige Vorläuferverbindungen getrennt in ein Projektil eingesetzt, sodass die hochtoxischen Endverbindungen erst beim Einsatz *in situ* gebildet werden (Pitschmann, 2014). Dies reduzierte die Vorsichtsmaßnahmen enorm, die beim Transport und der Lagerung der ursprünglichen Chemiewaffen getroffen werden mussten (Koelle, 1981). Zwischen 1970 und 1980 wurden solch binäre Chemiewaffen, z.B. GB-2, VX-2, IVA-2, in den USA entwickelt (Black, 2016; Pitschmann, 2014).

Die Sowjetunion reagierte darauf mit der Entwicklung binärer Kampfstoffe der vierten Generation. Dabei wurden im Rahmen des FOLIANT-Programms die sogenannten Novichok-Substanzen mit nochmals erhöhter Toxizität entdeckt (Bolt and Hengstler, 2022; Nepovimova and Kuca, 2018; Pitschmann, 2014). Lange waren die genauen Strukturen dieser Verbindungen unbekannt, doch in den letzten Jahren konnten einige durch spektroskopische und massenspektrometrische Studien entschlüsselt werden, sodass nun die allgemeine Strukturformel **8** zur Beschreibung der Novichok-Verbindungen gilt (siehe Abbildung 3) (Bhakhoa et al., 2019; Jeong et al., 2021; Lee et al., 2021).

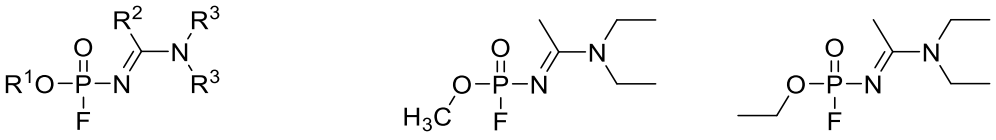

8

R^1 , R^2 = H or < C_{10} incl. cycloalkyl
R^3 = < C_{10} incl. cycloalkyl

9
A-232

10
A-234

Abbildung 3: Allgemeine Strukturformel der Novichok-Reihe (**8**), sowie explizit dargestellt A-232 (**9**) und A-234 (**10**).

Die Novichok-Verbindungen A-232 (**9**) bzw. A-234 (**10**), welche als binäre Kampfstoffe Novichok 5 bzw. Novichok 7 eingesetzt werden, sollen um ein Vielfaches toxischer sein als die Nervengifte Soman oder VX (Chai et al., 2018; Franca et al., 2019).

1.2 Vergiftungen mit phosphororganischen Verbindungen

1.2.1 Das cholinerge System

Das cholinerge System, das alle neuronalen Strukturen einschließt, die auf dem Neurotransmitter Acetylcholin (ACh) basieren (siehe Abbildung 4), spielt eine entscheidende Rolle im Nervensystem. Eine Vielzahl von physiologischen Prozessen, wie z.B. die Regulation der Herzfrequenz oder die Steuerung der Muskelkontraktion, wird durch cholinerge Rezeptoren, deren Verteilung sich sowohl über das zentrale als auch über das periphere Nervensystem erstreckt, beeinflusst.

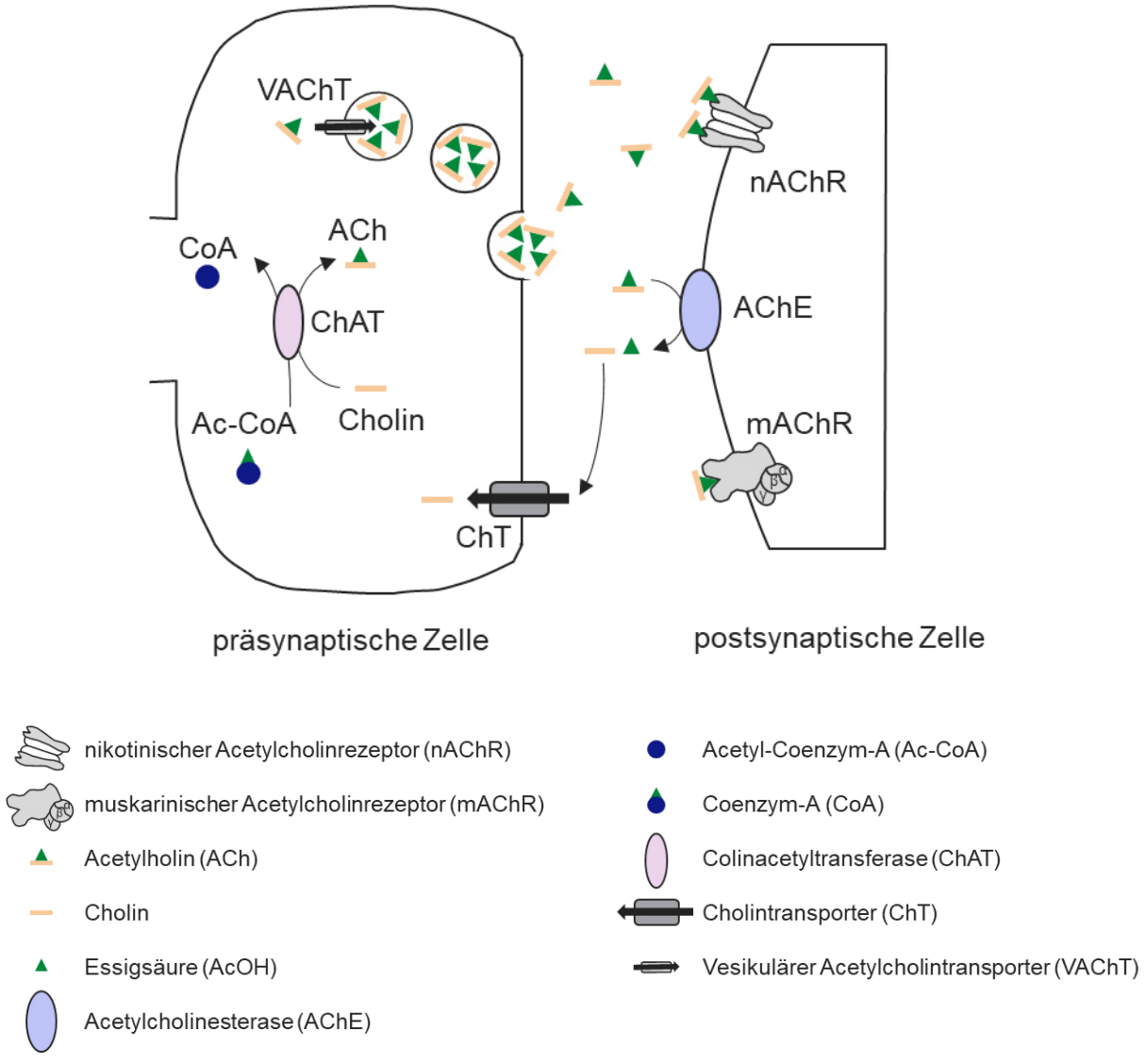

Abbildung 4: Vereinfachte Darstellung einer cholinergen Synapse nach Abreu-Villaça *et al.* (Abreu-Villaça et al., 2011).

Acetylcholin wird mit Hilfe der Cholinacetyltransferase (ChAT) enzymkatalysiert aus Cholin und Acetyl-Coenzym-A (Ac-CoA) im Cyctoplasma der Nervenzellen hergestellt. Dazu wird Cholin über Transporter (CHT) aus dem Extrazellulärraum in das Zytoplasma transportiert,

wohingegen Ac-CoA überwiegend aus dem Glucose- und Zitratstoffwechsel stammt. Anschließend wird das gebildete ACh über vesikuläre Acetylcholintransporter (VAChT) in die Vesikel aufgenommen. Bei der Reizübertragung, induziert durch Ca^{2+}-abhängige Exozytose, wird vesikulär gespeichertes ACh in den synaptischen Spalt freigesetzt. Dort löst es durch Bindung an postsynaptische nikotinische bzw. muskarinische Acetylcholinrezeptoren (nAChR bzw. mAChR) Folgeprozesse aus (Böhm, 2016). Nikotinische Acetylcholinrezeptoren als ionotrope Rezeptoren führen bei einer Aktivierung zu einer Öffnung des Ionenkanals, während eine Aktivierung von muskarinischen Acetylcholinrezeptoren als metabotrope Rezeptoren eine G-Protein gekoppelte Signalkaskade auslöst (Abreu-Villaça et al., 2011). Um eine Dauer-aktivierung der Rezeptoren zu verhindern, spaltet das im synaptischen Spalt lokalisierte Enzym Acetylcholinesterase (AChE) den Neurotransmitter ACh in einer extrem kurzen Reaktionszeit von nur 100 µs pro Molekül in die Bausteine Cholin und Acetat (Abreu-Villaça et al., 2011; Lawler, 1961; Zimmerman and Soreq, 2006). Die Hydrolyse wird durch eine katalytische Triade im aktiven Zentrum des Enzyms, bestehend aus den Aminosäuren Serin, Histidin und Glutamin, vermittelt.

1.2.2 Phosphororganische Vergiftungen und ihre Symptome

Phosphororganische Verbindungen wie z.B. Soman greifen am Abbau von ACh durch die AChE in das cholinerge System ein. Sie inhibieren die AChE durch kovalente Bindung eines Phosphat- oder Phosphonatrestes an die Hydroxylgruppe des Ser203 im aktiven Zentrum des Enzyms (Sirin and Zhang, 2014). Diese Enzym-OP-Komplexe werden im Unterschied zu den acetylierten Komplexen unter physiologischen Bedingungen nicht hydrolysiert und hemmen so irreversibel die katalytische Aktivität des Enzyms. Bei einigen phosphororganischen Verbindungen kommt es darüber hinaus zur Abspaltung eines Alkylsubstituenten, ein Vorgang, der als Aging bezeichnet wird. Dabei bilden sich aus den ursprünglich vorliegenden Phosphonsäurediestern die entsprechenden Monoester, die unter physiologischen Bedingungen deprotoniert vorliegen (Barak et al., 2000; Soukup et al., 2010). Vor allem bei verzweigtkettigen Alkylresten, wie sie z.B. bei Soman vorliegen, erfolgt diese exotherme Reaktion innerhalb weniger Minuten (Nachon et al., 2005; Sirin et al., 2012). Der Mechanismus der Phosphonylierung mit Soman sowie der anschließenden Dealkylierung ist in Schema 1 dargestellt.

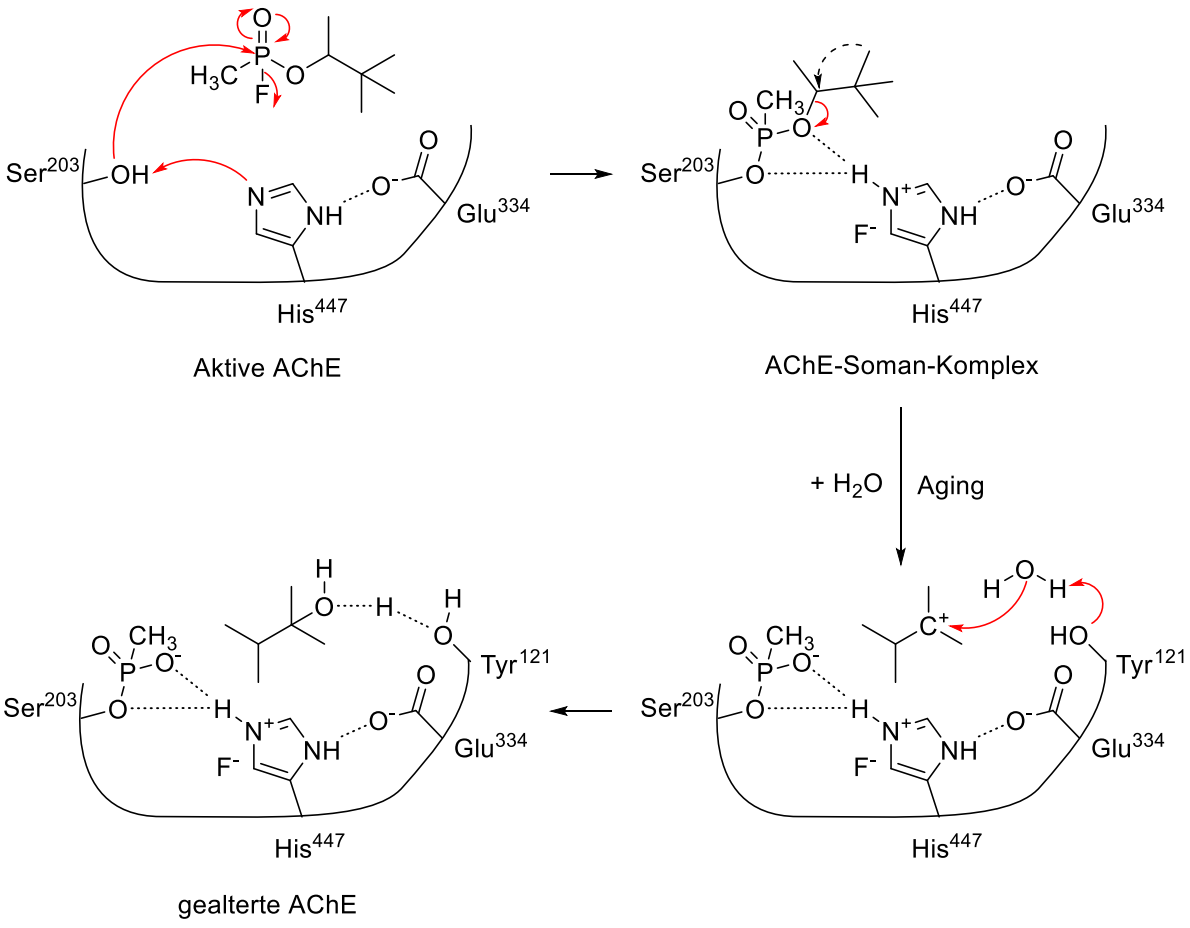

Schema 1: Mechanismus der Phosphonylierung des Ser203 im aktiven Zentrum der Acetylcholinesterase durch Soman sowie des anschließenden „Aging"-Prozesses (Sirin and Zhang, 2014; Sirin et al., 2012).

Infolge der irreversiblen Inhibition der AChE durch kovalente Bindung von Organophosphaten und der daraus resultierenden fehlenden ACh-Spaltung kommt es zu einer Akkumulation des Neurotransmitters im synaptischen Spalt. Dabei werden alle postsynaptischen ACh-Rezeptoren mit ACh gesättigt, sodass es zu einer Überstimulation der Rezeptoren kommt. Dies wird auch als cholinerge Krise bezeichnet (Soukup et al., 2010). Dabei äußert sich eine erhöhte Aktivierung des Parasympathikus über die muskarinischen Acetylcholin-rezeptoren unter anderem in übermäßiger Drüsensekretion, starker Bronchialsekretion und Bronchokonstriktion. Es sind jedoch vor allem die nikotinischen Effekte an der neuromuskulären Endplatte, die bei einer Vergiftung mit phosphororganischen Verbindungen lebensgefährlich sein können. Übermäßige nikotinische Stimulation führt zu einer raschen Depolarisation des Membranpotentials, was sich zunächst in Muskelfaszikulationen äußert. Bei anhaltender Stimulation verhindert eine Desensitisierung des Rezeptors eine Signal-weiterleitung, sodass es neben Schwindelgefühlen bis hin zu komatösen Zuständen auch zu Lähmungserscheinungen kommt. Bei akuten Vergiftungen wird Atemlähmung als häufigste Todesursache genannt (Rusyniak and Nañagas, 2004; Schecter, 2004).

1.2.3 Behandlungsmöglichkeiten bei Vergiftungen mit phosphororganischen Verbindungen

Aktuell werden drei verschiedene Klassen von Medikamenten zur Behandlung von Vergiftungen mit phosphororganischen Verbindungen eingesetzt: Parasympathomimetika, Oxime und Antikonvulsiva (Cannard, 2006). Direkt nach den ersten Maßnahmen, die bei Vergiftungsvorfällen mit phosphororganischen Verbindungen durchgeführt werden sollten (Entgiftung, Beatmung und Hämodialyse), wird Atropin verabreicht (Alozi and Rawas-Qalaji, 2020; Cannard, 2006). Natürlich vorkommend in der Tollkirsche, ist Atropin (**11**) (siehe Abbildung 5) ein Antagonist am mAChR und wirkt so gegen die durch eine Überstimulation der mAChRs ausgelösten anfänglichen Vergiftungserscheinungen (Alozi and Rawas-Qalaji, 2020; Böhm, 2016).

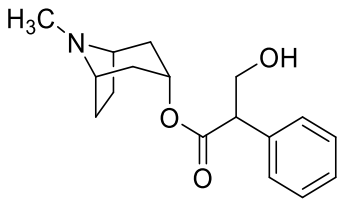

11

Abbildung 5: Strukturformel von Atropin (**11**).

Im Unterschied zu mAChR-Antagonisten sind kompetitive nAChR-Antagonisten aufgrund ihrer geringen therapeutischen Breite für die Behandlung von Nervenkampfstoffvergiftungen ungeeignet (Sheridan et al., 2005). Infolgedessen stellt die Reaktivierung inhibierter AChE durch Oxime, die zur Spaltung der Phosphat- bzw. Phosphonatester im aktiven Zentrum der AChE führen, den entscheidenden Schritt zur Beseitigung der nikotinischen Überstimulation dar. Unter den gebräuchlichen Oximen sind insbesondere das im Jahr 1955 entwickelte Pralidoxim (2-PAM) (**12**) und die strukturverwandte Bispyridinium-Verbindung Obidoxim (**13**) die bekanntesten Vertreter. Der Mechanismus der Spaltung der Phosphat- bzw. Phosphonatester sowie die Strukturformeln der genannten Oxime sind in Schema 2 dargestellt (Mercey et al., 2012; Worek et al., 2004).

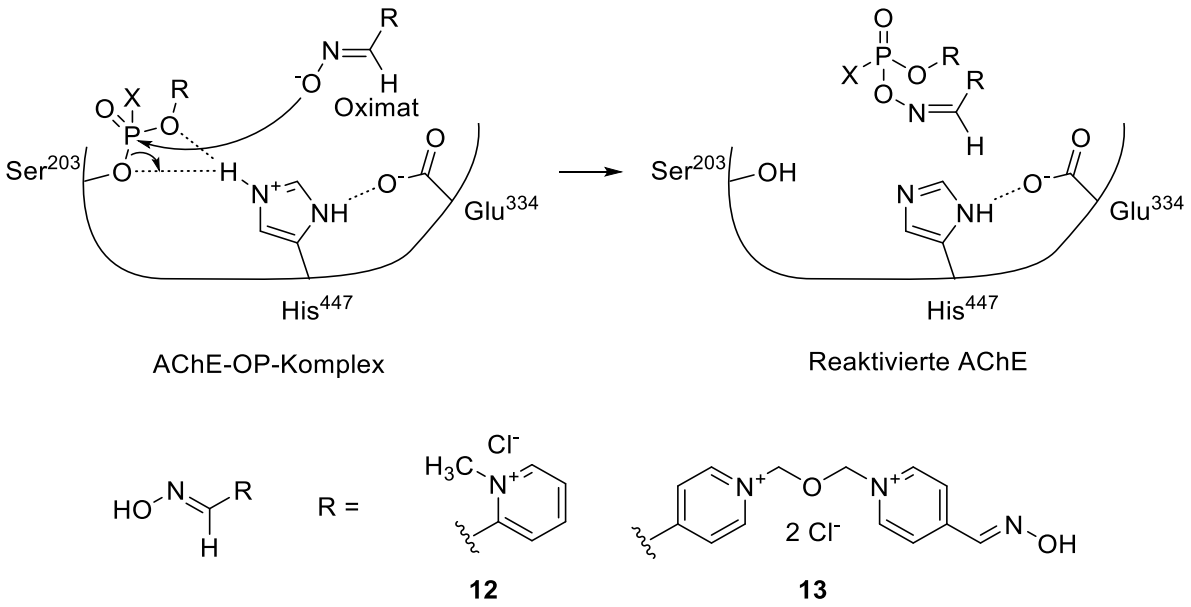

Schema 2: Mechanismus der Reaktivierung von inhibierter AChE durch Oxim-Phosphorylierung bzw. Phosphonylierung sowie die Strukturformeln der Oxime Pralidoxim (2-PAM) (**12**) und Obidoxim (**13**).

Innerhalb der ersten Stunden nach einer Vergiftung mit phosphororganischen Verbindungen werden in der Regel zusätzlich Benzodiazepine verabreicht, welche als Antikonvulsiva gegen Krampfanfälle wirken (Amend et al., 2020; Marrs, 2004). Dabei wurde lange Diazepam (**14**) eingesetzt, welches durch das strukturverwandte Midazolam (**15**) nach dessen Freigabe durch die FDA 2022 ersetzt werden soll (siehe Abbildung 6) (Gerecke, 1983; Joint Program Executive Office for Chemical, 2022; Newmark, 2019). Es zeichnet sich durch eine im Vergleich zu Diazepam schnellere und länger anhaltende, krampflösende Wirkung aus (Newmark, 2019).

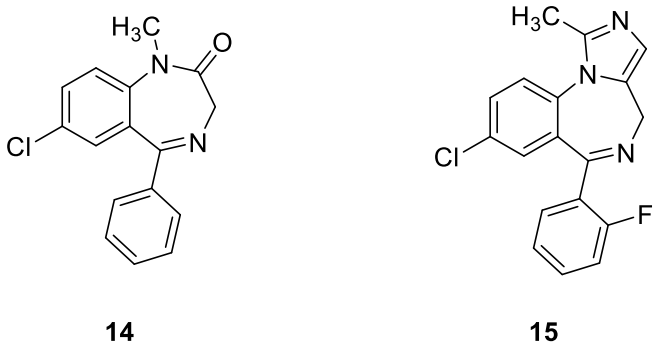

Abbildung 6: Strukturformeln von Diazepam (**14**) und Midazolam (**15**).

Zur Absicherung von Soldaten im Kampfeinsatz gegen Vergiftungen mit phosphororganischen Verbindungen werden unterschiedliche Strategien bzw. Entwicklungsansätze verfolgt. Ein erster Ansatz ist die Entwicklung von Bioscavengern, die die phosphororganischen Verbindungen entweder stöchiometrisch abfangen (z.B. Antikörper) oder sie katalytisch (Enzyme, wie z.B. Paraoxonasen) hydrolysieren. Dadurch wird eine Schädigung der AChE

durch Phosphorylierung oder Phosphonylierung bereits im Ansatz verhindert. Der zweite Ansatz basiert auf der Verwendung von indirekten Parasympathomimetika, die durch eine vorübergehende Bindung an die AChE eine irreversible Inhibition durch phosphororganische Verbindungen verhindern. Im militärischen Kontext werden hierfür Carbamate wie Pyridostigminbromid (**16**) oder Physostigmin (**17**) (siehe Abbildung 7) eingesetzt (Bajgar et al., 2020; Layish et al., 2005).

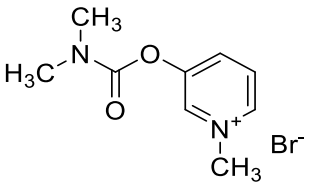

16

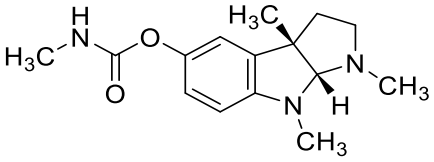

17

Abbildung 7: Pyridostigminbromid (**16**) und Physostigmin (**17**) als reversible AChE-Inhibitoren.

Trotz der vorhandenen Behandlungsansätze und langjähriger Forschung gibt es noch zahlreiche Schwierigkeiten und ungelöste Probleme. So ist eine rein präventive Behandlung mit indirekten Parasympathomimetika für große, gefährdete Bevölkerungsgruppen kaum umsetzbar (Bajgar et al., 2020). Problematisch ist außerdem, dass trotz jahrzehntelanger Bemühungen für manche Organophosphat- bzw. Organophosphonatvergiftungen bisher noch keine geeigneten Oximwirkstoffe entwickelt werden konnten (Worek et al., 2020). So ist zum Beispiel die Reaktivierungsrate für Tabun-inhibierte AChE bei der Behandlung mit gängigen Oximen nicht ausreichend (Worek et al., 2004). Zudem verlieren die Oxime bei gealterten Enzym-OP-Komplexen, wie sie z.B. bei Soman vorliegen (siehe Kapitel 1.2.2, Schema 1), ihre Wirkung (Worek et al., 2016). Und obwohl zahlreiche neue AChE-Reaktivatoren entwickelt wurden, wurde bisher keine Verbindung gefunden, die alle relevanten Nervenkampfstoffe und phosphororganischen Pestizide abdeckt und somit als Breitspektrum-Therapeutikum verwendet werden könnte (Thiermann et al., 2013; Worek and Thiermann, 2013). Derzeit wird eine kombinierte Oximtherapie angewandt, bei der eine Mischung unterschiedlicher Oxime mit einem daraus resultierenden breiteren Wirkungsspektrum verabreicht wird (Alozi and Rawas-Qalaji, 2020). Der therapeutische Wert von Atropin als Kompetitor von Acetylcholin an den Muskarinrezeptoren ist bis heute unumstritten und gehört deshalb zur Standardtherapie von phosphororganischen Vergiftungen. Die richtige Dosierung ist dabei jedoch von größter Bedeutung, da sich die Antagonisierung in einem schmalen therapeutischen Bereich bewegt: Atropin soll ACh von den muskarinischen Rezeptoren verdrängen, um eine normale Signaltransduktion zu gewährleisten, darf aber den Rezeptor auch nicht zu stark inhibieren, um einen gegenteiligen Effekt zu vermeiden (Thiermann et al., 2013).

Bei den nikotinischen Rezeptoren besteht nach wie vor eine große therapeutische Lücke. Ein erfolgversprechender Ansatzpunkt ist hier die direkte Adressierung der nAChRs durch

allosterische Modulatoren. Ziel ist es dabei, die überstimulierten Rezeptoren, die die post-synaptische Signaltransduktion blockieren, mit Hilfe von allosterischen Modulatoren, sogenannten Resensitizern, wieder in einen aktiven Zustand zu überführen. Um entsprechende Modulatoren gezielt für diesen Zweck entwickeln zu können, ist die Kenntnis der Struktur und das Verständnis der Wirkungsweise der betroffenen nAChRs essentiell (Amend et al., 2020).

1.3 Der nikotinische Acetylcholinrezeptor als Target zur Behandlung von Vergiftungen mit phosphororganischen Verbindungen

1.3.1 Aufbau und Struktur des nikotinischen Acetylcholinrezeptors

Der nikotinische Acetylcholinrezeptor ist ein ionotroper Rezeptor, welcher ligandenabhängig Ionenströme ermöglicht (Changeux, 2020). Er gehört, wie die $GABA_A$-, Glycin- und 5-HT_3-Rezeptoren, zu Rezeptoren der Cys-Loop-Superfamilie, welche alle aus fünf Untereinheiten bestehen. Die Untereinheiten des nikotinischen Acetylcholinrezeptors unterscheiden sich nicht nur untereinander, auch sind je nach Expressionsort verschiedene Zusammensetzungen dieser Untereinheiten bekannt. Jede der fünf Untereinheiten besteht aus einer extrazellulären Domäne, die hauptsächlich aus β-Faltblättern zusammengesetzt ist, einer Transmembrandomäne, die aus vier α-Helices gebildet wird, und einer kleinen intrazellulären Domäne, die im Wesentlichen aus einer α-Helix aufgebaut ist (Sine and Engel, 2006). Die kreisrunde Anordnung der fünf membrandurchspannenden Untereinheiten ermöglicht den Transport von Ca^{2+}-, Na^{2+}- oder K^+-Ionen durch die dabei gebildete Pore (Miyazawa et al., 2003; Sine and Engel, 2006).

Nikotinische Acetylcholinrezeptoren lassen sich in verschiedenen Zellen und Organen, vor allem in muskulärem oder neuronalem Gewebe, aber auch in der Haut, in Leukozyten oder in der Niere finden, wobei sie an einer Vielzahl von Prozessen im Körper beteiligt sind (Hurst et al., 2013). Sie werden je nach Hauptexpressionsort in muskuläre oder neuronale Subtypen unterteilt und unterscheiden sich wie bereits erwähnt in ihrer Zusammensetzung der Untereinheiten, was auch maßgebliche Unterschiede in der Pharmakologie zu Folge hat (Millar, 2003; Millar and Gotti, 2009). So sind zum Beispiel die heteropentameren Muskeltyp-nAChRs aus den Untereinheiten α1, δ, β, α1 und γ bzw. ε (bei der adulten Form des Rezeptors) aufgebaut (Mishina et al., 1986). Sie befinden sich an neuromuskulären Verbindungen der Skelettmuskulatur, wo sie neuromuskuläre Reize übertragen und damit die Kontraktion der Skelettmuskulatur ermöglichen. Die neuronalen nAChRs sind hingegen im peripheren und zentralen Nervensystem zu finden und damit Teil der schnellen synaptischen Übertragung von Reizen zur neuronalen Kommunikation. Neuronale nAChRs bestehen entweder aus verschiedenen Kombinationen der bisher identifizierten Untereinheiten α2, α3, α4, α5, α6, α7, α9, α10, β2, β3 oder β4 und liegen damit als Heteropentamere vor, oder sind, wie im Fall des neuronalen $(α7)_5$-Rezeptors, Homopentamere aus fünf identischen Untereinheiten (Albuquerque et al., 2009).

Bisher ist es noch nicht gelungen, die detaillierte Struktur von humanen nAChRs zu analysieren. Die bisher einzige vollständige dreidimensionale elektronenmikroskopische Aufnahme eines Modellsystems gelang Unwin *et al.* im Jahr 2005. Durch die Aufnahme von

359 elektronenmikroskopischen Bildern mit einer Auflösung von 4 Å konnte eine Strukturanalyse des *Torpedo marmorata*-nAChRs erstellt werden (siehe Abbildung 8) (Unwin, 2005). Der *Torpedo*-nAChR ist dem humanen Muskeltyp-nAChR (α1-ε-α1-δ-β) strukturell sehr ähnlich (α1-γ-α1-δ-β) und kommt in besonders hoher Expressionsdichte im Elektroorgan des Marmor-Zitterrochens der Familie *Torpedinidae* vor, was ihn zu einem geeigneten Modellsystem für *in silico*-Studien oder biologische Untersuchungen macht (Changeux, 2020).

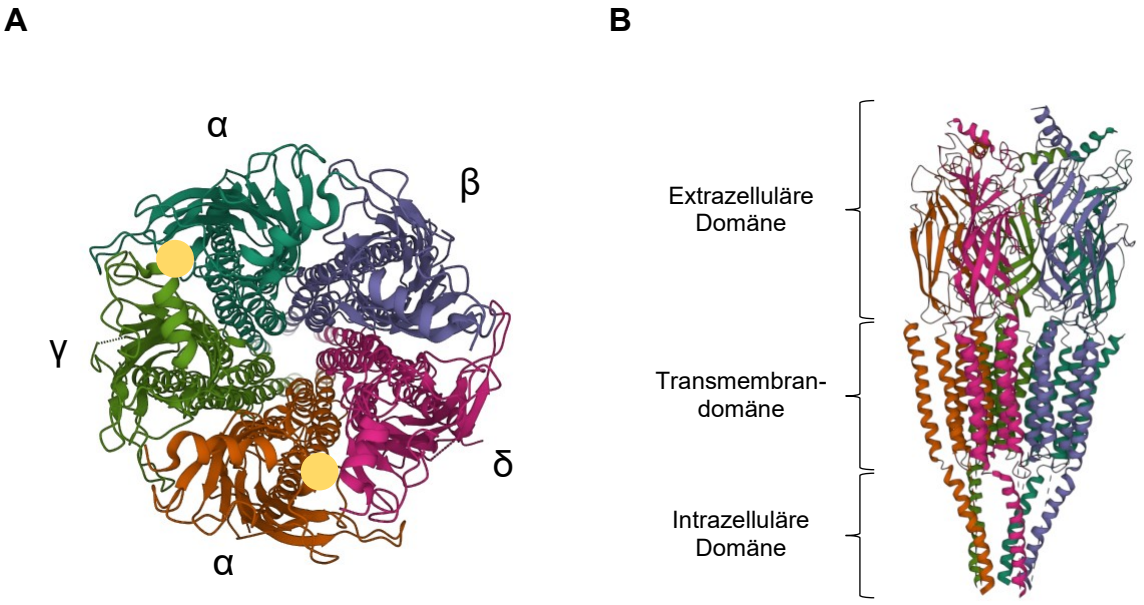

Abbildung 8: 3D-Strukturmodell des α1-γ-α1-δ-β-nAChR (Muskeltyp) aus dem Zitterrochen *Torpedo marmorata*, erstellt mithilfe von Elektronenmikroskopie, in Draufsicht (**A**) und Seitenansicht (**B**), veröffentlicht von Unwin *et al.* (Unwin, 2005). Die Struktur mit der ID 2BG9 wurde mithilfe des NGL-Viewers der Protein Datenbank (PDB) erstellt (Berman et al., 2000; Rose and Hildebrand, 2015). Zwischen den Untereinheiten α-γ und α-δ sind die Bindungsstellen des Neurotransmitters Acetylcholins farblich hervorgehoben (Hurst et al., 2013).

1.3.2 Funktionsweise des nAChRs im cholinergen System

Die orthosterischen Bindungsstellen für Acetylcholin bzw. Agonisten, wie z.B. Epibatidin oder Nikotin, befinden sich bei allen nAChR-Subtypen in einer hydrophoben aromatischen Tasche der extrazellulären Domäne, jeweils zwischen einer α-Untereinheit und einer benachbarten δ-, γ- oder ε-Untereinheit. Die Anzahl der orthosterischen Bindungsstellen ist somit von der Anzahl der α-Untereinheiten abhängig. Folglich gibt es am Muskeltyp-nAChR zwei Bindungsstellen, jeweils zwischen der α- und δ-Untereinheit sowie zwischen der α- und γ- bzw. ε-Untereinheit (Albuquerque et al., 2009; Papke, 2014).

Agonisten lösen beim Binden an den geschlossenen Rezeptor eine strukturelle Veränderung aus (Hogg et al., 2003; Monod et al., 1965). Es kommt zu einer Rotation in den α-Untereinheiten, sodass die Helices der intrazellulären Domäne, die in der Pore eine Barriere bilden und damit für einen geschlossenen Zustand sorgen, eine alternative Konformation einnehmen, wodurch ein ionendurchlässiger Kanal entsteht (Miyazawa et al., 2003; Unwin et al., 2002). Sobald der Rezeptor in den offenen Zustand übergeht, befindet er sich in einer weniger stabilen Konformation. Bei geringer ACh-Konzentration im synaptischen Spalt kehrt der Rezeptor deshalb nach Freisetzung des Agonisten wieder in den geschlossenen Zustand zurück (Karlin, 2002). Die Rezeptorkonformation hängt demnach maßgeblich von der ACh-Konzentration ab. Bei einer über einen langen Zeitraum aufrechterhaltenen, aber auch bei einer nur kurzen, jedoch hohen ACh-Konzentration, wird der Rezeptor überstimuliert und verfällt in einen desensitisierten Zustand, in dem er trotz Bindung des Agonisten dauerhaft geschlossen und inaktiv ist. Sinkt die Agonist-Konzentration im synaptischen Spalt, löst sich der gebundene Agonist vom desensitisierten Rezeptor, wodurch dieser in einen reaktivierten Zustand zurückkehren kann (Giniatullin et al., 2005). Zudem scheint es zwischen den drei beschrieben Rezeptorkonformationen diverse, subtypenabhängige Zwischenzustände zu geben, sodass sich noch kein vollständig aufgeklärtes Bild des Desensitisierungsmechanismus zeichnen lässt (Corradi and Bouzat, 2016). Ein vereinfachtes Modell der drei beschriebenen nAChR-Zustände ist in Abbildung 9 dargestellt.

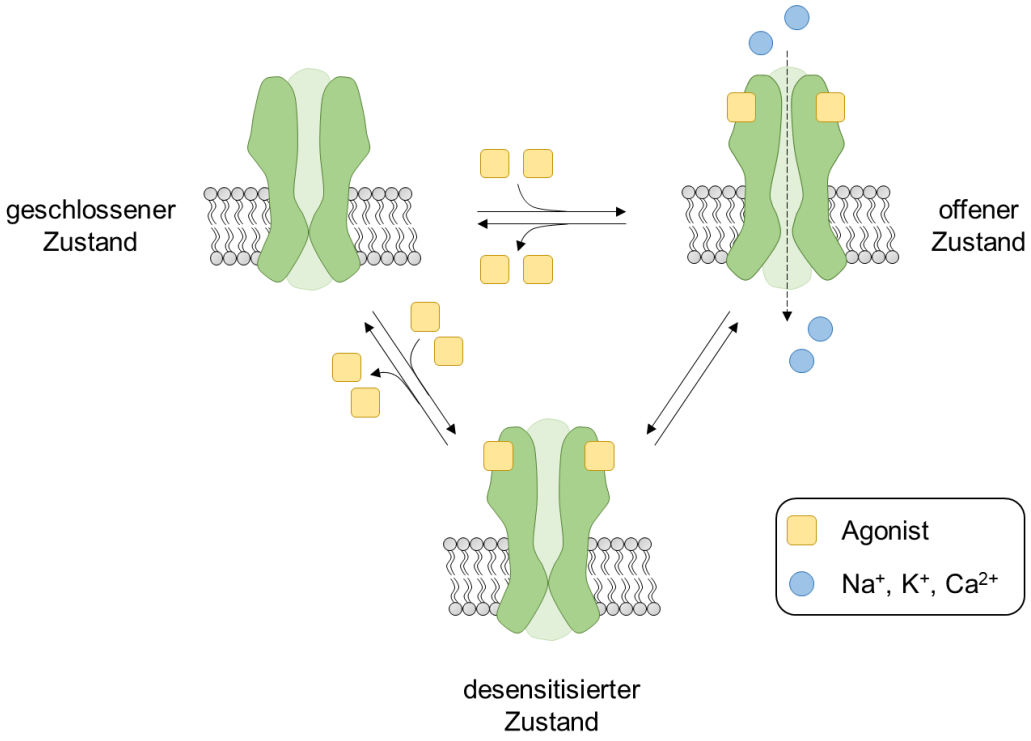

Abbildung 9: Darstellung der verschiedenen Konformationsänderungen des nAChRs in einem vereinfachten Modell nach Corradi *et al.* (Corradi and Bouzat, 2016).

Auch die Rolle der Rezeptor-Desensitisierung unter normalen physiologischen Bedingungen ist bei weitem noch nicht vollständig erforscht. Es handelt sich jedoch um eine bemerkenswerte rezeptorspezifische Kinetik, die den zeitlichen Verlauf, die Häufigkeit und die Stärke der zu übertragenden Signale zu beeinflussen scheint (Jones and Westbrook, 1996).

1.3.3 Der nAChR als Target bei Vergiftungen mit phosphororganischen Verbindungen

Bei Vergiftungen mit phosphororganischen Nervengiften kommt es, wie in Kapitel 1.2.2 und 1.3.2 beschrieben, durch die andauernd hohe Konzentration von ACh im synaptischen Spalt und der damit verbundenen Desensitisierung der nAChRs zu einer Unterbrechung der cholinergen Neurotransmission. Eine spontane Resensitisierung, der Übergang des Rezeptors zurück in den aktiven Zustand, ist bei einer hohen Agonist-Konzentration nicht möglich. Ein neuer vielversprechender Ansatzpunkt zur Therapie von Nervenkampfstoff-vergiftungen ist die Entwicklung von Verbindungen, die durch direkte Interaktion mit dem nAChR die Desensitisierung auch in Gegenwart hoher ACh-Konzentration aufheben und dadurch die Wiederherstellung der nikotinergen Neurotransmission bewirken können. Solche Verbindungen werden als positive allosterische Modulatoren (PAM) des Typs II bezeichnet. Durch Herabsetzen der Energiebarrieren zwischen den einzelnen Rezeptorkonformationen können sie eine Reaktivierung von desensitisierten Rezeptoren ermöglichen (Bertrand and Gopalakrishnan, 2007; Chatzidaki and Millar, 2015; Papke, 2014). Für neuronale nAChRs gibt es bereits eine Vielzahl von PAMs des Typs II, wie z.B. das auf den α7-Rezeptor selektiv wirkende PNU-120596, welches eine Resensitisierung desensitisierter Rezeptoren trotz hoher Agonist-Konzentration ermöglicht (Hogg et al., 2003; Hurst et al., 2005). Für die nAChRs des Muskeltyps ist bislang lediglich eine Substanzklasse bekannt, die einen positiv allosterischen Effekt auf den desensitisierten Rezeptor ausübt. Hierbei handelt es sich um Bispyridiniumsalze vom Typ des MB327, auf deren Grundlage bislang die Forschung an resensitisierenden Substanzen für desensitisierte muskuläre nikotinische Acetylcholinrezeptoren beruht.

1.4 Entwicklung von positiven allosterischen Modulatoren für den Muskeltyp-nAChR

Die Entwicklung von Bispyridiniumverbindungen als allosterische Modulatoren des nAChR gründet auf einer Zufallsentdeckung im Zuge der Forschung an Reaktivatoren der Acetylcholinesterase (AChE) in den 1970er Jahren. Dabei wurden zu Obidoxim (siehe Kapitel 1.2.3, Schema 2) strukturverwandte Verbindungen, die im Unterschied zu Obidoxim keine Oxim-Teilstrukturen aufwiesen, wie z.B. das Bispyridiniumsalz SAD 128 (siehe Abbildung 10), auf ihre pharmakologischen Eigenschaften hin untersucht.

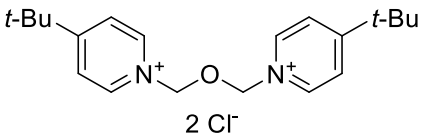

SAD-128

Abbildung 10: Strukturformel von SAD-128.

Entgegen den Erwartungen zeigte SAD-128, obwohl die für eine Reaktivierung von Organophosphat-vergifteter AChE erforderliche Oximteilstrukur fehlt, bei Nervenkampfstoffvergiftungen einen positiven Effekt. Bei *in vivo*-Versuchen mit Soman-vergifteten Mäusen führte diese Verbindung in Kombination mit Atropin im Vergleich zu einer Behandlung nur mit Atropin zu einer höheren Überlebensrate der Mäuse. Der Wirkungsmechanismus war lange Zeit unklar. Die Schutzwirkung konnte weder auf eine Inaktivierung des eingesetzten Somans noch auf eine Reaktivierung der phosphonylierten AChE zurückgeführt werden (Oldiges and Schoene, 1970). Erst knapp 20 Jahre später wurde für SAD-128 auf der Grundlage von Einzelkanalmessungen an Muskelpräparationen von Fröschen eine direkte Interaktion mit dem nAChR postuliert (Alkondon and Albuquerque, 1989). In *ex vivo*-Experimenten an Muskelpräparationen von Meerschweinchen, die mit Soman vergiftet wurden, konnte schließlich eine direkte pharmakologische Aktivität von Bispyridiniumverbindungen vom Typ des SAD-128 auf den Muskel nachgewiesen und damit der Muskeltyp-nAChR als Target für diese Klasse von Bispyridiniumverbindungen identifiziert werden (Tattersall, 1993).

1.4.1 Das Bispyridiniumsalz MB327 als Ausgangspunkt für die Entwicklung von positiven allosterischen Modulatoren für den Muskeltyp-nAChR

MB327 ist eine weitere Verbindung aus der oben genannten Klasse von Bispyridiniumverbindungen, die keine Oximfunktionen aufweisen. Sie unterscheidet sich von SAD-128 nur durch den Ersatz des Sauerstoffatoms im C3-Spacer durch eine Methylengruppe (siehe Abbildung 11). MB327 ist die hinsichtlich einer Interaktion mit dem nAChR bisher in *in vitro*-, *ex vivo*- und *in vivo*-Studien wohl am besten charakterisierte Verbindung.

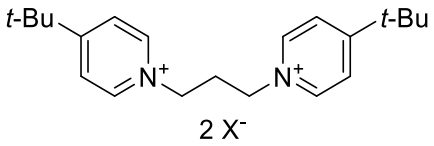

MB327 X = I^-
MB399 X = $MeSO_3^-$

Abbildung 11: Die Bispyridiniumverbindungen MB327 und MB399.

In vivo-Versuche haben gezeigt, dass MB399, das besser wasserlösliche Methansulfonat-Analogon zu MB327 (siehe Abbildung 11), in Kombination mit muskarinischen Antagonisten und indirekten Parasympathomimetika die Überlebensrate von mit Sarin, Soman, oder Tabun vergifteten Meerschweinchen verbessern kann. Dieser Effekt ist sowohl im Vergleich zu Versuchen ohne MB399-Zusatz aber auch im Vergleich zu einer entsprechenden Dreifachtherapie mit dem Oxim HI-6 anstelle von MB399 beobachtet worden (Timperley et al., 2012; Turner et al., 2011). Auch hier konnte, ähnlich wie im Falle von SAD-128 (s.o.), eine Reaktivierung der gehemmten AChE ausgeschlossen werden. Um die Wirkungsweise der Bispyridiniumverbindungen besser zu verstehen, wurde das Bindungsverhalten von MB327 am Muskeltyp-nAChR untersucht. [^{3}H]Epibatidin-Radioligand-Bindungsstudien, die an *Torpedo californica*-Präparationen durchgeführt wurden, zeigten dabei, dass MB327 in einem Konzentrationsbereich bis zu 100 µM keine wesentliche Affinität zur orthosterischen Bindungsstelle des nAChR aufweist (Niessen et al., 2011). Da für MB327 jedoch in *ex vivo*-Experimenten mit Soman-vergifteten Meerschweinchen- und Ratten-Diaphragmen sowie mit Soman-vergifteten humanen Interkostalmuskeln im entsprechenden Konzentrationsbereich eine signifikante Wiederherstellung der Muskelkraft gefunden wurde (Seeger et al., 2012; Turner et al., 2011), konnte ziemlich sicher ausgeschlossen werden, dass der reaktivierende Effekt durch Bindung an die orthosterische Bindungsstelle des nAChR hervorgerufen wird.

In Experimenten, die mit Hilfe der Surface-Electrogenic-Event-Reader-Technologie (SURFE^{2}R) durchgeführt wurden, konnte gezeigt werden, dass MB327 als positiver

allosterischer Modulator den Rezeptor aktiviert. So konnte MB327 bei zellfreien elektrophysiologischen Untersuchungen mit festkörpergestützten Membranen (Solid Supported Membranes, SSMs), bei welchen eine Messung von Ladungstranslokationen erfolgt, einer Carbachol-vermittelten Desensitisierung von *Torpedo califonica*-nAChR entgegenwirken (Niessen et al., 2016). Die spezifische Bindung von MB327 an den nAChR wurde schließlich in unserer Arbeitsgruppe mit Hilfe von Sättigungsexperimenten an *Torpedo*-nAChRs in einem MS-basierten Bindungsassay nachgewiesen. Dabei wurde in Kompetitionsexperimenten mit [$^2H_6$]MB327 als Reporterligand eine Bindungsaffinität von K_i = 18.3 ± 2.6 µmol/L ermittelt (Sichler et al., 2018).

Diese sehr vielversprechenden Ergebnisse wurden von *in vivo*-Versuchen getrübt, die zeigten, dass MB327 bei höheren Konzentrationen toxische Effekte aufweist. So führte die Verabreichung von 100 mg/kg MB327 bei gesunden Meerschweinchen zum Tod der Tiere (Price et al., 2016). Eine mögliche Erklärung hierfür ist die Inhibierung nikotinischer Acetylcholinrezeptoren durch Bindung von MB327 an die orthosterischen Bindungsstellen. Zwar wurde, wie bereits oben beschrieben, von Niessen *et al.* im [^{3}H]Epibatidin-Radioligand-Bindungsassay in einem Konzentrationsbereich bis 100 µM keine signifikante Bindung von MB327 an die orthosterische Bindungsstelle gefunden. In weiteren Untersuchungen zeigte sich jedoch bei höheren Konzentrationen (> 100 µM) eine relevante Affinität für diese Bindungsstellen (Niessen et al., 2018). Daraufhin wurden in erneuten *ex vivo*-Experimenten an Soman-vergifteten Ratten-Diaphragmen auch höhere Substanzkonzentrationen (bis zu 1000 µM) von MB327 untersucht. Dabei wurde bei Konzentrationen im Bereich von 100-300 µM wieder eine Reaktivierung der Muskelkraft beobachtet. Bei höheren Konzentrationen (> 300 µM) wurde dagegen ein gegenläufiger Effekt – eine Abnahme der Muskelkraft – festgestellt (Niessen et al., 2018). Dieser biphasische Verlauf der Konzentrations-Wirkungskurve wurde mit der bei höheren Konzentrationen signifikanten Affinität zur orthosterischen Bindungsstelle in Verbindung gebracht.

Diese Ergebnisse verdeutlichen, dass MB327 aufgrund einer zu geringen therapeutischen Breite für eine therapeutische Anwendung am Menschen nicht in Betracht kommt. Gleichwohl erschien die Verbindung als Ausgangspunkt für weitere Untersuchungen vielversprechend. So wurden ausgehend von MB327 weitere Bispyridiniumverbindungen untersucht, mit dem Ziel, Verbindungen mit einer höheren Affinität zur allosterischen Bindungsstelle zu entwickeln.

1.4.2 Entwicklung neuer Bispyridiniumverbindungen auf der Basis von MB327 als allosterische Modulatoren für den nAChR

Die Entwicklung weiterer allosterischer Modulatoren für den nAChR beruhte auf der systematischen Variation der Molekülstruktur von MB327. Zur Bestimmung der Bindungsaffinitäten sowie der intrinsischen Aktivitäten kamen dabei, wie in Kapitel 1.4.1 beschrieben, verschiedenste *in vitro*- und *ex vivo*-Assays zum Einsatz. Zusätzlich halfen *in silico*-Studien dabei, die Modulation des Rezeptors durch Ligandenbindung besser zu verstehen. Die Untersuchung vieler verschiedener Strukturanaloga mit vielfältigen Substitutionsmustern ist für die Ableitung von Struktur-Wirkungs-Beziehungen als Grundlage für die zielgerichtete Entwicklung von neuen, höher aktiven Verbindungen unabdingbar. Erst wenn die Zusammenhänge zwischen der Molekülstruktur und der Wirkung im biologischen System verstanden werden, kann zielgerichtet eine Optimierung hin zu verbesserten Wirkstoffen erfolgen.

Charakteristisch für die Struktur der Bispyridiniumverbindungen vom Typ des MB327 sind die beiden über die Ring-Stickstoffatome und einen Propan-1,3-diyl-Spacer (C3-Spacer) miteinander verbunden Pyridiniumringe. Erste Bestrebungen, verbesserte Modulatoren zu gewinnen, widmeten sich dem Abstand der kationischen Zentren und damit der Spacerlänge. So wurden MB327-Analoga mit C1- bis C10-Spacern in *in vitro*-Assays auf ihre Bindungsaffinität zur orthosterischen Bindungsstelle und in elektrophysiologischen Assays sowie *ex vivo*-Assays mit Soman-vergifteten Ratten-Diaphragmen hinsichtlich ihrer intrinsischen Aktivität untersucht. Dabei wurden für MB327 Assay-übergreifend die vielversprechendsten Ergebnisse erzielt: das Bispyridiniumsalz mit dem C3-Spacer zeigte nicht nur die niedrigste Affinität zur orthosterischen Bindungsstelle, sondern auch die höchsten intrinsischen Aktivitäten. Sowohl eine Kettenverkürzung als auch eine Kettenverlängerung führte zu einer Abnahme der intrinsischen Aktivität (Niessen et al., 2016; Niessen et al., 2013; Seeger et al., 2013).

Daraufhin wurde in unserer Arbeitsgruppe im Rahmen eines Vorläuferprojektes eine große Vielfalt von symmetrischen MB327-Analoga mit Propan-1,3-diyl-Spacer (siehe Abbildung 12) synthetisiert und im [$^2H_6$]MB327-MS-Bindungsassay auf ihre Affinität zur allosterischen Bindungsstelle untersucht (Rappenglück et al., 2018b). Es wurden dabei anstelle der *tert*-Butyl-Reste in 4-Position der Pyridiniumringe andere apolare (**18**) aber auch polare (**19**) Reste in die 2-, 3- oder 4-Position der Pyridiniumringe eingeführt, um deren sterischen Einfluss und/oder die Fähigkeit zur Ausbildung von Wasserstoffbrückenbindungen zur Bindungstasche zu untersuchen. Des Weiteren wurden von MB327 abgeleitete Verbindungen, die zusätzlich zu den *tert*-Butylresten in 4-Position Substituenten in der 2- oder 3-Position enthalten, synthetisiert (**20**). Um die strukturelle Vielfalt noch weiter zu erhöhen, wurden verschiedenste

N-Heterocyclen anstelle der für die Bispyridiniumverbindungen typischen Pyridiniumreste eingeführt (Verbindungen **21**).

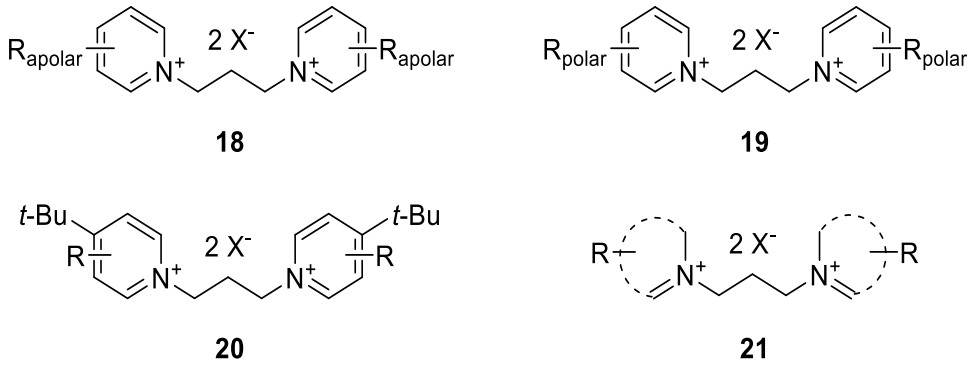

Abbildung 12: Symmetrische MB327-Analoga.

Insgesamt konnten für Verbindungen mit unpolaren Resten, die lipophile Wechselwirkungen erlauben (z.B. C≡CH, Me, *i*-Pr, *t*-Bu, Ph), höhere Bindungsaffinitäten erzielt werden, als für entsprechende Verbindungen mit polaren Resten (z.B. OMe, $CONMe_2$, COOEt). Die niedrigste Bindungsaffinität unter den untersuchten Verbindungen ($pK_i = 2.74 \pm 0.13$) wurde für die 3-Carboxyl-4-*tert*-Butyl-substituierte Verbindung PTM0028 gefunden (siehe Abbildung 13). Im Gegensatz dazu konnte für die lipophilste Verbindung, das 3-Phenyl-4-*tert*-Butyl-substituierte Bispyridiniumsalz PTM0022 (siehe Abbildung 13) die höchste Bindungsaffinität der untersuchten Substanzen ($pK_i = 5.16 \pm 0.07$) gemessen werden, womit im Vergleich zu MB327 ($pK_i = 4.73 \pm 0.03$) eine Erhöhung der Affinität um mehr als 0.4 log-Einheiten erzielt wurde. Für eine Bindung zum Target scheinen demnach zusätzliche lipophile Wechselwirkungen wie z.B. Van-der-Waals-, π-π- oder Kation-π-Wechselwirkungen relevant zu sein. Andererseits zeigte die in 3-Position NMe_2-substituierte Verbindung PTM0007 (siehe Abbildung 13) mit einem pK_i von 4.78 ± 0.05 als einzige der polar substituierten Verbindungen eine höhere Affinität als ein Großteil der unpolar substituierten Verbindungen, darunter auch das 3-*tert*-Butyl-substituierte Analogon PTM0001 ($pK_i = 4.44 \pm 0.10$, siehe Abbildung 13). Die stärker polare NMe_2-Gruppe scheint damit als bioisosterer Ersatz für die *tert*-Butylgruppe geeignet zu sein.

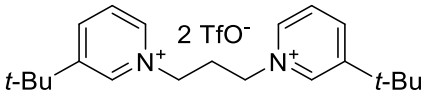

PTM0001

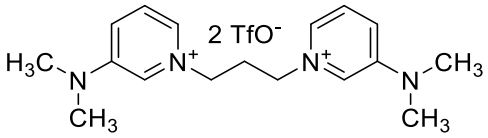

PTM0007

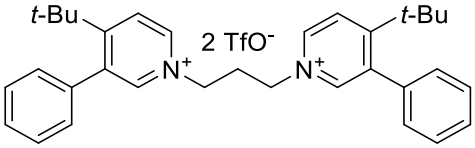

PTM0022

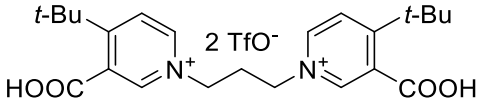

PTM0028

Abbildung 13: Strukturformeln von PTM0001, PTM0007, PTM0022 und PTM0028.

Erste Docking Studien mit MB327 an *Torpedo*-nAChR (Wein et al., 2018), die später nicht belegt werden konnten (Kaiser et al., 2023), legten nahe, dass die MB327-Bindungstasche im nAChR nicht, wie ursprünglich angenommen, symmetrisch aufgebaut ist, sondern eine eher polare und eine eher unpolare Seite aufweist. Von den daraufhin synthetisierten nicht-symmetrischen MB327-Analoga, die jeweils eine weniger polare und eine stärker polare Teilstruktur aufweisen (siehe Abbildung 14), wurden entsprechend höhere Bindungsaffinitäten erwartet (Rappenglück et al., 2018a). Die meisten Zielverbindungen wiesen zusätzlich zu einem 4-*tert*-Butylpyridiniumrest, unterschiedliche, überwiegend polar-substituierte Pyridiniumreste (**22**) oder *N*-Heterocyclen, wie z.B. *N*-Methylimidazolium-, 1,3-Thiazolium- oder Isoquinoliniumeinheiten (**23**) auf. Weitere Zielverbindungen (**24**) leiteten sich von 3-Methoxypyridin und einem zweiten, in 4-Position substituierten, Pyridin ab. Außerdem wurde die monokationische Verbindung **25** untersucht, welche anstelle einer 4-*tert*-Butylpyridiniumgruppe eine 4-*tert*-Butylphenylgruppe aufweist.

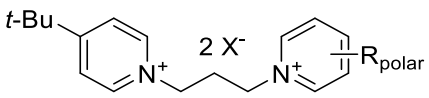

22

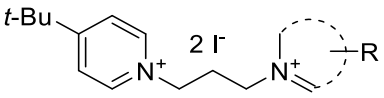

23

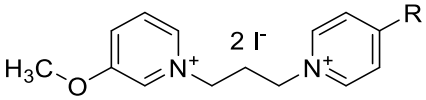

24

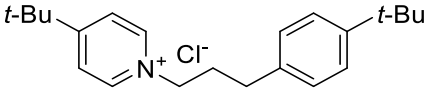

25

Abbildung 14: Nicht-symmetrische MB327-Analoga.

Obwohl einige der von Rappenglück *et al.* beschriebenen nicht-symmetrischen Verbindungen MB327 in seiner Affinität zur allosterischen Bindungsstelle übertrafen, erreichte keine eine vergleichbar hohe Bindungsaffinität wie die symmetrische Verbindung PTM0022 mit dem bis dato höchsten pK_i-Wert.

Um im Falle der Verbindungen **22** und **23** den Einfluss des Substituenten bzw. des *N*-Heterocyclus besser vergleichen zu können, wurde auch das MB327-Analogon PTM0029, das über eine unsubstituierte Pyridiniumeinheit verfügt, synthetisiert (siehe Abbildung 15). Für diese Verbindung konnte ein affinitätssteigernder Effekt von polaren Substituenten, wie z.B. NMe_2-Gruppen, gezeigt werden. So wiesen die beiden Verbindungen PTM0030 ($pK_i = 4.92 \pm 0.09$) und PTM0056 ($pK_i = 4.90 \pm 0.06$) im Vergleich zu PTM0029 ($pK_i = 4.52 \pm 0.06$) eine höhere Affinität auf. Die NMe_2-Gruppe von Verbindung PTM0056 zeigte dabei auch einen etwas stärkeren Effekt als die entsprechende 4-*tert*-Butylgruppe von MB327 ($pK_i = 4.73 \pm 0.03$). Der Austausch der *tert*-Butylgruppe an der 4-Position des zweiten Pyridiniumrings von PTM0056 durch eine Methoxygruppe an der 3-Position erwies sich dagegen als nachteilig. Für die entsprechende Zielverbindung PTM0042 wurde im Vergleich zu PTM0056 eine geringere Bindungsaffinität ($pK_i = 4.40 \pm 0.06$) festgestellt. Für das nur einfach positiv geladene Desaza-Analogon von MB327, PTM0060 (**25**), mit einem 4-*tert*-Butylphenylrest anstelle eines der beiden 4-*tert*-Butylpyridinium-Reste, wurde im Vergleich zu MB327 eine um knapp 0.4 log-Einheiten geringere Affinität gefunden ($pK_i = 4.34 \pm 0.04$), was die Bedeutung einer bis-kationischen Grundstruktur verdeutlicht. Unter den Verbindungen der allgemeinen Struktur **23**, die anstelle eines der beiden 4-*tert*-Butylpyridiniumreste von MB327 einen anderen *N*-Heterocyclus aufweisen, fanden sich ebenfalls Verbindungen mit etwas höherer Affinität als MB327. So wurde zum Beispiel für Verbindung PTM0054 mit einer Isoquinolinium-Teilstruktur ein pK_i-Wert von 4.90 ± 0.06 gefunden. Zusammengefasst wiesen die zu Beginn meiner Arbeit zu den Struktur-Wirkungs-Beziehungen von MB327-Analoga vorliegenden Erkenntnisse auf günstige Effekte einer nicht-symmetrischen bis-kationischen Grundstruktur, mit einer mehr polaren und einer mehr apolaren Hälfte, hin. Das Vorhandensein einer der beiden 4-*tert*-Butylpyridinium-Teilstrukturen von MB327 erschien ebenfalls günstig. Eine Steigerung der Bindungsaffinitäten ließ sich schließlich mit der Einführung von Phenylsubstituenten in die 3-Position der Pyridiniumringe erwarten.

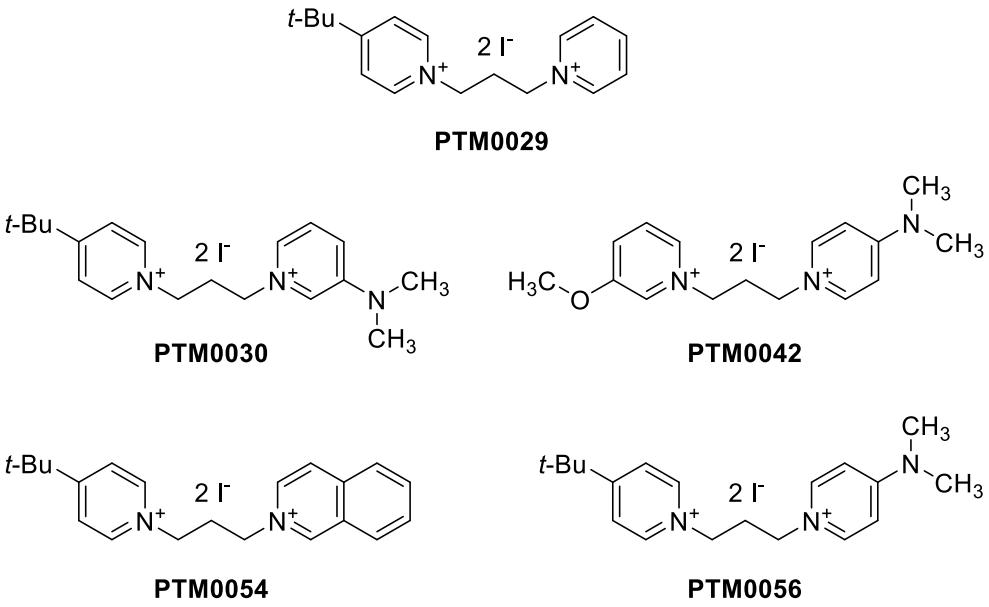

Abbildung 15: Strukturformeln der nicht-symmetrischen Bispyridiniumverbindungen PTM0029, PTM0030, PTM0042, PTM0054 und PTM0056.

Vor dem Hintergrund der im Vorgängerprojekt gewonnen Erkenntnissen zu den Struktur-Aktivitäts-Beziehungen der Bispyridiniumverbindungen bestand durchaus noch Entwicklungspotential, da keine der bisher untersuchten MB327-Analoga – mit Ausnahme von PTM0022 – eine im Vergleich zu MB327 deutlich höhere Affinität zur allosterischen MB327-Bindungstasche am nAChR aufwies. Um Verbindungen mit höheren Bindungsaffinitäten zu erzeugen ist die Einführung von stärker mit der Bindungstasche interagierenden Substituenten essenziell. Vor allem die im polaren Bereich der Bindungstasche angenommenen Aspartat-, Threonin- oder Tyrosin-Reste erschienen als Ansatzpunkt. Aufgrund ihrer Wasserstoffbrückendonor- und -akzeptor-Eigenschaften sind sie sehr wahrscheinlich von vielen Wassermolekülen umgeben (Kaiser et al., 2023; Wein et al., 2018). Idealerweise führt eine Verdrängung der Wassermoleküle aus der Bindungstasche durch polare Substituenten zu einer höheren Affinität. Die Herausforderung bei der Entwicklung von höher affinen Liganden bestand also darin, die Verbindungen so zu modifizieren, dass sie den polaren Teil der Bindungstasche möglichst vollständig ausfüllen.

Doch nicht nur die Affinitäten zur allosterischen MB327-Bindungsstelle, die im Rahmen des Vorgängerprojektes von Rappenglück und Sichler *et al.* untersucht wurden, sind für eine Wirkstoffoptimierung relevant (Rappenglück et al., 2018a, b). Auch die für die potenziellen Resensitizer im Ratten-Diaphragma-Assay an Soman-vergifteten Muskeln ermittelte *ex vivo*-Aktivität gibt wichtige Hinweise darauf, ob eine Verbindung als Startpunkt für eine weitere medizinalchemische Entwicklung von Interesse ist. So wurde kurz vor Projektstart für die 4-*N*,*N*-Dimethylamino-substituierte Verbindung PTM0056 (siehe Abbildung 15) eine auffallend hohe Muskelkraftwiederherstellung an Soman-vergifteten Ratten-Diaphragmen festgestellt

(Bernauer et al., 2024). Trotz einer im Vergleich zu MB327 nur etwas höheren Bindungsaffinität scheint PTM0056 den Muskel effektiver zu reaktivieren als MB327. Diese vielversprechenden Ergebnisse machten PTM0056 zu einem interessanten Ausgangspunkt für die weitere Entwicklung von nicht-symmetrischen Bispyridiniumverbindungen als Modulatoren desensitisierter nAChR.

1.4.3 UNC0646 und A366 als neue Ansatzpunkte für die Entwicklung von allosterischen Modulatoren für den Muskeltyp-nAChR

Neben der Entwicklung neuer Bispyridiniumverbindungen war das Screening von Substanzbibliotheken mit einem breiten Spektrum strukturell diverser, biologisch aktiver Verbindungen ein vielversprechender Ansatzpunkt für die Suche nach neuen Verbindungen mit einer möglichst hohen Affinität zur MB327-Bindungsstelle des nAChR. Neue Chemotypen, die im Vergleich zu MB327 idealerweise bereits eine deutlich höhere Affinität zur MB327-Bindungsstelle aufweisen, könnten eine günstigere Startposition für eine Wirkstoffentwicklung darstellen.

So wurde im Rahmen des Vorgängerprojekts unter Verwendung des zuvor entwickelten [$^2H_6$]MB327-MS-Bindungsassays ein Screening zweier Substanzbibliotheken durchgeführt (Sichler et al., 2024). Dabei wurde ein Pool aus über 1300 verschiedenen biologisch aktiven Substanzen aus der *Tocriscreen Plus*- und der *ChemDiv ion channel ligand*-Substanzbibliothek hinsichtlich der Bindungsaffinität an die MB327-Bindungsstelle des *Torpedo*-nAChR untersucht. Zehn Verbindungen konnten dabei identifiziert werden, welche bei einer Testsubstanzkonzentration von 10 µM den deuterierten [$^2H_6$]MB327-Marker (10 µM Markerkonzentration) zu mehr als 50% verdrängen konnten. Unter diesen als aktiv identifizierten Substanzen sind zwei Verbindungen besonders aufgefallen, UNC0646 und A366.

Das Chinazolin UNC0646, welches in der 2-, 4- und 7-Position unterschiedliche basische Reste enthaltende Substituenten trägt (siehe Abbildung 16), wurde von Liu *et al.* als selektiver Inhibitor für die Histon Methyltransferase G9a entwickelt (Liu et al., 2011). Im MS-Bindungsassay am nAChR von *Torpedo californica* mit [$^2H_6$]MB327 als Reporterligand zeigte die Verbindung mit einem pK_i-Wert von 6.23 ± 0.02 (Sichler et al., 2024) im Vergleich zu MB327 (pK_i = 4.73 ± 0.03) (Rappenglück et al., 2018b) eine mehr als eine Zehnerpotenz höhere Bindungsaffinität. UNC0646 war zu Beginn dieser Arbeit tatsächlich der Ligand mit der höchsten bekannten Affinität zur MB327-Bindungsstelle und erschien damit als ein sehr vielversprechender Ansatzpunkt für weitere Untersuchungen.

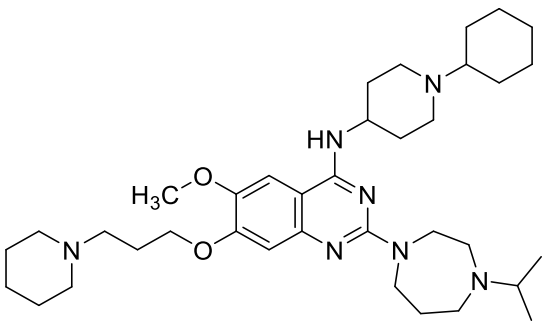

UNC0646

Abbildung 16: Strukturformel von UNC0646.

Der zweite vielversprechende Screening-Hit war das 2-Amino-3*H*-indol A366 (siehe Abbildung 17). Ursprünglich ebenfalls als Inhibitor der Methyltransferase G9a entwickelt (Sweis et al., 2014) fiel A366 durch eine im Vergleich zu MB327 um ca. 0.8 log-Einheiten höhere Affinität zur MB327-Bindungsstelle auf. Mit einem pK_i-Wert von 5.52 ± 0.15 (Sichler et al., 2024) bleibt A366 zwar hinsichtlich der Affinität hinter UNC0646 (pK_i = 6.23 ± 0.02) zurück, besitzt dafür aber eine deutlich geringere Molekülmasse (MW = 329.44 g/mol gegenüber 621.90 g/mol bei UNC0646) und erfüllt damit eher das in der Wirkstoffforschung besonders wichtige Kriterium einer hohen *ligand efficiency*. Diese Eigenschaften machten A366 ebenfalls zu einem attraktiven Ausgangspunkt für eine Wirkstoffoptimierung.

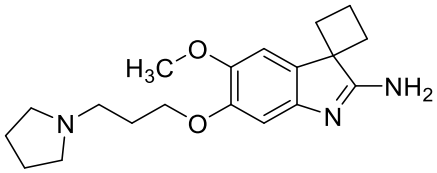

A366

Abbildung 17: Strukturformel von A366.

2 Ziele der Arbeit

Die Entwicklung von Resensitizern desensitisierter nikotinischer Acetylcholinrezeptoren ist ein vielversprechender neuer Ansatzpunkt zur Behandlung von Nervenkampfstoffvergiftungen. Da die prototypische Modellverbindung MB327 eine zu geringe Wirkstärke und entsprechend eine unzureichende therapeutische Breite aufweist, sollten im Rahmen meiner Arbeit ausgehend von 4-Amino-substituierten MB327-Analoga, wie z.B. PTM0056, und den beiden Screening-Hits UNC0646 und A366, neue Resensitizer entwickelt werden

2.1 Rationales Wirkstoffdesign

Die vorliegende Arbeit wurde im Rahmen des Forschungsvorhabens E/U2AD/KA019/IF558, finanziert durch das Bundesamt für Ausrüstung, Informationstechnik und Nutzung der Bundeswehr (BAAINBw), von Oktober 2019 bis März 2023 an der Ludwig-Maximilians-Universität München im Arbeitskreis von Prof. Dr. F. F. Paintner / Prof. Dr. K. T. Wanner im Bereich Medizinische Chemie angefertigt. Zusammen mit weiteren Forschungsarbeiten in unserer Arbeitsgruppe ist die vorliegende Arbeit Teil eines interdisziplinären Forschungsprojekts zur Entwicklung neuartiger Modulatoren zur Behandlung von Nervenkampfstoffvergiftungen. In einem iterativen Prozess wurden aufeinander aufbauend *in silico*- (Molecular Modeling), präparativ-synthetische, biologische und pharmakologische Methoden (MS-Bindungsassay, Ratten-Diaphragma-Assay) genutzt, um zielgerichtet neue potente Wirkstoffe zu entwickeln (siehe Abbildung 18).

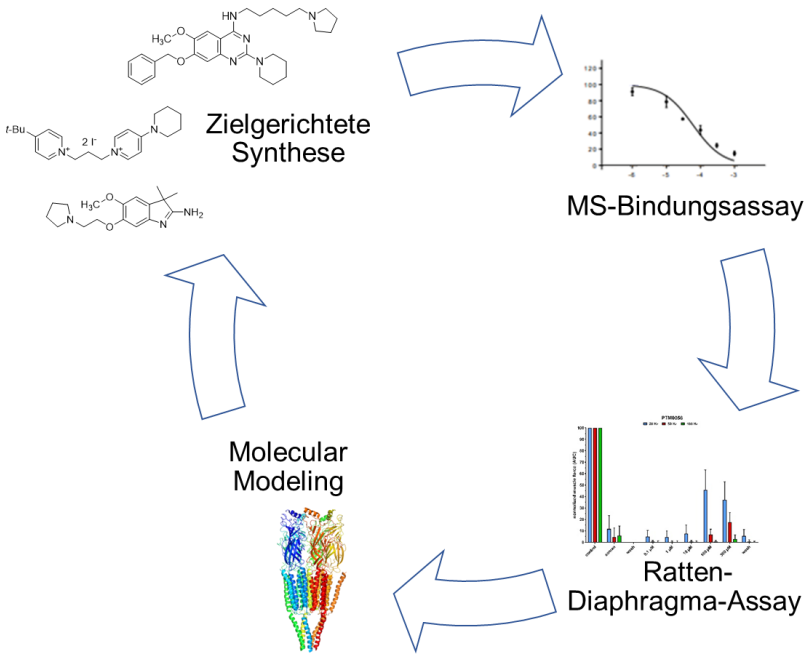

Abbildung 18: Darstellung des iterativen Forschungsprozesses innerhalb dieses Projekts.

Der MS-Bindungsassay, der im Vorgängerprojekt von S. Sichler entwickelt worden war, stellte zu Beginn des Projektes die effizienteste Methodik zu Charakterisierung von Struktur-Aktivitäts-Beziehungen von allosterischen Modulatoren an der MB327-Bindungsstelle des nAChRs dar (Sichler et al., 2018). Als Reporterligand zur Affinitätsbestimmung an *Torpedo californica* nAChR-Präparationen wurde dabei deuteriertes [$^{2}H_{6}$]MB327 verwendet. Im Rahmen des Forschungsprojekts sollte der Assay hinsichtlich seiner Effizienz und Robustheit weiterentwickelt werden. Sowohl die von mir synthetisierten Verbindungen als auch kommerziell verfügbare Analoga sollten damit im Verlauf des Projektes charakterisiert werden. Die Durchführung dieser biologischen Untersuchungen sollte an der Ludwig-Maximilians-Universität München im Arbeitskreis von Prof. Dr. F. F. Paintner / Prof. Dr. K. T. Wanner durch V. Nitsche stattfinden. In den MS-Bindungsassays als besonders affin erkannte Verbindungen sollten anschließend in Ratten-Diaphragma-Assays auf ihre Fähigkeit zur Muskelkraftwiederherstellung bei Soman-vergifteten Muskelpräparationen untersucht werden. Dies sollte in der Arbeitsgruppe von Dr. T. Seeger am Institut für Pharmakologie und Toxikologie der Bundeswehr München (InstPharmToxBw) erfolgen. Zusätzlich dazu sollte die Auswahl der Zielstrukturen in jeder Phase des Optimierungsprozesses von den Erkenntnissen begleitender *in silico*-Untersuchungen, durchgeführt von J. Kaiser im Arbeitskreis von Prof. Dr. H. Gohlke an der Heinrich-Heine-Universität Düsseldorf, geleitet werden. Ziel war es, neue tiefere Einblicke in die Struktur-Wirkungs-Beziehungen zu erhalten und auf dieser Grundlage mit Hilfe des *Computer Aided Drug Design* (CADD), Strukturvorschläge für die Weiterentwicklung der jeweiligen Hit-Substanzen, zu erzeugen. Die daran anknüpfenden chemischen Synthesen zur Darstellung neuer potenzieller Modulatoren wurden von mir geplant, durchgeführt und ausgewertet, und sind in dieser Arbeit niedergeschrieben.

2.2 Synthese nicht-symmetrischer MB327-Analoga

Im Rahmen der vorliegenden Arbeit stand zunächst die Synthese von Bispyridiniumverbindungen im Fokus. Dabei sollten für die Auswahl der Zielstrukturen sowohl Erkenntnisse zu Struktur-Wirkungs-Beziehungen aus bereits vorliegenden biologischen Untersuchungen als auch Ergebnisse von ersten *in silico*-Untersuchungen genutzt werden. Besonders vielversprechend erschienen dabei im Hinblick auf den nicht-symmetrischen Charakter der postulierten Bindungstaschen, mit jeweils einem sehr lipophilen und einem polaren Bereich, insbesondere nicht-symmetrische Bispyridiniumverbindungen mit jeweils einem unpolaren und einem polaren Rest an der 4- bzw. 4´-Position der Pyridiniumringe. Da bei Projektstart bereits erste vielversprechende Ergebnisse aus dem Ratten-Diaphragma-Assay für das im Vorgängerprojekt synthetisierte nicht-symmetrische MB327-Analogon PTM0056 (siehe Abbildung 15), mit einem *N,N*-Dimethylamino-Substituenten anstelle eines der *tert*-Butyl-Reste von MB327, vorlagen, sollten Struktur-Wirkungs-Beziehungen für Bispyridiniumverbindungen dieses Typs abgeleitet werden. Dafür sollten zunächst Analoga von PTM0056 mit modifizierten 4-Aminosubstituenten (**26**) dargestellt werden (siehe Abbildung 19). An die Stelle der *N,N*-Dimethylaminogruppe von PTM0056 sollten eine NH_2-Gruppe, eine *N*-Methylaminogruppe, unterschiedliche sekundäre Aminogruppen (z.B. $-NMe_2$, $-NBn_2$), cyclische Aminoreste [z.B. R^1, R^2 = $-(CH_2)_4-$] sowie Acylaminoreste (z.B. R^1 = H, R^2 = $COCH_3$) treten. Die Auswahl der Zielstrukturen sollte dabei in jeder Phase des Optimierungsprozesses von den Erkenntnissen begleitender *in silico*-Untersuchungen geleitet werden.

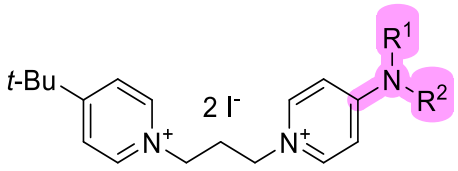

26

Abbildung 19: Allgemeine Strukturformel der MB327-Analoga **26**.

Die Zielverbindungen der allgemeinen Struktur **26** sollten sich, angelehnt an die etablierte Syntheseroute für nicht-symmetrische Bispyridiniumverbindungen von Rappenglück *et al.*, in zwei Schritten aufbauen lassen (siehe Schema 3) (Rappenglück et al., 2018a).

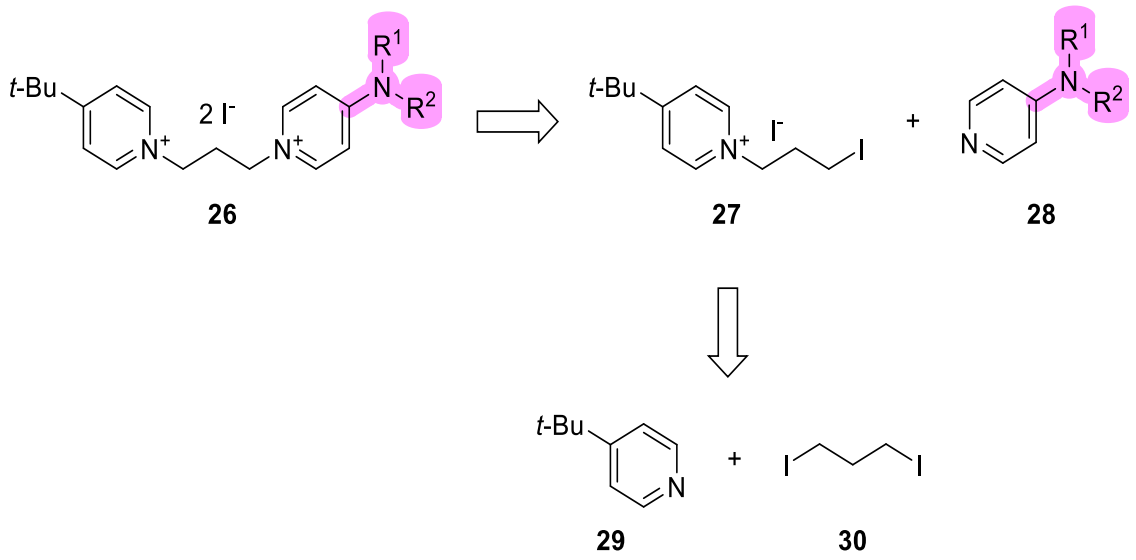

Schema 3: Retrosynthese der Zielverbindungen **26** aus den Bausteinen **28**, **29** und **30**.

Die Synthese der Zielverbindungen **26** erfolgt somit durch Monoalkylierung von 4-*tert*-Butylpyridin (**29**) mit 1,3-Diiodpropan (**30**) und nachfolgender Alkylierung der entsprechenden 4-Amino-substituierten Pyridine **28** mit dem als Zwischenprodukt erhaltenen 4-(*tert*-Butyl)-1-(3-iodopropyl)pyridin-1-iumiodid (**27**).

2.3 Synthese von UNC0646-Analoga

Ein weiterer Schwerpunkt dieser Arbeit sollte auf der Synthese von UNC0646-Analoga liegen. Das in 2-, 4- und 7-Position mit unterschiedlichen basischen Resten substituierte Chinazolin UNC0646 (siehe Abbildung 16) erschien wegen seiner zu Beginn dieser Arbeit höchsten bekannten Affinität zur MB327-Bindungsstelle des nAChRs (Sichler et al., 2024), als äußerst vielversprechender Ausgangspunkt für weitere Untersuchungen. Um die für die hohe Affinität verantwortlichen pharmakophoren Gruppen zu identifizieren, war beabsichtigt, die Struktur dieser Hit-Verbindung breit zu variieren. So sollten insbesondere die basischen Substituenten in 2-, 4- und 7-Position des Chinazolin-Grundkörpers von UNC0646, die potenziell starke Wechselwirkungen mit der Bindungsstelle eingehen können, systematisch abgewandelt werden. Strukturelle Abwandlungen sollten dabei den Austausch durch strukturverwandte Substituenten, aber auch durch solche mit reduziertem sterischen Anspruch bis hin zu einem Wasserstoffatom umfassen. Die Kenntnis der für diese Analoga ermittelten Bindungsaffinitäten sollte dann Ansatzpunkte für eine weitere Hit-Optimierung liefern.

Die im Rahmen dieser Arbeit geplanten Strukturvariationen lassen sich im Wesentlichen in drei Gruppen einteilen. In der ersten Gruppe sollte die basische Seitenkette von UNC0646 in der 7-Position unverändert beibehalten und die Substituenten in 2- und 4-Position breit variiert werden. Dabei sollten vor allem kleinere, Aminofunktionen enthaltende Reste zum Einsatz kommen. Die zweite Gruppe von Analoga sollte strukturell vereinfacht werden, in dem die basische Seitenkette in 7-Position durch eine Methoxygruppe ersetzt wird. Sollte das dabei erhaltene UNC0646-Analogon, bei dem die Substituenten in 2- und 4-Postion unverändert vorliegen, eine hinreichende Affinität zur MB327-Bindungsstelle aufweisen, sollten die Substituenten in 2- und 4-Position ähnlich wie in der ersten Gruppe breit abgewandelt werden. Die Zielverbindungen der dritten Gruppe sind durch den Ersatz des Aminosubstituenten in 2-Position durch ein Wasserstoffatom charakterisiert. Sollte das entsprechende UNC0646-Analogon, bei dem die Substituenten in 4- und 7-Postion unverändert vorliegen, eine hinreichende Affinität zur MB327-Bindungsstelle aufweisen, sollte der Substituent in 4-Position und insbesondere die basische Seitenkette in 7-Position breit abgewandelt werden (siehe Abbildung 20).

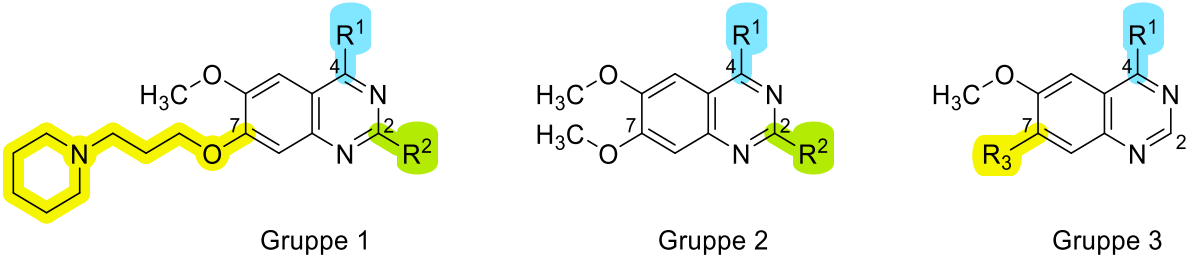

Abbildung 20: Allgemeine Strukturformeln von UNC0646-Analoga der Gruppen 1, 2 und 3.

Für die Synthesen der oben genannten Zielverbindungen sollten aufbauend auf literaturbekannten Arbeiten auf dem Gebiet der Synthese von Chinazolinderivaten vom Typ des UNC0646 (Liu et al., 2011; Liu et al., 2009; Liu et al., 2010; Sundriyal et al., 2017) effiziente konvergente Verfahren entwickelt werden, die breite Strukturvariationen an der 2-, 4- oder 7-Position erlauben. Ausgangspunkt sollten dabei entsprechende kommerziell erhältliche 2,4-Dichlor- oder 4-Chlorchinazolinbausteine sein.

Am Beispiel von Zielverbindungen der ersten Gruppe von UNC0646-Analoga mit variierenden Resten in der 2- und 4-Position des Chinazolingrundgerüsts ist die allgemeine Synthesestrategie in Schema 4 beschrieben. Als zentraler Synthesebaustein sollte hier jeweils der ausgehend von dem kommerziell erhältlichen 2,4-Dichlor-7-benzyloxy-6-methoxychinazolin (**34**) in zwei Syntheseschritten (hydrogenolytische Abspaltung der Benzylschutzgruppe und *Mitsunobu*-Reaktion zur Anknüpfung der basischen Seitenkette) zugängliche 2,4-Dichlor-substituierte Chinazolinbaustein **33** (Doig et al., 2014; Vital et al., 2023) dienen. Die schrittweise Substitution der Chloratome in der 2- und 4-Position sollte ausgehend von dem Schlüsselbaustein **33** in zwei Stufen gelingen. Bei der Umsetzung mit den jeweiligen primären oder sekundären Aminen sollte entsprechend der literaturbekannten Synthesen erst eine nukleophile Substitution in der 4-Position des Ringsystems und bei erneuter Reaktion unter forcierteren Bedingungen in der 2-Position erfolgen. So sollten entsprechende UNC0646-Analoga mit einem definierten Substituenten in der 4- und einem davon unterschiedlichen Substituenten in der 2-Position leicht zugänglich sein.

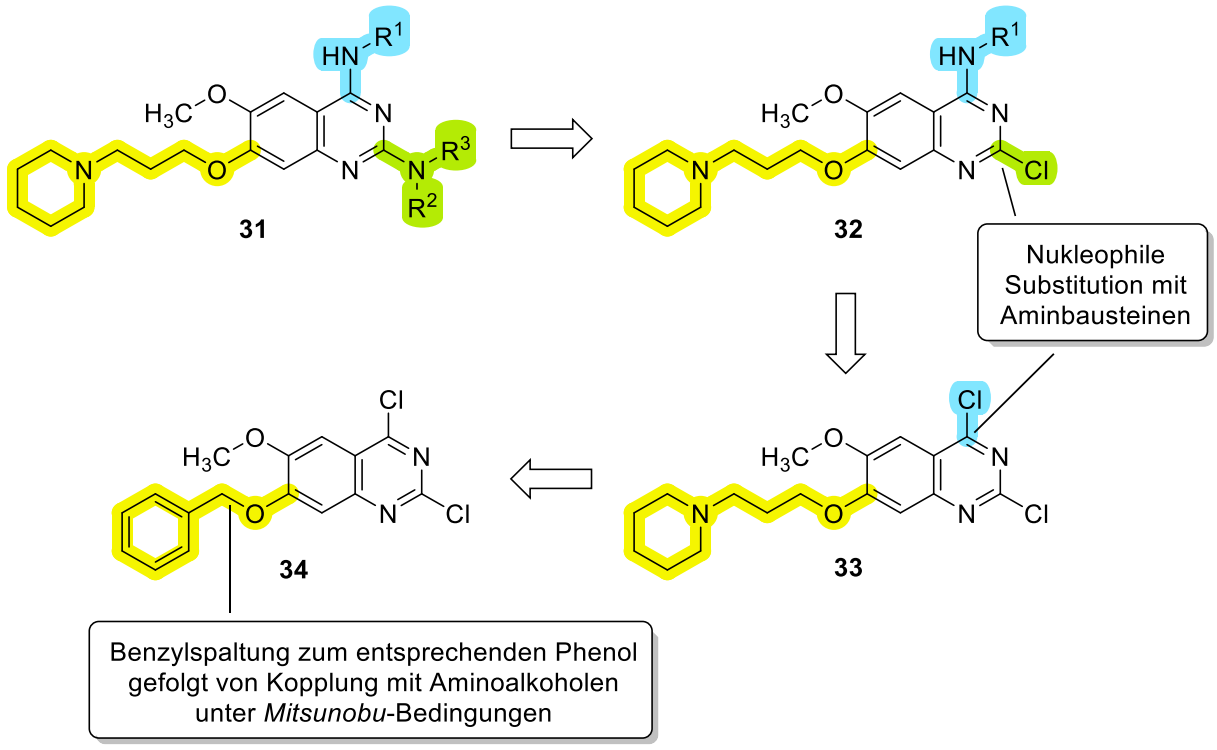

Schema 4: Retrosynthese der Zielverbindungen **31** ausgehend von **34** mit Beschreibung der Syntheseschritte.

Eine Herausforderung stellt vor diesem Hintergrund eine effiziente Gewinnung von UNC0646-Analoga mit definierten Substituenten in der 2- und unterschiedlichen Substituenten in der 4-Position dar. Hier sollte ein von Yoshida *et al.* für 2,4-Dichlorchinazolin **37** beschriebenes Verfahren untersucht werden, bei dem im ersten Schritt ein *N*-Methyl-substituiertes tertiäres Amin, wie z.B. *N*-Methylpiperidin, zum Einsatz kommt (Yoshida and Taguchi, 1992), das regioselektiv das Chloratom in 2-Position substituiert. Eine anschließende nukleophile Substitution des Chloratoms in 4-Position des Ringsystems von **36** mit entsprechenden Aminbausteinen sollte zur Gewinnung der Zielverbindungen **35** führen (siehe Schema 5).

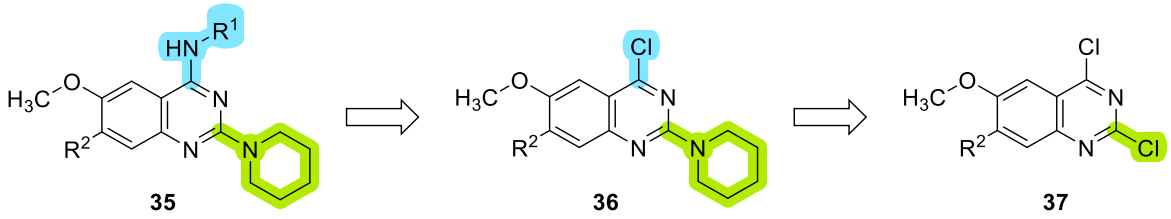

Schema 5: Retrosynthese der Zielverbindungen **35** ausgehend von 2,4-Dichlorchinazolin **37** unter Verwendung von *N*-Methylpiperidin.

6,7-Dimethoxy-substituierte Analoga **38** der zweiten Gruppe von Verbindungen sollten sich entsprechend der Zielverbindungen **31** und **35** ausgehend von dem kommerziell erhältlichen Baustein **39** gewinnen lassen (siehe Schema 6).

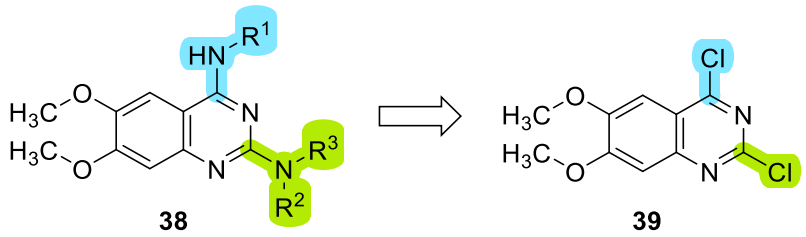

Schema 6: Retrosynthese der Chinazolin-Zielverbindungen **38** ausgehend von **39**.

In 2-Position unsubstituierte Chinazoline **40** der dritten Gruppe von Zielverbindungen mit einem Variationspunkt in der 7- oder 4-Position sollten ausgehend von den kommerziell erhältlichen Startmolekülen **42**, **44** bzw. **47** jeweils in zwei Schritten erhalten werden (siehe Schema 7). Dabei sollte im Falle von **42** (analog zu den bisherig vorgestellten Methoden) zunächst der Baustein **41** über nukleophile Substitution des Chloratoms gewonnen werden, bevor die basische Seitenkette via *Mitsunobu*-Reaktion angeknüpft werden könnte. In umgekehrter Reihenfolge sollte die Modifikation am Baustein **44** erfolgen: hier sollte zunächst die basische Seitenkette eingefügt werden, bevor dann am so erhaltenen Baustein **43** durch nukleophile Substitution des Chloratoms die Zielverbindungen **40** synthetisiert werden könnten. Für die Herstellung der zur Zielverbindung **40** äquivalenten, jedoch in 7-Position Amino-substituierten Chinazoline **45**, ist jedoch ein alternativer Syntheseweg von Nöten. Der kommerziell erhältliche 7-Fluor-substituierte Lactambaustein **47** sollte zunächst über eine

phosphoniumvermittelte S_NAr-Reaktion unter Verwendung von PyBOP/DBU und den jeweiligen Aminobausteinen zu den entsprechenden 4-Aminochinazolinen **46** umgesetzt werden. Das Fluoratom an der 7-Position sollte dann durch eine nukleophile Substitution mit den jeweiligen primären oder sekundären Aminobausteinen ersetzt werden können.

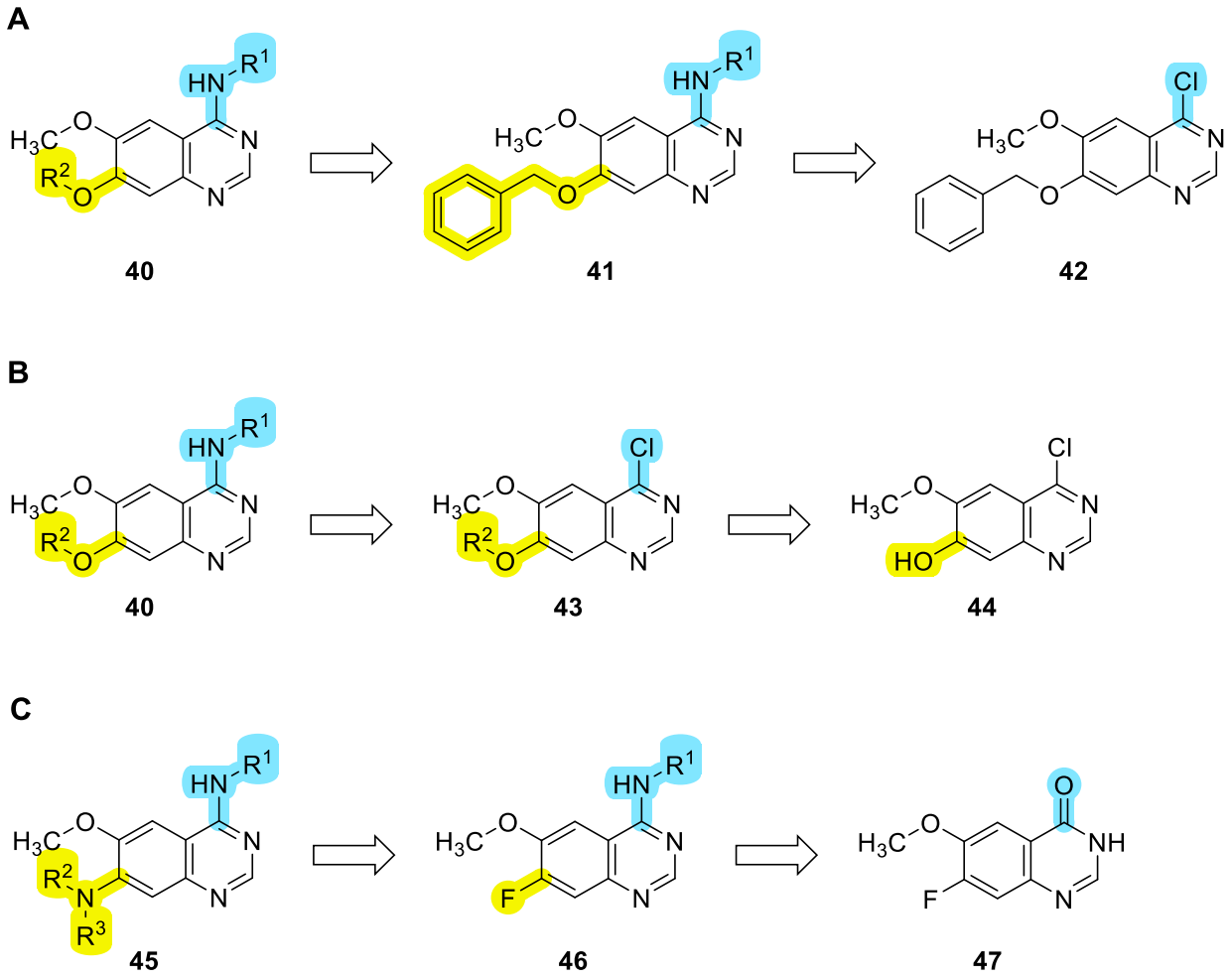

Schema 7: Retrosynthese der Chinazolin-Zielverbindungen der Gruppe 3 mit der allgemeinen Struktur **40** bzw. **45** ausgehend von **A**) **42** bzw. **B**) **44** und **C**) **47**.

2.4 Synthese von A366-Analoga

In einem dritten Projekt sollten Analoga des Screening-Hits A366 (siehe Abbildung 17) (Sichler et al., 2024) synthetisiert und auf ihre biologische Wirkung untersucht werden, um erste Einblicke in die Struktur-Aktivitäts-Beziehungen dieser Substanzklasse zu erhalten. Dabei sollte zunächst das synthetisch einfacher zugängliche A366-Analogon **48** [$R^1 = R^2 = CH_3$, R^3, R^4 = -$(CH_2)_4$-, n = 1], welches in 3-Position des 3*H*-Indol-Grundgerüsts anstelle des gespannten Cyclobutanrings von A366 zwei Methylreste aufweist, untersucht werden (siehe Abbildung 21). Sollte diese Verbindung eine vergleichbare Aktivität wie A366 am nAChR besitzen, würden weitere Strukturmodifikationen ausgehend von dieser Struktur erfolgen. Basierend auf der Struktur des genannten Analogons bzw. von A366 sollte in einem ersten Schritt zunächst die Kettenlänge der ω-Aminoalkoxyseitenkette (n = 0, 1 oder 2) und anschließend die Ringgröße des cyclischen Amins [z.B. Verbindungen der allgemeinen Struktur **48** mit R^3, R^4 = -$(CH_2)_3$- oder -$(CH_2)_5$-] variiert werden. Darüber hinaus war geplant, die Anknüpfungsposition der Seitenkette in 6-Position am 3*H*-Indol-Grundgerüst zu variieren. Von besonderem Interesse waren dabei Verbindungen der allgemeinen Struktur **49**, bei denen die beiden Substituenten in 5- bzw. 6-Position des Grundgerüsts von A366 vertauscht sind.

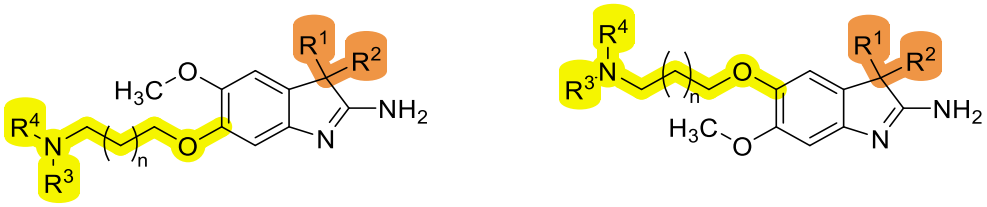

Abbildung 21: Allgemeine Strukturformeln der A366-Analoga **48** und **49**.

Das Synthesekonzept für eine kurze und effiziente Darstellung von A366-Analoga, das umfangreiche Strukturvariationen erlauben sollte, orientierte sich an den Arbeiten von Fagan *et al.* und Sweis *et al.* (Fagan et al., 2019; Sweis et al., 2014). Es beruht in den Schlüsselschritten auf einer Dialkylierung des Phenylacetonitrilbausteins **51** in α-Position zur Nitrilgruppe, einer selektiven Nitrierung des Phenylrings in 6-Position, der Einführung einer ω-Aminoalkoxyseitenkette in 4-Position des Phenylrings sowie dem finalen Ringschluss zum 2-Amino-3*H*-indol-Ringsystem (siehe Schema 8).

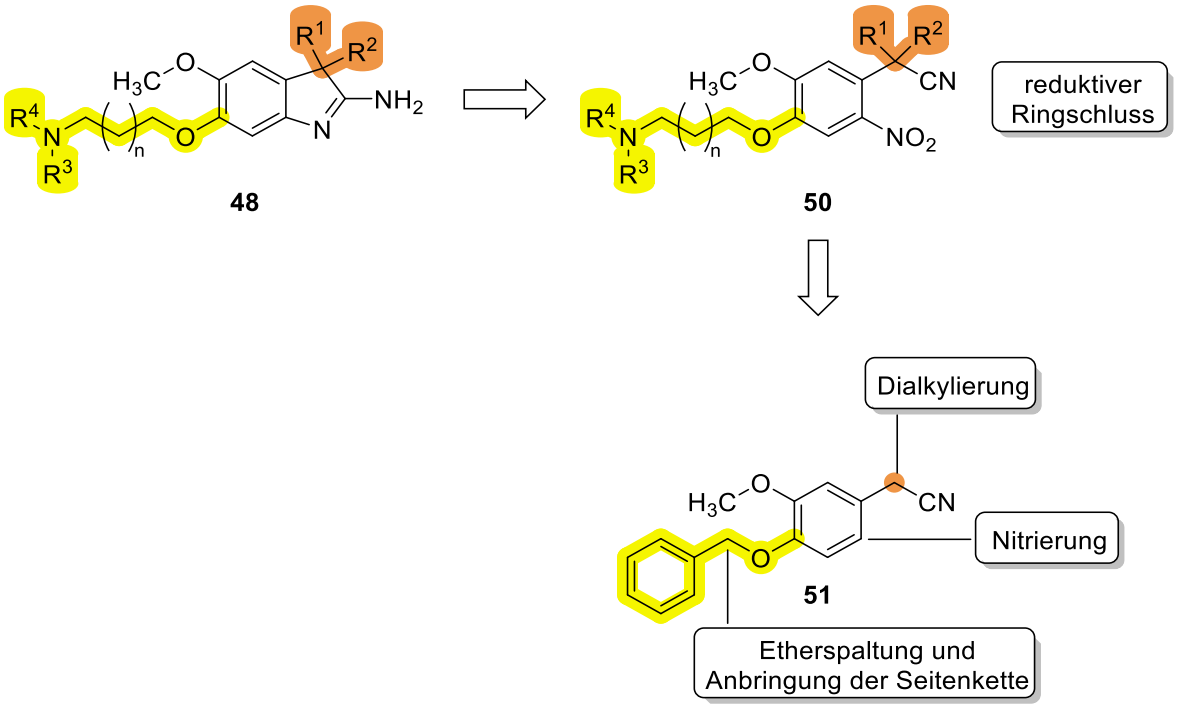

Schema 8: Retrosynthese für A366-Analoga der allgemeinen Struktur **48**.

Die A366-Analoga der allgemeinen Struktur **48** sollten demnach ausgehend von dem kommerziell erhältlichen Phenylacetonitrilbaustein **51** in jeweils fünf Schritten synthetisiert werden können. Im ersten Schritt sollte sich das entsprechende Dimethyl- oder Cyclobutyl-derivat durch eine Dialkylierungsreaktion mit Methyliodid bzw. 1,3-Dibrompropan erhalten lassen. Der nächste Schritt erfordert die regioselektive Nitrierung des jeweiligen Phenylrings in 6-Position. Fagan *et al.* und Sweis *et al.* (Fagan et al., 2019; Sweis et al., 2014) zeigten bereits, dass dies unter milden Bedingungen (70% HNO_3, Ac_2O, 0 °C) gelingen sollte. Alternativ ist auch eine inverse Abfolge der beiden ersten Syntheseschritte denkbar. Dies hätte den Vorteil, dass sich die Anzahl der linearen Syntheseschritte ab dem ersten Variationspunkt, der Dialkylierung des Nitrils, um einen Schritt verkürzen ließe. Im dritten Schritt muss die Benzyletherfunktion in 4-Position selektiv gespalten werden, um die entsprechenden Phenole zu erhalten. Dies sollte hydrogenolytisch (z.B. H_2, Pd/C) oder unter sauren Bedingungen (z.B. TFA) gelingen. Anschließend sollte dann im zweiten Variationspunkt der Synthese die Veretherung der phenolischen Hydroxylgruppe mit unterschiedlichen Aminoalkoholbausteinen unter *Mitsunobu*-Bedingungen erfolgen. Die so dargestellten Verbindungen **50** sollten sich dann im letzten Schritt durch Reduktion der Nitrogruppe zu den gewünschten Ziel-verbindungen **48** mit den für sie charakteristischen 2-Amino-3*H*-indol-Strukturen cyclisieren lassen.

Analoga der allgemeinen Struktur **49**, welche die basische Seitenkette in 5-Position des 3*H*-Indol-Ringsystem aufweisen, sollten ausgehend von dem entsprechenden Dimethoxy-substituierten Baustein **53** zugänglich sein (siehe Schema 9). Im Vergleich zu dem Synthese-baustein **51**, welcher Ausgangspunkt für die regioisomeren Verbindungen darstellt, verfügt die kommerziell erhältliche Verbindung **53** bereits über eine Nitrofunktion, so dass der Synthese-weg, um einen Schritt verkürzt werden kann.

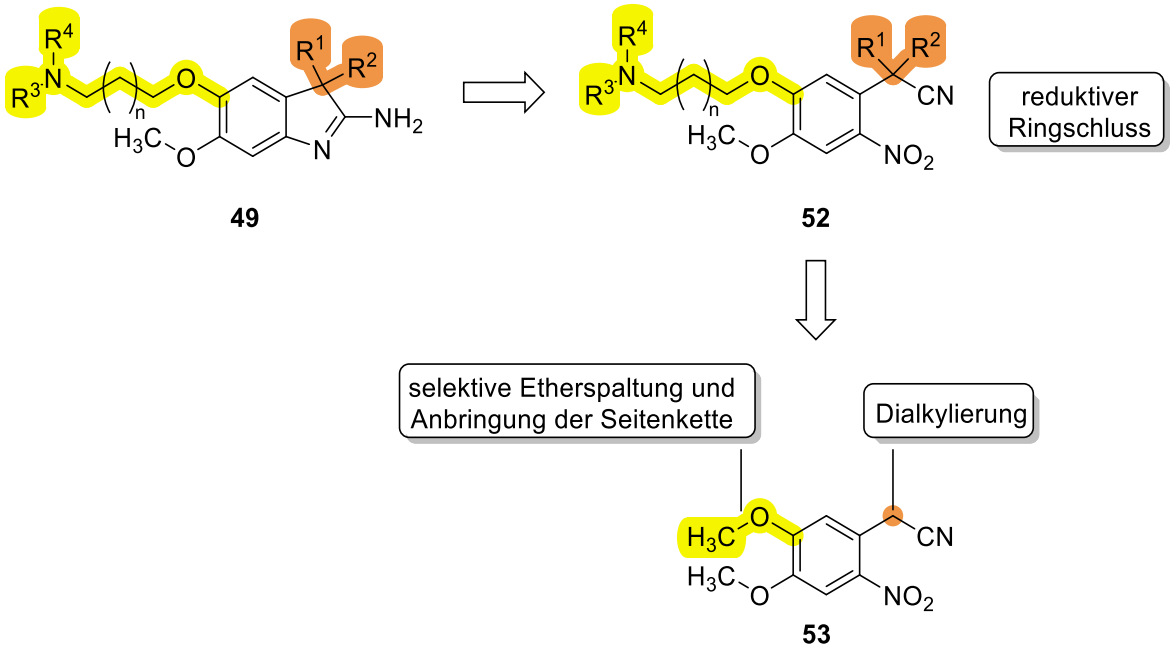

Schema 9: Retrosynthese für A366-Analoga der allgemeinen Struktur **49**.

Der entscheidende Schritt ist hier die selektive Spaltung des Methylethers in *para*-Position zur Nitrogruppe von Verbindung **53**. Wie an einer vergleichbaren Verbindung von Fagan *et al.* gezeigt wurde, sollte ein Angriff von Thiolat-Ionen aufgrund des elektronenziehenden Einflusses der Nitrogruppe, selektiv an der Methylgruppe in *para*-Stellung zur Nitrogruppe erfolgen und zu einer Spaltung des Ethers führen (Fagan et al., 2019). Anschließend sollten, wie bei den regioisomeren Bausteinen **51**, verschiedene ω-Aminoalkoxyseitenketten unter *Mitsunobu*-Bedingungen eingeführt werden können. Die Zielverbindungen **49** mit 2-Amino-3*H*-indol-Struktur sollten sich schließlich analog zu den Verbindungen **48** durch reduktive Cyclisierung der Bausteine **52** gewinnen lassen.

3 Veröffentlichungen

3.1 Erste Publikation: *A Novel Binding Site in the Nicotinic Acetylcholine Receptor for MB327 can Explain its Allosteric Modulation Relevant for Organophosphorus-Poisoning Treatment*

3.1.1 Zusammenfassung der Ergebnisse

Die Wiederherstellung der funktionalen Aktivität desensitisierter nikotinischer Acetylcholinrezeptoren (nAChR) durch allosterische Modulatoren, sogenannte Resensitizer, stellt einen erfolgversprechenden Ansatzpunkt in der Therapie von Vergiftungen mit Organophosphaten und -phosphonaten dar. Damit ließe sich die therapeutische Lücke schließen, die auftritt, wenn Oximreaktivatoren der Acetylcholinesterase unwirksam bleiben.

Als vielversprechende Substanzklasse gelten Bispyridiniumverbindungen vom Typ des MB327. *In vitro*-Untersuchungen an *Torpedo californica*-Präparationen sowie *ex vivo*-Untersuchungen an Soman-vergifteten Ratten-Diaphragmen und humanen Interkostalmuskeln haben gezeigt, dass MB327 und einige davon abgeleitete Derivate in der Lage sind, desensitisierte nAChR vom Muskeltyp wieder in den funktionalen Zustand zu überführen. Des Weiteren wurde in MS-Bindungsassays mit [$^2H_6$]MB327 als Reporterligand die spezifische Bindung von MB327 an *Torpedo californica*-nAChR charakterisiert.

Im Rahmen dieser Veröffentlichung konnte in *in silico*-Studien durch eine Kombination aus Blind-Docking-Experimenten und Molekulardynamik-Simulationen eine potenzielle allosterische Bindungstasche von MB327 am Muskeltyp-nAChR identifiziert werden, die als MB327-PAM-1 bezeichnet wurde. Sie befindet sich am Übergang von der extrazellulären zur transmembranären Region und zeigt für die mit MB327 interagierenden Aminosäuren ein hohes Maß an Konserviertheit zwischen den vier verschiedenen Untereinheiten der pentameren Rezeptoren. Darüber hinaus sind die entsprechenden Rezeptor-Untereinheiten auch zwischen verschiedenen Spezies hochkonserviert. Rigiditätsanalysen lassen den Schluss zu, dass nach Bindung von MB327 an die MB327-PAM-1-Bindungsstelle sowohl auf die orthosterische Bindungstasche als auch auf die Transmembrandomäne allosterische Effekte ausgeübt werden. In Moleküldynamik-Simulationen wurde auch eine gewisse Affinität von MB327 zur orthosterischen Bindungstasche gefunden, was die bei höheren Konzentrationen in *ex vivo*-Untersuchungen beobachtete muskelhemmende Aktivität erklären könnte.

Die Kenntnis der allosterischen Bindungstasche sowie des vorhergesagten Bindungsmodus ermöglichte die Vorhersage struktureller Modifikationen von MB327 mit dem Ziel, verbesserte Resensitizer zu erhalten. Die der Transmembrandomäne zugewandte *tert*-Butylgruppe von

MB327 ist in einem polaren Teil der Bindungstasche lokalisiert. Deshalb sollte der Austausch einer der beiden *tert*-Butylgruppen durch einen stärker polaren Substituenten die Bindungsaffinität erhöhen. Dementsprechend wurden zwei nicht-symmetrische MB327-Analoga vorgeschlagen, bei denen eine der beiden *tert*-Butylgruppen von MB327 durch eine Aminofunktion (PTM0062) bzw. *N*-Methylaminofunktion (PTM0063) ersetzt ist. Die beiden Zielverbindungen PTM0062 und PTM0063 wurden in einer Mikrowellen-unterstützten Synthese ausgehend von 1,3-Diiodpropan und den entsprechenden Pyridinbausteinen in zwei Schritten in hohen Ausbeuten gewonnen. In *ex vivo*-Untersuchungen an Soman-vergifteten Ratten-Diaphragmen konnte für die beiden Verbindungen im Vergleich zu MB327 tatsächlich eine deutlich stärkere Wiederherstellung der Muskelkraft beobachtet werden.

3.1.2 Darstellung des Eigenanteils

Alle *in silico*-Studien wurden von Jesko Kaiser durchgeführt, der bis auf einzelne ergänzende Beiträge von mir und Thomas Seeger auch das Manuskript verfasste. Die Synthesen der beiden MB327-Analoga PTM0062 und PTM0063 sowie die analytische Charakterisierung der Verbindungen, deren MS- und NMR-Spektren von der Analytikabteilung des Departments für Pharmazie gemessen wurden, wurden eigenständig von mir durchgeführt. Die *ex vivo*-Untersuchungen von PTM0062 und PTM0063 an Soman-vergifteten Ratten-Diaphragmen wurden von Thomas Seeger durchgeführt. Das Manuskript wurde von Jesko Kaiser gemeinsam mit Christoph G.W. Gertzen und Holger Gohlke konzipiert und das Manuskript im Wesentlichen von Holger Gohlke und Christoph G.W. Gertzen korrigiert. Darüber hinaus flossen Korrekturbeiträge von Georg Höfner, Karin V. Niessen, Franz Worek, Horst Thiermann, Franz F. Paintner und Klaus T. Wanner in das Manuskript ein.

Toxicology Letters 373 (2023) 160–171

Contents lists available at ScienceDirect

Toxicology Letters

journal homepage: www.journals.elsevier.com/toxicology-letters

A novel binding site in the nicotinic acetylcholine receptor for MB327 can explain its allosteric modulation relevant for organophosphorus-poisoning treatment

Jesko Kaiser[a,1], Christoph G.W. Gertzen[a,2], Tamara Bernauer[b,3], Georg Höfner[b], Karin V. Niessen[c], Thomas Seeger[c], Franz F. Paintner[b,4], Klaus T. Wanner[b,5], Franz Worek[c], Horst Thiermann[c], Holger Gohlke[a,d,*,6]

[a] Institute for Pharmaceutical and Medicinal Chemistry, Heinrich Heine University Düsseldorf, Düsseldorf, Germany
[b] Department of Pharmacy – Center for Drug Research, Ludwig-Maximilians-Universität München, München, Germany
[c] Bundeswehr Institute of Pharmacology and Toxicology, München, Germany
[d] John von Neumann Institute for Computing (NIC), Jülich Supercomputing Centre (JSC), Institute of Biological Information Processing (IBI-7: Structural Biochemistry) & Institute of Bio, and Geosciences (IBG-4: Bioinformatics), Forschungszentrum Jülich, Jülich, Germany

ARTICLE INFO

Editor: Dr. Angela Mally

Keywords:
nAChR
Cooperativity
Bispyridinium compounds
Blind docking
Molecular dynamics simulations
Rigidity analysis

ABSTRACT

Organophosphorus compounds (OPCs) are highly toxic compounds that can block acetylcholine esterase (AChE) and thereby indirectly lead to an overstimulation of muscarinic and nicotinic acetylcholine receptors (nAChRs). The current treatment with atropine and AChE reactivators (oximes) is insufficient to prevent toxic effects, such as respiratory paralysis, after poisonings with various OPCs. Thus, alternative treatment options are required to increase treatment efficacy. Novel therapeutics, such as the bispyridinium non-oxime MB327, have been found to reestablish neuromuscular transmission by interacting directly with nAChR, probably via allosteric mechanisms. To rationally design new, more potent drugs addressing nAChR, knowledge of the binding mode of MB327 is fundamental. However, the binding pocket of MB327 has remained elusive. Here, we identify a new potential allosteric binding pocket (MB327-PAM-1) of MB327 located at the transition of the extracellular to the transmembrane region using blind docking experiments and molecular dynamics simulations. MB327 forms striking interactions with the receptor at this site. The interacting amino acids are highly conserved among different subunits and different species. Correspondingly, MB327 can interact with several nAChR subtypes from different species. We predict by rigidity analysis that MB327 exerts an allosteric effect on the orthosteric binding pocket and the transmembrane domain after binding to MB327-PAM-1. Furthermore, free ligand diffusion MD simulations reveal that MB327 also has an affinity to the orthosteric binding pocket, which agrees with recently published results that related bispyridinium compounds show inhibitory effects via the orthosteric binding site. The newly identified binding site allowed us to predict structural modifications of MB327, resulting in the more potent resensitizers PTM0062 and PTM0063.

1. Introduction

Despite the aim to ban chemical warfare agents, they remain a serious threat to the military and civilian population (Wiener and Hoffman, 2004). The highly toxic organophosphorus (OPCs) nerve agents block acetylcholinesterase (AChE) and lead to an increase of

* Correspondence to: Universitätsstr. 1, 40225 Düsseldorf, Germany.
E-mail address: gohlke@uni-duesseldorf.de (H. Gohlke).
[1] ORCID: 0000-0002-6429-0911
[2] ORCID: 0000-0002-9562-7708
[3] ORCID: 0000-0001-9570-1253
[4] ORCID: 0000-0002-6795-586X
[5] ORCID: 0000-0003-4399-1425
[6] ORCID: 0000-0001-8613-1447

https://doi.org/10.1016/j.toxlet.2022.11.018
Received 7 October 2022; Accepted 25 November 2022
Available online 26 November 2022

acetylcholine at cholinergic synapses, followed by overstimulation of muscarinic (mAChR) and nicotinic (nAChR) acetylcholine receptors. This is associated with several serious toxic effects, such as respiratory paralysis, which can lead to death (Wiener and Hoffman, 2004; Holmstedt, 1959).

So far, the treatment of OPC-poisonings mainly focuses on reestablishing the function of AChE with oximes and competitive antagonism at mAChR (Thiermann et al., 2013). Although oximes can have a remarkable positive indirect effect on nAChR function by restoring AChE functionality in poisonings with several OPCs, they lack efficacy with others, e.g., tabun- and soman-inhibited AChE, which results in a substantial therapeutic gap (Worek et al., 2004). Novel therapeutic approaches focus on ligands that interact directly with nAChR (Sheridan et al., 2005; Turner et al., 2011). As such, the bispyridinium compound MB327, which modulates several nAChR subtypes from different species, has been reported to reestablish neuromuscular transmission in vitro (Seeger et al., 2012; Niessen et al., 2016; Scheffel et al., 2018; Sichler et al., 2018). Furthermore, it leads to increased protection against soman-poisoning in guinea pigs in combination with hyoscine and physostigmine (Turner et al., 2011). However, to improve the efficacy of such compounds in a knowledge-driven molecular design workflow, detailed information of the binding mode is of utmost importance.

So far, three potential binding sites for bispyridinium compounds have been reported in nAChR. Based on blind docking experiments, Wein et al. suggested two potential binding sites of MB327, one in the extracellular domain and one in the upper part of the transmembrane domain (Wein et al., 2018). Recently, Epstein et al. proposed that bispyridinium compounds can bind in the orthosteric binding pocket and its neighboring region between the α- and ε-subunits, exerting an inhibitory effect, and confirmed their *in silico* findings using mutational studies (Epstein et al., 2021). Although this data explains the inhibitory effect of bispyridinium compounds, our previous studies indicated that MB327 probably acts as an allosteric modulator to reestablish muscular function (Niessen et al., 2018). Furthermore, the affinities of analogs of the bispyridinium compound SAD-128 to the orthosteric binding pocket do not correlate with the improvement of neuromuscular transmission, suggesting that this effect is not mediated via binding to the orthosteric binding site (Niessen et al., 2011). Additionally, the displacement of the orthosteric ligand [^{3}H]epibatidine by MB327 results in an $IC_{50} > 100$ μM, although the affinity of [^{3}H]epibatidine to nAChR was already increased at lower concentrations of MB327 (Niessen et al., 2013). Finally, pharmacological effects have been recorded at low μM concentrations of MB327 in the presence of carbamoylcholine. In the absence of carbamoylcholine, no effect has been detected. The latter findings further indicate an allosteric effect (Niessen et al., 2016).

In this study, we describe a novel potential binding site for M327 in nAChR, termed MB327-PAM-1, which was identified by a combination of molecular docking experiments, molecular simulations, and rigidity analyses. To explore the ligand-receptor dynamics, we performed molecular dynamics (MD) simulations and identified important interactions of MB327 with the receptor. The interacting amino acids are highly conserved among different subunits and different species, which can explain the promiscuity of MB327 towards several nAChR subtypes in different species. Furthermore, constraint network analysis (CNA) reveals that MB327 can allosterically impact both the orthosteric binding pocket and the transmembrane domain after binding to MB327-PAM-1. Free ligand diffusion MD simulations imply that MB327 is also affine to the orthosteric binding site, which might contribute to the inhibitory effect on nAChR at higher concentrations (Scheffel et al., 2018; Niessen et al., 2018). Finally, based on the newly identified binding mode of MB327, we predicted structural modifications of MB327, resulting in the more potent resensitizers PTM0062 and PTM0063.

2. Materials and methods

2.1. Homology modeling

The homology models of nAChR were created using MODELLER, version 9.19 (Webb and Sali, 2016). For modeling the desensitized state of nAChR, we only included receptor structures of nAChRs where the transmembrane domain is resolved and that are described to be in a desensitized state. All receptors that, to the best of our knowledge, were available in the PDB at the point of model generation were included. Receptors deposited by Unwin et al. (PDB-IDs 2BG9 (Unwin, 2005), 4AQ5, and 4AQ9 (Unwin and Fujiyoshi, 2012)) were not considered because later structures and experiments showed that, due to low resolution, the structures were wrongly fitted in the transmembrane domain (Mnatsakanyan and Jansen, 2013; Morales-Perez et al., 2016). Furthermore, to neglect a bias of similar protein backbone conformations from one publication, we only included one structure from each publication. However, because all of these receptors show a resolution above 3.5 Å and we expect MB327 to bind in the extracellular domain, we also included the crystal structure of the acetylcholine-binding protein in complex with the partial agonist 4-OH-DMXBA (PDB-ID: 2WN9 (Hibbs et al., 2009)). Concluding, for the human desensitized muscle-type nAChR, the PDB structures 6PV8 (Gharpure et al., 2019), 5KXI (Morales-Perez et al., 2016), 2WN9 (Hibbs et al., 2009), and 6CNK (Walsh et al., 2018) were used as templates.

For the human α7-nAChR, the PDB structures 6PV8 (Gharpure et al., 2019), 5KXI (Morales-Perez et al., 2016), 2WN9 (Hibbs et al., 2009), 6CNK (Walsh et al., 2018), and 6UR8 (Mukherjee et al., 2020) were used as templates. While not stated explicitly in that publication, the cryoEM structure of the α4β2 nAChR in complex with the partial agonist varenicline (PDB-ID: 6UR8 (Mukherjee et al., 2020)) shows a transmembrane domain typical for the desensitized state (SI Fig. 1). Thus, after analyzing the transmembrane pore of this receptor, we also included the receptor in the later created alpha7 nAChR models.

For the human inactive muscle-type nAChR, the PDB structure 6UWZ (Rahman et al., 2020) was used as a template. This was, to the best of our knowledge, the only PDB structure of the inactive nAChR available in the PDB at the time of model generation. To compare the binding site of PNU-120596 in the human muscle-type nAChR with α7-nAChR, the structure of the α7-nAChR in complex with PNU-120596 was used as a template (PDB-ID: 7EKT (Zhao et al., 2021)).

The alignments were created using BLAST (Altschul et al., 1990) and verified using PROMALS3D (Pei et al., 2008). Water molecules and crystallization artifacts were removed. Amino acids at the N- and C-termini and in the intracellular loop not resolved in the templates were not included in the models. 50 models were generated for the human muscle-type and α7-nAChR, respectively, and the final model was selected based on the DOPE potential (Shen and Sali, 2006), TopScore (Mulnaes and Gohlke, 2018), and visual inspection. The selected homology models were protonated using PROPKA (Olsson et al., 2011; Sondergaard et al., 2011) as implemented in Maestro (Schrödinger, 2020) at a pH of 7.4, and the termini were capped with NME and ACE using Maestro (Schrödinger, 2020).

2.2. Docking

For the docking, 3D structures of the ligands were generated using Maestro (Schrödinger, 2020). MB327 was placed in the middle of the extracellular part of the pore so that we could generate a docking box including the extracellular part of the receptor (SI Fig. S2). The ligands were subsequently docked into the receptor using AutoDock3 (Morris et al., 1998) in combination with DrugScore^{2018} (Dittrich et al., 2019) as the scoring function. During the docking, default parameters were used, with the exception that the margin of the box was set to 35 Å and the grid spacing to 1 Å.

MB327, PTM0062, and PTM0063 were also docked into the newly

identified binding pocket using FRED (OpenEye Scientific Software, 2020) with default parameters. Therefore, conformers of MB327 were generated using OMEGA (OpenEye Scientific Software, 2020) with default parameters. The receptor was prepared using MakeReceptor (OpenEye Scientific Software, 2020) with the highest-ranked pose of MB327 after the initial docking for each pocket, and the ligands were subsequently docked into the receptor. To avoid a bias of the placement of MB327 based on the initial dockings, no constraints for protein-ligand interactions were selected, resulting in an independent placement of the ligands in the newly identified pocket. The best poses were selected based on their docking scores and visual inspection. For MD simulations, nicotine was docked to the orthosteric binding pocket using the same two-step procedure. For the simulations with MB327 bound to all five subunits, nicotine was added to nAChR by aligning the PDB structure of the α3β4-nAChR (PDB ID 6PV7 (Gharpure et al., 2019)) to the models and subsequently minimized in the orthosteric binding site using SZYBKI (OpenEye Scientific Software, 2020).

2.3. Molecular dynamics simulations

The structures were embedded in a membrane consisting of 1-palmitoyl-2-oleoyl-*sn*-glycero-3-phosphocholine (POPC) lipids and solvated in a rectangular box of OPC water (Izadi et al., 2014) using Packmol-Memgen (Schott-Verdugo and Gohlke, 2019), with the edge of the box at least 12 Å away from the solute atoms. For the MD simulations with MB327 bound to all five subunits, sodium was placed in the pore by aligning the sodium ion from the human α3β4-nAChR (PDB ID 6PV7 (Gharpure et al., 2019)). For the free ligand diffusion MD simulations, ten independent simulation systems were generated by placing MB327 at random positions within the rectangular box.

The AMBER package of molecular simulation software (Case et al., 2005) and the *ff19SB* force field (Tian et al., 2020) in combination with the Lipid17 force field (Gould et al., unpublished) was used to perform MD simulations. Ligand charges were calculated using Gaussian16 (Frisch et al. 2016). The "Particle Mesh Ewald" method was used to consider long-range interactions; for all bonds involving hydrogens, the SHAKE algorithm was applied (Darden et al., 1993; Ryckaert et al., 1977). During the thermalization period, the time step was set to 2 fs with a direct-space, nonbonded cutoff of 9 Å. During the production runs, hydrogen mass repartitioning was used, and the time step was set to 4 fs with a direct-space, nonbonded cutoff of 8 Å (Hopkins et al., 2015).

Initially, a combination of steepest descent and conjugate gradient minimization was performed; positional harmonic restraints were applied to protein and bound ligand atoms and gradually reduced from 5 (25 for the simulation with MB327 bound to all subunits) to 0 kcal mol^{-1} $Å^{-2}$. Next, the system was heated to 100 K during 50 ps (5 ps for the simulations of the docked structure) of NVT-MD (constant number of particles, volume, and temperature). Subsequently, 50 ps (115 ps for the simulations of the docked structure) of NPT-MD (constant number of particles, pressure, and temperature) were conducted to heat the system to 300 K. During these steps, harmonic restraints with a force constant of 1 kcal mol^{-1} $Å^{-2}$ (25 kcal mol^{-1} $Å^{-2}$ for the simulations with MB327 bound to all subunits) were applied to receptor and ligand atoms. The harmonic restraints were then gradually reduced to 0 kcal mol^{-1} $Å^{-2}$ during NPT-MD simulations.

Thereafter, the production runs of 900 ns length for the free ligand diffusion MD simulations (100 ns for the simulations of the docked structure) were performed. Subsequently, the distances of the ligand to the receptor were analyzed using the *nativecontacts mindist* function as implemented in CPPTRAJ (Roe and Cheatham, 2013). Representative binding poses were created by clustering the frames using the k-means clustering algorithm as implemented in CPPPTRAJ (Roe and Cheatham, 2013). The RMSD of the heavy atoms of the protein and the ligands have been used as a cluster criterion. The backbone RMSD and electron density values of the system during MD simulations were computed using CPPTRAJ (Roe and Cheatham, 2013). We computed the effective binding energy of MB327 in each binding pocket using the MM-GBSA method in combination with the OBC implicit water model, as implemented in AMBER (Case et al., 2005; Onufriev et al., 2004; Miller et al., 2012). We calculated the mean over all replicas x in which MB327 stays stable in MB327-PAM-1 and the standard error of the mean (SEM) using the following equation as done previously (Twizerimana et al., 2020):

$$SEM_{all} = \frac{1}{x}\sqrt{\sum_{i=1}^{x} SEM_i^2}$$

2.4. Constraint network analysis (CNA)

Frames were extracted from the MD simulations of nAChR with MB327 bound to all five subunits and nicotine bound to both orthosteric binding sites every 1 ns using CPPTRAJ (Roe and Cheatham, 2013). To investigate a potential functional coupling between the ligand binding sites as well as with the transmembrane domain, we performed perturbation runs as implemented in CNA (Pfleger et al., 2013a). The perturbation approach performs two runs of constraint dilution simulations of the protein in the presence and absence of the ligands and, thereby, calculates a per-residue decomposition $\Delta G_{i,CNA}$ that indicates the ligands' effect on the structural stability of residue i. We performed three calculations, one where only MB327 was extracted from the system (s1), one where only nicotine was extracted (s2), and one where both ligands where extracted (s1/s2) to investigate the respective impact of the ligands. To investigate the statistical independence of the frames, we computed the autocorrelation function (ACF(τ)) of the first replica for $\Delta G_{CNA,s1}$ (Case et al., 2005). As ACF(τ = 0.5 ns) = 0.2 < 1/e, the frames are statistically independent. To predict cooperative effects in the system, $\Delta G_{CNA,(s1/s2,\ s1,\ s2)}$ was computed as the sum over all $\Delta G_{i,CNA}$ for the respective state. Then, the cooperative free energy $\Delta\Delta G_{CNA,n}$ was computed according to Eq. 1 as done previously (Pfleger et al., 2021),

$$\Delta\Delta G_{CNA,n} = \Delta G_{CNA,s1/s2} - (\Delta G_{CNA,s1} + \Delta G_{CNA,s2}) \quad (1)$$

where positive values indicate a negative cooperativity while negative values indicate a positive cooperativity.

To analyze the impact of calcium on the system, we removed the ligands from nAChR and performed two CNA runs, one where we manually added additional restraints in the form of covalent bonds between the two glutamates involved in calcium binding in three subunits, and one without additional restraints. The former mimics the local rigidifying effect of a bound calcium ion. Then, we calculated the difference in $\Delta G_{i,CNA}$ between the CNA analyses for the systems with and without additional restraints for each residue i to compute the impact of calcium on the structural stability of nAChR.

2.5. Similarity analysis of the binding pocket

For the similarity analysis of the binding pocket, the PDB structure 1UW6 (Celie et al., 2004) of the acetylcholine binding protein of *Lymnaea stagnalis* was aligned to the human muscle-type nAChR model using UCSF Chimera (Pettersen et al., 2004), and amino acids within 5 Å of nicotine were compared to the respective region in the δ-β-subunit using BLAST (Altschul et al., 1990).

2.6. Electrostatic analysis

The electrostatics was analyzed by solving the linear *Poisson-Boltzman* equation as implemented in APBS (Jurrus et al., 2018) using the APBS Pymol Plugin in the presence of positively (charge +1, ion radius 1.8 Å) and negatively (charge −1, ion radius 2.0 Å) charged counter ions in a concentration of 0.15 M. The dielectric constant of the solvent and the protein were set to 78.0 and 2.0, respectively.

2.7. Image generation

Images of nAChR were generated using PyMol (Schrödinger, 2015), version 2.3.0.

2.8. Analysis of the transmembrane pore radius

The transmembrane pore radius of proteins was analyzed using the CAVER PyMol Plugin (Pavelka et al., 2016).

2.9. Synthesis of PTM0062 (3a) and PTM0063 (3b)

Microwave reactions were carried out on a Discover SP microwave system by CEM GmbH. All chemicals were used as purchased from commercial sources. Solvents used for purification were distilled before use. ^{1}H and ^{13}C NMR spectra were recorded on a Bruker BioSpin Avance III HD 400. MestReNova (Version 14.1.0) from Mestrelab Research S.L. 2019 was used for data processing, and for calibration, the solvent signal was used. The purity of the test compounds was > 99 %, determined by means of quantitative NMR using TraceCERT® ethyl 4-(dimethylamino) benzoate from Sigma Aldrich as an internal calibrant (Cushman et al., 2014; Pauli et al., 2014). High-resolution mass spectrometry was performed on a Finnigan LTQ FT (ESI). Melting points were determined with a Büchi 510 melting point instrument and are uncorrected. For IR spectroscopy, an FT-IR Spectrometer 1600 from PerkinElmer was used.

2.9.1. 4-Amino-1-{3-[4-(tert-butyl)pyridin-1-ium-1-yl]propyl}pyridin-1-ium diiodide (3a)

A solution of 4-(*tert*-butyl)– 1-(3-iodopropyl)pyridin-1-ium iodide (1) (Rappenglück, 2018) (216 mg, 0.500 mmol, 1.0 eq.) and pyridin-4-amine (2a) (51.8 mg, 0.550 mmol, 1.1 eq.) in acetonitrile (1 mL) was stirred under microwave irradiation (150 W) for 1 h at 90 °C. The reaction mixture was concentrated in vacuo and the residue purified by recrystallization from EtOAc/EtOH (2:3) yielding 3a (215 mg, 82 %) as yellow solid. mp.: 205 °C; IR (KBr): $\tilde{\nu}$= 3184, 1652, 1194, 839 cm^{-1}; ^{1}H NMR (400 MHz, CD_3OD): δ = 1.45 (s, 9 H, $C(CH_3)_3$), 2.58–2.70 (m, 2 H, NCH_2CH_2), 4.38 (t, *J* = 7.7 Hz, 2 H, $CH_2NCHCHCNH_2$), 4.75 (t, *J* = 7.8 Hz, 2 H, $CH_2NCHCHCC(CH_3)_3$), 6.82–6.90 (m, 2 H, $CHCNH_2$), 8.12–8.20 (m, 2 H, $CHCC(CH_3)_3$), 8.18–8.26 (m, 2 H, $CHCHCNH_2$), 8.93–9.00 (m, 2 H, $CHCHCC(CH_3)_3$); ^{13}C NMR (101 MHz, CD_3OD): δ = 30.22 [$C(CH_3)_3$], 33.11 (NCH_2CH_2), 37.66 ($C(CH_3)_3$), 55.54 ($CH_2NCHCHCNH_2$), 58.55 [$CH_2NCHCHCC(CH_3)_3$], 111.04 ($CHCNH_2$), 126.87 [$CHCC(CH_3)_3$], 144.08 ($CHCHCNH_2$), 145.39 [$CHCHCC(CH_3)_3$], 160.91 (CNH_2), 173.18 [$CC(CH_3)_3$]; HRMS-ESI *m/z* $[M\text{-}I]^+$ calcd for $C_{17}H_{25}N_3I$: 398.1093, found: 398.1082.

2.9.2. 4-(tert-Butyl)– 1-[3-(4-(methylamino)pyridin-1-ium-1-yl]propyl) pyridin-1-ium diiodide (3b)

Synthesis according to the procedure described above for the preparation of 3a from 4-(*tert*-butyl)–1-(3-iodopropyl)pyridin-1-ium iodide (1) (Rappenglück, 2018) (216 mg, 0.500 mmol, 1.0 eq.) and *N*-methylpyridin-4-amine (2b) (56.8 mg, 0.525 mmol, 1.05 eq.). Recrystallization from EtOAc/EtOH (2:1). 3b (210 mg, 78 %). Yellow solid. mp.: 180 °C; IR (KBr): $\tilde{\nu}$= 3013, 1654, 1194, 843 cm^{-1}; ^{1}H NMR (400 MHz, CD_3OD): δ = 1.45 [s, 9 H, $C(CH_3)_3$], 2.60–2.72 (m, 2 H, NCH_2CH_2), 2.99 (s, 3 H, NCH_3), 4.41 (t, *J* = 7.7 Hz, 2 H, $CH_2NCHCHCNHCH_3$), 4.78 [t, *J* = 7.8 Hz, 2 H, $CH_2NCHCHCC(CH_3)_3$)], 6.84–6.94 (m, 2 H, $CHCNHCH_3$), 8.13–8.22 [m, 3 H, $CHCHCNHCH_3$, $CHCC(CH_3)_3$], 8.33–8.40 (m, 1 H, $CHCHCNHCH_3$), 8.96–9.03 [m, 2 H, $CHCHCC(CH_3)_3$]; ^{13}C NMR (101 MHz, CD_3OD): δ = 29.80 (NCH_3), 30.23 [$C(CH_3)_3$], 33.19 (NCH_2CH_2), 37.65 [$C(CH_3)_3$], 55.39 ($CH_2NCHCHCNHCH_3$), 58.50 [$CH_2NCHCHCC(CH_3)_3$], 106.66 ($CHCNHCH_3$), 112.03 ($CHCNHCH_3$), 126.87 [$CHCC(CH_3)_3$], 142.39 ($CHCHCNHCH_3$), 144.92 ($CHCHCNHCH_3$), 145.40 [$CHCHCC(CH_3)_3$], 159.57 ($CNHCH_3$), 173.09 [$CC(CH_3)_3$]; HRMS-ESI *m/z* $[M\text{-}I]^+$ calcd for $C_{18}H_{27}N_3I$: 412.1250, found: 412.1230.

2.10. Rat diaphragm myography

All procedures using animals followed animal care regulations and were approved by the responsible ethics committee. Preparation of rat diaphragm hemispheres and experimental protocol of myography was performed as described before with slight modifications (Seeger et al., 2012, 2007). In short, for all procedures (including wash-out steps, preparation of soman and bispyridinium compound solutions) aerated Tyrode solution (125 mM NaCl, 24 mM $NaHCO_3$, 5.4 mM KCl, 1 mM $MgCl_2$, 1.8 mM $CaCl_2$, 10 mM glucose, 95 % O_2, 5 % CO_2; pH 7.4; 25 ± 0.5 °C) was used. After the recording of control muscle force, the muscle preparations were incubated in the Tyrode solution, containing 3 µM soman. Following a 20 min wash-out period, the test compounds PTM0062 or PTM0063 were added in ascending concentrations (1 µM, 10 µM, 100 µM, 300 µM). The incubation time was 20 min for each concentration. The electric field stimulation was performed with 10 µs pulse width and 0.2 A amplitudes. The titanic trains of 20 Hz, 50 Hz, 100 Hz were applied for 1 s and in 10 min intervals. Muscle force was calculated as a time-force integral (area under the curve, AUC) and constrained to values obtained for maximal force generation (muscle force in the presence of Tyrode solution without any additives; 100 %).

3. Results

3.1. Identifying a new potential binding site via blind docking

To identify a possible binding site of MB327 without bias towards any previously known binding site, we have used blind docking experiments. Here, binding to the complete extracellular domain and half of the transmembrane domain of the human adult muscle-type and the α7-nAChR was allowed (SI Fig. S2), as the permanently charged MB327 likely does not cross the plasma membrane in a notable quantity and, thus, likely does not interact with the intracellular parts of the receptor. Using AutoDock (Morris et al., 1998) and DrugScore^{2018} (Dittrich et al., 2019), we docked MB327 100 times to each subtype. This allows us to judge whether MB327 prefers the orthosteric binding site or alternative ones. The largest cluster, which was also the cluster with the best-ranked docking pose, placed MB327 in both receptors in a newly identified binding pocket, MB327-PAM-1, which is located in between two adjacent subunits at the transition from the extracellular to the transmembrane domain (Fig. 1, Fig. 2A, SI Table S1, SI Table S2). Since the α7-nAChR is a homopentamer, there are five potential, identical binding sites for MB327. The human muscle type nAChR is a heteropentamer containing 2 α_1, 1 β_1, 1 δ and 1 ε subunit. In 8 out of the 10 highest ranked clusters, MB327 binds to MB327-PAM-1 but in different subunits (SI Table S1) suggesting that MB327 can bind in the newly identified binding pocket between different subunits. By contrast, MB327 binds to the orthosteric binding site in the 28th and 34th highest ranked cluster only (SI Table S1). In comparison, in 58 out of 100 docking runs, including 30 poses in the highest ranked cluster, the orthosteric agonist acetylcholine was placed in the orthosteric binding pocket, confirming the quality of our predictions (SI Table S3).

3.2. MD simulations strengthen the suggestion of the new binding site

To consider receptor plasticity and assess the stability of the binding pose in the receptor, we performed 32 times 100 ns long MD simulations starting from the docked structure of MB327 in all five subunits of the human muscle-type nAChR embedded in an explicit bilayer membrane (SI Fig. S3). The initial blind docking procedure failed to place MB327 between the β- and α-subunit in the best 100 docked poses, however. Still, we expect that MB327 can bind in between all five subunits of the receptor because of the high sequence similarity of amino acids available for electrostatic interactions (Table 1). Hence, to enable simulations

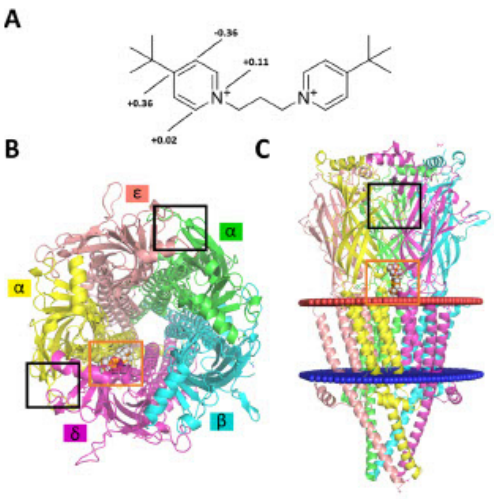

Fig. 1. Location of MB327-PAM-1 in the human adult muscle-type nAChR. (A) MB327 with restrained electrostatic potential (RESP) partial charges (Frisch et al., 2016; Bayly et al., 1993) of the nitrogen and carbons in the aromatic ring. nAChR is viewed from (B) the extracellular space and (C) the side. MB327 is displayed in orange spheres The orange box indicates the location of the newly identified allosteric binding site MB327-PAM-1. The orthosteric binding pocket is marked with a black box. The membrane is indicated with red (extracellular border) and blue (intracellular border) spheres. The membrane position was extracted from the α7-nAChR in a desensitized state (PDB ID 7KOQ (Noviello et al., 2021)) from the Orientations of Proteins in Membranes (OPM) database (Lomize et al., 2012).

with MB327 bound to all five subunits, we docked MB327 into MB327-PAM-1 between each subunit using FRED (OpenEye Scientific Software, 2020) (SI Fig. S4). Throughout the MD simulations, the receptor and the membrane remained structurally virtually invariant (SI Figs. S5, S6). To evaluate whether MB327 stays bound during the 100 ns long MD simulations, we evaluated the minimal distance of MB327 to the highly conserved isoleucine of β1 ($I61_\alpha$), located centrally in each respective subunit (Fig. 2A, SI Fig. S7). Since the largest distance among the docked structures in all five subunits of this isoleucine to MB327 is 4.2 Å (SI Table S4), we considered an unbinding of MB327 at distances above 5 Å. In 122 of 160 cases (32 replicas * 5 possible binding sites), MB327 stays bound in MB327-PAM-1. The unbinding events were mainly observed in between the β- and α-subunit (in 19/32 replicas) and in between the α- and ε-subunit (in 16/32 replicas), while we observed a rare unbinding in between the δ- and β-subunit (in 3/32 replicas) and no unbinding in between the α- and δ- as well as the ε- and α-subunit. This is in line with effective binding energy computations of MB327 in each subunit, revealing that MB327 binds most stably in between the α- and δ- (-23.01 ± 0.04 kcal mol^{-1}) and ε- and α-subunit (-24.43 ± 0.05 kcal mol^{-1}) and shows decreased free binding energies in between the δ- and β-subunit (-19.2 ± 0.05 kcal mol^{-1}), the α- and ε-subunit (-18.99 ± 0.07), and the β- and α-subunit (-14.30 ± 0.08 kcal mol^{-1}).

We next analyzed striking interactions with the receptor in the three binding pockets where MB327 remained predominantly bound. To do so, we computed the minimal distance of acidic side chains of the receptor to the partially positively charged atoms in MB327 when MB327 was bound. Because the nitrogen is part of an aromatic ring, its positive charge can be delocalized among the ring members. In fact, restrained electrostatic potential (RESP) partial charges (Frisch et al., 2016; Bayly et al., 1993) revealed that the positive charge is mainly located on the nitrogen and the carbon atom in *para* position (Fig. 1 A). Thus, we analyzed the minimal distance of these two atoms in each ring to the oxygen atoms of acidic side chains located in the binding pocket in each subunit where MB327 stays stable during the simulations (Fig. 2B, C, D). In between the α- and δ-subunit, MB327 mainly shows interactions with $E210_\delta$ located in loop F (Fig. 2B). This amino acid is highly conserved among different subunits of the heteropentamer. However, in between the δ- and β-subunit, this residue is mutated to glutamine (Table 1). There, MB327 shows almost no interactions with the side chain oxygen of this residue (SI Fig. S8C). However, in this subunit, MB327 forms good interactions with $E71_\delta$ located in the β1-β2-loop (Fig. 2C). In between the ε- and α-subunit, glutamates are present at both positions ($E220_\alpha$ and $E68_\varepsilon$, Fig. 2A). However, MB327 shows preferred interactions with $E68_\varepsilon$ located in the β1-β2-loop (Fig. 2D, SI Fig. S8D).

These results suggest the two acidic glutamates as major interaction partners for MB327. Both acidic amino acids are highly conserved among similar binding pockets in different subunits and different species (Table 1). In each subunit, at least one of the two acidic amino acids is present to stabilize MB327 in the binding pocket, strengthening the assumption that MB327 can bind in all subunits. This is in line with reports that MB327 can bind to nAChR of different species, e.g., *T. californica*, and to nAChRs containing different subunits, e.g., human α7-nAChR (Turner et al., 2011; Seeger et al., 2012; Niessen et al., 2016; Scheffel et al., 2018; Sichler et al., 2018). However, in our MD simulations, MB327 did not stay stable in the proposed binding pocket in two out of five subunits. There, MB327 might not have been placed correctly during the initial docking. In fact, in the two binding sites where MB327 unbound faster, the partially positively charged atoms of MB327 were more than 5 Å away from the carboxyl oxygens of the described amino acids, whereas in the other subunits, the distance to at least one oxygen is 4.5 Å or less (SI Table S4). Unsurprisingly, the effective binding energy is worst in between the β- and α-subunit where the ligand was placed farthest from the two glutamates in the binding site (SI Table S4). This further stresses the importance of these two amino acids. Thus, mutating one of these amino acids should lead to a significant decrease in binding affinity.

3.3. Allosteric impacts originating from the newly proposed binding pocket

To probe if the newly identified binding pocket MB327-PAM-1 couples functionally with other parts of nAChR, we applied a model of dynamic allostery introduced by us (Pfleger et al., 2013a, 2021) that describes allosteric effects due to ligand binding in terms of a free energy measure $\Delta G_{i,\mathrm{CNA}}$ computed from changes in biomolecular statics via CNA. To generate conformational ensembles for the analyses, we used the 32 times 100 ns long MD simulations with MB327 bound to all five subunits and nicotine bound to both orthosteric binding sites of the human muscle-type nAChR. However, due to the instability of MB327 in two subunits, we only considered the three subunits where MB327 remained stable in MB327-PAM-1. In 29 simulations, all three MB327 molecules were still bound after 100 ns; these replica were used to analyze the allosteric effect of MB327 binding on nAChR. For the perturbation run in CNA, all three MB327 molecules were removed to investigate the allosteric impact due to the ligand. Furthermore, to study the cooperative behavior of both ligands, two additional perturbation runs were performed: first, both nicotine molecules were removed; second, all stably bound ligands (three MB327 ligands and two nicotine molecules) were removed (SI Fig. S9).

CNA reveals that MB327 binding structurally stabilizes the extracellular domain, including amino acids in the orthosteric binding pocket (Fig. 3A, SI Fig. S10.). Interestingly, MB327 shows the largest impact in the orthosteric binding site on $W169_\alpha$, the only residue forming a hydrogen bond to the orthosteric ligand nicotine in the PDB structure of the human α3β4-nAChR (PDB-ID 6PV7) (Gharpure et al., 2019). MB327 transmits its allosteric information to the extracellular domain via both

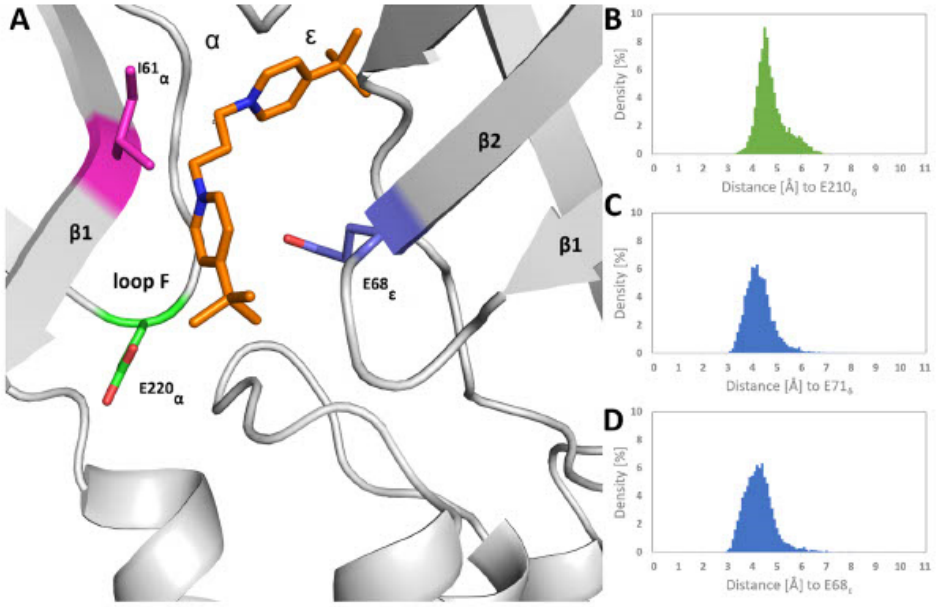

Fig. 2. Interactions of MB327 with nAChR in MB327-PAM-1. (A) Proposed binding mode of MB327 in MB327-PAM-1 between the ε- and α-subunits. The color of amino acids $E220_{\alpha}$ and $E68_{\varepsilon}$ relates to the figures in panels B-D. Minimum distance of the nitrogens and carbon atoms located in 4-position of MB327 to the carboxyl oxygens of (B) $E210_{\delta}$ of loop F in the α-δ-subunit (located at the same position as $E220_{\alpha}$, SI Fig. S4 B), (C) $E71_{\delta}$ of the β1-β2-loop in the δ-β-subunit (located at the same position as $E68_{\varepsilon}$, SI Fig. S4 C), and (D) $E68_{\varepsilon}$ of the β1-β2-loop in the α-ε-subunit.

Table 1
Sequence similarity of nAChR subunits in various species at specific positions in the MB327-PAM1 binding pockets.[a].

Human muscle type				α7	Torpedo marmorata				Rat			
α	β	δ	ε	α7	α	β	δ	γ	α	β	δ	ε
Q	E	E	E68	*Q*	*Q*	E	E	E	*Q*	E	E	E
E220	*Q*	E	E	E	E	*Q*	E	E	E	*Q*	E	E
I61	I	I	I	M	I	L	I	I	I	I	I	I

[a] Amino acids shown in Fig. 2A are represented with green shadings. Amino acids with deviating properties in other subunits are shown in italics.

adjacent subunits through the extracellular β-sheets (Fig. 3B). β-sheets have been demonstrated to be sensitive to changes in structural stability (Whiteley, 2005), and transition pathways along β-sheets have been reported previously (Pfleger et al., 2021, 2017). Especially, the stability of the three β-strands β1, β2, and β6 are affected by MB327 binding. β1 and the β1-β2-loop are both part of MB327-PAM-1. $W78_{\delta}$ in β2 is part of the highly conserved aromatic residues in which nicotine is enveloped according to the cryo-EM structure of the human α3β4-nAChR (PDB ID 6PV7 (Gharpure et al., 2019)). Additionally, via these three β-sheets, MB327 also impacts β7, β9, and β10. The loops of these three β-sheets form the orthosteric binding site. Because MB327 impacts both adjacent subunits, a binding of MB327 to each of the five possible binding pockets likely affects the binding of the orthosteric ligand since each binding site for MB327 features at least one subunit to which the orthosteric ligand binds. This qualitative observation suggests that MB327 addition can modulate cholinergic signals. Hence, we quantified cooperative effects between MB327 and nicotine binding according to Eq. 1 (Pfleger et al., 2021). Our results reveal a positive cooperative effect ($\Delta\Delta G_{CNA,n} = -3.97 \pm 0.71$ kcal mol^{-1}), in line with experimental findings that addition of MB327 leads to an enhancement of the cholinergic effect (Niessen et al., 2016). Therefore, binding of MB327 in MB327-PAM-1 is suggested to enhance cholinergic signals by increasing orthosteric ligand affinity.

Notably, a recently published PDB structure of the α7-nAChR (PDB ID 7KOX) shows calcium ions bound in the MB327-PAM-1 pocket (Noviello et al., 2021). Calcium binds in between E44 and E172. E172 is located in loop F, at the same position as $E220_{\alpha}$ (SI Fig. S11). A high concentration of calcium ions increases the cholinergic response in α7-nAChR, and our previous results suggest that the presence of divalent cations enhances the affinity of agonists in Torpedo nAChRs (Niessen et al., 2013; Galzi et al., 1996). Hence, we probed the effect of calcium binding in MB327-PAM-1 on the structural stability of the orthosteric site with CNA. To mimic the presence of the calcium ion which bridges two glutamates, we placed a constraint between the two carboxyl groups of E44 and E172. Similar to MB327, calcium leads to allosteric effects on the orthosteric binding site transmitted via the extracellular β-strands (SI Fig. S12). These findings strengthen the suggestion that positive allosteric modulation of the orthosteric ligand binding can originate

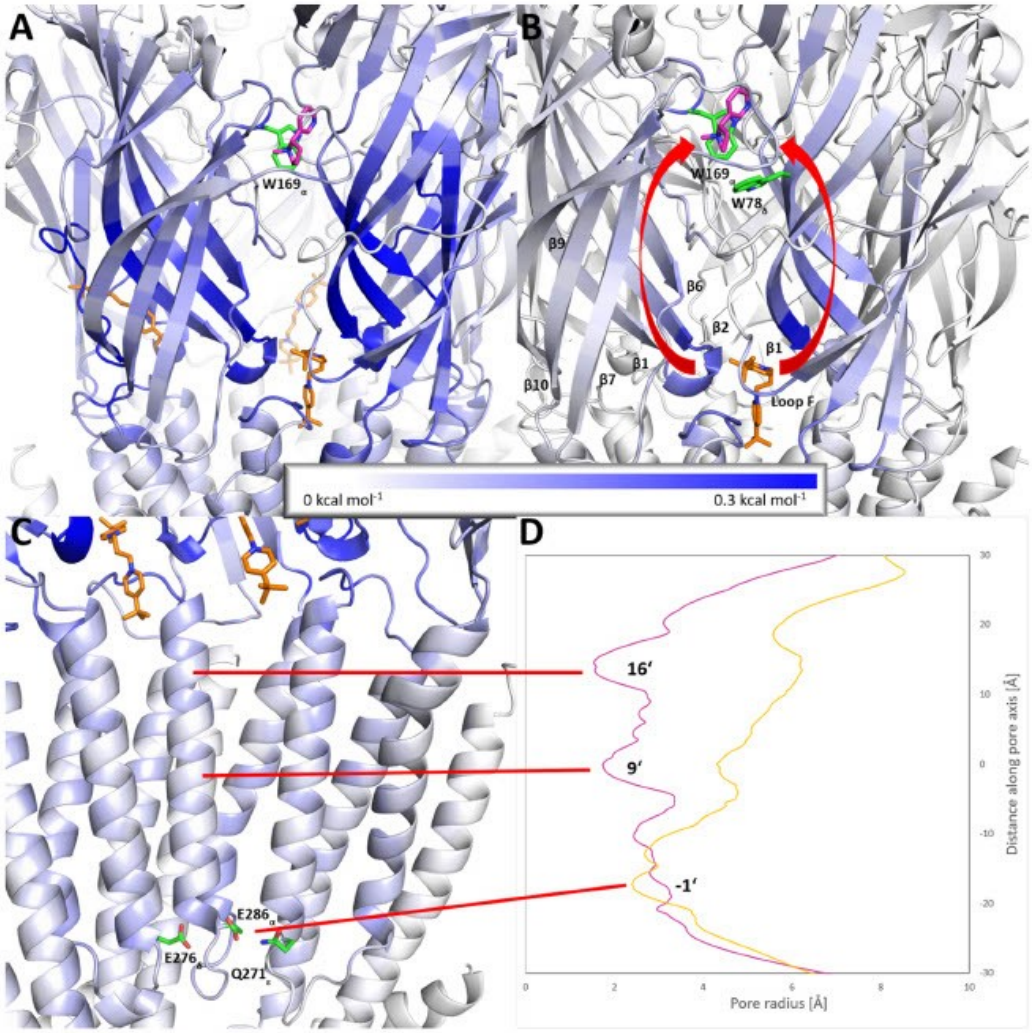

Fig. 3. Allosteric effect of MB327 (orange) on nAChR. Effect on the extracellular domain of (A) the three stable MB327 molecules and (B) MB327 located between the alpha- and ε-subunit. The receptor is colored according to the stabilizing impact of MB327 on the respective amino acid (bluish colors); darker colors indicate a higher impact. The pathway of the allosteric stabilization of the orthosteric binding pocket is indicated by red arrows. Nicotine (purple) is shown in the orthosteric binding pocket. $W169_{\alpha}$ and $W78_{\delta}$ are shown in green. (C) Allosteric effects of MB327 on the transmembrane domain of the human muscle type nAChR. For claritiy, only three subunits are shown. Amino acids at position − 1′ are shown in green. (D) Pore radii of the desensitized (yellow) and inactive (purple) nAChR. The desensitization gate at position − 1′ and the inactive gates at positions 9′ and 16′ are projected on the structure by red bars. The distance along the pore axis has been set to 0 Å at position 9′.

from binding to MB327-PAM-1.

MB327 binding to MB327-PAM-1 also modulates the structural stability of the transmembrane region, including the amino acids at position − 1′ in helices 2 (Fig. 3C, D). X-ray and cryo-EM structures of nAChRs reveal that this position acts as a desensitization gate (Morales-Perez et al., 2016; Gharpure et al., 2019; Walsh et al., 2018; Noviello et al., 2021). The effects on the position − 1′ ($\Delta G_{E286\alpha,CNA} = 0.075 \pm 0.005$ kcal mol^{-1}, $\Delta G_{E276\delta,CNA} = 0.076 \pm 0.004$ kcal mol^{-1}, $\Delta G_{Q271\varepsilon,CNA} = 0.041 \pm 0.003$ kcal mol^{-1}) are significant. The effect on $W169_{\alpha}$, located at a central position in the orthosteric binding pocket, is even larger ($\Delta G_{W169\alpha,CNA} = 0.224 \pm 0.017$ kcal mol^{-1}), which may be due to helices being more stable, and, hence, less receptive to stability changes, in general (Whiteley, 2005). Furthermore, we used the rigidity index to compute ΔG_{CNA}; this index was described to show minor effects on helices (Pfleger et al., 2013b). Overall, the impact on the N-terminal region of helices 2 suggests a mechanism for how MB327 binding reestablishes the muscle function after desensitization, a second effect exerted by MB327 on nAChR (Seeger et al., 2012).

3.4. MB327 shows affinity to the orthosteric binding site

Previous results indicate that related bispyridinium compounds transmit their inhibitory effect on nAChR via the orthosteric binding site (Epstein et al., 2021). An inhibitory effect of MB327 has been reported at concentrations above 70 µM (Scheffel et al., 2018). To further investigate a possible binding of MB327 to the orthosteric binding site, we performed ten additional replicas of 900 ns long unbiased free ligand diffusion MD simulations with one MB327 molecule (0.57 mM) placed at a random position within the simulation box around the human muscle-type nAChR. The inhibitory effect of bispyridinium compounds was described to occur via the orthosteric binding site between the α- and ε-subunits (Epstein et al., 2021). Thus, in order to observe a potential binding to this binding site, the orthosteric ligand nicotine was only placed in the orthosteric binding site between the α- and δ-subunits. In three out of ten replicas, MB327 entered the orthosteric binding pocket. In two replicas, MB327 stayed within the binding pocket until the end of the simulation (after its entrance at 54 and 760 ns). In both replicas, MB327 can interact with $Y131_{\varepsilon}$ after binding (Fig. 4A, B), which is important for the stabilization of bispyridinium compounds (Epstein et al., 2021). In the third replica, MB327 bound to the binding pocket after 211 ns and left it after additional 130 ns. However, in this replica, MB327 showed a slightly different binding mode not interacting with $Y131_{\varepsilon}$ (SI Fig. S13).

We also analyzed the electrostatics surrounding the orthosteric binding pocket by solving the linear Poisson-Boltzmann equation for the human muscle-type nAChR. Since the minimum distance of $W169_{\alpha}$, a central amino acid in the orthosteric binding site, to the membrane is 27 Å, the membrane was neglected in calculating the electrostatic properties around the orthosteric binding site. A strong electric field

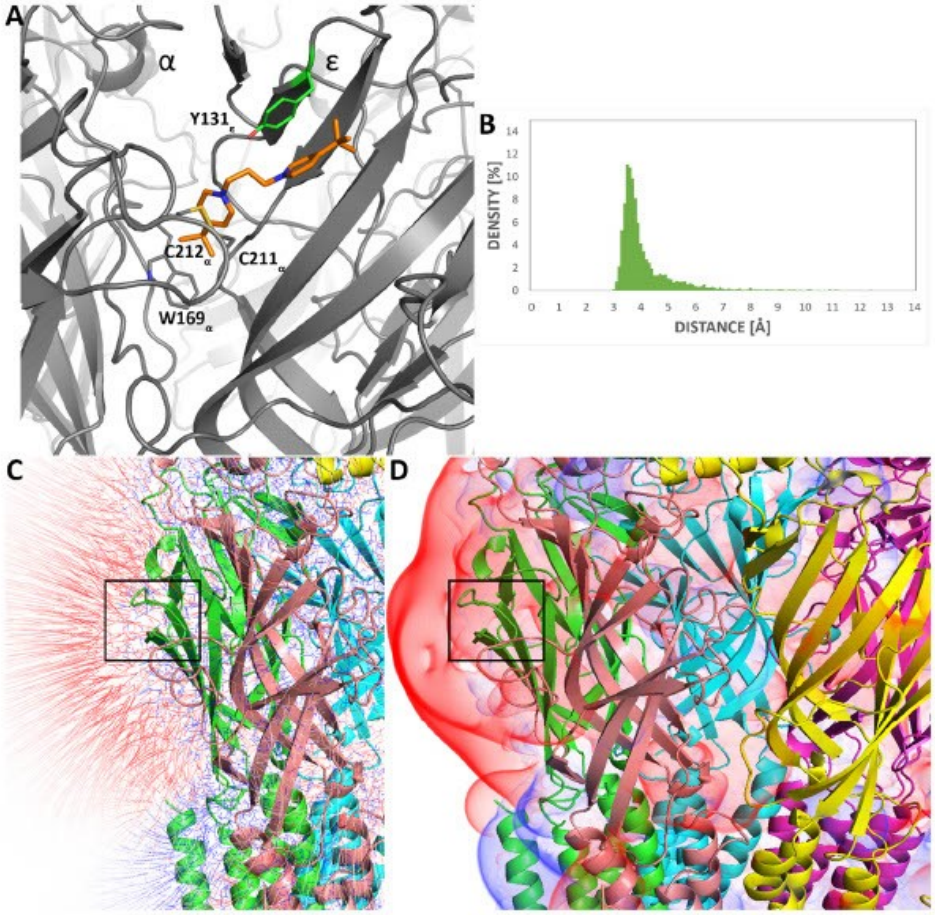

Fig. 4. Affinity of MB327 to the orthosteric binding site of nAChR. (A) Representative structure of MB327 (orange) bound to the orthosteric binding pocket and its adjacent region in between the α- and ε-subunit where no nicotine molecule was present during free ligand diffusion MD simulations. (B) Minimum distance of the heavy atoms of the aromatic ring of $Y131_{\varepsilon}$ as shown in (A) to the heavy atoms of the aromatic systems of MB327 while MB327 is bound. Electrostatics surrounding the orthosteric binding pocket between the α- (green) and ε- (salmon) subunits shown as (C) electric flux lines and (D) isocontour surfaces of the electrostatic potential. The location of the orthosteric binding pocket is marked with a black box. Notably, a strong electric field (red field lines) attractive to positively charged compounds such as MB327 surrounds the pocket entrance and leads towards the orthosteric binding pocket of the human nAChR.

attractive to positively charged compounds such as MB327 surrounds the pocket entrance and leads towards the orthosteric binding pocket. This may explain why bispyridinium compounds get dragged into this binding pocket (Fig. 4C,D).

3.5. Identification of MB327-PAM-1 allows rational design of more potent analogs

We used the knowledge gained from the binding mode of MB327 in MB327-PAM-1 to predict structural modifications of the ligand that should lead to more potent resensitizers. The *tert*-butyl group of MB327 facing toward the transmembrane domain is located in a polar part of the binding site (Fig. 5A). Thus, substituting the apolar with a polar substituent should increase the binding affinity (Fig. 5B). We, therefore, docked PTM0062 and PTM0063, which carry amino and methylamino groups, (Fig. 5C) in the binding site of all subunits. Both ligands were ranked better than MB327 in all but one subunit, respectively (Fig. 5B, SI Table S5). PTM0062 (3a) and PTM0063 (3b) were synthesized according to Rappenglück et al. by reacting 1 (Rappenglück, 2018) with pyridin-4-amine (2a) and *N*-methylpyridin-4-amine (2b), respectively, in acetonitrile under stirring and microwave irradiation for 1 h at 90 °C (Scheme 1) (Rappenglück, 2018). The bispyridinium salts were obtained

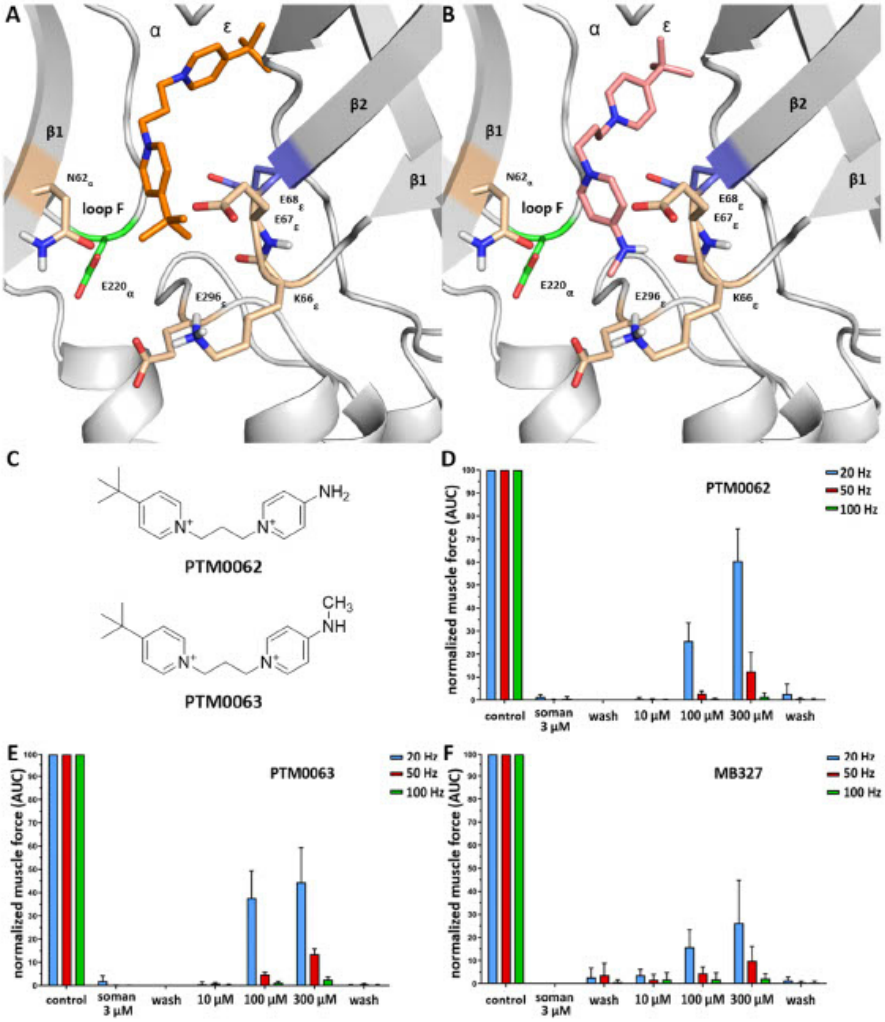

Fig. 5. Structure-based ligand design leads to novel compounds with increased resensitising effects on nAChR. (A) Binding mode of MB327 in between the α- and ε-subunit. The *tert*-butyl substituent facing towards the transmembrane region is located in a polar part of the binding site. (B) Proposed binding mode of PTM0063. Polar substituents can enhance the interactions with the receptor. (C) Structure of the two newly identified positive allosteric modulators PTM0062 and PTM0063. Restoration of the muscle force of soman-poisoned muscles after treatment with (D) PTM0062, (E) PTM0063, and (F) MB327. The error bars indicate the standard deviation.

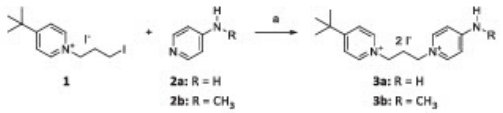

1 2a: R = H 2b: R = CH_3 3a: R = H 3b: R = CH_3

Scheme 1. Synthesis of PTM0062 (3a) and PTM0063 (3b): (a) 2a (1.1 equiv.) or 2b (1.05 equiv.), CH_3CN, microwave: 150 W, 90 °C, 1 h; 3a: 82 %; 3b: 78 %.

in good yields (3a: 82 %; 3b: 78 %) and high purities (> 99 %) by recrystallization of the residues resulting after the removal of the reaction solvent (Scheme 1). The compounds were subsequently evaluated in the rat diaphragm myography assay. PTM0062 (25.68 % ± 7.91 % (mean ± standard deviation) at 100 µM, 60.46 % ± 13.94 % at 300 µM) and PTM0063 (37.65 % ± 11.73 % at 100 µM, 44.43 % ± 14.88 % at 300 µM) both show increased resensitizing effects on muscles after OPC poisoning at a stimulation frequency of 20 Hz compared to MB327 (17.77% ± 7.5 % at 100 µM, 26.29 % ± 18.43 % at 300 µM) (Fig. 5D-F).

4. Discussion

We have identified a new potential binding site of MB327 in nAChR, MB327-PAM-1, using blind docking, MD simulations, and rigidity analyses. Previously, two allosteric and one orthosteric binding pocket were proposed for bispyridinium compounds using *in silico* methods (Wein et al., 2018; Epstein et al., 2021). MB327-PAM-1 is different from these three binding sites. Wein et al. suggested that MB327 might bind in between two adjacent subunits in the extracellular domain (MB327–1) or at the transition from the extracellular to the transmembrane domain (MB327–2) (Wein et al., 2018). In our blind dockings, we could also see a binding in the pocket MB327–1 but with worse docking scores compared to our newly identified binding pocket (SI Table S1). In the screening conducted to identify MB327–2, the structure of the *Torpedo marmorata* nAChR (PDB ID 2BG9 (Unwin, 2005)) was used (Wein et al., 2018). However, recently published structures and disulfide trapping experiments revealed that due to the structure's low resolution, the amino acids in the transmembrane domain were wrongly fitted, resulting in an amino acid shift (SI Fig. S14, SI Table S6) (Mnatsakanyan and Jansen, 2013; Morales-Perez et al., 2016). Without this shift, there is no MB327–2 pocket in nAChR (Wein et al., 2018).

During the MD simulations, MB327 is mainly stabilized via electrostatic interactions with glutamates located in the β1-β2 loop and loop F ($E220_\alpha$ and $E68_\varepsilon$ in Fig. 2A). These two amino acids are highly conserved among different subunits of the nAChR and different species. This corresponds to MB327 showing functional recovery of different types of nAChRs after overstimulation with agonists (Seeger et al., 2012; Niessen et al., 2016). Our newly identified binding pocket also occupies a region in which structural changes during desensitization occur (SI Fig. S15), which suggests that this binding site can be involved in allosteric modulation. Furthermore, CNA calculations show that MB327 might impact both the orthosteric binding site and the transmembrane domain after binding to MB327-PAM-1.

Several published structures of nAChRs and related Cys-loop receptors include allosteric modulators (Zhao et al., 2021; Noviello et al., 2021; Masiulis et al., 2019; Kim et al., 2020; Delbart et al., 2018; Spurny et al., 2013, 2015). A recent structure revealed that the binding site of a calcium ion overlaps with MB327-PAM-1 (Noviello et al., 2021). Calcium can act as a positive allosteric modulator of the α7-nAChR (Galzi et al., 1996). Additionally, mutating E172 of loop F to lysine in the α7-nAChR, which is located at the same position as $E220_\alpha$, leads to a loss of sensitivity to the orthosteric ligand acetylcholine (Zhang et al., 2015). A mutation of this amino acid in the α7-nAChR to glutamine also abolishes the enhancement of the physiological response to acetylcholine mediated through calcium ions (Galzi et al., 1996). These data underline the potential importance of this binding pocket in allosteric modulation. Mimicking the calcium ion in this binding pocket by including its interactions into the constraint network representation results in similar effects on the receptor as MB327 as shown with CNA computations. Notably, the calcium ion also exerts a similar effect on the transmembrane region, indicating that calcium might have a resensitizing effect on nAChR, too (SI Fig. S12).

Notably, the binding site of PNU-120596 has been revealed in an electron microscopy structure (PDB-ID: 7EKT (Zhao et al., 2021)) recently. This binding site overlaps with the newly identified allosteric binding site of diazepam in the $GABA_A$ receptor (PDB-IDs: 6X3X (Kim et al., 2020), 6HUP (Masiulis et al., 2019)). Because PNU-120596 also acts as a positive allosteric modulator (Hurst et al., 2005), we investigated whether MB327 may bind to this binding site. However, in the published PDB structure, no negatively charged amino acids are located within 5 Å of PNU-120596, which would lead to an insufficient stabilization of the double positively charged compound MB327 (SI Fig. S16A). Furthermore, PNU-120596 is a selective α7 modulator (Hurst et al., 2005). A reason for that may be that A298 is mutated to sterically larger amino acids in different subtypes of the receptor, which leads to a clash with PNU-120596. Thus, the binding site is critically smaller in other subtypes, including the human muscle-type nAChR (Fig. S16B). However, MB327 is known to bind to several subtypes of nAChR, including the muscle-type nAChR (Turner et al., 2011; Seeger et al., 2012; Niessen et al., 2016; Scheffel et al., 2018; Sichler et al., 2018). Therefore, binding of MB327 to the binding site of PNU-120596 is highly unlikely.

Furthermore, the multitude of binding sites and possible interactions within one binding site in the human muscle-type nAChR could lead to MB327 binding at lower concentrations to MB327-PAM-1 than to the orthosteric binding site. The binding of MB327 to the orthosteric binding pocket results in a binding pose where MB327 protrudes in part out of the pocket, but it completely fits into MB327-PAM-1. After poisoning with OPCs resulting in elevated levels of acetylcholine, MB327 would additionally need to displace acetylcholine in the orthosteric binding pocket because the binding pose of MB327 in the orthosteric pocket overlaps with the binding pose of the orthosteric ligand. Thus, binding to the orthosteric site would be expected at higher concentrations, where it can lead to an inhibitory effect. This inhibitory effect was shown by us in that an increase of MB327 concentration leads to a decrease of muscle force restoration after soman poisoning (Niessen et al., 2018). Furthermore, recent mutational studies showed that related bispyridinium compounds transfer their inhibitory effect via binding to the orthosteric pocket (Epstein et al., 2021).

Epstein et al. proposed that the therapeutic effect of bispyridinium compounds could be conducted via binding to the orthosteric binding site and its adjacent region (Epstein et al., 2021). We also see an affinity of MB327 to this binding site in our free ligand diffusion MD simulations. Epstein et al. performed docking experiments considering the orthosteric binding pocket and did not investigate binding to allosteric binding pockets. However, previous experimental results indicate that the bispyridinium compounds probably act as allosteric modulators of nAChR and, additionally, improvement of neuromuscular function is not correlated to their affinity to the orthosteric binding site (Niessen et al., 2016, 2018, 2011). Thus, although an inhibitory effect, detrimental to the therapeutic treatment, of the bispyridinium compounds might be conducted through binding to the orthosteric binding site at higher concentrations (Epstein et al., 2021; Niessen et al., 2018), our results suggest that for the allosteric modulation, relevant for treatment, MB327 binds to the newly identified binding pocket. This concentration-dependent binding to the allosteric and orthosteric binding site can also explain the therapeutic effect seen at lower concentrations of MB327 and the inhibition of the nAChR and loss of therapeutic effect at higher concentrations (Niessen et al., 2018). Thus, our results suggest that new drugs should show a high affinity to the newly identified binding pocket while showing a low affinity to the orthosteric binding site.

The knowledge of the binding mode is most important to predict

structure-based ligand modifications resulting in more potent resensitzers. Following this strategy, we predicted and validated PTM0062 and PTM0063, which are about two-fold more potent resensitizers than MB327. These findings further support that MB327 binds to MB327-PAM-1. Another way to enhance the affinity to the newly identified binding site might be to add chemical moieties that can form interactions via hydrogen bonds or salt bridges to the two glutamates $E220_{\alpha}$ and E68ε, while maintaining the apolar part of the compounds.

Taken together, our newly identified binding pocket can explain the allosteric effect mediated by MB327 and, together with a binding to the orthosteric site, the concentration dependence of the observed therapeutic effect.

Declaration of Competing Interest

The authors declare that they have no known competing financial interests or personal relationships that could have appeared to influence the work reported in this paper.

Data availability

Data will be made available on request.

Acknowledgments

This work was supported by the German Ministry of Defense (E/U2AD/KA019/IF558). We are grateful for computational support and infrastructure provided by the "Zentrum für Informations- und Medientechnologie" (ZIM) at the Heinrich Heine University Düsseldorf and the computing time provided by the John von Neumann Institute for Computing (NIC) to HG on the supercomputer JUWELS at Jülich Supercomputing Center (JSC) (user IDs: HKF7, VSK33, nAChR). HG is grateful to OpenEye Scientific Software for granting a Free Public Domain Research License.

Appendix A. Supporting Information

Supplementary data associated with this article can be found in the online version at doi:10.1016/j.toxlet.2022.11.018.

References

Altschul, S.F., et al., 1990. Basic local alignment search tool. J. Mol. Biol. 215 (3), 403–410.
Bayly, C.I., et al., 1993. A well-behaved electrostatic potential based method using charge restraints for deriving atomic charges: the RESP model. J. Phys. Chem. 97 (40), 10269–10280.
Case, D.A., et al., 2005. The Amber biomolecular simulation programs. J. Comput. Chem. 26 (16), 1668–1688.
Celie, P.H., et al., 2004. Nicotine and carbamylcholine binding to nicotinic acetylcholine receptors as studied in AChBP crystal structures. Neuron 41 (6), 907–914.
Cushman, M., et al., 2014. Absolute quantitative (1)h NMR spectroscopy for compound purity determination. J. Med Chem. 57 (22), 9219.
Darden, T., York, D., Pedersen, L., 1993. Particle mesh Ewald: an N·log(N) method for Ewald sums in large systems. J. Chem. Phys. 98 (12), 10089–10092.
OpenEye Scientific Software, I., *SZYBKI*. OpenEye Scientific Software: Santa Fe, NM.
Delbart, F., et al., 2018. An allosteric binding site of the alpha7 nicotinic acetylcholine receptor revealed in a humanized acetylcholine-binding protein. J. Biol. Chem. 293 (7), 2534–2545.
Dittrich, J., et al., 2019. Converging a knowledge-based scoring function: drugscore (2018). J. Chem. Inf. Model. 59 (1), 509–521.
Epstein, M., et al., 2021. Molecular determinants of binding of non-oxime bispyridinium nerve agent antidote compounds to the adult muscle nAChR. Toxicol. Lett. 340, 114–122.
M.J. Frisch, G.W.T, H.B. Schlegel, G.E. Scuseria, et al., Gaussian16. 2016, Gaussian Inc.: Wallingford CT.
Galzi, J.L., et al., 1996. Identification of calcium binding sites that regulate potentiation of a neuronal nicotinic acetylcholine receptor. EMBO J. 15 (21), 5824–5832.
Gharpure, A., et al., 2019. Agonist selectivity and ion permeation in the alpha3beta4 ganglionic nicotinic receptor. Neuron 104 (3), 501–511 e6.
Hibbs, R.E., et al., 2009. Structural determinants for interaction of partial agonists with acetylcholine binding protein and neuronal alpha7 nicotinic acetylcholine receptor. EMBO J. 28 (19), 3040–3051.
Holmstedt, B., 1959. Pharmacology of organophosphorus cholinesterase inhibitors. Pharm. Rev. 11, 567–688.
Hopkins, C.W., et al., 2015. Long-time-step molecular dynamics through hydrogen mass repartitioning. J. Chem. Theory Comput. 11 (4), 1864–1874.
Hurst, R.S., et al., 2005. A novel positive allosteric modulator of the alpha7 neuronal nicotinic acetylcholine receptor: in vitro and in vivo characterization. J. Neurosci. 25 (17), 4396–4405.
Izadi, S., Anandakrishnan, R., Onufriev, A.V., 2014. Building water models: a different approach. J. Phys. Chem. Lett. 5 (21), 3863–3871.
Jurrus, E., et al., 2018. Improvements to the APBS biomolecular solvation software suite. Protein Sci. 27 (1), 112–128.
Kim, J.J., et al., 2020. Shared structural mechanisms of general anaesthetics and benzodiazepines. Nature 585 (7824), 303–308.
Lomize, M.A., et al., 2012. OPM database and PPM web server: resources for positioning of proteins in membranes. Nucleic Acids Res. 40 (Database issue), D370–D376.
Masiulis, S., et al., 2019. GABAA receptor signalling mechanisms revealed by structural pharmacology. Nature 565 (7740), 454–459.
Miller 3rd, B.R., et al., 2012. MMPBSA.py: an efficient program for end-state free energy calculations. J. Chem. Theory Comput. 8 (9), 3314–3321.
Mnatsakanyan, N., Jansen, M., 2013. Experimental determination of the vertical alignment between the second and third transmembrane segments of muscle nicotinic acetylcholine receptors. J. Neurochem. 125 (6), 843–854.
Morales-Perez, C.L., Noviello, C.M., Hibbs, R.E., 2016. X-ray structure of the human alpha4beta2 nicotinic receptor. Nature 538 (7625), 411–415.
Morris, G.M., et al., 1998. Automated docking using a Lamarckian genetic algorithm and an empirical binding free energy function. J. Comput. Chem. 19 (14), 1639–1662.
Mukherjee, S., et al., 2020. Synthetic antibodies against BRIL as universal fiducial marks for single-particle cryoEM structure determination of membrane proteins. Nat. Commun. 11 (1), 1598.
Mulnaes, D., Gohlke, H., 2018. TopScore: using deep neural networks and large diverse data sets for accurate protein model quality assessment. J. Chem. Theory Comput. 14 (11), 6117–6126.
Niessen, K.V., et al., 2011. Interaction of bispyridinium compounds with the orthosteric binding site of human alpha7 and Torpedo californica nicotinic acetylcholine receptors (nAChRs). Toxicol. Lett. 206 (1), 100–104.
Niessen, K.V., et al., 2013. Affinities of bispyridinium non-oxime compounds to [(3)H] epibatidine binding sites of Torpedo californica nicotinic acetylcholine receptors depend on linker length. Chem. Biol. Interfaces 206 (3), 545–554.
Niessen, K.V., et al., 2016. Functional analysis of Torpedo californica nicotinic acetylcholine receptors in multiple activation states by SSM-based electrophysiology. Toxicol. Lett. 247, 1–10.
Niessen, K.V., et al., 2018. In vitro pharmacological characterization of the bispyridinium non-oxime compound MB327 and its 2- and 3-regioisomers. Toxicol. Lett. 293, 190–197.
Noviello, C.M., et al., 2021. Structure and gating mechanism of the alpha7 nicotinic acetylcholine receptor. Cell 184 (8), 2121–2134 e13.
OpenEye Scientific Software, I., OEDOCKING. 2020. Santa Fe, NM.
OpenEye Scientific Software, I., OMEGA. 2020. Santa Fe, NM.
Olsson, M.H., et al., 2011. PROPKA3: consistent treatment of internal and surface residues in empirical pKa predictions. J. Chem. Theory Comput. 7 (2), 525–537.
Onufriev, A., Bashford, D., Case, D.A., 2004. Exploring protein native states and large-scale conformational changes with a modified generalized born model. Proteins 55 (2), 383–394.
Pauli, G.F., et al., 2014. Importance of purity evaluation and the potential of quantitative (1)H NMR as a purity assay. J. Med. Chem. 57 (22), 9220–9231.
Pavelka, A., et al., 2016. CAVER: algorithms for analyzing dynamics of tunnels in macromolecules. IEEE/ACM Trans. Comput. Biol. Bioinform. 13 (3), 505–517.
Pei, J., Kim, B.H., Grishin, N.V., 2008. PROMALS3D: a tool for multiple protein sequence and structure alignments. Nucleic Acids Res. 36 (7), 2295–2300.
Pettersen, E.F., et al., 2004. UCSF Chimera – a visualization system for exploratory research and analysis. J. Comput. Chem. 25 (13), 1605–1612.
Pfleger, C., et al., 2013a. Constraint network analysis (CNA): a python software package for efficiently linking biomacromolecular structure, flexibility, (thermo-)stability, and function. J. Chem. Inf. Model. 53 (4), 1007–1015.
Pfleger, C., et al., 2013b. Global and local indices for characterizing biomolecular flexibility and rigidity. J. Comput. Chem. 34 (3), 220–233.
Pfleger, C., et al., 2017. Ensemble- and rigidity theory-based perturbation approach to analyze dynamic allostery. J. Chem. Theory Comput. 13 (12), 6343–6357.
Pfleger, C., et al., 2021. Allosteric signaling in C-linker and cyclic nucleotide-binding domain of HCN2 channels. Biophys. J. 120 (5), 950–963.
Rahman, M.M., et al., 2020. Structure of the native muscle-type nicotinic receptor and inhibition by snake venom toxins. Neuron 106 (6), 952–962 e5.
Rappenglück, S., et al., 2018. Synthesis of a series of non-symmetric bispyridinium and related compounds and their affinity characterization at the nicotinic acetylcholine receptor. ChemMedChem 13 (24), 2653–2663.
Roe, D.R., Cheatham 3rd, T.E., 2013. PTRAJ and CPPTRAJ: software for processing and analysis of molecular dynamics trajectory data. J. Chem. Theory Comput. 9 (7), 3084–3095.
Ryckaert, J.-P., Ciccotti, G., Berendsen, H.J.C., 1977. Numerical integration of the cartesian equations of motion of a system with constraints: molecular dynamics of n-alkanes. J. Comput. Phys. 23 (3), 327–341.
Scheffel, C., et al., 2018. Electrophysiological investigation of the effect of structurally different bispyridinium non-oxime compounds on human alpha7-nicotinic acetylcholine receptor activity – an in vitro structure-activity analysis. Toxicol. Lett. 293, 157–166.

Schott-Verdugo, S., Gohlke, H., 2019. PACKMOL-Memgen: a simple-to-use, generalized workflow for membrane-protein-lipid-bilayer system building. J. Chem. Inf. Model. 59 (6), 2522–2528.
Schrödinger, L.L.C., The PyMOL Molecular Graphics System, *Version 1.8.*, 2015.
Schrödinger, L.L.C., Maestro. 2020.
Seeger, T., et al., 2007. Reevaluation of indirect field stimulation technique to demonstrate oxime effectiveness in OP-poisoning in muscles in vitro. Toxicology 233 (1–3), 209–213.
Seeger, T., et al., 2012. Restoration of sonan-blocked neuromuscular transmission in human and rat muscle by the bispyridinium non-oxime MB327 in vitro. Toxicology 294 (2–3), 80–84.
Shen, M.Y., Sali, A., 2006. Statistical potential for assessment and prediction of protein structures. Protein Sci. 15 (11), 2507–2524.
Sheridan, R.D., et al., 2005. Nicotinic antagonists in the treatment of nerve agent intoxication. J. R. Soc. Med. 98 (3), 114–115.
Sichler, S., et al., 2018. Development of MS Binding Assays targeting the binding site of MB327 at the nicotinic acetylcholine receptor. Toxicol. Lett. 293, 172–183.
Sondergaard, C.R., et al., 2011. Improved treatment of ligands and coupling effects in empirical calculation and rationalization of pKa values. J. Chem. Theory Comput. 7 (7), 2284–2295.
Spurny, R., et al., 2013. Multisite binding of a general anesthetic to the prokaryotic pentameric Erwinia chrysanthemi ligand-gated ion channel (ELIC). J. Biol. Chem. 288 (12), 8355–8364.
Spurny, R., et al., 2015. Molecular blueprint of allosteric binding sites in a homologue of the agonist-binding domain of the alpha7 nicotinic acetylcholine receptor. Proc. Natl. Acad. Sci. USA 112 (19), E2543–E2552.
Thiermann, H., Worek, F., Kehe, K., 2013. Limitations and challenges in treatment of acute chemical warfare agent poisoning. Chem. Biol. Interfaces 206 (3), 435–443.
Tian, C., et al., 2020. ff19SB: amino-acid-specific protein backbone parameters trained against quantum mechanics energy surfaces in solution. J. Chem. Theory Comput. 16 (1), 528–552.
Turner, S.R., et al., 2011. Protection against nerve agent poisoning by a noncompetitive nicotinic antagonist. Toxicol. Lett. 206 (1), 105–111.
Twizerimana, A.P., et al., 2020. Cell type-dependent escape of capsid inhibitors by simian immunodeficiency virus SIVcpz. J. Virol. 94 (23).
Unwin, N., 2005. Refined structure of the nicotinic acetylcholine receptor at 4A resolution. J. Mol. Biol. 346 (4), 967–989.
Unwin, N., Fujiyoshi, Y., 2012. Gating movement of acetylcholine receptor caught by plunge-freezing. J. Mol. Biol. 422 (5), 617–634.
Walsh Jr., R.M., et al., 2018. Structural principles of distinct assemblies of the human alpha4beta2 nicotinic receptor. Nature 557 (7704), 261–265.
Webb, B., Sali, A., 2016. Comparative protein structure modeling using MODELLER. Curr. Protoc. Bioinform. 54 (5 6 1-5 6 37).
Wein, T., et al., 2018. Searching for putative binding sites of the bispyridinium compound MB327 in the nicotinic acetylcholine receptor. Toxicol. Lett. 293, 184–189.
Whiteley, W., 2005. Counting out to the flexibility of molecules. Phys. Biol. 2 (4), S116–S126.
Wiener, S.W., Hoffman, R.S., 2004. Nerve agents: a comprehensive review. J. Intensive Care Med. 19 (1), 22–37.
Worek, F., Thiermann, H., Szinicz, L., 2004. Reactivation and aging kinetics of human acetylcholinesterase inhibited by organophosphonylcholines. Arch. Toxicol. 78 (4), 212–217.
Zhang, Q., et al., 2015. Functional impact of 14 single nucleotide polymorphisms causing missense mutations of human alpha7 nicotinic receptor. PLOS One 10 (9), e0137588.
Zhao, Y., et al., 2021. Structural basis of human α7 nicotinic acetylcholine receptor activation. Cell Res. 31 (6), 713–716.

Supporting information

A novel binding site in the nicotinic acetylcholine receptor for MB327 can explain its allosteric modulation relevant for organophosphorus-poisoning treatment

Jesko Kaiser[1], Christoph G.W. Gertzen[1], Tamara Bernauer[2], Georg Höfner[2], Karin V. Niessen[3], Thomas Seeger[3], Franz F. Paintner[2], Klaus T. Wanner[2], Franz Worek[3], Horst Thiermann[3], Holger Gohlke[1,4,*]

[1]Institute for Pharmaceutical and Medicinal Chemistry, Heinrich Heine University Düsseldorf, Düsseldorf, Germany

[2]Department of Pharmacy, Ludwig-Maximilians-Universität München, München, Germany

[3]Bundeswehr Institute of Pharmacology and Toxicology, München, Germany

[4]John von Neumann Institute for Computing (NIC), Jülich Supercomputing Centre (JSC), Institute of Biological Information Processing (IBI-7: Structural Biochemistry) & Institute of Bio- and Geosciences (IBG-4: Bioinformatics), Forschungszentrum Jülich, Jülich, Germany

Table of content

Supplemental Figures and Tables

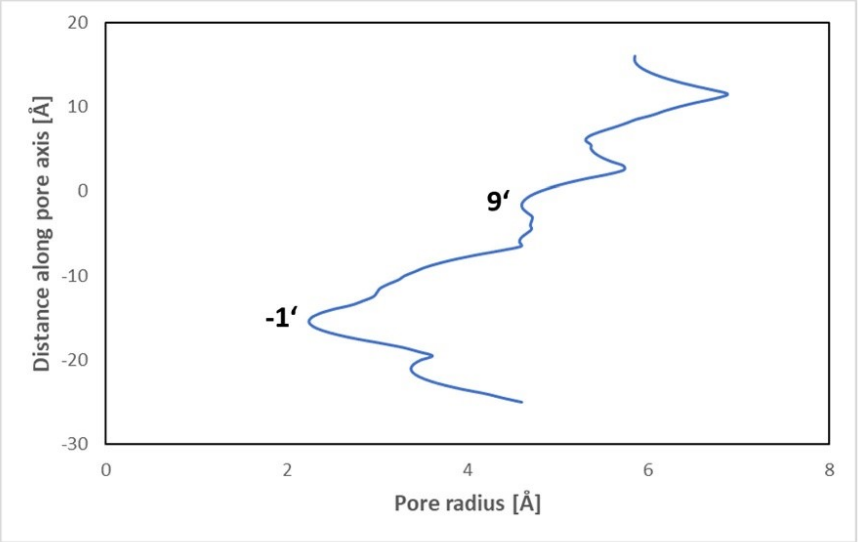

Figure S1: Pore radius of the α4β2 nAChR in complex with the partial agonist varenicline (PDB-ID: 6UR8[1]). The distance along the pore axis has been set to 0 Å at position 9'. The funnel-shaped structure with a gate at position -1' indicates a desensitized state.

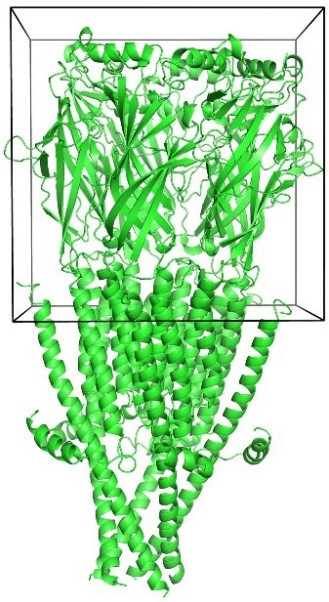

Figure S2: Model of the α7 nAChR. The displayed box indicates the part of the receptor that has been used to perform the blind docking experiments.

Table S1: Highest-ranked clusters of the blind docking experiments of MB327 in the human muscle-type nAChR.[a]

Cluster	Lowest docking energy [kcal/mol]	Number of poses in the cluster	Binding pocket	Subunits
1	-10.69	21	MB327-PAM-1	δ-β
2	-10.39	13	„orthosteric“[b]	δ-β
3	-9.83	5	MB327-PAM-1	ε-α
4	-9.70	1	MB327-PAM-1	α-ε
5	-9.56	10	MB327-PAM-1	α-δ
6	-9.48	2	MB327-PAM-1	δ-β
7	-9.39	8	MB327-PAM-1	α-δ
8	-8.8	1	MB327-PAM-1	α-ε
9	-8.73	1	MB327-PAM-1	α-δ
10	-8.60	1	„orthosteric“[b]	δ-β
11	-8.29	5	MB327-1	α-δ
28	-7.43	1	orthosteric	α-ε
34	-7.09	1	orthosteric	α-ε

[a] The ten highest-ranked clusters are shown. Additionally, the highest-ranked clusters where MB327 was placed in the orthosteric binding site (clusters 28 and 34) and MB327-1 as identified by Wein et al. [2] (cluster 11) are displayed.

[b] The orthosteric binding pocket is marked in quotes because the location of the binding pocket is identical between two neighboring subunits but acetylcholine only binds in between the α and its respective adjacent subunit. The sequence similarity of the “orthosteric” binding pocket between the δ- and β- subunits to the actual orthosteric binding pocket where nicotine binds (between the α- and δ-/ε- subunit)is 18%. MB327-PAM-1 refers to the newly identified pocket.

Table S2: Ten highest-ranked clusters of the blind docking of MB327 in the human α7-nAChR

Cluster	Lowest docking energy [kcal/mol]	Number of poses in the cluster	Binding pocket
1	-11.41	26	MB327-PAM-1
2	-10.91	1	MB327-PAM-1
3	-10.56	7	orthosteric
4	-9.69	11	MB327-PAM-1
5	-9.51	4	MB327-PAM-1
6	-9.32	5	orthosteric
7	-9.27	1	orthosteric
8	-9.27	15	MB327-1
9	-9.20	1	MB327-1
10	-9.11	1	MB327-1

Table S3: Four highest-ranked clusters of the blind docking experiments of acetylcholine in the human muscle-type nAChR.

Cluster	Lowest docking energy [kcal/mol]	Number of poses in the cluster	Binding pocket	Subunits
1	-6.51	30	orthosteric	α-ε
2	-6.44	10	„orthosteric“[a]	δ-β
3	-6.43	22	orthosteric	α-δ
4	-6.31	6	orthosteric	α-δ

[a] The orthosteric binding pocket is marked in quotes because the location of the binding pocket is identical between two neighboring subunits but acetylcholine only binds in between the α and its respective adjacent subunit. . The sequence similarity of the “orthosteric” binding pocket between the δ- and β- subunits to the actual orthosteric binding pocket where nicotine binds (between the α- and δ-/ε- subunit)is 18%. MB327-PAM-1 refers to the newly identified pocket.

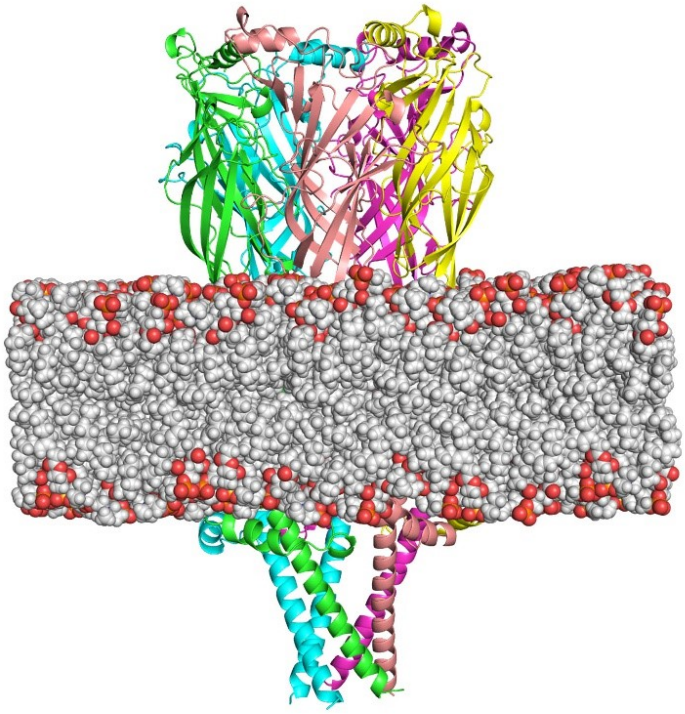

Figure S3: Starting structure for the MD simulations with MB327 bound to all five subunits. The membrane bilayer is shown as spheres. For clarity, water, potassium, and chloride molecules are not shown.

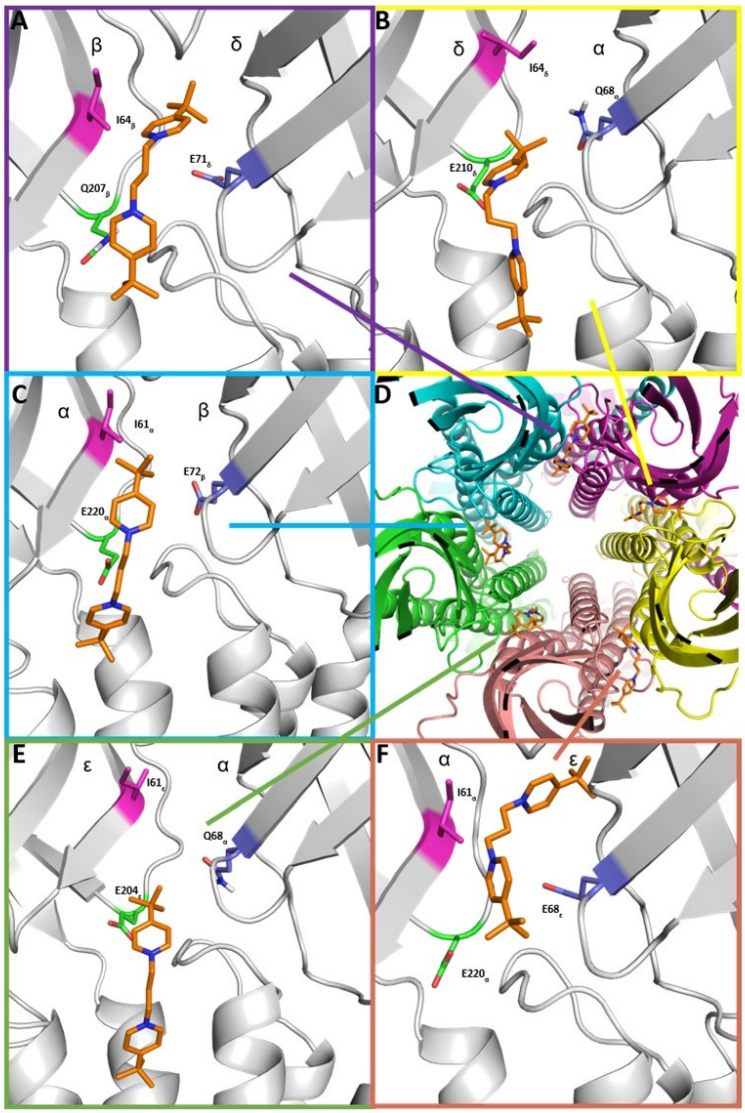

Figure S4: Docked binding mode of MB327 in MB327-PAM-1 in **A**) the β-δ-, **B**) δ-α-, **C**) α-β-, **E**) ε-α-, and **F**) α-ε-subunit. **D**) Extracellular view on MB327-PAM-1.

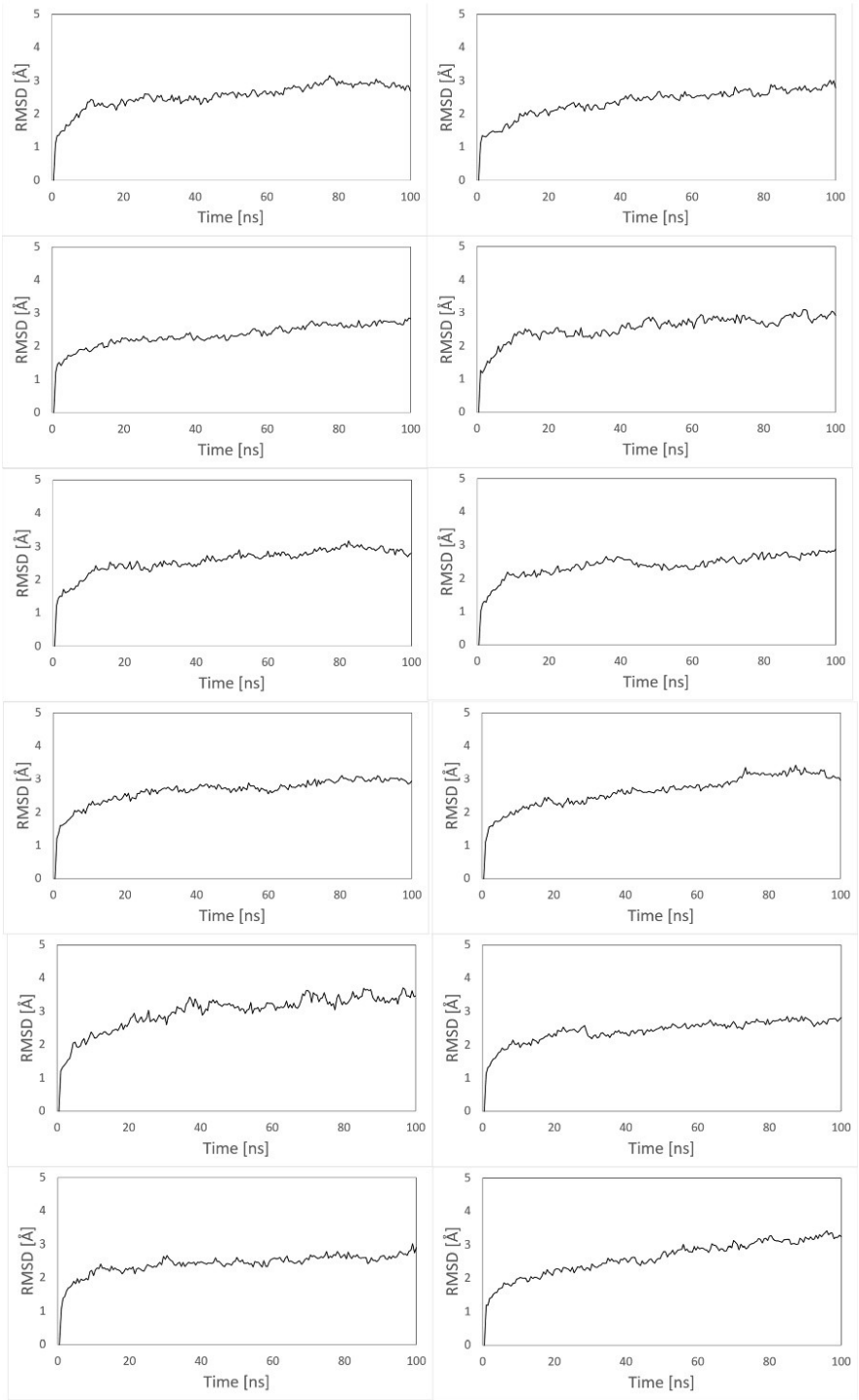

9

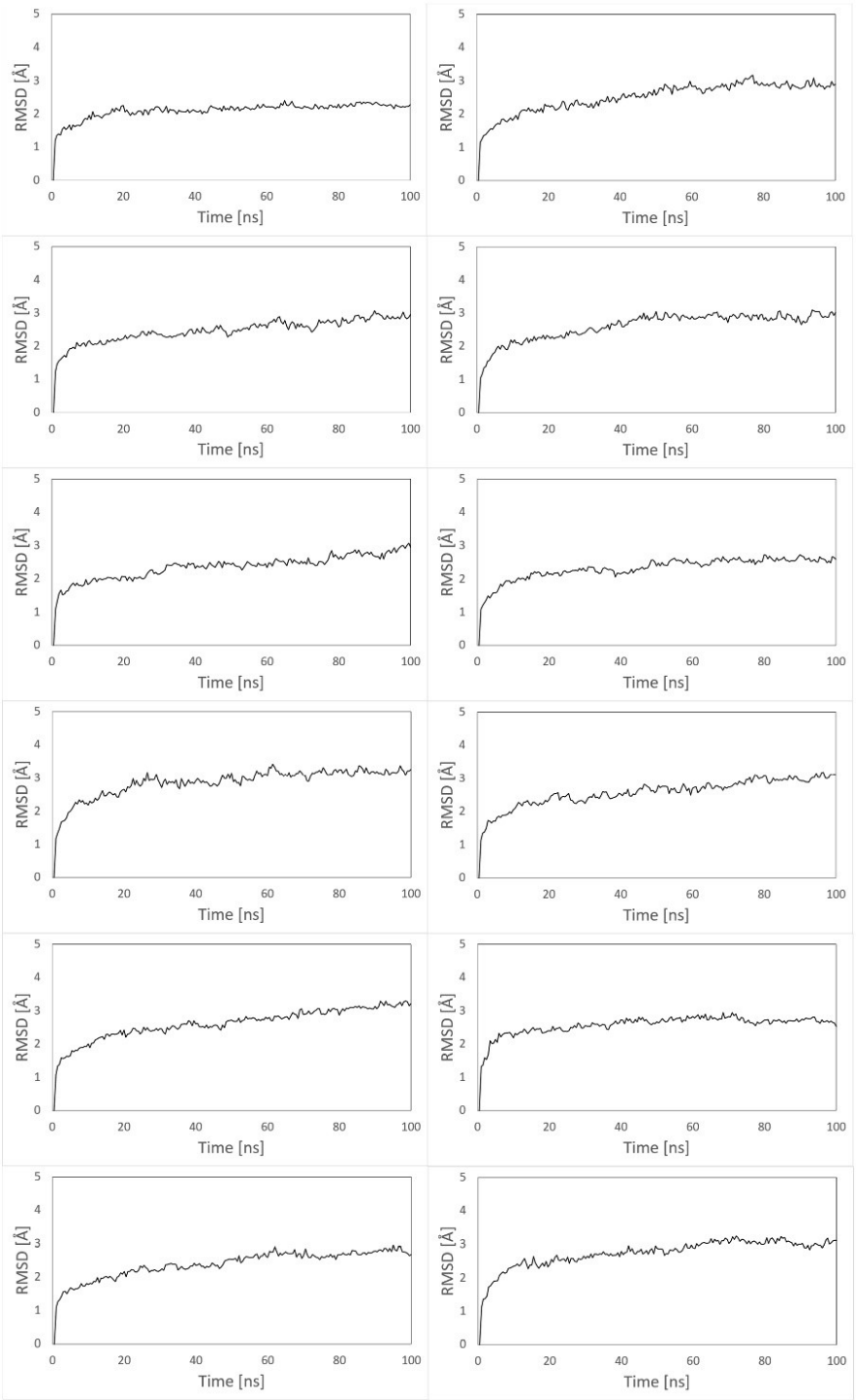

10

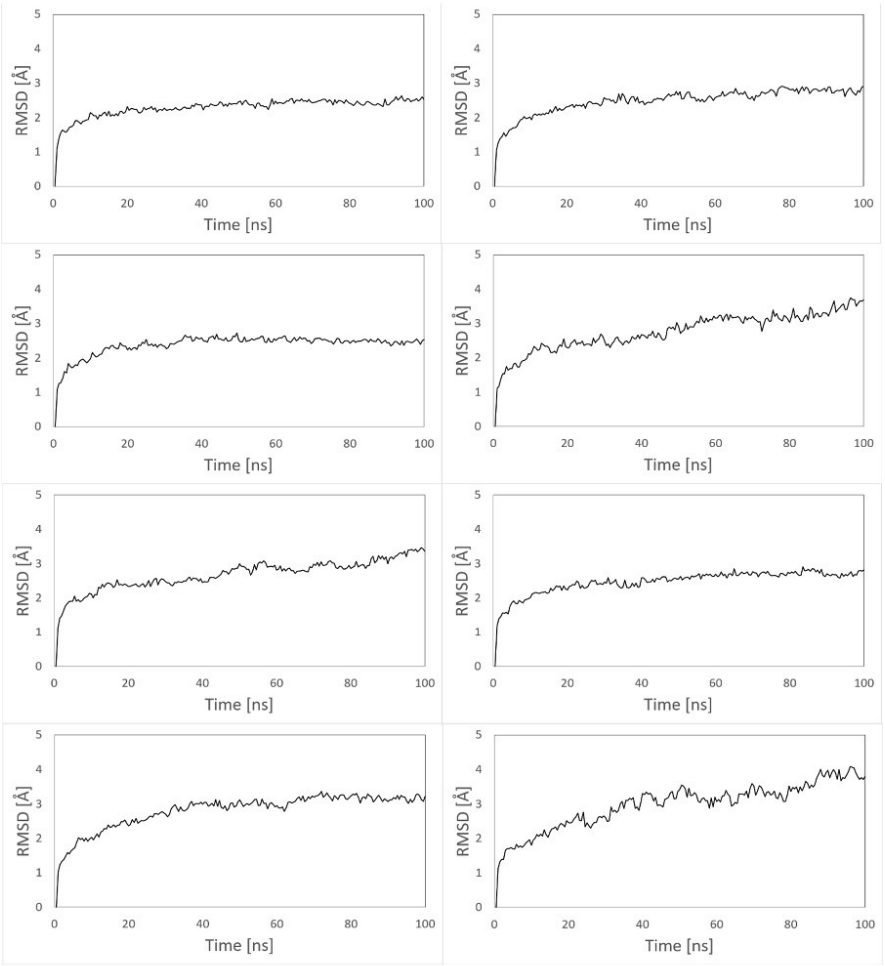

Figure S5: Backbone (C, CA, N) RMSD values of nAChR during 32 replicas of MD simulations with MB327 bound to all subunits.

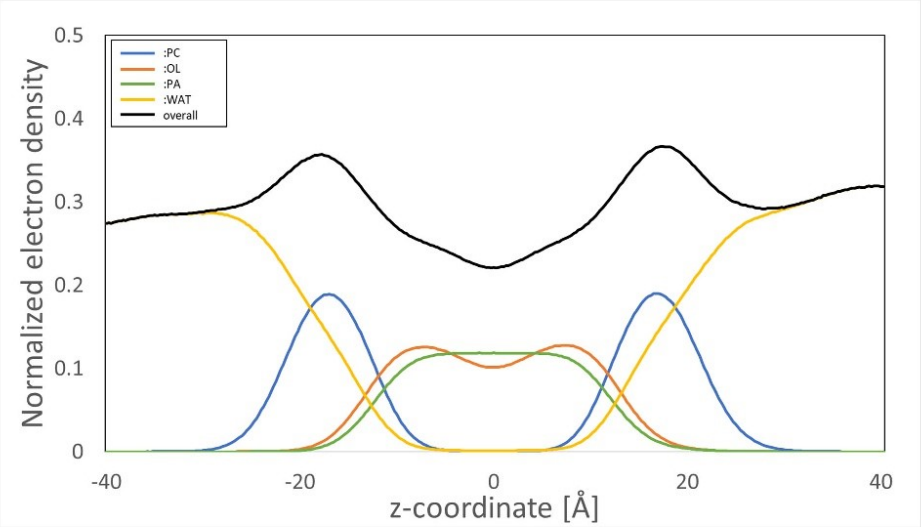

Figure S6: Electron density plot of membrane components and water based on all 32 replicas of the MD simulations with MB327 bound to nAChR. The electron density is plotted against the z-coordinate with the membrane centered at 0 Å for PC: phosphatidylcholine, OL: oleic acid, PA: palmitoylic acid, and WAT: water.

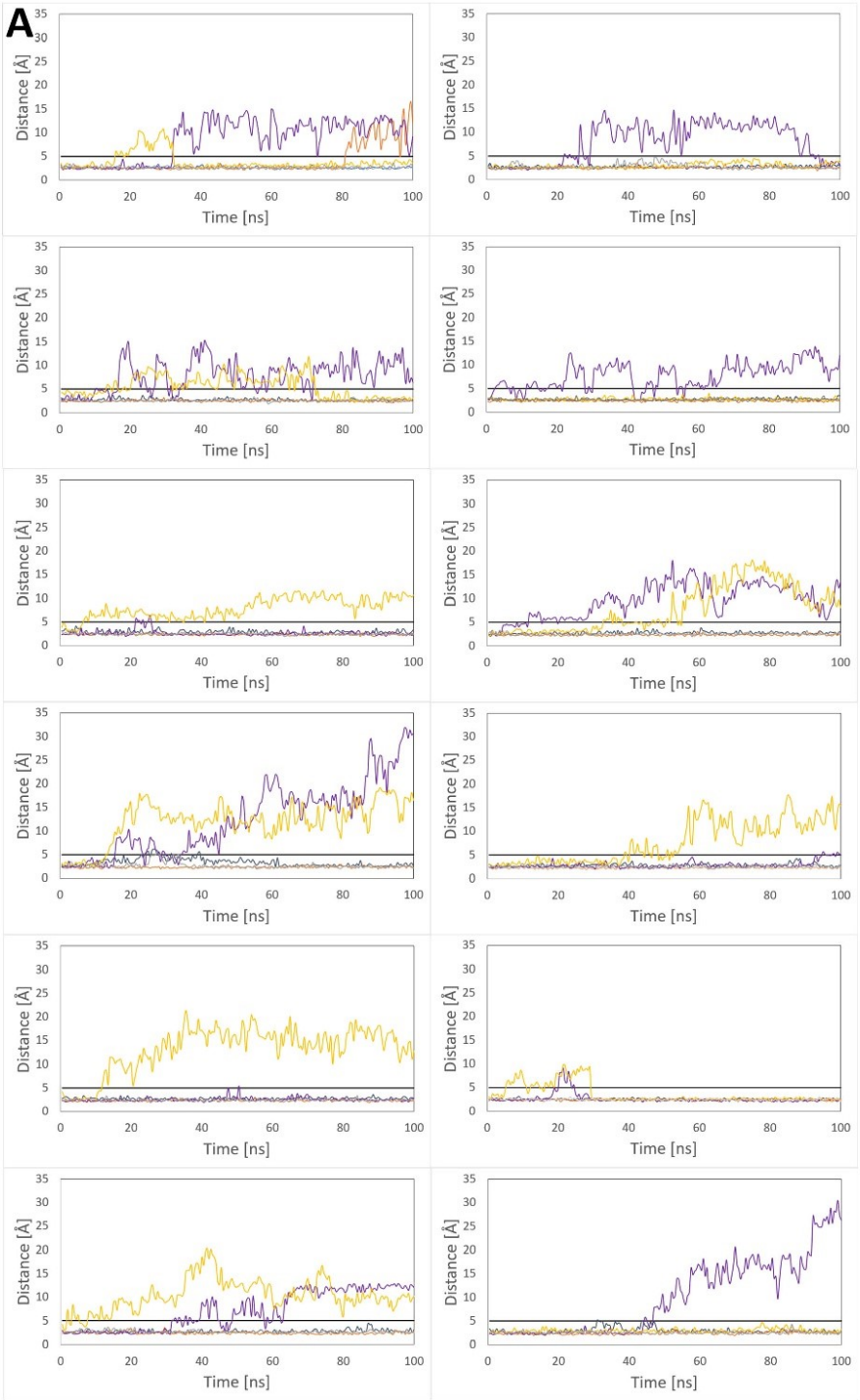

13

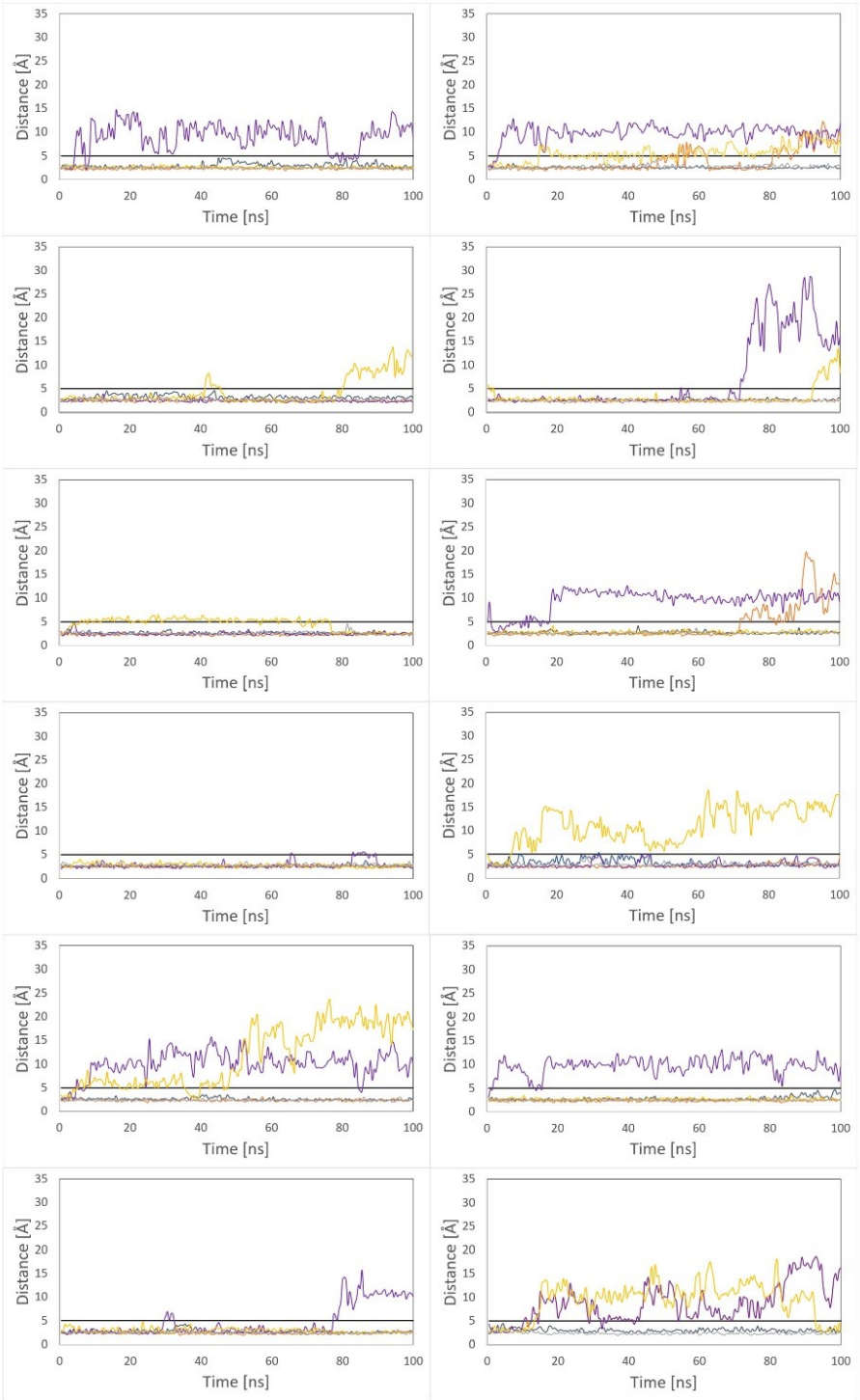

14

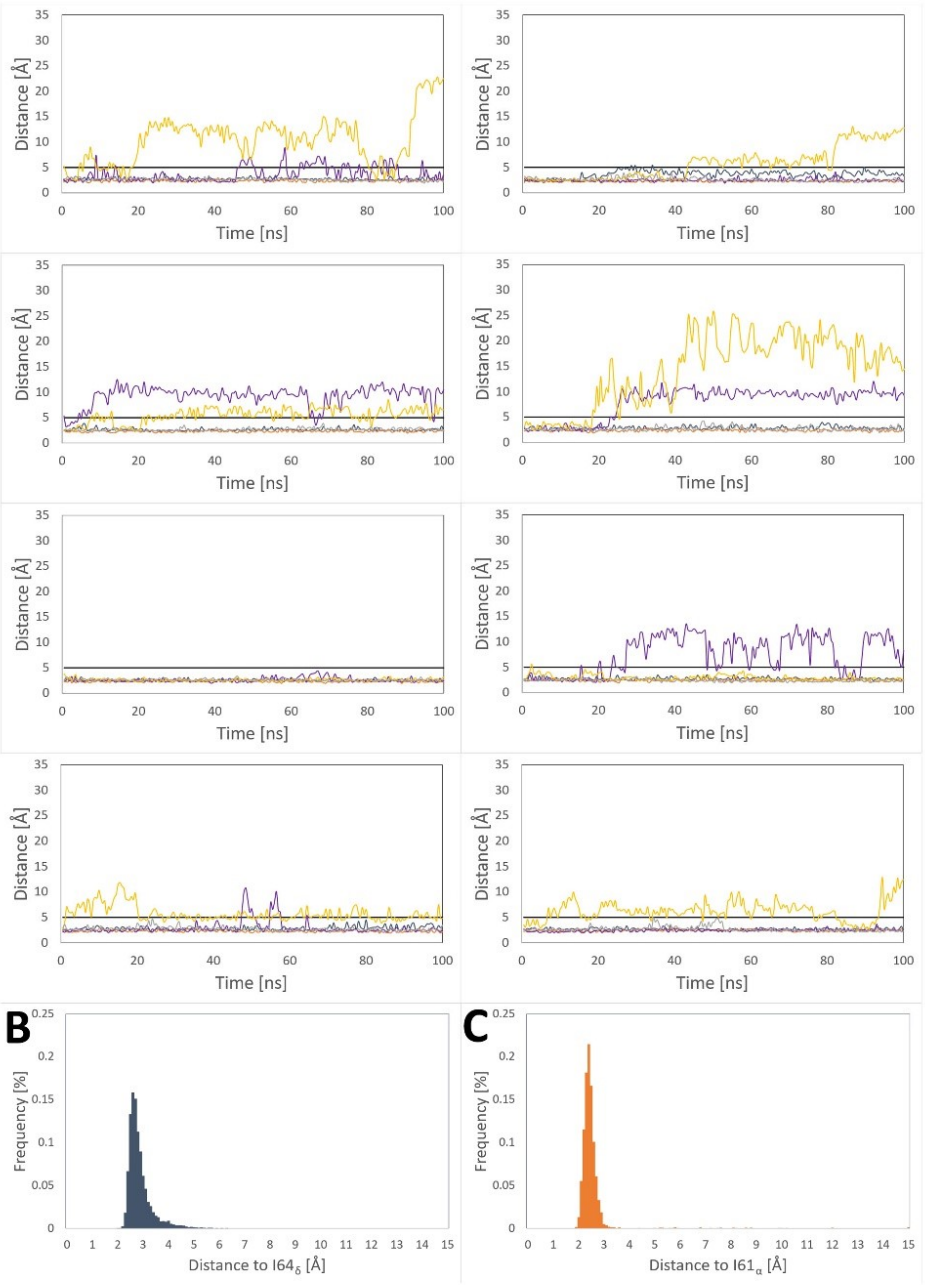
Distance [Å]
Time [ns]
B
Frequency [%]
Distance to I64$_{\delta}$ [Å]
C
Frequency [%]
Distance to I61$_{\alpha}$ [Å]

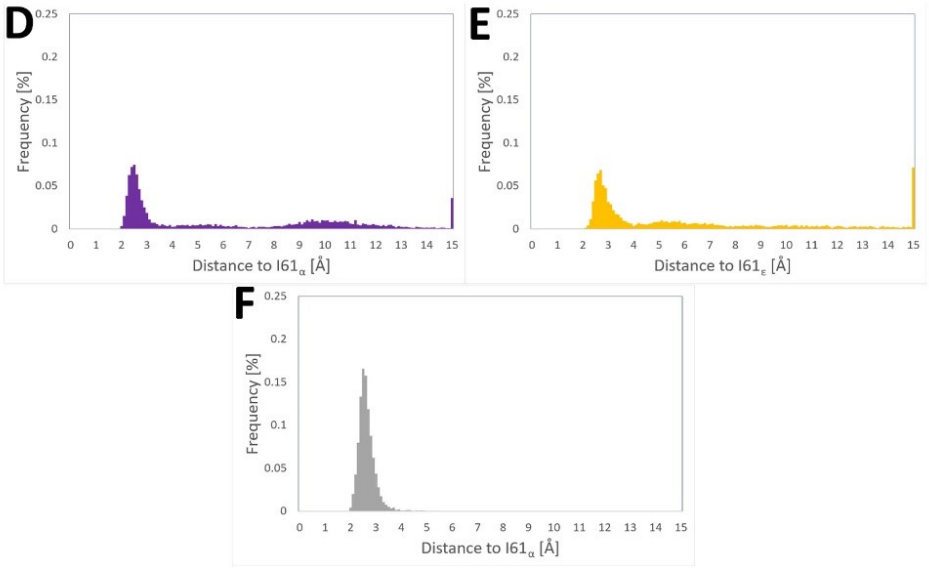

Figure S7: Distances of MB327 to the respective isoleucine in the binding site. **A)** The distance of MB327 of all 32 replicas during the simulations and the respective distance distributions **B)** in between the α- and δ-subunit to I64$_{\delta}$ is shown in dark blue, **C)** in between the δ- and β-subunit to I64$_{\beta}$ in orange, **D)** in between the β- and α-subunit to I61$_{\alpha}$ in purple, **E)** in between the α- and ε-subunit to I61$_{\varepsilon}$ in yellow, **F)** and in between the ε- and α-subunit to I61$_{\alpha}$ in grey. The distance cutoff of 5 Å is indicated by a black line in the distances plotted over the time during simulations. Values over 15 Å in the distance distributions are summarized in the last bin.

Table S4: Distances of docked MB327 to important amino acids in the binding site.[a]

Subunit	Distance to glutamate/glutamine in loop F[b]	Distance to glutamate/glutamine in β1-β2 loop[b]	Distance to isoleucine in β1[b]
α-δ	4.5	5.5	2.4
δ-β	6.1	3.9	1.1
β-α	7.4	10.6	1.5
α-ε	5.1	7.7	4.2
ε-α	4.9	3.2	3.0

[a] The distances to acidic sidechains represent the minimum distance of the partially positive charged atoms of the aromatic ring of MB327 (nitrogen and carbon in para position) to the oxygens of the respective sidechain. The distance to threonine represents the minimum distance to MB327.

[b] In Å.

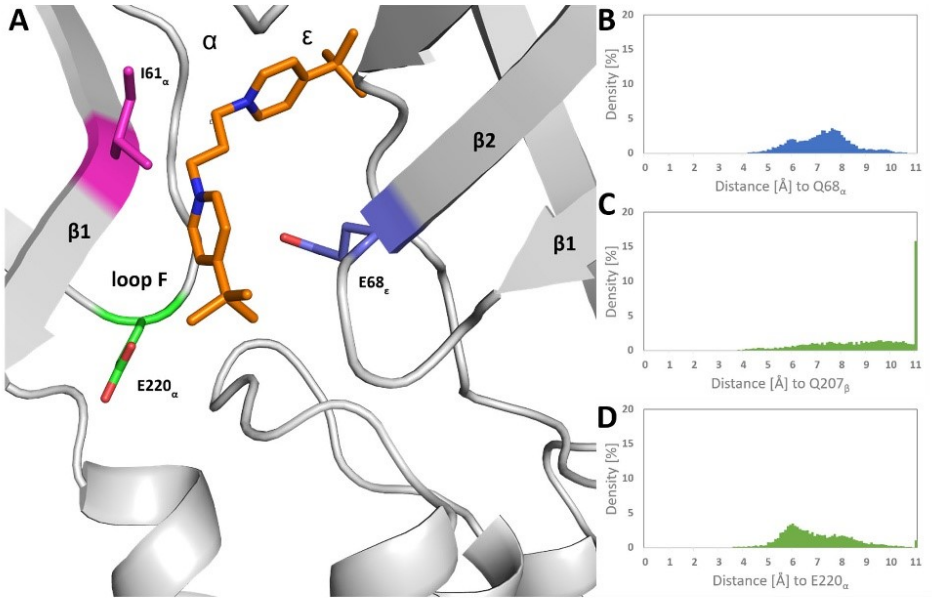

Figure S8: Distances of the nitrogens and carbon atoms in para position to the second acidic/polar residue in MB327-PAM-1. **A)** Proposed binding mode of MB327 in MB327-PAM-1 between the ε- and α-subunits. The color of amino acids E220 and E68 relates to the figures in panels B-D. Minimum distance of the nitrogens and carbon atoms located in the para position of MB327 to the side chain oxygens of **B)** $Q68_{\alpha}$, **C)** $Q207_{\beta}$, and **D)** $E220_{\alpha}$. Distances above 11 Å are summarized in the last bin.

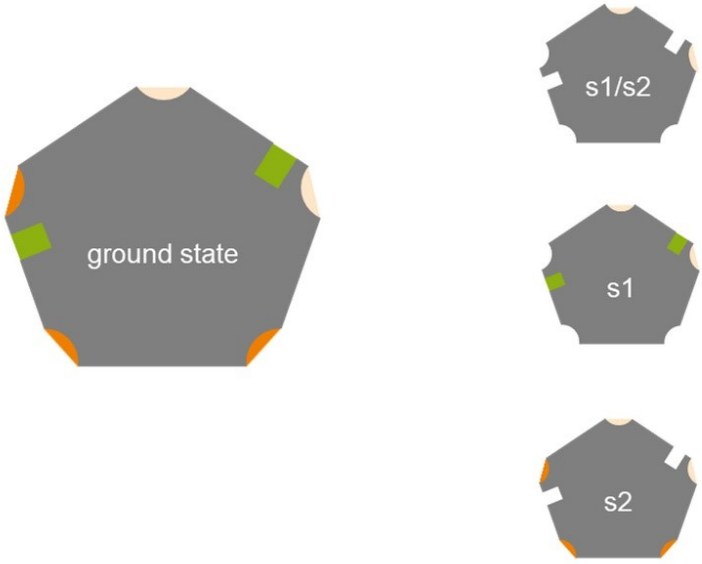

Figure S9: Performed perturbation runs in CNA to investigate the allosteric impact of MB327 and the cooperativity of binding of nicotine and MB327. The pentagon represents nAChR with its five subunits. During the MD simulations, MB327 is bound in all five possible binding sites, and nicotine is bound to both possible binding sites (left). The two MB327 molecules that did not stay stable in the binding site during MD simulations are shown in light orange. Three perturbation runs were performed: 1) s1/s2: all stable ligands were removed (top right); 2) s1: MB327 was removed in all stable binding sites (middle right); 3) s2: nicotine was removed in both binding sites (bottom right).

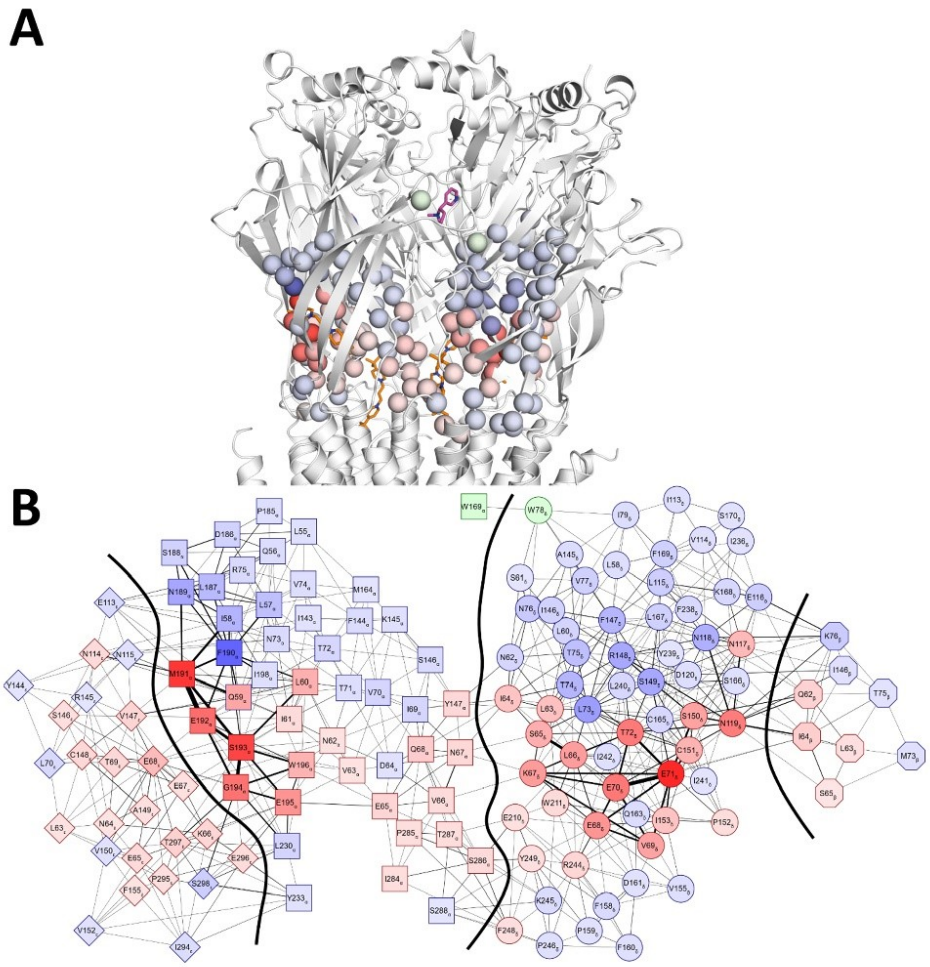

Figure S10: Allosteric effect of MB327 on the extracellular domain. **A)** Residues with significant changes of structural rigidity after removal of MB327 are shown as spheres. Residues located within 5 Å of MB327 are shown in red and those within 5 Å of the orthosteric ligand nicotine are shown in green. A cutoff of 0.15 kcal mol^{-1} was used to display residues. Thus, only an effect on the extracellular domain is shown. **B)** The information from (A) shown as a graph. The nodes represent residues, and edges the flow between these residues. Twisted squares represent residues from the ε-, squares residues from the α-, circles residues from the δ-, and octagons residues from the β-subunit.

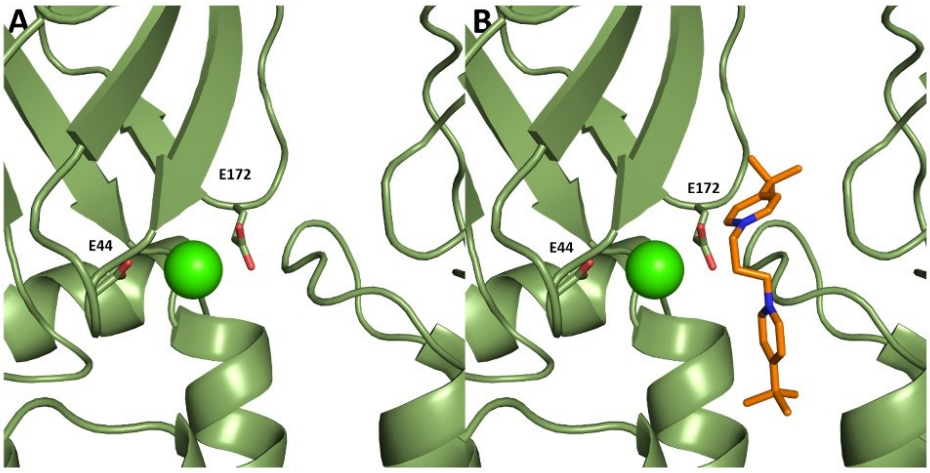

Figure S11: Location of calcium in MB327-PAM-1. **A**) Cryo-EM structure of α7-nAChR (PDB-ID: 7KOQ[3]) with calcium (green) located in between E44 and E172. **B**) Comparison of the calcium binding site to the docked binding mode of MB327 in the human muscle-type nAChR in MB327-PAM-1 between the α- and δ-subunit (orange) in α7-nAChR (PDB-ID: 7KOX [3]) after aligning the human muscle-type nAChR model to the cryo-EM structure of α7-nAChR.

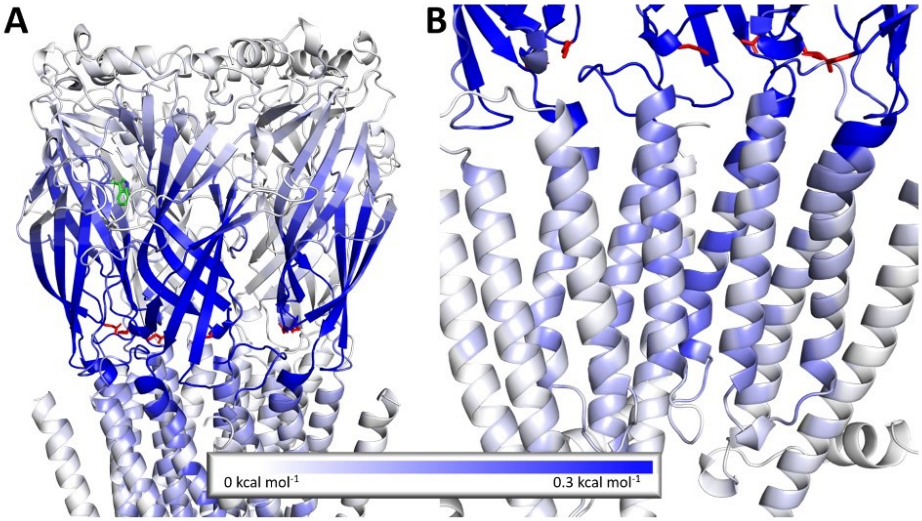

Figure S12: Allosteric effects of calcium on the **A**) the extracellular and **B**) the transmembrane domain of nAChR. The calcium ion was mimicked by setting constraints between the carboxy groups of the glutamates involved in calcium binding (shown in red). Blue colors indicate a stabilizing impact of calcium on the receptor. $W169_{\alpha}$, a central amino acid in the orthosteric binding site, is shown in green.

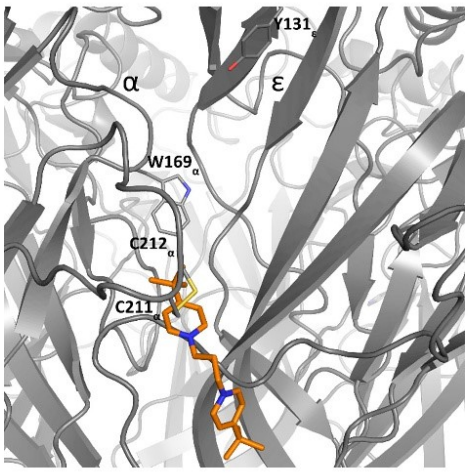

Figure S13: Representative binding mode of MB327 in the orthosteric binding pocket in the replica where MB327 stays only 130 ns within this pocket.

Table S5: Docking scores of MB327, PTM0062, and PTM0063 in all subunits of the muscle-type nAChR.

Subunit	Docking score of MB327	Docking score of PTM0062	Docking score of PTM0063
αδ	-8.62	-9.20	-8.51
δβ	-4.88	-5.76	-5.62
βα	-4.36	-6.17	-5.24
αε	-8.65	-8.13	-8.95
εα	-5.44	-6.01	-7.42

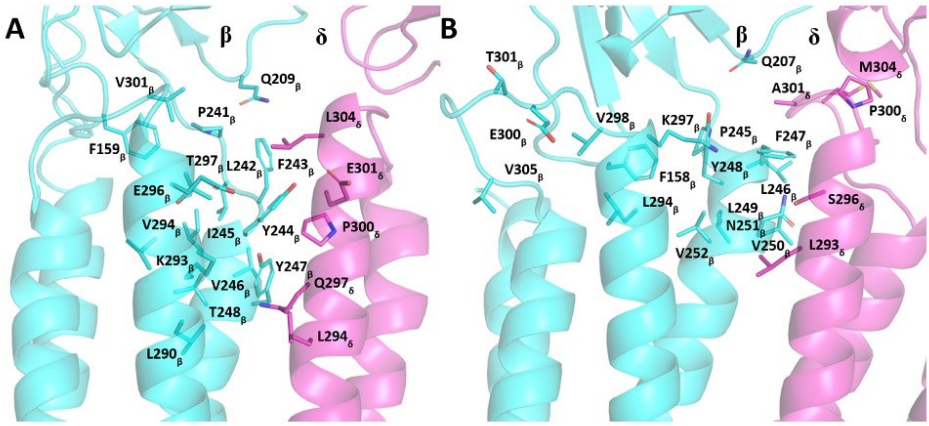

Figure S14: **A)** Amino acids that are part of the binding site MB327-2 in the PDB-structure 2BG9[4]. **B)** Amino acids that are part of M327-2 in our new models of the human muscle-type nAChR. The alignment of the amino acids is shown in Table S4.

Table S6: Alignment of the amino acids that are part of MB327-2 in the *Torpedo marmorata* and human muscle-type nAChR.

β		δ	
2BG9	human	2BG9	human
F159	F158	L294	L293
Q209	Q207	Q297	S296
P241	P245	P300	P300
L242	L246	E301	A301
F243	F247	L304	M304
Y244	Y248		
I245	L249		
V246	V250		
Y247	N251		
T248	V252		
L290	L294		
K293	K297		
V294	V298		
E296	E300		
T297	T301		
V301	V305		

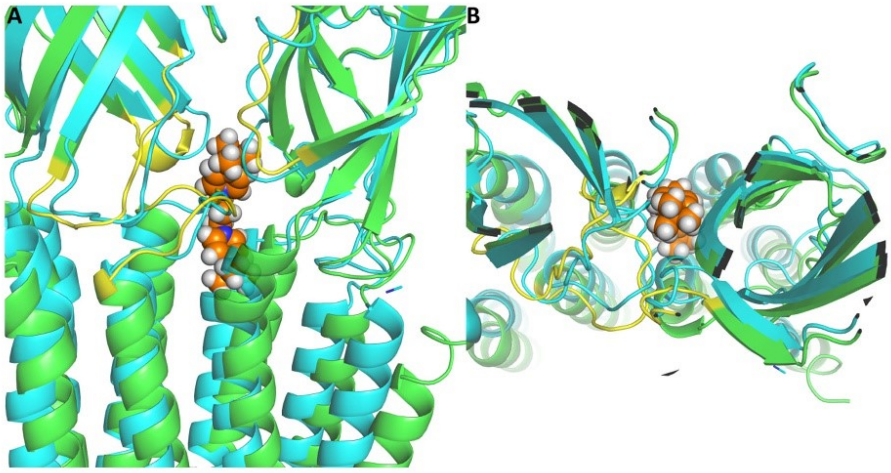

Figure S15: Aligned models of the human nAChR in the desensitized (green) and inactive (blue) state viewed from **A)** the side and **B)** the extracellular space. Structural changes that occur during desensitization in the region of the binding site of MB327 (orange spheres) are colored in yellow in the desensitized model. These regions are in line with the regions of structural changes in the glycine receptor, another pentameric ligand-gated ion channel, during desensitization[5]. For clarity, only two adjacent subunits (α and ε) are shown. Similar structural changes can be observed in all subunits of the receptor.

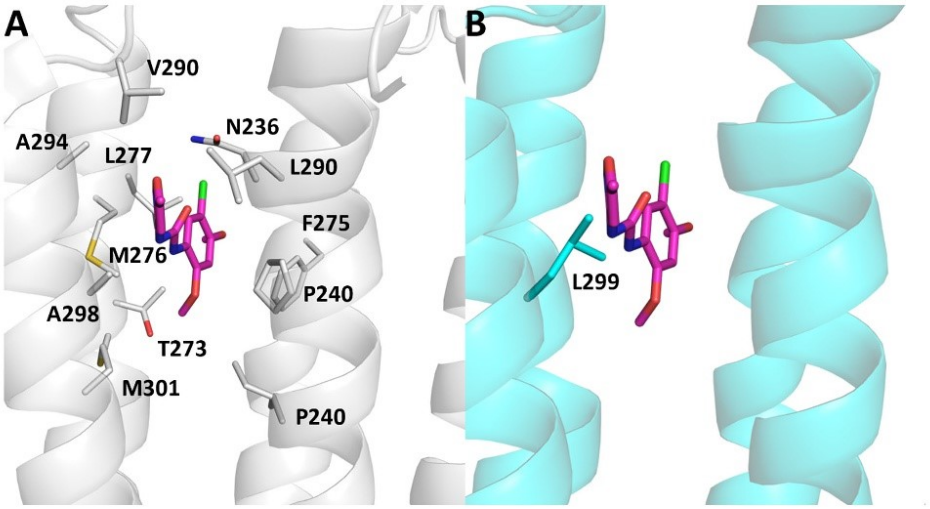

Figure S16: Comparison of the PNU-120596 binding site in the α7- and the human muscle-type nAChR. **A)** Amino acids located within 5 Å of PNU-120596 (purple) are shown as sticks. No charged amino acids are located in the binding site. **B)** A mutation of A298 in the α7-nAChR to L299 in the human muscle-type nAChR leads to a clash with the α7-selective modulator PNU-120596. The closest distance between heavy atoms of the ligand and heavy atoms of L299 is 0.9 Å.

Supplemental References

1. Mukherjee, S., et al., *Synthetic antibodies against BRIL as universal fiducial marks for single-particle cryoEM structure determination of membrane proteins.* Nat Commun, 2020. **11**(1): p. 1598.
2. Wein, T., et al., *Searching for putative binding sites of the bispyridinium compound MB327 in the nicotinic acetylcholine receptor.* Toxicol Lett, 2018. **293**: p. 184-189.
3. Noviello, C.M., et al., *Structure and gating mechanism of the alpha7 nicotinic acetylcholine receptor.* Cell, 2021. **184**(8): p. 2121-2134 e13.
4. Unwin, N., *Refined structure of the nicotinic acetylcholine receptor at 4A resolution.* J Mol Biol, 2005. **346**(4): p. 967-89.
5. Kumar, A., et al., *Mechanisms of activation and desensitization of full-length glycine receptor in lipid nanodiscs.* Nat Commun, 2020. **11**(1): p. 3752.

3.2 Zweite Publikation: *Synthesis and Biological Evaluation of Novel MB327 Analogs as Resensitizers for Desensitized Nicotinic Acetylcholine Receptors after Intoxication with Nerve Agents*

3.2.1 Zusammenfassung der Ergebnisse

Um die aktuell noch unzureichenden Behandlungsmöglichkeiten von Vergiftungen mit phosphororganischen Verbindungen zu verbessern, werden Substanzen untersucht, die als allosterische Modulatoren direkt mit desensitisierten nAChRs interagieren und diese resensitisieren. Die kürzlich entwickelten nicht-symmetrischen MB327-Analoga PTM0062, PTM0063 und PTM0056 konnten die Muskelkraft von mit Soman-vergifteten Ratten-Diaphragmen in bemerkenswertem Ausmaß wiederherstellen, wodurch sie erfolgversprechende Ausgangspunkte für die Entwicklung neuer Resensitizer desensitisierter nAChR darstellen.

Im Kontext dieser Veröffentlichung wurde eine Serie weiterer, von den oben genannten nicht-symmetrischen Bispyridiniumverbindungen abgeleiteter, Verbindungen synthetisiert, welche nicht nur hinsichtlich ihrer intrinsischen Aktivität, sondern auch mit Hilfe des UNC0642-MS-Bindungsassays hinsichtlich ihrer Affinität zur allosterischen MB327-PAM-1-Bindungstasche am nAChR untersucht wurden. Die Zielverbindungen, welche neben einer 4-*tert*-Butylpyridinium-Teilstruktur über unterschiedliche 4-Aminopyridinium-Teilstrukturen verfügen, konnten in einer Mikrowellen-unterstützten Synthese in ein bis zwei Schritten aus dem Schlüsselbaustein 4-(*tert*-Butyl)-1-(3-iodopropyl)pyridin-1-iumiodid und entsprechenden Pyridinbausteinen durchwegs in hohen Ausbeuten sowie hohen Reinheiten gewonnen werden.

Im Rahmen der biologischen Untersuchungen fielen vor allem die Piperidino-substituierte Verbindung PTM0069 sowie die *N*-Boc-Piperazino-substituierte Verbindung PTM0071 auf. Neben nennenswert höheren Affinitäten zur MB327-PAM-1-Bindungsstelle verglichen mit MB327, zeigten sie gleichzeitig einen deutlichen Muskelkraft-wiederherstellenden Effekt: Die untersuchten Substanzen erreichten nicht nur eine stärkere Reaktivierung der Muskeln nach Soman-Vergiftung, sondern sie bewirkten diesen Effekt bereits bei deutlich geringeren Konzentrationen als MB327. In höheren Konzentrationen wurde jedoch bei beiden Verbindungen eine Abnahme der Muskelkraft, bis zur vollständigen Hemmung der Muskeln, beobachtet. Interessanterweise zeigte PTM0069 bei Untersuchungen an nicht vergifteten Ratten-Diaphragmen genau in diesem Konzentrationsbereich eine reversible muskelhemmende Aktivität. Eine Erklärung für diesen inhibitorischen Effekt könnte eine bei höheren Konzentrationen auftretende Bindung von PTM0069 an die orthosterische Bindungsstelle des nAChR sein.

Zusätzlich zu den oben beschriebenen Bispyridiniumverbindungen mit 4-Aminopyridinium-Teilstrukturen wurden zwei, in *in silico*-Studien identifizierte, Hydroxy-substituierte MB327-Analoga synthetisiert. Basierend auf GIST-Berechnungen sollten Moleküle mit polaren Teilstrukturen durch Verdrängung von Wasser-Clustern aus der MB327-PAM-1-Bindungstasche eine erhöhte Affinität aufweisen. Tatsächlich konnte für die Verbindung PTMD90-0012, die eine 7-Hydroxychinazolinium-Teilstruktur aufweist, nicht nur eine erhöhte Affinität an die genannte Bindungsstelle, sondern auch eine im Vergleich zu MB327 leicht verbesserte intrinsische Aktivität gefunden werden.

3.2.2 Darstellung des Eigenanteils

Alle Synthesen sowie die analytische Charakterisierung der Verbindungen wurden von mir durchgeführt. Die technische Durchführung der MS- und NMR-Messungen wurde von der Analytikabteilung des Departments für Pharmazie übernommen. Die Bestimmungen der Bindungsaffinitäten mittels des UNC0642-MS-Bindungsassays wurden von Valentin Nitsche durchgeführt. Thomas Seeger übernahm die *ex vivo*-Untersuchungen der Substanzen an Soman-vergifteten Ratten-Diaphragmen. Die *in silico*-Studien wurden von Jesko Kaiser durchgeführt. Das Manuskript wurde von mir in Zusammenarbeit mit Klaus T. Wanner und Franz F. Paintner konzipiert und verfasst. Ergänzende Beiträge stammen von Valentin Nitsche, Jesko Kaiser und Thomas Seeger. Die Korrektur des Manuskripts übernahmen im Wesentlichen Franz F. Paintner sowie Klaus T. Wanner. Des Weiteren wurde das Manuskript von Georg Höfner, Christoph G. W. Gertzen, Holger Gohlke, Karin V. Niessen, Dirk Steinritz und Franz Worek korrigiert.

Toxicology Letters 397 (2024) 151–162

Contents lists available at ScienceDirect

Toxicology Letters

journal homepage: www.journals.elsevier.com/toxicology-letters

Synthesis and biological evaluation of novel MB327 analogs as resensitizers for desensitized nicotinic acetylcholine receptors after intoxication with nerve agents

Tamara Bernauer [a,1], Valentin Nitsche [a,2], Jesko Kaiser [b,3], Christoph G.W. Gertzen [b,4], Georg Höfner [a,5], Karin V. Niessen [c,6], Thomas Seeger [c,7], Dirk Steinritz [c,8], Franz Worek [c,9], Holger Gohlke [b,d,10], Klaus T. Wanner [a,11], Franz F. Paintner [a,*,12]

[a] Department of Pharmacy - Center for Drug Research, Ludwig-Maximilians-Universität München, Munich, Germany
[b] Institute for Pharmaceutical and Medicinal Chemistry, Heinrich Heine University Düsseldorf, Düsseldorf, Germany
[c] Bundeswehr Institute of Pharmacology and Toxicology, Munich, Germany
[d] John von Neumann Institute for Computing (NIC), Jülich Supercomputing Centre (JSC), Institute of Biological Information Processing (IBI-7: Structural Biochemistry) & Institute of Bio- and Geosciences (IBG-4: Bioinformatics), Forschungszentrum Jülich, Jülich, Germany

ARTICLE INFO

Editor: Dr. Angela Mally

Keywords:
Neurological agents
Nicotinic acetylcholine receptor
MB327-PAM-1 binding site
Bispyridinium salts
Resensitizer
In silico studies
Myographic studies

ABSTRACT

Poisoning with organophosphorus compounds, which can lead to a cholinergic crisis due to the inhibition of acetylcholinesterase and the subsequent accumulation of acetylcholine (ACh) in the synaptic cleft, is a serious problem for which treatment options are currently insufficient. Our approach to broadening the therapeutic spectrum is to use agents that interact directly with desensitized nicotinic acetylcholine receptors (nAChRs) in order to induce functional recovery after ACh overstimulation. Although MB327, one of the most prominent compounds investigated in this context, has already shown positive properties in terms of muscle force recovery, this compound is not suitable for use as a therapeutic agent due to its insufficient potency. By means of *in silico* studies based on our recently presented allosteric binding pocket at the nAChR, i.e. the MB327-PAM-1 binding site, three promising MB327 analogs with a 4-aminopyridinium ion partial structure (PTM0056, PTM0062, and PTM0063) were identified. In this study, we present the synthesis and biological evaluation of a series of new analogs of the aforementioned compounds with a 4-aminopyridinium ion partial structure (PTM0064-PTM0072), as well as hydroxy-substituted analogs of MB327 (PTMD90–0012 and PTMD90–0015) designed to substitute entropically unfavorable water clusters identified during molecular dynamics simulations. The compounds were characterized in terms of their binding affinity towards the aforementioned binding site by applying the UNC0642 MS Binding Assays and in terms of their muscle force reactivation in rat diaphragm myography. More potent compounds were identified compared to MB327, as some of them showed a higher affinity towards MB327-PAM-1 and also a higher recovery of neuromuscular transmission at lower compound concentrations. To

* Correspondence to: Butenandtstr. 5-13, 81377 München, Germany.
E-mail address: Franz.Paintner@cup.uni-muenchen.de (F.F. Paintner).
[1] ORCID 0000–0001-9570–1253
[2] ORCID 0009–0000-3351–1227
[3] ORCID 0000–0002-6429–0911
[4] ORCID 0000–0002-9562–7708
[5] ORCID 0000 0002 7957 4503
[6] ORCID 0009–0008-6810–5294
[7] ORCID0009–0007-5713–4367
[8] ORCID 0000–0002-2073–5683
[9] ORCID 0000–0003-3531–3616
[10] ORCID 0000–0001-8613–1447
[11] ORCID 0000–0003-4399–1425
[12] ORCID 0000–0002-6795–586X

https://doi.org/10.1016/j.toxlet.2024.05.011
Received 12 February 2024; Received in revised form 6 May 2024; Accepted 14 May 2024
Available online 15 May 2024

improve the treatment of organophosphate poisoning, direct targeting of nAChRs with appropriate compounds is a key step, and this study is an important contribution to this research.

1. Introduction

The verified use of sarin in the Syrian war in 2013 (Dolgin, 2013; Pita and Domingo, 2014) and 2017 (OPCW, 2017), as well as the politically motivated Novichok attack on Russian opposition politician Alexei Navalny in 2020 (Steindl et al., 2021), provide clear evidence that highly toxic organophosphorus nerve agents still pose a major threat to military personnel and civilians, even after their international ban by the Chemical Weapons Convention in 1997 (Thakur and Haru, 2007). Intoxication with organophosphorus compounds (OPCs) leads to the irreversible inhibition of acetylcholinesterase (AChE), resulting in an uncontrolled accumulation of acetylcholine (ACh) in the synaptic cleft of cholinergic neurons. As a result, cholinergic signaling is disrupted by overstimulation of muscarinic and nicotinic acetylcholine receptors (mAChRs and nAChRs, respectively) (Koelle, 1981; Maselli, Leung, 1993; Massoulié et al., 1993). This condition, known as a "cholinergic crisis", can be life-threatening due to respiratory paralysis as a result of the disruption of nAChR-mediated neuromuscular transmission (Brown and Brix, 1998; Thiermann et al., 2010). Standard treatment for nerve agent poisoning currently includes a muscarinic acetylcholine receptor antagonist, e.g. atropine, to reduce mAChR overstimulation and an oxime-based AChE reactivator, e.g. obidoxime. According to Sheridan et al. (Sheridan et al., 2005) neuromuscular blockers (competitive nAChR antagonists) are not suitable for the treatment of nerve agent poisoning. Hence, reactivation of inhibited AChE appears to be crucial to counteract nicotinic overstimulation. However, despite decades of effort, there is still no universally applicable AChE reactivator that can efficiently cleave all OPC-AChE conjugates (Worek et al., 2020). Therefore, there is an urgent need to develop novel antidotes to counteract desensitization of muscle-type nAChRs as a result of overstimulation. One approach is to use agents that directly target the nAChR to restore its function after it has been desensitized by overstimulation (Sheridan et al., 2005; Turner et al., 2011).

Indeed, a number of bispyridinium salts, such as the prototypical compound MB327 (Fig. 1), are able to restore the function of desensitized nAChR of *Torpedo californica* (recently reclassified as *Tetronarce californica*) in *in vitro* experiments by interacting directly with the receptor most likely via an allosteric mechanism (Niessen et al., 2016; Niessen et al., 2018; Seeger et al., 2012; Sichler et al., 2018). Since the *Torpedo californica* nAChR has a high sequence identity to the rat and human muscle-type nAChRs, it is reasonable to assume that MB327 has similar effects on the desensitized nAChRs of the latter species as well. Indeed, in *ex vivo* experiments, MB327 shows a muscle force-restoring effect on both soman-poisoned rat diaphragms and soman-poisoned human intercostal muscles, which is thought to be due to the resensitization of desensitized nAChR (Niessen et al., 2018; Seeger et al., 2012). In addition, MB327 (or the corresponding methanesulfonate salt MB399, respectively) in combination with the mAChR antagonist hyoscine and the indirect parasympathomimetic physostigmine, was shown to increase the survival rates of guinea pigs poisoned with sarin or tabun in *in vivo* studies (Timperley et al., 2012; Turner et al., 2011). Despite these promising results, MB327 is not suitable for human use due to its narrow therapeutic window. Nevertheless, MB327 is a promising starting point for further investigation.

Recently, based on blind docking experiments and molecular dynamics simulations, we proposed a new allosteric binding site of MB327 at the muscle-type nAChR, termed MB327-PAM-1 (Kaiser et al., 2023). This binding site is located at the transition from the extracellular to the trans-membrane region and, according to a rigidity analysis, is expected to exert an allosteric effect on the orthosteric binding pocket upon binding of MB327. The amino acids interacting with MB327 in this binding site, predominantly glutamate residues, are highly conserved within the different nAChR subunits as well as in different species. Accordingly, comparable resensitizing effects of MB327 should be observable on desensitized nAChR of different species (e.g. *Torpedo californica*, rats and humans).

However, recently published results also show that bispyridinium compounds related to MB327 have inhibitory activity on the nAChR, most likely mediated via the orthosteric binding site (Epstein et al., 2021). Indeed, free ligand diffusion MD simulations performed by us indicated that MB327 also has affinity for the orthosteric binding site (Kaiser et al., 2023). The fact that the muscle force restoring activity of MB327 on soman-poisoned rat diaphragms is lost at higher concentrations after a peak at 300 μM may be explained by this inhibitory activity (Niessen et al., 2018).

The binding mode of MB327 in the MB327-PAM-1 binding pocket indicates that one of the two *tert*-butyl groups projects into a polar region of the binding pocket. This allowed us to predict structural modifications of MB327 that led to the more potent resensitizers PTM0062 (1) and PTM0063 (2), which have a more polar substituent, i.e., an amino and a methylamino group, respectively, instead of one of the two *tert*-butyl residues of MB327 (Fig. 1) (Kaiser et al., 2023). Interestingly, the recently described dimethylamino analog PTM0056 (3) (Fig. 1), which has a less polar substituent than PTM0062 (1) or PTM0063 (2), also shows a slightly higher affinity for the MB327-PAM-1 binding site than MB327 (Rappenglück et al., 2018) and a muscle force-restoring activity comparable to PTM0062 (1) and PTM0063 (2) in preliminary, unpublished *ex vivo* studies with soman-poisoned rat diaphragm hemispheres. Therefore, PTM0056 (3) appeared to be a promising starting point for the development of new, possibly even more potent, resensitizers for the desensitizied muscle type nAChR.

In this study, we report the development of a series of non-symmetric MB327 analogs derived from PTM0062 (1), PTM0063 (2) and PTM0056 (3), respectively, as resensitizers for desensitized muscle-type nAChRs. To obtain a structurally diverse set of analogs, the 4-amino substituents of compounds 1-3 were replaced by either acylamino groups, dialkylamino groups previously not considered or cyclic amino groups (e.g. pyrrolidino, piperidino, morpholino and piperazino groups).

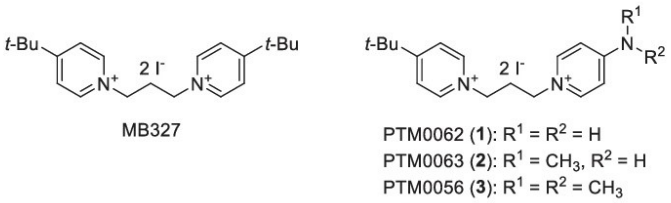

MB327

PTM0062 (**1**): $R^1 = R^2 = H$
PTM0063 (**2**): $R^1 = CH_3$, $R^2 = H$
PTM0056 (**3**): $R^1 = R^2 = CH_3$

Fig. 1. Chemical structures: MB327, PTM0062 (**1**), PTM0063 (**2**) and PTM0056 (**3**).

Furthermore, based on identifying entropically unfavorable water clusters in MB327-PAM-1 using molecular dynamics (MD) simulations in combination with Grid Inhomogeneous Solvent Theory (GIST) computations (Lazaridis, 1998; Nguyen et al., 2011; Nguyen et al., 2012; Ramsey et al., 2016), we designed novel MB327 analogs potentially able to substitute these water clusters. To determine the affinities of the newly developed compounds at the MB327-PAM-1 binding site of *Torpedo*-nAChR, our recently developed UHC0642 MS Binding Assays were applied. To gain insight into the intrinsic activity of some selected representatives of the newly developed compounds, their ability to restore muscle force was also investigated in *ex vivo* experiments with soman-poisoned rat diaphragms. Some of the newly developed compounds showed a slightly higher affinity for the MB327-PAM-1 binding site of *Torpedo*-nAChR than the prototypical compound MB327 and a comparable or even higher muscle force-restoring effect on soman-poisoned rat diaphragms at lower concentrations than MB327.

2. Material and methods

2.1. Synthesis of novel MB327 analogs

Microwave reactions were carried out on a Discover SP microwave system by *CEM GmbH* in glass vials. All chemicals used in the syntheses were used as purchased from commercial sources. Solvents used for crystallization were distilled before use. Melting points were determined with a Büchi 510 melting point apparatus and are uncorrected. For IR spectroscopy, an FT-IR Spectrometer 1600 from *PerkinElmer* was used. High-resolution mass spectrometry was performed on a Finnigan MAT 95 (EI) or a Finnigan LTQ FT (ESI). ^{1}H and ^{13}C NMR spectra were recorded on a Bruker BioSpin Avance III HD 400 and 500 MHz at 25 °C. For data processing, MestReNova (Version 14.1.0) from Mestrelab Research S.L. 2019, and for calibration, the solvent signal (CD_3OD) was used. See Supporting Information (SI, Figures S1-S11) for the NMR spectra of the bispyridinium compounds. Unless otherwise noted, the purity of the test compounds was ≥ 98%, determined using quantitative ^{1}H NMR spectroscopy using TraceCERTS® ethyl 4-(dimethylamino) benzoate from *Sigma Aldrich* as internal calibrant (Cushman et al., 2014; Pauli et al., 2014).

All target compounds synthesized in the context of this study were cataloged with a certain PTM and PTMD number, respectively (Pharmacy and Toxicology Munich and Pharmacy and Toxicology Munich and Düsseldorf, respectively).

General Procedure (GP): Synthesis of non-symmetric MB327 analogs by ***N***-alkylation with 4

A solution of 4-(*tert*-butyl)-1-(3-iodopropyl)pyridin-1-ium iodide (4) (Rappenglück et al., 2018) (1.0 equiv) and the corresponding 4-amino-substituted pyridine 5 (1.05–1.1 equiv) or 7-hydroxychinoline (7) in acetonitrile (2.0–2.7 mL/mmol) was stirred at 90 °C under microwave irradiation (150 W) for 1 h unless otherwise stated. The reaction mixture was concentrated in vacuo, and the residue was purified by recrystallization from different solvent mixtures.

Acetamido-1-{3- [4-(*tert*-butyl)pyridin-1-ium-1-yl] propyl}pyridin-1-ium diiodide (PTM0064, 6a)

According to the GP, with 4 (431 mg, 1.00 mmol, 1.0 equiv) and 5a (150 mg, 1.10 mmol, 1.1 equiv) in MeCN (2.0 mL). Recrystallization from EtOAc/EtOH/MeOH (1:2:1) afforded 6a (529 mg, 93%) as a yellow solid. m.p. 259 °C; ^{1}H NMR (400 MHz, CD_3OD): δ = 1.45 (s, 9 H), 2.27 (s, 3 H), 2.71–2.80 (m, 2 H), 4.66–4.72 (m, 2 H), 4.77–4.83 (m, 2 H), 8.12–8.16 (m, 2 H), 8.16–8.20 (m, 2 H), 8.79–8.86 (m, 2 H), 8.96–9.02 (m, 2 H); ^{13}C NMR (101 MHz, CD_3OD): δ = 24.61, 30.21, 33.27, 37.68, 57.42, 58.32, 116.48, 126.90, 145.43, 146.32, 154.33, 172.69, 173.27; IR (KBr): $\tilde{\nu}$ = 2964, 1645, 1518, 1207 cm^{-1}; HRMS (ESI): *m/z* calcd for $C_{19}H_{27}N_3OI_2$-I⁻: 440.1199 [*M*-I]$^{+}$; found: 440.1185.

4-[(*tert*-Butoxycarbonyl)amino] -1-{3- [4-(*tert*-butyl)pyridin-1-ium-1-yl] propyl}-pyridin-1-ium diiodide (PTM0065, 6b)

According to the GP, a solution of 4 (323 mg, 0.750 mmol, 1.0 equiv) and 5b (157 mg, 0.810 mmol, 1.08 equiv) in MeCN (2.0 mL) was stirred under microwave irradiation (150 W) at 60 °C for 15 h. Recrystallization from Et_2O/DMF (10:1) afforded 6b (431 mg, 92%) as a yellow solid. Purity: 94%. m.p. 117 °C; ^{1}H NMR (400 MHz, CD_3OD): δ = 1.45 (s, 9 H), 1.56 (s, 9 H), 2.67–2.79 (m, 2 H), 4.59–4.67 (m, 2 H), 4.74–4.82 (m, 2 H), 7.87–8.02 (m, 2 H), 8.20–8.14 (m, 2 H), 8.68–8.76 (m, 2 H), 8.91–9.01 (m, 2 H); ^{13}C NMR (101 MHz, CD_3OD): δ = 28.25, 30.21, 33.19, 37.68, 57.16, 58.38, 84.27, 115.30, 126.90, 145.41, 145.85, 153.10, 155.64, 173.30; IR (KBr): $\tilde{\nu}$ = 2967, 1643, 1531, 1148 cm^{-1}; HRMS (ESI): *m/z* calcd for $C_{22}H_{33}N_3O_2I_2$-I⁻: 498.1618 [*M*-I]$^{+}$; found: 498.1600.

4- [Benzyl(methyl)amino] -1-{3- [4-(*tert*-butyl)pyridin-1-ium-1-yl] propyl}pyridin-1-ium diiodide (PTM0066, 6c)

According to the GP, with 4 (323 mg, 0.750 mmol, 1.0 equiv) and 5c (164 mg, 0.830 mmol, 1.1 equiv) in MeCN (2.0 mL). Recrystallization from EtOAc/EtOH/MeOH (10:5:1) afforded 6c (354 mg, 75%) as a yellow solid. m.p. 185 °C; ^{1}H NMR (400 MHz, CD_3OD): δ = 1.45 (s, 9 H), 2.56–2.70 (m, 2 H), 3.34 (s, 3 H), 4.40 (t, *J* = 7.6 Hz, 1 H), 4.74 (t, *J* = 7.7 Hz, 2 H), 4.90 (s, 2 H), 7.03–7.19 (m, 2 H), 7.24–7.29 (m, 2 H), 7.29–7.41 (m, 3 H), 8.13–8.19 (m, 2 H), 8.20–8.40 (m, 2 H), 8.91–8.97 (m, 2 H); ^{13}C NMR (101 MHz, CD_3OD): δ = 30.20, 33.14, 37.67, 39.70, 55.41, 56.75, 58.52, 109.83, 126.86, 127.82, 129.11, 130.21, 136.21, 143.72, 145.38, 158.26, 173.24; IR (KBr): $\tilde{\nu}$ = 2967, 1645, 1556, 1193 cm^{-1}; HRMS (ESI): *m/z* calcd for $C_{25}H_{33}N_3I_2$-I⁻: 502.1719 [*M*-I]$^{+}$; found: 502.1703.

4-(*tert*-Butyl)-1-{3- [4-(diethylamino)pyridin-1-ium-1-yl] propyl}pyridin-1-ium diiodide (PTM0067, 6d)

According to the GP, with 4 (431 mg, 1.00 mmol, 1.0 equiv) and 5d (165 mg, 1.10 mmol, 1.1 equiv) in MeCN (2.0 mL). Recrystallization from EtOAc/EtOH (2.5:1) afforded 6d (419 mg, 72%) as a yellow solid. m.p. 217 °C; ^{1}H NMR (400 MHz, CD_3OD): δ = 1.27 (t, *J* = 7.2 Hz, 6 H), 1.45 (s, 9 H), 2.60–2.71 (m, 2 H), 3.64 (q, *J* = 7.2 Hz, 4 H), 4.41 (t, *J* = 7.7 Hz, 2 H), 4.78 (t, *J* = 7.8 Hz, 2 H), 7.01–7.08 (m, 2 H), 8.13–8.21 (m, 2 H), 8.24–8.31 (m, 2 H), 8.97–9.02 (m, 2 H); ^{13}C NMR (101 MHz, CD_3OD): δ = 12.21, 30.23, 33.20, 37.66, 46.46, 55.15, 58.49, 109.23, 126.86, 143.44, 145.41, 156.42, 173.11; IR (KBr): $\tilde{\nu}$ = 2968, 1648, 1561, 1197 cm^{-1}; HRMS (ESI): *m/z* calcd for $C_{21}H_{33}N_3I_2$-I⁻: 454.1719 [*M*-I]$^{+}$; found: 454.1704.

4-(*tert*-Butyl)-1-{3- [4-(pyrrolidin-1-yl)pyridin-1-ium-1-yl] propyl}pyridin-1-ium diiodide (PTM0068, 6e)

According to the GP, with 4 (431 mg, 1.00 mmol, 1.0 equiv) and 5e (159 mg, 1.05 mmol, 1.05 equiv) in MeCN (2.0 mL). Recrystallization from EtOAc/*i*-PrOH (1.1:1) afforded 6e (457 mg, 79%) as a yellow solid. m.p. 178 °C; ^{1}H NMR (400 MHz, CD_3OD): δ = 1.45 (s, 9 H), 2.10–2.15 (m, 4 H), 2.60–2.69 (m, 2 H), 3.55–3.60 (m, 4 H), 4.40 (t, *J* = 7.7 Hz, 2 H), 4.76 (t, *J* = 7.8 Hz, 2 H), 6.86–6.91 (m, 2 H), 8.15–8.18 (m, 2 H), 8.24–8.29 (m, 2 H), 8.96–9.00 (m, 2 H); ^{13}C NMR (101 MHz, CD_3OD): δ = 26.14, 30.21, 33.22, 37.66, 49.83, 55.26, 58.52, 109.87, 126.86, 143.01, 145.40, 155.23, 173.15; IR (KBr): $\tilde{\nu}$ = 2961, 1647, 1561, 1192 cm^{-1}; HRMS (ESI): *m/z* calcd for $C_{21}H_{31}N_3I_2$-I⁻: 452.1563 [*M*-I]$^{+}$; found: 452.1545.

4-(*tert*-Butyl)-1-{3- [4-(piperidin-1-yl)pyridin-1-ium-1-yl] propyl}pyridin-1-ium diiodide (PTM0069, 6f)

According to the GP, with 4 (216 mg, 0.500 mmol, 1.0 equiv) and 5 f (85.2 mg, 0.530 mmol, 1.05 equiv) in MeCN (1.0 mL). Recrystallization from EtOAc/*i*-PrOH (1:1.2) afforded 6 f (245 mg, 83%) as a yellow solid. m.p. 240 °C; ^{1}H NMR (400 MHz, CD_3OD): δ = 1.45 (s, 9 H), 1.69–1.76 (m, 4 H), 1.76–1.85 (m, 2 H), 2.58–2.71 (m, 2 H), 3.69–3.76 (m, 4 H), 4.39 (t, *J* = 7.6 Hz, 2 H), 4.77 (t, *J* = 7.7 Hz, 2 H), 7.12–7.20 (m, 2 H), 8.13–8.20 (m, 2 H), 8.21–8.29 (m, 2 H), 8.95–9.02 (m, 2 H); ^{13}C NMR (101 MHz, CD_3OD): δ = 24.93, 26.73, 30.22, 33.14, 37.66, 49.17, 55.07, 58.51, 109.45, 126.86, 143.58, 145.41, 156.92, 173.13; IR (KBr): $\tilde{\nu}$ = 2956, 1648, 1547, 1194 cm^{-1}; HRMS (ESI): *m/z* calcd for $C_{22}H_{33}N_3I_2$-I⁻: 466.1719 [*M*-I]$^{+}$; found: 466.1711.

4-(*tert*-Butyl)-1-[3-(4-morpholinopyridin-1-ium-1-yl)propyl] pyridin-1-ium diiodide (PTM0070, 6g)

According to the GP, with 4 (431 mg, 1.00 mmol, 1.00 equiv) and 5 g (172 mg, 1.10 mmol, 1.05 equiv) in MeCN (2.0 mL). Recrystallization from EtOAc/EtOH (1:1.4) afforded 6 g (518 mg, 87%) as a yellow solid. m.p. 222 °C; ^{1}H NMR (400 MHz, CD_3OD): δ = 1.45 (s, 9 H), 2.62–2.72 (m, 2 H), 3.69–3.76 (m, 4 H), 3.80–3.85 (m, 4 H), 4.45 (t, *J* = 7.7 Hz, 2 H), 4.78 (t, *J* = 7.8 Hz, 2 H), 7.13–7.27 (m, 2 H), 8.14–8.20 (m, 2 H), 8.33–8.40 (m, 2 H), 8.97–9.04 (m, 2 H); ^{13}C NMR (101 MHz, CD_3OD): δ = 30.23, 33.21, 37.66, 47.73, 55.33, 58.44, 67.15, 109.72, 126.86, 143.86, 145.41, 157.85, 173.11; IR (KBr): $\tilde{\nu}$ = 2964, 1650, 1545, 1193 cm^{-1}; HRMS (ESI): *m/z* calcd for $C_{21}H_{31}N_3OI_2$-I$^-$: 468.1512 [*M*-I]$^+$; found: 468.1493.

4-[4-(*tert*-Butoxycarbonyl)piperazin-1-yl]-1-{3-[4-(*tert*-butyl)pyridin-1-ium-1-yl]propyl}pyridin-1-ium diiodide (PTM0071, 6h)

According to the GP, with 4 (216 mg, 0.500 mmol, 1.0 equiv) and 5 h (145 mg, 0.550 mmol, 1.1 equiv) in MeCN (1.0 mL). Recrystallization from EtOAc/EtOH (2:1) afforded 6 h (320 mg, 92%) as a yellow solid. m.p. 149 °C; ^{1}H NMR (500 MHz, CD_3OD): δ = 1.45 (s, 9 H), 1.49 (s, 9 H), 2.61–2.69 (m, 2 H), 3.62–3.68 (m, 4 H), 3.76–3.80 (m, 4 H), 4.42 (t, *J* = 7.6 Hz, 2 H), 4.75 (t, *J* = 7.7 Hz, 2 H), 7.19–7.23 (m, 2 H), 8.15–8.19 (m, 2 H), 8.31–8.36 (m, 2 H), 8.95–8.99 (m, 2 H); ^{13}C NMR (126 MHz, CD_3OD): δ = 28.59, 30.21, 33.17, 37.67, 43.60, 47.12, 55.38, 58.48, 81.95, 109.85, 126.86, 143.79, 145.40, 156.17, 157.71, 173.22; IR (KBr): $\tilde{\nu}$ = 2967, 1649, 1416, 1169 cm^{-1}; HRMS (ESI): *m/z* calcd for $C_{26}H_{40}N_4O_2I_2$-I$^-$: 567.2196 [*M*-I]$^+$; found: 567.2180.

4-(1-{3-[4-(*tert*-Butyl)pyridin-1-ium-1-yl]propyl}pyridin-1-ium-4-yl)piperazin-1-ium triiodide (PTM0072, 6i)

A solution of 6 h (69.4 mg, 0.100 mmol, 1.0 equiv) and iodo(trimethyl)silane (80.0 mg, 0.400 mmol, 4.0 equiv) in MeCN (2.0 mL) was stirred under argon at rt for 2 h. 6i (71.3 mg, 99%) was afforded after filtration of the reaction mixture as a yellow solid. m.p. 109 °C; ^{1}H NMR (400 MHz, CD_3OD): δ = 1.45 (s, 9 H), 2.65–2.75 (m, 2 H), 3.47–3.55 (m, 4 H), 4.03–4.12 (m, 4 H), 4.52 (t, *J* = 7.5 Hz, 2 H), 4.77–4.83 (m, 2 H), 7.33–7.39 (m, 2 H), 8.14–8.20 (m, 2 H), 8.45–8.52 (m, 2 H), 9.01–9.06 (m, 2 H); ^{13}C NMR (101 MHz, CD_3OD): δ = 30.23, 33.27, 37.65, 44.04, 44.65, 55.66, 58.33, 110.83, 126.84, 144.37, 145.44, 158.02, 173.07; IR (KBr): $\tilde{\nu}$ = 2963, 1647, 1549, 1191 cm^{-1}; HRMS (ESI): *m/z* calcd for $C_{21}H_{33}N_4I_3$-H$^+$-2I$^-$: 467.1671 [*M*-I-I-H]$^+$; found: 467.1663.

1-{3-[4-(*tert*-Butyl)pyridin-1-ium-1-yl]propyl}-7-hydroxyquinolin-1-ium diiodide (PTMD90-0012, 8)

According to the GP, a solution of 4 (431 mg, 1.00 mmol, 1.0 equiv) and 7 (163 mg, 1.10 mmol, 1.1 equiv) in MeCN (2.0 mL) was stirred under microwave irradiation (150 W) at 90 °C for 3 h. Recrystallization from EtOH/EtOAc (2:1.5) afforded 8 (167 mg, 29%) as a yellow solid. m.p. 263 °C; ^{1}H NMR (400 MHz, CD_3OD): δ = 1.45 (s, 9 H), 2.76–2.89 (m, 2 H), 4.89–4.96 (m, 2 H), 5.09–5.19 (m, 2 H), 7.56 (dd, *J* = 9.0, 2.1 Hz, 1 H), 7.68 (d, *J* = 2.2 Hz, 1 H), 7.81 (dd, *J* = 8.1, 6.1 Hz, 1 H), 8.11–8.22 (m, 2 H), 8.29 (d, *J* = 9.1 Hz, 1 H), 8.95–9.04 (m, 3 H), 9.31 (dd, *J* = 6.1, 1.4 Hz, 1 H); ^{13}C NMR (101 MHz, CD_3OD): δ = 30.20, 31.59, 37.68, 54.85, 58.50, 101.59, 119.39, 123.77, 126.81, 126.88, 134.57, 142.53, 145.41, 148.20, 148.99, 167.19, 173.30; IR (film): $\tilde{\nu}$ = 2968, 1628, 1209, 849 cm^{-1}; HRMS (ESI): *m/z* calcd for $C_{21}H_{26}N_2OI_2$-H$^+$-2I$^-$: 321.1967 [*M*-I-I-H]$^+$; found: 321.1961.

1,1′-(2-Hydroxypropan-1,3-diyl)bis[4-(*tert*-butyl)pyridin-1-ium] dibromide (PTMD90-0015, 11)

A mixture of 9 (108 µL, 229 mg, 1.00 mmol, 1.0 equiv) and 10 (352 µL, 325 mg, 2.40 mmol, 2.4 equiv) was stirred at 145 °C for 2 h. The reaction mixture was concentrated in vacuo and the residue was purified by recrystallization from EtOAc/EtOH (1:2) to afford 11 (196 mg, 40%) as a colorless solid. m.p. 248 °C; ^{1}H NMR (400 MHz, CD_3OD): δ = 1.45 (s, 18 H), 4.43–4.69 (m, 3 H), 4.97–5.22 (m, 2 H), 8.11–8.24 (m, 4 H), 8.83–9.01 (m, 4 H); ^{13}C NMR (101 MHz, CD_3OD): δ = 30.19, 37.70, 63.74, 71.06, 126.42, 146.09, 173.58; IR (film): $\tilde{\nu}$ = 2972, 1643, 1468, 1117 cm^{-1}; HRMS (ESI): *m/z* calcd for $C_{21}H_{32}N_2OBr_2$-H$^+$-2Br$^-$: 327.2436 [*M*-Br-Br-H]$^+$; found: 327.2430.

2.2. UNC0642 MS Binding Assays

Competitive MS Binding Assays were performed as previously described (Kaiser et al., 2024; Hitsche et al., 2024) apart from one minor difference: in order to obtain competition curves for compounds bearing a 4-aminopyridinium moiety, the non-linear regression function "log (inhibitor) vs. normalized response – Variable slope" (Prism Software v. 6.07, GraphPad Software, La Jolla, CA, USA) was used instead of the recently used function "One site – fit Ki". Statistically significant differences were verified by a two-sided *t*-test (alpha = 0.05).

2.3. Rat diaphragm myography

All experiments were conducted at the Bundeswehr Institute of Pharmacology and Toxicology (InstPharmToxBw) which is the only institute in Germany authorized to use chemical warfare agents (CWA) for research in the areas of pathomechanisms, prevention, detection, treatment, and epidemiology of CWA-induced health disorders.

All procedures using animals followed animal care regulations. Preparation of rat diaphragm hemispheres from male Wistar rats (300 ± 50 g) and experimental protocol of myography was performed as previously described (Hitsche et al., 2024; Seeger et al., 2012). In brief, for all procedures (including wash-out steps, preparation of soman and test compound solutions) aerated Tyrode solution (125 mM NaCl, 24 mM $NaHCO_3$, 5.4 mM KCl, 1 mM $MgCl_2$, 1.8 mM $CaCl_2$, 10 mM glucose, 95% O_2, 5% CO_2; pH 7.4; 25 ± 0.5 °C) was used. The organophosphorus compound (OPC) soman (pinacolylmethylphosphonofluoridate; >93% by GC-MS, ^{1}H NMR and ^{31}P NMR) was provided by the German Ministry of Defence (Bonn, Germany). Soman stock solutions (0.1% v/v) were prepared in acetonitrile, stored at 20 °C and appropriately diluted in Tyrode buffer just before the experiment, and were kept at room temperature until use. All experiments were carried out in a chemical safety hood. After the recording of control muscle force one hour after preparation, the muscles were incubated in the Tyrode solution, containing 3 µM soman for 20 min. Following a 20 min wash-out period, the test compounds were added in ascending concentrations (0.1 µM to 300 µM). The incubation time was 20 min for each concentration. The electric field stimulation was performed with 10 µs pulse width and 2 A amplitudes. The titanic stimulation of 20 Hz, 50 Hz, 100 Hz were applied for 1 s and in 10 min intervals. Measurements on non-toxic muscle were carried out according to the same scheme. Instead of soman, pure Tyrode was incubated. Muscle force was calculated as a time-force integral (area under the curve, AUC) and constrained to values obtained for maximum force generation at the start of the measurements (muscle force in the presence of Tyrode solution without any additives; 100%). All results were expressed in means ± SD (n = 6–12). Prism 5.0 (GraphPad Software, San Diego, CA, USA) was used for data analysis.

2.4. MD simulations

The model of the human muscle type nAChR was generated using Modeller with the PDB structure of the α7-nAChR as the template (PDB ID: 7KOX (Noviello et al., 2021). The orthosteric ligand nicotine and a sodium ion in the transmembrane pore were included by aligning the structure of the α3β4-nAChR (PDB ID: 6PV7 (Gharpure et al., 2019) to the homology model. Nicotine was subsequently minimized using SZYBKI (OpenEye Scientific Software, 2021). MB327 was docked in MB327-PAM-1 using MOE with an induced-fit refinement using default parameters (Chemical Computing Group, 2020). Ligand charges were calculated using Gaussian16 (M. J. Frisch et al., 2016) at the HF/6–31 G* level of theory; force field parameters for the ligand were taken from the gaff force field (Wang et al., 2004). Using Packmol-Memgen (Schott-Verdugo and Gohlke, 2019), the system was embedded in a membrane containing 1-palmitoyl-2-oleoyl-*sn*-glycero-3-phosphocholine (POPC) lipids, solvated using the Optimal Point

Charge water model (Izadi et al., 2014) with a minimum distance of 12 Å between receptor atoms and the edge of the box, KCl was added in a concentration of 150 mM, and the system was neutralized using Cl^- ions. To perform MD simulations, the AMBER22 package of molecular simulations software (Case et al., 2005; Case et al., 2022), the ff19SB force field (Tian et al., 2020) for the protein, the Lipid17 force field (Gould et al., unpublished) for lipids, the gaff force field for the ligand, and the Joung and Cheatham parameters for monovalent ions were used (Joung and Cheatham, 2008). MD simulations were performed as described previously (Kaiser et al., 2023). In short, a combination of steepest descent and conjugate gradient minimization was performed while gradually decreasing positional harmonic restraints. The system was then heated in a stepwise manner to 300 K, and harmonic restraints on receptor and ligand atoms were gradually removed subsequently. Then, 12 replicas of 1 μs long unbiased MD simulations were performed in the NPT ensemble using semi-isotropic pressure adaptation with the Berendsen barostat. The RMSD, electron density profiles and representative binding modes were computed using CPPTRAJ (Roe and Cheatham, 2013), as implemented in AmberTools (Case et al., 2023).

2.5. GIST computations

GIST (Lazaridis, 1998; Nguyen et al., 2011, 2012; Ramsey et al., 2016) computations, as implemented in CPPTRAJ (Roe and Cheatham, 2013), were performed in replicas where MB327 remained in the binding site (distance to I64δ (respectively, I61ε, I61α, I64β) < 5 Å, as done previously) (Kaiser et al., 2023) during MD simulations. The backbone of each frame during these MD simulations was aligned to the starting structure of the simulations using CPPTRAJ (Roe and Cheatham, 2013). The middle carbon atom of the C3-linker in MB327 was used as the center of the box for GIST grid generations with grid dimensions of 40 increments along each axis and a grid spacing of 0.5 Å. In GIST, the entropy term of water in each voxel consists of both an orientational and translational contribution. Furthermore, for the energetic contribution the solute-water and water-water interaction is computed based on Lennard-Jones and electrostatic interactions. The results were filtered based on the density of oxygen centers in each voxel compared to bulk density (cutoff: > 1.75) and the solvent free energy (cutoff: > −0.25 kcal mol^{-1}). Visualization of water clusters and manual modification of MB327 to PTMD90–0012 (8) and PTMD90–0015 (11) was performed using MOE (Chemical Computing Group, 2020).

2.6. Image generation

Images of nAChR in complex with MB327 and its analogs were created using UCSF Chimera (Pettersen et al., 2004).

3. Results and discussion

3.1. Synthesis of novel MB327 analogs

To identify novel non-symmetric MB327 analogs that should exhibit higher binding affinities to the MB327-PAM-1 binding site as well as higher intrinsic activities compared to MB327, a series of non-symmetric bispyridinium compounds 6a-6i with a 4-aminopyridinium ion partial structure derived from compounds 1-3 was synthesized. In addition, based on modeling studies (see chapter 3.3), novel MB327 analogs 8 and 11 with an additional OH function were synthesized with the assumption that this modification should increase the binding affinity by displacing water molecules from the binding pocket.

3.1.1. Non-symmetric MB327 analogs PTM0064-PTM0072 (6a-6i) and PTMD90-0012 (8)

Non-symmetric MB327 analogs 6a-6 h bearing a 4-aminopyridinium ion moiety were readily accessible in one step by *N*-alkylation of 4-aminopyridines 5 with *N*-(3-iodopropyl)pyridinium building block 4, analogous to the method described by Rappenglück et al. (2018) (Scheme 1). To cover a wider variety of 4-amino substituents in the target compounds, the set of commercially available 4-aminopyridines 5a, 5b, and 5e-5 g was extended with some building blocks (5c, 5d and 5 h), synthesized according to literature (Hay et al., 2015; Price et al., 2006; Wang et al., 2019). *N*-Alkylation of the pyridines 5a and 5c-5 h with building block 4 (Rappenglück et al., 2018) was accomplished by stirring the components in acetonitrile at 90 °C under microwave irradiation for 1 h. After removing the reaction solvent, the resulting residues were purified by crystallization to yield the target compounds 6a and 6c-6 h in good to excellent yields (72–93%) and high purities (≥ 98%). Reaction with *tert*-butyl pyridin-4-ylcarbamate (5b), however, required a lower reaction temperature to prevent cleavage of the Boc group as a reaction at 90 °C for 1 h had led to a mixture of product 6b and 4-amino-analog 1 in a ratio of 3:1. By stirring 5b with building block 4 at 60 °Cfor 15 h no side product 1 was observed and the product 6b was afforded in excellent yield (92%) and sufficient purity (94%). To get the hydroiodide 6i, the Boc protecting group of 6 h was cleaved by stirring with trimethylsilyl iodide (TMSI) (4.0 equiv) in acetonitrile at room temperature for 1 h (Lott et al., 1979). Thus, compound 6i was isolated in quantitative yield (99%) and with high purity (100%).

PTMD90–0012 (8) was synthesized from building block 4 (Rappenglück et al., 2018) and 7-hydroxyquinoline (7) under the reaction conditions described for bispyridinium compounds 6a-6 h. However, the reaction time had to be increased to 3 h to compensate for the lower reactivity of the sterically more demanding quinoline 7 as compared to the 4-aminopyridines 5. That way, PTMD90–0012 (8) was obtained in 29% yield after recrystallization (purity ≥ 98%) (Scheme 2).

3.1.2. MB327 analog PTMD90-0015 (11)

The symmetric bispyridinium compound PTMD90–0015 (11) with a 2-hydroxypropyl linker between the two pyridinium rings, was synthesized by heating 1,3-dibromopropan-2-ol (9) with an excess of 4-*tert*-butylpyridine (10) to 145 °C for 2 h. Bis-alkylation product PTMD90–0015 (11) was obtained in 40% yield and in high purity (100%) after recrystallization (Scheme 3). In contrast, reaction of 8 with epichlorohydrine or 1,3-dichloropropan-2-ol under the reaction conditions described above led only to the corresponding monosubstituted products.

3.2. Biological evaluation

3.2.1. Affinity to the MB327-PAM-1 binding site of Torpedo californica nAChR

All of the newly developed compounds presented in this study, i.e. PTM0064-PTM0072 (6a-6i), PTMD90–0012 (8) and PTMD90–0015 (11) as well as MB327 and its recently reported analogs PTM0062 (1) (Kaiser et al., 2023), PTM0063 (2) (Kaiser et al., 2023) and PTM0056 (3) (Rappenglück et al., 2018) were evaluated for their binding affinity towards the MB327-PAM-1 binding site of *Torpedo californica* nAChR by means of the recently introduced UHC0642 MS Binding Assays (Table 1) (Kaiser et al., 2024; Hitsche et al., 2024). First, for economic reasons, all test compounds were studied at a single concentration of 10 μM and a reporter ligand concentration of 1 μM. For a set of selected compounds also the binding affinity constants (pK_i values) were determined in full-scale MS competition experiments.

Remaining reporter ligand binding in the presence of 10 μM of the respective compounds listed in Table 1 range from 102% ± 9% for MB327 (Table 1, entry 1) to 64% ± 8% for the *N*-Boc-piperazino derivative PTM0071 (6 h, Table 1, entry 12). For clarity reasons it may be stated that increasing binding affinities of the test compounds are reflected by decreasing values of the remaining reporter ligand binding. Substitution of one of the two 4-*tert*-butyl residues of MB327 by an amino [PTM0062 (1), 93% ± 5%, Table 1, entry 2], an *N*-methylamino [PTM0063 (2), 92% ± 1%, Table 1, entry 3], or dimethylamino group

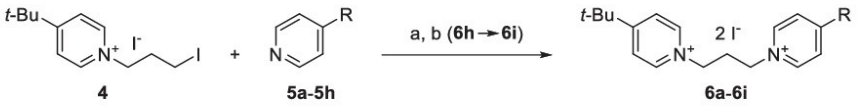

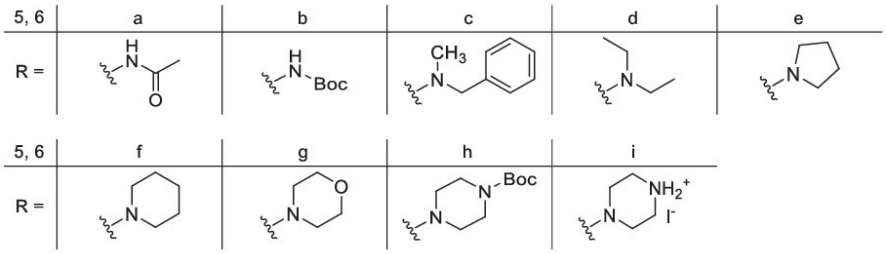

Scheme 1. Synthesis of **6a-6i**. Reagents and conditions: (a) 4-(*tert*-butyl)-1-(3-iodopropyl)pyridin-1-ium iodide (**4**) (1.0 equiv), pyridines **5a-5 h** (1.05–1.1 equiv), MeCN, microwave: 150 W, 60–90 °C, 1–15 h, 72–93%; (b) **6i**: **6 h** (1.0 equiv), TMSI (4.0 equiv), MeCN, rt, 1 h, 99%.

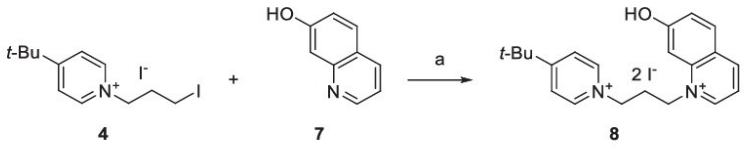

Scheme 2. Synthesis of PTMD90–0012 (**8**). Reagents and conditions: (a) 4-(*tert*-butyl)-1-(3-iodopropyl)pyridin-1-ium iodide (**4**) (1.0 equiv), 7-hydroxyquinoline (**7**) (1.1 equiv), MeCN, microwave: 150 W, 90 °C, 3 h, 29%.

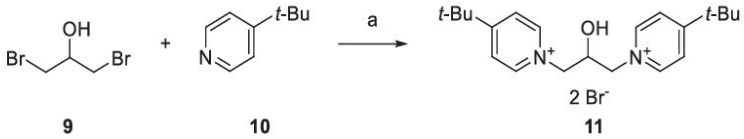

Scheme 3. Synthesis of PTMD90–0015 (**11**). Reagents and conditions: (a) 1,3-dibromopropan-2-ol (**9**) (1.0 equiv), 4-*tert*-butylpyridine (**10**) (2.4 equiv), 145 °C, 2 h, 40%.

[PTM0056 (3), 90% ± 5%, Table 1, entry 4] results in a nominal yet not statistically significant reduction of remaining reporter ligand binding as compared to MB327. This is also true for compounds PTM0064 (6a, 90% ± 6%, Table 1, entry 5) and PTM0065 (6b, 90% ± 4%, Table 1, entry 6) displaying an *N*-acetamido- and an *N*-*tert*-butoxycarbonylamino moiety, respectively effecting a reduction to 90% of remaining reporter ligand binding. According to the data obtained for 1-3 and 6a-6b the capability of the nitrogen substituents, present in these compounds to participate in hydrogen bonding seems to have only little if any influence on the binding affinities, the remaining reporter ligand binding amounting in any case to about 90%. Likewise, when the dimethylamino group in PTM0056 (3, 90% ± 5%, Table 1, entry 4) is replaced by a sterically more demanding *N*,*N*-diethylamino moiety, the binding affinity of the resulting PTM0067 (6d) remains with 91% ± 11% virtually unaltered (remaining reporter ligand binding, Table 1, entry 8). Although 1-3 as well as 6a, 6b and 6d effect remaining reporter ligand binding nominally below that of MB327 (Table 1, entry 1), for none of these compounds the observed differences are statistically significant. However, for the *N*-benzyl-*N*-methylamino derivative PTM0066 (6c) with an enlarged lipophilic domain, remaining reporter ligand binding reaches 85% ± 8% (Table 1, entry 7), which is statistically significantly lower than that of MB327 (102% ± 9%, Table 1, entry 1).

Notably, the pyrrolidino and the piperidino substituted derivatives PTM0068 (6e) and PTM0069 (6 f), of which the former can be considered as a cyclic analog of the diethylamino substituted 6d, reduce remaining reporter ligand binding to 85% ± 0.5% (Table 1, entry 9) and 73% ± 6% (Table 1, entry 10), both values being also statistically significantly below than that of MB327 (102% ± 9%, Table 1, entry 1).

Upon transition from the piperidino-substituted bispyridinium salt 6 f to the more polar morpholino-substituted analog PTM0070 (6 g), again a decline in binding affinity is observed with the remaining reporter ligand binding increasing to 90% ± 8% (Table 1, entry 11). However, for the nitrogen analog of the morpholino derivative 6 g, the piperazino derivative PTM0072 (6i), the decline in binding affinity compared to 6 f displaying a piperidino residue (73% ± 6%, Table 1, entry 10) was less pronounced, with the remaining reporter ligand binding amounting to 83% ± 5% (Table 1, entry 13). Obviously, the binding affinity-diminishing effect of the additional heteroatom seems to be less distinct for the piperazino derivative 6i than for the morpholino derivative 6 g (as compared to the piperidino analog 6 f). This can possibly be attributed to the capability of the terminal amino function of the piperazino group of 6i - present in free form or as a salt or both - to participate in a hydrogen bridge with the protein. Still, this ability to be part of a hydrogen bond appears to be of less overall

Table 1
Binding affinities of bispyridinium compounds for the MB327-PAM-1 binding site of *Torpedo californica* nAChR, determined in UNC0642 MS Binding Assays.

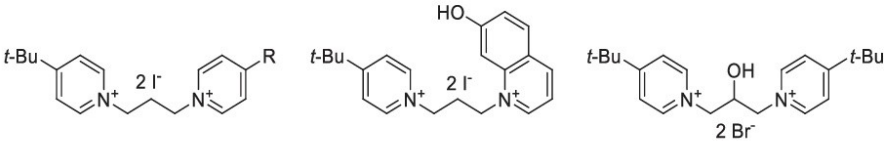

MB327, 1-3, 6a-6i **8** **11**

Entry	Compound	R	Remaining Reporter Ligand Binding [%] [a]	PTM code
1	**MB327**		102 ± 9 ($pK_i = 3.40 \pm 0.04$[b])	-
2	**1**		93 ± 5	0062[c]
3	**2**		92 ± 1	0063[c]
4	**3**		90 ± 5	0056[d]
5	**6a**		90 ± 6	0064
6	**6b**		90 ± 4	0065
7	**6c**	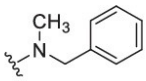	85 ± 8*	0066
8	**6d**		91 ± 11	0067
9	**6e**		85 ± 0.5*	0068
10	**6 f**		73 ± 6** ($pK_i = 3.96 \pm 0.08$)	0069
11	**6 g**	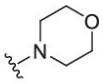	90 ± 8	0070
12	**6 h**	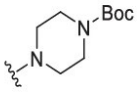	64 ± 8** ($pK_i = 4.17 \pm 0.02$)	0071
13[e]	**6i**	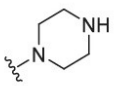	83 ± 5*	0072
14	**8**	-	93 ± 9 ($pK_i = 3.69 \pm 0.03$)	D90–0012
15	**11**	-	98 ± 5 ($pK_i = 3.29 \pm 0.05$)	D90–0015

Asterisks indicate statistically significantly lower values for the remaining reporter ligand binding of the respective compound compared to the MB327 value (* $p < 0.05$, ** $p < 0.01$, based on a two-sided *t*-test)

[a] The results of UNC0642 MS Binding Assays are given as percentages representing the remaining reporter ligand binding (UNC0642, 1 μM) in presence of 10 μM test compound as compared to 100% reporter ligand binding in the absence of a competitor. Values are given as means ± SD of triplicate experiments, except for MB327, which was determined in two experiments from a triplicate determination each. The pK_i values given in brackets represent means ± SEM of three independent experiments determined in UNC0642 MS Binding Assays in full scale competition experiments (mean Hill coefficient = 0.45–0.61).

[b] pK_i value of MB327 from (Nitsche et al., 2024).

[c] Compound from (Kaiser et al., 2023).

[d] Compound from (Rappenglück et al., 2018).

[e] Compound tested as hydroiodide.

importance, since although it is lost by the attachment of an *N*-Boc substituent to the piperazino moiety of 6i, resulting in PTM0071 (6 h, Table 1, entry 12), the binding affinity is distinctly improved. Thus, a remaining reporter ligand binding of 64% ± 8% could be measured for this compound, which is statistically significantly lower than that of the piperazino-substituted compound 6i (Table 1, entry 13). Hence, the piperidino-substituted compound 6 f (Table 1, entry 10) and the *N*-Boc-piperazino derivative 6 h (Table 1, entry 12) possess the highest binding affinities for the MB327-PAM-1 binding site of the nAChR of the compounds evaluated in this study.

Modeling studies (see chapter 3.3) indicated, that the presence of an OH function in ligands of the MB327-PAM-1 binding site might be favorable for the binding affinity by displacing water molecules present in the binding pocket. In particular, the MB327 analog 11 with an OH function in the spacer linking the two pyridinium subunits in the molecule as well as 8 with a 7-hydroxyquinolinium replacing one of the two pyridinium subunits in MB327 were expected to possess improved binding affinities. Hence, the binding affinities of PTMD90–0015 (11) and PTMD90–0012 (8) were studied. Both compounds, however, show no or only a negligible improvement of the binding affinity compared to MB327 (Table 1, entry 1), the remaining reporter ligand binding amounting to 98% ± 5% for 11 (Table 1, entry 15) and 93% ± 9% for 8 (Table 1, entry 14). Although no clear improvement of the binding affinity could be achieved with 11 and 8, the results indicate that the presence of an additional polar OH function is tolerated in the binding pocket.

Finally, for a small set of compounds, the pK_i values as a more accurate measure of the binding affinity were determined in full-scale competitive MS Binding Assays. This set comprised the two compounds 6 f and 6 h, which had shown the highest binding affinities in the single point determinations described above (reduction of the remaining reporter ligand binding to < 75%) as well as the two OH function-containing derivatives 8 and 11, which had emerged as candidate compounds for testing from modeling studies. Notably, the piperidino derivative 6 f (Table 1, entry 10) exhibits a pK_i of 3.96 ± 0.08, which was approximately 0.5 log units and thus statistically significantly higher than the pK_i of MB327 previously determined to be 3.40 ± 0.04 (Table 1, entry 1) (Nitsche et al., 2024). The *N*-Boc-piperazino derivative 6 h (Table 1, entry 12) showed an even higher pK_i of 4.17 ± 0.02, as to be expected from the preliminary binding data (remaining reporter ligand binding 64% ± 5%), exceeding that of MB327 by approximately 0.8 log units. For the MB327 analog 11 with an OH function as part of the propan-1,3-diyl spacer (Table 1, entry 15), the pK_i value (3.29 ± 0.05) matched that of MB327 within the limits of error. For the 7-hydroxyquinolinium derivative 8 (Table 1, entry 14), a pK_i value of 3.69 ± 0.03 was found, almost 0.3 log units higher than that of MB327, which is statistically significantly different, indicating the higher binding affinity of this compound compared to MB327.

3.2.2. Evaluation of muscle force recovery in soman-poisoned rat diaphragm hemispheres

In addition to the binding affinities, the intrinsic activities of a selection of the test compounds have been determined by means of an *ex vivo* assay based on rat diaphragm hemispheres. In this assay dissected rat diaphragm hemispheres are treated with a solution containing 3 μM soman. Whereas upon indirect electric field stimulation commonly carried out at frequencies of 20 Hz, 50 Hz and 100 Hz, unpoisoned rat diaphragms undergo muscle contractions, in case of poisoned samples no or only very faint contractions occur. This inhibition further does not vanish, when the poisoned samples are freed from the toxin by washing, typically performed as a control, as this has no effect on the irreversible inhibition of the AChE by the nerve agent. The positive intrinsic activity of the test compounds becomes apparent, when their addition to the poisoned muscle preparations, typically performed in increasing concentrations from 0.1 to 300 μM, affects a recovery of the muscle force of the soman-impaired rat diaphragm hemispheres. Muscle force inhibition reappears, when samples are subjected to a subsequent washout step, which is due to the irreversible inactivation of the AChE and indicative of the reversibility of the receptor-mediated resensitizing effect of the test compounds.

For the characterization of the muscle force restoring potency of soman-poisoned rat diaphragms in the aforementioned test system, the piperidino- and the *N*-Boc-piperazino derivatives 6 f and 6 h were selected as they had shown the highest binding affinities among the new test compounds presented in this study. In addition, the piperazino derivative 6i, closely related to 6 h, the *N,N*-dimethylamino-substituted compound 3 as parent compound, as well as the hydroxy-substituted compounds 8 and 11 as analogs of MB327 devoid of an amino-substituent were evaluated in this test system.

Since it is known, that the largest efficacy is observed at low stimulation frequencies (Seeger et al., 2012), only the results of experiments performed at 20 Hz will be presented (Fig. 2) and discussed in the following. The data of measurements carried out at higher frequencies (50 Hz, 100 Hz) can be found in the Supporting Information (SI, Figure S12).

As reference, the published data obtained for MB327 in the test system have been included in Fig. 2 (Hiessen et al., 2018). As previously reported, MB327 addition (Fig. 2A) leads to a concentration-dependent reactivation of soman-impaired muscle. The recovery gradually increases with the MB327 concentration (Fig. 2A). At a MB327 concentration of 100 μM, the muscle force recovery amounts to 14.8% ± 9.2%, reaches 30.2% ± 9.5% at 300 μM (both values statistically significantly different from the value obtained for the soman-poisoned muscle), to finally decrease to 4.2% ± 4.2% at 1000 μM MB327 (not shown in Fig. 2A)(Hiessen et al., 2018).

Similar to MB327, the analogs 3, 6 f, 6 h and 6i exhibiting a 4-amino group at one of the two pyridinium subunits instead of a *tert*-butyl moiety (present in MB327) lead to an increase of the regeneration of the muscle force of soman-poisoned rat diaphragms with increasing concentrations, whereas the onset and the size of this effect differ. The *N,N*-dimethylamino-substituted analog 3 shows its maximum recovery at a concentration of 100 μM (45.8% ± 17.4%), which statistically significantly exceeds that of MB327 ($p < 0.01$) at the same concentration (14.8% ± 9.2%). However, the reactivation decreases nominally at 300 μM to 37.0% ± 15.8%, approximating that of MB327 at the same concentration (30.2% ± 9.5%). At a compound concentration of 100 μM, the results for the piperidino- and the piperazino-substituted compounds 6 f (47.5% ± 29.8%) and 6i (47.3% ± 21.8%) are comparable to the value observed for the dimethylamino derivative 3, which are also nominally the highest values of all three compounds. At

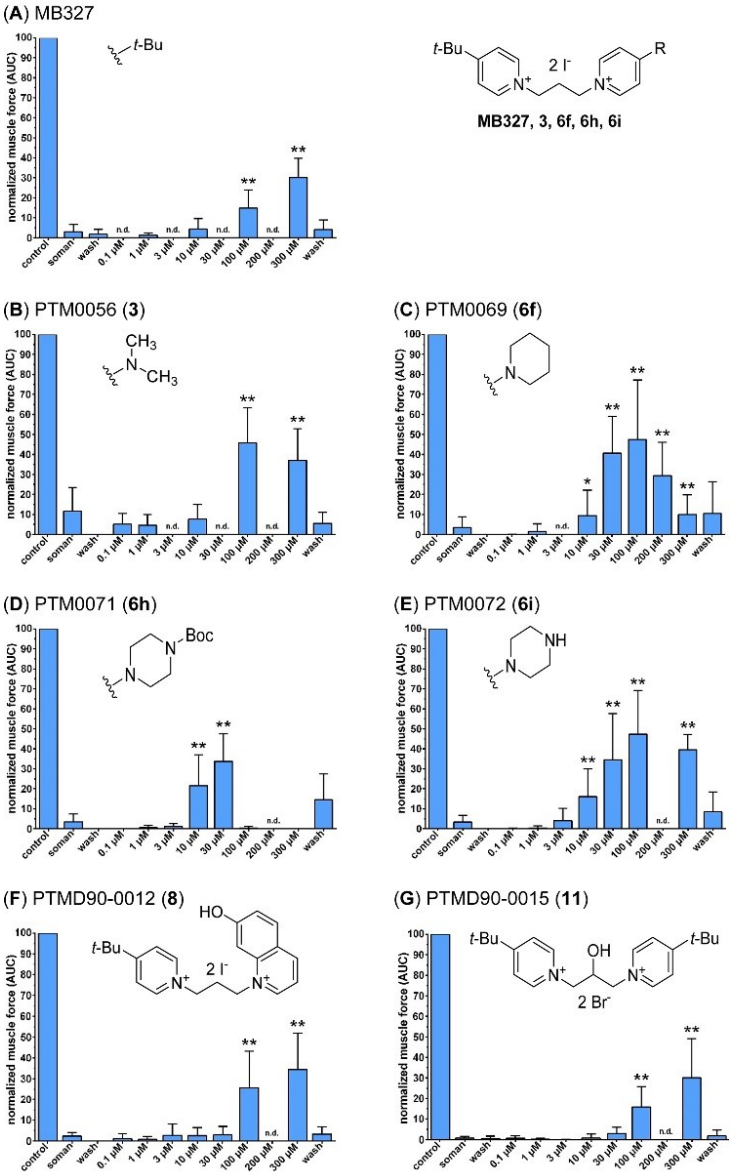

Fig. 2. Concentration-dependent restoration of muscle force of soman-poisoned rat diaphragms by (**A**) MB327 (Niessen et al., 2019), (**B**) PTM0056 (**3**), (**C**) PTM0069 (**6 f**), (**D**) PTM0071 (**6 h**), (**E**) PTM0072 (**6i**), (**F**) PTMD90–0012 (**8**) and (**G**) PTMD90–0015 (**11**). For indirect stimulation, a frequency of 20 Hz was applied. Data are shown as % of control and are given as mean ± SD (n = 4–25). Asterisks indicate statistically significantly higher values for the respective compound concentration compared to the soman value (* $p < 0.05$, ** $p < 0.01$, based on a two-sided *t*-test). n.d.: not determined.

concentrations above 100 μM, alike observed for the dimethylamino derivative 3, the muscle force declines again for 6 f as well as 6i, which is in the case of 6i with 39.5% ± 7.7% muscle force recovery at 300 μM compound concentration far less pronounced than for 6 f with 10.0% ± 9.8% (statistically significant, $p < 0.01$; 6 f at 200 μM 29.3% ± 16.8%).

The *N*-Boc-piperazino derivative 6 h induces a rather strong muscle force recovery already at 10 μM with a value amounting to 21.7% ± 15.3%, which is nominally the highest for all tested compounds at this concentration, which further increases at 30 μM to 33.8% ± 13.8% followed by a sharp drop to almost 0% (0.3% ± 0.8%) at 100 μM (0.0%

± 0.0% at 300 μM). This strong muscle force recovery effect of 6 h at a low concentration might be a result of its high binding affinity, which is the highest of all compounds studied.

Notably, all three MB327 analogs with cyclic amino residues exert already at a concentration of 10 μM a muscle force recovery that is statistically significantly higher than that of the soman-poisoned but untreated muscle, whereas this is neither the case for the dimethylamino derivative 3 nor for MB327. For the piperidino derivative 6 f, the respective recovery of muscle force at 10 μM amounts to 9.5% ± 12.7%, for the *N*-Boc-piperazino analog 6 h to 21.7% ± 15.3% and the piperazino derivative 6i to 16.0% ± 14.1%. Statistical significance of muscle force recovery over the soman-poisoned but untreated muscle as reference value is reached for these three compounds also at a test compound concentration of 30 μM (6 f, 40.6% ± 18.5%; 6 h, 33.8% ± 13.8%; 6i, 34.5% ± 23.2%). Yet, it remains unclear, whether this is also the case for the dimethylamino derivative 3 and MB327, as data for these two compounds when applied at 30 μM are missing.

The two MB327 analogs featuring an additional hydroxy group either in the spacer, 11, or as part of a quinolinium moiety, 8, show very similar effects in terms of muscle force regeneration after soman-intoxication. Also, muscle force recovery effected by 11 and 8 at concentrations of 100 μM and 300 μM is statistically significant as compared to the soman value. Thereby, the values for muscle force recovery of soman-poisoned muscle amounted for 11 to 15.9% ± 9.9% at 100 μM and to 30.1% ± 19.1% at 300 μM, whereas those for 8 are higher with 25.6% ± 17.5% at 100 μM and 34.3% ± 17.5% at 300 μM. For both compounds, no decrease in muscle force could be observed up to the highest concentration of 300 μM studied.

Finally, the effects of test compounds that were still available in sufficient amounts, i.e., of MB327 and the dimethylamino 3, the piperidino 6 f as well as the quinolinium derivative 8, on the muscle force of rat diaphragm hemispheres not been poisoned with soman were studied (SI, Figure S13). These experiments were carried out in analogy to those for the determination of muscle force recovery of soman-poisoned rat diaphragm hemispheres. Accordingly, the muscle force of rat diaphragm hemispheres not exposed to soman was measured as a function of increasing concentrations of the test compounds under indirect electric field stimulation at 20 Hz, 50 Hz and 100 Hz. Data from analogous experiments performed in parallel but without the application of test compounds served as reference by unveiling the loss of muscle force purely due to the washing steps. MB327 and dimethylamino derivative 3 showed no inhibitory effect up to the maximum concentration of 300 μM, as did the quinolinium derivative 8 up to 200 μM as the highest concentration still feasible due to a shortage of the compound. For the piperidino derivative 6 f, however, although the muscle force remained unaffected up to a concentration of 100 μM, a distinct reduction occurred at a concentration of 300 μM. The latter might explain the bell-shaped curve observed for this compound, 6 f, in the muscle force recovery experiments of soman-poisoned rat diaphragm hemispheres (Fig. 2C). The positive effect of 6 f on soman-poisoned rat diaphragms mediated by binding to the MB327-PAM-1 binding site of the nAChR might be counteracted by a direct negative effect on muscle force, mediated by different binding sites, which seems to become dominating at concentrations above 100 μM of 6 f, leading to the observed decline of muscle force recovery in soman-poisoned muscles (Fig. 2C) above this concentration.

3.3. *Substituting entropically unfavorable water clusters using in silico methods*

We performed unbiased MD simulations (12 replicas of 1 μs length each) of the human nAChR with MB327 bound to the recently identified allosteric binding site MB327-PAM-1 in all five subunits (Kaiser et al., 2023). During the simulations, the receptor and membrane stayed structurally invariant shortly after the simulations started (SI, Figure S14, S15). MB327 mostly or completely remained within the binding sites in between the α- and δ-subunits (ten out of twelve replicas) as well as in between the α- and ε-subunits (twelve out of twelve replicas) using the distance of heavy atoms of MB327 to heavy atoms of I64δ (respectively I61ε) to characterize unbinding as done previously (Kaiser et al., 2023). For these two binding sites, Grid Inhomogeneous Solvent Theory (GIST) computations (Lazaridis, 1998; Nguyen et al., 2011; Nguyen et al., 2012; Ramsey et al., 2016) were subsequently performed to identify potential entropically unfavorable water clusters (Fig. 3B, SI, Figure S16A). We then visualized the docked MB327 binding mode and representative MB327 structures from MD simulations in the presence of such water clusters and manually created new MB327 analogs with substituents replacing these water clusters. Initially, during the first few replicas (5 out of 12) of MD simulations and subsequent GIST computations, a network of entropically unfavorable water molecules near the linker of MB327 was identified between E65α, V66α, and Q68α (SI, Figure S17). Based on these preliminary results, PTMD90–0015 (11) was designed. However, after completion of the MD simulations, the hydroxyl group located at the C3-linker would not result in replacing entropically unfavorable water molecules as indicated by GIST. Hence, PTMD90–0012 (8) was designed based on the results after 1 μs long simulations (Fig. 3C, SI, Figure S16B), such that it should substitute entropically unfavorable water molecules in close proximity to I63ε, E65ε, and E204ε (respectively L66δ, E68δ, and E210δ). As only the analogs based on the docked structure [PTMD90–0012 (8)] and those based on the initial MD simulations results [PTMD90–0015 (11)] could be synthesized, they were subsequently tested for affinity and resensitizing potential.

4. Conclusion

The recently developed non-symmetric MB327 analogs PTM0062 (1), PTM0063 (2) and PTM0056 (3), which have an amino, methylamino or dimethylamino group in place of one of the two *tert*-butyl residues of MB327, respectively, show higher muscle force restoring activity on soman-poisoned rat diaphragms than MB327. They are therefore promising starting points for the development of new resensitizers for desensitized muscle-type nAChRs as antidots for OPC poisoning.

In the present study, a series of new non-symmetric MB327 analogs, PTM0064-PTM0072 (6a-6i), with a 4-amino-substituted pyridinium ion substructure derived from compounds 1-3, were synthesized and evaluated for their binding affinity towards the MB327-PAM-1 binding site of *Torpedo californica* nAChR using the recently introduced UNC0642 MS Binding Assays. In addition, selected compounds were evaluated for their intrinsic activity on soman-poisoned rat diaphragms in myography assays.

Among the compounds evaluated in this study, the piperidino derivative PTM0069 (6 f) and the *N*-Boc-piperazino derivative PTM0071 (6 h) showed the highest affinities for the MB327-PAM-1 binding site of the nAChR. The pK_i values for 6 f and 6 h exceeded that of MB327 by approximately 0.5 and 0.8 log units, respectively. PTMD90–0015 (11), designed to substitute unfavorable water clusters in MB327-PAM-1 after preliminary MD simulations, showed reduced affinity towards MB327-PAM-1 and no beneficial resensitizing effects compared to MB327. These results are concordant with that the hydroxy group located at the C3-linker would not result in replacing entropically unfavored water molecules as indicated by GIST after 1 μs long MD simulations. By contrast, PTMD90–0012 (8), designed using extended MD data, showed a statistically significant increase of affinity compared to MB327. Likely, this may result from replacing entropically unfavored water molecules close to $I63_\varepsilon$, $E65_\varepsilon$, and $E204_\varepsilon$ (or $L66_\delta$, $E68_\delta$, and $E210_\delta$) with the 7-hydroxy quinazoline moiety.

Ex vivo studies in soman-poisoned rat diaphragms showed a clear muscle force restoring activity for all compounds tested [PTM0069 (6 f), PTM0071 (6 h), PTM0056 (3), PTM0072 (6i), PTMD90–0012 (8), and

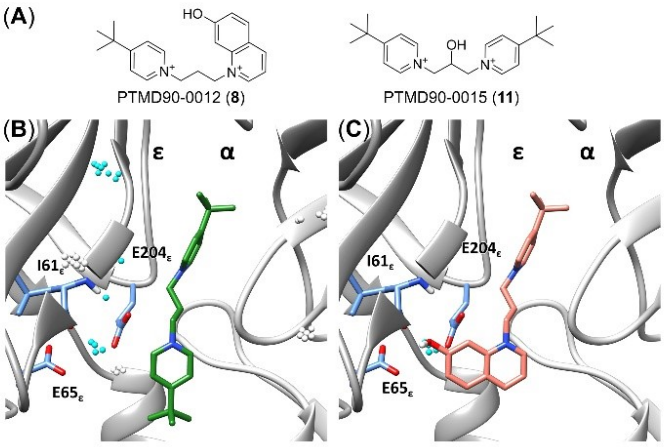

Fig. 3. Design of MB327 analogs based on substituting water clusters in MB327-PAM-1. **A)** Structure of the MB327 analogs PTMD90–0012 (**8**) and PTMD90–0015 (**11**). **B)** MB327 (green) binding in between the α- and ε-subunit. Water clusters identified during GIST computations are shown as spheres. Water clusters within 5 Å of MB327 are shown in cyan. **C)** Proposed binding mode of PTMD90–0012 (**8**) (salmon) in between the α- and ε-subunit. Modification of MB327 to PTMD90–0012 (**8**) (salmon) leads to a substitution of a water cluster located in proximity to $I63_\varepsilon$, $E65_\varepsilon$, and $E204_\varepsilon$; for $I61_\varepsilon$ the backbone atoms are shown in addition to the side chain.

PTMD90–0015 (11)]. In particular, compounds PTM0069 (6 f), PTM0071 (6 h) and PTM0072 (6i), which all have cyclic aliphatic amino substituents instead of one of the two *tert*-butyl residues of MB327, showed a statistically significantly higher activity at lower concentrations than MB327. Thus, to achieve muscle force recovery comparable to that of the aforementioned compounds, MB327 must be used at a tenfold higher concentration. This could be due to the fact that PTM0069 (6 f) and PTM0071 (6 h), in particular, but also PTM0072 (6i) have statistically significantly higher binding affinities for the MB327-PAM-1 binding site than MB327. It is noteworthy that the recovery of muscle force with PTM0069 (6 f) and PTM0071 (6 h) at higher concentrations decreased significantly immediately after reaching the maximum value, a phenomenon also observed for MB327. Experiments with PTM0069 (6 f) and rat diaphragms that had not been poisoned with soman showed that in the presence of higher concentrations of PTM0069 (6 f), a significant inhibition of muscle force occurs, which is reversible as it almost completely disappears after a subsequent washout step. Interestingly, this reversible inhibition occurs in the same concentration range in which the muscle force restoring effect of compound 6 f decreases in the experiments with soman-poisoned rat diaphragms.

Taken together, this indicates that the positive resensitizing effect mediated by binding to the MB327-PAM-1 binding site is counteracted by a muscle force inhibitory effect becoming generally prominent at higher concentrations that appears to be due to reversible binding to a different binding site.

Therefore, future efforts must focus, on the one hand, on further increasing the affinity of new compounds for the MB327-PAM-1 binding site and, on the other hand, on reducing the direct muscle inhibitory effect.

CRediT authorship contribution statement

Franz F. Paintner: Writing – review & editing, Supervision, Funding acquisition, Data curation, Conceptualization. **Holger Gohlke:** Writing – review & editing, Supervision, Software, Methodology, Conceptualization. **Klaus T. Wanner:** Writing – review & editing, Supervision, Funding acquisition, Conceptualization. **Dirk Steinritz:** Writing – review & editing. **Franz Worek:** Writing – review & editing. **Karin V. Niessen:** Writing – review & editing. **Thomas Seeger:** Writing – original draft, Methodology, Investigation. **Christoph G.W. Gertzen:** Writing – review & editing, Supervision, Methodology. **Georg Höfner:** Writing – review & editing, Methodology. **Valentin Nitsche:** Writing – original draft, Methodology, Investigation. **Jesko Kaiser:** Writing – original draft, Methodology, Investigation. **Tamara Bernauer:** Writing – original draft, Methodology, Investigation.

Declaration of Competing Interest

The authors declare that they have no known competing financial interests or personal relationships that could have appeared to influence the work reported in this paper.

Data availability

Data will be made available on request.

Acknowledgments

This work was supported by the German Ministry of Defence (E/U2AD/KA019/IF558). We are grateful for computational support and infrastructure provided by the "Zentrum für Informations- und Medientechnologie" (ZIM) at the Heinrich Heine University Düsseldorf and the computing time provided by the John von Neumann Institute for Computing (NIC) to HG on the supercomputer JUWELS at Jülich Supercomputing Center (JSC) (user IDs: HKF7, VSK33, nAChR). HG is grateful to OpenEye Scientific Software for granting a Free Public Domain Research License.

Appendix A. Supporting information

Supplementary data associated with this article can be found in the online version at doi:10.1016/j.toxlet.2024.05.011.

References

Brown, M.A., Brix, K.A., 1998. Review of health consequences from high-, intermediate- and low-level exposure to organophosphorus nerve agents. J. Appl. Toxicol. 18, 393–408.

Case, D.A., Aktulga, H.M., Belfon, K., Cerutti, D.S., Cisneros, G.A., Cruzeiro, V.W.D., Forouzesh, N., Giese, T.J., Götz, A.W., Gohlke, H., Izadi, S., Kasavajhala, K., Kaymak, M.C., King, E., Kurtzman, T., Lee, T.-S., Li, P., Liu, J., Luchko, T., Luo, R., Manathunga, M., Machado, M.R., Nguyen, H.M., O'Hearn, K.A., Onufriev, A.V., Pan, F., Pantano, S., Qi, R., Rahnamoun, A., Risheh, A., Schott-Verdugo, S., Shajan, A., Swails, J., Wang, J., Wei, H., Wu, X., Wu, Y., Zhang, S., Zhao, S., Zhu, Q., Cheatham III, T.E., Roe, D.R., Roitberg, A., Simmerling, C., York, D.M., Nagan, M.C., Merz Jr., K.M., 2023. AmberTools. J. Chem. Inf. Model. 63, 6183–6191.

Case, D.A., Cheatham 3rd, T.E., Darden, T., Gohlke, H., Luo, R., Merz Jr., K.M., Onufriev, A., Simmerling, C., Wang, B., Woods, R.J., 2005. The Amber biomolecular simulation programs. J. Comput. Chem. 26, 1668–1688.

Case, D.A., H.M, A., Belfon, K., Ben-Shalom, I.Y., Berryman, J.T., Brozell, S.R., Cerutti, D. S., Cheatham, T.E., 3rd, Cisneros, G.A., Cruzeiro, V.W.D., Darden, T.A., Duke, R.E., Giambasu, G., Gilson, M.K., Gohlke, H., Goetz, A.W., Harris, R., Izadi, S., Izmailov, S. A., Kasavajhala, K., Kaymak, M.C., King, E., Kovalenko, A., Kurtzmann, T., Lee, T.S., Le Grand, S., Li, P., Lin, C., Liu, J., Luchko, T., Luo, R., Machado, M., Man, V., Manathunga, M., Merz, K.M., Miao, Y., Mikhailovskii, O., Monard, G., Nguyen, H., O'Hearn, K.A., Onufriev, A., Pan, F., Pantano, S., Qi, R., Rahnamoun, A., Roe, D.R., Roitberg, A., Sagui, E., Schott-Verdugo, S., Shajan, A., Shen, J., Simmerling, C.L., Skrynnikov, N.R., Smith, J., Swails, J., Walker, R.C., Wang, J., Wang, J., Wei, H., Wolf, R.M., Wu, X., Xiong, Y., Xue, Y., York, D.M., Zhao, S., Kollmann, P.A., 2022. Amber 2022. vol. Amber 2022. University of California, San Francisco.

Chemical Computing Group, U., 2020. Molecular Operating Environment (MOE). vol. 2019.01, 1010 Sehrbooke St. West, Suite #910, Montreal, QC, Canada, H3A, 2R7.

Cushman, M., Georg, G.I., Holzgrabe, U., Wang, S., 2014. Absolute Quantitative 1H NMR spectroscopy for compound purity determination. J. Med. Chem. 57, 9219–9219.

Dolgin, E., 2013. Syrian gas attack reinforces need for better anti-sarin drugs. Nat. Med. 19, 1194–1195.

Epstein, M., Bali, K., Piggot, T.J., Green, A.C., Timperley, C.M., Bird, M., Tattersall, J.E. H., Bermudez, I., Biggin, P.C., 2021. Molecular determinants of binding of non-oxime bispyridinium nerve agent antidote compounds to the adult muscle nAChR. Toxicol. Lett. 340, 114–122.

Gharpure, A., Teng, J., Zhuang, Y., Noviello, C.M., Walsh Jr., R.M., Cabuco, R., Howard, R.J., Zaveri, N.T., Lindahl, E., Hibbs, R.E., 2019. Agonist selectivity and ion permeation in the alpha3beta4 ganglionic nicotinic receptor. Neuron 104 (501-511), e506.

Hay, D.A., Rogers, C.M., Fedorov, O., Tallant, C., Martin, S., Monteiro, O.P., Müller, S., Knapp, S., Schofield, C.J., Brennan, P.E., 2015. Design and synthesis of potent and selective inhibitors of BRD7 and BRD9 bromodomains. MedChemComm 6, 1381–1386.

Izadi, S., Anandakrishnan, R., Onufriev, A.V., 2014. Building water models: a different approach. J. Phys. Chem. Lett. 5, 3863–3871.

Joung, I.S., Cheatham III, T.E., 2008. Determination of alkali and halide monovalent ion parameters for use in explicitly solvated biomolecular simulations. J. Phys. Chem. B 112, 9020–9041.

Kaiser, J., Gertzen, C.G.W., Bernauer, T., Höfner, G., Niessen, K.V., Seeger, T., Paintner, F.F., Wanner, K.T., Worek, F., Thiermann, H., Gohlke, H., 2023. A novel binding site in the nicotinic acetylcholine receptor for MB327 can explain its allosteric modulation relevant for organophosphorus-poisoning treatment. Toxicol. Lett. 373, 160–171.

Kaiser, J., Gertzen, C.G.W., Bernauer, T., Nitsche, V., Höfner, G., Niessen, K.V., Seeger, T., Paintner, F.F., Wanner, K.T., Steinritz, D., Worek, F., Gohlke, H., 2024. Identification of ligands binding to MB327-PAM-1, a binding pocket relevant for resensitization of nAChRs. bioRxiv. https://doi.org/10.1101/2023.12.21.572862.

Koelle, G.B., 1981. Organophosphate poisoning—an overview. Fundam. Appl. Toxicol. 1, 129–134.

Lazaridis, T., 1998. Inhomogeneous fluid approach to solvation thermodynamics. 1. theory. J. Phys. Chem. B 102, 3531–3541.

Lott, R.S., Chauhan, V.S., Stammer, C.H., 1979. Trimethylsilyl iodide as a peptide deblocking agent. J. Chem. Soc., Chem. Commun. 495–496.

M.J. Frisch, G.W.T., H.B. Schlegel, G.E. Scuseria,, M.A. Robb, J.R.C, G. Scalmani, V. Barone, G.A. Petersson, H.N, X. Li, M. Caricato, A.V. Marenich, J. Bloino, B.G.J, R. Gomperts, B. Mennucci, H.P. Hratchian, J.V. Ortiz, A.F.I, J.L. Sonnenberg, D. Williams-Young, F. Ding, F.L, F. Egidi, J. Goings, B. Peng, A. Petrone, T. Henderson, D.R, V.G. Zakrzewski, J. Gao, N. Rega, G. Zheng, W.L, M. Hada, M. Ehara, K. Toyota, R. Fukuda, J. Hasegawa, M.I, T. Nakajima, Y. Honda, O. Kitao, H. Nakai,, T. Vreven, K.T, J.A. Montgomery, Jr., J.E. Peralta, F. Ogliaro, M.J.B, J.J. Heyd, E.N. Brothers, K. N. Kudin,, V.N. Staroverov, T.A.K, R. Kobayashi, J. Normand, K. Raghavachari, A.P. R, J.C. Burant, S.S. Iyengar, J. Tomasi, M.C, J.M. Millam, M. Klene, C. Adamo, R. Cammi, J.W. Ochterski, R.L.M, K. Morokuma, O. Farkas, J.B. Foresman, a.D.J.F, 2016. Gaussian16. vol. Revision A.03. Gaussian Inc., Wallingford CT.

Maselli, R.A., Leung, C., 1993. Analysis of anticholinesterase-induced neuromuscular transmission failure. Muscle Nerve 16, 548–553.

Massoulié, J., Pezzementi, L., Bon, S., Krejci, E., Vallette, F.-M., 1993. Molecular and cellular biology of cholinesterases. Prog. Neurobiol. 41, 31–91.

Nguyen, C., Gilson, M.K., Young, T., 2011. Structure and thermodynamics of molecular hydration via grid inhomogeneous solvation theory. arXiv 1108, 4876.

Nguyen, C.N., Young, T.K., Gilson, M.K., 2012. Grid inhomogeneous solvation theory: hydration structure and thermodynamics of the miniature receptor cucurbit[7]uril. J. Chem. Phys. 137, 044101.

Niessen, K.V., Muschik, S., Langguth, F., Rappengluck, S., Seeger, T., Thiermann, H., Worek, F., 2016. Functional analysis of Torpedo californica nicotinic acetylcholine receptors in multiple activation states by SSM-based electrophysiology. Toxicol. Lett. 247, 1–10.

Niessen, K.V., Seeger, T., Rappengluck, S., Wein, T., Höfner, G., Wanner, K.T., Thiermann, H., Worek, F., 2018. In vitro pharmacological characterization of the bispyridinium non-oxime compound MB327 and its 2- and 3-regioisomers. Toxicol. Lett. 293, 190–197.

Nitsche, V., Höfner, G., Kaiser, J., Gertzen, C.G.W., Seeger, T., Niessen, K.V., Steinritz, D., Worek, F., Gohlke, H., Paintner, F.F., Wanner, K.T., 2024. MS Binding Assays with UNC0642 as reporter ligand for the MB327 binding site of the nicotinic acetylcholine receptor. Toxicol. Lett. 392, 94–106.

Noviello, C.M., Gharpure, A., Mukhtasimova, N., Cabuco, R., Baxter, L., Borek, D., Sine, S.M., Hibbs, R.E., 2021. Structure and gating mechanism of the α7 nicotinic acetylcholine receptor. Cell 184, 2121–2134 e2113.

OPCW, 2017. OPCW Director-General Shares Incontrovertible Laboratory Results Concluding Exposure to Sarin, 19.04.2017.

OpenEye Scientific Software, I., 2021. SZYBKI. OpenEye Scientific Software, Santa Fe, NM.

Pauli, G.F., Chen, S.-N., Simmler, C., Lankin, D.C., Gödecke, T., Jaki, B.U., Friesen, J.B., McAlpine, J.B., Napolitano, J.G., 2014. Importance of purity evaluation and the potential of quantitative 1H NMR as a purity assay. J. Med. Chem. 57, 9220–9231.

Pettersen, E.F., Goddard, T.D., Huang, C.C., Couch, G.S., Greenblatt, D.M., Meng, E.C., Ferrin, T.E., 2004. UCSF Chimera—a visualization system for exploratory research and analysis. J. Comput. Chem. 25, 1605–1612.

Pita, R., Domingo, J., 2014. The use of chemical weapons in the syrian conflict. Toxics 2, 391–402.

Price, K.E., Mason, B.P., Bogdan, A.R., Broadwater, S.J., Steinbacher, J.L., McQuade, D. T., 2006. Microencapsulated Linear Polymers: "Soluble" Heterogeneous Catalysts. J. Am. Chem. Soc. 128, 10376–10377.

Ramsey, S., Nguyen, C., Salomon-Ferrer, R., Walker, R.C., Gilson, M.K., Kurtzman, T., 2016. Solvation thermodynamic mapping of molecular surfaces in AmberTools: GIST. J. Comput. Chem. 37, 2029–2037.

Rappengluck, S., Sichler, S., Höfner, G., Wein, T., Niessen, K.V., Seeger, T., Paintner, F.F., Worek, F., Thiermann, H., Wanner, K.T., 2018. Synthesis of a series of non-symmetric bispyridinium and related compounds and their affinity characterization at the nicotinic acetylcholine receptor. ChemMedChem 13, 2653–2663.

Roe, D.R., Cheatham 3rd, T.E., 2013. PTRAJ and CPPTRAJ: software for processing and analysis of molecular dynamics trajectory data. J. Chem. Theory Comput. 9, 3084–3095.

Schott-Verdugo, S., Gohlke, H., 2019. PACKMOL-Memgen: a simple-to-use, generalized workflow for membrane-protein-lipid-bilayer system building. J. Chem. Inf. Model 59, 2522–2528.

Seeger, T., Eichhorn, M., Lindner, M., Niessen, K.V., Tattersall, J.E.H., Timperley, C.M., Bird, M., Green, A.C., Thiermann, H., Worek, F., 2012. Restoration of soman-blocked neuromuscular transmission in human and rat muscle by the bispyridinium non-oxime MB327 in vitro. Toxicology 294, 80–84.

Sheridan, R.D., Smith, A.P., Turner, S.R., Tattersall, J.E.H., 2005. Nicotinic antagonists in the treatment of nerve agent intoxication. J. R. Soc. Med. 98, 114–115.

Sichler, S., Höfner, G., Rappengluck, S., Wein, T., Niessen, K.V., Seeger, T., Worek, F., Thiermann, H., Paintner, F.F., Wanner, K.T., 2018. Development of MS Binding Assays targeting the binding site of MB327 at the nicotinic acetylcholine receptor. Toxicol. Lett. 293, 172–183.

Steindl, D., Boehmerle, W., Körner, R., Praeger, D., Haug, M., Nee, J., Schreiber, A., Scheibe, F., Demin, K., Jacoby, P., Tauber, R., Hartwig, S., Endres, M., Eckardt, K.-U., 2021. Novichok nerve agent poisoning. Lancet 397, 249–252.

Thakur, R., Haru, E., 2007. The Chemical Weapons Convention: Implementation, Challenges, Opportunities.

Thiermann, H., Seeger, T., Gonder, S., Herkert, N., Antkowiak, B., Zilker, T., Eyer, F., Worek, F., 2010. Assessment of neuromuscular dysfunction during poisoning by organophosphorus compounds. Chem. -Biol. Interact. 187, 265–269.

Tian, C., Kasavajhala, K., Belfon, K.A.A., Raguette, L., Huang, H., Migues, A.N., Bickel, J., Wang, Y., Pincay, J., Wu, Q., Simmerling, C., 2020. ff19SB: amino-acid-specific protein backbone parameters trained against quantum mechanics energy surfaces in solution. J. Chem. Theory Comput. 16, 528–552.

Timperley, C.M., Bird, M., Green, C., Price, M.E., Chad, J.E., Turner, S.R., Tattersall, J.E., 2012. 1, 1'-(Propane-1, 3-diyl) bis (4-tert-butylpyridinium) di (methanesulfonate) protects guinea pigs from soman poisoning when used as part of a combined therapy. MedChemComm (3), 352–356.

Turner, S.R., Chad, J.E., Price, M., Timperley, C.M., Bird, M., Green, A.C., Tattersall, J.E. H., 2011. Protection against nerve agent poisoning by a noncompetitive nicotinic antagonist. Toxicol. Lett. 206, 105–111.

Wang, J., Wolf, R.M., Caldwell, J.W., Kollman, P.A., Case, D.A., 2004. Development and testing of a general amber force field. J. Comput. Chem. 25, 1157–1174.

Wang, X., Long, C.-Y., Su, M.-H., Qu, Y.-X., Li, S.-H., Zhang, X.-J., Huang, S.-J., Wang, X.-Q., 2019. Rapid amination of methoxy pyridines with aliphatic amines. Org. Process Res. Dev. 23, 1587–1593.

Worek, F., Thiermann, H., Wille, T., 2020. Organophosphorus compounds and oximes: a critical review. Arch. Toxicol. 94, 2275–2292.

Supporting Information

Synthesis and Biological Evaluation of Novel MB327 Analogs as Resensitizers for Desensitized Nicotinic Acetylcholine Receptors after Intoxication with Nerve Agents

Tamara Bernauer,[a] Valentin Nitsche,[a] Jesko Kaiser,[b] Christoph G.W. Gertzen,[b] Georg Höfner,[a] Karin V. Niessen,[c] Thomas Seeger,[c] Dirk Steinritz,[c] Franz Worek,[c] Holger Gohlke,[b,d] Klaus T. Wanner,[a] and Franz F. Paintner*[a]

[a] T. Bernauer, V. Nitsche, Dr. G. Höfner, Prof. Dr. K. T. Wanner, Prof. Dr. F. F. Paintner
Department of Pharmacy, Center for Drug Research
Ludwig-Maximilians-Universität München
Butenandtstrasse 5-13, 81377 Munich (Germany)
E-mail: Franz.Paintner@cup.uni-muenchen.de

[b] J. Kaiser, Dr. C. G. W. Gertzen, Prof. Dr. H. Gohlke
Institute for Pharmaceutical and Medicinal Chemistry
Heinrich Heine Universität Düsseldorf
Universitätsstrasse 1, 40225 Düsseldorf (Germany)

[c] Dr. K. V. Niessen, Dr. T. Seeger, Prof. Dr. D. Steinritz, Prof. Dr. F. Worek
Bundeswehr Institute of Pharmacology and Toxicology
Neuherbergstrasse 11, 80937 Munich (Germany)

[d] Prof. Dr. H. Gohlke
John von Neumann Institute for Computing (NIC), Jülich Supercomputing Centre (JSC), Institute of Biological Information Processing (IBI-7: Structural Biochemistry) & Institute of Bio- and Geosciences (IBG-4: Bioinformatics)
Forschungszentrum Jülich
Wilhelm-Johnen-Strasse, 52428 Jülich (Germany)

Table of Content

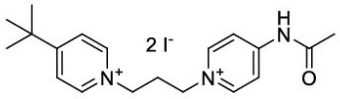

6a (PTM0064)

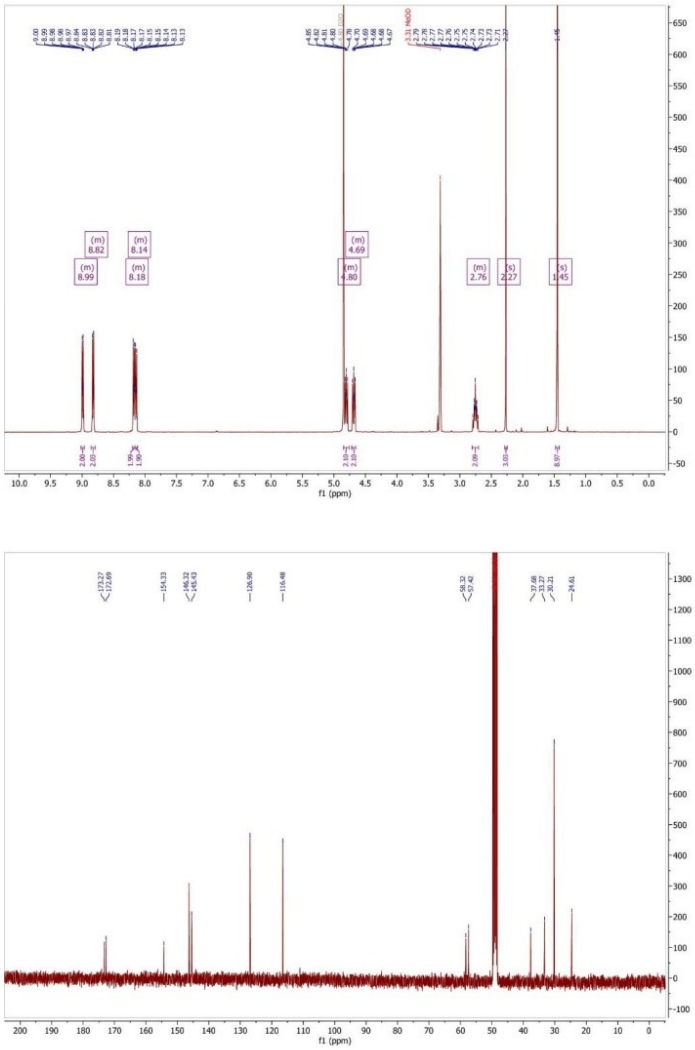

Figure S1: ^{1}H and ^{13}C NMR spectrum of **6a** (PTM0064).

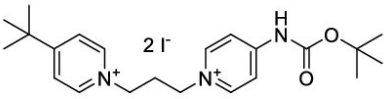

6b (PTM0065)

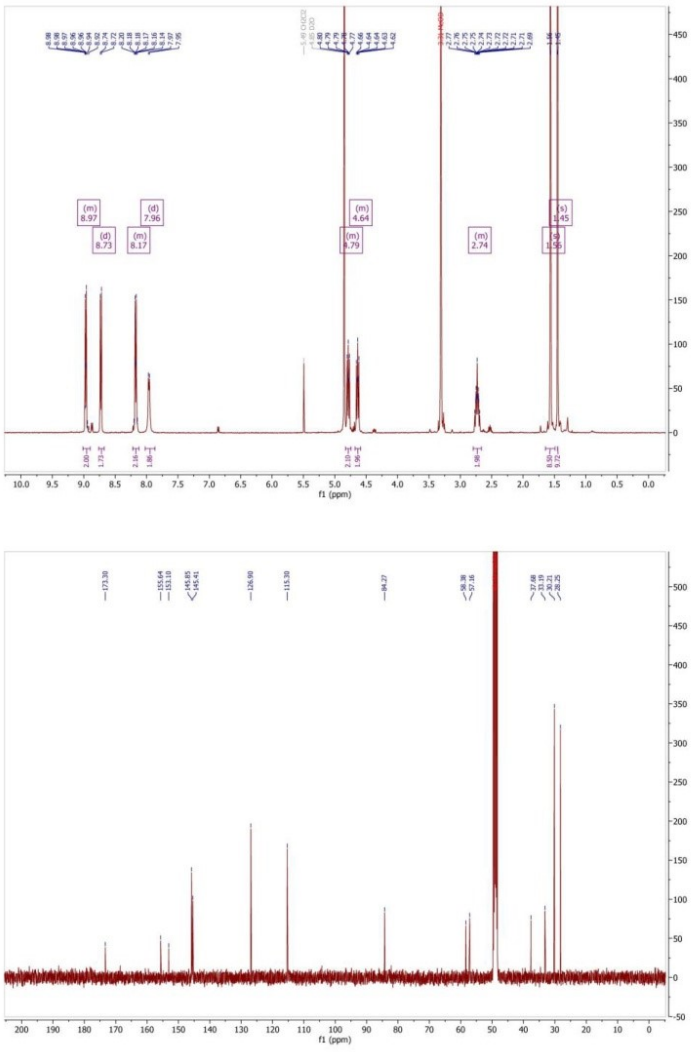

Figure S2: ^{1}H and ^{13}C NMR spectrum of **6b** (PTM0065).

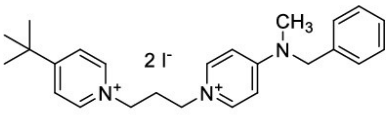

6c (PTM0066)

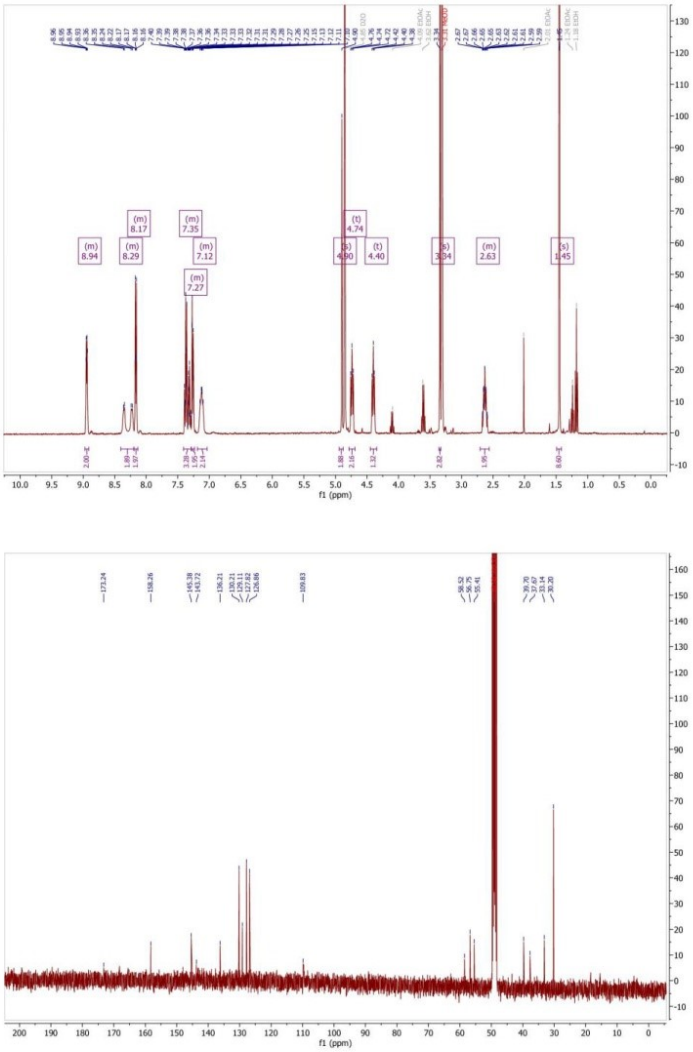

Figure S3: ^{1}H and ^{13}C NMR spectrum of **6c** (PTM0066).

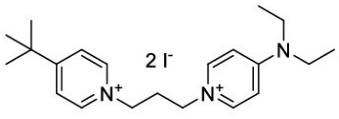

6d (PTM0067)

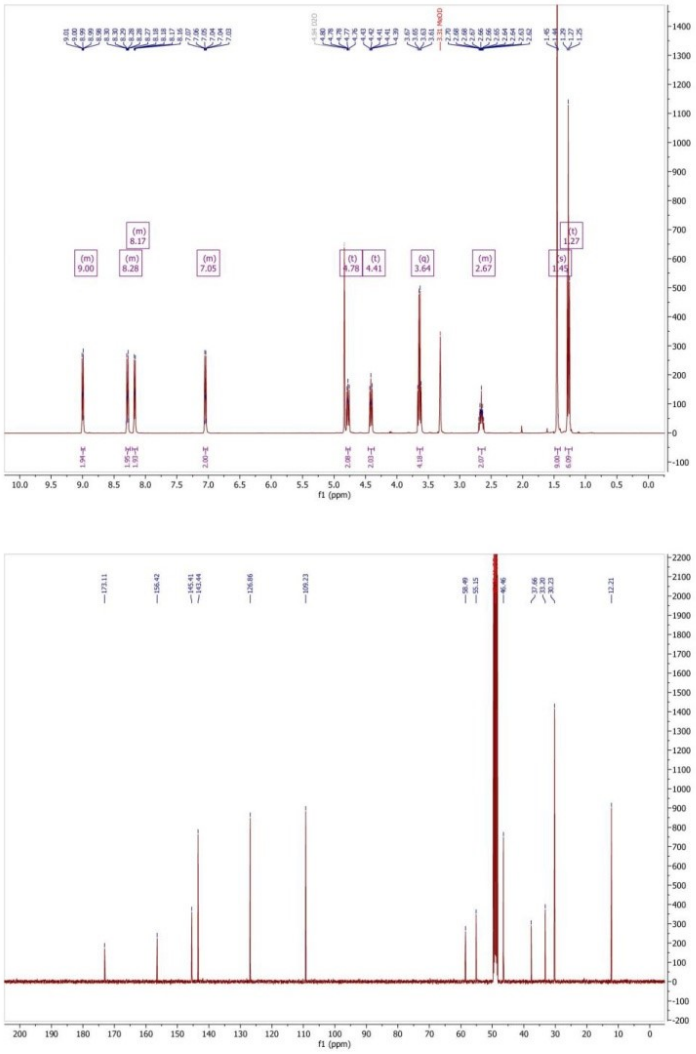

Figure S4: ^{1}H and ^{13}C NMR spectrum of **6d** (PTM0067).

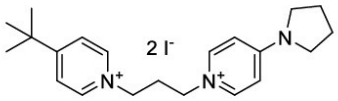

6e (PTM0068)

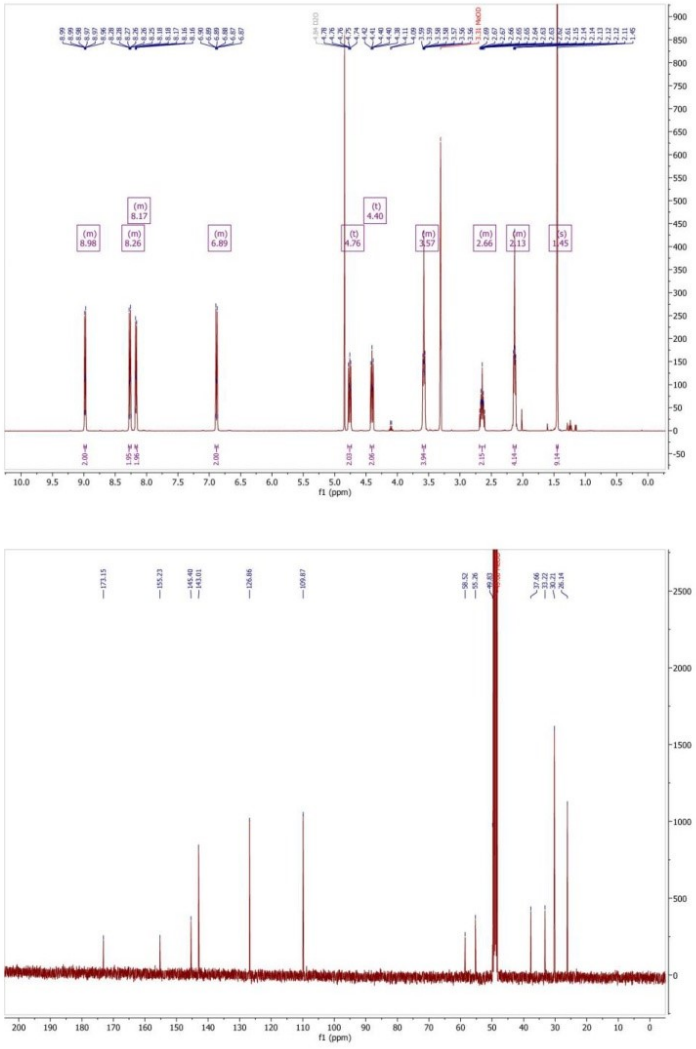

Figure S5: ^{1}H and ^{13}C NMR spectrum of **6e** (PTM0068).

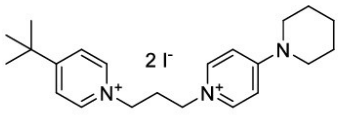

6f (PTM0069)

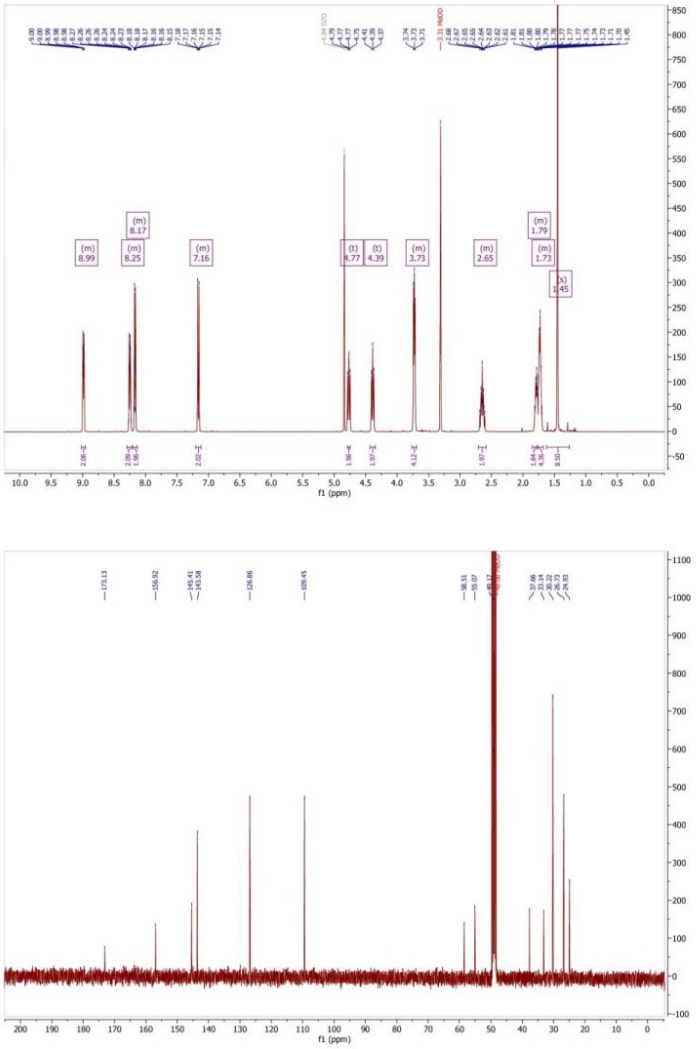

Figure S6: ^{1}H and ^{13}C NMR spectrum of **6f** (PTM0069).

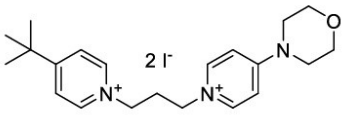

6g (PTM0070)

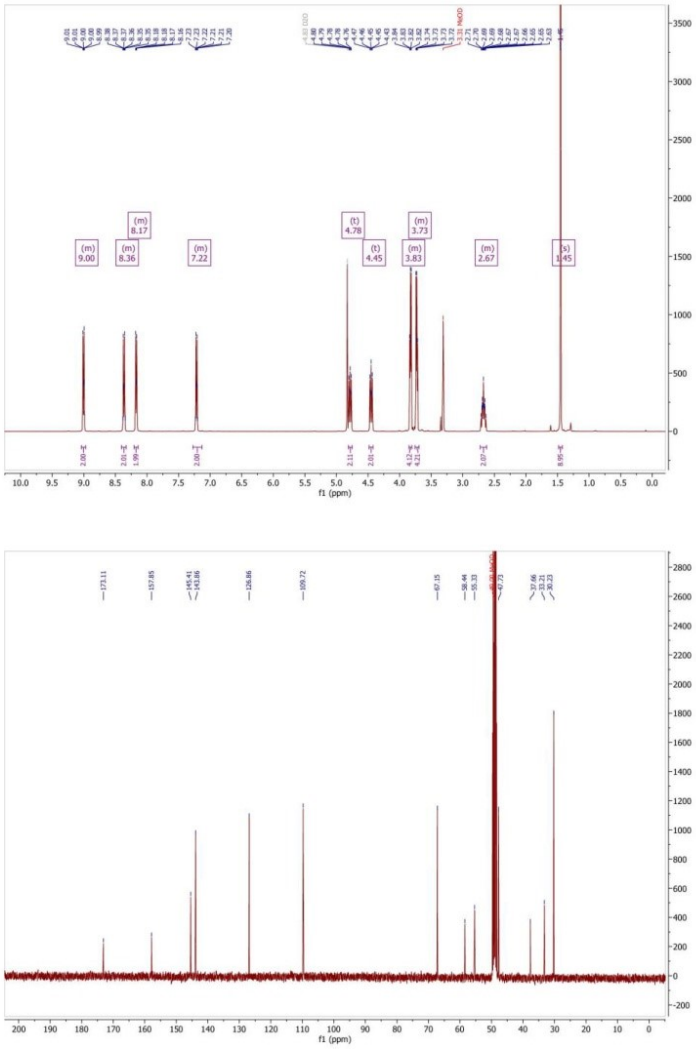

Figure S7: ^{1}H and ^{13}C NMR spectrum of **6g** (PTM0070).

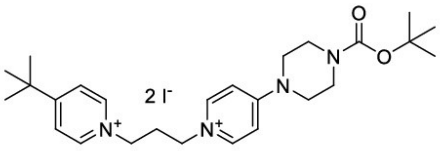

6h (PTM0071)

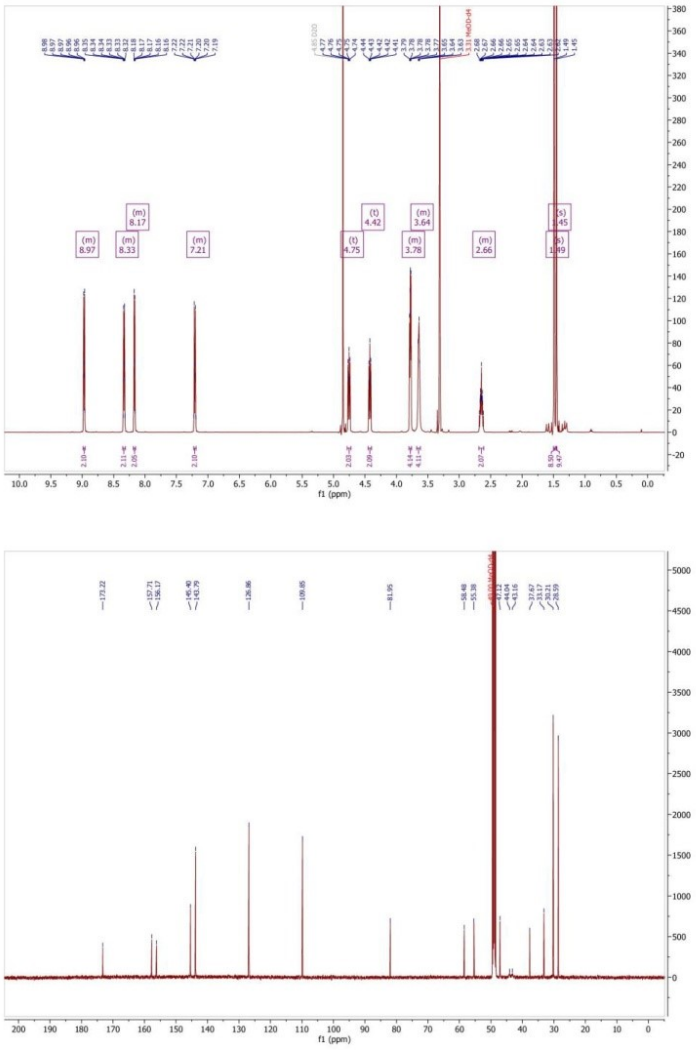

Figure S8: ^{1}H and ^{13}C NMR spectrum of **6h** (PTM0071).

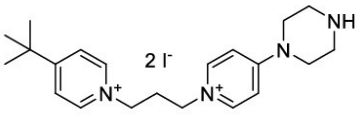

6i (PTM0072)

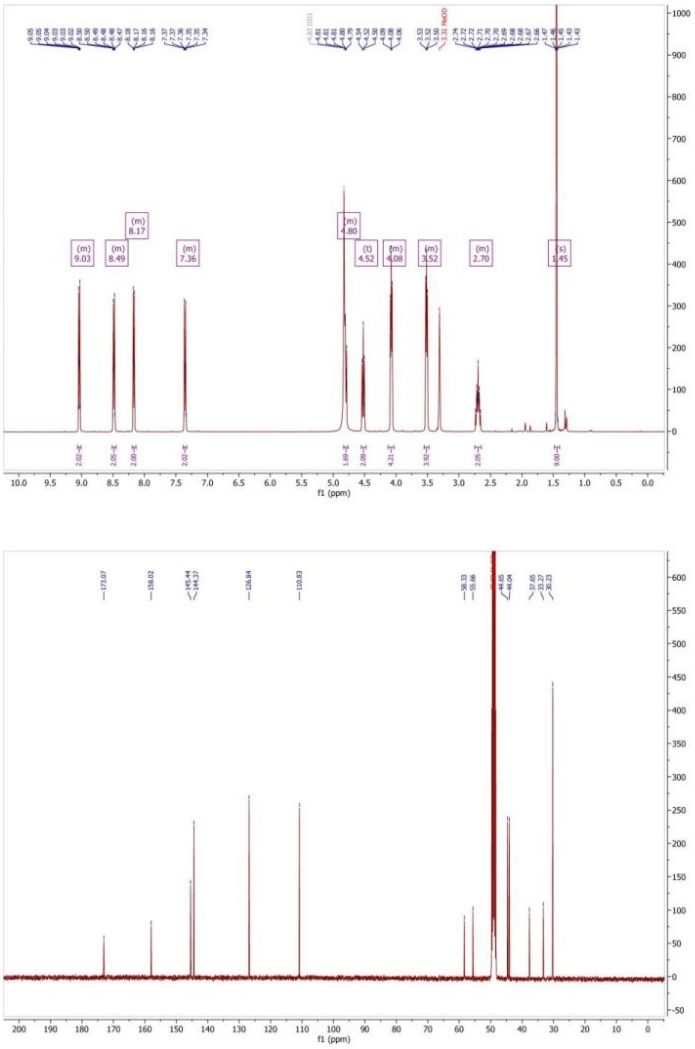

Figure S9: ^{1}H and ^{13}C NMR spectrum of **6i** (PTM0072).

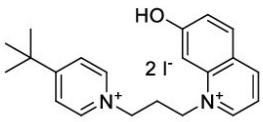

8 (PTMD90-0012)

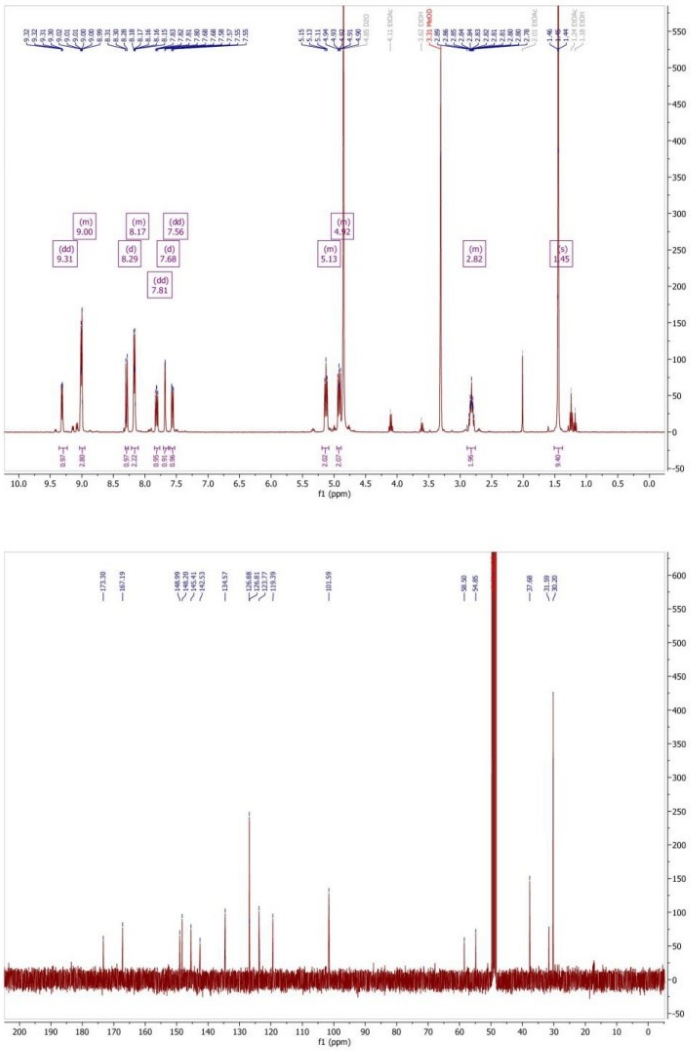

Figure S10: ^{1}H and ^{13}C NMR spectrum of **8** (PTMD90-0012).

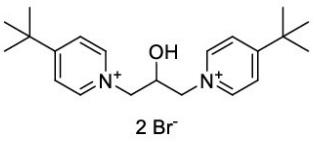

11 (PTMD90-0015)

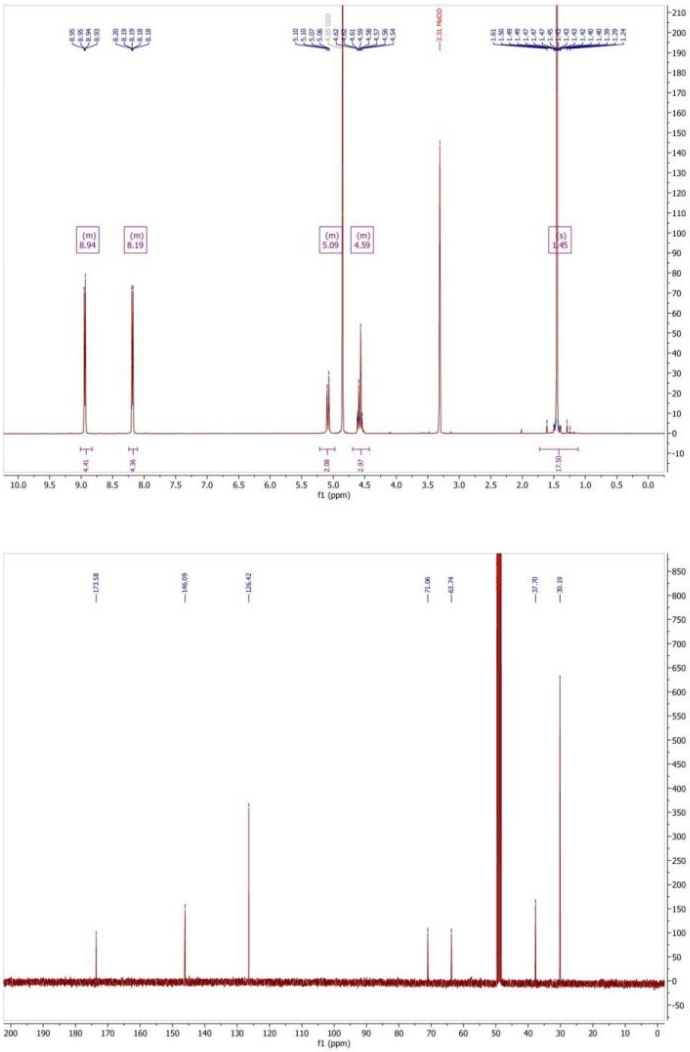

Figure S11: ^{1}H and ^{13}C NMR spectrum of **11** (PTMD90-0015).

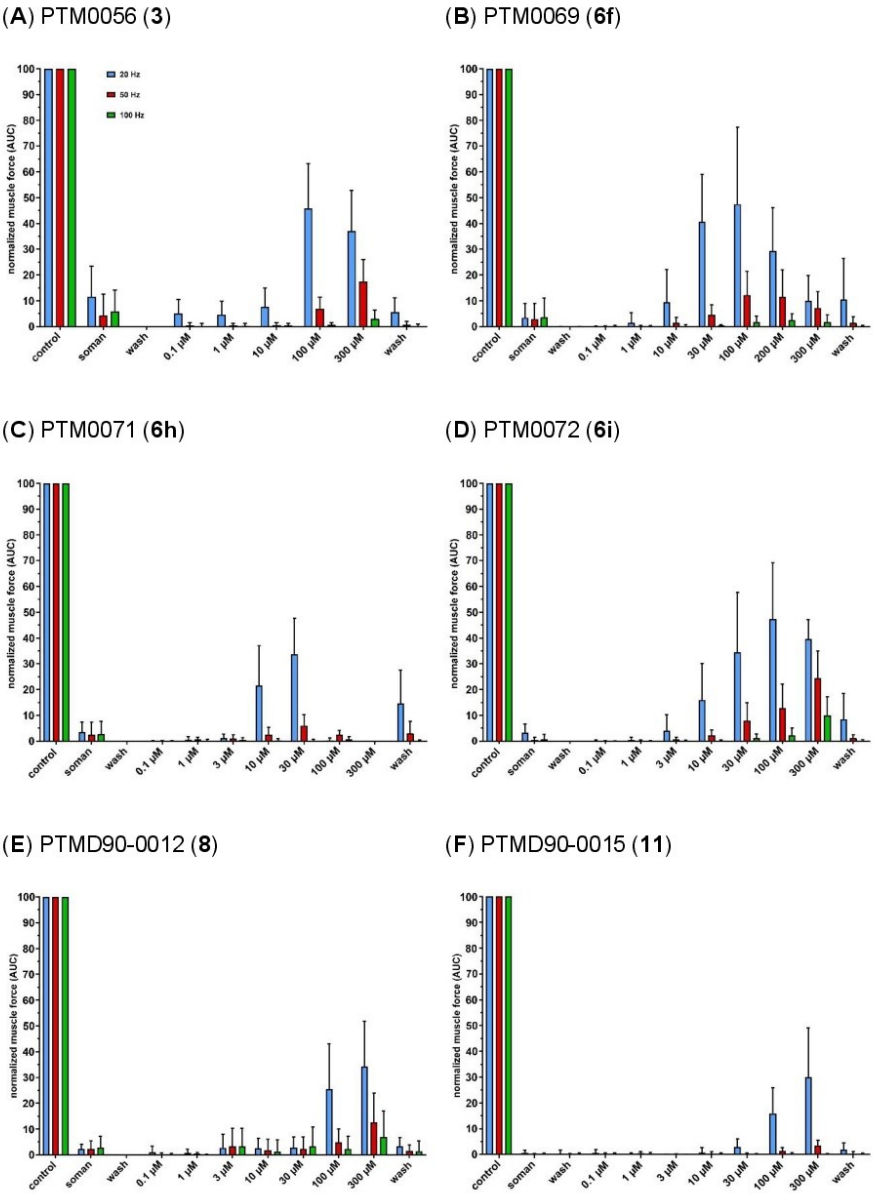

Figure S12: Concentration-dependent restoration of the muscle force by (**A**) PTM0056 (**3**), (**B**) PTM0069 (**6f**), (**C**) PTM0071 (**6h**), (**D**) PTM0072 (**6i**), (**E**) PTMD90-0012 (**8**), (**F**) PTMD90-0015 (**11**) of rat diaphragm preparations after poisoning with soman (3 µM). For indirect stimulation, a frequency of 20 Hz, 50 Hz and 100 Hz was applied. Data are shown as % of control and are given as mean ± SD (n = 4-25).

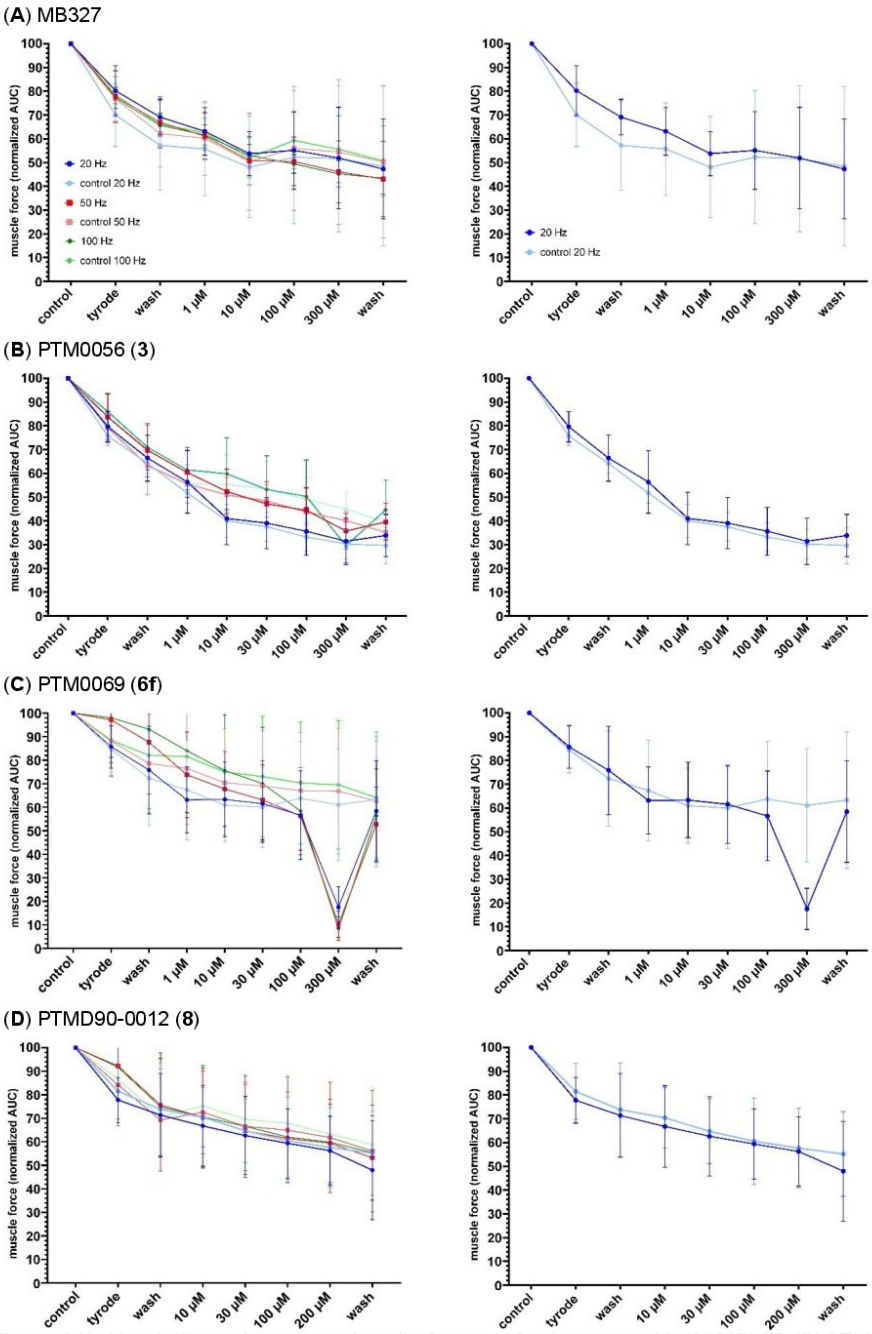

Figure S13: Muscle force of unpoisoned rat diaphragms after treatment with (**A**) MB327, (**B**) PTM0056 (**3**), (**C**) PTM0069 (**6f**) and (**D**) PTMD90-0012 (**8**). For indirect stimulation, a frequency of 20 Hz, 50 Hz and 100 Hz was applied. Muscle force generation was presented as the area under the curve normalized to muscle force under control conditions at the start of the measurement.

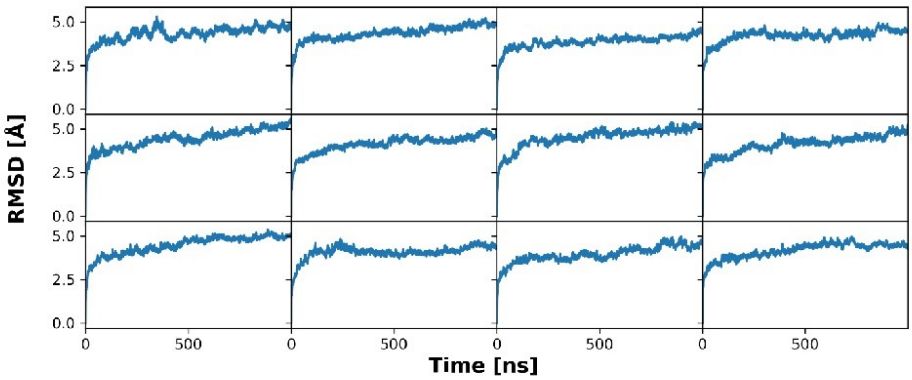

Figure S14: Backbone (C, CA, N) RMSD of 12 replicas of 1 µs long MD simulations of MB327 bound to the human nAChR compared to the first frame of each simulation.

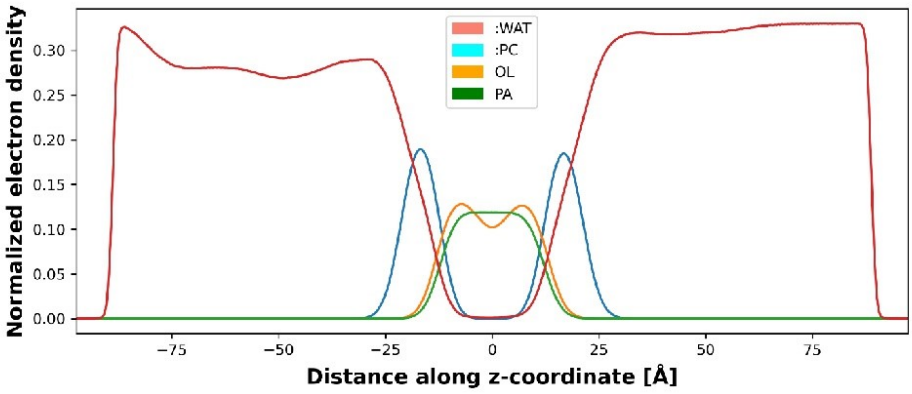

Figure S15: Normalized electron density of water and membrane components averaged over all replicas during MD simulations.

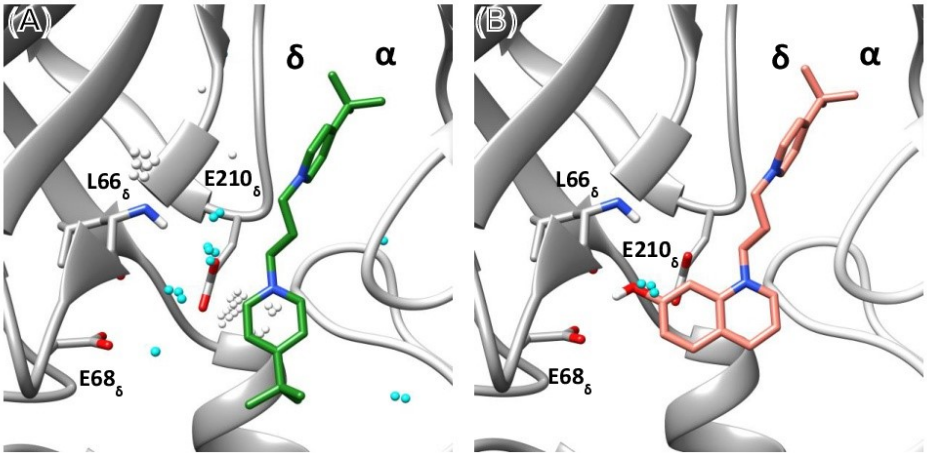

Figure S16: MB327 analog based on substituting water molecules in the allosteric MB327-PAM-1 binding pocket between the α- and δ-subunit. **A)** MB327 binding in between the α- and δ-subunit. Water clusters as identified by GIST are shown as spheres; clusters within 5 Å of MB327 are colored cyan. **B)** Proposed binding mode of PTMD90-0012 (salmon) in between the α- and δ-subunit. Modification of MB327 to PTMD90-0012 (salmon) leads to a substitution of a water cluster located in proximity to L66$_{\delta}$, E68$_{\delta}$, and E210$_{\delta}$. For L66$_{\delta}$, the backbone atoms are shown in addition to the side chain.

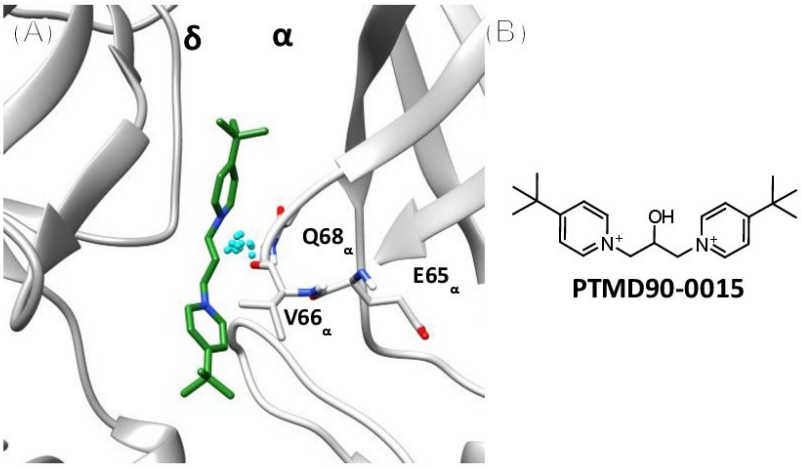

Figure S17: Initial water cluster leading to the design of PTMD90-0015. **A)** During the first few replicas (5 out of 12) of MD simulations of MB327 in MB327-PAM-1, an energetically unfavorable cluster of water molecules was identified in between the backbone atoms of E65$_{\alpha}$, V66$_{\alpha}$, and Q68$_{\alpha}$ close to the C3-linker of MB327 in a representative binding mode during MD simulations (*k*-means clustering based on MB327 atoms ligand between the α- and δ-subunit). Based on these preliminary results, **B)** PTMD90-0015 was designed. This water cluster was later only observed in between the δ- and α-subunit. However, there, no docked or representative structure from MD simulations was in the range to form interactions with the protein after modification of MB327 to PTMD90-0015.

3.3 Dritte Publikation: *Identification of Ligands Binding to MB327-PAM-1, a Binding Pocket Relevant for Resensitization of nAChRs*

3.3.1 Zusammenfassung der Ergebnisse

Allosterische Modulatoren an der MB327-PAM-1-Bindungsstelle des nikotinischen Acetylcholinrezeptors (nAChR) stellen Dank ihres resensitisierenden Effekts auf desensitisierte nAChRs eine vielversprechende Möglichkeit zur Behandlung phosphororganischer Vergiftungen dar. Aufgrund ihrer relativ geringen Affinität zum nAChR und der damit verbundenen geringen therapeutischen Breite sind die bisher hierzu untersuchten Bispyridiniumverbindungen, wie z.B. MB327, für einen Einsatz am Menschen jedoch ungeeignet.

Basierend auf dem kürzlich identifizierten, höheraffinen allosterischen Liganden UNC0646 sowie der kürzlich identifizierten potenziellen Bindungstasche MB327-PAM-1 am nAChR, konnte im Rahmen dieser Veröffentlichung neue vielversprechende Liganden entwickelt bzw. identifiziert werden. Der Einsatz von liganden- sowie strukturbasierten Screeningmethoden gefolgt von pharmakophorbasierten Dockingexperimenten diente, neben einer detaillierten Untersuchung der Bindungstasche im Hinblick auf den Chinazolin-Strukturraum, nicht nur zur Weiterentwicklung von chinazolinbasierten Liganden vom Typ des UNC0646 sondern auch zur Identifizierung weiterer erfolgversprechender Chemotypen.

Im Rahmen einer zweidimensionalen Ähnlichkeitssuche, basierend auf UNC0646, wurden zehn potenzielle Liganden identifiziert und hinsichtlich ihrer Bindungsaffinitäten an die MB327-PAM-1-Bindungstasche untersucht. Besonders vorteilhaft schienen dabei Chinazoline zu sein, die in der 4-Position des Chinazolinrings konformativ flexible, basische Reste enthaltende Substituenten aufweisen. Tatsächlich konnte für ein vor diesem Hintergrund synthetisiertes Chinazolin, PTMD01-0050, mit flexibler 5-(Pyrrolidin-1-yl)pentyl-Teilstruktur in der 4-Position, eine mit UNC0646 vergleichbare Bindungsaffinität festgestellt werden. Die Zielverbindung wurde über eine neu entwickelte zweistufige Synthesesequenz, ausgehend von 2,4-Dichlor-6-methoxy-7-[3-(piperidin-1-yl)propoxy]chinazolin, in guter Ausbeute gewonnen.

Die für die Bindung in der Bindungstasche relevante Konformation der Chinazolin-basierten Liganden, welche in die erste, zweidimensionale Ähnlichkeitssuche nicht mit einfloss, wurde in einem zweiten, dreidimensionalen Screening miteinbezogen. Dieses Screening wurde basierend auf dem in 2-Position unsubstituierten UNC0646-Analogon PTMD01-0004 durchgeführt. Diese Verbindung wurde aufgrund der, verglichen mit UNC0646, vorteilhafteren *ligand efficiency* ausgewählt. Unter den synthetisierten Hits des virtuellen Screenings fiel die Verbindung PTMD01-0043 mit einer deutlichen Reporterligandverdrängung im UNC0642-MS-Bindungsassay auf. Diese Verbindung weist, anstelle der über eine Alkoxyfunktion mit

dem Chinazolinrest verknüpften basischen Seitenkette der bislang untersuchten UNC0646-Analoga, eine 3-(Piperidin-1-ylmethyl)pyrrolidin-Teilstruktur in der 7-Position auf. Die Verbindung konnte ausgehend von dem kommerziell erhältlichen 7-Fluor-6-methoxy-chinazolin-4(3*H*)-on in nur zwei Schritten und in sehr guter Ausbeute gewonnen werden.

Auf der Suche nach neuen potenziellen Resensitizern wurden die virtuellen, ligandenbasierten Screenings schließlich durch strukturbasiertes Screening erweitert. Dabei konnten vier neue Chemotypen (PTMD99-0001C, PTMD99-0016C, PTMD99-0026C und Cycloguanil) identifiziert werden, die eine stärkere Bindung an die MB327-PAM-1-Bindungstasche aufweisen als MB327. Zudem wurden diese vier neuen Chemotypen zusammen mit UNC0646 mit Hilfe von *in silico*-Methoden hinsichtlich ihrer pharmakokinetischen und toxikologischen Eigenschaften charakterisiert. Im Gegensatz zu UNC0646, das unter anderem eine schlechte Zellpermeabilität und Verletzungen von zwei Regeln für die orale Bioverfügbarkeit (Lipinski's Rule of Five) aufweist, entsprechen die neu identifizierten chemischen Strukturen diesen Regeln und lassen insgesamt vielversprechendere pharmakokinetische und toxikologische Eigenschaften erwarten.

Cycloguanil, das unter den vier Substanzen die höchste Reporterligandverdrängung bewirkte, wurde anschließend im Hinblick auf seine intrinsische Aktivität im Ratten-Diaphragma-Assay untersucht. Tatsächlich zeigte es, und zwar bereits bei geringeren Konzentrationen, eine vergleichbare Reaktivierung von Soman-vergifteten Ratten-Diaphragmen wie MB327. Allerdings scheint auch Cycloguanil, ähnlich wie die Bispyridiniumverbindungen, in höheren Konzentrationen eine muskelhemmende Aktivität aufzuweisen.

3.3.2 Darstellung des Eigenanteils

Die Durchführung der *in silico*-Studien sowie die Erstellung des Manuskripts erfolgte durch Jesko Kaiser. Das Manuskript wurde durch Beiträge von mir, Valentin Nitsche und Thomas Seeger ergänzt. Alle Synthesen sowie die analytische Charakterisierung der Verbindungen wurden von mir durchgeführt. Die technische Durchführung der MS- und NMR-Messungen wurde von der Analytikabteilung des Departments für Pharmazie übernommen. Valentin Nitsche führte den UNC0642-MS-Bindungsassay durch. Thomas Seeger übernahm die *ex vivo*-Untersuchungen der Zielverbindungen an Soman-vergifteten Ratten-Diaphragmen. Das Manuskript wurde von Jesko Kaiser in Zusammenarbeit mit Christoph G.W. Gertzen und Holger Gohlke konzipiert und im Wesentlichen von Holger Gohlke und Christoph G.W. Gertzen korrigiert. Zusätzliche Korrekturbeiträge wurden von Georg Höfner, Karin V. Niessen, Dirk Steinritz und Franz Worek und insbesondere Franz F. Paintner und Klaus T. Wanner beigesteuert.

Toxicology Letters 398 (2024) 91–104

Contents lists available at ScienceDirect

Toxicology Letters

journal homepage: www.journals.elsevier.com/toxicology-letters

Identification of ligands binding to MB327-PAM-1, a binding pocket relevant for resensitization of nAChRs

Jesko Kaiser[a,1], Christoph G.W. Gertzen[a,2], Tamara Bernauer[b,3], Valentin Nitsche[b,4], Georg Höfner[b,5], Karin V. Niessen[c,6], Thomas Seeger[c,7], Franz F. Paintner[b,8], Klaus T. Wanner[b,9], Dirk Steinritz[c,10], Franz Worek[c,11], Holger Gohlke[a,d,*,12]

[a] Institute for Pharmaceutical and Medicinal Chemistry, Heinrich Heine University Düsseldorf, Düsseldorf, Germany
[b] Department of Pharmacy – Center for Drug Research, Ludwig-Maximilians-Universität München, Munich, Germany
[c] Bundeswehr Institute of Pharmacology and Toxicology, Munich, Germany
[d] Institute of Bio- and Geosciences (IBG-4: Bioinformatics), Forschungszentrum Jülich, Jülich, Germany

ARTICLE INFO

Editor: Dr. Angela Mally

Keywords:
nAChR
Virtual screening
Molecular dynamics simulations
MS Binding Assay

ABSTRACT

Desensitization of nicotinic acetylcholine receptors (nAChRs) can be induced by overstimulation with acetylcholine (ACh) caused by an insufficient degradation of ACh after poisoning with organophosphorus compounds (OPCs). Currently, there is no generally applicable treatment for OPC poisoning that directly targets the desensitized nAChR. The bispyridinium compound MB327, an allosteric modulator of nAChR, has been shown to act as a resensitizer of nAChRs, indicating that drugs binding directly to nAChRs can have beneficial effects after OPC poisoning. However, MB327 also acts as an inhibitor of nAChRs at higher concentrations and can thus not be used for OPC poisoning treatment. Consequently, novel, more potent resensitizers are required. To successfully design novel ligands, the knowledge of the binding site is of utmost importance. Recently, we performed *in silico* studies to identify a new potential binding site of MB327, MB327-PAM-1, for which a more affine ligand, UNC0646, has been described. In this work, we performed ligand-based screening approaches to identify novel analogs of UNC0646 to help further understand the structure-affinity relationship of this compound class. Furthermore, we used structure-based screenings and identified compounds representing four new chemotypes binding to MB327-PAM-1. One of these compounds, cycloguanil, is the active metabolite of the antimalaria drug proguanil and shows a higher affinity towards MB327-PAM-1 than MB327. Furthermore, cycloguanil can reestablish the muscle force in soman-inhibited rat muscles. These results can act as a starting point to develop more potent resensitizers of nAChR and to close the gap in the treatment after OPC poisoning.

* Correspondence to: Universitätsstr. 1, Düsseldorf 40225, Germany
E-mail address: gohlke@uni-duesseldorf.de (H. Gohlke).
[1] 0000-0002-6429-0911
[2] 0000-0002-9562-7708
[3] 0000-0001-9570-1253
[4] 0009-0000-3351-1227
[5] 0000 0002 7957 4503
[6] 0009-0008-6810-5294
[7] 0009-0007-5713-4367
[8] 0000-0002-6795-586X
[9] 0000-0003-4399-1425
[10] 0000-0002-2073-5683
[11] 0000-0003-3531-3616
[12] 0000-0001-8613-1447

https://doi.org/10.1016/j.toxlet.2024.05.013
Received 21 December 2023; Received in revised form 13 April 2024; Accepted 17 May 2024
Available online 18 May 2024

1. Introduction

Chemical warfare agents remain a serious threat to the military and civilian population. Organophosphorus compounds (OPCs) are one class of chemical warfare agents and block acetylcholinesterase (AChE) covalently (Wiener and Hoffman, 2004). This inhibits the decomposition of acetylcholine causing inflated acetylcholine (ACh) concentrations in the synaptic gap and, thereby, an overstimulation of muscarinic (mAChR) and nicotinic (nAChR) acetylcholine receptors. The overstimulation leads to structural rearrangements of nAChR, resulting in a non-functional, desensitized state (Wiener and Hoffman, 2004; Albuquerque et al., 2009; Unwin, 2013).

While the overstimulation of mAChRs can be treated with atropine, only antidotes (oximes) with insufficient efficiency are available to treat the overstimulation of nAChRs indirectly by reactivating AChE. However, these oximes are ineffective against several OPCs, in particular, when aging leads to altered OPC-enzyme complexes that are less susceptible to reactivation (Thiermann et al., 2013; Worek et al., 2005). Thus, novel antidotes are required to treat OPC poisonings.

The compound MB327 can reestablish the muscle force of OPC-poisoned muscles by interacting directly with nAChRs from several species via an allosteric modulation (Sichler et al., 2018; Scheffel et al., 2018; Niessen et al., 2016, 2018; Seeger et al., 2012). Furthermore, administration of MB327 can prolong the survival rates of guinea pigs after tabun poisoning compared to the oxime HI-6, both in combination with physostigmine and hyoscine (Turner et al., 2011). While these results are promising, MB327 cannot be used in the treatment of OPC poisoning so far because the therapeutic range is too narrow. Restoration of the muscle force in a rat diaphragm myography assay by MB327 increases up to concentrations of 300 µM but decreases at higher concentrations (Niessen et al., 2018; Seeger et al., 2012). Similarly, MB327 initially shows positive allosteric effects on nicotine binding, which decrease at micromolar concentrations. Likewise, MB327 increases the binding of the orthosteric ligand epibatidine up to micromolar concentrations but at higher concentrations decreases it (Scheffel et al., 2018; Niessen et al., 2018). These results indicate that MB327 transmits inhibitory effects on nAChR via binding to the orthosteric binding site, which has recently been experimentally validated for related bispyridinium compounds (Epstein et al., 2021). Additionally, we observed the binding of MB327 to the orthosteric binding site using free ligand diffusion molecular dynamics (MD) simulations (Kaiser et al., 2023). Hence, novel compounds that are more affine and more selective to the allosteric binding site than MB327 need to be identified. A first step in this direction was recently done by us by identifying UNC0646 as an allosteric nAChR ligand with a higher affinity than MB327 (Sichler et al., 2024).

One way to identify novel binders and improve the affinity of known ligands is by using computer-aided drug design methods (Leelananda and Lindert, 2016). In ligand-based screening, one can search for analogs based on two- (topological) or three- (structural) dimensional ligand representations. In two-dimensional similarity screening, the importance of the three-dimensional conformation in the binding site is not taken into account. This can lead to unsatisfactory results, especially for highly flexible ligands. Thus, three-dimensional ligand screening approaches can be more effective in identifying binders that can fit into the binding site and have been used for identifying novel binders successfully in the past (Metz et al., 2013; Dick et al., 2017; Porta et al., 2019; Huo et al., 2022; Ha et al., 2015; Menendez-Gonzalez et al., 2022). However, ligand-based screening approaches neglect explicit knowledge of the receptor structure. Additionally, ligand-based screening may only identify hits with more similar chemical scaffolds compared to the query. Thus, structure-based screening is a popular approach to identifying novel ligands for biological targets and can help to identify novel chemical scaffolds (Gunera et al., 2020; Park et al., 2022; Fink et al., 2022; Park et al., 2021; Benod et al., 2013; Song et al., 2013; Diao et al., 2012; Song et al., 2012). Recently, we identified a novel allosteric binding site of MB327 (MB327-PAM-1) and described a potential binding mode of UNC0646 in MB327-PAM-1 (Kaiser et al., 2023; Nitsche et al., 2024), providing necessary input for three-dimensional ligand-based screening and structure-based screening.

Here, we used this information to perform all three described screening approaches to increase the chance of success and validated hits by a mass spectrometry-based affinity determination (MS Binding Assay). We identified novel substituents (1a-k, 2b-e, 2g) at the UNC0646 quinazoline scaffold that lead to higher affinity and ligands with novel chemotypes [PTMD99–0001C (3), PTMD99–0016C (4), PTMD99–0026C (5), and cycloguanil (6)] binding to MB327-PAM-1.

2. Materials and methods

2.1. Two-dimensional similarity search

The MolPort database was searched for compounds similar to UNC0646 using a two-dimensional search as implemented on the MolPort website (https://molport.com, accessed on October 21st, 2020). All compounds identified by the similarity search using default parameters were selected. From 22 compounds identified, twelve compounds were ordered for testing in this study.

2.2. Homology modeling of nAChR

The homology modeling of the human and *Torpedo* (recently reclassified as *Tetronarce*) nAChR was performed as previously described (Kaiser et al., 2023). In short, homology models were generated using MODELER version 9.19 (Eswar et al., 2006) with the PDB structures 6PV8 (Gharpure et al., 2019), 5KXI (Morales-Perez et al., 2016), 2WH9 (Hibbs et al., 2009), and 6CHK (Walsh et al., 2018) as templates. Water molecules and molecules from the crystallization buffer were removed. Amino acids not resolved in the templates were not included in the models; these amino acids are located within the intracellular loop, the *N*- and *C*-terminal region and, hence, not in the region that forms the MB327-PAM-1 pocket. The final models were selected based on the DOPE potential (Shen and Sali, 2006), TopScore (Mulnaes and Gohlke, 2018), and visual inspection and subsequently protonated using PROPKA, v3.4.0 (Sondergaard et al., 2011; Olsson et al., 2011) as implemented in Schrödinger Maestro, v2021–1 (Schrödinger, 2020) at pH 7.4. The termini were capped with *N*-methyl amide (NME) and acetyl (ACE) groups, respectively.

2.3. Ligand-based screening with subsequent template-based docking

Based on our proposed binding mode of UNC0646 (Nitsche et al., 2024), we used the binding mode of PTMD01–0004 (2a) [Bernauer *et al.*, in preparation], a structurally reduced analog of UNC0646 that lacks the quinazoline substituent in 2-position, as input for ligand-based screening. We created a database from feasible organic reactions of building blocks of PTMD01–0004 (2a) with MolPort (https://molport.com) building blocks as implemented in the PINGUI webserver (https://scubidoo.pharmazie.uni-marburg.de/pingui/, accessed on May 19th, 2021) (SI Figure S1) (Chevillard et al., 2018), resulting in 69,223 in principle synthesizable compounds. We protonated the constituents of the database using OpenEye FixpKa, v2.1.1.0 (QUACPAC 2.1.1.0, 2020) and filtered the database to only use compounds that are at least double positively charged as PTMD01–0004 (2a), resulting in 14,396 compounds and generated conformers using OpenEye OMEGA, v4.1.1.0 (OMEGA 4.1.0.0, 2020; Hawkins et al., 2010) with default parameters except setting the *strictstereo* parameter to false. Initially, we used OpenEye vROCS, v3.4.1.0 (Hawkins et al., 2007; ROCS 3.4.1.0, 2020) (SI Figure S2) to filter the database by applying default parameters and the TanimotoCombo score. The best 1000 hits from the vROCS screening were further investigated using CCG MOE, v2020 (Chemical Computing Group and Molecular Operating Environment MOE, 2021) using a

template-based docking with an upstream pharmacophore filter (SI Figure S3). The hits were analyzed based on visual inspection, and four compounds were selected for synthesizing.

2.4. Synthesis

All target compounds synthesized in the context of this study were cataloged with a PTMD number (Pharmacy and Toxicology Munich and Düsseldorf). All chemicals were used as purchased from commercial sources. Solvents used for purification were distilled before use. 5-Pyrrolidin-1-ylpentan-1-amine, which could only be purchased as the respective hydrochloride salt was converted into the free base before use (Mellsted et al., 2016). Anhydrous reactions were carried out under an argon atmosphere in vacuum-dried glassware. For microwave reactions, a Discover SP microwave system by CEM GmbH was used. TLC-Analysis was performed on plates purchased from Merck (silica gel 60 F_{254} on aluminum sheet). Flash chromatography was carried out using silica gel 60 (40–63 mm mesh size) as stationary phase, purchased from Merck. All synthesized compounds were dried under a high vacuum. ^{1}H and ^{13}C NMR spectra were recorded with a Bruker BioSpin Avance III HD 400 and 500 MHz at 25 °C. For data processing, MestReNova (Version 14.1.0) from Mestrelab Research S.L. 2019, and for calibration, the solvent signal (CD_2Cl_2, CD_3OD or DMSO-d_6) was used. The purity of the test compounds was ≥ 95%, determined by means of quantitative NMR using TraceCERT® ethyl 4-(dimethylamino)benzoate from Merck as an internal calibrant (Pauli et al., 2014; Cushman et al., 2014). High-resolution mass spectra were recorded on a Finnigan MAT 95 (EI) or a Finnigan LTQ FT (ESI). Melting points were determined with a Büchi 510 melting point instrument and are uncorrected. For IR spectroscopy, an FT-IR Spectrometer 1600 from PerkinElmer was used. The analytical data of the synthesized compounds described below, obtained using the described methods, can be found in the Supporting Information.

Synthesis of 2,4-dichloro-6-methoxy-7-[3-(piperidin-1-yl)propoxy] quinazoline (7) recently reported by Vital et al. (2023). and of *N*-(1-cyclohexylpiperidin-4-yl)-6-methoxy-7-[3-(piperidin-1-yl)propoxy]-quinazolin-4-amine (2a) was accomplished according to Bernauer *et al.* [Bernauer *et al.*, in preparation].

General Procedure: Synthesis of quinazolin-4-amines (GP): A solution of the respective 4-chloroquinazoline (8) or (9) (1.0 equiv), the corresponding amine (2.0 equiv - 10 equiv) and *N,N*-diisopropylethylamine (DIEA) (3.0 equiv) in *i*-PrOH (5 mL/mmol) was stirred at 160 °C for 15–60 min under microwave irradiation (200 W). The reaction mixture was concentrated in vacuo and the crude product was purified by flash chromatography [5–15% 3 M NH_3 (in MeOH) in CH_2Cl_2 or 10% MeOH in CH_2Cl_2 + 0.5% DMEA].

6-Methoxy-2-(piperidin-1-yl)-7-[3-(piperidin-1-yl)propoxy] -***N***-[5-(pyrrolidin-1-yl)pentyl] quinazolin-4-amine (1k): According to GP with 8 (126 mg, 0.300 mmol, 1.0 equiv), 5-(pyrrolidin-1-yl)pentan-1-amine (93.8 mg, 0.600 mmol, 2.0 equiv) and DIEA (160 µL, 119 mg, 0.900 mmol, 3.0 equiv) in *i*-PrOH (1.5 mL) for 15 min. 1k (117 mg, 72% yield, 96% purity) was isolated by flash chromatography [7–15% 3 M NH_3 (in MeOH) in CH_2Cl_2] as a colorless solid.

***N*^{1}-Cyclohexyl-*N*^{2}-(6-methoxy-7-[3-(piperidin-1-yl)propoxy] quinazolin-4-yl)-*N*^{1}-methylethane-1,2-diamine (2b): According to GP with 9 (101 mg, 0.300 mmol, 1.0 equiv), N^1-cyclohexyl-N^1-methylethane-1,2-diamine (104 µL, 93.8 mg, 0.600 mmol, 2.0 equiv) and DIEA (160 µL, 119 mg, 0.900 mmol, 3.0 equiv) in *i*-PrOH (1.5 mL) for 1 h. 2b (127 mg, 93%) was isolated by flash chromatography [10% 3 M NH_3 (in MeOH) in CH_2Cl_2] as a yellow oil (96% purity).

6-Methoxy-***N***-[3-(4-methylpiperazin-1-yl)butyl] -7-[3-(piperidin-1-yl)propoxy] quinazolin-4-amine (2c): According to GP with 9 (101 mg, 0.300 mmol, 1.0 equiv), 3-(4-methylpiperazin-1-yl)butan-1-amine (114 µL, 108 mg, 0.600 mmol, 2.0 equiv) and DIEA (160 µL, 119 mg, 0.900 mmol, 3.0 equiv) in *i*-PrOH (1.5 mL) for 1 h. 2c (110 mg, 78% yield, 97% purity) was isolated by flash chromatography [10% 3 M NH_3 (in MeOH) in CH_2Cl_2] as a pale yellow solid.

6-Methoxy-7-[3-(piperidin-1-yl)propoxy] -4-[4-(pyrrolidin-1-yl)piperidin-1-yl] quinazoline (2d): According to GP with 9 (101 mg, 0.300 mmol, 1.0 equiv), 4-(pyrrolidin-1-yl)piperidine (97.4 mg, 0.600 mmol, 2.0 equiv) and DIEA (160 µL, 119 mg, 0.900 mmol, 3.0 equiv) in *i*-PrOH (1.5 mL) for 1 h. 2d (122 mg, 89%) was isolated by flash chromatography [10% 3 M NH_3 (in MeOH) in CH_2Cl_2] as a yellow oil (97% purity).

N-[1-(Azepan-1-yl)-2-methylpropan-2-yl] -6-methoxy-7-[3-(piperidin-1-yl)propoxy] quinazolin-4-amine (2e): According to GP with 9 (134 mg, 0.400 mmol, 1.0 equiv), 1-(azepan-1-yl)-2-methylpropan-2-amine (717 mg, 4.00 mmol, 10 equiv) and DIEA (213 µL, 158 mg, 1.20 mmol, 3.0 equiv) in *i*-PrOH (2.0 mL) for 1 h. 2e (46.4 mg, 25% yield, 97% purity) was isolated by flash chromatography [1. 10% 7 M NH_3 (in MeOH) in CH_2Cl_2, 2. 10% MeOH in CH_2Cl_2 + 0.5% DMEA] as a yellow oil. In addition, a further product fraction of lower purity was obtained (21% yield, 72% purity).

N-(1-Propan-2-ylpiperidin-4-yl)-6-methoxy-7-[3-(piperidin-1-yl)propoxy] quinazolin-4-amine(2f): According to GP with 9 (33.6 mg, 0.100 mmol, 1.0 equiv), 1-propan-2-ylpiperidin-4-amine (31.6 µL, 28.4 mg, 0.200 mmol, 2.0 equiv) and DIEA (53.3 µL, 39.6 mg, 0.300 mmol, 3.0 equiv) in *i*-PrOH (0.5 mL) for 15 min. 2f (41.2 mg, 93%) was isolated by flash chromatography [5–10% 3 M NH_3 (in MeOH) in CH_2Cl_2] as a colorless solid (96% purity).

N-(1-Propan-2-ylpiperidin-4-yl)-6-methoxy-7-[3-(piperidin-1-ylmethyl)pyrrolidin-1-yl] quinazolin-4-amine (2g): A mixture of 10 (111 mg, 0.350 mmol, 1.0 equiv), 1-(pyrrolidin-3-ylmethyl)piperidine (310 mg, 1.75 mmol, 5.0 equiv) and potassium carbonate (53.2 mg, 0.385 mmol, 1.1 equiv) in *N*-methyl-2-pyrrolidone (NMP) (455 µL) was stirred at 135 °C for 20 h. The reaction mixture was concentrated and purified by flash chromatography [5–20% 3 M NH_3 (in MeOH) in CH_2Cl_2] to afford 2g (147 mg, 90%) as a pale yellow solid (99% purity).

4-Chloro-6-methoxy-2-(piperidin-1-yl)-7-[3-(piperidin-1-yl) propoxy] quinazoline (8): A solution of 7 (370 mg, 1.00 mmol, 1.0 equiv) and 1-methylpiperidine (244 µL, 200 mg, 2.00 mmol, 2.0 equiv) in 1,4-dioxane (2.5 mL) was stirred at 150 °C for 1 h under microwave irradiation (300 W). 8 was isolated by flash chromatography (10–20% MeOH in CH_2Cl_2) as a yellow solid (327 mg, 78% yield, 95% purity).

4-Chloro-6-methoxy-7-[3-(piperidin-1-yl)propoxy] quinazoline (9) (Hennequin et al., 2000; Ravez et al., 2014): To a slurry of 11 (22.2 mg, 0.100 mmol, 1.0 equiv), 3-piperidin-1-ylpropan-1-ol (19.9 µL, 18.8 mg, 0.125 mmol, 1.25 equiv), PPh_3 (34.4 mg, 0.130 mmol, 1.3 equiv) and dry THF (1.0 mL) was added di-*tert*-butyl azodicarboxylate (DBAD) (30.5 mg, 0.130 mmol, 1.3 equiv) in portions at 0 °C. The resulting solution was stirred overnight at rt and concentrated under reduced pressure. Purification by flash chromatography [5% 3 M NH_3 (in MeOH) in CH_2Cl_2] afforded 9 as a pale yellow solid (34.5 mg, > 99% yield, 96% purity).

7-Fluoro-***N***-(1-propan-2-ylpiperidin-4-yl)-6-methoxyquinazolin-4-amine (10): A mixture of 12 (20.2 mg, 0.100 mmol, 1.0 equiv), PyBOP (69.0 mg, 0.130 mmol, 1.5 equiv), diazabicycloundecene (DBU) (22.9 µL, 23.3 mg, 0.150 mmol, 1.5 equiv) and 1-propan-2-ylpiperidin-4-amine (23.7 µL, 21.3 mg, 0.150 mmol, 1.5 equiv) in acetonitrile (0.5 mL) was stirred at rt for 1 h. The mixture was concentrated in vacuo. 10 (29.3 mg, 92%) was isolated after flash chromatography [5% 3 M NH_3 (in MeOH) in CH_2Cl_2] as a colorless solid (97% purity).

2.5. Structure-based screening

The SMILES codes of in-stock compounds in the lead-like (3,434,621 compounds) and the double-protonated (129,606 compounds) subsets were downloaded from the ZINC20 database (Irwin et al., 2020). All compounds were protonated using OpenEye FixpKa, v2.1.1.0, and conformers were generated using OpenEye OMEGA, v4.1.0.0 (OMEGA 4.1.0.0, 2020) with default parameters except setting the *strictstereo* parameter to false (OMEGA 4.1.0.0, 2020; Hawkins et al., 2010). The

human and *Torpedo* homology models of nAChR were prepared for docking using OpenEye MakeReceptor, v4.0.0.0, and all compounds were docked using OpenEye FRED, v4.0.0.0 (OEDOCKING 4.0.0.0, 2020; McGann, 2012, 2011), writing out a maximum of one pose per compound. The best 1000 hits in each binding pocket were visually inspected, and 30 compounds were ordered for testing.

2.6. Commercially obtained compounds

The 42 commercially obtainable compounds were purchased from several suppliers with purities of at least 85%. A corresponding, detailed list can be found in the Supporting Information (SI Table S1). For affinity testing in MS Binding Assays, the compounds were applied as described in SI Table S1.

2.7. Molecular dynamics simulations of cycloguanil bound to nAChR

The receptor with the docked ligand was embedded in a membrane of 1-palmitoyl-2-oleoyl-*sn*-glycero-3-phosphocholine (POPC) lipids and solvated using Packmol-Memgen (Schott-Verdugo and Gohlke, 2019) in a rectangular box of TIP3P water (Jorgensen et al., 1983). KCl was added at a concentration of 150 mM and the system was neutralized using Cl^- ions. The edge of the box was set to be at least 12 Å away from receptor atoms. The AMBER22 package of molecular simulations software (Case et al., 2005, 2022) was used in combination with the *ff14SB* force field for the protein (Maier et al., 2015), the Lipid21 force field for the lipids (Dickson et al., 2022), and the Joung and Cheatham parameters for monovalent ions (Joung and Cheatham, 2008). Ligand charges were calculated according to the RESP procedure (Bayly et al., 1993) with default parameters as implemented in antechamber (Wang et al., 2006) using electrostatic potentials generated by Gaussian16 (Frisch et al., 2016) at the HF/6–31G* level of theory; ligand force field parameters were derived from the gaff2 force field. Since cycloguanil (6) should carry one positive charge ($pK_a = 11.4$ (Charman et al., 2020)) on the nitrogen atoms in the 1,6-dihydro-1,3,5-triazine-2,4-diamine ring system, *N*-3 was protonated.

Molecular dynamics (MD) simulations were performed as described earlier (Kaiser et al., 2023) using AMBER22. In short, a combination of steepest descent and conjugate gradient minimization was performed while lowering positional restraints with force constants from 25 kcal mol^{-1} $Å^{-2}$ to zero. Stepwise heating to 300 K and a subsequent reduction of harmonic restraints from 25 kcal mol^{-1} $Å^{-2}$ to zero followed.

Subsequently, 10 replicas of 1 µs length each of unbiased MD simulations were performed; for temperature control, the Langevin dynamics were applied with a collision frequency of 2 ps^{-1}, and the Berendsen barostat with semi-isotropic pressure adaption was used.

Based on the four replicas in which cycloguanil (6) remained within the binding site, we computed representative binding structures of cycloguanil (6) using the *k*-means clustering algorithm, as implemented in CPPTRAJ (Roe and Cheatham, 2013). We then restarted simulations from the representative binding mode. Because the hydrogen bonds to $E62_\gamma$ and $E200_\gamma$ were highly conserved among all clusters except the largest one (containing 18.3% of all frames), we decided to restart simulations from the second largest cluster (containing 14.1% of all frames) (SI Figure S4). Therefore, we started directly with the production run with similar settings as for the docked structure. The first 10 ns of each replica were removed for further analysis.

All simulations were analyzed using CPPTRAJ (Roe and Cheatham, 2013).

2.8. Prediction of physicochemical and toxicological properties

Using OpenEye OMEGA, version 4.1.1.1 (Hawkins et al., 2010; OMEGA 4.1.1.1, 2021), three-dimensional conformations of the compounds based on the SMILES code were generated using the default setting with the exception that only one conformation was generated for each compound. Pharmacokinetic properties and hERG inhibition were predicted using Schrödinger QikProp, version 2022–2 (Schrödinger Release, 2022–2: QikProp, 2022).

For PAINS filtering, the PAINS-remover webserver, v0.99 (https://www.cbligand.org/PAINS/) (Baell and Holloway, 2010), was used. For the prediction of further toxicological properties, we used NEXUS Derek, v6.0.1 (Greene et al., 1999).

2.9. Image generation

Images of nAChR were created using UCSF Chimera (Pettersen et al., 2004).

2.10. Rat diaphragm myography

All procedures using animals followed animal care regulations and were approved by the responsible ethics committee. Preparation of rat diaphragm hemispheres and experimental protocol of myography were performed as described before (Hiessen et al., 2018). In short, for all procedures (including wash-out steps, preparation of soman and bispyridinium compound solutions) aerated Tyrode solution (125 mM NaCl, 24 mM $NaHCO_3$, 5.4 mM KCl, 1 mM $MgCl_2$, 1.8 mM $CaCl_2$, 10 mM glucose, 95% O_2, 5% CO_2; pH 7.4; 25 ± 0.5 °C) was used. After the recording of control muscle force, the muscle preparations were incubated in the Tyrode solution, containing 3 µM soman. Following a 20 min wash-out period, the test compound cycloguanil (Merck KGaA) was added in ascending concentrations (1 µM, 10 µM, 30 µM, 70 µM, 100 µM, 150 µM, 200 µM, 300 µM, 500 µM, 1000 µM). In each preparation, four concentrations were measured to avoid the fatigue effects of muscle force generation. The incubation time was 20 min for each concentration. The electric field stimulation was performed with 10 µs pulse width and 0.2 A amplitudes. The titanic trains of 20 Hz, 50 Hz, 100 Hz were applied for 1 s and in 10 min intervals. Measurements on non-poisoned muscles were carried out according to the same scheme. Instead of soman, pure Tyrode was incubated. Muscle force was calculated as a time-force integral (area under the curve, AUC) and constrained to values obtained for maximal force generation (muscle force in the presence of Tyrode solution without any additives; 100%).

2.11. UNC0642 MS Binding Assays

Competitive MS Binding Assays were performed as described previously (Hitsche et al., 2024). In short, the reporter ligand (UNC0642, 1 µM) and the corresponding test compound (varying concentrations) were incubated with aliquots of a membrane preparation from *Torpedo californica* electroplaque (approx. 75 µg protein per sample) in incubation buffer (120 mM NaCl, 5 mM KCl, 8.05 mM Na_2HPO_4 and 1.95 mM NaH_2PO_4, pH 7.4). Samples were generated in triplicates. After separating the protein-bound from the non-bound reporter ligand in the incubation mixture by centrifugation, the protein-bound portion of UNC0642 was liberated and finally quantified via LC-ESI-MS/MS. Total binding of UNC0642 was normalized to 100% (i.e. reporter ligand binding in the absence of test compound) and 0% (i.e. non-specific reporter ligand binding, determined by the presence of 100 µM UNC0646 instead of test compound). Applying the non-linear regression function "One site – fit Ki" yielded competition curves, which then revealed IC_{50} and K_i values, respectively (Prism software v. 6.07, GraphPad software, La Jolla, CA, USA). Top and bottom levels were fixed at 100% and 0%, respectively, for that purpose. K_i values are given as mean pK_i values from three experiments ± SEM, if not stated otherwise. Next to the full-scale competition experiments, also competition experiments with only a single concentration of test compound (i.e., 10 µM) have been performed in this study. Compared to full-scale competition experiments, the obtained data was not analyzed via non-linear regression in this case and only normalized as described above to reveal the remaining

reporter ligand binding as an indicator for the affinity of the respective test compound. If not stated otherwise, the remaining reporter ligand binding is given as the mean of triplicates ± SD.

3. Results and discussion

3.1. Screening strategy

We used different strategies to identify novel binders of MB327-PAM-1. First, we performed ligand-based screening to identify analogs of UNC0646 using a two-dimensional similarity search as implemented on the MolPort website (https://molport.com) to identify compounds with high similarity to UNC0646 (Fig. 1, blue scheme). Furthermore, we used PTMD01–0004 (2a), an analog with no substituent in the 2-position of the quinazoline ring, to perform ligand-based screening using its three-dimensional binding mode as a query using OpenEye vROCS (Hawkins et al., 2007; ROCS 3.4.1.0, 2020), followed by a pharmacophore-based docking of the best hits using CCG MOE (Chemical Computing Group and Molecular Operating Environment MOE, 2021) (Fig. 1, yellow scheme). Second, to reveal new binders with novel chemical scaffolds, we performed structure-based virtual screenings (Fig. 1, green scheme). There, we first docked a ZINC20 (Irwin et al., 2020) lead-like library (3,434,621 compounds) into the human muscle-type nAChR using OpenEye FRED (OEDOCKING 4.0.0.0, 2020; McGann, 2012, 2011). The lead-like library only includes compounds of a molecular weight between 250 and 350 g mol^{-1}. However, because a higher affinity of known ligands binding to MB327-PAM-1 generally correlates with a larger size of the ligands and most previously described binders feature at least two positive charges (Sichler et al., 2024; Hitsche et al., 2024; Rappengluck et al., 2018a,b), we performed an additional screening using a ZINC20 library (Irwin et al., 2020) of in-stock compounds bearing at least two positive charges (129,606 compounds). To exploit that the amino acids interacting with MB327 and UNC0646 are highly conserved among the human muscle-type and *Torpedo* nAChR (Kaiser et al., 2023; Hitsche et al., 2024) but that the conformations of the sidechains nevertheless vary, we now used the *Torpedo* nAChR for docking to increase the search space. Also, the *Torpedo* nAChR is used in our MS Binding Assays.

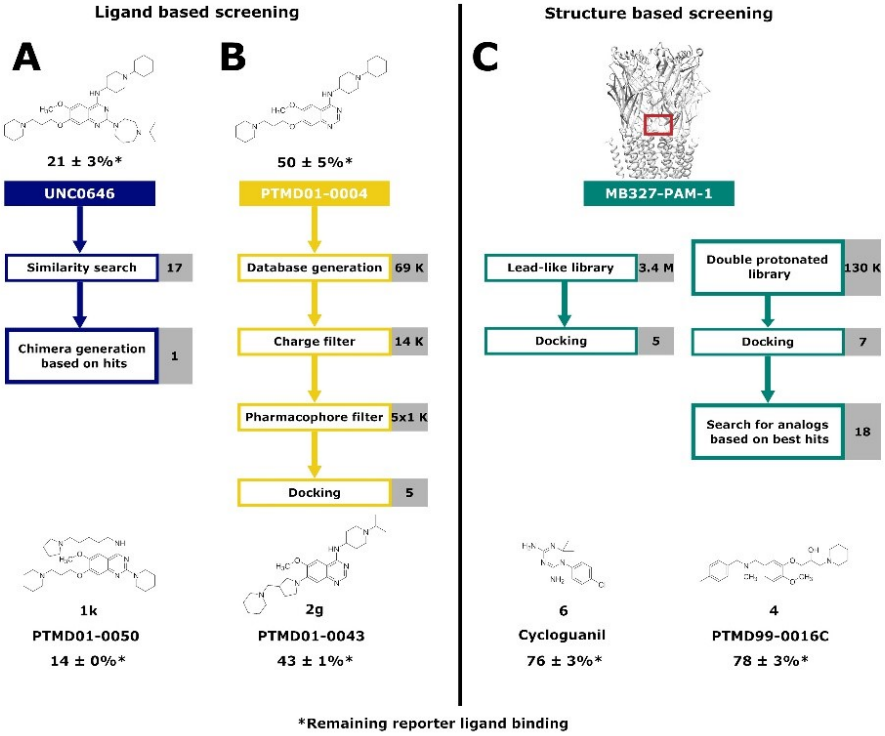

Fig. 1. : Screening strategies to identify novel binders of MB327-PAM-1. **A)** A two-dimensional similarity search using UNC0646 as a template was performed using MolPort (https://www.molport.com/). Based on the hits, one novel chimera compound was designed. **B)** Based on PTMD01–0004 (**2a**), a UNC0646-analog lacking the side chain in the 2-position, a database was generated based on feasible organic reactions (SI Fig. S1). After applying a charge filter and a pharmacophore filter, docking experiments led to five novel analogs of UNC0646. **C)** Based on structure-based screening experiments in the human muscle type and Torpedo nAChR, 5 respectively 7 compounds with novel chemotypes were ordered for affinity characterization in MS Binding Assays. After the first experimental results, 18 additional compounds based on three chemical scaffolds were selected from the initial screening and ordered. This resulted in the identification of cycloguanil (**6**) and PTMD99–0016C (**4**). For each screening strategy, the best hits are shown. Percentage values indicate the remaining reporter ligand binding in the presence of test compounds (at 10 μM concentration) as compared to 100% reporter ligand binding in the absence of a competitor using the reporter ligand UNC0642 in MS Binding Assays (1 μM UNC0642) (mean ± SD, $n = 3$).

3.2. Two-dimensional similarity search yields affine UNC0646 analogs with small substituents in 4-position

Based on a two-dimensional screening of the MolPort library using UNC0646 as a template (Fig. 1, blue scheme), 12 compounds were tested in our MS Binding Assay for MB327-PAM-1 (Nitsche et al., 2024). Of these, 10 compounds displaced the reporter ligand UNC0642 from the binding site at 10 μM (1a-1j; remaining reporter ligand binding at most 90 ± 7%, $n = 3$; Table 1, SI Table S2). The best result was obtained for PTMD01–0019C (1a). In contrast to previously described UNC0646 analogs (Sichler et al., 2024; Nitsche et al., 2024), this is the only compound that does not have a side chain in 7-position with an aliphatic amino group, although mainly acidic amino acid side chains are available for ligand binding in MB327-PAM-1 (Kaiser et al., 2023; Nitsche et al., 2024). However, a study with related 4-amino-2-(*N*,*N*-diethylamino)quinazoline derivatives revealed that the two amino substituents impact the pK_a values of quinazolines resulting in pK_a values of up to 8.31 (Zieliński and Kudelko, 2002) compared to 3.51 of the unsubstituted quinazoline (Armarego, 1963). Thus, PTMD01–0019C (1a) can still be protonated under experimental and physiological conditions, similar to all previously described binders in MB327-PAM-1 (Kaiser et al., 2023; Nitsche et al., 2024; Rappengluck et al., 2018a,b). Furthermore, 4-aminopyridine has a pK_a of 9.17, indicating that even the residue in the 2-position of PTMD01–0019C (1a) may be protonated (Albert et al., 1948). These results are in line with suggestions that a positive charge is crucial for binding in MB327-PAM-1 but also indicate that the location of the positive charge is less important, which can be explained by the many acidic amino acids in MB327-PAM-1 (SI Figure S6, SI Table S3) (Kaiser et al., 2023; Nitsche et al., 2024). To verify the results obtained from the competition experiments by applying a single concentration, we performed full-scale competition studies for the best-binding compound PTMD01–0019C (1a), resulting in a pK_i of 5.19 ± 0.05 (SI Figure S5).

The second strongest reduction of reporter ligand binding was observed for UNC0379 (1b), a ligand with a substituent with increased flexibility at the 4-position compared to UNC0646. Along these lines, the results for ZT-12–037–01 (1c), C-021 (1d), MS012 (1e), PTMD01–0020C (1 f), PTMD01–0021C (1 g), PTMD01–0024C (1 h), and PTMD01–0025C (1i) indicate that for affinity towards MB327-PAM-1, the positively charged amino side chain can be present at either position 2 or position 4 of the quinazoline building block. Furthermore, bunazosin (1j) has no basic side chains at the quinazoline ring but only the two electron donating groups in 2- and 4-positions, further indicating that the positive charge of the ligand might also be located within the heteroaromatic ring. This confirms the above observation that the location of the positive charge is not crucial for the binding of UNC0646 analogs. Based on these results, we synthesized PTMD01–0050 (1k), a chimera inspired by UNC0646, UNC0642, and UNC0379. The synthesis consisting of two steps started from 7 (Vital et al., 2023; Bernauer et al., 2024) (Scheme 1). In analogy to a procedure described in the literature (Yoshida and Taguchi, 1992), 7 was reacted with *N*-methylpiperidine (2.0 equiv) at 150 °C under microwave irradiation for 1 h affording the quinazoline 8 with a piperidine ring in 2-position after column chromatography in good yield (78%). For the subsequent substitution of chloride in 4-position, 8 was stirred with 5-(pyrrolidin-1-yl)pentan-1-amine (2.0 equiv) in the presence of DIEA (3.0 equiv) under microwave irradiation at 160 °C for 15 min. The desired product PTMD01–0050 (1k) could be isolated in good yield (72%). Notably, this compound shows a higher reporter ligand displacement than UNC0646 (Table 1).

3.3. Ligand-based screening using PTMD01-0004 (2a) as a template representing an analog of UNC0646 with a reduced molecular structure

While the two-dimensional similarity search based on UNC0646 yielded new, affine molecules binding to MB327-PAM-1, this approach did not consider the position and orientation of the ligand in MB327-PAM-1. Thus, we also performed a ligand-based screening in MB327-PAM-1 using PTMD01–0004 (2a) (Bernauer et al., 2024) as a template (Fig. 1, yellow scheme). We started with this analog of UNC0646 because the substituent in the 2-position of UNC0646 shows minor interactions with the receptor in our proposed binding mode (Nitsche et al., 2024), and UNC0646 violates the molecular weight rule of Lipinski's "rule of five" (Lipinski et al., 1997), in contrast to PTMD01–0004 (2a). Furthermore, the absence of an electron-donating group in the 2-position only has a minor impact on the affinity (Sichler et al., 2024).

We performed a two-step screening (see Materials and Methods) using a database of synthesizable compounds based on the building blocks of PTMD01–0004 (2a) (SI Figure S1). We selected five compounds that we synthesized (see below) and tested for affinity towards MB327-PAM-1 (2b-2e, 2g, Table 2). The substituents chosen for position 4 did not increase the affinity in any compound compared to PTMD01–0004 (2a). Still, slight modifications in this substituent can influence reporter ligand displacement significantly.

As to the UNC0646 building block, our two-dimensional similarity search revealed that substituting it with flexible linkers in the 4-position can lead to highly affine compounds as seen for PTMD01–0050 (1k). The compound with increased flexibility between the quinazoline ring and the basic side chain nitrogen located within the cyclohexyl ring, PTMD01–0032 (2b), has a higher affinity than PTMD01–0053 (2c). However, the piperazine ring of PTMD01–0053 (2c) might also result in an alternative distance between the positive charge of the side chain and the quinazoline moiety, depending on the protonation site. Still, the relation between linker flexibility and affinity is also observed in PTMD01–0027 (2d), PTMD01–0030 (2e), and PTMD01–0032 (2b), where the distance between the quinazoline ring to the positively charged nitrogen is 3–4 heavy atoms long. The increased flexibility potentially enables improved interactions with the side chains acting as hydrogen bond acceptors in the β1-β2 loop within MB327-PAM-1 ($E65_\gamma$ in SI Figure S6). However, this trend does not always apply. PTMD01–0053 (2c) with a more flexible side chain than PTMD01–0030 (2e) has a lower affinity. Thus, the additional polar atom and the additional methyl substituent of the piperazine ring as well as the different distance between the positive charge in the side chain and the quinazoline moiety of PTMD01–0053 (2c) may also lead to a decrease in affinity. Although experimentally observed structure-affinity relationships for UNC0646 analogs are based on measurements with the *Torpedo* nAChR, this knowledge is presumably transferable to the human muscle-type nAChR because of the high sequence identity within the binding site (SI Figure S6, SI Table S3). However, one limitation of these structure-affinity relationships is that MB327-PAM-1 can be present in five subunits of the heteropentamer. Thus, the relationships need to be considered as a representation over all five potential MB327-PAM-1 binding sites, and structure-affinity relationships between binding sites of one species might vary.

In the 7-position, we identified in PTMD01–0043 (2g), an alternative substituent that leads to a higher reporter ligand displacement than if the same substituent as in UNC0646 is used in the in 7-position [PTMD01–0005 (2f)]. PTMD01–0043 (2g) otherwise bears the same side chains as PTMD01–0005 (2f) except in the 7-position of the quinazoline ring. As for the assessment of the two-dimensional similarity search, we verified our results by characterizing the binding affinity of the most affine compound according to the single point determinations [PTMD01–0043 (2g); remaining reporter ligand binding 43 ± 1%] in a full-scale MS Binding Assay yielding a pK_i of 5.46 ± 0.04 (SI Figure S7).

3.3.1. Synthesis of compounds 2b-2g

Target compounds 2b-2f were easily accessible by a two-step synthesis from commercially available building block 11 (Scheme 2). First, key intermediate 9 (Hennequin et al., 2000) was obtained in quantitative yield (> 99%) by reaction of quinazoline derivative 11 with 1.25 equiv 3-(piperidin-1-yl)propan-1-ol under *Mitsunobu* conditions (1.3 equiv PPh_3, 1.3 equiv DBAD, THF, rt, 20 h) following a literature

Table 1
Selected analogs of UNC0646 identified by a two-dimensional similarity search and their affinities to MB327-PAM-1 in nAChR determined in MS Binding Assays.

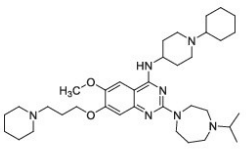

UNC0646

$pK_i = 5.83 \pm 0.05$[a]

Remaining reporter ligand binding: 21 ± 3 %[b]

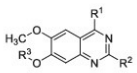

1a-k

Compound	Name / PTMD code	R^1	R^2	R^3	Remaining reporter ligand binding [%][b]
1a	PTMD01-0019C		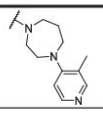		47 ± 3
1b	UNC0379	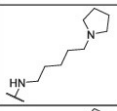			59 ± 4
1k	PTMD01-0050	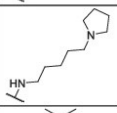			14 ± 0
1c	ZT-12-037-01	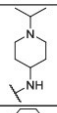			66 ± 5
1d	C-021		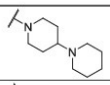		63 ± 2
1e	MS012	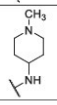	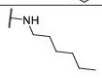		83 ± 6
1f	PTMD01-0020C		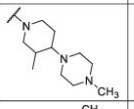		73 ± 7
1g	PTMD01-0021C		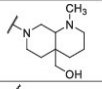		87 ± 2
1h	PTMD01-0024C		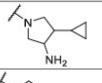		83 ± 4
1i	PTMD01-0025C		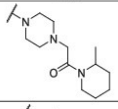		81 ± 5
1j	Bunazosin		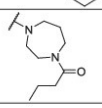		90 ± 7

[a] The pK_i value has been reported in ref (Nitsche et al., 2024).
[b] Characterized by UNC0642 MS Binding Assays; Percentage of remaining reporter ligand binding in the presence of test compounds as compared to 100% reporter ligand binding in the absence of a competitor. Results are based on thirty measurements for UNC0646 and three measurements for all other compounds at a test compound concentration of 10 μM and a reporter ligand concentration of 1 μM. Mean and standard deviation are displayed.

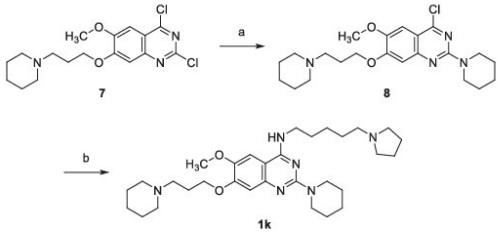

Scheme 1. : Reagents and conditions: (a) 1-methylpiperidine (2.0 equiv), 1,4-dioxane, 150 °C (300 W), 1 h, 78%; (b) 5-(pyrrolidin-1-yl)pentan-1-amine (2.0 equiv), DIEA (3.0 equiv), *i*-PrOH, microwave: 200 W, 160 °C, 15 min, 72%.

procedure (Tasler et al., 2009). In the second step, the 4-amino substituents were introduced to afford the target compounds 2b-2f. Nucleophilic displacement of the 4-chloro substituent was achieved according to a procedure reported in the literature (Liu et al., 2011) by heating 9 with the corresponding amines (2.0 equiv) in the presence of DIEA (3.0 equiv) to 160 °C under microwave irradiation. Thus, 4-aminoquinazolines 2b-2d and 2f were isolated in good to excellent yields (78–93%). However, the reaction with the sterically demanding amine 1-(azepan-1-yl)-2-methylpropan-2-amine to get 2e was sluggish. Hence, a higher excess of the amine (10 equiv) was applied. This led to the target compound, which could be isolated in a yield of 25% only, which is partly due to the fact, that also a small amount of a side-product had formed being difficult to separate.

The 7-aminoquinazoline 2g was synthesized in two steps starting from commercially available 7-fluoro substituted quinazoline-4(3*H*)-one 12 (Scheme 3). In the first step, the lactame 12 was converted to the 4-aminoquinazoline 10 by a phosphonium-mediated S_NAr reaction according to a procedure described in the literature (Wan et al., 2007). Thus, 12 was reacted with 1.5 equiv of 1-propan-2-ylpiperidin-4-amine, PyBOP and DBU in acetonitrile at rt for 1 h, to obtain product 10 in excellent yield (92%). The subsequent substitution of the fluorine in 7-position of 10 to afford target compound 2g was achieved by a reaction of 10 with a 5-fold excess of 1-(pyrrolidin-3-ylmethyl)piperidine in NMP at 135 °C in the presence of K_2CO_3 (1.1 equiv) according to a procedure reported in the literature (Harris et al., 2005). In this way, the product 2g could be isolated in 90% yield and high purity (99%).

Table 2
Selected analogs of PTMD01-0004 (**2a**) identified by a ligand-based screening followed by template-based docking and their affinities to MB327-PAM-1 in nAChR determined in MS Binding Assays.

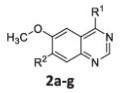

2a-g

Compound	PTMD code	R^1	R^2	Remaining reporter ligand binding [%][a]
2a	PTMD01-0004[b]	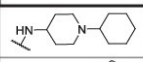	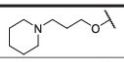	50 ± 5[c]
2b	PTMD01-0032	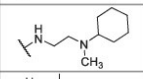	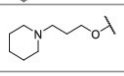	50 ± 7
2c	PTMD01-0053	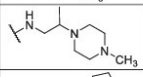	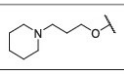	76 ± 7
2d	PTMD01-0027	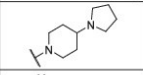	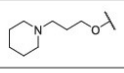	71 ± 3
2e	PTMD01-0030	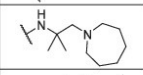	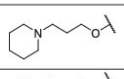	60 ± 3
2f	PTMD01-0005[b]	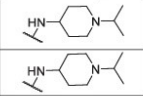	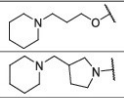	63 ± 4[d]
2g	PTMD01-0043		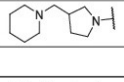	43 ± 1

[a] Characterized by UNC0642 MS Binding Assays; Percentage of remaining reporter ligand binding in the presence of test compounds as compared to 100% reporter ligand binding in the absence of a competitor. If not stated otherwise, results are based on three measurements at a test compound concentration of 10 μM and a reporter ligand concentration of 1 μM. Mean and standard deviation are displayed.
[b] PTMD01–0004 (**2a**) (Bernauer et al., 2024) and PTMD01–0005 (**2f**) were not identified in this study but are shown as reference structures to compare to PTMD01–0043 (**2g**).
[c,d] Results are based on twelve and six measurements, respectively, at a test compound concentration of 10 μM and a reporter ligand concentration of 1 μM. Mean and standard deviation are displayed.

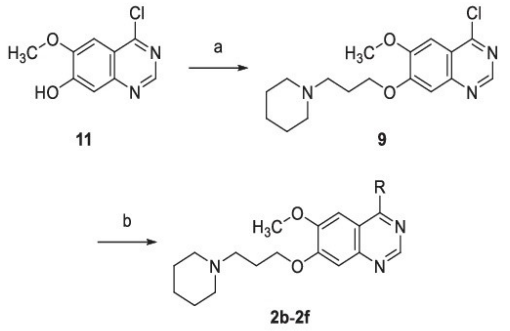

Scheme 2. : Reagents and conditions: (a) 3-piperidin-1-ylpropan-1-ol (1.25 equiv), PPh_3 (1.3 equiv), DBAD (1.3 equiv), THF, rt, 20 h, > 99%; (b) amines (2.0–10 equiv), DIEA (3.0 equiv), *i*-PrOH, microwave: 200 W, 160 °C, 15–60 min, **2b**: 93%, **2c**: 78%, **2d**: 89%, **2e**: 25%, **2f**: 93%.

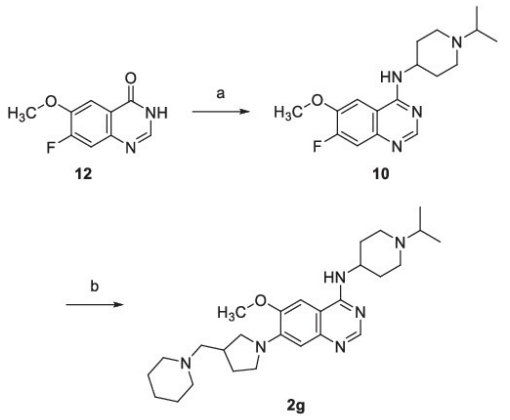

Scheme 3. : Reagents and conditions: (a) 1-propan-2ylpiperidin-4-amine (1.5 equiv), PyBOP (1.5 equiv), DBU (1.5 equiv), acetonitrile, rt, 1 h, 92%; (b) 1-(pyrrolidin-3-ylmethyl)piperidine (5.0 equiv), K_2CO_3 (1.1 equiv), NMP, 135 °C, 20 h, 90%.

3.4. Structure-based screening reveals new chemotypes with a higher affinity than MB327

We first screened the lead-like library of ZINC20 (Irwin et al., 2020) with 3434,621 molecules using the homology model of the human muscle-type nAChR and OpenEye FRED (OEDOCKING 4.0.0.0, 2020; McGann, 2012, 2011) as docking engine with default parameters (Fig. 1, green scheme). However, we know from previous work that larger molecules, such as UNC0646, usually bind to MB327-PAM-1 with a higher affinity than smaller ones, such as MB327. Furthermore, the two previously identified binders in MB327-PAM-1, UNC0646, and MB327, carry at least two positive charges. Thus, we decided to also screen a subset of the ZINC20 database (Irwin et al., 2020) containing all doubly protonated in-stock compounds (129,606 compounds) by docking into the *Torpedo* nAChR (see also above).

We ordered 12 compounds based on visual inspection of the best 1000 hits in MB327-PAM-1 in each subunit in each of the screenings (2 ×5×1000 = 10,000 hits in total) (Fig. 2, SI Table S4) (PTMD99–0001C – PTMD99–0015C). (In preliminary MS binding studies (the results of which had later on to be partly revised; for final results see SI Table S4), PTMD99–0006C (13), PTMD99–0010C (14), and PTMD99–0014C (15) showed the most promising results.) Thus, we decided to inspect the best 1000 hits in both screenings in each subunit again to find structurally similar chemotypes. We ordered three analogs of PTMD099–0006C (13), seven analogs of PTMD99–0010C (14), and eight analogs of PTMD99–0014C (15) (SI Table S5). In each group, at least one compound (at 10 μM concentration) displaced the reporter ligand UNC0642 (at 1 μM concentrations) from MB327-PAM-1 during single-concentration MS Binding Assay experiments indicating that these compounds show a higher affinity towards MB327-PAM-1 than MB327, which shows a remaining marker ligand binding of 102 ± 9% ($n = 6$) under identical conditions (1 μM reporter ligand, 10 μM test ligand) (Bernauer et al., 2024). In total, four new chemotypes, all containing at least one positive charge, were identified that displace UNC0642 from MB327-PAM-1 at concentrations of 10 μM (reporter ligand concentration of 1 μM) to any appreciable extent. However, for two of these compounds the remaining reporter ligand binding values are slightly not significantly different from 100%, while the two other compounds differ significantly from 100% {$p < 0.05$ according to a two-sided one-sample *t*-test; p [PTMD99–0001C (3)] = 0.064, p [PTMD99–0016C (4)] = 0.005, p [PTMD99–0026C (5)] = 0.079, p [cycloguanil (6)] = 0.006}.

Of the analogs based on PTMD99–0006C (13), PTMD99–0016C (4) shows the highest affinity within this group and is the only compound able to displace UNC0642 to any appreciable extent during measurements with test compound concentrations of 10 μM and reporter ligand concentrations of 1 μM. Small changes in the 4-methylbenzyl group can have a high impact on affinity. For example, PTMD99–0020C (16) (SI Table S5), bearing a (3-methylpyridin-4-yl)methyl substituent instead of the 4-methylbenzyl group, does not show a displacement of the reporter ligand to any appreciable extent anymore under identical experimental conditions. In fact, all compounds bearing a heteroaromatic ring instead of the 4-methylbenzyl group fail to displace UNC0642 to any appreciable extent under identical experimental conditions to a reasonable extent.

Based on the initial results for PTMD99–0010C (14), we identified PTMD99–0026C (5), able to displace the reporter ligand (concentration 1 μM) to any appreciable extent at 10 μM test compound concentration. However, compounds with an amide group in 3-position to the nitrogen at position 2 of the 2,8-diazaspiro[4.5]decane system do not displace the reporter ligand UNC0642 under similar experimental conditions to any appreciable extent (PTMD99–0010C (14), PTMD99–0023 C (17), PTMD99–0024C (18), PTMD99–0025C (19), PTMD99–0028C (20) (SI Table S4, S5)). Furthermore, replacing the quinolinyl substituent by a 5-(*tert*-butyl)-pyrazol-3-yl substituent (PTMD99–0031C (21) (SI Table S5)) also abrogates the reporter ligand displacement indicating that hydrogen bond donors as substituents of the 2,8-diazaspiro[4.5] decane ring might be unfavorable.

Additionally, as the fourth novel chemotype binding to MB327-PAM-1, the 1,6-dihydro-1,3,5-triazine-2,4-diamine building block was identified. Most interesting, the compound showing the highest affinity, cycloguanil (6, 10 μM test compound concentration at 1 μM reporter ligand concentration, Fig. 2D), is the active metabolite of the antimalarial drug proguanil. In competitive MS binding experiments, we observed a pK_i value for cycloguanil (6) of 3.64 ± 0.03 (SI Figure S8), significantly higher compared to MB327 [pK_i (MB327) = 3.40 ± 0.04 (Hitsche et al., 2024), $p < 0.01$, according to a two-sided *t*-test]. Cycloguanil (6) forms salt bridges both with $E62_\gamma$ and $E200_\gamma$ in the docked pose (Fig. 2D). These two amino acids are highly conserved among different subunits of several species (Table 3), including the *Torpedo* nAChR, which is used in our MS Binding Assay, the rat muscle nAChR, which is used in our rat diaphragm assays, and in the human nAChR, in which the compounds need to exhibit an effect after OPC poisoning. Furthermore, these glutamates are crucial for the stabilization of the calcium ion in the α7 nAChR that can act as a positive allosteric modulator (Hiessen et al., 2013; Galzi et al., 1996; Hoviello et al.,

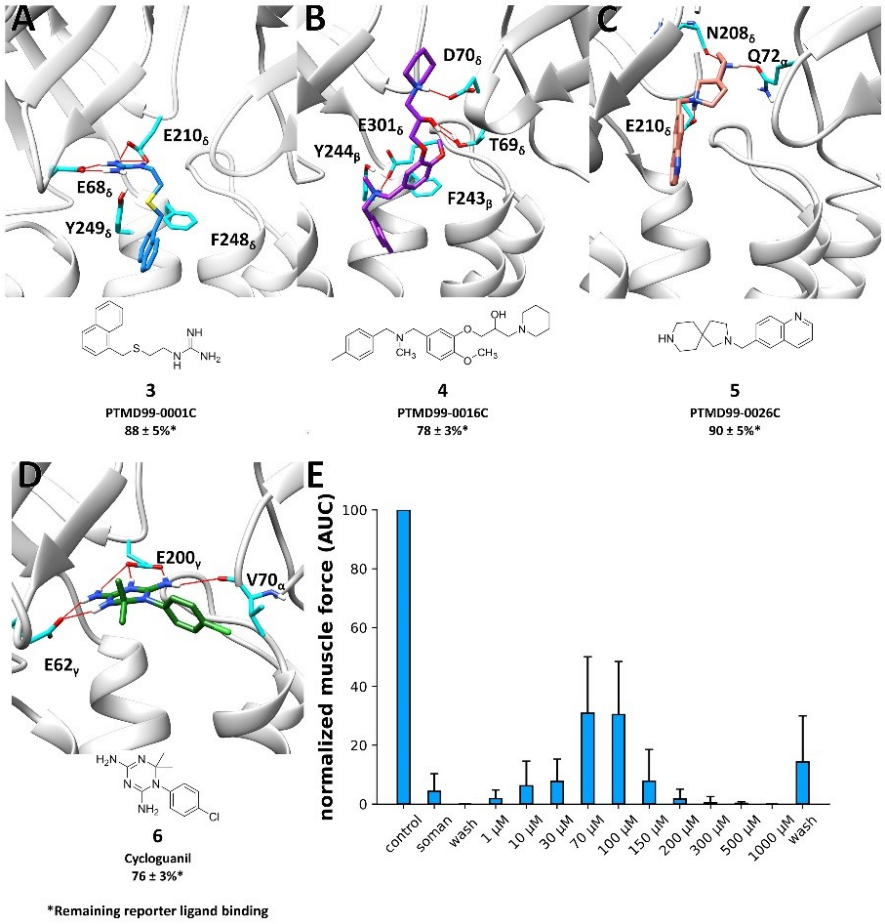

Fig. 2. : Docked binding mode and MS Binding Assay affinity data of selected hits from a structure-based screening in different subunits and species of nAChR. Docked binding mode of **(A)** PTMD99–0001C (**3**) in between the α- and δ-subunits of the human nAChR, **(B)** PTMD99–0016C (**4**) in between the δ- and β-subunits of the *Torpedo* nAChR, **(C)** PTMD99–0026C (**5**) in between the α- and δ-subunits of the *Torpedo* nAChR, and **(D)** cycloguanil (**6**) in between the α- and γ-subunits of *Torpedo* nAChR. Red lines indicate hydrogen bonds. Percentage values indicate the remaining reporter ligand binding in the presence of test compounds (at 10 µM concentration) as compared to 100% reporter ligand binding in the absence of a competitor using the reporter ligand UNC0642 in MS Binding Assays (1 µM UNC0642) (mean ± SD, $n = 3$). Compounds displaying chirality were tested as racemats. **(E)** Resoration of muscle force of soman-inhibited muscles after treatment with cycloguanil (**6**). Error bars indicate the standard deviation (n is between 5 and 27). Since the largest efficacies are observed at low stimulation frequencies (Seeger et al., 2012), results are only shown for a stimulation frequency of 20 Hz (see SI Table S6 for all stimulation frequencies applied).

Table 3
Sequence conservation of $E62_\gamma$ and $E200_\gamma$ (green shadings) in the human muscle-type, *Torpedo*, and rat nAChR with respect to structurally homologous positions in the γ-subunit of the *Torpedo* nAChR.[a]

Human muscle type				*Torpedo*				Rat			
α	β	δ	ε	α	β	δ	γ	α	β	δ	ε
E	E	E	E	E	E	E	E62	E	E	E	E
E	Q	E	E	E	Q	E	E200	E	Q	E	E

[a] $E62_\gamma$ and $E200_\gamma$ are important for interactions with cycloguanil (**6**) in the docked binding mode and during MD simulations (Fig. 3; see also text).

2021). According to our screening results, we can, in general, see that larger substituents at both rings of cycloguanil (**6**) lead to a decrease in affinity (22-28, SI Table S5). Compounds based on the 1,3,5-triazin-2, 4-diamin building block are overall much smaller than UNC0646 (M [UNC0646] = 621.93 g mol^{-1}; M [Cycloguanil (**6**)] = 251.72 g mol^{-1}), leading to compounds with an improved ligand efficiency.

Enough substance to conduct competition experiments with varying ligand concentrations and to perform rat diaphragm assays in order to investigate the restoration of muscle force after soman poisoning was only commercially available for cycloguanil (**6**). Treatment with cycloguanil (**6**) led to significant restoration of muscle force in rat diaphragm hemispheres after soman inhibition (Fig. 2E, SI Table S6). The maximum restoration at stimulation frequencies of 20 Hz is comparable to the

maximum restoration when using MB327 as a treatment option. However, while concentrations of 300 μM are necessary for the maximum effect of MB327 [26.29 ± 18.43% (mean ± SD; $n = 27$) restoration of muscle force, values taken from ref (Kaiser et al., 2023).], cycloguanil (6) exerts a comparable effect at concentrations of 70 μM (30.87 ± 19.23%; $n = 5$). At a concentration of 100 μM, cycloguanil (6) leads to a significantly increased restoration of muscle force compared to MB327 [30.42 ± 18.04% vs. 17.77 ± 7.5%, values for MB327 taken from ref (Kaiser et al., 2023)., $p < 0.01$ according to a two-sided t-test ($n = 27$)]. Like MB327, cycloguanil (6) has a small therapeutic index, leading to muscle force inhibition at concentrations ≥ 300 μM (Fig. 2E, SI Figure S9). To compare the therapeutic range of cycloguanil to that of MB327, we compared the muscle force reestablishing capabilities of both compounds. Therefore, we calculated at which concentrations cycloguanil significantly reestablishes the muscle force after soman poisoning compared to the first wash-out, as done previously for MB327 (Iliessen et al., 2018). Starting at concentrations of 10 μM [6.2 ± 8.4% ($n = 18$; $p = 0.02$)] (100 μM for MB327 [25.7 ± 17.7%] (Iliessen et al., 2018)), cycloguanil significantly and earlier than MB327 reestablishes the muscle force. The effect increases dose-dependently at concentrations of 30 and 70 μM to a maximum at 100 μM [30.4 ± 18.0% ($n = 27$)], whereas the maximum is reached at 300 μM [33.2 ± 27.7%] for MB327 (Iliessen et al., 2018)). At this concentration, the reestablishing capabilities of cycloguanil vanish, whereas this is observed for MB327 at 700 μM (Iliessen et al., 2018) (SI Table S6). Considering that experiments were performed at precise compound concentrations with missing data for intermediate concentrations, this implies that cycloguanil and MB327 have comparable concentration-dependent and maximal reestablishing capabilities as well as therapeutic ranges, although the effect of cycloguanil is shifted to lower concentrations. Thus, cycloguanil (6) currently cannot be considered as a treatment option but as a novel lead structure for treating OPC poisoning.

To further investigate the binding mode of cycloguanil (6), we performed MD simulations starting from the docked conformation. In 6 out of 10 replicas over 1 μs simulation time each, the ligand left the binding site (SI Figure S10). In the replicas where cycloguanil (6) remained in the binding site, the binding mode shifted. Whereas the interaction with the two glutamates persisted, the aromatic system of cycloguanil (6) moved towards the transmembrane region of nAChR in the direction of $Y239_\gamma$ (Fig. 3A). This amino acid is located in a hydrophobic part of the binding site. Thus, we clustered the replica in which cycloguanil (6) remained in the binding site and performed additional 10 replicas of 1 μs long MD simulations starting from a representative structure. During the simulations, the membrane and receptor remained structurally virtually invariant (SI Figure S11, S12). Cycloguanil (6) continued to remain in the binding site in all replicas and showed highly conserved interactions with $E62_\gamma$ and $E200_\gamma$ (Fig. 3B, C). Thus, we conclude that according to the MD-optimized binding mode, the interactions with the two glutamates persist and the hydrophobic interactions with amino acids close to $Y239_\gamma$ are important for ligand stabilization.

3.5. Prediction of pharmacokinetic and toxicological properties of best hits

UNC0646, the best hits of both ligand-based screenings [PTMD01–0050 (1k), PTMD01–0043 (2 g)], and the best hit of each novel chemotype from the structure-based screening [PTMD99–0001C (3), PTMD99–0016C (4), PTMD99–0026C (5), and cycloguanil (6)] were initially probed in a pan interference compounds (PAINS) filter as implemented in the PAINS-remover webserver (Baell and Holloway, 2010); all compounds passed this filter, suggesting that they are less likely to react nonspecifically with biological targets. We further predicted the pharmacokinetic and toxicological properties using Schrödinger QikProp (Schrödinger Release, 2022–2: QikProp, 2022) and NEXUS Derek (Greene et al., 1999) (Table 4, Table 5). By far the most predictions for UNC0646 fall outside a 95% range for values of known drugs, questioning the drug-like properties of this compound. Along these lines, UNC0646 shows the worst Caco-2 cell permeability prediction as a model for gut-blood barrier permeation among all tested compounds and also violates two rules of Lipinski's rule of five and one rule of Jorgensen's rule of three, which are used as indicators for oral bioavailability. By contrast, all newly identified chemotypes show no violations of Lipinski's rule of five, and only PTMD99–0026C (5) violates one rule of Jorgensen's rule of three. Note, however, that the violated pharmacokinetic descriptors describe oral availability, whereas in the case of OPC poisoning drugs may be injected. On the other hand, improved oral bioavailability and reduced side effects might lead to the possibility to provide the antidote to a broader group of civilians and

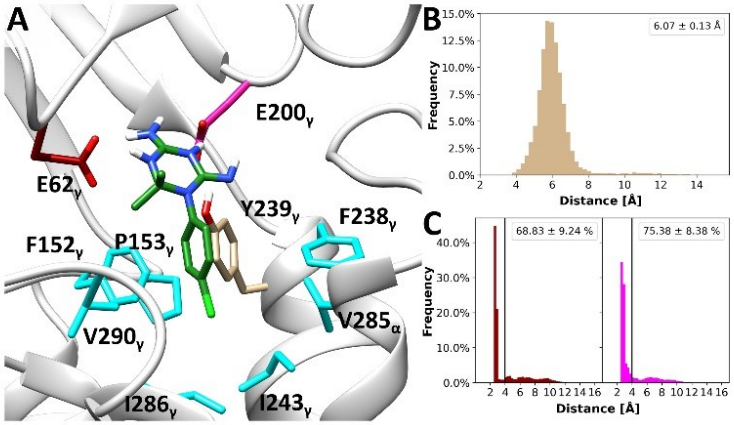

Fig. 3. : Binding mode of cycloguanil during MD simulations. **A)** Representative (according to a k-means clustering based on receptor and ligand atoms; the biggest cluster containing 48.2% of all frames is shown) binding mode of cycloguanil during 10 replicas of 1 μs long unbiased MD simulations starting from the docked conformation. **B)** Distance of the center of mass (COM) of the phenyl ring of cycloguanil to the phenyl ring of $Y239_\gamma$. The mean ± SEM distance is displayed as a legend. **C)** Distance of the nitrogens that can act as hydrogen bond donors of cycloguanil to the side chain oxygens of $E62_\gamma$ (dark red) and $E200_\gamma$ (pink). The frequency of contacts (distance < 4 Å; mean ± SEM) is displayed as a legend.

Table 4
Predicted pharmacokinetic properties of the best screening hits.

Compound	#stars[a]	QPlogPo/w[b]	QPPCaco[c]	RuleOfFive[d]	RuleOfThree[e]
UNC0646	7	6.014	125.427	2	1
PTMD01–0050 (**1k**)	1	5.609	428.531	2	0
PTMD01–0043 (**2g**)	0	4.541	297.484	0	0
PTMD99–0001C (**3**)	0	2.568	615.239	0	0
PTMD99–0016C (**4**)	0	3.718	277.071	0	1
PTMD99–0026C (**5**)	0	2.446	201.628	0	0
Cycloguanil (**6**)	1	1.592	446.492	0	0

[a] Number of properties falling outside the 95% range of similar values for known drugs.
[b] Octanol/water partition coefficient (recommended values: −2.0 – 6.5).
[c] Caco-2 cell permeability [nm/s] as a model for gut-blood barrier permeation (values < 25 poor, > 500 great).
[d] Number of violations of Lipinski's rule of five.
[e] Number of violations of Jorgensen's rule of three.

Table 5
Predicted toxicological properties of the best screening hits.

Compound	QPlogHERG[a]	Toxicological alert count[b]	Bacterial mutagenicity[d]
UNC0646	-8.224	4	EQUIVOCAL
PTMD01–0050 (**1k**)	-6.109	2	EQUIVOCAL
PTMD01–0043 (**2g**)	-7.460	4	EQUIVOCAL
PTMD99–0001C (**3**)	-4.980	0	INACTIVE
PTMD99–0016C (**4**)	-6.125	2	INACTIVE
PTMD99–0026C (**5**)	-6.528	4	PLAUSIBLE
Cycloguanil (**6**)	-3.989	1	INACTIVE

[c] Bacterial mutagenicity in vitro.
[a] IC_{50} value for blockage of HERG K^+ channels (recommended values: above −5).
[b] Number of alerts for toxicological predictions. For further information see SI Table S6.

military members in the case of a high risk of OPC poisoning. Finally, the newly identified chemotypes [PTMD99–0001C (3), PTMD99–0016C (4), PTMD99–0026C (5), and cycloguanil (6)] show a reduced predicted affinity towards the HERG K^+ channel and a reduced toxicological alert count compared to UNC0646 and its analogs [PTMD01–0050 (1k), PTMD01–0043 (2g)]. Also, for the new chemotypes – except PTMD99–0026C (5) – no bacterial mutagenicity is predicted. To overcome the predicted mutagenicity of UNC0646 and its analogs, the substituted 4-anilinoquinazoline would need to be substituted, which is a common building block in all UNC0646 analogs tested in our binding assays so far (Hiltsche et al., 2024). In that respect, all novel compounds identified from the screenings show improved predicted pharmacokinetic properties compared to UNC0646 (Table 4) and, besides PTMD99–0026C (5), all novel chemotypes also display improved predicted toxicological properties (Table 5). Particularly, PTMD99–0001C (3) does not present any toxicologic alerts. PTM99–0016C (4) only shows toxicologic alerts regarding HERG channel inhibition (SI Table S7), however, the predicted IC_{50} is higher than for UNC0646. Because this parameter is problematic for nearly all compounds, it needs to be thoroughly investigated and experimentally validated during lead optimization. PTMD99–0026C (5) raises toxicological concerns regarding mammal mutagenicity and androgen receptor modulation – two parameters where no other compounds show toxicological alerts. Noteworthy, the reason for these toxicological alerts is the quinoline building block. Lastly, cycloguanil raises toxicological concerns regarding nephrotoxicity because of the halogenated benzene. However, proguanil, the prodrug of cycloguanil, is already used in malaria treatment and is considered well tolerated. Thus, in further approaches to optimize these new lead structures, the quinoline substructure of PTM99–0026 C (5) and the halogenated benzene of cycloguanil (6) would need to be modified to avoid these toxicological alerts. Both building blocks are not involved in any hydrogen bonds in the docked binding mode and, thus, might be replaced without compromising affinity towards MB327-PAM-1.

4. Conclusion

To find new compounds representing novel chemotypes that bind to MB327-PAM-1 and to better understand structure-affinity relationships of the known binder UNC0646, we performed exhaustive virtual screening followed by an MS Binding Assay. As to the importance of the substituents of UNC0646 analogs, overall, beneficial substituents in position 4 are also more flexible, suggesting that conformational adaptability may be favorable compared to the loss of conformational entropy. Furthermore, while all compounds known to bind to MB327-PAM-1 carry at least one positive charge, our results indicate that the location of the positive charge plays a minor role. Based on our results, we developed PTMD01–0050 (1k), which leads to a higher reporter ligand displacement at test compound concentrations of 10 μM than UNC0646.

UNC0646 analogs in general show increased binding affinity with increased molecular weight and size. Due to concerns for oral bioavailability and because for some pharmacokinetic and toxicological predictions UNC0646 lies outside the recommended value range, together with the fact that despite an increased affinity UNC0646 and its analogs show no increased muscle force restoration compared to MB327 (Hiltsche et al., 2024), we also aimed to find novel chemotypes binding to MB327-PAM-1. The identified compounds with four novel chemotypes can displace UNC0642 from MB327-PAM-1 (mean ± SD < 100%) at test compound concentrations of 10 μM and reporter ligand concentrations of 1 μM. While one compound (PTMD99–0016C (4)) already has a molecular weight > 400 Da, the other three hits have a molecular weight < 300 Da. These compounds can be used as a starting point for optimization in terms of affinity, pharmacokinetics, and resensitization capability of a desensitized nAChR. Because only for one of those compounds, cycloguanil (6), enough substance was available to perform rat diaphragm myography assays, it was tested for its resensitizing capabilities in soman-inhibited rat muscles and led to a significant muscle force restoration at a concentration of 1 μM. Furthermore, the muscle force restoration was significantly increased compared to MB327 at a concentration of 100 μM. Thus, the cycloguanil building block can be a

promising starting point for further ligand optimization with a focus on annihilating the inhibitory effect at higher concentrations. All novel chemotypes display acceptable predicted pharmacokinetic properties. Cycloguanil already is described to be well-tolerated and shows the least risk for HERG inhibition based on the predictions of toxicological parameters, followed by PTMD99–0001C (3). PTMD99–0016C (4) and PTMD99–0026 (5) lie outside the recommended range. Additionally, PTM99–0026C (5) raises further toxicological concerns regarding mutagenicity and androgen receptor modulation. Taken together, cycloguanil and PTMD99–0001C (3) are the most promising lead structures, followed by PTMD99–0016C (4) because of its size and potential HERG inhibition. PTMD99–0026C (5) already raises several toxicological concerns, which might make lead optimization demanding. However, which novel chemotype is ultimately most promising and should be favored in further studies highly depends on rat diaphragm myography assays for the remaining three compounds.

The identification of more potent resensitizers of nAChR is of utmost importance to improve the currently insufficient treatment after OPC poisonings. Identifying novel chemotypes by structure-based screening and showing with our MS Binding Assay that these compounds can bind in the same binding site as MB327 suggests that the hits also bind to the allosteric binding site MB327-PAM-1.

CRediT authorship contribution statement

Klaus T. Wanner: Writing – review & editing, Supervision, Resources, Project administration, Investigation, Funding acquisition. Karin V. Niessen: Writing – review & editing, Resources, Project administration. Georg Höfner: Supervision, Investigation, Formal analysis. Franz F. Paintner: Writing – review & editing, Supervision, Resources, Project administration, Investigation, Funding acquisition, Formal analysis. Thomas Seeger: Writing – review & editing, Resources, Methodology, Investigation, Formal analysis. Christoph G.W. Gertzen: Writing – review & editing, Validation, Investigation, Formal analysis. Holger Gohlke: Writing – original draft, Supervision, Software, Resources, Project administration, Funding acquisition, Formal analysis, Conceptualization. Jesko Kaiser: Writing – original draft, Visualization, Methodology, Investigation, Formal analysis. Valentin Nitsche: Writing – review & editing, Methodology, Investigation, Formal analysis. Tamara Bernauer: Writing – review & editing, Methodology, Investigation, Formal analysis. Franz Worek: Resources, Project administration, Funding acquisition. Dirk Steinritz: Resources, Project administration, Funding acquisition.

Declaration of Competing Interest

The authors declare that they have no known competing financial interests or personal relationships that could have appeared to influence the work reported in this paper.

Data availability

Data will be made available on request.

Acknowledgments

This work was supported by the German Ministry of Defense (E/U2AD/KA019/IF558). We are grateful for computational support and infrastructure provided by the "Zentrum für Informations- und Medientechnologie" (ZIM) at the Heinrich Heine University Düsseldorf and the computing time provided by the John von Neumann Institute for Computing (NIC) to HG on the supercomputer JUWELS at Jülich Supercomputing Center (JSC) (user IDs: VSK33, nAChR). HG is grateful to OpenEye Scientific Software for granting a Free Public Domain Research License.

Appendix A. Supporting information

Supplementary data associated with this article can be found in the online version at doi:10.1016/j.toxlet.2024.05.013.

References

Albert, A., Goldacre, R., Phillips, J., 1948. 455. The strength of heterocyclic bases. J. Chem. Soc. 0, 2240–2249.
Albuquerque, E.X., et al., 2009. Mammalian nicotinic acetylcholine receptors: from structure to function. Physiol. Rev. 89 (1), 73–120.
Armarego, W.L.F., 1963. Quinazolines. In: Katritzky, R. (Ed.), Adv. Heterocycl. Chem., A. Academic Press, pp. 253–309.
Baell, J.B., Holloway, G.A., 2010. New substructure filters for removal of pan assay interference compounds (PAINS) from screening libraries and for their exclusion in bioassays. J. Med. Chem. 53 (7), 2719–2740.
Bayly, C.I., et al., 1993. A well-behaved electrostatic potential based method using charge restraints for deriving atomic charges: the RESP model. J. Phys. Chem. 97 (40), 10269–10280.
Benod, C., et al., 2013. Structure-based discovery of antagonists of nuclear receptor LRH-1. J. Biol. Chem. 288 (27), 19830–19844.
Bernauer, T., et al., 2024. Synthesis and biological evaluation of novel MB327 analogs as resensitizers for desensitized nicotinic acetylcholine receptors after intoxication with nerve agents. bioRxiv, 2024.02.09.579646.
Case, D.A., et al., 2005. The Amber biomolecular simulation programs. J. Comput. Chem. 26 (16), 1668–1688.
Case, D.A., et al., Amber 2022. 2022, University of California: San Francisco.
Charman, S.A., et al., 2020. An in vitro toolbox to accelerate anti-malarial drug discovery and development. Malar. J. 19 (1), 1.
Chemical Computing Group, U., 2021. Molecular Operating Environment (MOE). 1010 Sehrbooke St. West, Suite #910, Montreal, QC, Canada, H3A, 2R7..
Chevillard, F., et al., 2018. Binding-site compatible fragment growing applied to the design of beta2-adrenergic receptor ligands. J. Med. Chem. 61 (3), 1118–1129.
Cushman, M., et al., 2014. Absolute quantitative ^{1}H NMR spectroscopy for compound purity determination. J. Med. Chem. 57 (22), 9219–9219.
Diao, Y., et al., 2012. Discovery of diverse human dihydroorotate dehydrogenase inhibitors as immunosuppressive agents by structure-based virtual screening. J. Med. Chem. 55 (19), 8341–8349.
Dick, M., et al., 2017. Pyrazolidine-3,5-dione-based inhibitors of phosphoenolpyruvate carboxylase as a new class of potential C4 plant herbicides. FEBS Lett. 591 (20), 3369–3377.
Dickson, C.J., Walker, R.C., Gould, I.R., 2022. Lipid21: complex lipid membrane simulations with AMBER. J. Chem. Theory Comput. 18 (3), 1726–1736.
Epstein, M., et al., 2021. Molecular determinants of binding of non-oxime bispyridinium nerve agent antidote compounds to the adult muscle nAChR. Toxicol. Lett. 340, 114–122.
Eswar, N., et al., 2006. Comparative protein structure modeling using Modeller. Curr. Protoc. Bioinforma.
Fink, E.A., et al., Structure-based discovery of nonopioid analgesics acting through the x3b1;2A-adrenergic receptor. Science, 2022. 377(6614): p. eabn7065.
Frisch, M.J., G.W.T, Schlegel, H.B., Scuseria, G.E., et al., 2016. Gaussian16. Gaussian Inc, Wallingford CT.
Galzi, J.L., et al., 1996. Identification of calcium binding sites that regulate potentiation of a neuronal nicotinic acetylcholine receptor. EMBO J. 15 (21).
Gharpure, A., et al., Agonist selectivity and ion permeation in the x3b1;3×3b2;4 ganglionic nicotinic receptor. Neuron, 2019. 104(3): p. 501-511.e6.
Greene, N., et al., 1999. Knowledge-based expert systems for toxicity and metabolism prediction: DEREK, StAR and METEOR. SAR QSAR Environ. Res 10 (2-3), 299–314.
Gunera, J., et al., 2020. Structure-based discovery of novel ligands for the orexin 2 receptor. J. Med. Chem. 63 (19), 11045–11053.
Ha, H., et al., 2015. Discovery of novel CXCR2 inhibitors using ligand-based pharmacophore models. J. Chem. Inf. Model. 55 (8), 1720–1738.
Harris, C.S., Kettle, J.G., Williams, E.J., 2005. Facile synthesis of 7-amino anilinoquinazolines via direct amination of the quinazoline core. Tetrahedron Lett. 46 (43), 7381–7384.
Hawkins, P.C.D., et al., 2010. Conformer generation with OMEGA: algorithm and validation using high quality structures from the protein databank and Cambridge structural database. J. Chem. Inf. Model. 50 (4), 572–584.
Hawkins, P.C., Skillman, A.G., Nicholls, A., 2007. Comparison of shape-matching and docking as virtual screening tools. J. Med. Chem. 50 (1), 74–82.
Hennequin, L.F., et al., 2000. Quinazoline Derivatives as Angiogenesis Inhibitors (WO-2000047212-A1). W.I.P. Organization.
Hibbs, R.E., et al., 2009. Structural determinants for interaction of partial agonists with acetylcholine binding protein and neuronal α7 nicotinic acetylcholine receptor. EMBO J. 28 (19), 3040–3051.
Huo, D., et al., 2022. Discovery of novel epidermal growth factor receptor (EGFR) inhibitors using computational approaches. J. Chem. Inf. Model. 62 (21), 5149–5164.
Irwin, J.J., et al., 2020. ZINC20-a free ultralarge-scale chemical database for ligand discovery. J. Chem. Inf. Model. 60 (12), 6065–6073.
Jorgensen, W.L., et al., 1983. Comparison of simple potential functions for simulating liquid water. J. Chem. Phys. 79 (2), 926–935.

Joung, I.S., Cheatham, T.E., 2008. Determination of alkali and halide monovalent ion parameters for use in explicitly solvated biomolecular simulations. J. Phys. Chem. B 112 (30), 9020–9041.
Kaiser, J., et al., 2023. A novel binding site in the nicotinic acetylcholine receptor for MB327 can explain its allosteric modulation relevant for organophosphorus-poisoning treatment. Toxicol. Lett. 373, 160–171.
Leelananda, S.P., Lindert, S., 2016. Computational methods in drug discovery. Beilstein J. Org. Chem. 12, 2694–2718.
Lipinski, C.A., et al., 1997. Experimental and computational approaches to estimate solubility and permeability in drug discovery and development settings. Adv. Drug Del. Rev. 23 (1), 3–25.
Liu, F., et al., 2011. Optimization of cellular activity of G9a inhibitors 7-aminoalkoxy-quinazolines. J. Med. Chem. 54 (17), 6139–6150.
Maier, J.A., et al., 2015. ff14SB: improving the accuracy of protein side chain and backbone parameters from ff99SB. J. Chem. Theory Comput. 11 (8), 3696–3713.
McGann, M., 2011. FRED pose prediction and virtual screening accuracy. J. Chem. Inf. Model. 51 (3), 578–596.
McGann, M., 2012. FRED and HYBRID docking performance on standardized datasets. J. Comput. Aided Mol. Des. 26 (8), 897–906.
Mellsted, H., et al., 2016. 2-phenyl-3H-imidazo [4, 5-B] pyridine derivates useful as inhibitors of mammalian tyrosine kinase ROR1 activity. W.I.P. Organization.
Menendez-Gonzalez, J.B., et al., 2022. Ligand-based discovery of a novel GATA2 inhibitor targeting acute myeloid leukemia cells. Front. Drug Discov. 2.
Metz, A., et al., 2013. From determinants of RUNX1/ETO tetramerization to small-molecule protein-protein interaction inhibitors targeting acute myeloid leukemia. J. Chem. Inf. Model. 53 (9), 2197–2202.
Morales-Perez, C.L., Noviello, C.M., Hibbs, R.E., 2016. X-ray structure of the human α4β2 nicotinic receptor. Nature 538 (7625), 411–415.
Mulnaes, D., Gohlke, H., 2018. TopScore: using deep neural networks and large diverse data sets for accurate protein model quality assessment. J. Chem. Theory Comput. 14 (11), 6117–6126.
Niessen, K.V., et al., 2013. Affinities of bispyridinium non-oxime compounds to [(3)H] epibatidine binding sites of Torpedo californica nicotinic acetylcholine receptors depend on linker length. Chem. Biol. Interact. 206 (3), 545–554.
Niessen, K.V., et al., 2016. Functional analysis of Torpedo californica nicotinic acetylcholine receptors in multiple activation states by SSM-based electrophysiology. Toxicol. Lett. 247, 1–10.
Niessen, K.V., et al., 2018. In vitro pharmacological characterization of the bispyridinium non-oxime compound MB327 and its 2- and 3-regioisomers. Toxicol. Lett. 293, 190–197.
Nitsche, V., et al., 2024. MS Binding Assays with UNC0642 as reporter ligand for the MB327 binding site of the nicotinic acetylcholine receptor. Toxicol. Lett. 392, 94–106.
Noviello, C.M., et al., 2021. Structure and gating mechanism of the alpha7 nicotinic acetylcholine receptor. Cell 184 (8), 2121–2134 e13.
OEDOCKING 4.0.0.0. 2020, OpenEye Scientific Software: Santa Fe, NM, USA.
Olsson, M.H., et al., 2011. PROPKA3: consistent treatment of internal and surface residues in empirical pKa predictions. J. Chem. Theory Comput. 7 (2), 525–537.
OMEGA 4.1.0.0. 2020, Openeye Scientific Software: Santa Fe, NM, USA.
OMEGA 4.1.1.1. 2021, Openeye Scientific Software: Santa Fe, NM, USA.
Park, H., et al., 2021. Structure-based virtual screening and De Novo design of PIM1 inhibitors with anticancer activity from natural products. Pharmaceuticals 14 (3), 275.
Park, H., et al., 2022. Structure-based virtual screening and De Novo design to identify submicromolar inhibitors of G2019S mutant of leucine-rich repeat kinase 2. Int. J. Mol. Sci. 23 (21), 12825.
Pauli, G.F., et al., 2014. Importance of purity evaluation and the potential of quantitative ^{1}H NMR as a purity assay. J. Med. Chem. 57 (22), 9220–9231.
Pettersen, E.F., et al., 2004. UCSF Chimera—a visualization system for exploratory research and analysis. J. Comput. Chem. 25 (13), 1605–1612.
Porta, N., et al., 2019. Small-molecule inhibitors of nisin resistance protein NSR from the human pathogen Streptococcus agalactiae. Biorg. Med. Chem. 27 (20), 115079.
QUACPAC 2.1.1.0. 2020, OpenEye Scientific Software: Santa Fe, NM.
Rappengluck, S., et al., 2018b. Synthesis of a series of structurally diverse MB327 derivatives and their affinity characterization at the nicotinic acetylcholine receptor. ChemMedChem 13 (17), 1806–1816.
Rappengluck, S., et al., 2018a. Synthesis of a series of non-symmetric bispyridinium and related compounds and their affinity characterization at the nicotinic acetylcholine receptor. ChemMedChem 13 (24), 2653–2663.
Ravez, S., et al., 2014. Inhibition of tumor cell growth and angiogenesis by 7-Aminoalkoxy-4-aryloxy-quinazoline ureas, a novel series of multi-tyrosine kinase inhibitors. Eur. J. Med. Chem. 79, 369–381.
ROCS 3.4.1.0. OpenEye Scientific Software: Santa Fe, NM. 2020.
Roe, D.R., Cheatham 3rd, T.E., 2013. PTRAJ and CPPTRAJ: software for processing and analysis of molecular dynamics trajectory data. J. Chem. Theory Comput. 9 (7), 3084–3095.
Scheffel, C., et al., 2018. Electrophysiological investigation of the effect of structurally different bispyridinium non-oxime compounds on human alpha7-nicotinic acetylcholine receptor activity-an in vitro structure-activity analysis. Toxicol. Lett. 293, 157–166.
Schott-Verdugo, S., Gohlke, H., 2019. PACKMOL-Memgen: a simple-to-use, generalized workflow for membrane-protein-lipid-bilayer system building. J. Chem. Inf. Model. 59 (6), 2522–2528.
Schrödinger, Maestro, 2020. Schrödinger, LLC.: New York, NY, USA..
Schrödinger Release 2022-2: QikProp. 2022, Schrödinger, LLC: New York, NY.
Seeger, T., et al., 2012. Restoration of soman-blocked neuromuscular transmission in human and rat muscle by the bispyridinium non-oxime MB327 in vitro. Toxicology 294 (2-3), 80–84.
Shen, M.Y., Sali, A., 2006. Statistical potential for assessment and prediction of protein structures. Protein Sci. 15 (11), 2507–2524.
Sichler, S., et al., 2018. Development of MS binding assays targeting the binding site of MB327 at the nicotinic acetylcholine receptor. Toxicol. Lett. 293, 172–183.
Sichler, S., et al., 2024. Screening for new ligands of the MB327-PAM-1 binding site of the nicotinic acetylcholine receptor. Toxicol. Lett. 394, 23–31.
Sondergaard, C.R., et al., 2011. Improved treatment of ligands and coupling effects in empirical calculation and rationalization of pKa values. J. Chem. Theory Comput. 7 (7), 2284–2295.
Song, C.-H., et al., 2012. Structure-based virtual screening and identification of a novel androgen receptor antagonist. J. Biol. Chem. 287 (36), 30769–30780.
Song, Y., et al., 2013. Discovery of non-peptide inhibitors of Plasmepsin II by structure-based virtual screening. Bioorg. Med. Chem. Lett. 23 (7), 2078–2082.
Tasler, S., et al., 2009. Substituted 2-arylbenzothiazoles as kinase inhibitors: Hit-to-lead optimization. Biorg. Med. Chem. 17 (18), 6728–6737.
Thiermann, H., Worek, F., Kehe, K., 2013. Limitations and challenges in treatment of acute chemical warfare agent poisoning. Chem. Biol. Interact. 206 (3), 435–443.
Turner, S.R., et al., 2011. Protection against nerve agent poisoning by a noncompetitive nicotinic antagonist. Toxicol. Lett. 206 (1), 105–111.
Unwin, N., 2013. Nicotinic acetylcholine receptor and the structural basis of neuromuscular transmission: insights from Torpedo postsynaptic membranes. Q. Rev. Biophys. 46 (4), 283–322.
Vital, T., et al., 2023. MS0621, a novel small-molecule modulator of Ewing sarcoma chromatin accessibility, interacts with an RNA-associated macromolecular complex and influences RNA splicing. Front. Oncol. 13, 1099550.
Walsh, R.M., et al., 2018. Structural principles of distinct assemblies of the human α4β2 nicotinic receptor. Nature 557 (7704), 261–265.
Wan, Z.-K., et al., 2007. The scope and mechanism of phosphonium-mediated SNAr reactions in heterocyclic amides and ureas. J. Org. Chem. 72 (26), 10194–10210.
Wang, J., et al., 2006. Automatic atom type and bond type perception in molecular mechanical calculations. J. Mol. Graph. Model. 25 (2), 247–260.
Wiener, S.W., Hoffman, R.S., 2004. Nerve agents: a comprehensive review. J. Intensive Care Med. 19 (1), 22–37.
Worek, F., et al., 2005. Evaluation of oxime efficacy in nerve agent poisoning: development of a kinetic-based dynamic model. Toxicol. Appl. Pharmacol. 209 (3), 193–202.
Yoshida, K., Taguchi, M., 1992. Reaction of N-substituted cyclic amines with 2,4-dichloroquinazoline, 2,4-dichloropyrimidine, and its 5-methyl derivative. J. Chem. Soc., Perkin Trans. 1 (7), 919–922.
Zieliński, W., Kudelko, A., 2002. A study concerning the synthesis, basicity and hydrolysis of 4-amino-2-(N,N-diethylamino)quinazoline derivatives. J. Heterocycl. Chem. 39 (6), 1289–1292.

Supporting Information

Identification of ligands binding to MB327-PAM-1, a binding pocket relevant for resensitization of nAChRs

Jesko Kaiser[1], Christoph G.W. Gertzen[1], Tamara Bernauer[2], Valentin Nitsche[2], Georg Höfner[2], Karin V. Niessen[3], Thomas Seeger[3], Franz F. Paintner[2], Klaus T. Wanner[2], Dirk Steinritz[3], Franz Worek[3], Holger Gohlke[1,4,*]

[1]Institute for Pharmaceutical and Medicinal Chemistry, Heinrich Heine University Düsseldorf, Düsseldorf, Germany

[2]Department of Pharmacy – Center for Drug Research, Ludwig-Maximilians-Universität München, München, Germany

[3]Bundeswehr Institute of Pharmacology and Toxicology, München, Germany

[4]Institute of Bio- and Geosciences (IBG-4: Bioinformatics), Forschungszentrum Jülich, Jülich, Germany

Table of Content

Supplemental Figures

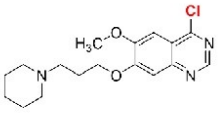

Buchwald-Hartwig
Heck
Negishi
Stille

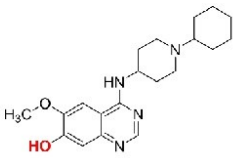

Mitsunobu

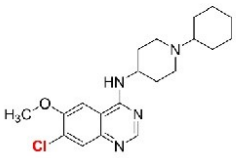

Buchwald-Hartwig
Heck
Negishi
Stille
Suzuki

Figure S1: Building blocks of PTMD01-0004 (**2a**) for the generation of a virtual database. For each building block, the stated virtual syntheses have been performed with building blocks available on MolPort (https://molport.com) using PINGUI [1]. Functional groups that participate in the respective reaction are shown in red.

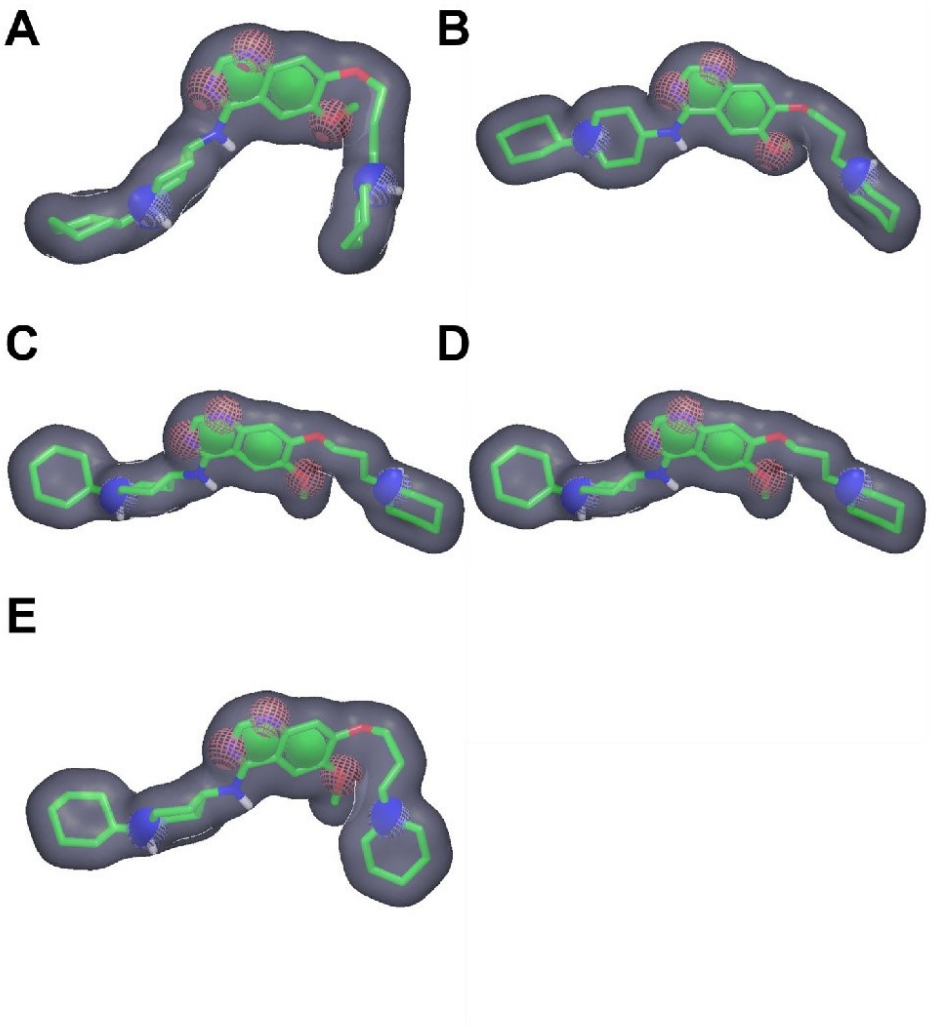

Figure S2: Pharmacophore models used for database filtering during template-based docking. Conformations of PTMD01-0004 (**2a**) (green) are shown as sticks between the **A)** α- and δ-, **B)** δ- and β-, **C)** β- and α-, **D)** α- and γ-, and **E)** γ- and α-subunits. Colored elements indicate pharmacophore filters: the grey surface indicates the ligand surface, green circles indicate aromatic systems, blue circles indicate hydrogen bond donor cations, and red circles indicate hydrogen bond acceptors. Figures were generated using OpenEye vROCS [2].

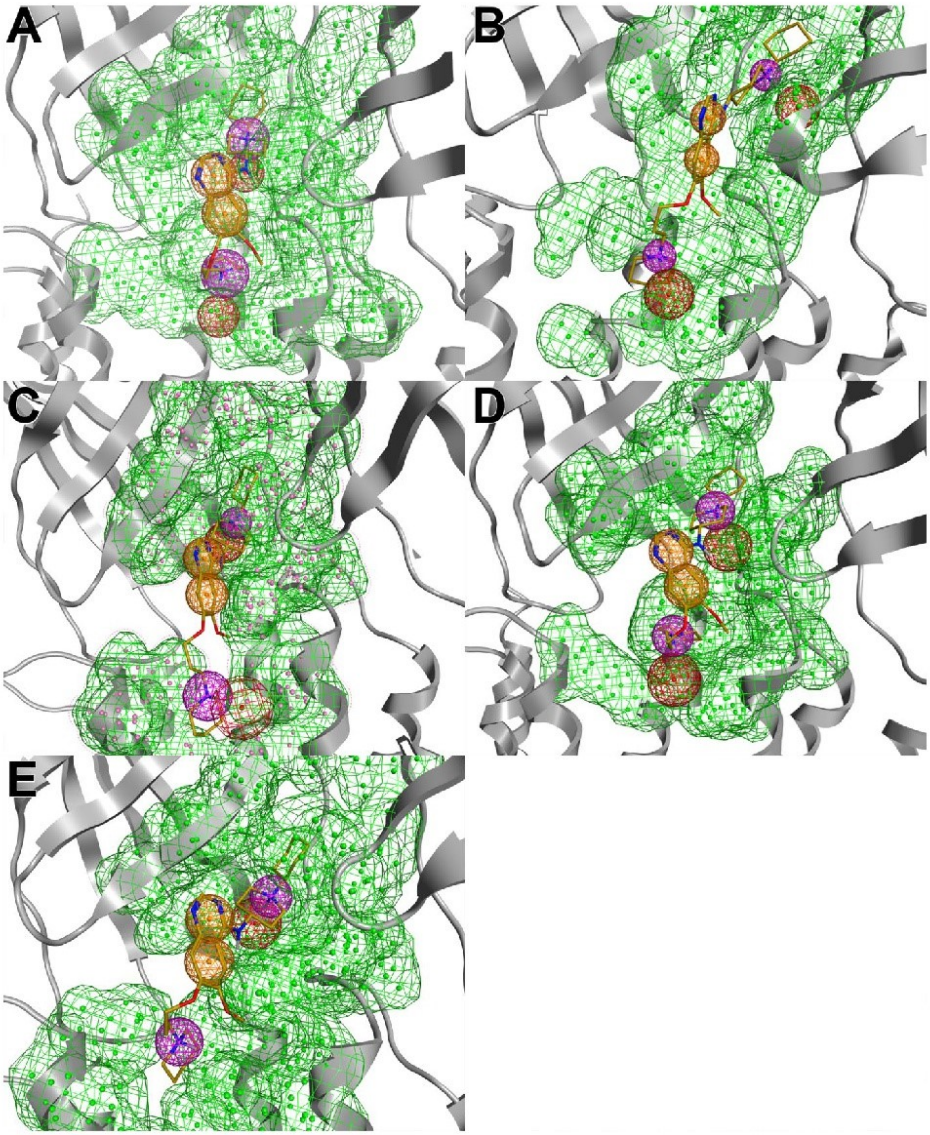

Figure S3: Binding mode of and pharmacophore model for template-based docking based on PTMD01-0004 (**2a**) (gold) shown between the **A)** α- and δ-, **B)** δ- and β-, **C)** β- and α-, **D)** α- and γ-, and **E)** γ- and α-subunits. Colored mesh areas indicate features of the pharmacophore filter: green area indicates the surface of the receptor where no atoms of the ligands are allowed to overlap, orange circles indicate the presence of an aromatic system, purple circles indicate the presence of a cation donor, and red circles indicate the direction of the hydrogen bond donor orientation. Figures were generated using Chemical Computing Group MOE [3].

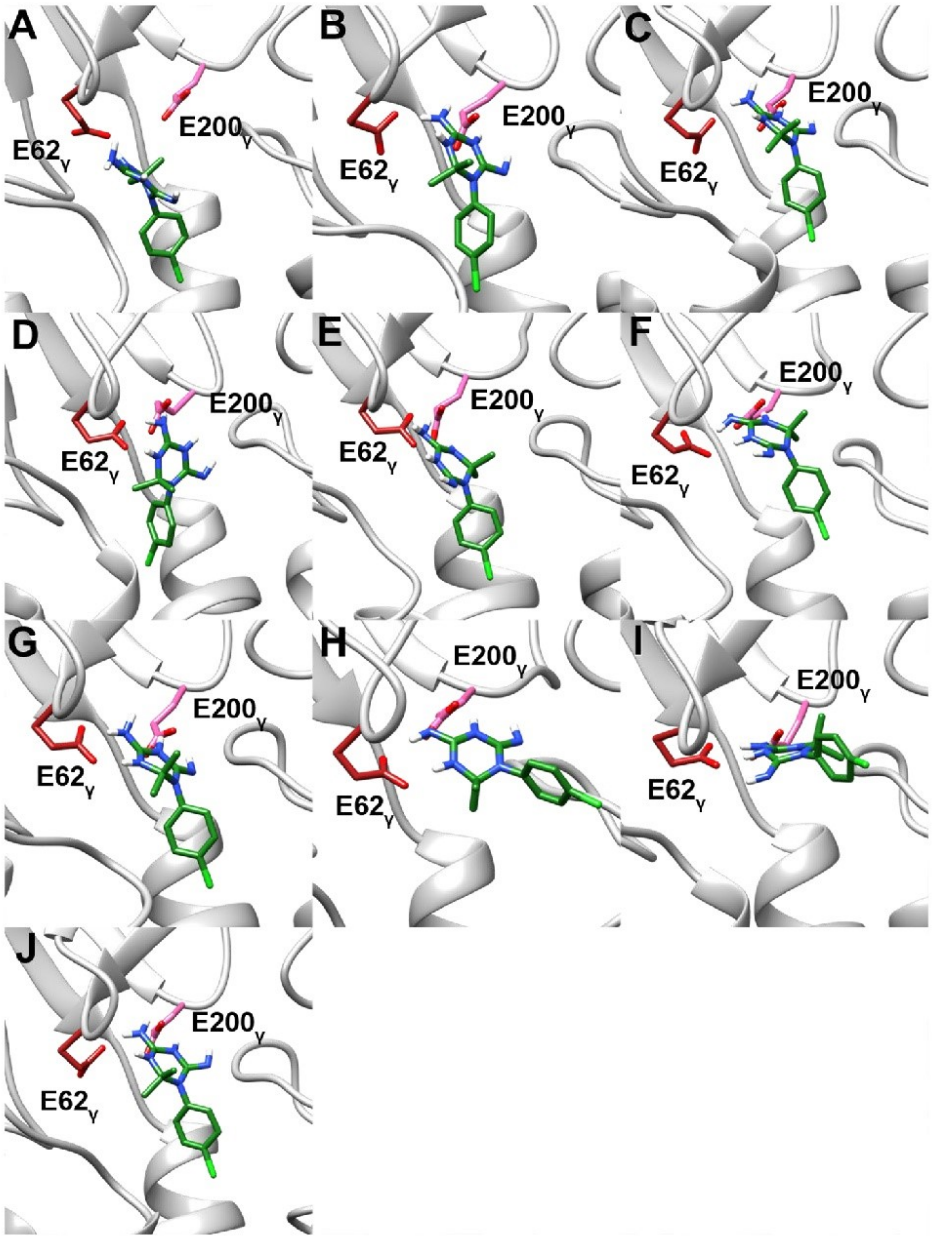

Figure S4: Representative binding modes of cycloguanil in MD simulations starting from the docked binding mode after clustering using the *k-means* algorithm as implemented in CPPTRAJ [4]. **A)** Only in the largest cluster (containing 18.3% of all frames) cycloguanil is not interacting with $E200_{\gamma}$. In the **B)** second (containing 14.1% of all frames), **C)** third (containing 12.4 % of all frames, **D)** fourth (containing 10.9% of all frames), **E)** fifth (containing 10.8% of all frames), **F)** sixth (containing 10.5% of all frames), **G)** seventh (containing 10.1% of all frames), **H)** eight (containing 6.7% of all frames), **I)** ninth (containing 3.6% of all frames), and **J)** tenth (containing 2.5% of all frames) largest cluster, cycloguanil is interacting with $E200_{\gamma}$ and $E62_{\gamma}$.

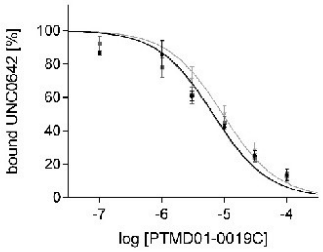

Figure S5: Competition curves obtained for PTMD01-0019C (**1a**) in UNC0642 MS Binding Assays. Data points (mean ± SD, $n = 3$) represent the specific binding of UNC0642.

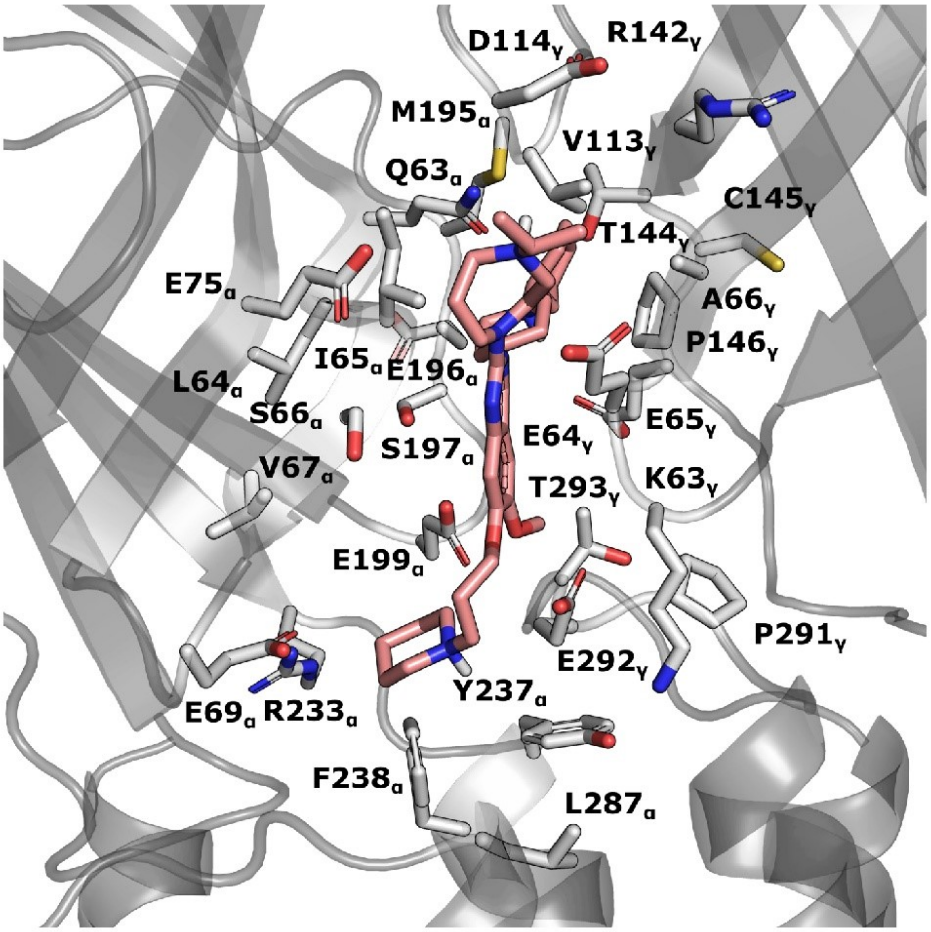

Figure S6: Amino acids within 5 Å of UNC0646 in the recently proposed binding mode of UNC0646 [5].

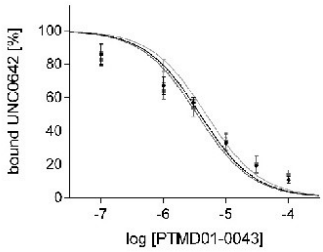

Figure S7: Competition curves obtained for PTMD01-0043 (**2g**) in UNC0642 MS Binding Assays. Data points (mean ± SD, *n* = 3) represent the specific binding of UNC0642.

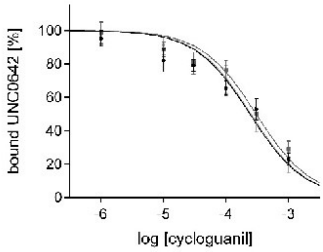

Figure S8: Competition curves obtained for cycloguanil (**6**) in UNC0642 MS Binding Assays. Data points (mean ± SD, *n* = 3) represent the specific binding of UNC0642.

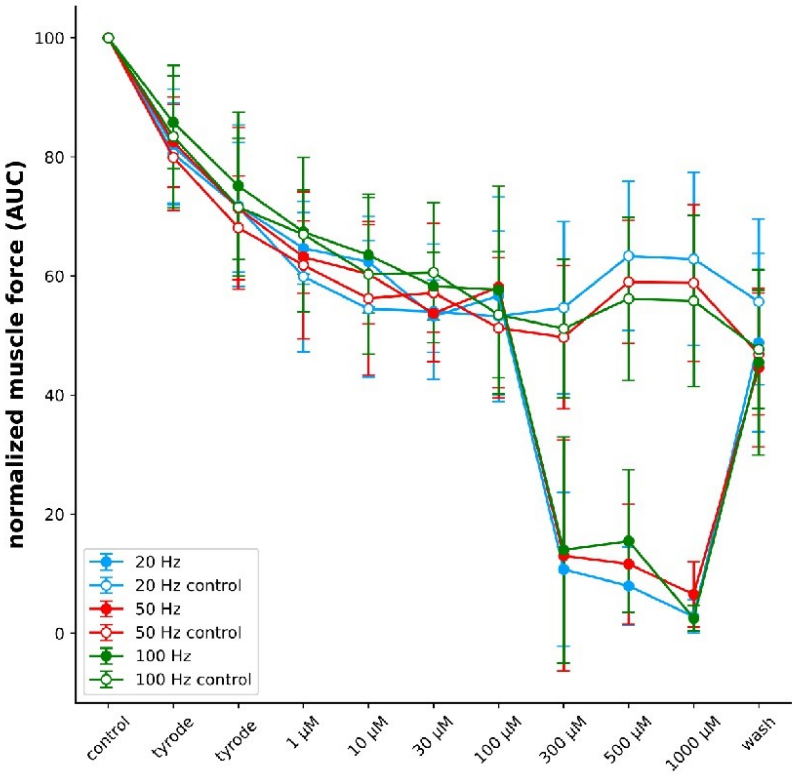

Figure S9: Normalized rat muscle force in the presence of increasing cycloguanil (**6**) concentrations and in the absence of cycloguanil (**6**) (control) during indirect electric field stimulations of 20, 50, and 100 Hz. Error bars indicate the standard deviation (*n* is between 3 and 13).

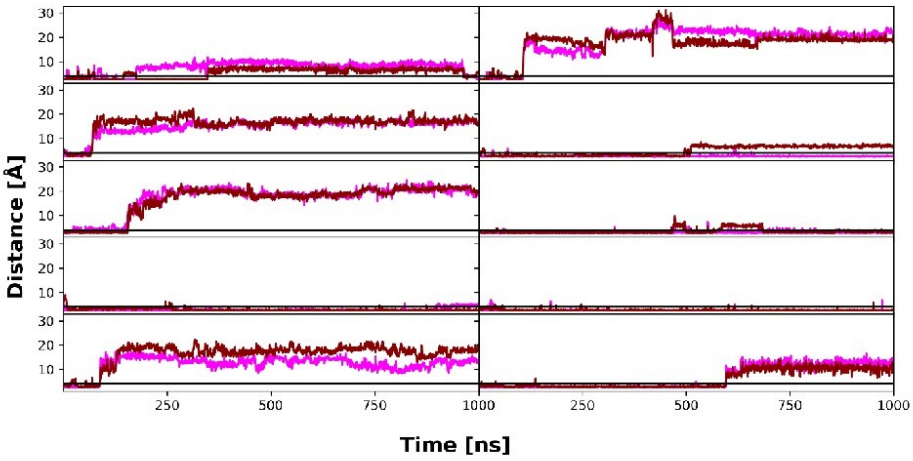

Figure S10: Distance of nitrogens that can act as hydrogen bond donors of cycloguanil to side chain oxygens of $E62_\gamma$ (pink) and $E200_\gamma$ (dark red) during 10 replicas of unbiased MD simulations.

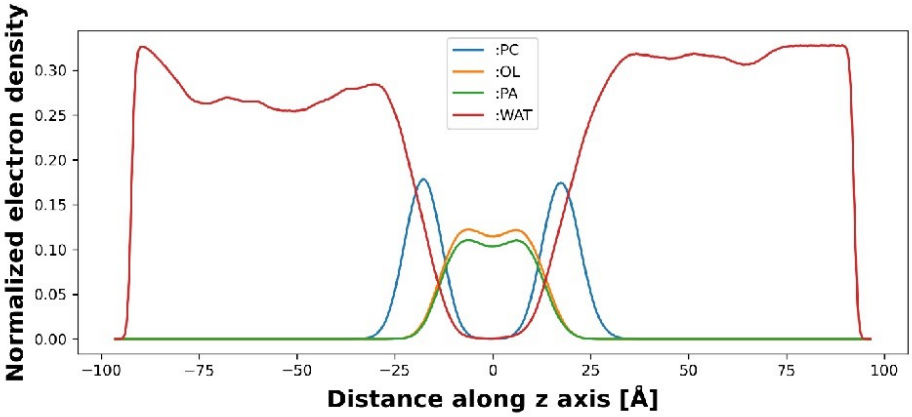

Figure S11: Normalized (number of electrons per volume [$e^-/Å^3$]) electron density of membrane components and water averaged over all 10 replicas of 1 µs long MD simulations. The electron density is plotted against the z-coordinate, which is parallel to the membrane normal. The membrane is centered at 0 Å for phosphatidylcholine (:PC), oleic acid (:OL), palmitoyl acid (:PA), and water (:WAT).

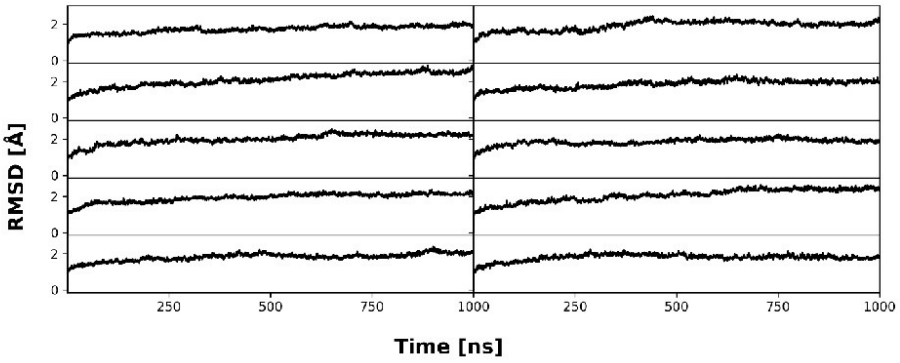

Figure S12: Backbone (C, CA, N) RMSD of nAChR during 10 replicas of 1 µs long MD simulations with respect to the first frame of the production run.

Supplemental Tables

Table S1: List of commercially obtained test compounds.

#	Compound	Salt	Purity	Supplier
1	Bunazosin	-	≥ 95%	Angene (Honk Kong, China)
2	C-021	-	≥ 97%	BIONET – KeyOrganics Ltd (Cornwall, United Kingdom)
3	Cycloguanil	HCl	≥ 95%	Otava Ltd (Kiew, Ukraine)
4	MS012	-	≥ 90%	TimTec, LLC (Newark, United States)
5	PTMD01-0019C	-	≥ 85%	ChemBridge Corporation (San Diego, United States)
6	PTMD01-0020C	-	≥ 90%	Enamine Ltd (Kiew, Ukraine)
7	PTMD01-0021C	-	≥ 85%	ChemBridge Corporation (San Diego, United States)
8	PTMD01-0022C	-	≥ 85%	ChemBridge Corporation (San Diego, United States)
9	PTMD01-0023C	-	≥ 90%	Enamine Ltd (Kiew, Ukraine)
10	PTMD01-0024C	-	≥ 85%	ChemBridge Corporation (San Diego, United States)
11	PTMD01-0025C	-	≥ 90%	Enamine Ltd (Kiew, Ukraine)
12	PTMD99-0001C	HI	≥ 90%	Enamine Ltd (Kiew, Ukraine)
13	PTMD99-0002C	-	≥ 90%	UkrOrgSynthesis Ltd. (Kiew, Ukraine)
14	PTMD99-0004C	2 HCl	≥ 85%	ChemBridge Corporation (San Diego, United States)
15	PTMD99-0005C	-	≥ 90%	ChemBridge Corporation (San Diego, United States)
16	PTMD99-0006C	-	≥ 85%	ChemBridge Corporation (San Diego, United States)
17	PTMD99-0008C	H_2SO_4	≥ 90%	Vitas-M Laboratory Ltd (Causeway Bay, Hong Kong)
18	PTMD99-0009C	HBr	≥ 90%	Enamine Ltd (Kiew, Ukraine)
19	PTMD99-0010C	2 HCl	≥ 85%	ChemBridge Corporation (San Diego, United States)
20	PTMD99-0011C	-	≥ 85%	ChemBridge Corporation (San Diego, United States)
21	PTMD99-0013C	HCl	≥ 90%	ChemBridge Corporation (San Diego, United States)
22	PTMD99-0014C	HCl	≥ 90%	Enamine Ltd (Kiew, Ukraine)
23	PTMD99-0015C	-	≥ 85%	ChemBridge Corporation (San Diego, United States)
24	PTMD99-0016C	-	≥ 85%	ChemBridge Corporation (San Diego, United States)
25	PTMD99-0020C	-	≥ 85%	ChemBridge Corporation (San Diego, United States)
26	PTMD99-0021C	-	≥ 85%	ChemBridge Corporation (San Diego, United States)
27	PTMD99-0023C	2 HCl	≥ 85%	ChemBridge Corporation (San Diego, United States)
28	PTMD99-0024C	2 HCl	≥ 85%	ChemBridge Corporation (San Diego, United States)
29	PTMD99-0025C	2 HCl	≥ 85%	ChemBridge Corporation (San Diego, United States)
30	PTMD99-0026C	2 HCl	≥ 85%	ChemBridge Corporation (San Diego, United States)
31	PTMD99-0028C	2 HCl	≥ 85%	ChemBridge Corporation (San Diego, United States)
32	PTMD99-0029C	2 HCl	≥ 85%	ChemBridge Corporation (San Diego, United States)
33	PTMD99-0031C	2 HCl	≥ 85%	ChemBridge Corporation (San Diego, United States)
34	PTMD99-0032C	HCl	≥ 90%	Maybridge Ltd (Cornwall, United Kingdom)
35	PTMD99-0035C	HCl	≥ 90%	Otava Ltd (Kiew, Ukraine)
36	PTMD99-0036C	HCl	≥ 90%	ChemBridge Corporation (San Diego, United States)
37	PTMD99-0038C	HCl	≥ 95%	Otava Ltd (Kiew, Ukraine)
38	PTMD99-0041C	HCl	≥ 85%	ChemBridge Corporation (San Diego, United States)
39	PTMD99-0044C	HCl	≥ 90%	Maybridge Ltd (Cornwall, United Kingdom)
40	PTMD99-0045C	HCl	≥ 90%	Maybridge Ltd (Cornwall, United Kingdom)
41	UNC0379	-	≥ 98%	TargetMol (Boston, United States)
42	ZT-12-037-01	-	≥ 98%	TargetMol (Boston, United States)

Table S2: All analogs of UNC0646 tested for affinity to MB327-PAM-1 in nAChR determined in MS Binding Assays based on a two-dimensional similarity search.

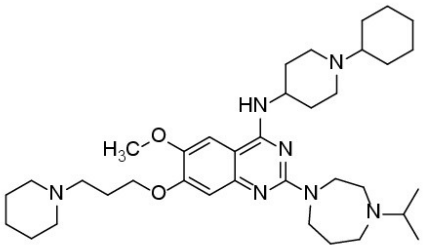

UNC0646
pK_i = 5.83 ± 0.05[a]

Remaining reporter ligand binding: 21 ± 3 %[b]

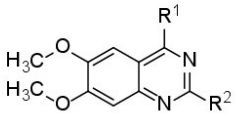

Compound	R^1	R^2	Remaining reporter ligand binding [%][b]
C-021	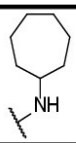	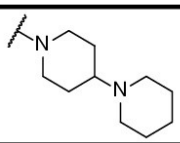	63 ± 2
ZT-12-037-01	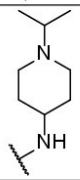		66 ± 5
MS012	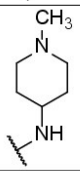	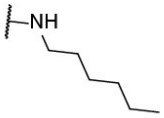	83 ± 6
UNC0379	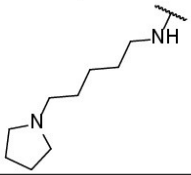		59 ± 4
Bunazosin		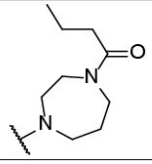	90 ± 7

PTMD01-0019C		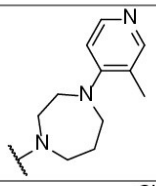	47 ± 3
PTMD01-0020C		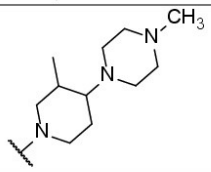	73 ± 7
PTMD01-0021C		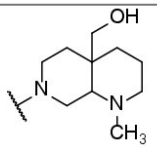	87 ± 2
PTMD01-0022C		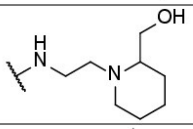	108 ± 10
PTMD01-0023C		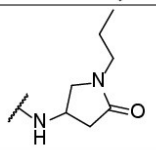	98 ± 3
PTMD01-0024C		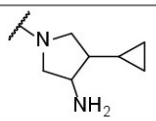	83 ± 4
PTMD01-0025C		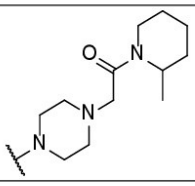	81 ± 5

[a] The pK_i value of UNC0646 has been reported in ref. [6].

[b] Characterized by UNC0642 MS Binding Assays; Percentage of remaining reporter ligand binding in the presence of test compounds as compared to 100% reporter ligand binding in the absence of a competitor. Results are based on thirty measurements for UNC0646 and three measurements for all other compounds at a test compound concentration of 10 µM and a reporter ligand concentration of 1 µM. Mean and standard deviation are displayed.

Table S3: Sequence similarity between the *Torpedo* and human muscle-type nAChR.[a]

α - subunit		β - subunit		δ - subunit		γ - subunit		ε - subunit
Torpedo	human	*Torpedo*	human	*Torpedo*	human	*Torpedo*	human	human
Q63	Q	N	Q	N	N	N	N	N
L64	L	L	L	L	L	L	L	L
I65	I	L	I	I	I	I	I	I
S66	N	I	S	S	S	S	S	S
V67	V	L	L	L	L	L	L	L
E69	E	E	E	E	E	E	E	E
E75	T	T	S	T	T	T	T	T
M195	M	T	I	T	T	T	T	T
E196	E	E	E	E	E	E	E	E
S197	S	N	N	N	N	N	N	N
E199	E	Q	Q	E	E	E	E	E
R233	R	R	R	R	R	R	R	R
Y237	Y	F	F	F	F	F	F	F
F238	F	Y	Y	Y	Y	Y	Y	Y
L287	L	K	K	R	R	K	K	K
V	V	K	K	T	V	K63	R	K
N	N	I	D	D	E	E64	E	E
Q	Q	E	E	E	E	E65	E	E
I	I	E	E	T	T	A66	A	T
A	A	N	N	N	N	V113	V	I
D	D	D	D	D	D	D114	D	D
K	K	R	R	R	R	R142	R	R
Y	Y	S	S	S	S	T144	A	V
C	C	C	C	C	C	C145	C	C
E	E	T	S	P	P	P146	S	A
P	P	P	P	P	P	P291	P	P
S	S	E	E	E	A	E292	E	E
T	T	T	T	T	T	T293	T	T

[a] Numbered amino acids are also shown in Figure 2. Amino acid differences between *Torpedo* and human muscle-type nAChR are colored blue for identical chemical properties and orange for deviating chemical properties.

Table S4: Results of affinity testing to MB327-PAM-1 in nAChR determined in MS Binding Assays of initial compounds ordered based on structure-based screening.

Name	Structure	Remaining reporter ligand binding [%][a]
PTMD99-0001C (**3**)	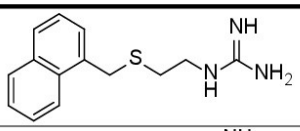	88 ± 5
PTMD99-0002C	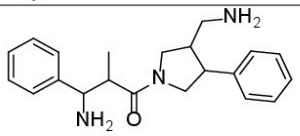	101 ± 9
PTMD99-0004C	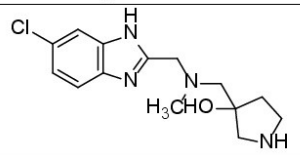	92 ±7
PTMD99-0005C	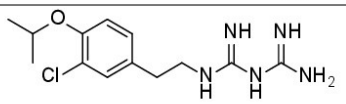	101 ± 3
PTMD99-0006C (**13**)	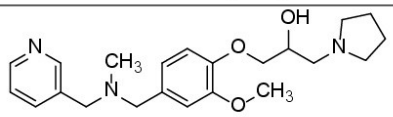	93 ± 7
PTMD99-0008C	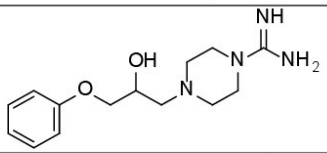	95 ± 4
PTMD99-0009C	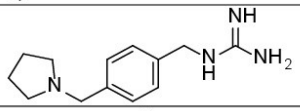	92 ± 9
PTMD99-0010C (**14**)	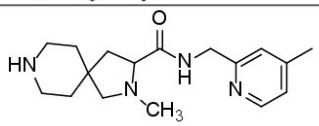	96 ± 5
PTMD99-0011C	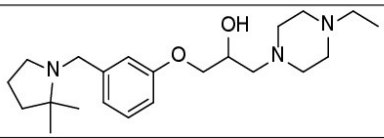	95 ± 7
PTMD99-0013C	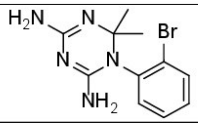	101 ± 6

PTMD99-0014C (**15**)	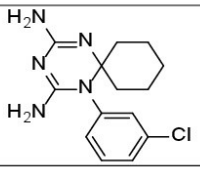	94 ± 6
PTMD99-0015C	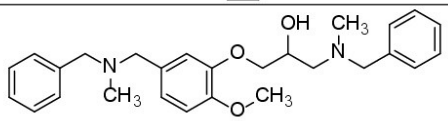	98 ± 8

[a] Characterized by UNC0642 MS Binding Assays; Percentage of remaining reporter ligand binding in the presence of test compounds as compared to 100% reporter ligand binding in the absence of a competitor. If not stated otherwise, results are based on three measurements at a test compound concentration of 10 µM and a reporter ligand concentration of 1 µM. Mean and standard deviation are displayed.

Table S5: Results of affinity testing of compounds analogous to the best hits from the initially ordered compounds based on structure-based screening.

Name	Structure	Remaining reporter ligand binding [%][a]
PTMD99-0016C (**4**)	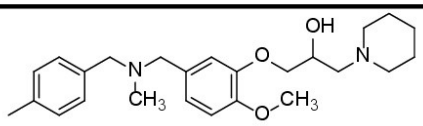	78 ± 3
PTMD99-0020C (**16**)	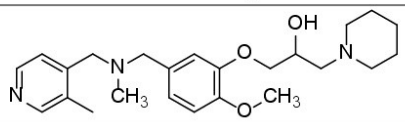	97 ± 4
PTMD99-0021C	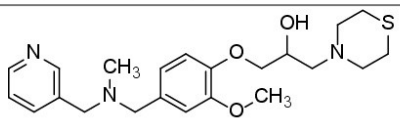	107 ± 11
PTMD99-0023C (**17**)	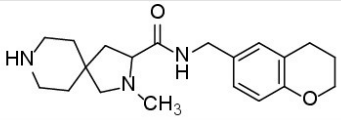	108 ± 4
PTMD99-0024C (**18**)	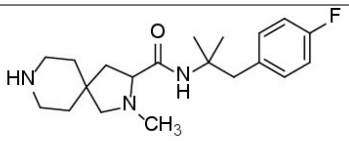	99 ± 6
PTMD99-0025C (**19**)	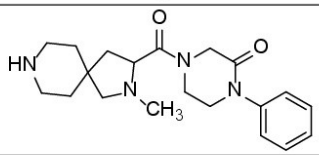	100 ± 6
PTMD99-0026C (**5**)	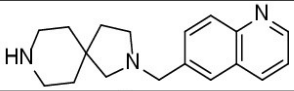	90 ± 5
PTMD99-0028C (**20**)	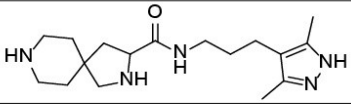	101 ± 7
PTMD99-0029C	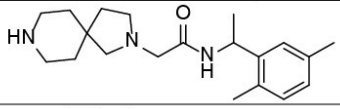	98 ± 4
PTMD99-0031C (**21**)	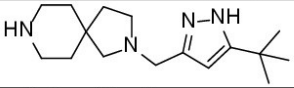	101 ± 8
PTMD99-0032C (**22**)	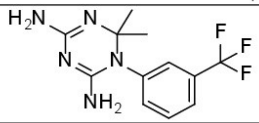	98 ± 6

PTMD99-0035C (**23**)	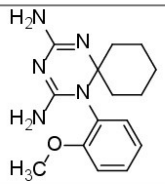	109 ± 8
PTMD99-0036C (**24**)	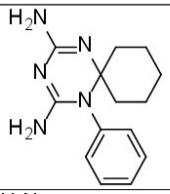	93 ± 4
PTMD99-0038C (**25**)	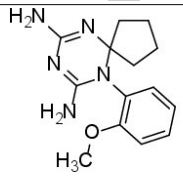	100 ± 4
Cycloguanil (**6**)	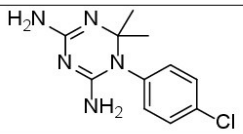	76 ± 3
PTMD99-0041C (**26**)	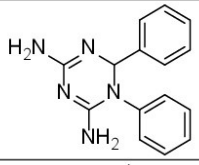	81 ± 3
PTMD99-0044C (**27**)	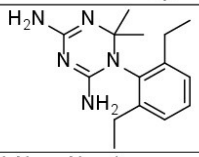	106 ± 6
PTMD99-0045C (**28**)	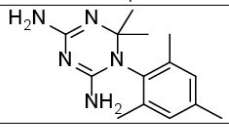	95 ± 8

[a] Characterized by UNC0642 MS Binding Assays; Percentage of remaining reporter ligand binding in the presence of test compounds as compared to 100% reporter ligand binding in the absence of a competitor. If not stated otherwise, results are based on three measurements at a test compound concentration of 10 µM and a reporter ligand concentration of 1 µM. Mean and standard deviation are displayed.

Table S6: Restoration of muscle force in soman-inhibited rat muscles after cyclouanil (**6**) treatment.[a]

	20 Hz			50 Hz			100 Hz		
	Mean [%]	SD [%]	n	Mean [%]	SD [%]	n	Mean [%]	SD [%]	n
control	100.00	0.00	27	100.00	0.00	27	100.00	0.00	27
soman	4.30	6.02	27	3.86	8.36	27	4.51	8.95	27
wash	0.00	0.00	27	0.00	0.00	27	0.00	0.00	27
1 µM	1.86	2.91	13	0.64	1.29	13	0.40	1.00	13
10 µM	6.20	8.40	18	0.82	1.28	18	0.25	0.56	18
30 µM	7.66	7.64	5	1.38	2.34	5	1.14	2.51	5
70 µM	30.87	19.23	5	2.76	3.51	5	0.68	1.32	5
100 µM	30.42	18.04	27	4.68	4.76	27	1.29	2.72	27
150 µM	7.78	10.79	9	0.85	1.33	9	0.28	0.57	9
200 µM	1.69	3.35	4	0.23	0.41	4	0.00	0.00	4
300 µM	0.51	2.09	17	0.51	1.69	17	0.71	2.44	17
500 µM	0.24	0.53	5	1.37	3.05	5	1.67	3.73	5
1000 µM	0.00	0.00	5	0.73	1.62	5	1.05	2.35	5
wash	14.30	15.66	27	2.43	3.89	27	0.39	1.44	27

[a] For the stimulation frequencies of 20, 50, and 100 Hz, the mean muscle force restoration, the standard deviation (SD), and the number of experiments (*n*) are displayed at each testing point.

Table S7: Breakdown of the toxicological alert count of the best screening hits.[a]

Compound	HERG channel inhibition *in vitro* mammal alert count	Mutagenicity *in vitro* bacterium alert count	Phospho-lipidosis mammal alert count	Androgen receptor modulation mammal alert count	Mutagenicity *in vivo* mammal alert count	Nephrotoxicity mammal alert count
UNC0646	2	1	1	0	0	0
PTMD01-0050 (**1k**)	1	1	0	0	0	0
PTMD01-0043 (**2g**)	2	1	1	0	0	0
PTMD99-0001C (**3**)	0	0	0	0	0	0
PTMD99-0016C (**4**)	2	0	0	0	0	0
PTMD99-0026C (**5**)	1	1	0	1	1	0
Cycloguanil (**6**)	0	0	0	0	0	1

[a] Predictions where no compound displays alert counts (Skin sensitization mammal alert count, Teratogenicity mammal alert count) are not shown as a column.

Analytical Data

6-Methoxy-2-(piperidin-1-yl)-7-[3-(piperidin-1-yl)propoxy]-*N*-[5-(pyrrolidin-1-yl)pentyl]quinazolin-4-amine (1k): mp.: 54 °C. R_f = 0.34 [10% 3 M NH_3 (in MeOH) in CH_2Cl_2]. IR (film): $\tilde{\nu}$ = 2935, 1581, 1493, 1244, 754 cm^{-1}. ^1H NMR (500 MHz, CD_2Cl_2): δ = 1.37-1.47 (m, 2 H, CH_2CH$_2$CH$_2$NCH$_2$CH$_2$CH$_2$O), 1.48-1.55 (m, 2 H, CH_2CH$_2$CH$_2$NH), 1.55-1.61 (m, 8 H, CH$_2$CH_2CH$_2$NC, CH$_2$CH_2CH$_2$NCH$_2$CH$_2$CH$_2$O), 1.62-1.70 (m, 4 H, CH_2CH$_2$CH$_2$NC, CH_2CH$_2$CH$_2$CH$_2$NH), 1.74 (p, J = 7.0 Hz, 2 H, CH_2CH$_2$NH), 1.80-1.89 [m, 4 H, CH_2CH$_2$N(CH$_2$)$_5$NH], 2.00 (p, J = 6.9 Hz, 2 H, CH_2CH$_2$O), 2.22-2.42 (m, 4 H, CH_2NCH$_2$CH$_2$CH$_2$O), 2.42-2.48 (m, 2 H, CH_2CH$_2$CH$_2$O), 2.57-2.66 [m, 2 H, CH_2(CH$_2$)$_4$NH], 2.66-2.84 [m, 4 H, CH_2N(CH$_2$)$_5$NH], 3.53-3.64 (m, 2 H, CH_2NH), 3.73-3.84 (m, 4 H, CH$_2$NC), 3.89 (s, 3 H, CH$_3$O), 4.11 (t, J = 6.7 Hz, 2 H, CH$_2$O), 5.77 (s, 1 H, NH), 6.84 (s, 1 H, C*H*COCH$_2$), 6.98 (s, 1 H, C*H*COCH$_3$). ^{13}C NMR (126 MHz, CD_2Cl_2): δ = 23.82 [*C*H$_2$CH$_2$N(CH$_2$)$_5$NH], 24.94 (*C*H$_2$CH$_2$CH$_2$NCH$_2$CH$_2$CH$_2$O), 25.17 (*C*H$_2$CH$_2$CH$_2$NH), 25.57 (*C*H$_2$CH$_2$CH$_2$NC), 26.41 (*C*H$_2$CH$_2$NCH$_2$CH$_2$CH$_2$O)*, 26.46 (*C*H$_2$CH$_2$NC)*, 27.05 (*C*H$_2$CH$_2$O), 28.02 [*C*H$_2$(CH$_2$)$_3$NH], 29.19 (*C*H$_2$CH$_2$NH), 41.36 (*C*H$_2$NH), 45.39 (*C*H$_2$NC), 54.41 [*C*H$_2$N(CH$_2$)$_5$NH], 55.00 (*C*H$_2$NCH$_2$CH$_2$CH$_2$O), 55.97 (*C*H$_2$CH$_2$CH$_2$O), 56.31 [*C*H$_2$(CH$_2$)$_4$NH], 56.96 (CH$_3$O), 67.57 (CH$_2$O), 102.41 (*C*HCOCH$_3$), 103.30 (*C*CNH), 106.82 (*C*HCOCH$_2$), 145.83 (*C*OCH$_3$), 149.62 (*C*CCNH), 154.35 (*C*OCH$_2$), 159.04 (*C*NCNH), 159.49 (CNH). HRMS-EI m/z [M]$^+$ calcd. for $C_{31}H_{50}N_6O_2$: 538.3995, found: 538.3989.

***N*^{1}-Cyclohexyl-*N*^{2}-{6-methoxy-7-[3-(piperidin-1-yl)propoxy]quinazolin-4-yl}-*N*^{1}-methylethane-1,2-diamine (2b):** R_f = 0.38 [10% 3 M NH_3 (in MeOH) in CH_2Cl_2]. IR (film): $\tilde{\nu}$ = 3020, 1641, 1215 cm^{-1}. ^1H NMR (500 MHz, CD_2Cl_2): δ = 1.03-1.16 (m, 1 H, CH_2CH$_2$CH$_2$CHN), 1.19-1.37 (m, 4 H, CH_2CH_2CHN), 1.37-1.47 (m, 2 H, CH_2CH$_2$CH$_2$NCH$_2$CH$_2$CH$_2$O), 1.47-1.59 (m, 4 H, CH_2CH$_2$NCH$_2$CH$_2$CH$_2$O), 1.59-1.66 (m, 1 H, CH_2CH$_2$CH$_2$CHN), 1.77-1.87 (m, 4 H, CH_2CH_2CHN), 2.02 (p, J = 6.8 Hz, 2 H, CH_2CH$_2$O), 2.32 (s, 3 H, CH$_3$N), 2.34-2.43 (m, 4 H, CH_2NCH$_2$CH$_2$CH$_2$O), 2.43-2.52 (m, 3 H, CH_2CH$_2$CH$_2$O, CH$_2$C*H*N), 2.68-2.88 (m, 2 H, CH_2CH$_2$NH), 3.53-3.67 (m, 2 H, CH_2NH), 3.94 (s, 3 H, CH$_3$O), 4.16 (t, J = 6.7 Hz, 2 H, CH$_2$O), 6.50 (d, J = 13.6 Hz, 1 H, NH), 6.95 (s, 1 H, C*H*COCH$_3$), 7.14 (s, 1 H, C*H*COCH$_2$), 8.43 (s, 1 H, C*H*NCNH). ^{13}C NMR (126 MHz, CD_2Cl_2): δ = 24.97 (*C*H$_2$CH$_2$CH$_2$NCH$_2$CH$_2$CH$_2$O), 26.35 (*C*H$_2$CH$_2$CHN), 26.52 (*C*H$_2$CH$_2$NCH$_2$CH$_2$CH$_2$O), 26.68 (*C*H$_2$CH$_2$O), 27.02 (*C*H$_2$CH$_2$CH$_2$CHN), 29.26 (*C*H$_2$CHN), 37.08 (CH$_3$N), 38.38 (CH$_2$NH), 52.08 (*C*H$_2$CH$_2$NH), 55.03 (*C*H$_2$NCH$_2$CH$_2$CH$_2$O), 55.91 (*C*H$_2$CH$_2$CH$_2$O), 56.39 (CH$_3$O), 63.59 (CH$_2$*C*HN), 67.87 (CH$_2$O), 100.42 (*C*HCOCH$_3$), 108.83 (*C*HCOCH$_2$), 109.02 (14), 146.84 (15), 149.46 (12), 154.21 (11), 154.49 (*C*HNCNH), 158.65 (19). HRMS-ESI m/z [M+H]$^+$ calcd. for $C_{26}H_{42}N_5O_2$: 456.3339, found: 456.3334.

6-Methoxy-*N*-[3-(4-methylpiperazin-1-yl)butyl]-7-[3-(piperidin-1-yl)propoxy]quinazolin-4-amine (2c): mp.: 85 °C. R_f = 0.22 [10% 3 M NH_3 (in MeOH) in CH_2Cl_2]. IR (film): $\tilde{\nu}$ = 2100, 1622, 1504, 1338, 1217 cm^{-1}. ^1H NMR (500 MHz, CD_2Cl_2): δ = 1.05 (d, J = 6.6 Hz, 3 H, CH_3CH), 1.37-1.49 (m, 2 H, CH_2CH$_2$CH$_2$NCH$_2$CH$_2$CH$_2$O), 1.51-1.61 (m, 4 H, CH_2CH$_2$NCH$_2$CH$_2$CH$_2$O), 1.65-1.97 (m, 2 H, CH_2CH$_2$NH), 1.98-2.08 (m, 2 H, CH_2CH$_2$O), 2.26 (s, 3 H, CH$_3$N), 2.28-2.62 (m, 12 H, CH_2CH_2NCH$_3$, CH_2NCH_2CH$_2$CH$_2$O), 2.64-2.77 (m, 2 H, CH_2CH$_2$NCH$_3$), 2.78-2.96 (m, 1 H, C*H*CH$_3$), 3.58-3.70 (m, 1 H, CH_2NH), 3.72-3.85 (m, 1 H, CH_2NH), 3.97 (s, 3 H, CH$_3$O), 4.17 (t, J = 6.6 Hz, 2 H, CH$_2$O), 6.71 (s, 1 H, NH), 7.05 (s, 1 H, C*H*COCH$_3$), 7.15 (s, 1 H, C*H*COCH$_2$), 8.43 (s, 1 H, C*H*NCNH). ^{13}C NMR (126 MHz, CD_2Cl_2): δ = 13.74 (*C*H$_3$CH), 24.92 (*C*H$_2$CH$_2$CH$_2$NCH$_2$CH$_2$CH$_2$O), 26.47 (*C*H$_2$CH$_2$NCH$_2$CH$_2$CH$_2$O), 26.98 (*C*H$_2$CH$_2$O), 32.20 (*C*H$_2$CH$_2$NH), 40.71 (CH$_2$NH), 46.07 (CH$_3$N), 48.75 (*C*H$_2$CH$_2$NCH$_3$), 55.01 (*C*H$_2$NCH$_2$CH$_2$CH$_2$O), 55.93 (*C*H$_2$NCH$_3$, *C*H$_2$CH$_2$CH$_2$O), 57.61 (CH$_3$O), 59.32 (*C*HCH$_3$), 67.81 (CH$_2$O), 102.33 (*C*HCOCH$_3$), 108.99 (*C*HCOCH$_2$), 109.06 (*C*CNH), 147.20 (*C*CCNH), 149.40 (*C*OCH$_3$), 154.51 (*C*HNCNH, *C*OCH$_2$), 158.94 (CNH). HRMS-ESI m/z [M+H]$^+$ calcd. for $C_{26}H_{43}N_6O_2$: 471.3447, found: 471.3443.

6-Methoxy-7-[3-(piperidin-1-yl)propoxy]-4-[4-(pyrrolidin-1-yl)piperidin-1-yl]quinazoline (2d): IR (film): $\tilde{\nu}$ = 2937, 1643, 1504, 1209 cm^{-1}. ^1H NMR (500 MHz, CD_2Cl_2): δ = 1.36-1.49 (m, 2 H, CH_2CH$_2$CH$_2$NCH$_2$CH$_2$CH$_2$O), 1.49-1.59 (m, 4 H, CH_2CH$_2$NCH$_2$CH$_2$CH$_2$O), 1.69-1.82 (m, 6 H, CH_2CHN, CH_2CH$_2$NCH), 1.98-2.10 (m, 4 H, CH_2CHN, CH_2CH$_2$O), 2.28 (tt, *J* = 10.2, 4.0 Hz, 1 H, C*H*NCH$_2$), 2.32-2.43 (m, 4 H, CH_2NCH$_2$CH$_2$CH$_2$O), 2.46 (t, *J* = 7.1 Hz, 2 H, CH_2CH$_2$CH$_2$O), 2.51-2.64 (m, 4 H, CH_2NCH), 3.04-3.15 (m, 2 H, CH$_2$NC), 3.94 (s, 3 H, CH$_3$O), 4.04-4.14 (m, 2 H, CH$_2$NC), 4.18 (t, *J* = 6.7 Hz, 2 H, CH$_2$O), 7.11 (s, 1 H, C*H*COCH$_3$), 7.19 (s, 1 H, C*H*COCH$_2$), 8.55 (s, 1 H, CHNCN). ^{13}C NMR (126 MHz, CD_2Cl_2): δ = 23.74 (*C*H$_2$CH$_2$NCH), 24.96 (*C*H$_2$CH$_2$CH$_2$NCH$_2$CH$_2$CH$_2$O), 26.52 (*C*H$_2$CH$_2$NCH$_2$CH$_2$CH$_2$O), 26.98 (*C*H$_2$CH$_2$O), 32.07 (*C*H$_2$CHN), 49.09 (*C*H$_2$CH$_2$CHN), 51.78 (*C*H$_2$NCH), 55.03 (*C*H$_2$NCH$_2$CH$_2$CH$_2$O), 55.89 (*C*H$_2$CH$_2$CH$_2$O), 56.31 (CH$_3$O), 62.21 (*C*HNCH$_2$), 67.92 (CH$_2$O), 103.89 (*C*HCOCH$_3$), 108.49 (*C*HCOCH$_2$), 111.84 (*C*CHCOCH$_3$), 149.03 (*C*OCH$_3$), 149.47 (*C*CCNCH$_2$), 153.34 (*C*HNCN), 154.41 (*C*OCH$_2$), 164.49 (*C*NCH$_2$). HRMS-ESI m/z $[M+H]^+$ calcd. for $C_{26}H_{40}N_5O_2$: 454.3182, found: 454.3177.

***N*-[1-(Azepan-1-yl)-2-methylpropan-2-yl]-6-methoxy-7-[3-(piperidin-1-yl)propoxy]quinazolin-4-amine (2e):** Hygroscopic. R_f = 0.30 [5% 7 M NH_3 (in MeOH) in CH_2Cl_2]. IR (film): $\tilde{\nu}$ = 2926, 1643, 1498 cm^{-1}. ^1H NMR (500 MHz, CD_2Cl_2): δ = 1.38-1.47 (m, 2 H, CH_2CH$_2$CH$_2$NCH$_2$CH$_2$CH$_2$O), 1.52-1.62 (m, 10 H, CH$_3$C, CH_2CH$_2$NCH$_2$CH$_2$CH$_2$O), 1.62-1.78 (m, 8 H, CH_2CH_2CH$_2$NCH$_2$CNH), 2.03 (p, *J* = 6.9 Hz, 2 H, CH_2CH$_2$O), 2.26-2.46 (m, 4 H, CH_2NCH$_2$CH$_2$CH$_2$O), 2.46-2.57 (m, 2 H, CH_2CH$_2$CH$_2$O), 2.75 (s, 2 H, CH_2CNH), 2.82-2.96 (m, 4 H, CH_2NCH$_2$CNH), 3.95 (s, 3 H, CH$_3$O), 4.16 (t, *J* = 6.6 Hz, 2 H, CH$_2$O), 6.84 (s, 1 H, NH), 6.93 (s, 1 H, C*H*COCH$_3$), 7.12 (s, 1 H, C*H*COCH$_2$), 8.40 (s, 1 H, C*H*NCNH). ^{13}C NMR (126 MHz, CD_2Cl_2): δ = 24.91 (*C*H$_2$CH$_2$CH$_2$NCH$_2$CH$_2$CH$_2$O), 25.77 (*C*H$_3$C), 26.45 (*C*H$_2$CH$_2$NCH$_2$CH$_2$CH$_2$O), 26.97 (*C*H$_2$CH$_2$O), 27.51 (*C*H$_2$CH$_2$CH$_2$NCH$_2$CNH), 29.59 (*C*H$_2$CH$_2$NCH$_2$CNH), 54.36 (CH$_3$*C*), 55.00 (*C*H$_2$NCH$_2$CH$_2$CH$_2$O), 55.91 (*C*H$_2$CH$_2$CH$_2$O), 56.38 (CH$_3$O), 58.82 (*C*H$_2$NCH$_2$CNH), 67.81 (CH$_2$O), 69.97 (*C*H$_2$CNH), 100.45 (*C*HCOCH$_3$), 109.02 (*C*HCOCH$_2$), 109.86 (*C*CNH), 146.93 (*C*CCNH), 149.32 (*C*OCH$_3$), 153.88 (*C*OCH$_2$), 154.04 (*C*HNCNH), 158.64 (NCNH). HRMS-ESI m/z $[M+H]^+$ calcd. for $C_{27}H_{44}N_5O_2$: 470.3495, found: 470.3492.

***N*-(1-Propan-2-ylpiperidin-4-yl)-6-methoxy-7-[3-(piperidin-1-yl)propoxy]quinazolin-4-amine (2f):** mp.: 166 °C. R_f = 0.18 [10% 4 M NH_3 (in MeOH) in CH_2Cl_2]. IR (film): $\tilde{\nu}$ = 2933, 1593, 1506, 1254 cm^{-1}. ^1H NMR (500 MHz, CD_3OD): δ = 1.14 (d, *J* = 6.6 Hz, 6 H, CH_3CH), 1.45-1.56 (m, 2 H, CH_2CH$_2$CH$_2$NCH$_2$CH$_2$CH$_2$O), 1.57-1.69 (m, 4 H, CH_2CH$_2$NCH$_2$CH$_2$CH$_2$O), 1.69-1.81 (m, 2 H, CH_2CHNH), 2.04-2.18 (m, 4 H, CH_2CH$_2$O, CH_2CHNH), 2.38-2.48 (m, 2 H, CH_2NCH), 2.48-2.60 (m, 4 H, CH_2NCH$_2$CH$_2$CH$_2$O), 2.60-2.69 (m, 2 H, CH_2CH$_2$CH$_2$O), 2.82 (hept, *J* = 6.5 Hz, 1 H, CH$_3$C*H*), 2.98-3.09 (m, 2 H, CH_2NCH), 3.97 (s, 3 H, CH$_3$O), 4.09-4.30 (m, 3 H, CH$_2$O, C*H*NH), 7.07 (s, 1 H, CHCN), 7.60 (s, 1 H, CHCCN), 8.30 (s, 1 H, CHNCNH). ^{13}C NMR (126 MHz, CD_3OD): δ = 18.47 (*C*H$_3$CH), 25.04 (*C*H$_2$CH$_2$CH$_2$NCH$_2$CH$_2$CH$_2$O), 26.38 (*C*H$_2$CH$_2$NCH$_2$CH$_2$CH$_2$O), 27.00 (*C*H$_2$CH$_2$O), 32.37 (*C*H$_2$CHNH), 48.83 (*C*H$_2$NCH), 49.84 (*C*HNH), 55.46 (*C*H$_2$NCH$_2$CH$_2$CH$_2$O), 56.06 (CH$_3$*C*H), 56.82 (CH$_3$O), 57.00 (*C*H$_2$CH$_2$CH$_2$O), 68.32 (CH$_2$O), 102.94 (*C*HCCN), 107.81 (*C*HCN), 110.17 (*C*CNH), 146.65 (*C*CCNH), 150.87 (CH$_3$O*C*), 154.28 (*C*HNCNH), 155.48 (CH$_2$O*C*), 159.65 (CNH). HRMS-ESI m/z $[M+H]^+$ calcd. for $C_{25}H_{40}N_5O_2$: 442.3182, found: 442.3175.

***N*-(1-Propan-2-ylpiperidin-4-yl)-6-methoxy-7-[3-(piperidin-1-ylmethyl)pyrrolidin-1-yl]quinazolin-4-amine (2g):** mp.: 244 °C. R_f = 0.35 [10% 3 M NH_3 (in MeOH) in CH_2Cl_2]. IR (film): $\tilde{\nu}$ = 2935, 1612, 1504, 1363 cm^{-1}. ^1H NMR (500 MHz, CD_2Cl_2): δ = 1.04 (d, *J* = 6.6 Hz, 6 H, CH_3CH), 1.33-1.47 (m, 2 H, CH_2CH$_2$CH$_2$N), 1.47-1.60 (m, 6 H, CH$_2$CH_2CH$_2$N, CH_2CHNH), 1.60-1.78 (m, 1 H, CH$_2$CH_2CHCH$_2$N), 2.02-2.09 (m, 1 H, CH$_2$CH_2CHCH$_2$N), 2.09-2.17 (m, 2 H, CH_2CHNH), 2.19-2.44 (m, 8 H, CH_2NCH_2CHCH$_2$N,

C*H*$_2$CH$_2$CHNH), 2.49 (hept, *J* = 7.0 Hz, 1 H, C*H*CH$_2$N), 2.76 (hept, *J* = 6.4 Hz, 1 H, CH$_3$C*H*), 2.83-2.93 (m, 2 H, C*H*$_2$CH$_2$CHNH), 3.26 (dd, *J* = 10.2, 7.2 Hz, 1 H, CHC*H*$_2$NC), 3.51-3.62 (m, 3 H, C*H*$_2$NC), 3.90 (s, 3 H, CH$_3$O), 4.10-4.26 (m, 1 H, C*H*NH), 5.01-5.18 (m, 1 H, NH), 6.76 (s, 1 H, C*H*COCH$_3$), 6.79 (s, 1 H, C*H*CNCH$_2$), 8.34 (s, 1 H, CHNC). ^{13}C NMR (126 MHz, CD_2Cl_2): δ = 18.46 (*C*H$_3$CH), 24.97 (*C*H$_2$CH$_2$CH$_2$N), 26.55 (CH$_2$*C*H$_2$CH$_2$N), 30.45 (*C*H$_2$CHCH$_2$N), 33.37 (*C*H$_2$CHNH), 36.58 (*C*HCH$_2$N), 48.05 (*C*H$_2$CH$_2$CHNH), 48.85 (CHNH), 50.56 (*C*H$_2$CH$_2$CHCH$_2$N), 54.85 (CH$_3$*C*H), 55.41 (CH$_2$CH$_2$*C*H$_2$N), 55.84 (CN*C*H$_2$CH), 56.33 (CH$_3$O), 63.20 (*C*H$_2$CHCH$_2$NC), 100.12 (*C*HCOCH$_3$), 106.53 (*C*CNH), 109.46 (*C*HCNCH$_2$), 145.49 (*C*NCH$_2$), 147.48 (*C*CCNH), 150.16 (*C*OCH$_3$), 154.18 (*C*HNCNH), 157.71 (CNH). HRMS-ESI m/z [M+H]$^+$ calcd. for $C_{27}H_{43}N_6O$: 467.3498; found: 467.3489.

4-Chloro-6-methoxy-2-(piperidin-1-yl)-7-[3-(piperidin-1-yl)propoxy]quinazoline (8): mp.: 138 °C. R_f = 0.35 (15% MeOH in CH_2Cl_2 IR (film): ṽ = 2931, 1626, 1585, 1495, 1238, 754 cm^{-1}. ^{1}H NMR (500 MHz, CD_3OD): δ = 1.59-1.70 (m, 6 H, C*H*$_2$CH$_2$CH$_2$NCH$_2$CH$_2$CH$_2$O, C*H*$_2$CH$_2$NC), 1.70-1.77 (m, 2 H, C*H*$_2$CH$_2$CH$_2$NC), 1.77-1.89 (m, 4 H, C*H*$_2$CH$_2$NCH$_2$CH$_2$CH$_2$O), 2.15-2.37 (m, 2 H, C*H*$_2$CH$_2$O), 2.87-3.17 (m, 6 H, C*H*$_2$NC*H*$_2$CH$_2$CH$_2$O), 3.81-3.88 (m, 4 H, CH$_2$NC), 3.95 (s, 3 H, CH$_3$O), 4.25 (t, *J* = 5.8 Hz, 2 H, CH$_2$O), 7.00 (s, 1 H, CHCOCH$_2$), 7.26 (s, 1 H, C*H*COCH$_3$). ^{13}C NMR (126 MHz, CD_3OD): δ = 23.72 (*C*H$_2$CH$_2$CH$_2$NCH$_2$CH$_2$CH$_2$O), 25.29 (*C*H$_2$CH$_2$NCH$_2$CH$_2$CH$_2$O), 25.74 (*C*H$_2$CH$_2$O)*, 25.92 (*C*H$_2$CH$_2$CH$_2$NC)*, 26.88 (*C*H$_2$CH$_2$NC), 46.31 (*C*H$_2$NC), 55.01 (*C*H$_2$NCH$_2$CH$_2$CH$_2$O), 56.54 (CH$_3$O), 56.73 (*C*H$_2$CH$_2$CH$_2$O), 68.09 (CH$_2$O), 104.82 (*C*HCOCH$_3$), 106.56 (*C*HCOCH$_2$), 113.18 (*C*CCl), 148.82 (*C*OCH$_3$), 152.67 (*C*CCCl), 157.42 (*C*OCH$_2$), 158.93 (*C*NCH$_2$), 160.90 (CCl). HRMS-ESI m/z [M+H]$^+$ calcd. for $C_{22}H_{32}ClN_4O_2$: 419.224, found: 419.2206.

4-Chloro-6-methoxy-7-[3-(piperidin-1-yl)propoxy]quinazoline (9) [7, 8]**:** mp.: 106 °C. R_f = 0.21 [5% 4 M NH_3 (in MeOH) in CH_2Cl_2]. IR (film): ṽ = 2933, 2358, 1500, 1232, 1020 cm^{-1}. ^{1}H NMR (500 MHz, DMSO-d_6) δ = 1.31-1.43 (m, 2 H, C*H*$_2$CH$_2$CH$_2$NCH$_2$CH$_2$CH$_2$O), 1.45-1.54 (m, 4 H, C*H*$_2$CH$_2$NCH$_2$CH$_2$CH$_2$O), 1.95 (p, *J* = 6.7 Hz, 2 H, C*H*$_2$CH$_2$O), 2.26-2.38 (m, 4 H, C*H*$_2$NCH$_2$CH$_2$CH$_2$O), 2.38-2.43 (m, 2 H, C*H*$_2$CH$_2$CH$_2$O), 4.00 (s, 3 H, CH$_3$O), 4.25 (t, *J* = 6.4 Hz, 2 H, CH$_2$O), 7.38 (s, 1 H, CHCN), 7.44 (s, 1 H, CHCCN), 8.86 (s, 1 H, CHN). ^{13}C NMR (126 MHz, DMSO-d_6) δ = 24.13 (*C*H$_2$CH$_2$CH$_2$NCH$_2$CH$_2$CH$_2$O), 25.60 (*C*H$_2$CH$_2$NCH$_2$CH$_2$CH$_2$O), 25.92 (*C*H$_2$CH$_2$O), 54.11 (*C*H$_2$NCH$_2$CH$_2$CH$_2$O), 54.93 (*C*H$_2$CH$_2$CH$_2$O), 56.21 (*C*H$_3$O), 67.65 (CH$_2$O), 102.30 (*C*HCCN), 107.32 (*C*HCN), 118.48 (*C*CCl), 148.60 (*C*CCCl), 151.49 (CH$_3$O*C*), 152.19 (CHN), 156.11 (CH$_2$O*C*), 157.84 (CCl). HRMS-ESI m/z [M+H]$^+$ calcd. for $C_{17}H_{23}ClN_3O_2$: 336.1479, found: 336.1476. The analytical data agree with those previously reported in the literature [7, 8].

7-Fluoro-*N*-(1-propan-2-ylpiperidin-4-yl)-6-methoxyquinazolin-4-amine (10): mp.: 233 °C (decomposition). R_f = 0.48 [10% 3 M NH_3 (in MeOH) in CH_2Cl_2]. IR (film): ṽ = 2968, 1593, 1537, 1045 cm^{-1}. ^{1}H NMR (500 MHz, CD_2Cl_2): δ = 1.04 (d, *J* = 6.6 Hz, 6 H, C*H*$_3$CH), 1.52-1.64 (m, 2 H, C*H*$_2$CHNH), 2.11-2.20 (m, 2 H, C*H*$_2$CHNH), 2.31-2.42 (m, 2 H, C*H*$_2$CH$_2$CHNH), 2.71-2.84 (m, 1 H, CH$_3$C*H*), 2.83-2.96 (m, 2 H, C*H*$_2$CH$_2$CHNH), 4.00 (s, 3 H, CH$_3$O), 4.15-4.31 (m, 1 H, C*H*NH), 5.43 (d, *J* = 7.6 Hz, 1 H, NH), 7.02 (d, *J* = 8.6 Hz, 1 H, C*H*COCH$_3$), 7.44 (d, *J* = 12.0 Hz, 1 H, CHCF), 8.48 (s, 1 H, C*H*NCNH). ^{13}C NMR (126 MHz, CD_2Cl_2): δ = 18.43 (*C*H$_3$CH), 33.01 (*C*H$_2$CHNH), 48.00 (CH$_2$CH$_2$CHNH), 49.23 (CHNH), 54.86 (CH$_3$*C*H), 56.96 (CH$_3$O), 102.29 (d, *J* = 3.5 Hz, *C*HCOCH$_3$), 111.90 (*C*CNH), 114.04 (d, *J* = 17.6 Hz, *C*HCF), 146.26 (d, *J* = 12.0 Hz, *C*CHCF), 147.82 (d, *J* = 13.0 Hz, *C*OCH$_3$), 154.79 (*C*HNCNH), 156.64 (d, *J* = 255.1 Hz, CF), 158.12 (CNH). HRMS-ESI m/z [M+H]$^+$ calcd. for $C_{17}H_{24}FN_4O$: 319.1934, found: 319.1929.

* Due to signal overlap in 2D-NMR, signals could not be unambiguously assigned.

Supplemental References

1. Chevillard, F., et al., *Binding-Site Compatible Fragment Growing Applied to the Design of beta2-Adrenergic Receptor Ligands.* J. Med. Chem., 2018. **61**(3): p. 1118-1129.
2. *ROCS 3.4.1.0.* OpenEye Scientific Software: Santa Fe, NM.
3. Chemical Computing Group, U., *Molecular Operating Environment (MOE)*. 2021: 1010 Sehrbooke St. West, Suite #910, Montreal, QC, Canada, H3A, 2R7.
4. Roe, D.R. and T.E. Cheatham, 3rd, *PTRAJ and CPPTRAJ: Software for Processing and Analysis of Molecular Dynamics Trajectory Data.* J. Chem. Theory Comput., 2013. **9**(7): p. 3084-95.
5. Nitsche, V., et al., *MS Binding Assays with UNC0642 as reporter ligand for the MB327 binding site of the nicotinic acetylcholine receptor.* Toxicol. Lett., 2024. **392**: p. 94-106.
6. Nitsche, V., et al., *MS Binding Assays with UNC0642 as reporter ligand for the MB327 binding site of the nicotinic acetylcholine receptor.* bioRxiv, 2023: p. 2023.11.15.567260.
7. Hennequin, L.F., et al., *Quinazoline Derivatives as Angiogenesis Inhibitors (WO-2000047212-A1)*, W.I.P. Organization, Editor. 2000.
8. Ravez, S., et al., *Inhibition of tumor cell growth and angiogenesis by 7-Aminoalkoxy-4-aryloxy-quinazoline ureas, a novel series of multi-tyrosine kinase inhibitors.* Eur. J. Med. Chem., 2014. **79**: p. 369-381.

3.4 Manuskript zur vierten Publikation: *Structure-Affinity Relationship of Quinazoline Derivatives as Potential Resensitizers for Desensitized nAChRs After Nerve Agent Intoxication*

3.4.1 Zusammenfassung der Ergebnisse

Allosterischer Modulatoren, die desensitisierte nikotinische Acetylcholinrezeptoren bei einer Überstimulation mit Acetylcholin wieder in einen funktionalen Zustand überführen können (sog. Resensitizer), gelten als vielversprechende Behandlungsoptionen bei Vergiftungen mit phosphororganischen Verbindungen. Chinazoline, wie das vor kurzem bei einem Library-Screening als Hit identifizierte UNC0646 erscheinen hierfür aufgrund ihrer hohen Affinität für die MB327-PAM-1-Bindungstasche als erfolgversprechende Ausgangspunkte. Um die für die hohe Affinität verantwortlichen pharmakophoren Gruppen zu identifizieren, wurde die Struktur von UNC646 hinsichtlich der in den Positionen 2, 4 und 7 des Chinazolin-Grundkörpers vorhanden, basische Gruppen enthaltender Substituenten, die gemeinhin starke Interaktionen mit der Bindungstasche erwarten lassen, systematisch variiert. In einer ersten Gruppe von Verbindungen wurde das Substitutionsmuster von UNC0646 in den Positionen 6 und 7 unverändert beibehalten und die Substituenten in 2- und 4-Position breit variiert. Die strukturellen Abwandlungen umfassten dabei den Austausch der Reste durch strukturverwandte Substituenten, aber auch durch solche mit deutlich reduziertem sterischen Anspruch bis hin zu einem Wasserstoffatom. Bei einer zweiten Gruppe von Verbindungen wurden die Strukturen weiter vereinfacht, indem die basische Seitenkette in 7-Position durch einen Methoxysubstituenten ersetzt wurde, während die Substituenten in der 2- und 4-Postion ähnlich wie in der ersten Gruppe abgewandelt wurden. Bei der dritten Gruppe von Verbindungen wurde schließlich die Aminofunktion in der 2-Position durch ein Wasserstoffatom ersetzt, und der so vereinfachte Grundkörper einmal hinsichtlich der 4-Position oder der 7-Position strukturell abgewandelt.

Für die Synthesen der Zielverbindungen wurden sehr effiziente und leistungsfähige Verfahren entwickelt, die eine breite Auswahl an einzuführenden Substituenten zulassen und hinsichtlich der Reihenfolge der Einführung der Substituenten eine hohe Flexibilität erlauben.

In den meisten Fällen kamen 2,4-Dichlorchinazolinbausteine zum Einsatz, bei denen ggf. im ersten Schritt noch eine basische Seitenkette an die phenolische Hydroxylgruppe in der 7-Position angeknüpft wurde. Dies erfolgte sehr effizient über *Mitsunobu*-Reaktionen mit entsprechenden, zumeist kommerziell verfügbaren Aminoalkoholen. Bei anschließenden Umsetzungen mit primären oder sekundären Aminen erfolgte dann erst eine nukleophile Substitution in der 4-Position des Ringsystems und bei neuerlicher Reaktion mit einem Aminderivat unter etwas stärker forcierenden Reaktionsbedingungen in der 2-Position. So ließen

sich insbesondere Untergruppen von Substanzen mit einem definierten Rest in 4- und unterschiedlichen Substituenten in der 2-Position der Chinazolinbausteine leicht herstellen. Das Verfahren konnte aber auch so abgewandelt werden, dass Untergruppen von Substanzen mit einem vorgegebenen Rest in 2-Position und variierenden Substituenten in 4-Position entstehen. Hierzu musste im ersten Substitutionsschritt lediglich ein tertiäres Amin, das über einen *N*-Methylsubstituenten verfügt, eingesetzt werden. Dies führte zu einer selektiven Substitution in 2-Position, woraufhin eine Zweitsubstitution in 4-Position erfolgen konnte.

Die zahlreichen so gewonnenen UNC0646-Analoga wurden hinsichtlich ihrer Affinität zur MB327-PAM-1-Bindungsstelle mit Hilfe des neu entwickelten UNC0642-MS-Bindungsassay untersucht. In die Untersuchungen wurden zudem auch einige zu UNC0646 strukturverwandte kommerziell erhältliche Chinazoline miteinbezogen. Unter den über 50 getesteten Verbindungen war mit UNC0631, das sich von UNC0646 nur durch eine zusätzliche Methylengruppe unterscheidet, nur eine, die UNC0646 in ihrer Affinität zur MB327-PAM-1-Bindungsstelle etwas übertraf ($pK_i = 6.04 \pm 0.04$ vs. $pK_i = 5.83 \pm 0.05$). Eine weitere Verbindung, PTMD01-0049, die im Unterschied zu UNC0646 in der 2-Position anstelle eines *N*-Isopropyl-substituierten 1,4-Diazepanrestes einen Piperidinrest aufweist, zeigte eine mit UNC0646 vergleichbare Affinität ($pK_i = 5.83 \pm 0.02$). Unabhängig davon wurden mit der Untersuchung der zahlreichen in 2-, 4- und 7-Position modifizierten UNC0646-Analoga wertvolle Einblicke in die Struktur-Affinitäts-Beziehungen dieser Substanzklasse gewonnen, die als Ausgangspunkt für weitere Strukturoptimierungen dienen können.

3.4.2 Darstellung des Eigenanteils

Die Erstellung des Manuskripts erfolgte zu gleichen Teilen durch Valentin Nitsche und mich. Alle Synthesen sowie die analytische Charakterisierung der Verbindungen, deren NMR- und MS-Spektren von der Analytikabteilung des Departments für Pharmazie gemessen wurden, wurden eigenständig von mir durchgeführt. Die technische Durchführung der MS- und NMR-Messungen wurde von der Analytikabteilung des Departments für Pharmazie übernommen. Valentin Nitsche führte die UNC0642-MS-Bindungsassays durch. Die Korrektur des Manuskripts übernahmen Klaus T. Wanner und Franz F. Paintner. Weitere Korrekturbeiträge erfolgten durch Georg Höfner. Das Manuskript soll zusätzlich um einen Beitrag zu *in silico*-Studien von Jesko Kaiser, Christoph G. W. Gertzen und Holger Gohlke erweitert werden. Anschließend sollen Korrekturbeiträge von Thomas Seeger, Karin V. Niessen, Dirk Steinritz und Franz Worek einfließen. Schließlich ist geplant, das Manuskript bei Toxicology Letters einzureichen.

Structure-Affinity Relationship of Quinazoline Derivatives as Potential Resensitizers of Desensitized nAChRs After Nerve Agent Intoxication

Tamara Bernauer[+][a], Valentin Nitsche[+][a], Georg Höfner[a], Karin V. Niessen[b], Thomas Seeger[b], Dirk Steinritz[b], Franz Worek[b], Klaus T. Wanner[a] and Franz F. Paintner*[a]

[a] T. Bernauer, V. Nitsche, Dr. G. Höfner, Prof. Dr. K. T. Wanner, Prof. Dr. F. F. Paintner
Department of Pharmacy - Center for Drug Research
Ludwig-Maximilians-Universität München
Butenandtstrasse 5-13, 81377 Munich (Germany)
E-mail: Franz.Paintner@cup.uni-muenchen.de

[b] Dr. K. V. Niessen, Dr. T. Seeger, Prof. Dr. D. Steinritz, Prof. Dr. F. Worek
Bundeswehr Institute of Pharmacology and Toxicology
Neuherbergstrasse 11, 80937 Munich (Germany)

[+] These authors contributed equally to this work.

Author ORCID

Tamara Bernauer: 0000-0001-9570-1253

Valentin Nitsche: 0009-0000-3351-1227

Georg Höfner: 0000 0002 7957 4503

Karin Niessen: 0009-0008-6810-5294

Thomas Seeger: 0009-0007-5713-4367

Dirk Steinritz: 0000-0002-2073-5683

Franz Worek: 0000-0003-3531-3616

Klaus Wanner: 0000-0003-4399-1425

Franz Paintner: 0000-0002-6795-586X

Abstract

In order to improve the therapy in case of organophosphorus compound poisoning, which eventually leads to death if not treated properly, one promising approach seems to be the development of allosteric modulators of the nicotinic acetylcholine receptor (nAChR), so called resensitizers. Recently, it was found that quinazoline-based compounds may propose very promising candidates for this purpose, as several of them, for example UNC0646, display the highest yet known affinities for the corresponding binding site of the nAChR. With the intention to gain a better understanding regarding structure-affinity relationships within this class of compounds, we present the syntheses and the evaluation (via MS binding experiments) of a remarkable number of UNC0646 analogs in this study. On the one hand, our results show, how to easily access a variety of UNC0646 analogs with different substituents in positions 2, 4 and 7 of the quinazoline. Furthermore, the results of MS Binding Assays for this plethora of compounds are of great value regarding the specific design of novel, ideally more affine (and therefore hopefully more potent) quinazoline-based compounds in the future.

1 Introduction

Organophosphorus compounds (OPCs), commonly used as pesticides (Freire and Koifman, 2013) but also as chemical weapons, e.g. in the brutal civil war in Syria (Dolgin, 2013; OPCW, 2017; Pita and Domingo, 2014), can cause severe health damage upon exposure. They interfere with the cholinergic system, where the formed OPC-acetylcholinesterase (AChE) complexes prevent the necessary cleavage of the neurotransmitter acetylcholine (ACh) in the synaptic cleft of cholinergic neurons, so that the accumulated ACh triggers overstimulation of the associated muscarinic (mAChRs) and nicotinic acetylcholine receptors (nAChRs) (Brown and Brix, 1998; Maselli and Leung, 1993; Massoulié et al., 1993; Thiermann et al., 2010). The resulting so-called "cholinergic crisis" manifests itself in mild poisoning, e.g. by abdominal cramping and vomiting; severe poisoning is life-threatening if medical treatment is inadequate because of the onset of respiratory arrest (Newmark, 2007). The most common approach to counteract overstimulation of the affected receptors involves, on the one hand, the degradation of ACh catalyzed by AChE reactivated by oxime drugs and, on the other hand, the antagonization of ACh at the mAChR by administration of atropine to reduce neuronal signal transduction (Shih et al., 2007; Thiermann and Worek, 2022; Worek et al., 2005). However, the current treatment approach has major gaps, as present oxime drugs show only limited efficacy on specific OPC-AChE complexes, and despite extensive research in this field, no universal oxime therapy has yet been presented (Worek et al., 2020). At the same time, there are no competitive nAChR antagonists that act directly on the corresponding receptors, which is why the receptors rapidly enter a desensitized state with interrupted cholinergic signal transduction (Papke, 2014). Therefore, an important approach to improve OPC treatment is to directly address the nAChR with allosteric ligands, so-called resensitizers, in order to reactivate the inactive nAChRs (Sheridan et al., 2005; Turner et al., 2011).

Initially, bispyridinium compounds such as MB327 were investigated for this purpose, whereby beneficial pharmacological aspects could be detected in various *in vitro*, *ex vivo* as well as *in vivo* experiments (Niessen et al., 2016; Niessen et al., 2018; Seeger et al., 2012; Timperley et al., 2012; Turner et al., 2011). Nevertheless, both the affinity to the nAChR and the potency of MB327, were insufficient to be applicable as a therapeutic agent (Kassa et al., 2022; Price et al., 2016). Detailed *in silico* studies of the binding mode led to the identification of an allosteric binding pocket (MB327-PAM-1) (Kaiser et al., 2023). And even while our recently synthesized MB327 analogs have shown that the development of more potent bispyridinium compounds with higher binding affinity to the nAChR and higher muscle reactivation ability is possible (Bernauer et al., 2024; Kaiser et al., 2023; Rappenglück et al., 2018a, b), it again became clear that the potency of the compounds is far from meeting the requirements for a drug candidate.

Moving away from the syntheses of compounds based on MB327, we have therefore dedicated ourselves to the search for a new compound class with higher affinity towards the MB327-PAM-1 binding site, which would benefit their use as therapeutic agents. To this purpose, we recently screened two compound libraries with our [$^{2}H_{6}$]MB327 MS Binding Assay, identifying a series of quinazoline derivatives, specifically UNC0646 (**1**), UNC0642 (**2**), and UNC0638 (**3**), which have a distinctly higher affinity towards the MB327-PAM-1 binding site than the so far investigated bispyridinium compounds, showing K_i values around low micromolar concentrations (Figure 1) (Sichler et al., 2024). Based on these new quinazoline-based ligands, with the highest yet known affinities towards the binding site of interest, we developed an alternative MS Binding Assay with UNC0642 (**2**) as the reporter ligand and UNC0638 (**3**) as the internal standard, which provides a valuable alternative for characterizing binding

affinities of ligands towards the MB327-PAM-1 binding site of *Torpedo*-nAChR (Nitsche et al., 2024). Applying this assay, it was proven, that UNC0646 (**1**) is the allosteric ligand with the highest yet known binding affinity of $pK_i = 5.83 \pm 0.05$ making this compound an indispensable candidate as a new scaffold structure for the development of new derivatives.

Initial *in silico* studies involving flexible docking studies and MD simulations to analyze the binding behavior of UNC0646 (**1**) to the receptor identified strong binding interactions (in the form of salt bridge binding) of the substituent in the 4-position with glutamate residues in the binding pocket. Further, but probably weaker interactions between the ligand and the glutamate residues are conceivable, whereby the diazepane in the 2-position appears to be the less important (Nitsche et al., 2024). Broadening the spectrum of consideration by synthesizing and characterizing structurally different UNC0646 analogs in our MS Binding Assay showed that some increased flexibility of the substituents in the 4-position was beneficial in terms of binding, and thus even replacing the basic side chain in the 7-position with a methoxy residue was tolerated in this case (Kaiser et al., 2024). These initial indications of the binding behavior of UNC0646 (**1**) are helpful, but for further development of more comprehensive structure-affinity relationships the characterization of a large group of analogs with systematic structural variations is essential so that new potential allosteric nAChR modulators can be designed rationally. Especially considering that UNC0646 (**1**) does not meet the standard criteria for a drug candidate in terms of molecular weight, it is of great importance to find out, which components of the molecule are particularly important for its affinity, in order to reduce its size and ideally further enhance its affinity.

In this work, we synthesized a variety of UNC0646 analogs with quinazoline scaffold and varying substituents in the 2-, 4-, and 7-position. These compounds, along with commercially acquired ones, were then investigated using the newly developed UNC0642 MS Binding Assay, evaluating their binding affinities towards the *Torpedo*-nAChR. First, by systematic structural simplification of the individual substituents starting from UNC0646 (**1**), their relevance concerning binding affinity was investigated. In addition, we generated simplified, rapidly synthesizable quinazoline compounds in which either the 2-position was unsubstituted, or the basic side chain in the 7-position was reduced in size in order to improve the efficiency of the investigation of the binding behavior of UNC0646 analogs.

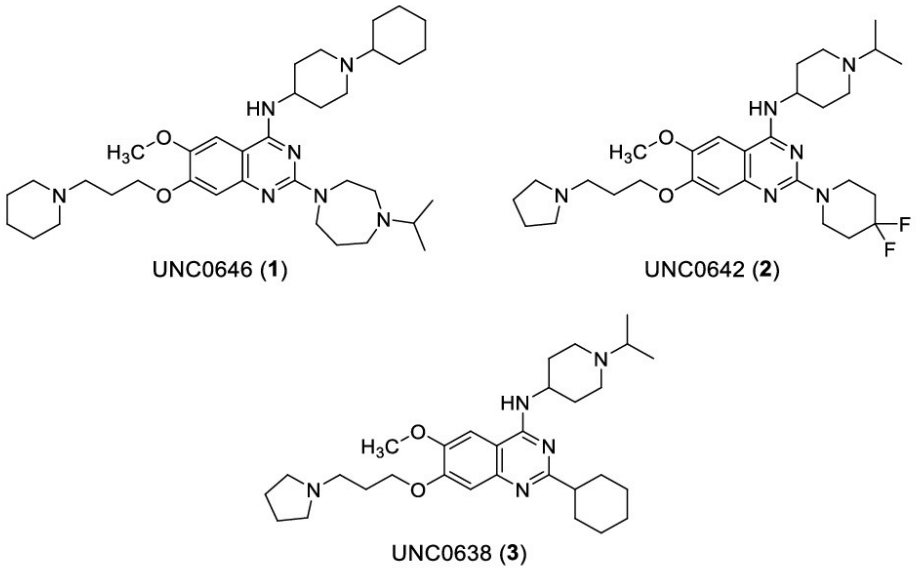

Figure 1. Quinazoline-based ligands towards MB327-PAM-1: UNC0646 (**1**), UNC0642 (**2**) and UNC0638 (**3**).

2 Material and Methods

All target compounds synthesized in the context of this study were cataloged with a certain PTMD number (Pharmacy and Toxicology Munich and Düsseldorf).

2.1 Chemistry

All chemicals were used as purchased from commercial sources. Solvents used for purification were distilled before use. Amines, which could only be purchased as the respective hydrochloride salts (1-cyclohexylpiperidin-4-amine dihydrochloride, 1-(cyclohexylmethyl)-piperidin-4-amine dihydrochloride and 5-pyrrolidin-1-ylpentan-1-amine dihydrochloride) were converted into the free bases before use (Mellstedt et al., 2020). Anhydrous reactions were carried out under argon atmosphere in vacuum-dried glassware. For Microwave reactions, a Discover SP microwave system by CEM GmbH was used. TLC-Analysis was performed on plates purchased from Merck (silica gel $60F_{254}$ on aluminum sheet). Flash chromatography was carried out using Merck silica gel 60 (40-63 mm mesh size) as stationary phase. Melting points were determined with a Büchi 510 melting point instrument and are uncorrected. IR spectra were recorded on a PerkinElmer FT-IR Spectrometer 1600 as films. ^{1}H and ^{13}C NMR spectra were recorded with a Bruker BioSpin Avance III HD 400 and 500 MHz at 25 °C. For data processing, MestReNova (Version 14.1.0) from Mestrelab Research S.L. 2019, and for calibration, the solvent signal (CD_2Cl_2, CD_3OD or $CDCl_3$) was used. Due to signal overlap in 2D-NMR, signals that could not be unambiguously assigned were marked with *. The purity of all test compounds was ≥ 95% as determined using quantitative NMR using TraceCERT® ethyl 4-(dimethylamino)benzoate from Merck as internal calibrant (Cushman et al., 2014; Pauli et al., 2014). High-resolution MS spectra were recorded with a Finnigan MAT 95 (EI) or a Finnigan LTQ FT (ESI). The analytical data of the synthesized compounds described below, obtained using the described methods, can be found in the Supporting Information.

The following compounds were prepared according to literature:

4-Chloro-6-methoxy-2-(piperidin-1-yl)-7-[3-(piperidin-1-yl)propoxy]quinazoline (**8**) (Kaiser et al., 2024), 4-chloro-6-methoxy-7-[3-(piperidin-1-yl)propoxy]quinazoline (**15**) (Kaiser et al., 2024), 7-fluoro-*N*-(1-isopropylpiperidin-4-yl)-6-methoxyquinazolin-4-amine (**22**) (Kaiser et al., 2024), 4-(*tert*-butyl)-1-(3-iodopropyl)pyridin-1-ium iodide (Rappenglück et al., 2018a).

General procedures

Synthesis of 4-amino-substituted 2-chloroquinazolines (GP1): A solution of the respective 2,4-dichloroquinazoline **6** or **24** (1.0 equiv), the corresponding amine (1.1 equiv) and *N*,*N*-diisopropylethylamine (DIEA) (3.0 equiv) in dry THF (4 mL/mmol) was stirred at rt for 48 h. The reaction mixture was concentrated in vacuo and the crude product was purified by flash chromatography [5% to 15% 3 M NH_3 (in MeOH) in CH_2Cl_2]. Synthesized compounds: **7** (yellow solid, 64% yield, 96% purity), **10a** (yellow solid, 86% yield, 99% purity), **10b** (yellow solid, 48% yield, 97% purity), **10c** (colorless solid, 86% yield, 96% purity), **25** (colorless solid,

81% yield, 95% purity), **26** (colorless solid, 65% yield, 99% purity), **27** (pale yellow solid, 98% yield, 98% purity).

Synthesis of 2,4-diamino-substituted quinazolines (GP2): A mixture of the respective 4-amino-substituted 2-chloroquinazoline **7**, **10**, **12**, **25**, **26** or **27** (1.0 equiv) and the corresponding amine (5.0 equiv) in toluene (2-5 mL/mmol) was stirred at 130 °C under microwave irradiation (300 W) for 50 min. The reaction mixture was concentrated in vacuo and the crude product was purified by flash chromatography [5% to 20% 3 M NH_3 (in MeOH) in CH_2Cl_2]. Synthesized compounds: **9a** (colorless solid, 89% yield, 97% purity), **9b** (colorless solid, 89% yield, 99% purity), **11a** (pale yellow solid, 89% yield, 95% purity), **11b** (colorless solid, 62% yield, 98% purity), **11c** (red solid, 91% yield, 98% purity), **14** (yellow oil, 99% yield, 97% purity), **28a** (yellow, hygroscopic solid, 90% yield, 97% purity), **28b** (yellow solid, 94% yield, 97% purity), **28c** (yellow solid, 97% yield, 97% purity), **31** (red solid, > 99% yield, 95% purity), **32a** (pale yellow solid, 91% yield, 95% purity), **32b** (pale yellow solid, 67% yield, 98% purity), **32c** (pale yellow solid, 84% yield, 98% purity), **32d** (colorless solid, 97% yield, 98% purity).

Synthesis of 4-amino-substituted quinazolin-2-amines (GP3): A solution of the respective 4-amino-substituted 2-chloroquinazoline **7** or **27** (1.0 equiv) and NaN_3 (1.1 equiv) in EtOH/AcOH (4:1) (6.7 mL/mmol) was stirred at 90 °C for 2 h. After cooling down, 10% Pd/C (0.10 equiv) and hydrazine hydrate (1.5 equiv) were gradually added and the mixture was again stirred at 90 °C for 2 h. The cold reaction mixture was filtered over a pad of celite, washed with EtOH and the solvent was removed in vacuo. The crude product was purified by flash chromatography [10% 3 M NH_3 (in MeOH) in CH_2Cl_2 or 5% to 10% 7 M NH_3 (in MeOH) in CH_2Cl_2]. Synthesized compounds: **9e** (colorless solid, 49% yield, 99% purity) and **16b** (colorless solid, 16% yield, 97% purity) as a side-product, **32e** (colorless solid, 78% yield, 96% purity) and **32f** (colorless solid, 5% yield, 95% purity) as a side-product.

Synthesis of 4-amino-substituted quinazolines (GP4): A solution of the respective 4-chloroquinazoline **8**, **15**, **17**, **29** or **33** (1.0 equiv), the corresponding amine (2.0 equiv) and *N*,*N*-diisopropylethylamine (DIEA) (3.0 equiv) in *i*-PrOH (5 mL/mmol) was stirred at 160 °C under microwave irradiation (200 W) for 15 min to 1 h. The reaction mixture was concentrated in vacuo and the crude product was purified by flash chromatography [5% to 15% 3 M NH_3 (in MeOH) in CH_2Cl_2]. Synthesized compounds: **9c** (colorless solid, 70% yield, 98% purity), **9f** (colorless solid, 58% yield, 99% purity), **16a** (colorless solid, 62% yield, 98% purity), **16b** (yellow solid, 94% yield, 95% purity), **16c** (colorless solid, 69% yield, 97% purity), **16d** (colorless solid, 82% yield, 100% purity), **16e** (colorless solid, 85% yield, 99% purity), **16f** (pale yellow solid, 83% yield, 98% purity), **18** (colorless solid, > 99% yield, 96% purity), **30a** (pale yellow, hygroscopic solid, 84% yield, 95% purity), **30b** (colorless solid, 64% yield, 97% purity), **34a** (pale yellow, hygroscopic solid, 86% yield, 99% purity), **34b** (colorless solid, 68% yield, 99% purity), **34c** (colorless solid, 73% yield, 97% purity).

***Mitsunobu*-reaction on quinazolin-7-ol 19 (GP5):** To a slurry of quinazolin-7-ol **19** (1.0 equiv), the corresponding alcohol (3.5-4.0 equiv) and PPh_3 (5.5 equiv) in dry THF (14.5 mL/mmol) at 0 °C diisopropyl azodicarboxylate (DIAD; 5.0 equiv) was added in portions. The resulting solution was stirred at rt for 20 h. The reaction mixture was concentrated in vacuo and the crude product was purified by flash chromatography [20% MeOH in CH_2Cl_2 or 10% 3 M NH_3 (in MeOH) in CH_2Cl_2]. Synthesized compounds: **20a** (colorless solid, 63% yield, 99% purity), **20c** (colorless solid, 79% yield, 99% purity), **20d** (colorless solid, 69% yield, 98%

purity), **20e** (colorless solid, 59% yield, 97% purity), **20f** (colorless solid, 46% yield, 100% purity), **20g** (colorless solid, 58% yield, 95% purity), **20h** (colorless solid, 78% yield, 96% purity), **21** (colorless solid, 92% yield, 99% purity).

Synthesis of 7-amino-substituted quinazolines (GP6): A mixture of 7-fluoroquinazolin-4-amine **22** (1.0 equiv), the corresponding amine (5.0 equiv) and K_2CO_3 (1.1 equiv) in *N*-methyl-2-pyrrolidone (NMP) (1.3 mL/mmol) was stirred at 135 °C for 20 h. The reaction mixture was concentrated in vacuo and the crude product was purified by flash chromatography [5% to 20% 3 or 7 M NH_3 (in MeOH) in CH_2Cl_2]. Synthesized compounds: **23a** (pale yellow solid, 78% yield, 95% purity), **23b** (pale yellow solid, 84% yield, 97% purity), **23c** (colorless solid, 24% yield, 98% purity).

Synthesis of 4-chlor-2-(piperidin-1-yl)quinazolines (GP7): A solution of the respective 2,4-dichloroquinazoline **4** or **24** (1.0 equiv) and 1-methylpiperidine (1.2-2.0 equiv) in 1,4-dioxane (2.5 mL/mmol) was stirred at 150 °C under microwave irradiation (300 W) for 1 h. The reaction mixture was concentrated in vacuo and the crude product was purified by flash chromatography (CH_2Cl_2). Synthesized compounds: **33** (yellow solid, 132 mg, 86% yield, 100% purity) and **29** (yellow solid, 81% yield, 95% purity).

2,4-Dichloro-6-methoxyquinazolin-7-ol (5) (Doig et al., 2014)**:** A mixture of **4** (3.35 g, 10.0 mmol, 1.0 equiv) and 5% Pd on alumina (1.70 g, 0.800 mmol, 0.08 equiv) in THF (130 mL) was stirred under H_2 atmosphere (1 bar) on ice for 6 h. The mixture was filtered and concentrated in vacuo to give **5** without further purification as a pale yellow solid (2.48 g, > 99% yield, 95% purity).

2,4-Dichloro-6-methoxy-7-[3-(piperidin-1-yl)propoxy]quinazoline (6) (Vital et al., 2023)**:** To a slurry of **5** (245 mg, 1.00 mmol, 1.0 equiv), PPh_3 (344 mg, 1.30 mmol, 1.3 equiv), 3-piperidin-1-ylpropan-1-ol (200 µL, 188 mg, 1.25 mmol, 1.25 equiv) and dry THF (2.0 mL) was added di-tert-butyl azodicarboxylate (DBAD) (305 mg, 1.30 mmol, 1.3 equiv) in portions at 0 °C. The resulting solution was stirred overnight at rt and concentrated under reduced pressure. Purification by flash chromatography (10% MeOH in CH_2Cl_2) afforded **6** as a red solid (301 mg, 81% yield, 97% purity).

***N*⁴-(1-Cyclohexylpiperidin-4-yl)-6-methoxy-*N*²,*N*²-dimethyl-7-[3-(piperidin-1-yl)propoxy]-quinazoline-2,4-diamine (9d):** A mixture of **7** (98.1 mg, 0.190 mmol, 1.0 equiv) solved in dimethylamine (2 M in THF) (0.95 µL, 1.90 mmol, 10 equiv) was heated for 48 h at 100 °C in a pressure vessel. The mixture was cooled down and concentrated in vacuo. **9d** was purified with flash chromatography [7% 3 M NH_3 (in MeOH) in CH_2Cl_2] and obtained as a red solid (84.8 mg, 85% yield, 96% purity).

2-Chloro-6-methoxy-7-[3-(piperidin-1-yl)propoxy]quinazoline (12) and 6-methoxy-7-[3-(piperidin-1-yl)propoxy]quinazoline (13): A mixture of **6** (370 mg, 1.00 mmol, 1.0 equiv), 10% Pd/C (23.7 mg, 20.0 µmol, 0.02 equiv) and NEt_3 (209 µL, 152 mg, 1.50 mmol, 1.5 equiv) in EtOAc (2.0 mL) was stirred under H_2 atmosphere at rt for 4 h. The mixture was filtered and concentrated in vacuo. **12** (203 mg, 61% yield, 98% purity) and **13** (57.8 mg, 19% yield, 96% purity) were isolated after flash chromatography [5% 3 M NH_3 (in MeOH) in CH_2Cl_2] as colorless resp. pale yellow solids.

4-[(1-Isopropylpiperidin-4-yl)oxy]-6-methoxy-7-[3-(piperidin-1-yl)propoxy]quinazoline (16g): NaH (60% in mineral oil, 24.0 mg, 0.600 mmol, 2.0 equiv) was added at 0 °C to a

solution of 1-propan-2-ylpiperidin-4-ol (92.7 µL, 90.5 mg, 0.600 mmol, 2.0 equiv) in THF (1.1 mL). After stirring for 20 min, **15** (101 mg, 0.300 mmol, 1.0 equiv) was added and the mixture was stirred for a further 3 h at 0 °C. The reaction mixture was quenched with H_2O (0.5 mL). The phases were separated and the aqueous phase was washed with CH_2Cl_2 (3 × 1 mL). The combined organic phases were washed with brine (2 mL), dried over Na_2SO_4, filtrated and concentrated. **16g** (122 mg, 92% yield, 95% purity) was isolated after flash chromatography [7% 3 M NH_3 (in MeOH) in CH_2Cl_2] as a pale yellow solid.

4-[(1-Isopropylpiperidin-4-yl)amino]-6-methoxyquinazolin-7-ol (19): A suspension of **18** (1.42 g, 3.50 mmol, 1.0 equiv), cyclohexa-1,4-diene (3.41 mL, 2.89 g, 35.0 mmol, 10 equiv) and 10% Pd/C (518 mg, 438 µmol, 0.125 equiv) in EtOH (34 mL) was stirred under reflux for 2 h. After cooling, the catalyst was filtered off and the filtrate was concentrated in vacuo to yield **19** (1.16 g, > 99% yield, 95% purity) without further purification as a yellow solid.

***N*-(1-Isopropylpiperidin-4-yl)-6-methoxy-7-[4-(piperidin-1-yl)butoxy]quinazolin-4-amine (20b):** A mixture of **21** (102 mg, 0.250 mmol, 1.0 equiv) and KI (83.0 mg, 0.500 mmol, 2.0 equiv) in piperidine (2.49 mL, 2.15 g, 25.0 mmol, 100 equiv) was stirred at 50 °C for 48 h. **20b** (98.0 mg, 86% yield, 98% purity) was isolated by flash chromatography [10% 3 M NH_3 (in MeOH) in CH_2Cl_2] as a colorless solid.

4-(*tert*-Butyl)-1-[3-({4-[(1-isopropylpiperidin-4-yl)amino]-6-methoxyquinazolin-7-yl}oxy)-propyl]pyridin-1-ium chloride (20i) A mixture of **19** (79.1 mg, 0.250 mmol, 1.0 equiv), 4-(*tert*-butyl)-1-(3-iodopropyl)pyridin-1-ium iodide (119 mg, 0.275 mmol, 1.1 equiv) and K_2CO_3 (173 mg, 1.25 mmol, 5.0 equiv) in DMF (0.625 mL) was stirred overnight at rt. The reaction mixture was filtrated, concentrated and purified by flash chromatography [10% 3 M NH_3 (in MeOH) in CH_2Cl_2]. To obtain the product as chloride salt, the isolated quinazoline was resolved in CH_2Cl_2 (2 mL) and extracted with NaCl (958 mg, 10.0 mmol, 40 equiv) in NaOH solution (8 M, 10 mL). The aqueous phase was extracted with CH_2Cl_2 (3 × 10 mL). The combined organic phase was dried over $MgSO_4$, filtrated, and concentrated to yield **20i** (39.1 mg, 30% yield, 97% purity) as a brown solid.

2.2 Determination of Binding Affinities

The affinity of the test compounds for the MB327-PAM-1 binding site of *Torpedo*nAChR was determined by a competitive UNC0642 MS Binding Assay as described previously (Kaiser et al., 2024; Nitsche et al., 2024). General information on the test compounds from commercial sources can be found in the Supporting Information (Table S1). These were employed in the form given in Table S1.

3 Results and Discussion

3.1 Chemistry

To gain further insight into the structure-affinity relationships of UNC0646 analogs regarding their binding to the MB327-PAM-1 binding site of nAChR, a series of related quinazoline derivatives was synthesized. While retaining the 5,8-unsubstituted 6-methoxyquinazoline scaffold, the UNC0646 structure was varied at the 2-, 4-, and/or 7-positions.

The first two sets of compounds investigated (**9a-9e** and **16b** and **11a-11c** and **14**, respectively) consist of structurally closely related analogs of UNC0646 (**1**), in which the residues at either the 2- or 4-position have been gradually reduced in size, as shown in Figure 2.

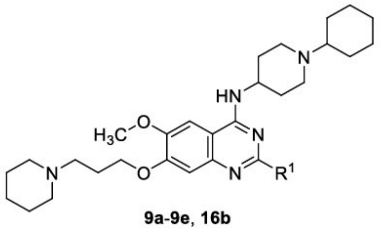

9a-9e, 16b

	9a	**9b**	**9c**
R^1 =	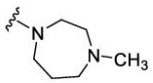	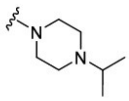	

	9d	**9e**	**16b**
R^1 =			

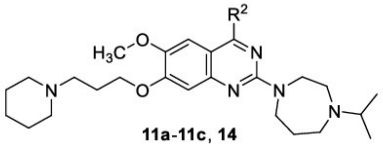

11a-11c, 14

	11a	**11b**	**11c**	**14**
R^2 =	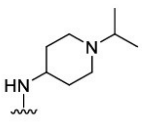	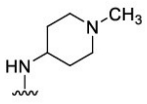		

Figure 2. Structures of target compounds **9a-9e**, **11a-11c**, **14** and **16**.

The key building block for the target compounds **9a**, **9b**, **9d** and **9e**, which differ from UNC0646 (**1**) only in the substituents at the 2-position, is the 2-chloroquinazoline **7**, which was readily accessible in three steps starting from the commercially available building block **4** (Scheme 1).

In the first step, the benzyl ether protecting group was cleaved with hydrogen over a Pd/Al catalyst according to a method described in the literature. (Doig et al., 2014). The yield of 2,4-dichloroquinazolin-7-ol (**5**) was thereby increased from 77% to nearly 100% by extending the reaction time from 2 h as described by Doig et al. to 6 h in this work. In the next step, starting from compound **5**, the 3-(piperidin-1-yl)propoxy side chain was introduced at position 7 of the quinazoline scaffold via a *Mitsunobu* reaction. Accordingly, the quinazolin-7-ol **5** was reacted with 1.25 equivalents of 3-(piperidin-1-yl)propan-1-ol and 1.3 equivalents each of PPh_3 and DBAD (THF, rt, 20 h) to give compound **6** (Vital et al., 2023) in very good yield (81%). Finally, the chlorine atom at the 4-position of 2,4-dichloquinazoline **6** was selectively substituted by reaction with 1.1 equivalents of 1-cyclohexylpiperidin-4-amine under well-established reaction conditions (3.0 equivalents of DIEA, THF, rt, 48 h) (Liu et al., 2011) to give the desired product **7** in 64% yield.

The UNC0646 analogs **9a** and **9b**, which contain a 1-methyl-1,4-diazepane and 1-propan-2-ylpiperazino group, respectively, at the 2-position of the quinazoline ring, were readily obtained starting from building block **7** by microwave-assisted reaction with the corresponding secondary amines (Kaiser et al., 2024; Sundriyal et al., 2017). With a 5-fold excess of secondary amine (toluene, microwave irradiation, 300 W, 130 °C, 50 min), the 2,4-diamino-quinazoline derivatives **9a** (Liu et al., 2011) and **9b** were obtained in high yields of 89% each. The synthesis of compound **9d**, which has a dimethylamino group at the 2-position, required adapted reaction conditions due to the volatility of dimethylamine, as a microwave synthesis as described for **9a** and **9b** was not possible due to the high pressure developed. Therefore, compound **7** was reacted in a conventional manner with dimethylamine in a pressure tube (Venkatesan et al., 2008). The reaction with a tenfold excess of dimethylamine at 100 °C (THF, 48 h) afforded the target compound **9d** in a very good yield (85%). To obtain the 2-aminoquinazoline **9e** starting from **7**, a two-step one-pot strategy known from the literature (Mohamed and Rao, 2015) based on an azide intermediate was used, since the direct reaction of 4-amino-substituted 2-chloroquinazolines, such as intermediate **7**, with ammonia usually gives poor yields (Aubin et al., 2010; Borzenko et al., 2015). Therefore, the chlorine atom was first replaced by an azide group by reacting **7** with 1.1 equivalents of NaN_3 (EtOH, AcOH, rt to 90 °C, 2 h). The resulting crude azide product was then reduced with 1.5 equivalents of hydrazine hydrate in the presence of Pd/C (rt to 90 °C, 2 h) to give the primary amine **9e**. In addition to the desired target compound **9e**, which was obtained in 49% yield, the by-product **16b** was also formed (16% yield).

Finally, the target compounds **9c** and **9f**, which have a piperidine residue at the 2-position, **9f** being an analog of UNC0631 (**35**) (see Table 1), were readily accessible in one step from the recently described 4-chloroquinazoline building block **8** (Kaiser et al., 2024). Thus, heating of compound **8** with 2.0 equivalents of the corresponding 4-aminopiperidines under microwave irradiation (3.0 equivalents DIEA, *i*-PrOH, 160 °C, 15 min) (Kaiser et al., 2024) afforded **9c** and **9f** in 70% and 58% yields, respectively.

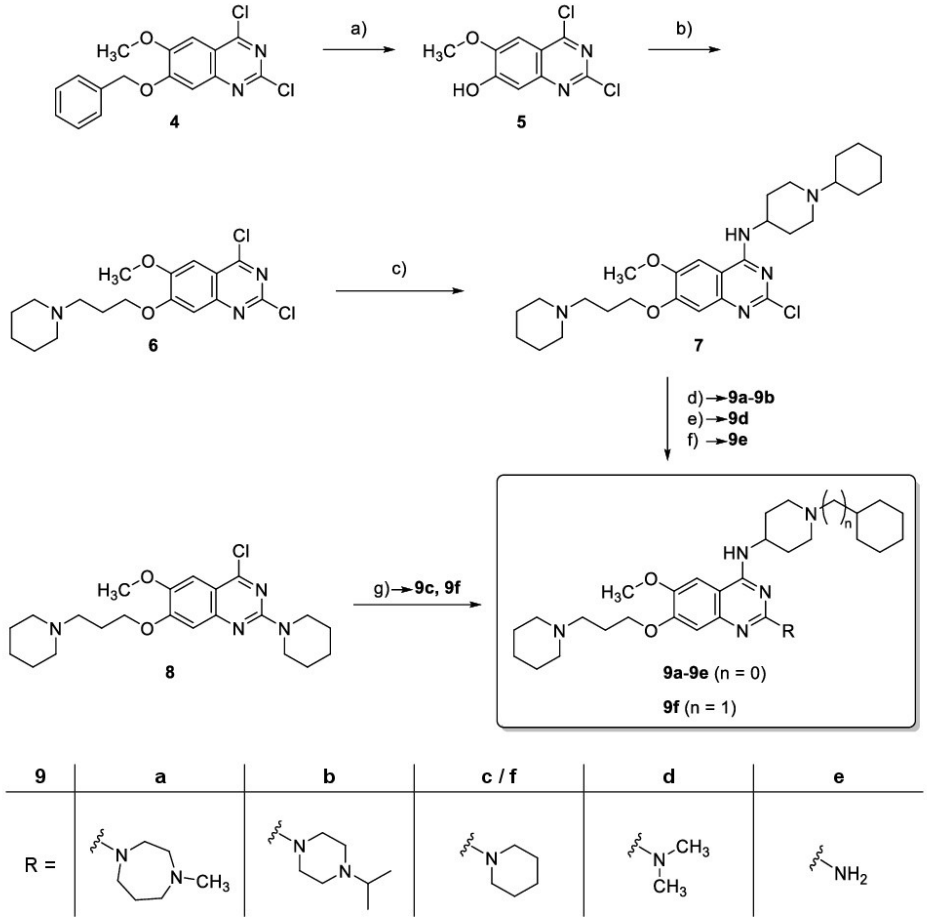

Scheme 1. Reagents and conditions: (a) H_2, 5% Pd/Al (0.08 equiv), THF, 0 °C, 6 h, > 99%; (b) 3-piperidin-1-ylpropan-1-ol (1.25 equiv), PPh_3 (1.3 equiv), DBAD (1.3 equiv), THF, rt, 20 h, 81%; (c) 1-cyclohexylpiperidin-4-amine (1.1 equiv), DIEA (3.0 equiv), THF, rt, 48 h, 64%; (d) 1-methyl-1,4-diazepane or 1-propan-2-ylpiperazine (5.0 equiv), toluene, microwave: 300 W, 130 °C, 50 min; **9a**: 89%, **9b**: 89% (e) dimethylamine (10 equiv), THF, 100 °C, 48 h, 85%; (f) 1. NaN_3 (1.1 equiv), 4:1 EtOH, glacial AcOH, rt to 90 °C, 2 h; 2. 10% Pd/C (0.01 equiv), hydrazine hydrate (1.5 equiv), rt to 90 °C, 2 h, 49% (over two steps); (g) 1-cyclohexylpiperidin-4-amine or 1-(cyclohexylmethyl)piperidin-4-amine (2.0 equiv), DIEA (3.0 equiv), *i*-PrOH, microwave: 200 W, 160 °C, 15 min; **9c**: 70%, **9f**: 58%.

The desired UNC0646 analogs **11a** (UNC618) (Jiang et al., 2017; Liu et al., 2011), **11b** and **11c**, which have amine residues at the 4-position that are gradually reduced in size compared to those of UNC0646 (**1**), were prepared analogously to compounds **9a** and **9b**. First, the intermediates **10a** (Davis et al., 2016; Vital et al., 2023), **10b** and **10c**, which are analogous to compound **7** (see above), were prepared by reacting compound **6** with 1-isopropylpiperidin-4-amine, 1-methylpiperidin-4-amine and methylamine, respectively. The desired compounds **10a-10c** were obtained in 48-86% yields. Intermediates **10a-10c** were then reacted with 1-isopropyl-1,4-diazepane to afford the target compounds **11a-11c** in fair to excellent yields (62-91%) (Scheme 2).

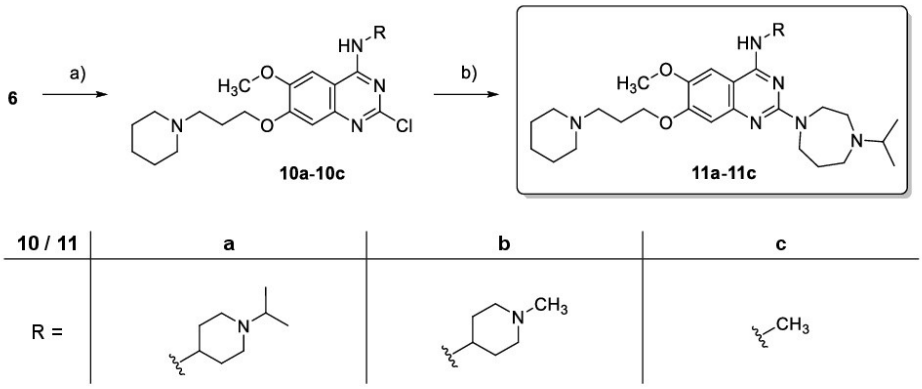

Scheme 2. Reagents and conditions: (a) 1-propan-2-ylpiperidin-4-amine or 1-methylpiperidin-4-amine or methanamine (1.1 equiv), DIEA (3.0 equiv), THF, rt, 48 h, **10a**: 86%, **10b**: 48%, **10c**: 86%; (b) 1-propan-2yl-1,4-diazepane (5.0 equiv), toluene, microwave: 300 W, 130 °C, 50 min; **11a**: 89%, **11b**: 62%, **11c**: 91%.

The synthesis of the 4-unsubstituted UNC0646 analog **14** was carried out starting from the 2,4-dichloroquinazoline building block **6**, as no appropriate 4-unsubstituted 2-chloro-quinazoline building block was commercially available (Scheme 3). Since it is generally not possible to selectively replace the chloro substituent at the 2-position of 2,4-dichloro-quinazolines by reaction with secondary amine nucleophiles, since the 4-substituted products are preferentially formed (see above) (Yamamoto and Shinnkai, 2004), the chloro substituent at the 4-position first had to be selectively removed by reductive means. This was accomplished according to a procedure described in the literature (Abe et al., 1998), by hydrogenolysis with hydrogen over Pd/C in the presence of NEt_3, yielding 2-chloroquinazoline **12** as the major product (61% yield) and the double reduction product **13** as a minor component (19% yield). Finally, the desired product **14** was prepared from **12** and 1-isopropyl-1,4-diazepane under the same reaction conditions as described for the syntheses of **11a**-**11c**, whereby **14** could be isolated in quantitative yield.

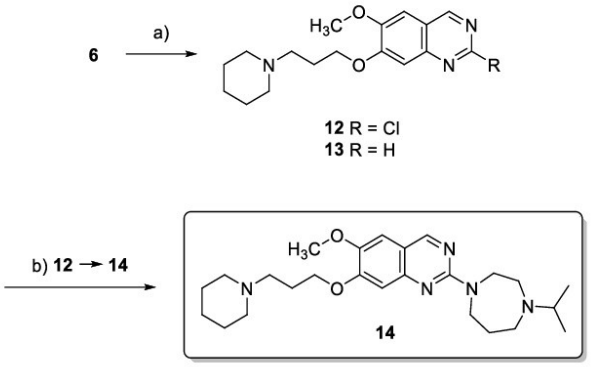

Scheme 3. Reagents and conditions: (a) H_2, 10% Pd/C (0.02 equiv), NEt_3 (1.5 equiv), EtOAc, rt, 4 h, **12**: 61%, **13**: 19%; (b) 1-isopropyl-1,4-diazepane (5.0 equiv), toluene, microwave: 300 W, 130 °C, 50 min, 99%.

As we have recently shown (Kaiser et al., 2024), 2-unsubstituted UNC0646 analogs also exhibit a distinct affinity for the MB327-PAM-1 binding site. Therefore, two series of additional 2-unsubstituted UNC0646 analogs were synthesized in which the substituents at the 4-position (**16a**-**16g**) and at the 7-position (**20a**-**20i** and **23a**-**23c**), respectively, were varied (Table 2 and Table 3).

Starting from building block **15** known from the literature (Kaiser et al., 2024), the target compounds **16a**-**16f** were readily accessible in one step (62-94% yield) by reacting **15** with 2.0 equivalents of the corresponding amines using well-established microwave-assisted reaction conditions (3.0 equivalents DIEA, *i*-PrOH, 160 °C, 15-60 min) (Kaiser et al., 2024; Liu et al., 2011) (Scheme 4). Quinazoline derivative **16g** bearing a (1-isopropylpiperidin-4-yl)oxy-substituent at the 4-position was obtained in 92% yield by reacting **15** with 2.0 equivalents of 1-propan-2-ylpiperidin-4-ol in the presence of NaH (2.0 equivalents, THF, rt, 3 h) (Scheme 4) (Gharat et al., 2015).

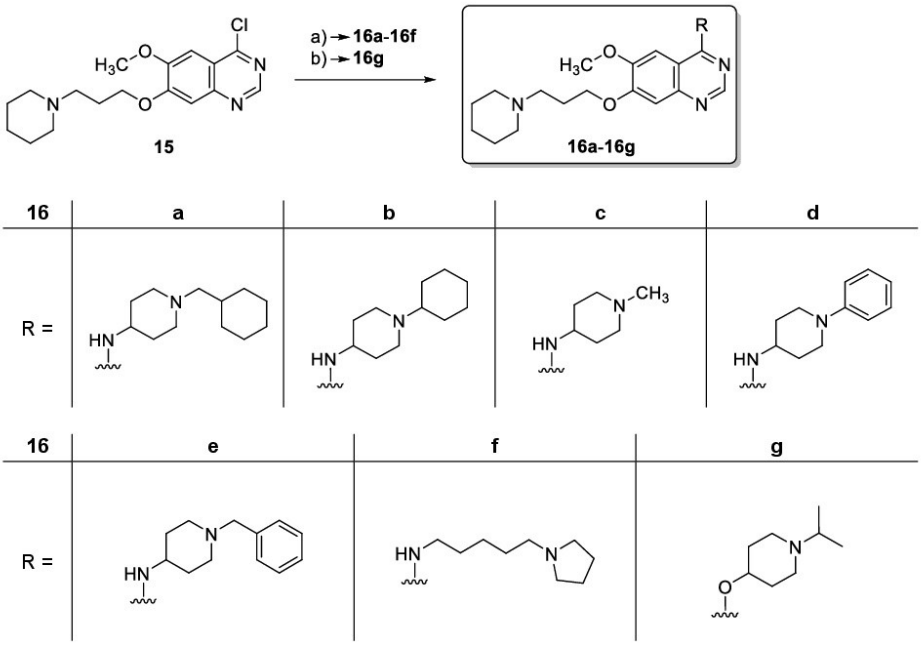

Scheme 4. Reagents and conditions: (a) corresponding amines (2.0 equiv), DIEA (3.0 equiv), *i*-PrOH, microwave: 200 W, 160 °C, 15-60 min, **16a**: 62%, **16b**: 94%, **16c**: 69%, **16d**: 82%, **16e**: 85%, **16f**: 83%; (b) 1-propan-2-ylpiperidin-4-ol (2.0 equiv), NaH (60%, 2.0 equiv), THF, rt, 3 h, 92%.

In addition to the UNC0646 analogs **16a**-**16g**, the 2-unsubstituted quinazoline derivatives **20a**-**20i** and **23a**-**23c** were synthesized, bearing a uniform (1-isopropypiperidin-4-yl)amino residue at the 4-position and varying basic side chains at the 7-position. These side chains are not only linked to the quinazoline backbone via an ether function (compounds **20a**-**20i**), but also via amino functions (compounds **23a**-**23c**).

The key building block **19** for the synthesis of the compounds **20a**-**20i** was prepared in only two steps and in almost quantitative yield from the commercially available building block **17** (Scheme 5). In the first step, the substitution of the chlorine at the 4-position was achieved quantitatively by reaction with 2.0 equivalents of 1-propan-2-ylpiperidin-4-amine (3.0 equivalents DIEA, *i*-PrOH, microwave irradiation, 160 °C, 15 min). In a second step, the benzyl ether protecting group of the resulting building block **18** was cleaved using 10 equivalents of cyclohexa-1,4-diene over a Pd/C catalyst (EtOH, reflux, 2 h) (Liu et al., 2010), to give quinazolin-7-ol **19**.The subsequent introduction of the basic side chains at the 7-position of the quinazoline to generate the target compounds **20a** (Kaiser et al., 2024) and **20c**-**20h** was accomplished in one step via a *Mitsunobu* reaction (5.5 equivalents PPh_3, 5.0 equivalents DIAD, THF, rt, 20 h) (Liu et al., 2011) using 3.5-4.0 equivalents of the corresponding aminoalcohols (46-79% yield). Target compound **20b**, bearing a 4-(piperidin-1-yl)butoxy side chain, was prepared in an alternative two-step procedure. A *Mitsunobu* reaction with the corresponding amino alcohol 4-(piperidin-1-yl)butan-1-ol is not possible in this case, since the intermediate alkoxyphosphonium ion formed from it cyclizes to a 5-azaspiro[4.5]decan-5-ium ion, which is not reactive enough for alkylation reactions (Gmeiner et al., 1994). Therefore, in a first step, quinazolin-7-ol **19** was converted to the 7-(4-chlorobutoxy)quinazoline **21** via a *Mitsunobu* reaction with 4.0 equivalents of 4-chloro-butan-1-ol (5.5 equivalents PPh_3, 5.0 equivalents DIAD, THF, rt, 20 h) (Liu et al., 2011). The subsequent reaction with piperidine (2.0 equivalents, KI, 50 °C, 20 h) (Fagan et al., 2019) then afforded the desired product **20b** in good overall yield (79% over two steps). The synthesis of the hybrid compound **20i**, which carries a partial structure of the prototypical ligand MB327 as a side chain, was also carried out starting from the key building block **19**. Thus, quinazolin-7-ol **19** was first alkylated with 1.1 equivalents of 4-(*tert*-butyl)-1-(3-iodopropyl)pyridin-1-ium iodide (Rappenglück et al., 2018a) (5.0 equivalents K_2CO_3, DMF, rt, 20 h) to obtain the corresponding iodine salt as crude product. After basic extraction of this salt (aqueous NaOH, CH_2Cl_2) in the presence of a large excess of sodium chloride, the desired product **20i** was obtained as the chloride salt (30% yield).

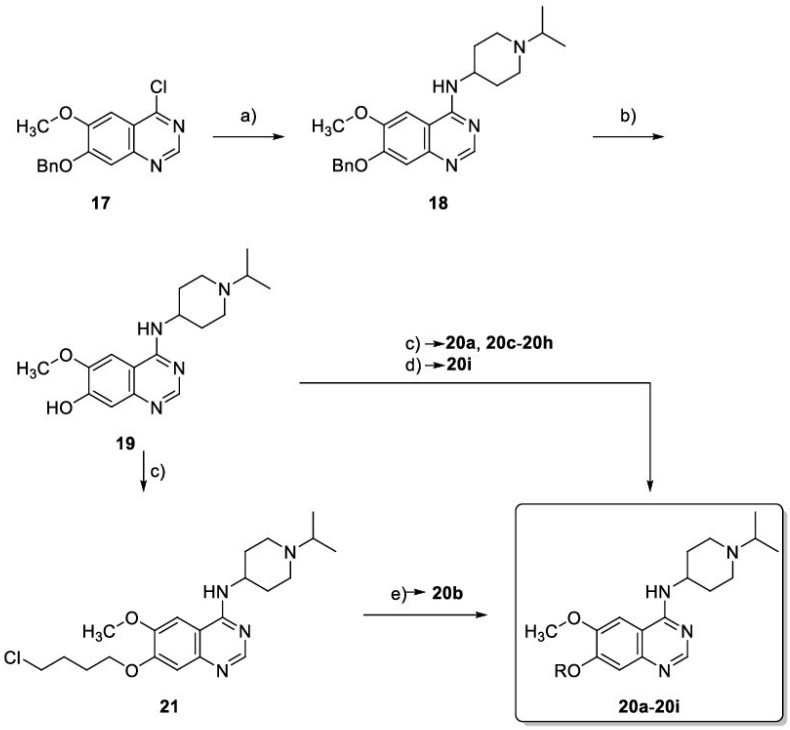

20	a	b	c
R =	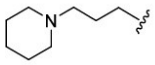	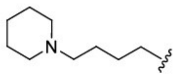	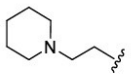

20	d	e	f
R =	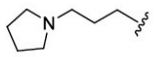	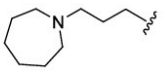	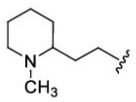

20	g	h	i
R =	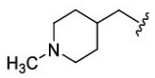	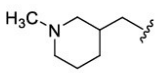	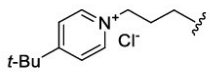

Scheme 5. Reagents and conditions: (a) 1-propan-2-ylpiperidin-4-amine (2.0 equiv), DIEA (3.0 equiv), *i*-PrOH, microwave: 200 W, 160 °C, 15 min, > 99%; (b) cyclohexa-1,4-diene (10 equiv), 10% Pd/C (0.125 equiv), EtOH, reflux, 2 h, > 99%; (c) corresponding aminoalcohols (3.5-4.0 equiv) or 4-chlorobutan-1-ol (4.0 equiv), PPh_3 (5.5 equiv), DIAD (5.0 equiv), THF, rt, 20 h, **20a**: 63%, **20c**: 79%, **20d**: 69%, **20e**: 59%, **20f**: 46%, **20g**: 58%, **20h**: 78%, **21**: 92%; (d) 1. 4-(*tert*-butyl)-1-(3-iodopropyl)pyridin-1-ium iodide (1.1 equiv), K_2CO_3 (5.0 equiv), DMF, rt, 20 h; 2. NaCl, NaOH (8 M), rt, 30% (over two steps); (e) KI (2.0 equiv), piperidine, 50 °C, 20 h, 86%.

Finally, the 7-amino-substituted target compounds **23a-23c** were readily accessible in a single step starting from the recently described 7-fluoroquinazoline building block **22** (Kaiser et al., 2024). Nucleophilic substitution of the fluorine atom with 5.0 equivalents of the corresponding primary or secondary amine (1.1 equivalents K_2CO_3, NMP, 135 °C, 20 h) (Harris et al., 2005; Kaiser et al., 2024) afforded the desired products **23a-23c** in 24-84% yields (Scheme 6).

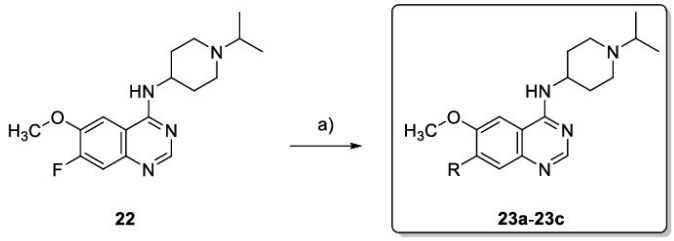

23	a	b	c
R =	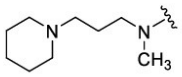	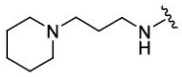	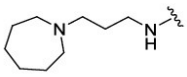

Scheme 6. Reagents and conditions: (a) 3-piperidin-1-ylpropan-1-amine, *N*-methyl-3-piperidin-1-ylpropan-1-amine or 3-(azepan-1-yl)propan-1-amine (5.0 equiv), K_2CO_3 (1.1 equiv), NMP, 135 °C, 20 h, **23a**: 78%, **23b**: 84%, **23c**: 24%.

In addition to the UNC0646 analogs with gradually reduced residues at the 2- and 4-positions (**9a**-**9e**, **11a**-**11c**, **14** and **16b**), the UNC0646 analog **31**, which in contrast to UNC0646 (**1**) bears a methoxy substituent at the 7-position instead of a basic 3-(piperidin-1-yl)propoxy side chain, was of particular interest. As we have recently shown, individual UNC0646 analogs with a 6,7-dimethoxyquinazoline scaffold also exhibit remarkable binding affinities to the MB327-PAM-1 binding site of nAChR (Kaiser et al., 2024). To further investigate the binding behavior of such compounds, we prepared a series of additional UNC0646 analogs with a 6,7-dimethoxyquinazoline scaffold and various substituents at the 2- and 4-positions (**28a**-**28c**, **30a**-**30b**, **31** and **32a**-**32f**) (Table 4). Most of these compounds were accessible in a simple two-step procedure starting from the commercially available 2,4-dichloroquinazoline **24** (Scheme 7 and Scheme 8).

By reaction **24** with 1.1 equivalents of the corresponding primary amines under same reaction conditions as described for the synthesis of **7** from **6** (see above), the intermediates **25**-**27** were prepared according to literature (Ma et al., 2014; Somnarin et al., 2022; Sundriyal et al., 2017; Wang et al., 2019). Deviating from the literature procedures, the reaction time was increased from 2-20 h (47-86% yield) to 48 h, which clearly increased the yields (65-98% yield).The subsequent reaction of the intermediates **25**-**27** with 5.0 equivalents of 1-methyl-1,4-diazepane or 1-propan-2-yl-1,4-diazepane under the established reaction conditions (see above for synthesis of **9a** and **9b**) afforded the desired products **28a**, **28b**-**28c** (Sundriyal et al., 2017) and **31** in excellent yield (94 to > 99%).

For an efficient synthesis of a structurally diverse series of 2,4-diaminoquinazolines starting from readily available 2,4-dichloroquinazolines, it would be of great advantage to be able to replace the chlorine atoms at the 2- and 4-positions by amino groups in any order. As already observed in the synthesis of intermediates **7**, **10a**-**10c** and **25**-**27**, reactions of 2,4-dichloro-quinazolines with primary and secondary amines are highly regioselective at the 4-position. However, Yoshida et al. showed that in the case of 2,4-dichloroquinazoline, the chlorine atom at the 2-position is selectively substituted with amino groups by reaction with tertiary *N*-methylamines with cleavage of the methyl group (Yoshida and Taguchi, 1992). Indeed, the reaction of 2,4-dichloroquinazoline **24** with 2.0 equivalents of 1-methylpiperidine under adapted, microwave-assisted reaction conditions (1,4-dioxane, 300 W, 150 °C, 1 h) (Kaiser et al., 2024) afforded 2-piperidinoquinazoline **29** as the sole product in 81% yield. With intermediate **29** in hand, the desired compounds **30a** (Ma et al., 2014) and **30b** (Sundriyal et al., 2017) were prepared in good yields (84% and 64%, respectively) by reaction with 2.0 equivalents of 5-pyrrolidin-1-ylpentan-1-amine and 1-propan-2-ylpiperidin-4-amine, respectively, under the same reaction conditions as described for the synthesis of **9c** and **9f** (see above).

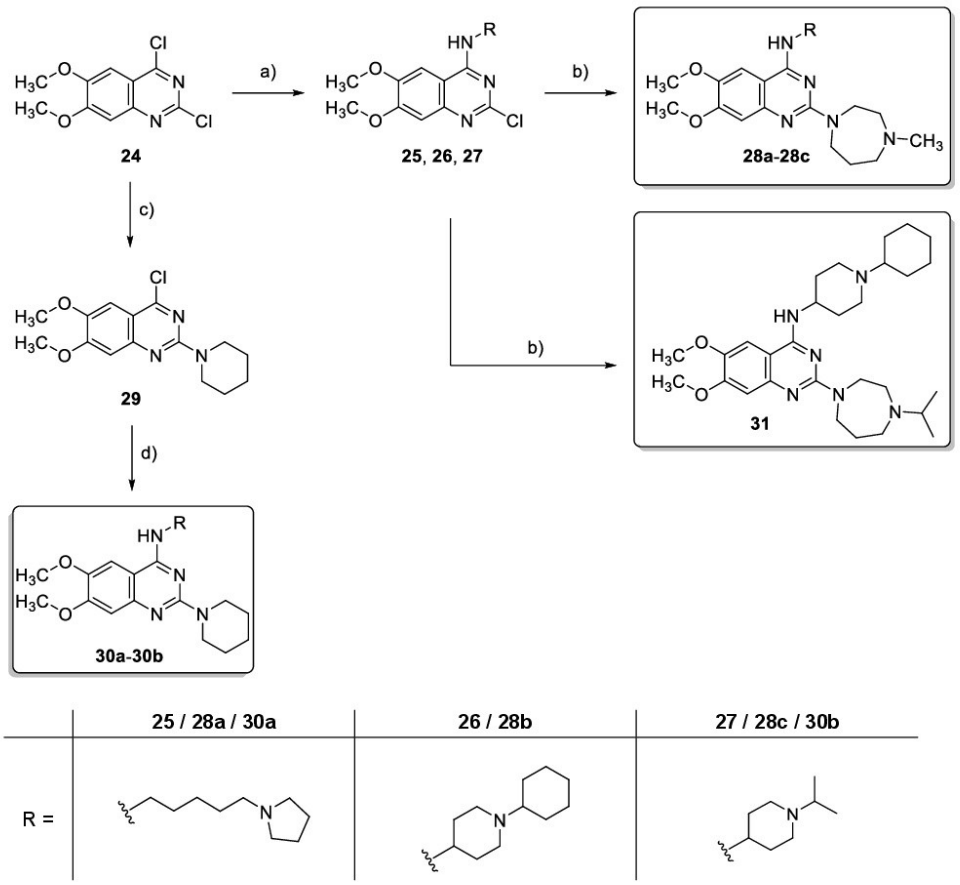

Scheme 7. Reagents and conditions: (a) 5-pyrrolidin-1-ylpentan-1-amine, 1-cyclohexylpiperidin-4-amine or 1-propan-2-ylpiperidin-4-amine (1.1 equiv), DIEA (3.0 equiv), THF, rt, 48 h, **25**: 81%, **26**: 65%, **27**: 98%; (b) 1-methyl-1,4-diazepane or 1-propan-2-yl-1,4-diazepane (5.0 equiv), toluene, microwave: 300 W, 130 °C, 50 min; **28a**: 90%, **28b**: 94%, **28c**: 97%, **31**: > 99%; (c) 1-methylpiperidine (2.0 equiv), 1,4-dioxane, microwave: 300 W, 150 °C, 1 h, 81%; (d) 5-pyrrolidin-1-ylpentan-1-amine or 1-propan-2-ylpiperidin-4-amine (2.0 equiv), DIEA (3.0 equiv), *i*-PrOH, microwave: 200 W, 160 °C, 15 min, **30a**: 84%, **30b**: 64%.

To investigate the effects of different amino substituents at the 2-position (Kaiser et al., 2024) on the binding affinity of 2,4-diamino-substituted 6,7-dimethoxyquinazolines, a series of compounds **32a-32f** derived from compounds **28c** and **30b**, respectively, were synthesized (Scheme 8). Using the known substitution procedure, compounds **32a-32d** were readily obtained by analogy with compound **28c** starting from intermediate **27**. Thus, reacting **27** with a 5-fold excess of the corresponding secondary amines gave the desired compounds **32a-32c** and **32d** (Cui et al., 2020) in 67 to 97% yield. The synthesis of 2-aminoquinazoline **32e** followed a two-step, one-pot azide-based procedure analogous to the synthesis of compound **9e** described above. By replacing the chlorine atom of **27** with an azide group and subsequent reduction of the intermediate, the primary amine **32e** was obtained in good yield (78%). As in the analogous synthesis of **9e**, the corresponding 2-unsubstituted by-product was also formed here (**32f**, 5% yield).

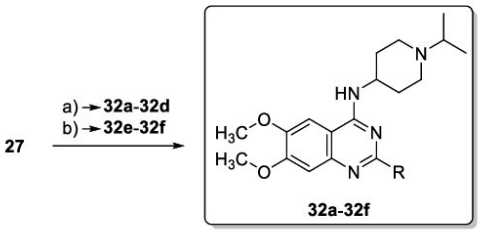

32	a	b	c
R =	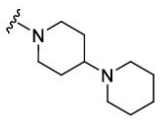	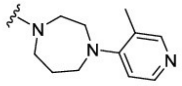	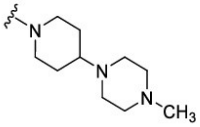

32	d	e	f
R =	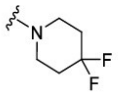		

Scheme 8. Reagents and conditions: (a) corresponding amines (5.0 equiv), toluene, microwave: 130 °C, 50 min; **32a**: 91%, **32b**: 67%, **32c**: 84%, **32d**: 97%; (b) 1. NaN_3 (1.1 equiv), 4:1 EtOH, glacial AcOH, rt to 90 °C, 2 h; 2. 10% Pd/C (0.01 equiv), hydrazine hydrate (1.5 equiv), rt to 90 °C, 2 h, **32e**: 78% (two steps), **32f**: 5% (two steps).

The last series of test compounds, 4-amino-substituted 2-piperidinoquinazolines bearing a benzyloxy group at the 7-position, **34a**-**34c** (Table 5), were synthesized in two steps starting from the commercially available building block **4** analogously to the compounds **30a**-**30b** described above. Intermediate **33** was obtained in 86% yield by regioselective nucleophilic displacement of the 2-chloro substituent of **4** with 1.2 equivalents of 1-methylpiperidine. Subsequent reaction with 2.0 equivalents of the corresponding amines afforded the target compounds **34a**-**34c** in good to high yield (68-86%) (Scheme 9).

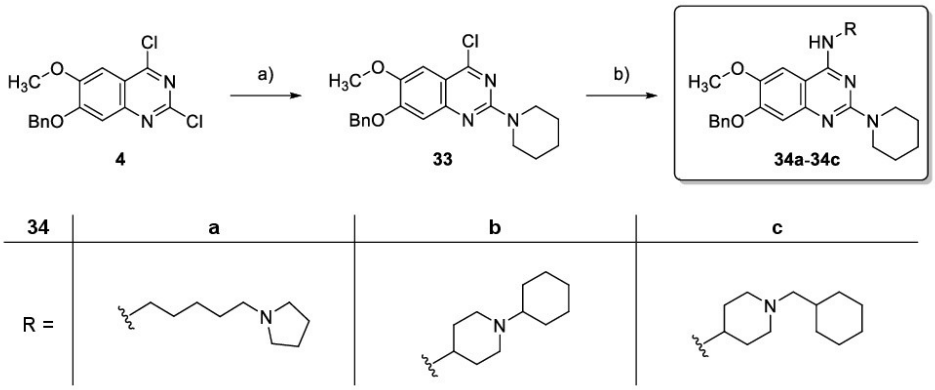

Scheme 9. Reagents and conditions: (a) 1-methylpiperidine (1.2 equiv), 1,4-dioxane, 150 °C (300 W), 1 h, 86%; (b) 5-pyrrolidin-1-ylpentan-1-amine, 1-cyclohexylpiperidin-4-amine or 1-(cyclohexylmethyl)-piperidin-4-amine (2.0 equiv), DIEA (3.0 equiv), *i*-PrOH, microwave: 200 W, 160 °C, 15 min, **34a**: 86%, **34b**: 68%, **34c**: 73%.

3.2 Biological evaluation

All compounds synthesized as part of this study supplemented by compounds from commercial sources, that appeared of interest because of structural relations, were characterized regarding their affinity towards the MB327 binding site of the nAChR. To this end the recently developed UNC0642 MS Binding Assay for the MB327-PAM-1 binding site was used. Based on the obtained data first structure-affinity relationships for the studied quinazoline derivatives were established. For economic reasons test compounds were studied at a single concentration, i.e. of 10 µM, in the UNC0642 MS Binding Assays with the concentration of the reporter ligand UNC0642 (**2**) being set to 1 µM. As deduced from affinity calculation for competitive binding and as known from previous studies based on this setup, it can be assumed that compounds with binding affinities comparable to that of UNC0646 (**1**, $pK_i = 5.83 \pm 0.05$) lead to a distinct reduction of specific reporter ligand binding, i.e. to about ~ 20% (Kaiser et al., 2024). Accordingly, compounds with binding affinities in the range of that of UNC0646 (**1**) including those with binding affinities up to nearly 100 µM should be clearly identifiable. In the following the discussion and interpretation of the test results is divided into five categories corresponding to the respective compound classes with the data being listed in five individual tables.

At first, compounds derived from UNC0646 (**1**), exhibiting the highest yet known affinity towards the MB327-PAM-1 binding site of the nAChR, by varying the structure and in particular reducing the size of the substituents in 2- and 4-position were studied (see Table 1).

In one set of compounds the substituents of UNC0646 (**1**, Table 1, Entry 1) in 4-, 6- and 7-position remained unchanged whereas the 4-isopropyl-1,4-diazepan-1-yl residue of UNC0646 (**1**) in 2-position of the quinazoline scaffold was gradually reduced in size. In the individual compounds thus in this position either a 4-methyl-1,4-diazepan-1-yl (**9a**, Table 1, Entry 2), a 4-isopropylpiperazin-1-yl (**9b**, Table 1, Entry 3) or a piperidin-1-yl residue (**9c**, Table 1, Entry 4) is present. Furthermore, compounds with even smaller substituents in the 2-position, i.e. a *N*,*N*-dimethylamino (**9d**, Table 1, Entry 5), an amino function (**9e**, Table 1, Entry 6) or just hydrogen were studied (**16b**, Table 1, Entry 7). In the latest case with only hydrogen in 2-position the lowest binding affinity in this series of compounds is observed, which is still characterized by a significant reduction of reporter ligand binding down to 50 ± 5% (Table 1, Entry 7). Remarkably, for the test compounds with a 1,4-diazepan-1-yl (**9a**), a piperazin-1-yl (**9b**), a dimethylamino (**9d**) and an amino residue (**9e**) the remaining reporter ligand binding ranged from 23% to 27% (Table 1, Entries 2, 3, 5, 6). The binding affinities of these compounds are thus very similar to each other and to that of UNC0646 (**1**, 21 ± 3%). In case of the 2-piperidin-1-yl substituted quinazoline derivative **9c** the affinity to the MB327-PAM-1 binding site seems somewhat higher with the remaining reporter ligand binding amounting to 11 ± 3% (Table 1, Entry 4). Though this value is even below the remaining reporter ligand binding of UNC0646 (**1**) as competitor (21 ± 3%, Table 1, Entry 1), the pK_i values determined for **9c** ($pK_i = 5.83 \pm 0.02$) and UNC0646 (**1**, $pK_i = 5.83 \pm 0.05$) (in full scale competition experiments) indicate, that the binding affinities for both compounds are the same.

According to the result from recent *in silico* studies, residues in 2-position of the quinazoline derivatives exhibit only minor interactions with the receptor (Kaiser et al., 2024; Nitsche et al., 2024). This may explain the very similar binding affinities observed for **1** and **9a**-**9e**. The

relatively strong decline of the binding affinity in case of **16b** might be due to the decreased basicity of the quinazoline ring resulting from the lack of an amino group in 2-position as a mesomeric donor.

The second set of compounds comprises derivatives of UNC0646 (**1**) in which the substituent in 2-position is left unchanged whereas the substituents in 4-position are delineated from the original 1-cyclohexylpiperidin-4-amino residue by a stepwise reduction of the size of the latter. Thus, in 4-position a 1-isopropylpiperidin-4-amino (**11a**, Table 1, Entry 8), a 1-methylpiperidin-4-amino (**11b**, Table 1, Entry 9) a *N*-methylamino residue (**11c**, Table 1, Entry 10), or only a hydrogen (**14**, Table 1, Entry 11) is present. Upon reduction of the terminal *N*-cyclohexyl residue within the substituent in 4-position (**1**, Table 1, Entry 1) to an isopropyl moiety (**11a**, Table 1, Entry 8) or methyl group (**11b**, Table 1 Entry 9), a nominal increase of the remaining reporter ligand binding from 21 ± 3% to 33 ± 6% and 37 ± 4%, respectively, is observed. This nominal increase of remaining reporter ligand binding corresponding to a decrease of binding affinity further continued when only a *N*-methylamino group (**11c**, 39 ± 5%, Table 1, Entry 10) or finally only a hydrogen atom (**14**, 44 ± 8%, Table 1, Entry 11) was present. Thus, a comparably large *N*-alkyl residue attached to the piperidin-4-amino substituent in 4-position of the quinazoline skeleton as in **1** appears favorable for the binding affinity for the MB327-PAM-1 binding site (compare binding affinity of **1** to binding affinity of **11a** and **11b**), though the influence of the 4-substituent overall is moderate (compare binding affinity of **1** to binding affinity of **11c** and **14**). This trend of larger *N*-alkyl residues attached to the piperidine nitrogen of the 4-substituent of the quinazoline moiety resulting in higher binding affinities continued for the UNC0646 analog UNC0631 (**35**, Table 1, Entry 13). The latter by exhibiting a cyclohexylmethyl residue instead of the smaller cyclohexyl moiety present in UNC0646 (**1**) gives rise to a remaining reporter ligand binding of 12 ± 0.5%, which is significantly lower than that of UNC0646 (**1**, 21 ± 3%). The higher binding affinity of **35** as compared to **1** is further corroborated by the pK_i value determined for this compound, which by amounting to 6.04 ± 0.04 (pK_i, **35**) is significantly higher than that of **1** (pK_i = 5.83 ± 0.05).

Having studied the influence of the substituents in 2- and 4-position of the quinazoline ring on the affinity of the UNC0646 analogs, also the relevance of the side chain in 7-position, in particular of the terminal piperidine ring should be evaluated. To this end, the 3-(piperidin-1-yl)propoxy substituent in this position was replaced by a methoxy group. According to the remaining reporter ligand binding of 65 ± 7% found for the respective compound, the UNC0646 analog **31** (Table 1, Entry 12), the binding affinity of this compound is distinctly lower than that of UNC0646 (**1**, remaining reporter ligand binding 21 ± 3%) but still significant. Hence, the 7-substituent in UNC0646 (**1**) significantly contributes to the binding affinity of this compound, but may be partly omitted, i.e. reduced to a methoxy group, while still a reasonable binding affinity remains.

As in preliminary experiments a substitution of the residue in 2-position of the original quinazoline derivative UNC0646 (**1**) with a piperidino moiety and an exchange of the terminal cyclohexyl group in the 4-substituent of **1** by a cyclohexylmethyl residue had yielded a reduction of remaining reporter ligand binding indicating the potential to enhance binding affinities, it was assumed that a combination of both measures might further improve the binding affinity (compare remaining reporter ligand binding of **9c** and **35** with **1**). For compound **9f** (Table 1, Entry 14) comprising the aforementioned structural adaptations a value of 6 ± 1% for the remaining reporter ligand was found, which is distinctly lower than the values observed for **9c** (11 ± 3%) and **35** (12 ± 0.5%) and thus points to an increase in binding affinity as

compared to the aforementioned compounds as well as of UNC0646 (**1**). According to the pK_i value, that has finally been determined in full scale competition experiments for the hybrid compound **9f**, the binding affinity of this compound, **9f**, by amounting to 5.84 ± 0.03 (pK_i) is, however, in the same range as that of the precursor compounds **9c** (pK_i = 5.83 ± 0.02) and **35** (pK_i = 6.04 ± 0.04) as well as of the reference compound UNC0646 (**1**, pK_i = 5.83 ± 0.05).

Table 1: Binding affinities of analogues of UNC0646 (**1**) with varying structures of the substituents in 2- and 4-position for the MB327-PAM-1 binding site of *Torpedo*-nAChR. [a] 'reporter ligand binding' refers to the remaining binding of the reporter ligand (UNC0642, 1 µM) in presence of the respective test compound (10 µM) as % value ± SD; see Material and Methods for details. [b] 'reporter ligand binding' and/or pK_i value have been reported previously (Kaiser et al., 2024; Nitsche et al., 2024).

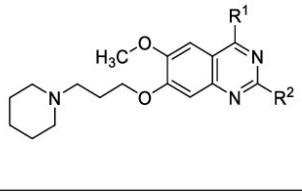	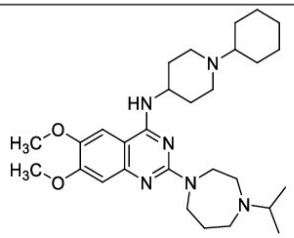
1, **9a-9f**, **11a-11c**, **14**, **16b**, **35**	**31**

Entry	Compound	R^1	R^2	reporter ligand binding [%] [a]	PTMD01 code
1	**1** (UNC0646)	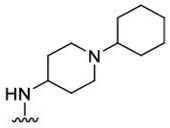	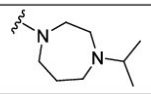	21 ± 3 (n = 30) pK_i = 5.83 ± 0.05 [b]	-
2	**9a**		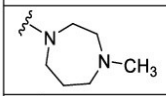	23 ± 2	47L
3	**9b**		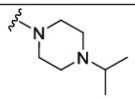	26 ± 5	71
4	**9c**			11 ± 3 pK_i = 5.83 ± 0.02	49
5	**9d**			23 ± 4	48
6	**9e**			27 ± 2	65
7	**16b**			50 ± 5 (n = 12) [b]	04

Continued next page

Table 1 *(continued)*

Entry	Compound	R^1	R^2	reporter ligand binding [%] [a]	PTMD01 code
8	**11a** (UNC618)	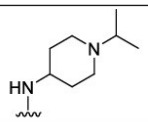	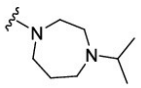	33 ± 6	-
9	**11b**	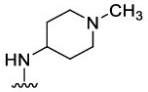		37 ± 4	45
10	**11c**			39 ± 5	46
11	**14**			44 ± 8	40
12	**31**	-	-	65 ± 7 (n = 9)	01
13	**35** (UNC0631)	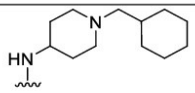	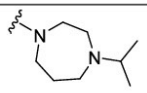	12 ± 0.5 pK_i = 6.04 ± 0.04	-
14	**9f**	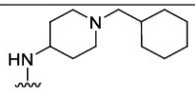		6 ± 1 pK_i = 5.84 ± 0.03	70

For the UNC0646 (**1**) analog **16b** differing from **1** by the lack of a 2-substituent the remaining reporter ligand binding by amounting to 50 ± 5% was found as described above to be distinctly higher than that of the reference compound UNC0646 (**1**, 21 ± 3%; see Table 1, Entry 1 and 7). Though the binding affinity of **16b** is thus significantly lower than that of **1**, it is still of a decent size. Hence, analogs of this compound, **16b**, with varying substituents in 4-position should be studied with regard to their binding affinities, as this might supplement the so far established structure affinity relationships. The compounds selected in this context, the synthesis of which is comparably easy to accomplish, are listed in Table 2.

The first subset of compounds to be discussed regarding their binding affinities comprises the quinazoline derivatives **16b**, **20a**, **16c** and **16a** (Table 2, Entries 1-4). These compounds differ with regard to their *N*-alkyl substituents attached to the terminal amino group of the piperidin-4-amino residue in 4-position of the quinazoline system, which are a cyclohexyl, an isopropyl, a methyl and a cyclohexylmethyl group. As observed before for the UNC0646 analogs **11a**-**11c** and **35** (see Table 1) also for **16b**, **20a**, **16c** and **16a** (Table 2, Entries 1-4) the binding affinity increases, which is mirrored by a decrease in remaining reporter ligand binding, in parallel to the increasing size of the aforementioned *N*-alkyl substituents. Thus, while **16a** with a *N*-cyclohexylmethyl residue effects a remaining reporter ligand binding of 41 ± 4%, this value goes continuously up to 50 ± 5% for the *N*-cyclohexyl (**16b**), 63 ± 4% for the *N*-isopropyl (**20a**) and finally to 80 ± 2% for the *N*-methyl derivative (**16c**).

In addition, the effect of the substitution of the *N*-cyclohexyl residue present in **16a** and the *N*-cyclohexylmethyl moiety in **16b** by a phenyl (→ **16d**) and a benzyl group (→ **16e**),

respectively, on the remaining reporter ligand binding has been evaluated. These structural variations have, however, no significant effect on the binding affinity, the remaining reporter ligand binding amounting to 50 ± 3% for the phenyl and 46 ± 3% for the benzyl derivative **16d** and **16e**, respectively, which values are identical or at least very close to those observed for the saturated analogs **16b** (50 ± 5%, Table 2, Entry 2) and **16a** (41 ± 4%, Table 2, Entry 1).

In a recent study a quinazoline derivative with a 5-(pyrrolidin-1-yl)pentan-1-amino residue in the 4-position of **9c** instead of the 1-cyclohexylpiperidin-4-amino residue was found to remain a similar binding affinity as the original compound **9c** (Kaiser et al., 2024). When an analogous exchange was undertaken for **16b** the binding affinity of the resulting compound **16f** (remaining reporter ligand binding 65 ± 5%, Table 2, Entry 7) was, to some extent lower than that of the reference compound (**16b**, remaining reporter ligand binding 50 ± 5%, Table 2, Entry 2).

When the secondary amino function attached to the 4-position of **20a** was replaced by an ether oxygen, to expand the structure affinity relationship study, the thus modified compound **16g** showed a decreased binding affinity (as compared to **20a**, 63 ± 4%, Table 2, Entry 2). Interestingly, with 74 ± 4% the value of the remaining reporter ligand binding for this compound, **16g** (Table 2, Entry 8), is still of a reasonable size indicating that even an ether function instead of an amino function is tolerated in 4-position of the quinazoline. When, however, a substituent in 4-position of the quinazoline ring is omitted in this series of compounds listed in Table 2, then as can be seen from the data obtained for **13** any binding affinity appears to be lost (remaining reporter ligand binding 100 ± 7%, Table 2, Entry 9).

Finally, also the commercially available drug Tandutinib (**36**) structurally related to the compounds in Table 2 was included in this study. The remaining reporter ligand binding for this compound describing its affinity amounted to 66 ± 6% (Table 2, Entry 10). Though, this binding affinity is relatively low, it is still of reasonable size, indicating that Tandutinib (**36**) known as an inhibitor of the FMS-like tyrosine kinase 3, is also as a ligand of the MB327-PAM-1 binding site of the nAChR.

Table 2: Binding affinities of UNC0646 analogs devoid of a 2-substituent but with varying 4-substituents for the MB327-PAM-1 binding site of the *Torpedo*-nAChR. [a] 'reporter ligand binding' refers to the remaining binding of the reporter ligand (UNC0642, 1 µM) in presence of the respective test compound (10 µM) as % value ± SD; see Material and Methods for details. [b] 'reporter ligand binding' has been reported previously (Kaiser et al., 2024).

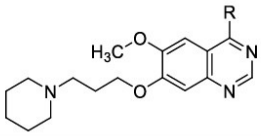

13, 16a-16g, 20a, 36

Entry	Compound	R	reporter ligand binding [%] [a]	PTMD01 code
1	**16a**	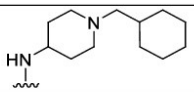	41 ± 4	07

Continued next page

Table 2 *(continued)*

Entry	Compound	R	reporter ligand binding [%] [a]	PTMD01 code
2	**16b**	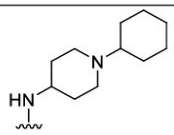	50 ± 5 (n = 12) [b]	04
3	**20a**	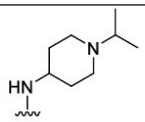	63 ± 4 (n = 6) [b]	05
4	**16c**	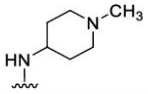	80 ± 2	06
5	**16d**	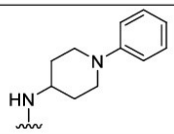	50 ± 3	08
6	**16e**	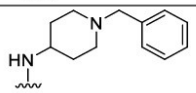	46 ± 3	09
7	**16f**	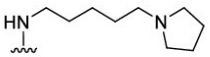	65 ± 5	51
8	**16g**	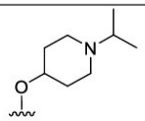	74 ± 4	54
9	**13**		100 ± 7	52
10	**36** (Tandutinib)	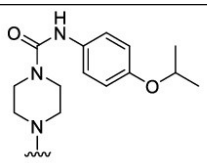	66 ± 6	-

Next, the binding affinities of UNC0646 analogs devoid of a 2-substituent but with varying 7-substituents for the MB327-PAM-1 binding site were studied. The structures of these analogs and their binding affinities again determined by means of UNC0642 MS Binding Assays are listed in Table 3.

First, the influence of the chain length of the spacer between the ether and the amino function of the side chain in 7-position of the quinazoline scaffold on the binding affinity was studied by extending as well as shortening it by one methylene group leading from **20a** with a propan-1,3-diyl (Table 3, Entry 1) to **20b** with a butan-1,4-diyl (Table 3, Entry 2) and **20c** with an ethan-1,2-diyl chain (Table 3, Entry 3), respectively. This, however, did not have any significant effect

on the binding affinity, the remaining reporter ligand binding amounting to 63 ± 4% (**20a**), 64 ± 3% (**20b**) and 63 ± 2% (**20c**), respectively, and thus stays almost constant.

Furthermore, the effect of the terminal heterocycle of the side chain in the 7-position of **20a** on the binding affinity was studied. When the respective piperidine ring of **20a** is exchanged by a pyrrolidine-1-yl and azepan-1-yl moiety resulting in **20d** and **20e**, respectively, the remaining reporter ligand binding of **20a** of 63 ± 4% (Table 3, Entry 1) increases to 76 ± 5% for **20d** (Table 3, Entry 4) whereas it descends to 55 ± 5% for **20e** (Table 3, Entry 5). Hence, there is a clear trend, according to which an increase of the ring size of the terminal azaheterocycle of the 7-substituent in these quinazoline derivatives gives rise to improved binding affinities.

In the compounds **20f**, **20g** and **20h**, the attachment point of the spacer in the 7-substituent of the quinazoline derivative **20a** is shifted from the nitrogen to the 2-, 4- and 3-position of the terminal piperidine ring, respectively, in combination with adapted spacer lengths. Whereas for the derivative **20g** (Table 3, Entry 7), in which the piperidine ring is linked via the 4-position with the rest of the molecule, the remaining reporter ligand is with 63 ± 1% nominally identical with that of **20a** (63 ± 4%, Table 3, Entry 1), that of **20f** and **20h** attached via the 2- and 3-position, respectively, is higher (**20f**, 71 ± 7%, Table 3, Entry 6; **20h**, 79 ± 7%, Table 3, Entry 8). Thus, these variations appear to have no (**20g**) or only a negative effect on the binding affinity (**20f** and **20h**).

To gain insight on the significance of the ether function in the 7-position of **20a** for the binding affinity, a set of derivatives of **20a**, in which the ether function had been replaced by an amino group, was included in this study as well. When this ether function is replaced by a methylamino group leading to **23a** with a tertiary amino function a clear decrease of binding affinity with the remaining reporter ligand binding ascending to 71 ± 1% occurs (Table 3, Entry 10) as compared to 63 ± 4% for **20a** (Table 3, Entry 1). Interestingly, for **23b** the remaining reporter ligand binding is significantly lower (54 ± 4%; Table 3, Entry 11) than that of the original compound **20a** (63 ± 4%). A further decline of the remaining reporter ligand binding to 45 ± 7% and thus increase of the binding affinity is even observed for the azepan-1-yl analog **23c** (Table 3, Entry 12). The latter improvement is likely to be assigned to the presence of the azepane ring, which also in case of the quinazoline derivative **20a** (Table 3, Entry 1) with an ether function gives rise to an increase in binding affinity when the piperidine ring (in **20a**) is enlarged to an azepane ring (→ **20e**, Table 3, Entry 5). In any case, a secondary amino group instead of an ether function in 7-position of the quinazoline scaffold is according to the above-described results well tolerated giving even rise to a slight increase of the binding affinity.

With MB327 as a prototypic ligand of the MB327-PAM-1 binding site, well characterized in various *in vitro* and *in vivo* assays, in mind we thought it worthwhile to replace the piperidine ring in the side chain in 7-position of **20a** by a 4-*tert*-butylpyridinium group and to thus partly mimic MB327 as a bispyridinium salt comprising two such moieties. The remaining reporter ligand binding found for the respective hybrid compound **20i** (Table 3, Entry 9) is by amounting to 79 ± 2%, however, distinctly higher than that of **20a** (Table 3, Entry 1, 63 ± 4%), thus indicating the reduced binding affinity effected by the performed modification.

To shed some light on the question of the importance of the side chain in 7-position comprising a piperidino moiety for the binding affinity of **20a**, the more basically substituted compounds **18**, **32f** and **22** (Table 3, Entries 13-15) with a benzyloxy, methoxy or a fluoro substituent in

this position, respectively, were also included in this study. The remaining reporter ligand binding found for these compounds are by amounting to 96 ± 2% (**18**), 92 ± 8% (**32f**) and 88 ± 2% (**22**) far higher than that of **20a** (63 ± 4%) indicating a distinct loss of binding affinity due to the structural variations, the binding affinities becoming very low to negligible.

Table 3: Binding affinities of UNC0646 analogs devoid of a 2-substituent but with varying 7-substituents for the MB327 binding site of the *Torpedo*-nAChR. [a] 'reporter ligand binding' refers to the remaining binding of the reporter ligand (UNC0642, 1 µM) in presence of the respective test compound (10 µM) as % value ± SD; see Material and Methods for details. [b] 'reporter ligand binding' has been reported previously (Kaiser et al., 2024).

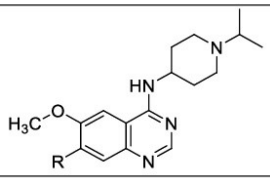

18, **20a-20i**, **22**, **23a-23c**, **32f**

Entry	Compound	R	reporter ligand binding [%] [a]	PTMD01 code
1	**20a**	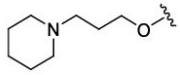	63 ± 4 (n = 6) [b]	05
2	**20b**	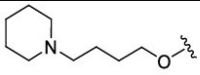	64 ± 3	16
3	**20c**	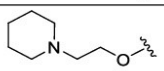	63 ± 2	10
4	**20d**	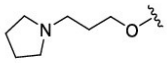	76 ± 5	12
5	**20e**	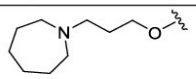	55 ± 5	11
6	**20f**	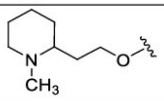	71 ± 7	13
7	**20g**	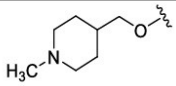	63 ± 1	14
8	**20h**	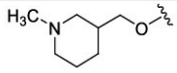	79 ± 7	15
9	**20i**	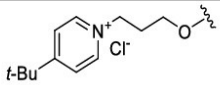	79 ± 2	17
10	**23a**	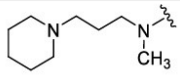	71 ± 1	41

Continued next page

Table 3 *(continued)*

Entry	Compound	R	reporter ligand binding [%] [a]	PTMD01 code
11	**23b**	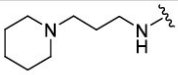	54 ± 4 (n = 6)	42
12	**23c**	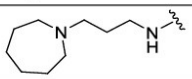	45 ± 7	63
13	**18**	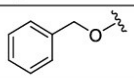	96 ± 2	68
14	**32f**		92 ± 8	69
15	**22**		88 ± 2	72

For the transformation of UNC0646 (**1**) into its analog **31** by exchange of the 3-(piperidin-1-yl)propoxy group in 7-position by a methoxy substituent, as already outlined above, a distinct decline in binding affinity has been observed reflected by an increase of the remaining reporter ligand binding from 21 ± 3% for **1** to 65 ± 7% for **31**. But for a compound of this size, **31** being notably smaller than **1**, this binding affinity is still reasonable. Moreover, for some analogs of **31** promising results had been reported in a recent study (Kaiser et al., 2024). Hence, a set of analogs of **31** for which the substituents in 2- and 4-position are varied but the 6,7-dimethoxyquinazoline scaffold is kept constant should be studied for their binding affinity for the MB327-PAM-1 binding site.

When as a first measure, the 4-isopropyl-1,4-diazepan-1-yl substituent in 2-position was reduced in size by replacing the isopropyl by a methyl group, the remaining reporter ligand binding goes nominally down from 65 ± 7% for **31** to 57 ± 4% for **28b** (Table 4, Entry 4). Though this might indicate an increase in binding affinity, this change lacks statistical significance.

A reduction of the size of the 4-substituent in **28b** by replacement of the terminal hexyl by an isopropyl group, however, leads to a distinct decrease in binding affinity, the remaining reporter ligand binding increasing from 57 ± 4% for **28b** (Table 4, Entry 4) to 74 ± 1% for **28c** (Table 4, Entry 6). This is in line with a former observation, according to which large *N*-alkyl residues as in the 1-cyclohexylpiperidin-4-amino rest in 4-position are more favorable for higher binding affinities (compare listed data for **16a**-**16c** and **20a**, Table 2, and in addition the listed data for **11a**, **11b**, **1** and **35**, Table 1). Similarly, as already observed for the analogs **16b** and **16e** (Table 2, Entry 2 and 6) differing by the terminal *N*-substituent of the piperidin-4-amino residue in 4-position of the quinazoline scaffold, i.e. a cyclohexyl versus a benzyl group, this switch has here, as well, no significant influence on the binding affinity. Thus, whereas for the *N*-cyclohexyl analog **28b** the remaining reporter ligand binding amounts 57 ± 4%, the *N*-benzyl analog **37**, gives rise to a nominal increase to 64 ± 4% (Table 4, Entry 3) which is, however, not statistically significant.

In a two-dimensional *in silico* similarity search for UNC0646 analogs, among 6,7-dimethoxyquinazoline derivatives one compound (UNC0379) with a 5-(pyrrolidin-1-yl)pentan-

1-amino moiety in 4-position with promising binding affinity has been found. In the present set of compounds, **28a** exhibiting the same residue (5-(pyrrolidin-1-yl)pentan-1-amino moiety) the remaining reporter ligand binding amounted 56 ± 3% that is in the same range as for **28b** (57 ± 4%) with a 1-cyclohexylpiperidin-4-amino residue known from UNC0646. For **30a**, which is formally deduced from **28a** by exchange of the 4-methyl-1,4-diazepan-1-yl by a piperidine residue in 2-position a decrease of the remaining reporter ligand binding from 56 ± 3% (for **28a**) to 48 ± 5% (for **30a**) is observed. This change, however, does not reflect an increase in binding affinity, as the difference does lack statistical significance. Still, a positive effect of the presence of the 5-(pyrrolidin-1-yl)pentan-1-amino moiety on the binding affinity becomes apparent, when compound **30a** is compared to **30b**, both exhibiting a piperidine ring in 2-position. Here, the exchange of the substituent in 2-position, i.e. of the 1-isopropylhexylpiperidin-4-amino (in **30b**) by a 5-(pyrrolidin-1-yl)pentan-1-amino residue (in **30a**) leads to a decline of the remaining reporter ligand binding from 66 ± 5% (**30b**, Table 4, Entry 11) to 48 ± 5% (**30a**, Table 4, Entry 1) indicating an increase in binding affinity.

As already described above, for the quinazoline derivative **28c** exhibiting a 4-methyl-1,4-diazepan-1-yl moiety in 2- and a 1-isopropylpiperidin-4-amino residue in 4-position only a modest binding affinity has been found (remaining reporter ligand binding 74 ± 1%, Table 4, Entry 6). Yet, it seemed of interest to explore to what extent the binding affinity of this compound, **28c**, depends on the structure of the substituent in 2-position. Hence, we investigated the binding affinity of analogs of **28c**, for which the structure of the 2-substituent was altered, whereas that of all other substituent was kept constant.

For **32a** with an 1,4´-bipiperidine moiety, **32c** with an 4-(4-methlypiperazin1-yl)piperidine moiety, **32d** with a 4,4-difluoropiperidine and **30b** with a piperidine ring in 2-position the remaining reporter ligand binding varied only to a small extent, the values reaching from 64% to 66%. Thus, the binding affinities of these derivatives delineated from **28c** are very similar to that of the original compound, **28c**, exhibiting a remaining reporter ligand binding of 74 ± 1% (Table 4, Entry 6).

In a related study the (3-methylpyridin-4-yl)-1,4-diazepan-1-yl located in in the 4-position of a quinazoline derivative has been found to mediate a positive effect on the binding affinity of the respective test compound (Kaiser et al., 2024). Interestingly, this is the case here, too, as compound **32b** with the aforementioned substituent in 2-position exhibits a distinct increase in binding affinity as compared to **28c**, the remaining reporter ligand binding of **32b** ranging with 41 ± 9% (Table 4, Entry 8) significantly below the 74 ± 1% of **28c** (Table 4, Entry 6).

For the two UNC0646 (**1**, Table 1, Entry 1) analogs **9e** (Table 1, Entry 6) and **16b** (Table 1, Entry 7), in which the 4-isopropyl-1,4-diazepane residue of **1** in the 2-position of the molecule has been replaced by a primary amino group (**9e**) or just an hydrogen (**16b**), the binding affinity remained in the first case almost unchanged (remaining reporter ligand binding 27 ± 2%) or in the second case was lowered but remained still reasonable (50 ± 5%). A similar trend is observed upon transition from **28c** to its analogs **32e** and **32f**, that can be considered as parent compounds. When instead of the 4-methyl-1,4-diazepane substituent in 2-position of **28c** a primary amino group is present (**32e**) the remaining reporter ligand binding is with 75 ± 2% almost identical with that of **28c** (74 ± 1%). In case of the in 2-position unsubstituted analog of **28c**, **32f**, the binding affinity decreases and as it starts already at a low level for **28c** (remaining reporter ligand binding 74 ± 1%) it this time almost vanishes (remaining reporter ligand binding 92 ± 8%).

By exhibiting a primary amino function in 2- and 4-position of 6,7-dimethoxyquinazoline compound **40** it comprises all of the most fundamental structural features of the compound listed in Table 4. As this compound, **40**, as well its analogs **38** and **39** with more complex amino substituents in the 2-position, a piperazine ring and a 4-furanoylpiperazine moiety, were commercially available, they were included in this study. Whereas the diamino substituted quinazoline derivative **40** seems to be devoid of any binding affinity (remaining reporter ligand binding 95 ± 8%), the presence of the two larger substituents in **38** and **39** appears to mediate a slight increase of the binding affinity which remains, however, still modest (remaining reporter ligand binding 83 ± 7% and 85 ± 5% for **38** and **39**, respectively).

Table 4: Binding affinities of 6,7-dimethoxyquinazoline analogs of UNC0646 for the MB327 binding site of the *Torpedo*-nAChR. [a] 'reporter ligand binding' refers to the remaining binding of the reporter ligand (UNC0642, 1 µM) in presence of the respective test compound (10 µM) as % value ± SD; see Material and Methods for details.

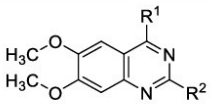

28a-28c, **30a-30b**, **31**, **32a-32f**, **37-40**

Entry	Compound	R^1	R^2	reporter ligand binding [%] [a]	PTMD01 code
1	**30a**	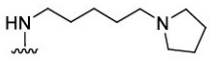		48 ± 5	61L
2	**28a**	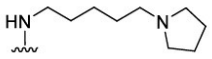	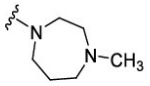	56 ± 3	59
3	**37** (BIX01294)	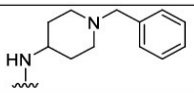		64 ± 4	-
4	**28b**	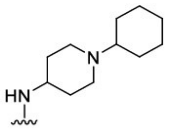		57 ± 4	02
5	**31**		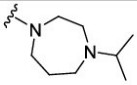	65 ± 7 (n = 9)	01

Continued next page

Table 3 *(continued)*

Entry	Compound	R^1	R^2	reporter ligand binding [%] [a]	PTMD01 code
6	**28c**	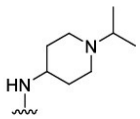	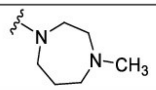	74 ± 1	03
7	**32a**		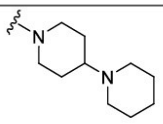	64 ± 6	55
8	**32b**		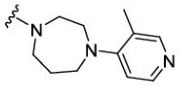	41 ± 9	56
9	**32c**		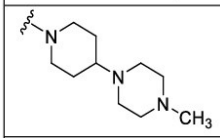	64 ± 8	57
10	**32d**		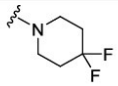	70 ± 2 (n = 2)	58L
11	**30b**			66 ± 5	60L
12	**32e**			75 ± 2	64
13	**32f**			92 ± 8	69
14	**38**		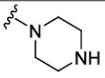	83 ± 7	18C
15	**39** (Prazosin)		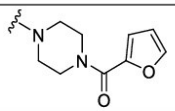	85 ± 5	-
16	**40**			95 ± 8	73C

During this study various analogs of UNC0646 (**1**) have been synthesized using 7-benzyloxy-2,4-dichloro-6-methoxyquinazoline (**4**) as a key compound. Thereby, the 7-benzyloxy residue in **4** served as starting point for the establishment of various ω-aminoalkoxy side chains in this position of the final test compounds as they are common for UNC0646 (**1**) and respective analogs. With the building block **4** at hand, it seemed worthwhile to also study the binding affinities of UNC0646 analogs that can be directly delineated from **4** leaving the substituents in 6- and 7-position unchanged. That was expected to provide further information regarding the necessity of a basic side chain in 7-position of quinazoline analogs of UNC0646 (**1**) for effecting reasonable binding affinities. Hence, the test compounds **34a**-**34c** were studied, all of which are characterized by a 6-methoxy-7-benzyloxyquinazoline substructure, a piperidine ring in 2-position and various basic residues in 4-position. The piperidine ring in 2-position had been chosen, as it mediates a similar binding affinity as the 4-isopropyl-1,4-diazepan-1-yl substituent in UNC0646 though it is distinctly smaller (Table 1, Entries 1 and 4). As the UNC0646 analog **9c** also the 7-benzyloxy substituted quinazoline derivative **34b** contains a 1-cyclohexylpiperidin-4-amino residue in 4-position as does UNC0646 (**1**). Remarkably, compound **34b** exerts a reduction of reporter ligand binding down to 26 ± 1%, which is in the same range as the remaining reporter ligand binding of UNC0646 (**1**, 21 ± 3%, Table 1, Entry 1) and **9c** (11 ± 3%, Table 1, Entry 4). Upon substitution of the 1-cyclohexylpiperidin-4-amino group in 4-position by a 5-(pyrrolidin-1-yl)pentan-1-amino residue the binding affinity even further increases, the remaining reporter ligand binding decreasing to 15 ± 1% (Table 5, Entry 1). Hence, high binding affinities may even be reached without a basic group being part of the substituent in 7-position of the quinazoline system.

For the UNC0646 analog **9c** upon transition to **9f** with an extra methylene group in the side chain in 4-position (1-cyclohexylmethylpiperidin-4-amino instead of a 1-cyclohexylpiperidin-4-amino residue) the high binding affinity is retained [remaining reporter ligand binding of **9c**, 11 ± 3% (pK_i = 5.83 ± 0.02) for **9f**, 6 ± 1% (pK_i = 5.84 ± 0.03)]. In contrast, for **34c** a lower binding affinity than for **34b** is observed, though the former differs from the latter in the same way as **9f** and **9c** by an extra methylene group in the 4-substituent of the quinazoline system. These different trends might possibly arise from different binding modes for quinazoline derivatives with a basic group as part of the 7-substituent and those with a 7-benzyloxy group.

Being commercially available the quinazoline derivative **41** (Table 5, Entry 4) with a 7-benzyloxy residue alike **34a**-**34c** was included in this study, as well. With a remaining reporter ligand binding of 67 ± 3% (Table 5, Entry 4) the binding affinity of this compound with a 4-substituent that was now smaller than that of **34b** (1-methylpiperidin-4-amino instead of a 1-cyclohexylpiperidin-4-amino group) and which carried a 1,4-diazepane instead of a piperidine ring in 2-position was poor, too.

In any case, considering these results, quinazoline derivatives related to UNC0646 (**1**) but equipped with a benzyloxy residue instead of a side chain with an amino function in 7-position appear to deserve further exploration as ligands of the MB327 binding site.

Table 5: Binding affinities of 2,4-disubstituted 7-(benzyloxy)-6-methoxyquinazoline derivatives for the MB327 binding site of the *Torpedo*-nAChR. [a] 'reporter ligand binding' refers to the remaining binding of the reporter ligand (UNC0642, 1 µM) in presence of the respective test compound (10 µM) as % value ± SD; see Material and Methods for details.

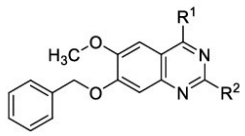

34a-34c, **41**

Entry	Compound	R^1	R^2	reporter ligand binding [%] [a]	PTMD01 code
1	**34a**	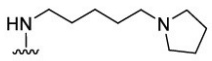		15 ± 1	62
2	**34b**	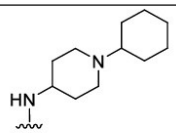		26 ± 1	66
3	**34c**	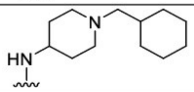		53 ± 2	67
4	**41** (TM2-115)	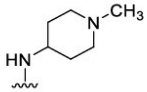	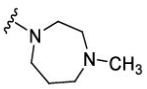	67 ± 3	-

4 Conclusion

In this study we successfully synthesized a remarkable number of yet unknown analogs of UNC0646 (**1**), which represented the compound with the highest known affinity towards the MB327-PAM-1 binding site of the nAChR at the begin of this study. This binding site is of great interest as it is thought that organophosphorus compound poisoning therapy will benefit from compounds mediating allosteric effects through this binding site.

Adapting literature known methods, this plethora of compounds could be synthesized with high efficiency in one- to four-step syntheses, introducing a wide variety of substituents to positions 2, 4 and 7 of the quinazoline scaffold. By applying this strategy, we were able to, on the one hand, get access to strategically, only slightly modified UNC0646 analogs to subsequently examine the influence of the corresponding substituents. On the other hand, we accomplished the synthesis of quinazoline-based compounds that structurally differed a little more from UNC0646 (**1**) in order to further explore the chemical space around UNC0646 (**1**).

Expanded with structurally matching compounds that were commercially available, all compounds synthesized in this study were evaluated regarding their affinity towards the above-mentioned binding site. For this purpose, a recently developed MS Binding Assay, utilizing UNC0642 (**2**) as reporter ligand, was applied. Even though here only one compound, UNC0631 (**35**) ($pK_i = 6.04 \pm 0.04$), showed an increased affinity compared to UNC0646 (**1**) ($pK_i = 5.83 \pm 0.05$), the generated data is of great value. This is because the results of the competitive MS binding experiments at a single test compound concentration, which investigated more than 50 quinazoline-based compounds, allow to draw conclusions regarding structure-affinity relationships within this class of compounds, not yet possible to this extent.

The gained information is crucial in order to purposefully design new quinazoline-based compounds, ideally addressing the MB327-PAM-1 binding site with high affinity plus ideally having lower molecular weight than UNC0646 (**1**). These compounds would then display promising candidates to be further evaluated in terms of other characteristics, e.g. regarding their intrinsic activity in order to develop novel therapeutics against organophosphorus intoxications.

5 Supporting Information

Supplementary data associated with this article can be found in the online version at doi: xxx.

6 Acknowledgments

This work was supported by the German Ministry of Defence (E/ U2AD/KA019/IF558).

7 Conflict of interest

The authors declare no conflict of interest.

8 Keywords

neurological agents • nicotinic acetylcholine receptor • quinazolines • structure-affinity relationships • MS Binding Assay

9 References

Abe, Y., Kayakiri, H., Satoh, S., Inoue, T., Sawada, Y., Inamura, N., Asano, M., Aramori, I., Hatori, C., Sawai, H., Oku, T., Tanaka, H., 1998. A Novel Class of Orally Active Non-Peptide Bradykinin B2 Receptor Antagonists. 3. Discovering Bioisosteres of the Imidazo[1,2-a]pyridine Moiety. Journal of Medicinal Chemistry 41, 4062-4079.

Aubin, Y., Fischmeister, C., Thomas, C.M., Renaud, J.-L., 2010. Direct amination of aryl halides with ammonia. Chemical Society Reviews 39, 4130-4145.

Bernauer, T., Nitsche, V., Kaiser, J., Gertzen, C.G.W., Höfner, G., Niessen, K.V., Seeger, T., Steinritz, D., Worek, F., Gohlke, H., Wanner, K.T., Paintner, F.F., 2024. Synthesis and Biological Evaluation of Novel MB327 Analogs as Resensitizers for Desensitized Nicotinic Acetylcholine Receptors after Intoxication with Nerve Agents. bioRxiv, 2024.2002.2009.579646.

Borzenko, A., Rotta-Loria, N.L., MacQueen, P.M., Lavoie, C.M., McDonald, R., Stradiotto, M., 2015. Nickel-Catalyzed Monoarylation of Ammonia. Angewandte Chemie 127, 3844-3848.

Brown, M.A., Brix, K.A., 1998. Review of health consequences from high-, intermediate- and low-level exposure to organophosphorus nerve agents. Journal of Applied Toxicology 18, 393-408.

Cui, R., Yin, C., Deng, X., Zhang, T., 2020. STK19 inhibitors for treatment of cancer. Trustees of Boston University, Xiamen University.

Cushman, M., Georg, G.I., Holzgrabe, U., Wang, S., 2014. Absolute Quantitative 1H NMR Spectroscopy for Compound Purity Determination. Journal of Medicinal Chemistry 57, 9219-9219.

Davis, I., Jin, J., Janzen, W.P., Pattenden, S., Jayakody, C., 2016. A novel compound for the treatment of ewing sarcoma and high-throughput assays for identifying small molecules that modulate aberrant chromatin accessibility. Google Patents.

Doig, P., Boriack-Sjodin, P.A., Dumas, J., Hu, J., Itoh, K., Johnson, K., Kazmirski, S., Kinoshita, T., Kuroda, S., Sato, T.-o., Sugimoto, K., Tohyama, K., Aoi, H., Wakamatsu, K., Wang, H., 2014. Rational design of inhibitors of the bacterial cell wall synthetic enzyme GlmU using virtual screening and lead-hopping. Bioorganic & Medicinal Chemistry 22, 6256-6269.

Dolgin, E., 2013. Syrian gas attack reinforces need for better anti-sarin drugs. Nature Medicine 19, 1194-1195.

Fagan, V., Johansson, C., Gileadi, C., Monteiro, O., Dunford, J.E., Nibhani, R., Philpott, M., Malzahn, J., Wells, G., Faram, R., Cribbs, A.P., Halidi, N., Li, F., Chau, I., Greschik, H., Velupillai, S., Allali-Hassani, A., Bennett, J., Christott, T., Giroud, C., Lewis, A.M., Huber,

K.V.M., Athanasou, N., Bountra, C., Jung, M., Schüle, R., Vedadi, M., Arrowsmith, C., Xiong, Y., Jin, J., Fedorov, O., Farnie, G., Brennan, P.E., Oppermann, U., 2019. A Chemical Probe for Tudor Domain Protein Spindlin1 to Investigate Chromatin Function. Journal of Medicinal Chemistry 62, 9008-9025.

Freire, C., Koifman, S., 2013. Pesticides, depression and suicide: a systematic review of the epidemiological evidence. International journal of hygiene and environmental health 216, 445-460.

Gharat, L.A., Banerjee, A., Khairatkar-Joshi, N., Kattige, V.G., 2015. Bicyclic compounds as mPGES-1 inhibitors. Google Patents.

Gmeiner, P., Junge, D., Kaertner, A., 1994. Enantiomerically pure amino alcohols and diamino alcohols from L-aspartic acid. Application to the synthesis of epi-and diepislaframine. The Journal of Organic Chemistry 59, 6766-6776.

Harris, C.S., Kettle, J.G., Williams, E.J., 2005. Facile synthesis of 7-amino anilinoquinazolines via direct amination of the quinazoline core. Tetrahedron Letters 46, 7381-7384.

Jiang, Y.-H., Kim, Y., Lee, H.-M., Jin, J., Roth, B.L., 2017. Preparation of quinazolin-4-amine derivatives as histone methyltransferase G9a inhibitors and methods for the treatment of Prader-willi syndrome. Duke University, The University of North Carolina at Chapel Hill.

Kaiser, J., Gertzen, C.G.W., Bernauer, T., Höfner, G., Niessen, K.V., Seeger, T., Paintner, F.F., Wanner, K.T., Worek, F., Thiermann, H., Gohlke, H., 2023. A novel binding site in the nicotinic acetylcholine receptor for MB327 can explain its allosteric modulation relevant for organophosphorus-poisoning treatment. Toxicology Letters 373, 160-171.

Kaiser, J., Gertzen, C.G.W., Bernauer, T., Nitsche, V., Höfner, G., Niessen, K.V., Seeger, T., Paintner, F.F., Wanner, K.T., Steinritz, D., Worek, F., Gohlke, H., 2024. Identification of ligands binding to MB327-PAM-1, a binding pocket relevant for resensitization of nAChRs. bioRxiv, p. 2023.2012.2021.572862.

Kassa, J., Timperley, C.M., Bird, M., Green, A.C., Tattersall, J.E.H., 2022. Influence of Experimental End Point on the Therapeutic Efficacy of Essential and Additional Antidotes in Organophosphorus Nerve Agent-Intoxicated Mice. Toxics, vol. 10.

Liu, F., Barsyte-Lovejoy, D., Allali-Hassani, A., He, Y., Herold, J.M., Chen, X., Yates, C.M., Frye, S.V., Brown, P.J., Huang, J., Vedadi, M., Arrowsmith, C.H., Jin, J., 2011. Optimization of Cellular Activity of G9a Inhibitors 7-Aminoalkoxy-quinazolines. Journal of Medicinal Chemistry 54, 6139-6150.

Liu, F., Chen, X., Allali-Hassani, A., Quinn, A.M., Wigle, T.J., Wasney, G.A., Dong, A., Senisterra, G., Chau, I., Siarheyeva, A., Norris, J.L., Kireev, D.B., Jadhav, A., Herold, J.M., Janzen, W.P., Arrowsmith, C.H., Frye, S.V., Brown, P.J., Simeonov, A., Vedadi, M., Jin, J., 2010. Protein Lysine Methyltransferase G9a Inhibitors: Design, Synthesis, and Structure Activity Relationships of 2,4-Diamino-7-aminoalkoxy-quinazolines. Journal of Medicinal Chemistry 53, 5844-5857.

Ma, A., Yu, W., Li, F., Bleich, R.M., Herold, J.M., Butler, K.V., Norris, J.L., Korboukh, V., Tripathy, A., Janzen, W.P., 2014. Discovery of a selective, substrate-competitive inhibitor of the lysine methyltransferase SETD8. Journal of medicinal chemistry 57, 6822-6833.

Maselli, R.A., Leung, C., 1993. Analysis of anticholinesterase-induced neuromuscular transmission failure. Muscle & Nerve 16, 548-553.

Massoulié, J., Pezzementi, L., Bon, S., Krejci, E., Vallette, F.-M., 1993. Molecular and cellular biology of cholinesterases. Progress in Neurobiology 41, 31-91.

Mellstedt, H., Bystrom, S., Vagberg, J., Olsson, E., 2020. 2-phenyl-3H-imidazo [4, 5-B] pyridine derivates useful as inhibitors of mammalian tyrosine kinase ROR1 activity. Google Patents.

Mohamed, T., Rao, P.P., 2015. Facile approaches toward the synthesis of N4-monosubstituted quinazolin-2, 4-diamines. Tetrahedron letters 56, 6882-6885.

Newmark, J., 2007. Nerve Agents. The Neurologist 13, 20-32.

Niessen, K.V., Muschik, S., Langguth, F., Rappenglück, S., Seeger, T., Thiermann, H., Worek, F., 2016. Functional analysis of Torpedo californica nicotinic acetylcholine receptors in multiple activation states by SSM-based electrophysiology. Toxicology Letters 247, 1-10.

Niessen, K.V., Seeger, T., Rappenglück, S., Wein, T., Höfner, G., Wanner, K.T., Thiermann, H., Worek, F., 2018. In vitro pharmacological characterization of the bispyridinium non-oxime compound MB327 and its 2- and 3-regioisomers. Toxicology Letters 293, 190-197.

Nitsche, V., Höfner, G., Kaiser, J., Gertzen, C.G.W., Seeger, T., Niessen, K.V., Steinritz, D., Worek, F., Gohlke, H., Paintner, F.F., Wanner, K.T., 2024. MS Binding Assays with UNC0642 as reporter ligand for the MB327 binding site of the nicotinic acetylcholine receptor. Toxicology Letters 392, 94-106.

OPCW, 2017. OPCW Director-General Shares Incontrovertible Laboratory Results Concluding Exposure to Sarin, 19.04.2017.

Papke, R.L., 2014. Merging old and new perspectives on nicotinic acetylcholine receptors. Biochemical Pharmacology 89, 1-11.

Pauli, G.F., Chen, S.-N., Simmler, C., Lankin, D.C., Gödecke, T., Jaki, B.U., Friesen, J.B., McAlpine, J.B., Napolitano, J.G., 2014. Importance of Purity Evaluation and the Potential of Quantitative 1H NMR as a Purity Assay. Journal of Medicinal Chemistry 57, 9220-9231.

Pita, R., Domingo, J., 2014. The Use of Chemical Weapons in the Syrian Conflict. Toxics 2, 391-402.

Price, M.E., Docx, C.J., Rice, H., Fairhall, S.J., Poole, S.J.C., Bird, M., Whiley, L., Flint, D.P., Green, A.C., Timperley, C.M., Tattersall, J.E.H., 2016. Pharmacokinetic profile and quantitation of protection against soman poisoning by the antinicotinic compound MB327 in the guinea-pig. Toxicology Letters 244, 154-160.

Rappenglück, S., Sichler, S., Höfner, G., Wein, T., Niessen, K.V., Seeger, T., Paintner, F.F., Worek, F., Thiermann, H., Wanner, K.T., 2018a. Synthesis of a Series of Non-Symmetric Bispyridinium and Related Compounds and Their Affinity Characterization at the Nicotinic Acetylcholine Receptor. ChemMedChem 13, 2653-2663.

Rappenglück, S., Sichler, S., Höfner, G., Wein, T., Niessen, K.V., Seeger, T., Paintner, F.F., Worek, F., Thiermann, H., Wanner, K.T., 2018b. Synthesis of a Series of Structurally Diverse MB327 Derivatives and Their Affinity Characterization at the Nicotinic Acetylcholine Receptor. ChemMedChem 13, 1806-1816.

Seeger, T., Eichhorn, M., Lindner, M., Niessen, K.V., Tattersall, J.E.H., Timperley, C.M., Bird, M., Green, A.C., Thiermann, H., Worek, F., 2012. Restoration of soman-blocked neuromuscular transmission in human and rat muscle by the bispyridinium non-oxime MB327 in vitro. Toxicology 294, 80-84.

Sheridan, R.D., Smith, A.P., Turner, S.R., Tattersall, J.E.H., 2005. Nicotinic Antagonists in the Treatment of Nerve Agent Intoxication. Journal of the Royal Society of Medicine 98, 114-115.

Shih, T.-M., Rowland, T.C., McDonough, J.H., 2007. Anticonvulsants for Nerve Agent-Induced Seizures: The Influence of the Therapeutic Dose of Atropine. Journal of Pharmacology and Experimental Therapeutics 320, 154.

Sichler, S., Höfner, G., Nitsche, V., Niessen, K.V., Seeger, T., Worek, F., Paintner, F.F., Wanner, K.T., 2024. Screening for new ligands of the MB327-PAM-1 binding site of the nicotinic acetylcholine receptor. Toxicology Letters 394, 23-31.

Somnarin, T., Pobsuk, N., Chantakul, R., Panklai, T., Temkitthawon, P., Hannongbua, S., Chootip, K., Ingkaninan, K., Boonyarattanakalin, K., Gleeson, D., Paul Gleeson, M., 2022. Computational design, synthesis and biological evaluation of PDE5 inhibitors based on N2,N4-diaminoquinazoline and N2,N6-diaminopurine scaffolds. Bioorganic & Medicinal Chemistry 76, 117092.

Sundriyal, S., Chen, P.B., Lubin, A.S., Lueg, G.A., Li, F., White, A.J.P., Malmquist, N.A., Vedadi, M., Scherf, A., Fuchter, M.J., 2017. Histone lysine methyltransferase structure activity relationships that allow for segregation of G9a inhibition and anti-Plasmodium activity. MedChemComm 8, 1069-1092.

Thiermann, H., Seeger, T., Gonder, S., Herkert, N., Antkowiak, B., Zilker, T., Eyer, F., Worek, F., 2010. Assessment of neuromuscular dysfunction during poisoning by organophosphorus compounds. Chemico-Biological Interactions 187, 265-269.

Thiermann, H., Worek, F., 2022. Pro: Oximes should be used routinely in organophosphate poisoning. British Journal of Clinical Pharmacology 88, 5064-5069.

Timperley, C.M., Bird, M., Green, C., Price, M.E., Chad, J.E., Turner, S.R., Tattersall, J.E., 2012. 1, 1′-(Propane-1, 3-diyl) bis (4-tert-butylpyridinium) di (methanesulfonate) protects guinea pigs from soman poisoning when used as part of a combined therapy. MedChemComm 3, 352-356.

Turner, S.R., Chad, J.E., Price, M., Timperley, C.M., Bird, M., Green, A.C., Tattersall, J.E.H., 2011. Protection against nerve agent poisoning by a noncompetitive nicotinic antagonist. Toxicology Letters 206, 105-111.

Venkatesan, A.M., Dehnhardt, C., Chen, Z., Santos, O.D., Santos, E.D., Curran, K., Ayral-Kaloustian, S., Chen, L., 2008. Amino-substituted quinazoline derivatives as inhibitors of β-cantenin/Tcf-4 pathway and cancer treatment agents and their preparation. Wyeth.

Vital, T., Wali, A., Butler, K.V., Xiong, Y., Foster, J.P., Marcel, S.S., McFadden, A.W., Nguyen, V.U., Bailey, B.M., Lamb, K.N., 2023. MS0621, a novel small-molecule modulator of Ewing sarcoma chromatin accessibility, interacts with an RNA-associated macromolecular complex and influences RNA splicing. Frontiers in Oncology 13.

Wang, P.G., Kondengaden, M.S., Zhang, Q., Zang, L., 2019. Histone deacetylase and histone methyltransferase inhibitors and methods of making and use of the same. Google Patents.

Worek, F., Szinicz, L., Eyer, P., Thiermann, H., 2005. Evaluation of oxime efficacy in nerve agent poisoning: Development of a kinetic-based dynamic model. Toxicology and Applied Pharmacology 209, 193-202.

Worek, F., Thiermann, H., Wille, T., 2020. Organophosphorus compounds and oximes: a critical review. Archives of Toxicology 94, 2275-2292.

Yamamoto, Y., Shinnkai, I., 2004. Science of Synthesis - Category 2, Hetarenes and Related Ring Systems, Stuttgart, pp. 573-749.

Yoshida, K., Taguchi, M., 1992. Reaction of N-substituted cyclic amines with 2, 4-dichloroquinazoline, 2, 4-dichloropyrimidine, and its 5-methyl derivative. Journal of the Chemical Society, Perkin Transactions 1, 919-922.

Supporting Information

Structure-Affinity Relationship of Quinazoline Derivatives as Potential Resensitizers of Desensitized nAChRs After Nerve Agent Intoxication

Tamara Bernauer[+][a], Valentin Nitsche[+][a], Georg Höfner[a], Karin V. Niessen[b], Thomas Seeger[b], Dirk Steinritz[b], Franz Worek[b], Klaus T. Wanner[a] and Franz F. Paintner*[a]

[a] T. Bernauer, V. Nitsche, Dr. G. Höfner, Prof. Dr. K. T. Wanner, Prof. Dr. F. F. Paintner
Department of Pharmacy - Center for Drug Research
Ludwig-Maximilians-Universität München
Butenandtstrasse 5-13, 81377 Munich (Germany)
E-mail: Franz.Paintner@cup.uni-muenchen.de

[b] Dr. K. V. Niessen, Dr. T. Seeger, Prof. Dr. D. Steinritz, Prof. Dr. F. Worek
Bundeswehr Institute of Pharmacology and Toxicology
Neuherbergstrasse 11, 80937 Munich (Germany)

[*] These authors contributed equally to this work.

Table of Content

Table S1: Commercially obtained test compounds.

#	Compound	Salt	Purity	Supplier
1	BIX01294	3 HCl	≥ 97%	Activate Scientific GmbH (Prien, Germany)
2	Prazosin	HCl	≥ 99%	Angene (Honk Kong, China)
3	PTMD01-0018C	-	≥ 98%	Merck (Darmstadt, Germany)
4	PTMD01-0073C	2 HCl	≥ 95%	BLDpharm (Kaiserslautern, Germany)
5	Tandutinib	-	≥ 98%	MedChemExpess (New Jersey, USA)
6	TM2-115	-	≥ 99%	Excenen Pharma & Tech (Guangzhou, China)
7	UNC0631	-	≥ 99%	MedChemExpess (New Jersey, USA)

Experimental Procedures and Analytical Data of Synthesized Compounds

2,4-Dichloro-6-methoxyquinazolin-7-ol (5) (Doig et al., 2014)

mp.: 184 °C. IR (film): $\tilde{\nu}$ = 1632, 1514, 1257, 1180 cm^{-1}. ^{1}H NMR (500 MHz, CD_3OD): δ = 4.06 (s, 3 H, CH_3O), 7.15 (s, 1 H, C*H*COH), 7.42 (s, 1 H, C*H*COCH$_3$). ^{13}C NMR (126 MHz, CD_3OD): δ = 56.95 (CH_3O), 103.98 (*C*HCOCH$_3$), 109.96 (*C*HCOH), 118.35 (*C*CHCOCH$_3$), 151.82 (*C*CHCOH), 152.78 (*C*OCH$_3$), 154.05 (*C*NCCHCOH), 158.62 (*C*CCHCOCH$_3$), 161.12 (COH). HRMS-EI m/z [M]$^+$ calcd. for $C_9H_6Cl_2N_2O_2$: 243.9806, found: 243.9803.

2,4-Dichloro-6-methoxy-7-[3-(piperidin-1-yl)propoxy]quinazoline (6) (Vital et al., 2023)

mp.: 106 °C. R_f = 0.27 (10% MeOH in CH_2Cl_2). IR (film): $\tilde{\nu}$ = 2935, 1643, 1506, 1240 cm^{-1}. ^{1}H NMR (500 MHz, CD_3OD): δ = 1.43–1.58 [m, 2 H, C*H*$_2$CH$_2$CH$_2$N(CH$_2$)$_3$O], 1.58–1.75 [m, 4 H, C*H*$_2$CH$_2$N(CH$_2$)$_3$O], 2.09–2.20 (m, 2 H, C*H*$_2$CH$_2$O), 2.45–2.63 [m, 4 H, C*H*$_2$N(CH$_2$)$_3$O], 2.63–2.72 (m, 2 H, *C*H$_2$CH$_2$CH$_2$O), 4.03 (s, 3 H, CH_3O), 4.28 (t, *J* = 6.1 Hz, 2 H, CH_2O), 7.30 (s, 1 H, C*H*COCH$_2$), 7.45 (s, 1 H, C*H*COCH$_3$). ^{13}C NMR (126 MHz, CD_3OD): δ = 24.83 [*C*H$_2$CH$_2$CH$_2$N(CH$_2$)$_3$O], 26.22 [*C*H$_2$CH$_2$N(CH$_2$)$_3$O], 26.67 (*C*H$_2$CH$_2$O), 55.39 [*C*H$_2$N(CH$_2$)$_3$O], 56.76 (*C*H$_2$CH$_2$CH$_2$O), 56.95 (CH_3O), 69.09 (CH_2O), 103.74 (*C*HCOCH$_3$), 107.54 (*C*HCOCH$_2$), 118.97 (*C*CCl), 151.82 (*C*CCCl), 153.58 (*C*OCH$_3$), 154.22 (C*C*Cl), 159.06 (*C*OCH$_2$), 161.19 (CHCN*C*Cl). HRMS-ESI m/z [M+H]$^+$ calcd. for $C_{17}H_{22}Cl_2N_3O_2$: 370.1089, found: 370.1087.

2-Chloro-*N*-(1-cyclohexylpiperidin-4-yl)-6-methoxy-7-[3-(piperidin-1-yl)propoxy]quinazolin-4-amine (7)

According to GP1 with **6** (278 mg, 0.750 mmol, 1.0 equiv), 1-cyclohexylpiperidin-4-amine (150 mg, 0.825 mmol, 1.1 equiv) and DIEA (400 µL, 297 mg, 2.25 mmol, 3.0 equiv) in THF (3 mL). Purification by flash chromatography [5% to 10% 3 M NH_3 (in MeOH) in CH_2Cl_2] afforded **7** as yellow solid (249 mg, 64% yield, 96% purity). mp.: 89 °C. R_f = 0.32 [10% 3 M NH_3 (in MeOH) in CH_2Cl_2]. IR (film): $\tilde{\nu}$ = 2927, 2360, 1587, 1510, 1443, 1255 cm^{-1}. ^{1}H NMR (500 MHz, CD_2Cl_2): δ = 1.03–1.17 (m, 1 H, 10), 1.18–1.32 (m, 4 H, CH$_2$C*H*$_2$C*H*$_2$CHN), 1.35–1.48 [m, 2 H, C*H*$_2$CH$_2$CH$_2$N(CH$_2$)$_3$O], 1.49–1.66 [m, 6 H, C*H*$_2$CHNH, C*H*$_2$CH$_2$CH$_2$CHN, C*H*$_2$CH$_2$N(CH$_2$)$_3$O], 1.74–1.88 (m, 4 H, CH$_2$C*H*$_2$C*H*$_2$CHN), 2.00 (p, *J* = 6.8 Hz, 2 H, C*H*$_2$CH$_2$O), 2.06–2.19 (m, 2 H, C*H*$_2$CHNH), 2.25–2.40 [m, 5 H, C*H*$_2$N(CH$_2$)$_3$O, CHN], 2.41–2.54 (m, 4 H, C*H*$_2$CH$_2$CHNH, C*H*$_2$CH$_2$CH$_2$O), 2.81–2.97 (m, 2 H, C*H*$_2$CH$_2$CHNH), 3.94 (s, 3 H, CH_3), 4.10–4.26 (m, 3 H, CH_2O, CHNH), 5.44 (d, *J* = 7.8 Hz, 1 H, NH), 6.83 (s, 1 H, C*H*COCH$_3$), 7.08 (s, 1 H, C*H*COCH$_2$). ^{13}C NMR (126 MHz, CD_2Cl_2): δ = 24.97 [*C*H$_2$CH$_2$CH$_2$N(CH$_2$)$_3$O], 26.51 [*C*H$_2$CH$_2$N(CH$_2$)$_3$O]*, 26.54 (CH$_2$*C*H$_2$CH$_2$CHN)*, 26.85 (*C*H$_2$CH$_2$CH$_2$CHN)**, 26.94 (*C*H$_2$CH$_2$O)**, 29.29 (CH$_2$CH$_2$*C*H$_2$CHN), 33.27 (CH$_2$*C*H$_2$CHNH), 48.34 (*C*H$_2$CH$_2$CHNH), 49.41 (CHNH), 55.03 [*C*H$_2$N(CH$_2$)$_3$O], 55.83 (*C*H$_2$CH$_2$CH$_2$O), 56.76 (CH_3O), 64.09 (CHN), 68.04 (CH_2O), 100.38 (*C*HCOCH$_3$), 106.91 (*C*CHCOCH$_3$), 108.37 (*C*HCOCH$_2$), 148.49 (*C*CCNH), 149.72 (*C*OCH$_3$), 155.07 (*C*OCH$_2$), 156.29 (CCl), 159.52 (CNH). HRMS-ESI m/z [M+H]$^+$ calcd. for $C_{28}H_{43}ClN_5O_2$: 516.3105, found: 516.3096.

***N*-(1-Cyclohexylpiperidin-4-yl)-6-methoxy-2-(4-methyl-1,4-diazepan-1-yl)-7-[3-(piperidin-1-yl)propoxy]quinazolin-4-amine (9a)** (Liu et al., 2011)

According to GP2 with **7** (92.9 mg, 0.180 mmol, 1.0 equiv) and 1-methyl-1,4-diazepane (115 µL, 106 mg, 0.900 mmol, 5.0 equiv) in toluene (0.9 mL). **9a** was isolated by flash chromatography [10% to 20% 3 M NH_3 (in MeOH) in CH_2Cl_2] as colorless solid (95.0 mg, 89% yield, 97% purity). mp.: 82 °C. R_f = 0.22 [10% 3 M NH_3 (in MeOH) in CH_2Cl_2]. IR (film): $\tilde{\nu}$ = 2933, 2854, 1579, 1495, 1246 cm^{-1}. ^1H NMR (500 MHz, CD_2Cl_2): δ = 1.05–1.18 (m, 1 H, C*H*$_2$CH$_2$CH$_2$CHN), 1.21–1.33 (m, 4 H, CH$_2$C*H*$_2$C*H*$_2$CHN), 1.37–1.49 [m, 2 H, C*H*$_2$CH$_2$CH$_2$N(CH$_2$)$_3$O], 1.52–1.71 [m, 7 H, C*H*$_2$CH$_2$N(CH$_2$)$_3$O, CH$_2$C*H*$_2$CHNH, C*H*$_2$CH$_2$CH$_2$CHN], 1.78–1.82 (m, 2 H, CH$_2$C*H*$_2$CH$_2$CHN), 1.84–1.92 (m, 2 H, CH$_2$CH$_2$C*H*$_2$CHN), 1.93–2.06 (m, 4 H, C*H*$_2$CH$_2$O, CH$_3$NCH$_2$C*H*$_2$CH$_2$N), 2.09–2.24 (m, 2 H, CH$_2$C*H*$_2$CHNH), 2.34 (s, 3 H, CH$_3$N), 2.35–2.50 (m, 9 H, C*H*$_2$NC*H*$_2$CH$_2$CH$_2$O, CHN, C*H*$_2$CH$_2$CHNH), 2.51–2.57 (m, 2 H, CH$_3$NC*H*$_2$CH$_2$CH$_2$N), 2.64–2.72 (m, 2 H, CH$_3$NC*H*$_2$CH$_2$N), 2.84–3.04 (m, 2 H, C*H*$_2$CH$_2$CHNH), 3.83 (t, *J* = 6.4 Hz, 2 H, CH$_3$NCH$_2$CH$_2$C*H*$_2$N), 3.88 (s, 3 H, CH$_3$O), 3.89–3.96 (m, 2 H, CH$_3$NCH$_2$C*H*$_2$N), 4.02–4.09 (m, 1 H, C*H*NH), 4.11 (t, *J* = 6.7 Hz, 2 H, CH$_2$O), 5.07 (d, *J* = 7.2 Hz, 1 H, NH), 6.75 (s, 1 H, C*H*COCH$_3$), 6.82 (s, 1 H, C*H*COCH$_2$). ^{13}C NMR (126 MHz, CD_2Cl_2): δ = 24.94 [*C*H$_2$CH$_2$CH$_2$N(CH$_2$)$_3$O], 26.43 (CH$_2$*C*H$_2$CH$_2$CHN)*, 26.46 [CH$_2$*C*H$_2$N(CH$_2$)$_3$O]*, 26.76 (*C*H$_2$CH$_2$O), 27.05 (CH$_2$*C*H$_2$CH$_2$CHN), 28.26 (CH$_3$NCH$_2$*C*H$_2$CH$_2$N), 29.13 (CH$_2$CH$_2$*C*H$_2$CHN), 32.99 (CH$_2$*C*H$_2$CHNH), 46.20 (CH$_3$NCH$_2$CH$_2$*C*H$_2$N)**, 46.26 (CH$_3$NCH$_2$*C*H$_2$N)**, 46.83 (CH$_3$N), 48.55 (*C*H$_2$CH$_2$CHNH), 49.10 (CHNH), 55.01 [*C*H$_2$N(CH$_2$)$_3$O], 55.96 (*C*H$_2$CH$_2$CH$_2$O), 56.88 (CH$_3$O), 57.60 (CH$_3$N*C*H$_2$CH$_2$CH$_2$N), 59.11 (CH$_3$N*C*H$_2$CH$_2$N), 64.30 (CHN), 67.59 (*C*H$_2$O), 101.89 (*C*HCOCH$_3$), 102.95 (*C*CNH), 107.02 (*C*HCOCH$_2$), 145.63 (*C*OCH$_3$), 150.55 (*C*CCNH), 154.52 (*C*OCH$_2$), 158.47 (CNH), 159.31 (*C*NCNH). HRMS-ESI m/z $[M+H]^+$ calcd. for $C_{34}H_{56}N_7O_2$: 594.4495, found: 594.4488.

***N*-(1-Cyclohexylpiperidin-4-yl)-2-(4-isopropylpiperazin-1-yl)-6-methoxy-7-[3-(piperidin-1-yl)propoxy]quinazolin-4-amine (9b)**

According to GP2 with **7** (206 mg, 0.400 mmol, 1.0 eq) and 1-propan-2-ylpiperazine (292 µL, 262 mg, 2.00 mmol, 5.0 equiv) in toluene (2.0 mL). **9b** was isolated by flash chromatography [10% to 15% 3 M NH_3 (in MeOH) in CH_2Cl_2] as colorless solid (216 mg, 89% yield, 99% purity). mp.: 83 °C. R_f = 0.51 [10% 3 M NH_3 (in MeOH) in CH_2Cl_2]. IR (film): $\tilde{\nu}$ = 2098, 1626, 1448, 1245 cm^{-1}. ^1H NMR (500 MHz, CD_2Cl_2): δ = 1.05 (d, *J* = 6.5 Hz, 6 H, C*H*$_3$CH), 1.07–1.19 (m, 1 H, C*H*$_2$CH$_2$CH$_2$CHN), 1.20–1.34 (m, 4 H, CH$_2$C*H*$_2$C*H*$_2$CHN), 1.35–1.47 [m, 2 H, C*H*$_2$CH$_2$CH$_2$N(CH$_2$)$_3$O], 1.47–1.58 [m, 6 H, C*H*$_2$CHNH, C*H*$_2$CH$_2$N(CH$_2$)$_3$O], 1.58–1.66 (m, 1 H, C*H*$_2$CH$_2$CH$_2$CHN), 1.75–1.88 (m, 4 H, CH$_2$C*H*$_2$C*H*$_2$CHN), 1.99 (p, *J* = 6.8 Hz, 2 H, C*H*$_2$CH$_2$O), 2.07–2.19 (m, 2 H, C*H*$_2$CHNH), 2.24–2.48 (m, 9 H, C*H*NC*H*$_2$CH$_2$CHNH, C*H*$_2$NC*H*$_2$CH$_2$CH$_2$O), 2.49–2.59 (m, 4 H, C*H*$_2$NCHCH$_3$), 2.70 (hept, *J* = 6.6 Hz, 1 H, CH$_3$C*H*), 2.84–2.99 (m, 2 H, C*H*$_2$CH$_2$CHNH), 3.61–3.81 (m, 4 H, CH$_2$NC), 3.88 (s, 3 H, CH$_3$O), 3.97–4.19 (m, 3 H, C*H*NH, CH$_2$O), 5.05 (d, *J* = 7.2 Hz, 1 H, NH), 6.74 (s, 1 H, C*H*COCH$_3$), 6.82 (s, 1 H, C*H*COCH$_2$). ^{13}C NMR (126 MHz, CD_2Cl_2): δ = 18.65 (*C*H$_3$CH), 24.99 [*C*H$_2$CH$_2$CH$_2$N(CH$_2$)$_3$O], 26.52 (CH$_2$*C*H$_2$CH$_2$CHN)*, 26.55 [*C*H$_2$CH$_2$N(CH$_2$)$_3$O]*, 26.88 (CH$_2$*C*H$_2$CH$_2$CHN), 27.11 (CH$_2$CH$_2$O), 29.32 (CH$_2$CH$_2$*C*H$_2$CHN), 33.32 (*C*H$_2$CHNH), 44.88 (*C*H$_2$NC), 48.54 (*C*H$_2$CH$_2$CHNH), 49.19 (*C*H$_2$NCHCH$_3$), 49.20 (CHNH), 54.93 (CH$_3$*C*H), 55.04 [*C*H$_2$N(CH$_2$)$_3$O], 55.96 (*C*H$_2$CH$_2$CH$_2$O), 56.85 (CH$_3$O), 64.13 (CH$_2$CH$_2$CH$_2$*C*HN), 67.62 (CH$_2$O), 101.79 (*C*HCOCH$_3$), 103.29 (*C*CNH),

107.18 (*C*HCOCH$_2$), 145.98 (*C*OCH$_3$), 149.72 (*C*CCNH), 154.54 (*C*OCH$_2$), 158.58 (CNH), 159.27 (*C*NCNH). HRMS-ESI m/z [M+H$^+$]$^+$ calcd. for $C_{35}H_{58}N_7O_2$: 608.4652; found: 608.4662.

_N_-(1-Cyclohexylpiperidin-4-yl)-6-methoxy-2-(piperidin-1-yl)-7-[3-(piperidin-1-yl)propoxy]quinazolin-4-amine (9c)

According to GP4 with **8** (83.8 mg, 0.200 mmol, 1.0 equiv), 1-cyclohexylpiperidin-4-amine (72.9 mg, 0.400 mmol, 2.0 equiv) and DIEA (107 µL, 79.1 mg, 0.600 mmol, 3.0 equiv) in *i*-PrOH (1.0 mL) for 15 min. **9c** (78.8 mg, 70% yield, 98% purity) was isolated by flash chromatography [7% to 15% 3 M NH_3 (in MeOH) in CH_2Cl_2] as colorless solid. mp.: 92 °C. R_f = 0.38 [10% 3 M NH_3 (in MeOH) in CH_2Cl_2]. IR (film): $\tilde{\nu}$ = 2929, 1579, 1491, 1244, 754 cm^{-1}. ^{1}H NMR (500 MHz, CD_2Cl_2): δ = 1.04–1.18 (m, 1 H, C*H*$_2$CH$_2$CH$_2$CHN), 1.22–1.28 (m, 4 H, CH$_2$C*H*$_2$C*H*$_2$CHN), 1.38–1.46 [m, 2 H, C*H*$_2$CH$_2$CH$_2$N(CH$_2$)$_3$O], 1.47–1.54 (m, 2 H, C*H*$_2$CHNH), 1.54–1.62 [m, 8 H, C*H*$_2$CH$_2$NC, C*H*$_2$CH$_2$N(CH$_2$)$_3$O], 1.62–1.68 (m, 2 H, C*H*$_2$CH$_2$CH$_2$NC), 1.68–1.74 (m, 1 H, C*H*$_2$CH$_2$CH$_2$CHN), 1.75–1.88 (m, 4 H, CH$_2$C*H*$_2$C*H*$_2$CHN), 1.99 (p, *J* = 6.9 Hz, 2 H, C*H*$_2$CH$_2$O), 2.08–2.19 (m, 2 H, C*H*$_2$CHNH), 2.27–2.49 (m, 9 H, C*H*$_2$CH$_2$CHNH, C*H*$_2$NC*H*$_2$CH$_2$CH$_2$O, CHN), 2.82–2.96 (m, 2 H, C*H*$_2$CH$_2$CHNH), 3.74–3.79 (m, 4 H, CH$_2$NC), 3.87 (s, 3 H, CH$_3$O), 4.01–4.15 (m, 3 H, C*H*NH, CH$_2$O), 5.02 (d, *J* = 7.2 Hz, 1 H, NH), 6.74 (s, 1 H, C*H*COCH$_3$), 6.81 (s, 1 H, C*H*COCH$_2$). ^{13}C NMR (126 MHz, CD_2Cl_2): δ = 24.99 [*C*H$_2$CH$_2$CH$_2$N(CH$_2$)$_3$O], 25.60 (*C*H$_2$CH$_2$CH$_2$NC), 26.40 (*C*H$_2$CH$_2$NC)*, 26.52 (*C*H$_2$CH$_2$CHN)*, 26.54 [*C*H$_2$CH$_2$N(CH$_2$)$_3$O]*, 26.87 (*C*H$_2$CH$_2$CH$_2$CHN)*, 27.11 (*C*H$_2$CH$_2$O), 29.31 (*C*H$_2$CHN), 33.30 (*C*H$_2$CHNH), 45.36 (*C*H$_2$NC), 48.54 (*C*H$_2$CH$_2$CHNH), 49.16 (CHNH), 55.04 [*C*H$_2$N(CH$_2$)$_3$O], 55.98 (*C*H$_2$CH$_2$CH$_2$O), 56.87 (CH$_3$O), 64.14 (CHN), 67.60 (CH$_2$O), 101.87 (*C*HCOCH$_3$), 103.05 (*C*CNH), 107.11 (*C*HCOCH$_2$), 145.77 (*C*OCH$_3$), 149.92 (*C*CCNH), 154.49 (*C*OCH$_2$), 158.58 (CNH), 159.26 (CNCNH). HRMS-ESI m/z [M+H]$^+$ calcd. for $C_{33}H_{53}N_6O_2$: 565.4230, found: 565.4229.

_N_^{4}-(1-Cyclohexylpiperidin-4-yl)-6-methoxy-_N_^{2},_N_^{2}-dimethyl-7-[3-(piperidin-1-yl)propoxy]-quinazoline-2,4-diamine (9d)

mp.: 84 °C. R_f = 0.32 [10% 3 M NH_3 (in MeOH) in CH_2Cl_2]. IR (film): $\tilde{\nu}$ = 2931, 1628, 1581, 1427, 1246 cm^{-1}. ^{1}H NMR (500 MHz, CD_2Cl_2): δ = 1.03–1.19 (m, 1 H, C*H*$_2$CH$_2$CH$_2$CH), 1.21–1.34 (m, 4 H, CH$_2$C*H*$_2$C*H*$_2$CH), 1.42 [t, *J* = 5.9 Hz, 2 H, C*H*$_2$CH$_2$CH$_2$N(CH$_2$)$_3$O], 1.47–1.69 [m, 7 H, C*H*$_2$CHNH, C*H*$_2$CH$_2$CH$_2$CH, C*H*$_2$CH$_2$N(CH$_2$)$_3$O], 1.70–1.89 (m, 4 H, CH$_2$C*H*$_2$C*H*$_2$CH), 1.99 (p, *J* = 6.9 Hz, 2 H, C*H*$_2$CH$_2$O), 2.09–2.22 (m, 2 H, C*H*$_2$CHNH), 2.24–2.52 (m, 9 H, C*H*$_2$CH$_2$CHNH, C*H*N, C*H*$_2$NC*H*$_2$CH$_2$CH$_2$O), 2.87–3.00 (m, 2 H, C*H*$_2$CH$_2$CHNH), 3.16 (s, 6 H, CH$_3$N), 3.87 (s, 3 H, CH$_3$O), 4.05–4.21 (m, 3 H, CH$_2$O, C*H*NH), 5.04 (d, *J* = 7.2 Hz, 1 H, NH), 6.74 (s, 1 H, C*H*COCH$_3$), 6.83 (s, 1 H, C*H*COCH$_2$). ^{13}C NMR (126 MHz, CD_2Cl_2): δ = 24.98 [*C*H$_2$CH$_2$CH$_2$N(CH$_2$)$_3$O], 26.49 (CH$_2$*C*H$_2$CH$_2$CH)*, 26.52 [*C*H$_2$CH$_2$N(CH$_2$)$_3$O]*, 26.84 (*C*H$_2$CH$_2$CH$_2$CH), 27.10 (*C*H$_2$CH$_2$O), 29.24 (CH$_2$CH$_2$*C*H$_2$CH), 33.21 (*C*H$_2$CHNH), 37.12 (CH$_3$N), 48.57 (*C*H$_2$CH$_2$CHNH), 49.18 (CHNH), 55.03 [*C*H$_2$N(CH$_2$)$_3$O], 55.97 (*C*H$_2$CH$_2$CH$_2$O), 56.88 (CH$_3$O), 64.19 (CHN), 67.61 (*C*H$_2$O), 101.91 (*C*HCOCH$_3$), 102.77 (*C*CNH), 107.04 (*C*HCOCH$_2$), 145.66 (*C*OCH$_3$), 149.93 (*C*CCNH), 154.52 (*C*OCH$_2$), 158.43 (CNH), 159.93 (*C*NCH$_3$). HRMS-ESI m/z [M+H]$^+$ calcd. for $C_{30}H_{49}N_6O_2$: 525.3917, found: 525.3909.

N^4-(1-Cyclohexylpiperidin-4-yl)-6-methoxy-7-[3-(piperidin-1-yl)propoxy]quinazoline-2,4-diamine (9e) and *N*-(1-cyclohexylpiperidin-4-yl)-6-methoxy-7-[3-(piperidin-1-yl)propoxy]quinazolin-4-amine (16b)

According to a GP3, with **7** (196 mg, 0.380 mmol, 1.0 equiv) and NaN_3 (27.2 mg, 0.418 mmol, 1.1 equiv) in EtOH/AcOH (4:1) (2.54 mL) and afterwards 10% Pd/C (45.0 mg, 38.0 µmol, 0.10 equiv) and hydrazine hydrate (28.5 µL, 28.5 mg, 0.570 mmol, 1.5 equiv). **9e** (92.6 mg, 49% yield, 99% purity) and **16b** (29.6 mg, 16% yield, 97% purity, analytic see below) were isolated by flash chromatography [10% 3 M NH_3 (in MeOH) in CH_2Cl_2] as colorless solids. **9e**: mp.: 143 °C. R_f = 0.32 [10% 3 M NH_3 (in MeOH) in CH_2Cl_2]. IR (film): $\tilde{\nu}$ = 2935, 2089, 1624, 1454, 1213, 754 cm^{-1}. ^1H NMR (500 MHz, CD_2Cl_2): δ = 1.04–1.19 (m, 1 H, CH_2CH$_2$CH$_2$CH), 1.20–1.32 (m, 4 H, CH$_2$CH_2CH_2CH), 1.35–1.46 [m, 2 H, CH_2CH$_2$CH$_2$N(CH$_2$)$_3$O], 1.53–1.65 [m, 7 H, CH_2CHNH, CH_2CH$_2$CH$_2$CH, CH_2CH$_2$N(CH$_2$)$_3$O], 1.66–1.90 (m, 4 H, CH$_2$CH_2CH_2CH), 2.00 (p, *J* = 6.8 Hz, 2 H, CH_2CH$_2$O), 2.07–2.16 (m, 2 H, CH_2CHNH), 2.21–2.52 (m, 9 H, CH_2NC*H*, CH_2NCH_2CH$_2$CH$_2$O), 2.87–3.00 (m, 2 H, CH_2NCH), 3.89 (s, 3 H, CH$_3$O), 4.10 (t, *J* = 6.6 Hz, 2 H, CH$_2$O), 4.12–4.21 (m, 1 H, C*H*NH), 4.84 (s, 2 H, NH$_2$), 5.38 (s, 1 H, NH), 6.79 (s, 1 H, C*H*COCH$_2$), 6.82 (s, 1 H, C*H*COCH$_3$). ^{13}C NMR (126 MHz, CD_2Cl_2): δ = 24.92 [CH$_2$CH$_2$CH$_2$N(CH$_2$)$_3$O], 26.42 (CH$_2$CH_2CH$_2$CH)*, 26.45 [CH_2CH$_2$N(CH$_2$)$_3$O]*, 26.77 (CH_2CH$_2$CH$_2$CH)**, 26.95 (CH_2CH$_2$O)**, 29.13 (CH$_2$CH$_2$CH_2CH), 32.99 (CH_2CHNH), 48.53 (CH_2NCH), 48.73 (CHNH), 54.99 [CH_2N(CH$_2$)$_3$O], 55.91 (CH_2CH$_2$CH$_2$O), 56.87 (CH$_3$O), 64.22 (CH$_2$CH$_2$CH$_2$CH), 67.66 (CH$_2$O), 101.94 (*C*HCOCH$_3$), 103.84 (*C*CNH), 106.07 (*C*HCOCH$_2$), 146.56 (*C*OCH$_3$), 148.01 (*CC*CNH), 154.72 (*C*OCH$_2$), 159.36 (CNH), 159.77 (CNH$_2$). HRMS-EI m/z $[M]^+$ calcd. for $C_{28}H_{44}N_6O_2$: 496.3526; found: 496.3524.

***N*-[1-(Cyclohexylmethyl)piperidin-4-yl]-6-methoxy-2-(piperidin-1-yl)-7-[3-(piperidin-1-yl)propoxy]quinazolin-4-amine (9f)**

According to GP4 with **8** (168 mg, 0.400 mmol, 1.0 equiv), 1-(cyclohexylmethyl)piperidin-4-amine (157 mg, 0.800 mmol, 2.0 equiv) and DIEA (213 µL, 158 mg, 1.20 mmol, 3.0 equiv) in *i*-PrOH (2.0 mL) for 15 min. **9f** (134 mg, 58% yield, 99% purity) was isolated by flash chromatography [7% 3 M NH_3 (in MeOH) in CH_2Cl_2] as colorless solid. mp.: 75 °C. R_f = 0.49 [10% 3 M NH_3 (in MeOH) in CH_2Cl_2]. IR (film): $\tilde{\nu}$ = 2931, 1579, 1493, 1244, 756 cm^{-1}. ^1H NMR (500 MHz, CD_2Cl_2): δ = 0.77–0.96 (m, 2 H, CH$_2$CH$_2$CH_2CH), 1.10–1.33 (m, 3 H, CH_2CH_2CH$_2$CH), 1.40–1.45 (m, 2 H, CH_2CH$_2$CH$_2$NCH$_2$), 1.46–1.53 (m, 1 H, CH$_2$CH$_2$CH$_2$C*H*), 1.53–1.74 (m, 15 H, CH_2CH_2CH$_2$NC, CH_2CHNH, CH$_2$CH_2CH$_2$NCH$_2$, CH_2CH_2CH$_2$CH), 1.74–1.81 (m, 2 H, CH$_2$CH$_2$CH_2CH), 1.99 (p, *J* = 6.9 Hz, 2 H, CH$_2$CH_2CH$_2$O), 2.04–2.18 (m, 6 H, CH_2NCH_2CH_2CHNH), 2.38 (s, 4 H, CH$_2$CH$_2$CH_2NCH$_2$), 2.44 (t, *J* = 7.1 Hz, 2 H, CH_2CH$_2$CH$_2$O), 2.72–2.98 (m, 2 H, CH_2CH$_2$CHNH), 3.73–3.81 (m, 4 H, CH$_2$CH$_2$CH_2NC), 3.87 (s, 3 H, CH$_3$O), 4.11 (t, *J* = 6.7 Hz, 3 H, C*H*NH, CH$_2$CH$_2$CH_2O), 5.04 (d, *J* = 7.2 Hz, 1 H, NH), 6.74 (s, 1 H, C*H*COCH$_3$), 6.81 (s, 1 H, C*H*COCH$_2$). ^{13}C NMR (126 MHz, CD_2Cl_2): δ = 24.96 (CH$_2$CH$_2$CH$_2$NCH$_2$), 25.59 (CH_2CH$_2$CH$_2$NC), 26.40 (CH$_2$CH_2CH$_2$NCH$_2$)*, 26.49 (CH$_2$CH$_2$CH$_2$NC)*, 26.62 (CH$_2$CH_2CH$_2$CH), 27.07 (CH$_2$CH_2CH$_2$O), 27.30 (CH_2CH$_2$CH$_2$CH), 32.28 (CH$_2$CH$_2$CH_2CH), 32.75 (CH_2CHNH), 35.79 (CH$_2$CH$_2$CH$_2$CH), 45.37 (CH$_2$CH$_2$CH_2NC), 48.85 (CHNH), 53.55 (CH_2CH$_2$CHNH), 55.02 (CH$_2$CH$_2$CH_2NCH$_2$), 55.97 (CH_2CH$_2$CH$_2$O), 56.85 (CH$_3$O), 66.08 (CHCH_2N), 67.59 (CH$_2$CH$_2$CH_2O), 101.84 (*C*HCOCH$_3$), 103.06 (*C*CNH), 107.09 (*C*HCOCH$_2$), 145.78 (*C*OCH$_3$), 149.87 (*CC*CNH), 154.49 (*C*OCH$_2$), 158.61 (CNH), 159.22 (*C*NCNH). HRMS-ESI m/z $[M+H^+]^+$ calcd. for $C_{34}H_{55}N_6O_2$: 579.4386; found: 579.4392.

2-Chloro-*N*-(1-isopropylpiperidin-4-yl)-6-methoxy-7-[3-(piperidin-1-yl)propoxy]quinazolin-4-amine (10a) (Davis et al., 2016; Vital et al., 2023)

According to GP1 with **6** (43.3 mg, 0.110 mmol, 1.0 equiv), 1-propan-2-ylpiperidin-4-amine (19.1 µL, 17.2 mg, 0.121 mmol, 1.1 equiv) and DIEA (58.7 µL, 43.5 mg, 0.330 mmol, 3.0 equiv) in THF (440 µL). Purification by flash chromatography [5% to 10% 3 M NH_3 (in MeOH) in CH_2Cl_2] afforded **10a** as yellow solid (45.1 mg, 86% yield, 99% purity). mp.: 81 °C. R_f = 0.27 [10% 3 M NH_3 (in MeOH) in CH_2Cl_2]. IR (film): $\tilde{\nu}$ = 2931, 1622, 1589, 1510, 1443 cm^{-1}. ^1H NMR (500 MHz, CD_2Cl_2): δ = 1.07 (d, *J* = 6.6 Hz, 6 H, CH_3CH), 1.37–1.48 [m, 2 H, CH_2CH$_2$CH$_2$N(CH$_2$)$_3$O], 1.51–1.59 [m, 4 H, CH_2CH$_2$N(CH$_2$)$_3$O], 1.59–1.81 (m, 2 H, CH_2CHNH), 2.01 (p, *J* = 6.8 Hz, 2 H, CH_2CH$_2$O), 2.09–2.19 (m, 2 H, CH_2CHNH), 2.24–2.53 (m, 8 H, CH_2CH$_2$CHNH, CH_2NCH_2CH$_2$CH$_2$O), 2.81 (h, *J* = 6.6 Hz, 1 H, CH$_3$C*H*), 2.88–2.99 (m, 2 H, CH_2CH$_2$CHNH), 3.96 (s, 3 H, CH$_3$O), 4.15 (t, *J* = 6.6 Hz, 2 H, CH$_2$O), 4.17–4.29 (m, 1 H, C*H*NH), 5.45 (d, *J* = 7.9 Hz, 1 H, NH), 6.83 (s, 1 H, C*H*COCH$_3$), 7.08 (s, 1 H, C*H*COCH$_2$). ^{13}C NMR (126 MHz, CD_2Cl_2): δ = 18.35 (*C*H$_3$CH), 24.93 [*C*H$_2$CH$_2$CH$_2$N(CH$_2$)$_3$O], 26.49 [*C*H$_2$CH$_2$N(CH$_2$)$_3$O], 26.90 (*C*H$_2$CH$_2$O), 32.83 (*C*H$_2$CHNH), 47.86 (*C*H$_2$CH$_2$CHNH), 49.18 (CHNH), 55.01 [*C*H$_2$N(CH$_2$)$_3$O], 55.04 (CH$_3$*C*H), 55.82 (*C*H$_2$CH$_2$CH$_2$O), 56.79 (CH$_3$O), 68.03 (CH$_2$O), 100.36 (*C*HCOCH$_3$), 106.91 (*C*CNH), 108.39 (*C*HCOCH$_2$), 148.51 (*C*CCNH), 149.75 (*C*OCH$_3$), 155.08 (*C*OCH$_2$), 156.25 (CCl), 159.52 (CNH). HRMS-ESI m/z $[M+H]^+$ calcd. for $C_{25}H_{39}ClN_5O_2$: 476.2792, found: 476.2797.

2-Chloro-6-methoxy-*N*-(1-methylpiperidin-4-yl)-7-[3-(piperidin-1-yl)propoxy]quinazolin-4-amine (10b)

According to GP1 with **6** (148 mg, 0.400 mmol, 1.0 equiv), 1-methylpiperidin-4-amine (58.1 µL, 52.9 mg, 0.440 mmol, 1.1 equiv) and DIEA (213 µL, 158 mg, 1.20 mmol, 3.0 equiv) in THF (1.6 mL). Purification by flash chromatography [5% to 10% 3 M NH_3 (in MeOH) in CH_2Cl_2] afforded **10b** as yellow solid (86.1 mg, 48% yield, 97% purity). mp.: 82 °C. R_f = 0.24 [10% 3 M NH_3 (in MeOH) in CH_2Cl_2]. IR (film): $\tilde{\nu}$ = 2929, 1587, 1510, 1441, 1255 cm^{-1}. ^1H NMR (500 MHz, CD_2Cl_2): δ = 1.37–1.50 [m, 2 H, CH_2CH$_2$CH$_2$N(CH$_2$)$_3$O], 1.50–1.59 [m, 4 H, CH_2CH$_2$N(CH$_2$)$_3$O], 1.59–1.70 (m, 2 H, CH$_2$CH_2CHNH), 2.01 (p, *J* = 6.8 Hz, 2 H, CH_2CH$_2$O), 2.07–2.14 (m, 2 H, CH$_2$CH_2CHNH), 2.14–2.23 (m, 2 H, CH_2CH$_2$CHNH), 2.28 (s, 3 H, CH$_3$N), 2.38 [s, 4 H, CH_2N(CH$_2$)$_3$O], 2.46 (t, *J* = 7.1 Hz, 2 H, CH_2CH$_2$CH$_2$O), 2.69–2.97 (m, 2 H, CH_2CH$_2$CHNH), 3.95 (s, 3 H, CH$_3$O), 4.15 (t, *J* = 6.6 Hz, 2 H, CH$_2$O), 4.17–4.25 (m, 1 H, C*H*NH), 5.43 (d, *J* = 7.7 Hz, 1 H, NH), 6.84 (s, 1 H, C*H*COCH$_3$), 7.08 (s, 1 H, C*H*COCH$_2$). ^{13}C NMR (126 MHz, CD_2Cl_2): δ = 24.91 [*C*H$_2$CH$_2$CH$_2$N(CH$_2$)$_3$O], 26.46 [*C*H$_2$CH$_2$N(CH$_2$)$_3$O], 26.87 (*C*H$_2$CH$_2$O), 32.58 (*C*H$_2$CHNH), 46.37 (CH$_3$N), 48.51 (CHNH), 54.96 (*C*H$_2$CH$_2$CHNH), 55.00 [*C*H$_2$N(CH$_2$)$_3$O], 55.81 (*C*H$_2$CH$_2$CH$_2$O), 56.78 (CH$_3$O), 68.02 (CH$_2$O), 100.36 (*C*HCOCH$_3$), 106.93 (*C*CNH), 108.38 (*C*HCOCH$_2$), 148.50 (*C*CCNH), 149.75 (*C*OCH$_3$), 155.08 (*C*OCH$_2$), 156.25 (CCl), 159.57 (CNH). HRMS-ESI m/z $[M+H]^+$ calcd. for $C_{23}H_{35}ClN_5O_2$: 448.2479, found: 448.2474.

2-Chloro-6-methoxy-*N*-methyl-7-[3-(piperidin-1-yl)propoxy]quinazolin-4-amine (10c)

According to GP1 with **6** (222 mg, 0.600 mmol, 1.0 equiv), methanamine (2 M in THF) (330 µL, 0.660 mmol, 1.1 equiv) and DIEA (320 µL, 237 mg, 1.80 mmol, 3.0 equiv) in THF (2.07 mL).

Purification by flash chromatography [5% 3 M NH_3 (in MeOH) in CH_2Cl_2] afforded **10c** as colorless solid (187 mg, 86% yield, 96% purity). mp.: 63 °C. R_f = 0.34 [10% 3 M NH_3 (in MeOH) in CH_2Cl_2]. IR (film): $\tilde{\nu}$ = 1624, 1510, 1244, 1022 cm^{-1}. ^1H NMR (500 MHz, CD_2Cl_2): δ = 1.34–1.47 [m, 2 H, $CH_2CH_2CH_2N(CH_2)_3O$], 1.48–1.66 [m, 4 H, $CH_2CH_2N(CH_2)_3O$], 2.01 (p, J = 6.8 Hz, 2 H, CH_2CH_2O), 2.32–2.41 [m, 4 H, $CH_2N(CH_2)_3O$], 2.45 (t, J = 7.1 Hz, 2 H, $CH_2CH_2CH_2O$), 3.16 (d, J = 4.8 Hz, 3 H, CH_3NH), 3.93 (s, 3 H, CH_3O), 4.15 (t, J = 6.6 Hz, 2 H, CH_2O), 5.59–5.78 (m, 1 H, NH), 6.85 (s, 1 H, $CHCOCH_3$), 7.09 (s, 1 H, $CHCOCH_2$). ^{13}C NMR (126 MHz, CD_2Cl_2): δ = 25.11 [$CH_2CH_2CH_2N(CH_2)_3O$], 26.67 [$CH_2CH_2N(CH_2)_3O$], 27.07 (CH_2CH_2O), 28.81 (CH_3NH), 55.18 [$CH_2N(CH_2)_3O$], 55.98 ($CH_2CH_2CH_2O$), 56.76 (CH_3O), 68.20 (CH_2O), 100.41 ($CHCOCH_3$), 107.25 (*C*CNH), 108.51 ($CHCOCH_2$), 148.35 (*C*CCNH), 149.96 ($COCH_3$), 155.19 ($COCH_2$), 156.45 (CCl), 161.05 (CNH). HRMS-ESI m/z $[M+H]^+$ calcd. for $C_{18}H_{26}ClN_4O_2$: 365.1744, found: 365.1740.

2-(4-Isopropyl-1,4-diazepan-1-yl)-*N*-(1-isopropylpiperidin-4-yl)-6-methoxy-7-[3-(piperidin-1-yl)propoxy]quinazolin-4-amine (11a) (Jiang et al., 2017; Liu et al., 2011)

According to GP2 with **10a** (100 mg, 0.210 mmol, 1.0 equiv) and 1-propan-2-yl-1,4-diazepane (170 µL, 152 mg, 1.05 mmol, 5.0 equiv) in toluene (1.0 mL). **11a** was isolated by flash chromatography [10% to 15% 3 M NH_3 (in MeOH) in CH_2Cl_2] as pale yellow solid (109 mg, 89% yield, 95% purity). mp.: 52 °C. R_f = 0.25 [10% 3 M NH_3 (in MeOH) in CH_2Cl_2]. IR (film): $\tilde{\nu}$ = 2931, 2094, 1630, 1248 cm^{-1}. ^1H NMR (500 MHz, CD_2Cl_2): δ = 1.00 (d, J = 6.6 Hz, 6 H, $CH_3CHNCH_2CH_2N$), 1.05 (d, J = 6.6 Hz, 6 H, $CH_3CHNCH_2CH_2CH$), 1.37–1.48 [m, 2 H, $CH_2CH_2CH_2N(CH_2)_3O$], 1.50–1.65 (m, 6 H, $CH_2CH_2NCH_2CH_2CH_2O$, CH_2CHNH), 1.89 (p, J = 6.1 Hz, 2 H, $CH_2CH_2CH_2NC$), 1.99 (p, J = 6.9 Hz, 2 H, CH_2CH_2O), 2.13–2.18 (m, 2 H, CH_2CHNH), 2.29–2.42 [m, 6 H, CH_2CH_2CHNH, $CH_2N(CH_2)_3O$], 2.44 (t, J = 7.1 Hz, 2 H, $CH_2CH_2CH_2O$), 2.53–2.62 (m, 2 H, $CH_2CH_2CH_2NC$), 2.72–2.82 (m, 3 H, $CH_3CHNCH_2CH_2CHNH$, NCH_2CH_2NC), 2.85–2.92 (m, 2 H, CH_2CH_2CHNH), 2.92–2.98 (m, 1 H, $CH_3CHNCH_2CH_2NC$), 3.81–3.85 (m, 2 H, $NCH_2CH_2CH_2NC$), 3.85–3.93 (m, 5 H, CH_3O, NCH_2CH_2NC), 4.00–4.17 (m, 3 H, CH_2O, $CHNH$), 5.12 (d, J = 7.1 Hz, 1 H, NH), 6.78 (s, 1 H, $CHCOCH_3$), 6.82 (s, 1 H, $CHCOCH_2$). ^{13}C NMR (126 MHz, CD_2Cl_2): δ = 18.45 ($CH_3CHNCH_2CH_2NC$), 18.45 ($CH_3CHNCH_2CH_2CHNH$), 24.95 [$CH_2CH_2CH_2N(CH_2)_3O$], 26.48 [$CH_2CH_2N(CH_2)_3O$], 27.06 (CH_2CH_2O), 29.03 ($NCH_2CH_2CH_2NC$), 33.00 (NCH_2CH_2CHNH), 45.89 ($NCH_2CH_2CH_2NC$), 48.08 (NCH_2CH_2NC, CH_2CH_2CHNH), 49.17 (*C*HNH), 50.89 ($NCH_2CH_2CH_2NC$), 52.45 (NCH_2CH_2NC), 54.97 ($CH_3CHNCH_2CH_2CHNH$), 55.01 [$CH_2N(CH_2)_3O$], 55.96 ($CH_2CH_2CH_2O$), 56.06 ($CH_3CHNCH_2CH_2NC$), 56.88 (CH_3O), 67.59 (CH_2O), 102.01 ($CHCOCH_3$), 102.98 (*C*CNH), 106.99 ($CHCOCH_2$), 145.56 ($COCH_3$), 149.95 (*C*CCNH), 154.48 ($COCH_2$), 158.54 (CNH), 158.83 (*C*NCNH). HRMS-ESI m/z $[M+H]^+$ calcd. for $C_{33}H_{56}N_7O_2$: 582.4495, found: 582.4488.

2-(4-Isopropyl-1,4-diazepan-1-yl)-6-methoxy-*N*-(1-methylpiperidin-4-yl)-7-[3-(piperidin-1-yl)propoxy]quinazolin-4-amine (11b)

According to GP2 with **10b** (58.2 mg, 0.130 mmol, 1.0 equiv) and 1-propan-2-yl-1,4-diazepane (105 µL, 94.3 mg, 0.650 mmol, 5.0 equiv) in toluene (0.6 mL). **11b** was isolated by flash chromatography [10% to 15% 3 M NH_3 (in MeOH) in CH_2Cl_2] as colorless solid (44.9 mg, 62% yield, 98% purity). mp.: 68 °C. R_f = 0.15 [10% 3 M NH_3 (in MeOH) in CH_2Cl_2]. IR (film): $\tilde{\nu}$ = 2935, 1628, 1579, 1497, 1248 cm^{-1}. ^1H NMR (500 MHz, CD_3OD): δ = 1.07 (d, J = 6.6 Hz,

6 H, CH_3CH), 1.45–1.58 [m, 2 H, CH_2CH$_2$CH$_2$N(CH$_2$)$_3$O], 1.60–1.69 [m, 4 H, CH_2CH$_2$N(CH$_2$)$_3$O], 1.69–1.82 (m, 2 H, CH_2CHNH), 1.90–2.01 (m, 2 H, CH$_2$CH_2CH$_2$NC), 2.03–2.15 (m, 4 H, CH_2CHNH, CH_2CH$_2$O), 2.16–2.24 (m, 2 H, CH_2NCH$_3$), 2.33 (s, 3 H, CH$_3$N), 2.54 [s, 4 H, CH_2N(CH$_2$)$_3$O], 2.59–2.65 (m, 2 H, CH_2CH$_2$CH$_2$O), 2.65–2.75 (m, 2 H, CH_2CH$_2$CH$_2$NC), 2.79–2.93 (m, 2 H, NCH_2CH$_2$NC), 2.93–3.05 (m, 3 H, CH$_3$CH, CH_2NCH$_3$), 3.86 (t, J = 6.2 Hz, 2 H, CH$_2$CH$_2$CH_2NC), 3.89 (s, 5 H, CH$_3$O, NCH$_2$CH_2NC), 4.08–4.26 (m, 3 H, CH$_2$O, CHNH), 6.91 (s, 1 H, CHCOCH$_2$), 7.42 (s, 1 H, CHCOCH$_3$). ^{13}C NMR (126 MHz, CD$_3$OD): δ = 18.31 (*C*H$_3$CH), 25.07 [*C*H$_2$CH$_2$CH$_2$N(CH$_2$)$_3$O], 26.40 [*C*H$_2$CH$_2$N(CH$_2$)$_3$O], 27.06 (*C*H$_2$CH$_2$O), 29.11 (CH$_2$*C*H$_2$CH$_2$NC), 32.34 (*C*H$_2$CHNH), 46.24 (CH$_3$N), 46.50 (CH$_2$CH$_2$*C*H$_2$NC), 47.99 (NCH$_2$*C*H$_2$NC), 48.49 (CHNH), 51.73 (*C*H$_2$CH$_2$CH$_2$NC), 52.68 (NCH$_2$CH$_2$NC), 55.47 [*C*H$_2$N(CH$_2$)$_3$O], 56.04 (*C*H$_2$NCH$_3$), 56.62 (CH$_3$*C*H), 56.87 (CH$_3$O), 57.08 (*C*H$_2$CH$_2$CH$_2$O), 68.06 (CH$_2$O), 104.31 (*C*HCOCH$_3$), 104.77 (*C*CNH), 106.27 (*C*HCOCH$_2$), 147.03 (*C*OCH$_3$), 149.18 (*C*CCNH), 155.18 (*C*OCH$_2$), 159.60 (*C*NCNH), 160.13 (CNH). HRMS-ESI m/z [M+H]$^+$ calcd. for C$_{31}$H$_{52}$N$_7$O$_2$: 554.4182, found: 554.4176.

2-(4-Isopropyl-1,4-diazepan-1-yl)-6-methoxy-*N*-methyl-7-[3-(piperidin-1-yl)propoxy]quinazolin-4-amine (11c)

According to GP2 with **10c** (146 mg, 0.400 mmol, 1.0 equiv) and 1-propan-2-yl-1,4-diazepane (324 µL, 290 mg, 2.00 mmol, 5.0 equiv) in toluene (2.0 mL). **11c** was isolated by flash chromatography [10% 3 M NH$_3$ (in MeOH) in CH$_2$Cl$_2$] as red solid (171 mg, 91% yield, 98% purity). mp.: 66 °C. R_f = 0.29 [10% 3 M NH$_3$ (in MeOH) in CH$_2$Cl$_2$]. IR (film): ṽ = 2937, 2360, 1585, 1497, 1215 cm^{-1}. ^{1}H NMR (400 MHz, CD$_2$Cl$_2$): δ = 0.99 (d, J = 6.6 Hz, 6 H, CH_3CH), 1.36–1.47 [m, 2 H, CH_2CH$_2$CH$_2$N(CH$_2$)$_3$O], 1.52–1.61 [m, 4 H, CH_2CH$_2$N(CH$_2$)$_3$O], 1.80–1.93 (m, 2 H, CH$_2$CH_2CH$_2$NC), 1.99 (p, J = 6.9 Hz, 2 H, CH_2CH$_2$O), 2.25–2.40 [m, 4 H, CH_2N(CH$_2$)$_3$O], 2.43 (t, J = 7.1 Hz, 2 H, CH_2CH$_2$CH$_2$O), 2.50–2.65 (m, 2 H, CH_2CH$_2$CH$_2$NC), 2.67–2.81 (m, 2 H, NCH_2CH$_2$NC), 2.83–3.01 (m, 1 H, CH$_3$CH), 3.09 (d, J = 4.7 Hz, 3 H, CH_3NH), 3.76–3.99 (m, 7 H, CH$_2$NC, CH$_3$O), 4.11 (t, J = 6.7 Hz, 2 H, CH$_2$O), 5.18–5.29 (m, 1 H, NH), 6.76 (s, 1 H, CHCOCH$_3$), 6.81 (s, 1 H, CHCOCH$_2$). ^{13}C NMR (101 MHz, CD$_2$Cl$_2$): δ = 18.52 (*C*H$_3$CH), 25.00 [*C*H$_2$CH$_2$CH$_2$N(CH$_2$)$_3$O], 26.55 [*C*H$_2$CH$_2$N(CH$_2$)$_3$O], 27.13 (*C*H$_2$CH$_2$O), 28.24 (CH$_3$NH), 29.30 (CH$_2$*C*H$_2$CH$_2$NC), 45.97 (CH$_2$CH$_2$*C*H$_2$NC), 48.45 (NCH$_2$*C*H$_2$NC), 51.03 (*C*H$_2$CH$_2$CH$_2$NC), 52.46 (NCH$_2$CH$_2$NC), 55.04 [*C*H$_2$N(CH$_2$)$_3$O], 55.94 (CH$_3$*C*H), 55.98 (*C*H$_2$CH$_2$CH$_2$O), 56.68 (CH$_3$O), 67.61 (*C*H$_2$O), 101.78 (*C*HCOCH$_3$), 103.12 (*C*CNH), 107.02 (*C*HCOCH$_2$), 145.54 (*C*OCH$_3$), 149.80 (*C*CCNH), 154.42 (*C*OCH$_2$), 159.01 (*C*NCN$_2$), 159.89 (CNH). HRMS-ESI m/z [M+H]$^+$ calcd. for C$_{26}$H$_{43}$N$_6$O$_2$: 471.3447, found: 471.3442.

2-Chloro-6-methoxy-7-[3-(piperidin-1-yl)propoxy]quinazoline (12)

mp.: 127 °C. R_f = 0.59 [10% 3 M NH$_3$ (in MeOH) in CH$_2$Cl$_2$]. IR (film): ṽ = 2935, 1616, 1504, 1246 cm^{-1}. ^{1}H NMR (500 MHz, CD$_2$Cl$_2$): δ = 1.38–1.48 [m, 2 H, CH_2CH$_2$CH$_2$N(CH$_2$)$_3$O], 1.53–1.58 [m, 4 H, CH_2CH$_2$N(CH$_2$)$_3$O], 2.05 (p, J = 6.8 Hz, 2 H, CH_2CH$_2$O), 2.38 [s, 4 H, CH_2N(CH$_2$)$_3$O], 2.46 (t, J = 7.1 Hz, 2 H, CH_2CH$_2$CH$_2$O), 3.99 (s, 3 H, CH$_3$O), 4.24 (t, J = 6.6 Hz, 2 H, CH$_2$O), 7.12 (s, 1 H, CHCOCH$_3$), 7.25 (s, 1 H, CHCOCH$_2$), 9.00 (s, 1 H, CHNCCl). ^{13}C NMR (126 MHz, CD$_2$Cl$_2$): δ = 24.94 [CH$_2$CH$_2$CH$_2$N(CH$_2$)$_3$O], 26.51 [*C*H$_2$CH$_2$N(CH$_2$)$_3$O], 26.80 (*C*H$_2$CH$_2$O), 55.02 [CH$_2$N(CH$_2$)$_3$O], 55.72 (CH$_2$CH$_2$CH$_2$O), 56.60 (CH$_3$O), 68.48 (CH$_2$O),

104.17 (*C*HCOCH$_3$), 106.77 (*C*HCOCH$_2$), 119.77 (*C*CHCOCH$_3$), 150.59 (*C*CHCOCH$_2$), 151.66 (*C*OCH$_3$), 156.21 (CCl), 157.43 (*C*OCH$_2$), 159.45 (*C*HNCCl). HRMS-ESI m/z [M+H]$^+$ calcd. for $C_{17}H_{23}ClN_3O_2$: 336.1479, found: 336.1471.

6-Methoxy-7-[3-(piperidin-1-yl)propoxy]quinazoline (13)

mp.: 98 °C. R_f = 0.49 [10% 3 M NH$_3$ (in MeOH) in CH$_2$Cl$_2$]. IR (film): $\tilde{\nu}$ = 2937, 1618, 1502, 1234 cm^{-1}. ^{1}H NMR (500 MHz, CD$_2$Cl$_2$): δ = 1.39–1.46 [m, 2 H, C*H*$_2$CH$_2$CH$_2$N(CH$_2$)$_3$O], 1.53–1.59 [m, 4 H, C*H*$_2$CH$_2$N(CH$_2$)$_3$O], 2.05 (p, *J* = 6.8 Hz, 2 H, C*H*$_2$CH$_2$O), 2.25–2.43 [m, 4 H, C*H*$_2$N(CH$_2$)$_3$O], 2.47 (t, *J* = 7.1 Hz, 2 H, C*H*$_2$CH$_2$CH$_2$O), 3.99 (s, 3 H, CH$_3$O), 4.24 (t, *J* = 6.7 Hz, 2 H, CH$_2$O), 7.11 (s, 1 H, C*H*COCH$_3$), 7.31 (s, 1 H, C*H*COCH$_2$), 9.06 (s, 1 H, C*H*NCCHCOCH$_2$), 9.12 (s, 1 H, C*H*CCHCOCH$_3$). ^{13}C NMR (126 MHz, CD$_2$Cl$_2$): δ = 24.95 [*C*H$_2$CH$_2$CH$_2$N(CH$_2$)$_3$O], 26.52 [*C*H$_2$CH$_2$N(CH$_2$)$_3$O], 26.89 (*C*H$_2$CH$_2$O), 55.02 [CH$_2$N(CH$_2$)$_3$O], 55.80 (CH$_2$CH$_2$CH$_2$O), 56.49 (CH$_3$O), 68.24 (CH$_2$O), 104.23 (*C*HCOCH$_3$), 107.49 (*C*HCOCH$_2$), 121.32 (*C*CHCOCH$_3$), 148.46 (*C*CHCOCH$_2$), 151.35 (*C*OCH$_3$), 154.34 (*C*HNCCHCOCH$_2$), 156.25 (*C*OCH$_2$), 156.93 (*C*HCCHCOCH$_3$). HRMS-ESI m/z [M+H]$^+$ calcd. for $C_{17}H_{24}N_3O_2$: 302.1869, found: 302.1861.

2-(4-Isopropyl-1,4-diazepan-1-yl)-6-methoxy-7-[3-(piperidin-1-yl)propoxy]quinazoline (14)

According to GP2 with **12** (101 mg, 0.300 mmol, 1.0 equiv) and 1-isopropyl-1,4-diazepane (243 µL, 218 mg, 1.50 mmol, 5.0 equiv) in toluene (1.5 mL). **14** was isolated by flash chromatography [10% 3 M NH$_3$ (in MeOH) in CH$_2$Cl$_2$] as yellow oil (131 mg, 99% yield, 97% purity). Hygroscopic. R_f = 0.33 [10% 3 M NH$_3$ (in MeOH) in CH$_2$Cl$_2$]. IR (film): $\tilde{\nu}$ = 2931, 1593, 1493, 1223, 1153 cm^{-1}. ^{1}H NMR (500 MHz, CD$_2$Cl$_2$): δ = 0.98 (d, *J* = 6.6 Hz, 6 H, C*H*$_3$CH), 1.36–1.51 [m, 2 H, C*H*$_2$CH$_2$CH$_2$N(CH$_2$)$_3$O], 1.51–1.60 [m, 4 H, C*H*$_2$CH$_2$N(CH$_2$)$_3$O], 1.80–1.94 (m, 2 H, CNCH$_2$C*H*$_2$CH$_2$N), 2.01 (p, *J* = 6.9 Hz, 2 H, C*H*$_2$CH$_2$O), 2.38 [s, 4 H, C*H*$_2$N(CH$_2$)$_3$O], 2.44 (t, *J* = 7.1 Hz, 2 H, C*H*$_2$CH$_2$CH$_2$O), 2.51–2.63 (m, 2 H, CNCH$_2$CH$_2$C*H*$_2$N), 2.67–2.82 (m, 2 H, CNCH$_2$C*H*$_2$N), 2.90 (hept, *J* = 6.6 Hz, 1 H, CH$_3$C*H*), 3.79–3.96 (m, 7 H, CNCH$_2$, CH$_3$O), 4.17 (t, *J* = 6.8 Hz, 2 H, CH$_2$O), 6.89 (s, 1 H, C*H*COCH$_2$), 6.90 (s, 1 H, C*H*COCH$_3$), 8.74 (s, 1 H, CHNC). ^{13}C NMR (126 MHz, CD$_2$Cl$_2$): δ = 18.52 (*C*H$_3$CH), 24.99 [*C*H$_2$CH$_2$CH$_2$N(CH$_2$)$_3$O], 26.55 [*C*H$_2$CH$_2$N(CH$_2$)$_3$O], 27.01 (*C*H$_2$CH$_2$O), 29.12 (CNCH$_2$*C*H$_2$CH$_2$N), 46.19 (CN*C*H$_2$CH$_2$CH$_2$N), 48.68 (CN*C*H$_2$CH$_2$N), 51.15 (CNCH$_2$CH$_2$*C*H$_2$N), 52.08 (CNCH$_2$*C*H$_2$N), 55.05 [*C*H$_2$N(CH$_2$)$_3$O], 55.88 (*C*H$_2$CH$_2$CH$_2$O), 55.93 (CH$_3$*C*H), 56.32 (CH$_3$O), 67.88 (CH$_2$O), 105.55 (CHCO)*, 105.76 (CHCO)*, 114.18 (*C*CHCOCH$_3$), 147.10 (*C*OCH$_3$), 150.66 (*C*CHCOCH$_2$), 156.21 (*C*OCH$_2$), 158.43 (*C*HNC), 159.44 (*C*NCH$_2$). HRMS-ESI m/z [M+H]$^+$ calcd. for $C_{25}H_{40}N_5O_2$, 442.3182, found: 442.3177.

***N*-[1-(Cyclohexylmethyl)piperidin-4-yl]-6-methoxy-7-[3-(piperidin-1-yl)propoxy]-quinazolin-4-amine (16a)**

According to GP4 with **15** (67.2 mg, 0.200 mmol, 1.0 equiv), 1-(cyclohexylmethyl)piperidin-4-amine (78.5 mg, 0.400 mmol, 2.0 equiv) and DIEA (107 µL, 79.1 mg, 0.600 mmol, 3.0 equiv)

in *i*-PrOH (1.0 mL) for 15 min. **16a** (61.8 mg, 62% yield, 98% purity) was isolated by flash chromatography [7% to 8% 3 M NH_3 (in MeOH) in CH_2Cl_2] as colorless solid. mp.: 194 °C. R_f = 0.43 [10% 3 M NH_3 (in MeOH) in CH_2Cl_2]. IR (film): $\tilde{\nu}$ = 2927, 1589, 1504, 1458, 1252, 754 cm^{-1}. ^1H NMR (500 MHz, CD_2Cl_2): δ = 0.78–0.96 (m, 2 H, CH_2CHCH$_2$N), 1.12–1.34 (m, 3 H, CH_2CH_2CH$_2$CHCH$_2$N), 1.36–1.46 [m, 2 H, CH_2CH$_2$CH$_2$N(CH$_2$)$_3$O], 1.46–1.53 (m, 1 H, CHCH$_2$N), 1.53–1.59 [m, 4 H, CH_2CH$_2$N(CH$_2$)$_3$O], 1.59–1.63 (m, 2 H, CH$_2$CH_2CHNH), 1.63–1.74 (m, 3 H, CH_2CH_2CH$_2$CHCH$_2$N), 1.74–1.82 (m, 2 H, CH_2CHCH$_2$N), 1.96–2.05 (m, 2 H, CH_2CH$_2$O), 2.05–2.18 (m, 6 H, CH_2NCH_2CH_2CHNH), 2.29–2.42 [m, 4, CH_2N(CH$_2$)$_3$O], 2.45 (t, *J* = 7.1 Hz, 2 H, CH_2CH$_2$CH$_2$O), 2.78–2.93 (m, 2 H, CH_2CH$_2$CHNH), 3.95 (s, 3 H, CH$_3$O), 4.16 (t, *J* = 6.6 Hz, 2 H, CH$_2$O), 4.18–4.28 (m, 2 H, CHNH), 5.24 (d, *J* = 7.7 Hz, 1 H, NH), 6.85 (s, 1 H, CHCCNH), 7.15 (s, 1 H, CHCCCNH), 8.43 (s, 1 H, CHNCNH). ^{13}C NMR (126 MHz, CD_2Cl_2): δ = 24.96 [CH$_2$CH$_2$CH$_2$N(CH$_2$)$_3$O], 26.52 [CH$_2$CH$_2$N(CH$_2$)$_3$O], 26.61 (CH_2CH$_2$CHCH$_2$N), 27.01 (CH$_2$CH$_2$O), 27.31 (CH_2CH$_2$CH$_2$CH), 32.26 (CH_2CHCH$_2$N), 32.90 (CH$_2$CHNH), 35.79 (CHCH$_2$N), 48.76 (CHNH), 53.49 (CH$_2$CH$_2$CHNH), 55.03 [CH$_2$N(CH$_2$)$_3$O], 55.90 (CH$_2$CH$_2$CH$_2$O), 56.68 (CH$_3$O), 66.00 (CHCH$_2$N), 67.90 (CH$_2$O), 100.09 (CHCCNH), 108.69 (CCNH), 108.97(CHCCCNH), 147.17 (CCCNH), 149.57 (COCH$_3$), 154.29 (CHNCNH), 154.33 (COCH$_2$), 157.98 (CNH). HRMS-ESI m/z $[M+H]^+$ calcd. for $C_{29}H_{46}N_5O_2$: 496.3651, found: 496.3644.

_N_-(1-Cyclohexylpiperidin-4-yl)-6-methoxy-7-[3-(piperidin-1-yl)propoxy]-quinazolin-4-amine (16b)

According to GP4 with **15** (33.6 mg, 0.100 mmol, 1.0 equiv), 1-cyclohexylpiperidin-4-amine (36.5 mg, 0.200 mmol, 2.0 equiv) and DIEA (53.3 µL, 39.6 mg, 0.300 mmol, 3.0 equiv) in *i*-PrOH (0.5 mL) for 15 min. **16b** (45.2 mg, 94% yield, 95% purity) was isolated by flash chromatography [5% to 10% 3 M NH_3 (in MeOH) in CH_2Cl_2] as yellow solid. mp.: 168 °C. R_f = 0.50 [10% 4 M NH_3 (in MeOH) in CH_2Cl_2]. IR (film): $\tilde{\nu}$ = 2929, 1620, 1504, 1217, 735 cm^{-1}. ^1H NMR (400 MHz, CD_3OD): δ = 1.09–1.23 (m, 1 H, CH_2CH$_2$CH$_2$CHN), 1.25–1.42 (m, 4 H, CH_2CH_2CHN), 1.44–1.58 [m, 2 H, CH_2CH$_2$CH$_2$N(CH$_2$)$_3$O], 1.61–1.72 [m, 5 H, CH_2CH$_2$CH$_2$CHN, CH_2CH$_2$N(CH$_2$)$_3$O], 1.72–1.83 (m, 2 H, CH_2CHNH), 1.83–1.92 (m, 2 H, CH_2CH$_2$CHN), 1.92–2.05 (m, 2 H, CH_2CHN), 2.06–2.17 (m, 4 H, CH_2CHNH, CH_2CH$_2$O), 2.38–2.47 (m, 1 H, CH$_2$CHN), 2.47–2.55 (m, 2 H, CH_2CH$_2$CHNH), 2.55–2.62 [m, 4 H, CH_2N(CH$_2$)$_3$O], 2.62–2.70 (m, 2 H, CH_2CH$_2$CH$_2$O), 3.02–3.13 (m, 2 H, CH_2CH$_2$CHNH), 3.97 (s, 3 H, CH$_3$O), 4.13–4.20 (m, 3 H, CHNH, CH$_2$O), 7.07 (s, 1 H, CHCCCNH), 7.60 (s, 1 H, CHCCNH), 8.30 (s, 1 H, CHNCNH). ^{13}C NMR (101 MHz, CD_3OD): δ = 25.00 [CH$_2$CH$_2$CH$_2$N(CH$_2$)$_3$O], 26.35 [CH$_2$CH$_2$N(CH$_2$)$_3$O], 26.97 (CH$_2$CH$_2$O), 27.09 (CH$_2$CH$_2$CHN), 27.29 (CH$_2$CH$_2$CH$_2$CHN), 29.52 (CH$_2$CHN), 32.41 (CH$_2$CHNH), 49.28 (CH$_2$CH$_2$CHNH), 49.85 (CHNH), 55.45 [CH$_2$N(CH$_2$)$_3$O], 56.82 (CH$_3$O), 56.99 (CH$_2$CH$_2$CH$_2$O), 65.28 (CH$_2$CHN), 68.31 (CH$_2$O), 102.94 (CHCCNH), 107.82 (CHCCCNH), 110.17 (CCNH), 146.65 (CCCNH), 150.87 (CH$_3$OC), 154.28 (CNCNH), 155.47 (CH$_2$OC), 159.64 (CNH). HRMS-ESI m/z $[M+H]^+$ calcd. for $C_{28}H_{44}N_5O_2$: 482.3495, found: 482.3490.

6-Methoxy-_N_-(1-methylpiperidin-4-yl)-7-[3-(piperidin-1-yl)propoxy]quinazolin-4-amine (16c)

According to GP4 with **15** (33.6 mg, 0.100 mmol, 1.0 equiv), 1-methylpiperidin-4-amine (26.4 µL, 24.5 mg, 0.200 mmol, 2.0 equiv) and DIEA (53.3 µL, 39.6 mg, 0.300 mmol,

3.0 equiv) in *i*-PrOH (0.5 mL) for 15 min. **16c** (28.7 mg, 69% yield, 97% purity) was isolated by flash chromatography [5% to 10% 3 M NH_3 (in MeOH) in CH_2Cl_2] as colorless solid. mp.: 210 °C (decomposition). R_f = 0.26 [10% 4 M NH_3 (in MeOH) in CH_2Cl_2]. IR (film): $\tilde{\nu}$ = 2931, 1591, 1254, 1049 cm^{-1}. ^1H NMR (500 MHz, CD_3OD): δ = 1.48–1.59 [m, 2 H, CH_2CH$_2$CH$_2$N(CH$_2$)$_3$O], 1.63–1.72 [m, 4 H, CH_2CH$_2$N(CH$_2$)$_3$O], 1.73–1.85 (m, 2 H, CH_2CHNH), 2.04–2.11 (m, 2 H, CH_2CHNH), 2.11–2.17 (m, 2 H, CH_2CH$_2$O), 2.21–2.28 (m, 2 H, CH_2NCH$_3$), 2.35 (s, 3 H, CH_3N), 2.64 [bs, 4 H, CH_2N(CH$_2$)$_3$O], 2.68–2.76 (m, 2 H, CH_2CH$_2$CH$_2$O), 2.93–3.04 (m, 2 H, CH_2NCH$_3$), 3.98 (s, 3 H, CH_3O), 4.14–4.26 (m, 3 H, CH_2O, C*H*NH), 7.07 (s, 1 H, C*H*CCNH), 7.60 (s, 1 H, C*H*CCNH), 8.31 (s, 1 H, C*H*NCNH). ^{13}C NMR (126 MHz, CD_3OD): δ = 24.78 [$CH_2CH_2CH_2N(CH_2)_3O$], 26.16 [$CH_2CH_2N(CH_2)_3O$], 26.76 (CH_2CH_2O), 32.26 (CH_2CHNH), 46.18 (CH_3N), 55.37 [$CH_2N(CH_2)_3O$], 55.92 (CH_2NCH_3), 56.82 (CH_3O), 56.95 ($CH_2CH_2CH_2O$), 68.24 (CH_2O), 102.93 (*C*HCCNH), 107.83 (*C*HCCCNH), 110.22 (*C*CNH), 146.63 (*C*CCNH), 150.84 (CH_3OC), 154.30 (*C*HNCNH), 155.40 (CH_2OC), 159.69 (CNH). HRMS-ESI m/z $[M+H]^+$ calcd. for $C_{23}H_{36}N_5O_2$: 414.1869, found: 414.2864.

6-Methoxy-*N*-(1-phenylpiperidin-4-yl)-7-[3-(piperidin-1-yl)propoxy]quinazolin-4-amine (16d)

According to GP4 with **15** (67.2 mg, 0.200 mmol, 1.0 equiv), 1-phenylpiperidin-4-amine (74.2 mg, 0.400 mmol, 2.0 equiv) and DIEA (107 µL, 79.1 mg, 0.600 mmol, 3.0 equiv) in *i*-PrOH (1.0 mL) for 15 min. **16d** (77.7 mg, 82% yield, 100% purity) was isolated by flash chromatography [10% 3 M NH_3 (in MeOH) in CH_2Cl_2] as colorless solid. mp.: 207 °C (decomposition). R_f = 0.49 [10% 4 M NH_3 (in MeOH) in CH_2Cl_2]. IR (film): $\tilde{\nu}$ = 2935, 1589, 1504, 1215, 756 cm^{-1}. ^1H NMR (500 MHz, CD_2Cl_2): δ = 1.37–1.47 [m, 2 H, CH_2CH$_2$CH$_2$N(CH$_2$)$_3$O], 1.49–1.63 [m, 4 H, CH_2CH$_2$N(CH$_2$)$_3$O], 1.74 (qd, *J* = 11.9, 11.9, 11.9, 4.0 Hz, 2 H, CH_2CHNH), 2.03 (p, *J* = 6.9, 6.9, .9, 6.9 Hz, 2 H, CH_2CH$_2$O), 2.21–2.30 (m, 2 H, CH_2CHNH), 2.39 [s, 4 H, CH_2N(CH$_2$)$_3$O], 2.44–2.52 (m, 2 H, CH_2CH$_2$CH$_2$O), 2.97 (td, *J* = 12.4, 12.4, 2.5 Hz, 2 H, CH_2CH$_2$CHNH), 3.69–3.78 (m, 2 H, CH_2CH$_2$CHNH), 3.94 (s, 3 H, CH_3O), 4.16 (t, *J* = 6.7, 6.7 Hz, 2 H, CH_2O), 4.36–4.50 (m, 1 H, C*H*NH), 5.34 (s, 1 H, NH), 6.82 (t, *J* = 7.3, 7.3 Hz, 1 H, C*H*CHCHCN), 6.88 (s, 1 H, C*H*CCNH), 6.93–7.01 (m, 2 H, CHC*H*CHCN), 7.16 (s, 1 H, C*H*CCCNH), 7.21–7.30 (m, 2 H, CHCHC*H*CN), 8.46 (s, 1 H, C*H*NCNH). ^{13}C NMR (126 MHz, CD_2Cl_2): δ = 24.90 [$CH_2CH_2N(CH_2)_3O$], 26.44 [$CH_2N(CH_2)_3O$], 26.92 (CH_2CH_2O), 32.34 (CH_2CH_2CHNH), 48.57 (CHNH), 49.14 (CH_2CH_2CHNH), 54.99 [$CH_2N(CH_2)_3O$], 55.87 ($CH_2CH_2CH_2O$), 56.67 (CH_3O), 67.88 (CH_2O), 100.06 (*C*HCCNH), 108.72 (*C*CNH), 108.98 (*C*HCCCNH), 116.75 (CH*C*HCHCN), 119.61 (*C*HCHCHCN), 129.46 (CHCH*C*HCN), 147.22 (*C*CCNH), 149.64 ($COCH_3$), 151.76 (CHCHCH*C*N), 154.24 (*C*HNCNH), 154.37 ($COCH_2$), 157.94 (CNH). HRMS-ESI m/z $[M+H]^+$ calcd. for $C_{28}H_{38}N_5O_2$: 476.3026, found: 476.3019.

***N*-(1-Benzylpiperidin-4-yl)-6-methoxy-7-[3-(piperidin-1-yl)propoxy]quinazolin-4-amine (16e)**

According to GP4 with **15** (67.2 mg, 0.200 mmol, 1.0 equiv), 1-benzylpiperidin-4-amine (83.2 µL, 77.7 mg, 0.400 mmol, 2.0 equiv) and DIEA (107 µL, 79.1 mg, 0.600 mmol, 3.0 equiv) in *i*-PrOH (1.0 mL) for 15 min. **16e** (83.1 mg, 85% yield, 99% purity) was isolated by flash chromatography [10% 3 M NH_3 (in MeOH) in CH_2Cl_2] as colorless solid. mp.: 164 °C. R_f = 0.32 [10% 4 M NH_3 (in MeOH) in CH_2Cl_2]. IR (film): $\tilde{\nu}$ = 2931, 1589, 1504, 1458, 1217, 746 cm^{-1}. ^1H NMR (400 MHz, CD_2Cl_2): δ = 1.37–1.48 [m, 2 H, CH_2CH$_2$CH$_2$N(CH$_2$)$_3$O], 1.48–1.75 [m, 6 H,

CH_2CH_2CHNH, $CH_2CH_2N(CH_2)_3O$], 1.97–2.08 (m, 2 H, CH_2CH_2O), 2.08–2.17 (m, 2 H, CH_2CH_2CHNH), 2.17–2.27 (m, 2 H, CH_2CH_2CHNH), 2.29–2.43 [m, 4 H, $CH_2N(CH_2)_3O$], 2.43–2.53 (m, 2 H, $CH_2CH_2CH_2O$), 2.84–2.98 (m, 2 H, CH_2CH_2CHNH), 3.53 (s, 2 H, CCH_2N), 3.95 (s, 3 H, CH_3O), 4.16 (t, J = 6.6 Hz, 2 H, CH_2O), 4.19–4.31 (m, 1 H, CHNH), 5.18–5.26 (m, 1 H, NH), 6.85 (s, 1 H, CHCCNH), 7.15 (s, 1 H, CHCCCNH), 7.21–7.28 (m, 1 H, CHCHCHCCH$_2$N), 7.28–7.37 (m, 4 H, $CHCHCCH_2N$), 8.43 (s, 1 H, CHNCNH). ^{13}C NMR (101 MHz, CD_2Cl_2): δ = 24.90 [$CH_2CH_2CH_2N(CH_2)_3O$], 26.43 [$CH_2CH_2N(CH_2)_3O$], 26.92 (CH_2CH_2O), 32.85 (CH_2CH_2CHNH), 48.62 (CH_2CH_2CHNH), 52.93 (CH_2CH_2CHNH), 54.99 [$CH_2N(CH_2)_3O$], 55.87 ($CH_2CH_2CH_2O$), 56.68 (CH_3O), 63.31 (CCH_2N), 67.85 (CH_2O), 100.05 (CHCCNH), 108.69 (CCNH), 108.99 (CHCCCNH), 127.28 (CHCHCHCCH$_2$N), 128.53 (CHCHCCH$_2$N), 129.38 ($CHCCH_2N$), 139.39 (CCH_2N), 147.18 (CCCNH), 149.57 ($COCH_3$), 154.27 (CHNCNH), 154.31 ($COCH_2$), 157.96 (CNH). HRMS-ESI m/z $[M+H]^+$ calcd. for $C_{29}H_{40}N_5O_2$: 490.3182, found: 490.3176.

6-Methoxy-7-[3-(piperidin-1-yl)propoxy]-*N*-[5-(pyrrolidin-1-yl)pentyl]quinazolin-4-amine (16f)

According to GP4 with **15** (101 mg, 0.300 mmol, 1.0 equiv), 5-pyrrolidin-1-ylpentan-1-amine (93.8 mg, 0.600 mmol, 2.0 equiv) and DIEA (160 µL, 119 mg, 0.900 mmol, 3.0 equiv) in *i*-PrOH (1.5 mL) for 1 h. **16f** (114 mg, 83% yield, 98% purity) was isolated by flash chromatography [10% to 15% 3 M NH_3 (in MeOH) in CH_2Cl_2] as pale yellow solid. mp.: 103 °C. R_f = 0.41 [15% 3 M NH_3 (in MeOH) in CH_2Cl_2]. IR (film): ṽ = 2937, 1593, 1460, 1217, 754 cm^{-1}. ^{1}H NMR (500 MHz, CD_2Cl_2): δ = 1.38–1.46 [m, 2 H, $CH_2CH_2CH_2N(CH_2)_3O$], 1.47–1.53 (m, 2 H, $CH_2CH_2CH_2NH$), 1.54–1.58 [m, 4 H, $CH_2CH_2N(CH_2)_3O$], 1.58–1.65 [m, 2 H, $CH_2(CH_2)_3NH$], 1.69–1.76 (m, 2 H, CH_2CH_2NH), 1.76–1.84 [m, 4 H, $CH_2CH_2N(CH_2)_5NH$], 2.01 (p, J = 6.9 Hz, 2 H, CH_2CH_2O), 2.31–2.42 [m, 4 H, $CH_2N(CH_2)_3O$], 2.45 (t, J = 7.2 Hz, 2 H, $CH_2CH_2CH_2O$), 2.53 [t, J = 7.2 Hz, 2 H, $CH_2(CH_2)_4NH$], 2.56–2.62 [m, 4 H, $CH_2N(CH_2)_5NH$], 3.56–3.71 (m, 2 H, CH_2NH), 3.95 (s, 3 H, CH_3O), 4.15 (t, J = 6.7 Hz, 2 H, CH_2O), 5.90 (t, J = 5.6 Hz, 1 H, NH), 7.07 (s, 1 H, $CHCOCH_3$), 7.14 (s, 1 H, $CHCOCH_2$), 8.43 (s, 1 H, CHNCNH). ^{13}C NMR (126 MHz, CD_2Cl_2): δ = 23.82 [$CH_2CH_2N(CH_2)_5NH$], 24.96 [$CH_2CH_2CH_2N(CH_2)_3O$], 25.22 ($CH_2CH_2CH_2NH$), 26.51 [$CH_2CH_2N(CH_2)_3O$], 27.00 (CH_2CH_2O), 28.52 [$CH_2(CH_2)_3NH$], 29.43 (CH_2CH_2NH), 41.58 (CH_2NH), 54.47 [$CH_2N(CH_2)_5NH$], 55.02 [$CH_2N(CH_2)_3O$], 55.90 ($CH_2CH_2CH_2O$), 56.39 [$CH_2(CH_2)_4NH$], 56.79 (CH_3O), 67.85 (CH_2O), 100.72 ($CHCOCH_3$), 108.83 ($CHCOCH_2$), 108.91 (CCNH), 146.98 (CCCNH), 149.52 ($COCH_3$), 154.21 ($COCH_2$), 154.32 (CHNCNH), 158.84 (CNH). HRMS-ESI m/z $[M+H]^+$ calcd. for $C_{26}H_{42}N_5O_2$: 456.3339, found: 456.3333.

4-[(1-Isopropylpiperidin-4-yl)oxy]-6-methoxy-7-[3-(piperidin-1-yl)propoxy]quinazoline (16g)

mp.: 93 °C. R_f = 0.38 [7% 3 M NH_3 (in MeOH) in CH_2Cl_2]. IR (film): ṽ = 2935, 1502, 1427, 1211, 754 cm^{-1}. ^{1}H NMR (500 MHz, CD_2Cl_2): δ = 1.05 (d, J = 6.5 Hz, 6 H, CH_3CH), 1.32–1.48 [m, 2 H, $CH_2CH_2CH_2N(CH_2)_3O$], 1.49–1.62 [m, 4 H, $CH_2CH_2N(CH_2)_3O$], 1.83–1.93 (m, 2 H, CH_2CHO), 2.03 (p, J = 6.8 Hz, 2 H, CH_2CH_2O), 2.08–2.18 (m, 2 H, CH_2CHO), 2.25–2.42 [m, 4 H, $CH_2N(CH_2)_3O$], 2.42–2.52 (m, 4 H, $CH_2CH_2CH_2O$, CH_2CH_2CHO), 2.76 (h, J = 6.6 Hz, 1 H, CH_3CH), 2.80–2.91 (m, 2 H, CH_2CH_2CHO), 3.97 (s, 3 H, CH_3O), 4.19 (t, J = 6.7 Hz, 2 H, CH_2O), 5.35 (dt, J = 8.5, 4.2 Hz, 1 H, CHO), 7.23 (s, 1 H, $CHCOCH_2$), 7.36 (s, 1 H, $CHCOCH_3$),

8.56 (s, 1 H, CHNCO). ^{13}C NMR (126 MHz, CD_2Cl_2): δ = 18.46 (*C*H_3CH), 24.96 [$CH_2CH_2CH_2N(CH_2)_3O$], 26.52 [$CH_2CH_2N(CH_2)_3O$], 26.97 (*C*H_2CH_2O), 31.82 (*C*H_2CHO), 46.44 (*C*H_2CH_2CHO), 54.77 (CH_3CH), 55.03 [$CH_2N(CH_2)_3O$], 55.87 (*C*$H_2CH_2CH_2O$), 56.42 (CH_3O), 68.01 (CH_2O), 73.20 (CHO), 101.69 (*C*HCOCH$_3$), 107.87 (*C*HCOCH$_2$), 111.30 (*C*CCO), 149.00 (*C*CCO), 150.27 (*C*OCH$_3$), 153.30 (*C*HNCO), 155.28 (*C*OCH$_2$), 165.09 (*C*OCH). HRMS-ESI m/z $[M+H]^+$ calcd. for $C_{25}H_{39}N_4O_3$: 443.3022, found: 443.3019.

7-Benzyloxy-*N*-(1-isopropylpiperidin-4-yl)-6-methoxyquinazolin-4-amine (18)

According to GP4 with **17** (1.27 g, 4.00 mmol, 1.0 equiv), 1-propan-2-ylpiperidin-4-amine (1.29 mL, 1.16 g, 8.00 mmol, 2.0 equiv) and DIEA (2.08 mL, 1.58 g, 12.0 mmol, 3.0 equiv) in *i*-PrOH (20 mL) for 15 min. **18** (1.63 g, > 99% yield, 96% purity) was isolated by flash chromatography [10% 3 M NH_3 (in MeOH) in CH_2Cl_2] as colorless solid. mp.: 192 °C (decomposition). R_f = 0.35 [10% 4 M NH_3 (in MeOH) in CH_2Cl_2]. IR (film): $\tilde{\nu}$ = 2966, 1589, 1504, 1252, 752 cm^{-1}. ^{1}H NMR (500 MHz, $CDCl_3$): δ = 1.07 (d, *J* = 6.6 Hz, 6 H, C*H*$_3$CH), 1.52–1.73 (m, 2 H, C*H*$_2$CH), 2.11–2.23 (m, 2 H, C*H*$_2$CH), 2.34–2.45 (m, 2 H, C*H*$_2$CH$_2$CH), 2.70–2.83 (m, 1 H, CH$_3$C*H*), 2.87–2.97 (m, 2 H, C*H*$_2$CH$_2$CH), 4.01 (s, 3 H, CH_3O), 4.18–4.29 (m, 1 H, C*H*NH), 5.12 (d, *J* = 7.7 Hz, 1 H, NH), 5.27 (s, 2 H, CH_2O), 6.81 (s, 1 H, C*H*CCNH), 7.22 (s, 1 H, *C*HCCCNH), 7.29–7.34 (m, 1 H, C*H*CHCHCCH$_2$O), 7.35–7.41 (m, 2 H, C*H*CHCCH$_2$O), 7.44–7.51 (m, 2 H, C*H*CCH$_2$O), 8.52 (s, 1 H, C*H*NCNH). ^{13}C NMR (126 MHz, $CDCl_3$): δ = 18.59 (*C*H$_3$C), 32.99 (*C*H$_2$CH), 47.82 (*C*H$_2$CH$_2$CH), 48.63 (CHNH), 54.65 (CH$_3$*C*), 56.59 (CH_3O), 70.91 (CH_2O), 99.77 (*C*HCCNH), 108.78 (*C*CNH), 109.69 (*C*HCCCNH), 127.57 (*C*HCCH$_2$O), 128.35 (*C*HCHCHCCH$_2$O), 128.86 (*C*HCHCCH$_2$O), 135.60 (*C*CH$_2$O), 146.70 (*C*CCNH), 149.46 (CH$_3$O*C*), 153.59 (CH$_2$O*C*), 154.23 (*C*HNCNH), 157.70 (CNH). HRMS-ESI m/z $[M+H]^+$ calcd. for $C_{24}H_{31}N_4O_2$: 407.2447, found: 407.2441.

4-[(1-Isopropylpiperidin-4-yl)amino]-6-methoxyquinazolin-7-ol (19)

mp.: 166 °C. R_f = 0.18 [15% 4 M NH_3 (in MeOH) in CH_2Cl_2]. IR (film): $\tilde{\nu}$ = 2359, 1633, 1489, 1427, 1352 cm^{-1}. ^{1}H NMR (400 MHz, CD_3OD): δ = 1.15 (d, *J* = 6.6 Hz, 6 H, C*H*$_3$CH), 1.65–1.83 (m, 2 H, C*H*$_2$CHNH), 2.02–2.21 (m, 2 H, C*H*$_2$CHNH), 2.34–2.53 (m, 2 H, CH_2N), 2.85 (hept, *J* = 6.6 Hz, 1 H, CH$_3$C*H*), 2.94–3.12 (m, 2 H, CH_2N), 4.00 (s, 3 H, CH_3O), 4.21 (tt, *J* = 11.4, 4.2 Hz, 1 H, C*H*NH), 6.94 (s, 1 H, C*H*COH), 7.57 (s, 1 H, C*H*CCNH), 8.25 (s, 1 H, C*H*NCNH). ^{13}C NMR (126 MHz, CD_3OD): δ = 18.40 (*C*H$_3$CH), 32.29 (*C*H$_2$CHNH), 49.17 (CH_2N), 49.74 (CHNH), 56.20 (CH$_3$*C*H), 56.65 (CH_3O), 102.49 (*C*HCCNH), 108.41 (*C*CNH), 109.53 (*C*HCOH), 145.87 (*C*CCNH), 151.00 (CH$_3$O*C*), 153.21 (*C*HNCNH), 156.86 (COH), 159.59 (CNH). HRMS-ESI m/z $[M+H]^+$ calcd. for $C_{17}H_{25}N_4O_2$: 317.1978, found: 317.1973.

***N*-(1-Propan-2-ylpiperidin-4-yl)-6-methoxy-7-[3-(piperidin-1-yl)propoxy]quinazolin-4-amine (20a)** (Kaiser et al., 2024).

According to GP5, with **19** (127 mg, 0.400 mmol, 1.0 equiv), 3-piperidin-1-ylpropan-1-ol (224 µL, 211 mg, 1.40 mmol, 3.5 equiv), PPh_3 (0.589 g, 2.20 mmol, 5.5 equiv) and DIAD (413 µL, 426 mg, 2.00 mmol, 5.0 equiv) in THF (5.8 mL). Purification by flash chromatography [10% 3 M NH_3 (in MeOH) in CH_2Cl_2] afforded **20a** (111 mg, 63% yield, 99% purity) as colorless solid. The characterization data of **20a** match the reported (Kaiser et al., 2024).

_N_-(1-Isopropylpiperidin-4-yl)-6-methoxy-7-[4-(piperidin-1-yl)butoxy]quinazolin-4-amine (20b)

mp.: 191 °C. R_f = 0.41 [10% 4 M NH_3 (in MeOH) in CH_2Cl_2]. IR (film): $\tilde{\nu}$ = 2927, 1624, 1504, 1460, 1252 cm^{-1}. ^1H NMR (500 MHz, CD_2Cl_2): δ = 1.04 (d, J = 6.6 Hz, 6 H, CH_3CH), 1.36–1.46 [m, 2 H, CH_2CH$_2$CH$_2$N(CH$_2$)$_4$O], 1.48–1.61 [m, 6 H, CH_2CH$_2$N(CH$_2$)$_4$O, CH_2CHNH], 1.62–1.75 (m, 2 H, CH_2CH$_2$CH$_2$O), 1.82–1.94 (m, 2 H, CH_2CH$_2$O), 2.09–2.18 (m, 2 H, CH_2CHNH), 2.20–2.54 [m, 8 H, CH_2NCH_2(CH$_2$)$_3$O, CH_2CH$_2$CHNH], 2.76 (hept, J = 6.6 Hz, 1 H, CH$_3$CH), 2.83–2.93 (m, 2 H, CH_2CH$_2$CHNH), 3.95 (s, 3 H, CH$_3$O), 4.13 (t, J = 6.7 Hz, 2 H, CH$_2$O), 4.15–4.26 (m, 1 H, CHNH), 5.25 (d, J = 7.7 Hz, 1 H, NH), 6.86 (s, 1 H, CHCCNH), 7.13 (s, 1 H, CHCCCNH), 8.43 (s, 1 H, CHNCNH). ^{13}C NMR (126 MHz, CD_2Cl_2): δ = 18.45 (CH_3CH), 23.81 (CH_2CH$_2$CH$_2$O), 25.01 [CH_2CH$_2$CH$_2$N(CH$_2$)$_4$O], 26.53 [CH_2CH$_2$N(CH$_2$)$_4$O], 27.37 (CH_2CH$_2$O), 33.23 (CH_2CHNH), 48.02 (CH_2CH$_2$CHNH), 49.04 (CHNH), 54.85 (CH$_3$CH), 55.01 [CH_2N(CH$_2$)$_4$O], 56.69 (CH$_3$O), 59.16 [CH_2(CH$_2$)$_3$O], 69.26 (CH$_2$O), 100.10 (CHCCNH), 108.67 (CCNH), 108.87 (CHCCCNH), 147.17 (CCCNH), 149.58 (CH$_3$OC), 154.28 (CHNCNH), 154.33 (CH$_2$OC), 157.97 (CNH). HRMS-ESI m/z [M+H]$^+$ calcd. for $C_{26}H_{42}N_5O_2$: 456.3339, found: 456.3331.

_N_-(1-Isopropylpiperidin-4-yl)-6-methoxy-7-[2-(piperidin-1-yl)ethoxy]quinazolin-4-amine (20c)

According to GP5, with **19** (127 mg, 0.400 mmol, 1.0 equiv), 2-piperidin-1-ylethan-1-ol (215 µL, 209 mg, 1.60 mmol, 4.0 equiv), PPh_3 (0.589 g, 2.20 mmol, 5.5 equiv) and DIAD (413 µL, 426 mg, 2.00 mmol, 5.0 equiv) in THF (5.8 mL). Purification by flash chromatography [10% 3 M NH_3 (in MeOH) in CH_2Cl_2] afforded **20c** (136 mg, 79% yield, 99% purity) as colorless solid. mp.: 185 °C. R_f = 0.21 [15% 4 M NH_3 (in MeOH) in CH_2Cl_2]. IR (film): $\tilde{\nu}$ = 1643, 1460, 1252 cm^{-1}. ^1H NMR (500 MHz, CD_2Cl_2): δ = 1.04 (d, J = 6.6 Hz, 6 H, CH_3CH), 1.36–1.47 (m, 2 H, CH_2CH$_2$CH$_2$NCH$_2$CH$_2$O), 1.54–1.63 (m, 6 H, CH_2CHNH, CH_2CH$_2$NCH$_2$CH$_2$O), 2.12–2.17 (m, 2 H, CH_2CHNH), 2.32–2.40 (m, 2 H, CH_2CH$_2$CHNH), 2.42–2.54 (m, 4 H, CH_2NCH$_2$CH$_2$O), 2.78 (s, 1 H, CH$_3$CH), 2.78–2.81 (m, 2 H, CH_2CH$_2$O), 2.84–2.93 (m, 2 H, CH_2CH$_2$CHNH), 3.96 (s, 3 H, CH$_3$O), 4.15–4.27 (m, 3 H, CH$_2$O, CHNH), 5.27 (d, J = 7.7 Hz, 1 H, NH), 6.87 (s, 1 H, CHCCNH), 7.14 (s, 1 H, CHCCCNH), 8.43 (s, 1 H, CHNCNH). ^{13}C NMR (126 MHz, CD_2Cl_2): δ = 18.45 (CH_3CH), 24.71 (CH_2CH$_2$CH$_2$NCH$_2$CH$_2$O), 26.43 (CH_2CH$_2$NCH$_2$CH$_2$O), 33.22 (CH_2CHNH), 48.02 (CH_2CH$_2$CHNH), 49.06 (CHNH), 54.84 (CH$_3$CH), 55.43 (CH_2NCH$_2$CH$_2$O), 56.68 (CH$_3$O), 58.02 (CH_2CH$_2$O), 67.04 (CH$_2$O), 100.19 (CHCCNH), 108.80 (CCNH), 109.01 (CHCCCNH), 147.13 (CCCNH), 149.49 (CH$_3$OC), 153.75 (CH$_2$OC), 154.33 (CHNCNH), 157.98 (CNH). HRMS-ESI m/z [M+H]$^+$ calcd. for $C_{24}H_{38}N_5O_2$: 428.3026, found: 428.3020.

_N_-(1-Isopropylpiperidin-4-yl)-6-methoxy-7-[3-(pyrrolidin-1-yl)propoxy]-quinazolin-4-amine (20d)

According to GP5, with **19** (127 mg, 0.400 mmol, 1.0 equiv), 3-pyrrolidin-1-ylpropan-1-ol (227 µL, 218 mg, 1.60 mmol, 4.0 equiv), PPh_3 (0.589 g, 2.20 mmol, 5.5 equiv) and DIAD (413 µL, 426 mg, 2.00 mmol, 5.0 equiv) in THF (5.8 mL). Purification by flash chromatography [10% 3 M NH_3 (in MeOH) in CH_2Cl_2] afforded **20d** (119 mg, 69% yield, 98% purity) as colorless solid. mp.: 162 °C. R_f = 0.18 [15% 4 M NH_3 (in MeOH) in CH_2Cl_2]. IR (film): $\tilde{\nu}$ = 2964, 1593,

1506, 1254 cm^{-1}. ^1H NMR (500 MHz, CD_2Cl_2): δ = 1.11 (d, *J* = 6.6 Hz, 6 H, C*H*$_3$CH), 1.69–1.78 (m, 2 H, C*H*$_2$CHNH), 1.77–1.82 [m, 4 H, C*H*$_2$CH$_2$N(CH$_2$)$_3$O], 2.09 (p, *J* = 6.8 Hz, 2 H, C*H*$_2$CH$_2$O), 2.12–2.21 (m, 2 H, C*H*$_2$CHNH), 2.38–2.53 (m, 2 H, C*H*$_2$CH$_2$CHNH), 2.53–2.62 [m, 4 H, C*H*$_2$N(CH$_2$)$_3$O], 2.61–2.73 (m, 2 H, C*H*$_2$CH$_2$CH$_2$O), 2.90 (hept, *J* = 6.6 Hz, 1 H, CH$_3$C*H*), 2.96–3.10 (m, 2 H, C*H*$_2$CH$_2$CHNH), 3.96 (s, 3 H, CH$_3$O), 4.19 (t, *J* = 6.6 Hz, 3 H, CH$_2$O), 4.22–4.37 (m, 1 H, C*H*NH), 5.44 (d, *J* = 7.7 Hz, 1 H, NH), 6.91 (s, 1 H, C*H*CCNH), 7.15 (s, 1 H, C*H*CCCNH), 8.42 (s, 1 H, C*H*NCNH). ^{13}C NMR (126 MHz, CD_2Cl_2): δ = 18.14 (*C*H$_3$CH), 23.90 [*C*H$_2$CH$_2$N(CH$_2$)$_3$O], 28.61 (*C*H$_2$CH$_2$O), 32.36 (*C*H$_2$CHNH), 48.07 (*C*H$_2$CH$_2$CHNH), 48.44 (CHNH), 53.05 (*C*H$_2$CH$_2$CH$_2$O), 54.46 [*C*H$_2$N(CH$_2$)$_3$O], 55.51 (CH$_3$*C*H), 56.73 (CH$_3$O), 67.65 (CH$_2$O), 100.27 (*C*HCCNH), 108.79 (*C*CNH), 108.91 (*C*HCCCNH), 147.13 (*C*CCNH), 149.59 (CH$_3$O*C*), 154.20 (*C*HNCNH), 154.27 (CH$_2$O*C*), 157.98 (CNH). HRMS-ESI m/z $[M+H]^+$ calcd. for $C_{24}H_{38}N_5O_2$: 428.3026, found: 428.3021.

7-[3-(Azepan-1-yl)propoxy]-*N*-(1-isopropylpiperidin-4-yl)-6-methoxyquinazolin-4-amine (20e)

According to GP5, with **19** (127 mg, 0.400 mmol, 1.0 equiv), 3-(azepan-1-yl)propan-1-ol (273 µL, 265 mg, 1.60 mmol, 4.0 equiv), PPh_3 (0.589 g, 2.20 mmol, 5.5 equiv) and DIAD (413 µL, 426 mg, 2.00 mmol, 5.0 equiv) in THF (5.8 mL). Purification by flash chromatography [10% 3 M NH_3 (in MeOH) in CH_2Cl_2] afforded **20e** (108 mg, 59% yield, 97% purity) as colorless solid. mp.: 167 °C. R_f = 0.44 [15% 4 M NH_3 (in MeOH) in CH_2Cl_2]. IR (film): $\tilde{\nu}$ = 2926, 1622, 1593, 1460, 1252 cm^{-1}. ^1H NMR (500 MHz, CD_2Cl_2): δ = 1.05 (d, *J* = 6.6 Hz, 6 H, C*H*$_3$CH), 1.48–1.80 [m, 10 H, C*H*$_2$CHNH, C*H*$_2$C*H*$_2$CH$_2$N(CH$_2$)$_3$O], 2.00 (p, *J* = 6.8 Hz, 2 H, C*H*$_2$CH$_2$O), 2.08–2.23 (m, 2 H, C*H*$_2$CHNH), 2.28–2.45 (m, 2 H, C*H*$_2$CH$_2$CHNH), 2.58–2.67 (m, 6 H, C*H*$_2$NC*H*$_2$CH$_2$CH$_2$O), 2.72–2.84 (m, 1 H, CH$_3$C*H*), 2.86–2.96 (m, 2 H, C*H*$_2$CH$_2$CHNH), 3.96 (s, 3 H, CH$_3$O), 4.11–4.28 (m, 3 H, C*H*NH, CH$_2$O), 5.27–5.31 (m, 1 H, NH), 6.88 (s, 1 H, C*H*CCNH), 7.15 (s, 1 H, C*H*CCCNH), 8.42 (s, 1 H, C*H*NCNH). ^{13}C NMR (126 MHz, CD_2Cl_2): δ = 18.40 (*C*H$_3$CH), 27.43 [*C*H$_2$CH$_2$CH$_2$N(CH$_2$)$_3$O], 27.81 (*C*H$_2$CH$_2$O), 28.82 [*C*H$_2$CH$_2$N(CH$_2$)$_3$O], 33.04 (*C*H$_2$CHNH), 48.04 (*C*H$_2$CH$_2$CHNH), 48.92 (*C*HNH), 54.93 (*C*H$_2$CH$_2$CH$_2$O), 54.93 (CH$_3$*C*H), 55.86 [*C*H$_2$N(CH$_2$)$_3$O], 56.70 (CH$_3$O), 67.84 (CH$_2$O), 100.18 (*C*HCCNH), 108.70 (*C*CNH), 108.88 (*C*HCCCNH), 147.13 (*C*CCNH), 149.58 (CH$_3$O*C*), 154.25 (*C*HNCNH), 154.39 (CH$_2$O*C*), 157.99 (CNH). HRMS-ESI m/z $[M+H]^+$ calcd. for $C_{26}H_{42}N_5O_2$: 456.3339, found: 456.3334.

***N*-(1-Isopropylpiperidin-4-yl)-6-methoxy-7-[2-(1-methylpiperidin-2-yl)ethoxy]-quinazolin-4-amine (20f)**

According to GP5, with **19** (127 mg, 0.400 mmol, 1.0 equiv), 2-(1-methylpiperidin-2-yl)ethan-1-ol (246 µL, 241 mg, 1.60 mmol, 4.0 equiv), PPh_3 (0.589 g, 2.20 mmol, 5.5 equiv) and DIAD (413 µL, 426 mg, 2.00 mmol, 5.0 equiv) in THF (5.8 mL). Purification by flash chromatography [10% 3 M NH_3 (in MeOH) in CH_2Cl_2] afforded **20f** (81.0 mg, 46% yield, 100% purity) as colorless solid. mp.: 208 °C. R_f = 0.56 [15% 4 M NH_3 (in MeOH) in CH_2Cl_2]. IR (film): $\tilde{\nu}$ = 1624, 1506, 1252, 1217 cm^{-1}. ^1H NMR (500 MHz, CD_2Cl_2): δ = 1.04 (d, *J* = 6.6 Hz, 6 H, C*H*$_3$CH), 1.21–1.34 (m, 1 H, C*H*$_2$CH$_2$CH$_2$NCH$_3$), 1.36–1.47 [m, 1 H, C*H*$_2$(CH$_2$)$_3$NCH$_3$], 1.47–1.76 (m, 7 H, C*H*$_2$CHNH, C*H*$_2$C*H*$_2$C*H*$_2$CHC*H*$_2$CH$_2$O), 1.93–2.04 (m, 1 H, C*H*$_2$CH$_2$O), 2.04–2.18 (m, 4 H, C*H*$_2$CHNH, C*H*NC*H*$_2$), 2.26 (s, 3 H, CH$_3$N), 2.32–2.42 (m, 2 H, C*H*$_2$CH$_2$CHNH), 2.71–2.78 (m, 1 H, CH$_3$C*H*), 2.78–2.84 (m, 1 H, CH$_3$NC*H*$_2$), 2.84–2.94 (m, 2 H, C*H*$_2$CH$_2$CHNH), 3.95 (s, 3 H,

CH_3O), 4.11–4.28 (m, 3 H, C*H*NH, CH_2O), 5.22–5.29 (m, 1 H, NH), 6.86 (s, 1 H, C*H*CCNH), 7.15 (s, 1 H, C*H*CCCNH), 8.43 (s, 1 H, C*H*NCNH). ^{13}C NMR (126 MHz, CD_2Cl_2): δ = 18.46 (*C*H_3CH), 24.74 (*C*H_2CH$_2$CH$_2$NCH$_3$), 26.11 (*C*H_2CH$_2$NCH$_3$), 31.40 [*C*H_2(CH$_2$)$_3$NCH$_3$], 32.32 (*C*H_2CH$_2$O), 33.23 (*C*H_2CHNH), 43.23 (CH_3N), 48.02 (*C*H_2CH$_2$CHNH), 49.05 (CHNH), 54.82 (CH$_3$*C*H), 56.69 (CH_3O), 57.25 (*C*H_2NCH$_3$), 61.46 (*C*HNCH$_3$), 66.58 (CH_2O), 100.14 (*C*HCCNH), 108.71 (*C*CNH), 108.96 (*C*HCCCNH), 147.16 (*C*CCNH), 149.53 (CH$_3$O*C*), 154.29 (CH$_2$O*C*), 154.30 (*C*HNCNH), 157.98 (CNH). HRMS-ESI m/z [M+H]$^+$ calcd. for $C_{25}H_{40}N_5O_2$: 442.3182, found: 442.2176.

_N_-(1-Isopropylpiperidin-4-yl)-6-methoxy-7-[(1-methylpiperidin-4-yl)methoxy]-quinazolin-4-amine (20g)

According to GP5, with **19** (127 mg, 0.400 mmol, 1.0 equiv), (1-methylpiperidin-4-yl)methanol (200 µL, 218 mg, 1.60 mmol, 4.0 equiv), PPh_3 (0.589 g, 2.20 mmol, 5.5 equiv) and DIAD (413 µL, 426 mg, 2.00 mmol, 5.0 equiv) in THF (5.8 mL). Purification by flash chromatography [10% 3 M NH_3 (in MeOH) in CH_2Cl_2] afforded **20g** (99.6 mg, 58% yield, 95% purity) as colorless solid. mp.: 156 °C. R_f = 0.31 [15% 4 M NH_3 (in MeOH) in CH_2Cl_2]. IR (film): $\tilde{\nu}$ = 1643, 1504, 1254 cm^{-1}. ^{1}H NMR (500 MHz, CD_2Cl_2): δ = 1.06 (d, *J* = 6.6 Hz, 6 H, C*H*$_3$CH), 1.36–1.47 (m, 2 H, C*H*$_2$CHCH$_2$O), 1.59–1.68 (m, 2 H, C*H*$_2$CHNH), 1.72–1.91 (m, 3 H, C*H*$_2$C*H*CH$_2$O), 1.91–1.99 (m, 2 H, C*H*$_2$NCH$_3$), 2.09–2.18 (m, 2 H, C*H*$_2$CHNH), 2.23 (s, 3 H, CH_3N), 2.32–2.47 (m, 2 H, C*H*$_2$CH$_2$CHNH), 2.75–2.83 (m, 1 H, CH$_3$C*H*), 2.83–2.88 (m, 2 H, C*H*$_2$NCH$_3$), 2.88–2.97 (m, 2 H, C*H*$_2$CH$_2$CHNH), 3.92–3.99 (m, 5 H, CH_3O, CH_2O), 4.15–4.31 (m, 1 H, C*H*NH), 5.34–5.36 (m, 1 H, NH), 6.88 (s, 1 H, C*H*CCNH), 7.11 (s, 1 H, C*H*CCCNH), 8.42 (s, 1 H, C*H*NCNH). ^{13}C NMR (126 MHz, CD_2Cl_2): δ = 18.35 (*C*H_3CH), 29.48 (*C*H_2CCH$_2$O), 32.92 (*C*H_2CHNH), 35.41 (*C*HCH$_2$O), 46.62 (CH_3N), 48.03 (CH$_2$CH$_2$CHNH), 48.85 (CHNH), 55.06 (CH$_3$*C*H), 55.72 (*C*H_2NCH$_3$), 56.76 (CH_3O), 73.88 (CH_2O), 100.31 (*C*HCCNH), 108.73 (*C*CNH), 108.90 (*C*HCCCNH), 147.14 (*C*CCNH), 149.64 (CH$_3$O*C*), 154.26 (*C*HNCNH), 154.38 (CH$_2$O*C*), 157.98 (CNH). HRMS-ESI m/z [M+H]$^+$ calcd. for $C_{24}H_{38}N_5O_2$: 428.3026, found: 428.3020.

_N_-(1-Isopropylpiperidin-4-yl)-6-methoxy-7-[(1-methylpiperidin-3-yl)methoxy]-quinazolin-4-amine (20h)

According to GP5, with **19** (127 mg, 0.400 mmol, 1.0 equiv), (1-methylpiperidin-3-yl)methanol (213 µL, 215 mg, 1.60 mmol, 4.0 equiv), PPh_3 (0.589 g, 2.20 mmol, 5.5 equiv) and DIAD (413 µL, 426 mg, 2.00 mmol, 5.0 equiv) in THF (5.8 mL). Purification by flash chromatography [10% 3 M NH_3 (in MeOH) in CH_2Cl_2] afforded **20h** (133 mg, 78% yield, 96% purity) as colorless solid. mp.: 169 °C. R_f = 0.31 [15% 4 M NH_3 (in MeOH) in CH_2Cl_2]. IR (film): $\tilde{\nu}$ = 1643, 1506, 1460, 1254 cm^{1}. ^{1}H NMR (500 MHz, CD_2Cl_2): δ = 1.04 (d, *J* = 6.6 Hz, 6 H, C*H*$_3$CH), 1.07–1.16 (m, 1 H, C*H*$_2$CH$_2$CH$_2$NCH$_3$), 1.53–1.59 (m, 2 H, C*H*$_2$CHNH), 1.59–1.74 (m, 2 H, C*H*$_2$CH$_2$NCH$_3$), 1.76–1.87 (m, 2 H, C*H*$_2$CH$_2$CH$_2$NCH$_3$, CHC*H*$_2$NCH$_3$), 1.93–2.01 (m, 1 H, CH$_2$CH$_2$C*H*$_2$NCH$_3$), 2.09–2.17 (m, 2 H, C*H*$_2$CHNH), 2.17–2.21 (m, 1 H, C*H*CH$_2$O), 2.23 (s, 3 H, CH_3N), 2.32–2.42 (m, 2 H, C*H*$_2$CH$_2$CHNH), 2.62–2.72 (m, 1 H, C*H*$_2$NCH$_3$), 2.77 (hept, *J* = 6.6 Hz, 1 H, CH$_3$C*H*), 2.84–2.96 (m, 3 H, C*H*$_2$CH$_2$CHNH, CHC*H*$_2$NCH$_3$), 3.87–4.03 (m, 5 H, CH_3O, CH_2O), 4.12–4.28 (m, 1 H, C*H*NH), 5.25 (d, *J* = 7.7 Hz, 1 H, NH), 6.86 (s, 1 H, C*H*CCNH), 7.12 (s, 1 H, C*H*CCCNH), 8.43 (s, 1 H, C*H*NCHNH). ^{13}C NMR (126 MHz, CD_2Cl_2): δ = 18.45 (*C*H_3CH), 25.17 (CH$_2$*C*H$_2$CH$_2$NCH$_3$), 27.20 (*C*H_2CH$_2$CH$_2$NCH$_3$), 33.21 (*C*H_2CHNH), 36.52 (*C*HCH$_2$O), 46.92 (CH_3N), 48.02 (*C*H_2CH$_2$CHNH), 49.04 (*C*HNH), 54.86 (CH$_3$*C*H), 56.64

($CH_2CH_2CH_2NCH_3$), 56.78 (CH_3O), 59.53 ($CHCH_2NCH_3$), 72.30 (CH_2O), 100.27 (*C*HCCNH), 108.74 (*C*CNH), 108.98 (*C*HCCCNH), 147.16 (*CC*CNH), 149.63 (CH_3OC), 154.29 (*C*HNCNH), 154.37 (CH_2OC), 157.97 (CNH). HRMS-ESI m/z $[M+H]^+$ calcd. for $C_{24}H_{38}N_5O_2$: 428.3026, found: 428.3020.

4-(*tert*-Butyl)-1-[3-({4-[(1-isopropylpiperidin-4-yl)amino]-6-methoxyquinazolin-7-yl}oxy)-propyl]pyridin-1-ium chloride (20i)

mp.: 182 °C (decomposition). R_f = 0.23 [20% 3 M NH_3 (in MeOH) in CH_2Cl_2]. IR (film): $\tilde{\nu}$ = 1641, 1506, 1462, 1254, 1217 cm^{-1}. ^1H NMR (500 MHz, CD_2Cl_2): δ = 1.04 (d, *J* = 6.6 Hz, 6 H, CH_3CH), 1.40 (s, 9 H, CH_3C), 1.62–1.69 (m, 2 H, CH_2CHNH), 2.06–2.15 (m, 2 H, CH_2CHNH), 2.31–2.42 (m, 2 H, CH_2CH_2CHNH), 2.68 (p, *J* = 6.2 Hz, 2 H, CH_2CH_2O), 2.76 (h, *J* = 6.6 Hz, 1 H, CH_3CH), 2.83–2.94 (m, 2 H, CH_2CH_2CHNH), 4.00 (s, 3 H, CH_3O), 4.13–4.31 (m, 3 H, $CHNH$, CH_2O), 5.11 (t, *J* = 6.7 Hz, 2 H, $CH_2CH_2CH_2O$), 5.58 (d, *J* = 7.7 Hz, 1 H, NH), 7.03 (s, 1 H, $CHCOCH_3$), 7.11 (s, 1 H, $CHCOCH_2$), 7.90–8.01 (m, 2 H, $CHCCCH_3$), 8.43 (s, 1 H, CHNCNH), 9.19–9.27 (m, 2 H, $CHCHCCCH_3$). ^{13}C NMR (126 MHz, CD_2Cl_2): δ = 18.45 (CH_3CH), 30.15 (CH_3C), 30.87 (CH_2CH_2O), 33.09 (CH_2CHNH), 37.08 (CH_3C), 48.09 (CH_2CH_2CHNH), 49.23 (CHNH), 54.81 (CH_3C), 57.13 (CH_3O), 58.52 ($CH_2CH_2CH_2O$), 65.11 (CH_2O), 101.12 ($CHCOCH_3$), 109.56 (*C*CNH), 109.68 ($CHCOCH_2$), 125.80 ($CHCCCH_3$), 144.70 ($CHCHCCCH_3$), 146.85 (*CC*CNH), 149.20 ($COCH_3$), 152.88 ($COCH_2$), 154.52 (*C*HNCNH), 158.09 (CNH), 172.18 ($CCCH_3$). HRMS-ESI m/z $[M-Cl]^+$ calcd. for $C_{29}H_{42}N_5O_2$: 492.33385; found: 492.3327.

7-(4-Chlorobutoxy)-*N*-(1-isopropylpiperidin-4-yl)-6-methoxyquinazolin-4-amine (21)

According to GP5, with **19** (127 mg, 0.400 mmol, 1.0 equiv), 4-chlorobutan-1-ol (188 µL, 204 mg, 1.60 mmol, 4.0 equiv) PPh_3 (0.589 g, 2.20 mmol, 5.5 equiv) and DIAD (413 µL, 426 mg, 2.00 mmol, 5.0 equiv) in THF (5.8 mL). Purification by flash chromatography (20% MeOH in CH_2Cl_2) afforded **21** (150 mg, 92% yield, 99% purity) as colorless solid. mp.: 187 °C. R_f = 0.43 (20% MeOH in CH_2Cl_2). IR (film): $\tilde{\nu}$ = 2964, 1622, 1593, 1460, 1252 cm^{-1}. ^1H NMR (500 MHz, CD_2Cl_2): δ = 1.06 (d, *J* = 6.6 Hz, 6 H, CH_3CH), 1.58–1.67 (m, 2 H, CH_2CHNH), 1.94–2.08 (m, 4 H, $ClCH_2CH_2CH_2CH_2O$), 2.12–2.20 (m, 2 H, CH_2CHNH), 2.31–2.46 (m, 2 H, CH_2CH_2CHNH), 2.74–2.86 (m, 1 H, CH_3CH), 2.87–2.97 (m, 2 H, CH_2CH_2CHNH), 3.63–3.69 (m, 2 H, $ClCH_2$), 3.96 (s, 3 H, CH_3O), 4.13–4.17 (m, 2 H, CH_2O), 4.17–4.28 (m, 1 H, $CHNH$), 5.30 (bs, 1 H, NH), 6.88 (s, 1 H, CHCCNH), 7.13 (s, 1 H, CHCCCNH), 8.43 (s, 1 H, CHNCNH). ^{13}C NMR (126 MHz, CD_2Cl_2): δ = 18.52 (CH_3CH), 26.96 ($ClCH_2CH_2$), 29.98 ($ClCH_2CH_2CH_2$), 33.13 (CH_2CHNH), 45.46 ($ClCH_2$), 48.18 (CH_2CH_2CHNH), 49.05 (CHNH), 55.18 (CH_3CH), 56.87 (CH_3O), 68.67 (CH_2O), 100.38 (CHCCNH), 109.00 (*C*CNH), 109.10 (CHCCCNH), 147.26 (*CC*CNH), 149.72 (CH_3OC), 154.28 (CH_2OC), 154.46 (*C*HNCNH), 158.14 (CNH). HRMS-ESI m/z $[M+H]^+$ calcd. for $C_{21}H_{31}ClN_4O_2$: 407.2214, found: 407.2207.

N^4-(1-Isopropylpiperidin-4-yl)-6-methoxy-N^7-methyl-N^7-[3-(piperidin-1-yl)propyl]quinazoline-4,7-diamine (23a)

According to GP6, with **22** (159 mg, 0.500 mmol, 1.0 equiv), *N*-methyl-3-piperidin-1-ylpropan-1-amine (457 µL, 411 mg, 2.50 mmol, 5.0 equiv) and K_2CO_3 (76.0 mg, 0.550 mmol, 1.1 equiv)

in NMP (650 µL). Purification by flash chromatography [7% to 15% 3 M NH_3 (in MeOH) in CH_2Cl_2] afforded **23a** (176 mg, 78% yield, 95% purity) as pale yellow solid. mp.: 242 °C. R_f = 0.28 [10% 3 M NH_3 (in MeOH) in CH_2Cl_2]. IR (film): $\tilde{\nu}$ = 2927, 1643, 1502, 1244 cm^{-1}. ^1H NMR (500 MHz, CD_2Cl_2): δ = 1.04 (d, J = 6.6 Hz, 6 H, CH_3CH), 1.34–1.46 [m, 2 H, CH_2CH$_2$CH$_2$N(CH$_2$)$_3$NC], 1.46–1.64 [m, 6 H, CH_2CHNH, CH_2CH$_2$N(CH$_2$)$_3$NC], 1.74 (tt, J = 9.5, 6.5 Hz, 2 H, CH_2CH$_2$NC), 2.09–2.18 (m, 2 H, CH_2CHNH), 2.18–2.46 (m, 8 H, CH_2CH$_2$CHNH, CH_2NCH_2CH$_2$CH$_2$NC), 2.77 (hept, J = 6.6 Hz, 1 H, CH$_3$CH), 2.83–2.97 (m, 5 H, CH_2CH$_2$CHNH, CH$_3$N), 3.19–3.32 (m, 2 H, CH$_2$NC), 3.95 (s, 3 H, CH$_3$O), 4.13–4.26 (m, 1 H, CHNH), 5.21 (d, J = 7.7 Hz, 1 H, NH), 6.80 (s, 1 H, CHCOCH$_3$), 7.07 (s, 1 H, CHCNCH$_3$), 8.39 (s, 1 H, CHNCNH). ^{13}C NMR (126 MHz, CD_2Cl_2): δ = 18.44 (CH_3CH), 24.96 [CH_2CH$_2$CH$_2$N(CH$_2$)$_3$NC], 25.21 (CH_2CH$_2$NC), 26.49 [CH_2CH$_2$N(CH$_2$)$_3$NC], 33.24 (CH_2CHNH), 40.10 (CH_3NC), 48.03 (CH_2CH$_2$CHNH), 48.91 (CHNH), 53.37 (CH_2NC), 54.88 (CH$_3$CH), 54.95 [CH_2N(CH$_2$)$_3$NC], 56.17 (CH$_3$O), 57.15 (CH_2CH$_2$CH$_2$NC), 99.84 (CHCOCH$_3$), 108.71 (*C*CNH), 114.71 (CHCNCH$_3$), 146.88 (*C*CCNH), 148.29 (*C*NCH$_3$), 151.96 (*C*OCH$_3$), 154.09 (*C*NCNH), 157.86 (CNH). HRMS-ESI m/z [M+H]$^+$ calcd. for $C_{26}H_{43}N_6O$: 455.3498; found: 455.3492.

N^4-(1-Isopropylpiperidin-4-yl)-6-methoxy-N^7-[3-(piperidin-1-yl)propyl]quinazoline-4,7-diamine (23b)

According to GP6, with **22** (127 mg, 0.400 mmol, 1.0 eq), 3-piperidin-1-ylpropan-1-amine (328 µL, 293 mg, 2.00 mmol, 5.0 equiv) and K_2CO_3 (60.8 mg, 0.440 mmol, 1.1 equiv) in NMP (520 µL). Purification by flash chromatography [5% to 15% 3 M NH_3 (in MeOH) in CH_2Cl_2] afforded **23b** (148 mg, 84% yield, 97% purity) as pale yellow solid. mp.: 251 °C. R_f = 0.32 [10% 3 M NH_3 (in MeOH) in CH_2Cl_2]. IR (film): $\tilde{\nu}$ = 2935, 1620, 1525, 1433, 1213 cm^{-1}. ^1H NMR (500 MHz, CD_2Cl_2): δ = 1.05 (d, J = 6.6 Hz, 6 H, CH_3CH), 1.41–1.52 [m, 2 H, CH_2CH$_2$CH$_2$N(CH$_2$)$_3$NH], 1.52–1.60 (m, 2 H, CH_2CHNH), 1.60–1.67 [m, 4 H, CH_2CH$_2$N(CH$_2$)$_3$NH], 1.85 (p, J = 6.1 Hz, 2 H, CH_2CH$_2$NH), 2.08–2.18 (m, 2 H, CH_2CHNH), 2.30–2.45 [m, 6 H, CH_2CH$_2$CHNH, CH_2N(CH$_2$)$_3$NH], 2.47 (t, J = 6.1 Hz, 2 H, CH_2CH$_2$CH$_2$NH), 2.78 (hept, J = 6.6 Hz, 1 H, CH$_3$CH), 2.83–2.97 (m, 2 H, CH_2CH$_2$CHNH), 3.29 (t, J = 6.2 Hz, 2 H, CH_2NH), 3.96 (s, 3 H, CH$_3$O), 4.18 (tdt, J = 11.5, 8.1, 4.3 Hz, 1 H, CHNH), 5.00–5.18 (m, 1 H, CHNH), 6.38–6.63 (m, 1 H, NHCH$_2$), 6.66 (s, 1 H, CHCNH), 6.71 (s, 1 H, CHCOCH$_3$), 8.34 (s, 1 H, CHNCNH). ^{13}C NMR (126 MHz, CD_2Cl_2): δ = 18.42 (CH_3CH), 24.98 [CH_2CH$_2$CH$_2$N(CH$_2$)$_3$NH], 25.23 (CH_2CH$_2$NH), 26.42 [CH_2CH$_2$N(CH$_2$)$_3$NH], 33.33 (CH_2CHNH), 43.97 (CH$_2$NH), 48.08 (CH_2CH$_2$CHNH), 48.81 (CHNH), 54.94 (CH$_3$CH), 55.20 [CH_2N(CH$_2$)$_3$NH], 55.98 (CH$_3$O), 58.89 (CH_2CH$_2$CH$_2$NH), 97.46 (CHCOCH$_3$), 103.13 (CHCNH), 104.94 (*C*CNHCH), 144.68 (*C*NHCH$_2$), 147.66 (*C*CCNHCH), 147.93 (*C*OCH$_3$), 153.90 (CHNCNH), 157.88 (*C*NHCH). HRMS-EI m/z [M]$^+$ calcd. for $C_{25}H_{40}N_6O$: 440.3264; found: 440.3259.

N^7-[3-(Azepan-1-yl)propyl]-N^4-(1-isopropylpiperidin-4-yl)-6-methoxyquinazoline-4,7-diamine (23c)

According to GP6, with **22** (111 mg, 0.350 mmol, 1.0 equiv), 3-(azepan-1-yl)propan-1-amine (320 µL, 288 mg, 1.75 mmol, 5.0 equiv) and K_2CO_3 (53.2 mg, 0.385 mmol, 1.1 equiv) in NMP (455 µL). Purification by flash chromatography [7% to 12% (7 M NH_3 (in MeOH) in CH_2Cl_2] afforded **23c** (38.0 mg, 24% yield, 98% purity) as colorless solid. mp.: 220 °C (decomposition). R_f = 0.42 [10% (7 M NH_3 (in MeOH) in CH_2Cl_2]. IR (film): $\tilde{\nu}$ = 2929, 1620, 1527, 1215, 754 cm^{-1}.

^{1}H NMR (500 MHz, CD_2Cl_2): δ = 1.03 (d, *J* = 6.6 Hz, 6 H, C*H*$_3$CH), 1.49–1.58 (m, 2 H, C*H*$_2$CHNH), 1.62–1.73 (m, 8 H, C*H*$_2$C*H*$_2$CH$_2$N(CH$_2$)$_3$NH), 1.83 (p, *J* = 6.2 Hz, 2 H, C*H*$_2$CH$_2$NH), 2.08–2.16 (m, 2 H, C*H*$_2$CHNH), 2.31–2.41 (m, 2 H, C*H*$_2$CH$_2$CHNH), 2.59–2.65 (m, 6 H, C*H*$_2$NC*H*$_2$CH$_2$CH$_2$NH), 2.69–2.80 (m, 1 H, CH$_3$C*H*), 2.84–2.91 (m, 2 H, C*H*$_2$CH$_2$CHNH), 3.27–3.33 (m, 2 H, C*H*$_2$NH), 3.96 (s, 3 H, CH$_3$O), 4.17 (tdt, *J* = 11.6, 8.3, 4.3 Hz, 1 H, C*H*NH), 5.07 (d, *J* = 7.7 Hz, 1 H, CHN*H*), 6.11 (t, *J* = 4.9 Hz, 1 H, CH$_2$N*H*), 6.68 (s, 1 H, C*H*CCNH), 6.70 (s, 1 H, C*H*CCNH), 8.34 (s, 1 H, C*H*NCNH). ^{13}C NMR (126 MHz, CD_2Cl_2): δ = 18.47 (*C*H$_3$CH), 26.50 (*C*H$_2$CH$_2$NH), 27.32 [*C*H$_2$CH$_2$CH$_2$N(CH$_2$)$_3$NH]*, 28.65 [CH$_2$*C*H$_2$CH$_2$N(CH$_2$)$_3$NH]*, 33.44 (*C*H$_2$CHNH), 43.72 (*C*H$_2$NH), 48.07 (*C*H$_2$CH$_2$CHNH), 48.86 (*C*HNH), 54.81 (CH$_3$*C*H), 56.08 (CH$_3$O), 56.36 [*C*H$_2$N(CH$_2$)$_3$NH], 58.01 (*C*H$_2$CH$_2$CH$_2$NH), 97.51 (*C*HCCNH), 103.42 (*C*HCCCNH), 105.04 (*C*CNHCH), 144.53 (*C*NHCH$_2$), 147.59 (*C*OCH$_3$), 148.02 (*C*CCNHCH), 154.01 (*C*HNCNH), 157.89 (*C*NHCH). HRMS-EI m/z [M]$^+$ calcd. for $C_{26}H_{42}N_6O$: 454.3420; found: 454.3423.

2-Chloro-6,7-dimethoxy-*N*-[5-(pyrrolidin-1-yl)pentyl]quinazolin-4-amine (25) (Ma et al., 2014)

According to GP1 with **24** (264 mg, 1.00 mmol, 1.0 equiv), 5-pyrrolidin-1-ylpentan-1-amine (172 mg, 1.10 mmol, 1.1 equiv) and DIEA (533 µL, 396 mg, 3.00 mmol, 3.0 equiv) in THF (4.0 mL). Purification by flash chromatography [10% to 15% 3 M NH_3 (in MeOH) in CH_2Cl_2] afforded **25** as colorless solid (308 mg, 81% yield, 95% purity). mp.: 54 °C. R_f = 0.30 [10% 3 M in NH_3 MeOH) in CH_2Cl_2]. IR (film): ṽ = 1624, 1512, 1429, 1244 cm^{-1}. ^{1}H NMR (500 MHz, CD_2Cl_2): δ = 1.42–1.52 (m, 2 H, C*H*$_2$CH$_2$CH$_2$NH), 1.52–1.62 [m, 2 H, C*H*$_2$(CH$_2$)$_3$NH], 1.68–1.79 [m, 6 H, C*H*$_2$(CH$_2$)$_3$NCH$_2$C*H*$_2$], 2.36–2.52 (m, 6 H, C*H*$_2$NC*H*$_2$), 3.62 (td, *J* = 7.1, 5.4 Hz, 2 H, C*H*$_2$NH), 3.93 (d, *J* = 1.5 Hz, 6 H, CH$_3$O), 5.99 (t, *J* = 5.5 Hz, 1 H, NH), 6.97 (s, 1 H, C*H*CCNH), 7.06 (s, 1 H, C*H*CCCNH). ^{13}C NMR (126 MHz, CD_2Cl_2): δ = 23.82 (*C*H$_2$CH$_2$N(CH$_2$)$_5$NH), 25.23 (*C*H$_2$CH$_2$CH$_2$NH), 28.94 [*C*H$_2$(CH$_2$)$_3$NH], 29.36 (*C*H$_2$CH$_2$NH), 41.97 (CH$_2$NH), 54.47 (*C*H$_2$N(CH$_2$)$_5$NH), 56.39 (*C*H$_2$(CH$_2$)$_4$NH), 56.47 (CH$_3$O)*, 56.65 (CH$_3$O)*, 100.58 (C*H*CCNH), 107.25 (*C*CNH), 107.51 (*C*HCCCNH), 148.29 (*C*CCNH), 149.54 (*C*CHCCNH), 155.44 (*C*CHCCCNH), 156.40 (CCl), 160.42 (CNH). HRMS-ESI m/z [M+H]$^+$ calcd. for $C_{19}H_{28}ClN_4O_2$: 379.1901, found: 379.1894.

2-Chloro-*N*-(1-cyclohexylpiperidin-4-yl)-6,7-dimethoxyquinazolin-4-amine (26) (Sundriyal et al., 2017)

According to GP1 with **24** (132 mg, 0.500 mmol, 1.0 equiv), 1-cyclohexylpiperidin-4-amine (102 mg, 0.550 mmol, 1.1 equiv) and DIEA (267 µL, 198 mg, 1.50 mmol, 3.0 equiv) in THF (2.0 mL). Purification by flash chromatography [5% 3 M NH_3 (in MeOH) in CH_2Cl_2] afforded **26** as colorless solid (132 mg, 65% yield, 99% purity). mp.: 169 °C. R_f = 0.23 [5% 4 M NH_3 (in MeOH) in CH_2Cl_2]. IR (film): ṽ = 2925, 2360, 1585, 1508, 1254 cm^{-1}. ^{1}H NMR (500 MHz, $CDCl_3$): δ = 1.03–1.18 (m, 1 H, C*H*$_2$CH$_2$CH$_2$CHN), 1.18–1.32 (m, 4 H, C*H*$_2$C*H*$_2$CHN), 1.53–1.70 (m, 3 H, C*H*$_2$CH$_2$CH$_2$CHN, C*H*$_2$CHNH), 1.74–1.93 (m, 4 H, C*H*$_2$C*H*$_2$CHN), 2.13–2.22 (m, 2 H, C*H*$_2$CHNH), 2.29–2.40 (m, 1 H, CHN), 2.40–2.53 (m, 2 H, CH$_2$N), 2.90–3.00 (m, 2 H, CH$_2$N), 3.97 (s, 3 H, C*H*$_3$OCCHCN), 3.99 (s, 3 H, C*H*$_3$OCCHCCN), 4.16–4.32 (m, 1 H, C*H*NH), 5.26–5.35 (m, 1 H, NH), 6.77 (s, 1 H, C*H*CCNH), 7.13 (s, 1 H, C*H*CCCNH). ^{13}C NMR (126 MHz, $CDCl_3$): δ = 26.20 (*C*H$_2$CH$_2$CHN), 26.50 (*C*H$_2$CH$_2$CH$_2$CHN), 29.05 (*C*H$_2$CHN), 32.91 (*C*H$_2$CHNH), 48.07 (CH$_2$N), 48.8 (*C*HNH), 56.40 (CH$_3$O), 56.52(CH$_3$O), 63.95 (CHN),

99.62 (*C*HCCNH), 106.78 (*C*CNH), 107.56 (*C*HCCCNH), 148.25 (*C*CCNH), 149.17 ($CH_3OCCHCCNH$), 155.11 ($CH_3OCCHCCCNH$), 156.38 (CCl), 159.20 (CNH). The characterization data of **26** match the reported (Sundriyal et al., 2017).

2-Chloro-*N*-(1-isopropylpiperidin-4-yl)-6,7-dimethoxyquinazolin-4-amine (27) (Somnarin et al., 2022; Wang et al., 2019)

According to GP1 with **24** (1.32 g, 5.00 mmol, 1.0 equiv), 1-propan-2-ylpiperidin-4-amine (869 mL, 782 mg, 5.50 mmol, 1.1 equiv) and DIEA (2.67 mL, 1.98 g, 15.0 mmol, 3.0 equiv) in THF (20 mL). Purification by flash chromatography [5% to 10% 3 M NH_3 (in MeOH) in CH_2Cl_2] afforded **27** as pale yellow solid (1.79 g, 98% yield, 98% purity). mp.: 106 °C. R_f = 0.32 [10% 3 M NH_3 (in MeOH) in CH_2Cl_2]. IR (film): $\tilde{\nu}$ = 2964, 1585, 1512, 1254 cm^{-1}. ^1H NMR (500 MHz, $CDCl_3$): δ = 1.04 (d, *J* = 6.6 Hz, 6 H, CH_3CH), 1.59 (qd, *J* = 11.8, 3.8 Hz, 2 H, CH_2CHNH), 2.07–2.19 (m, 2 H, CH_2CHNH), 2.34 (td, *J* = 11.8, 2.5 Hz, 2 H, CH_2N), 2.75 (hept, *J* = 6.6 Hz, 1 H, CH_3CH), 2.87 (dt, *J* = 12.1, 3.8 Hz, 2 H, CH_2N), 3.92 (d, *J* = 4.0 Hz, 6 H, CH_3O), 4.23 (tdt, *J* = 11.6, 8.2, 4.2 Hz, 1 H, C*H*NH), 5.71 (d, *J* = 7.8 Hz, 1 H, NH), 6.90 (s, 1 H, *CH*CCNH), 7.07 (s, 1 H, CHCN). ^{13}C NMR (126 MHz, $CDCl_3$): δ = 18.47 (CH_3CH), 32.57 (CH_2CHNH), 47.66 (CH_2N), 48.91 (CHNH), 54.62 (CH_3CH), 56.31 (CH_3O), 56.41 (CH_3O), 100.03 (*C*HCCNH), 106.88 (*C*CNH), 107.26 (*C*HCN), 148.10 (*C*CCNH), 149.07 (*C*CHCCNH), 155.00 (*C*CHCN), 156.30 (CCl), 159.29 (CNH). HRMS-ESI m/z $[M+H]^+$ calcd. for $C_{18}H_{26}ClN_4O_2$: 365.1744, found: 365.1741.

6,7-Dimethoxy-2-(4-methyl-1,4-diazepan-1-yl)-*N*-[5-(pyrrolidin-1-yl)pentyl]quinazolin-4-amine (28a)

According to GP2 with **25** (152 mg, 0.400 mmol, 1.0 equiv) and 1-methyl-1,4-diazepane (256 µL, 235 mg, 2.00 mmol, 5.0 equiv) in toluene (2.0 mL). **28a** was isolated by flash chromatography [7% to 12% 3 M NH_3 (in MeOH) in CH_2Cl_2] as yellow, hygroscopic solid (165 mg, 90% yield, 97% purity). mp.: 57 °C. R_f = 0.22 [10% 3 M NH_3 (in MeOH) in CH_2Cl_2]. IR (film): $\tilde{\nu}$ = 2935, 1630, 1583, 1495, 1240, 752 cm^{-1}. ^1H NMR (500 MHz, CD_2Cl_2): δ = 1.42–1.51 (m, 2 H, C$H_2CH_2CH_2NH$), 1.52–1.62 [m, 2 H, C$H_2(CH_2)_8NH$], 1.66–1.78 [m, 6 H, C$H_2CH_2N(CH_2)_3CH_2$], 1.91–2.01 (m, 2 H, $NCH_2CH_2CH_2NC$), 2.32 (s, 3 H, CH_3N), 2.42–2.55 [m, 8 H, N$CH_2CH_2CH_2NC$, C$H_2NCH_2(CH_2)_4NH$], 2.62–2.69 (m, 2 H, NCH_2CH_2NC), 3.53–3.60 (m, 2 H, CH_2NH), 3.81–3.86 (m, 2 H, $NCH_2CH_2CH_2NC$), 3.87 (s, 3 H, $CH_3OCCHCCNH$), 3.90 (s, 3 H, $CH_3OCCHCCCNH$), 3.91–3.96 (m, 2 H, NCH_2CH_2NC), 5.38 (s, 1 H, NH), 6.79 (s, 1 H, *CH*CCNH), 6.80 (s, 1 H, C*H*CCNH). ^{13}C NMR (126 MHz, CD_2Cl_2): δ = 23.85 ($CH_2CH_2N(CH_2)_5NH$), 25.52 ($CH_2CH_2CH_2NH$), 28.43 ($NCH_2CH_2CH_2NC$), 29.03 [$CH_2(CH_2)_3NH$], 29.80 (CH_2CH_2NH), 41.61 (CH_2NH), 46.28 ($NCH_2CH_2CH_2NC$), 46.36 (NCH_2CH_2NC), 46.94 (CH_3N), 54.49 ($CH_2N(CH_2)_5NH$), 56.14 ($CH_3OCCHCCCNH$), 56.65 ($CH_2(CH_2)_4NH$, $CH_3OCCHCCNH$), 57.68 ($NCH_2CH_2CH_2NC$), 59.20 (NCH_2CH_2NC), 101.62 (*C*HCCNH), 103.14 (*C*CNH), 106.20 (*C*HCCCNH), 145.43 (*C*CHCCNH), 149.90 (*C*CCNH), 154.86 (*C*CHCCCNH), 159.02 (*C*NCNH), 159.26 (CNH). HRMS-EI m/z $[M]^+$ calcd. for $C_{25}H_{40}N_6O_2$: 456.3213, found: 456.3210.

***N*-(1-Cyclohexylpiperidin-4-yl)-6,7-dimethoxy-2-(4-methyl-1,4-diazepan-1-yl)quinazolin-4-amine (28b)** (Sundriyal et al., 2017)

According to GP2 with **26** (60.7 mg, 0.150 mmol, 1.0 equiv) and 1-methyl-1,4-diazepane (96.2 µL, 88.3 mg, 0.750 mmol, 5.0 equiv) in toluene (0.3 mL). **28b** was isolated by flash chromatography [10% 3 M NH_3 (in MeOH) in CH_2Cl_2] as yellow solid (67.8 mg, 94% yield, 97% purity). mp.: 94 °C. R_f = 0.49 [10% 4 M NH_3 (in MeOH) in CH_2Cl_2]. IR (film): $\tilde{\nu}$ = 2931, 1579, 1427, 1246 cm^{-1}. ^1H NMR (500 MHz, CD_2Cl_2): δ = 1.05–1.17 (m, 1 H, CH_2CH$_2$CH$_2$CHN), 1.19–1.34 (m, 4 H, CH$_2$CH_2CH_2CHN), 1.46–1.58 (m, 2 H, CH$_2$CH_2CHNH), 1.58–1.66 (m, 1 H, CH_2CH$_2$CH$_2$CHN), 1.75–1.86 (m, 4 H, CH$_2$CH_2CH_2CHN), 1.89–1.99 (m, 2 H, CH$_3$NCH$_2$CH_2CH$_2$N), 2.09–2.20 (m, 2 H, CH$_2$CH_2CHNH), 2.27–2.36 (m, 4 H, CH$_3$N, CHN), 2.36–2.44 (m, 2 H, CH_2CH$_2$CHNH), 2.47–2.55 (m, 2 H, CH$_3$NCH_2CH$_2$CH$_2$N), 2.61–2.68 (m, 2 H, CH$_3$NCH_2CH$_2$N), 2.87–2.95 (m, 2 H, CH_2CH$_2$CHNH), 3.83 (t, *J* = 6.4, 6.4 Hz, 2 H, CH$_3$NCH$_2$CH$_2$CH_2N), 3.87 (s, 3 H, CH_3OCCHCCNH), 3.88–3.94 (m, 5 H, CH$_3$NCH$_2$CH_2N, CH_3OCCHCCCNH), 3.97–4.12 (m, 1 H, C*H*NH), 5.08 (d, *J* = 7.2 Hz, 1 H, NH), 6.75 (s, 1 H, C*H*CCNH), 6.79 (s, 1 H, C*H*CCCNH). ^{13}C NMR (126 MHz, CD_2Cl_2): δ = 26.51 (CH$_2$CH$_2$CH$_2$CHN), 26.86 (*C*H$_2$CH$_2$CH$_2$CHN), 28.41 (CH$_3$NCH$_2$*C*H$_2$CH$_2$N), 29.30 (CH$_2$CH$_2$*C*H$_2$CHN), 33.31 (CH$_2$*C*H$_2$CHNH), 46.25 (CH$_3$NCH$_2$CH$_2$*C*H$_2$N), 46.41 (CH$_3$NCH$_2$*C*H$_2$N), 46.92 (CH$_3$N), 48.56 (*C*H$_2$CH$_2$CHNH), 49.34 (CH$_2$CH$_2$*C*HNH), 56.13 (*C*H$_3$OCCHCCCNH), 56.67 (*C*H$_3$OCCHCCNH), 57.65 (CH$_3$NCH$_2$CH$_2$CH$_2$N), 59.15 (CH$_3$N*C*H$_2$CH$_2$N), 64.13 (CHN), 101.56 (*C*HCCNH), 103.05 (*C*CNH), 106.23 (*C*HCCCNH), 145.42 (CH$_3$O*C*CHCCNH), 150.03 (*C*CCNH), 154.91 (CH$_3$O*C*CHCCCNH), 158.49 (CNH), 158.98 (*C*NCNH). HRMS-ESI m/z $[M+H]^+$ calcd. for $C_{27}H_{43}N_6O_2$: 483.3447, found: 483.3442.

_N_-(1-Isopropylpiperidin-4-yl)-6,7-dimethoxy-2-(4-methyl-1,4-diazepan-1-yl)-quinazolin-4-amine (28c) (Sundriyal et al., 2017)

According to GP2 with **27** (91.2 mg, 0.250 mmol, 1.0 equiv) and 1-methyl-1,4-diazepane (160 µL, 147 mg, 1.25 mmol, 5.0 equiv) in toluene (0.5 mL). **28c** was isolated by flash chromatography [5% 3 M NH_3 (in MeOH) in CH_2Cl_2] as yellow solid (107 mg, 97% yield, 97% purity). mp.: 89 °C. R_f = 0.57 [15% 3 M NH_3 (in MeOH) in CH_2Cl_2]. IR (film): $\tilde{\nu}$ = 2935, 1579, 1495, 1246 cm^{-1}. ^1H NMR (500 MHz, $CDCl_3$): δ = 1.09 (d, *J* = 6.6 Hz, 6 H, CH_3CH), 1.55–1.69 (m, 2 H, CH_2CHNH), 2.02 (p, *J* = 6.2 Hz, 2 H, CH_2CH$_2$NCH$_3$), 2.13–2.22 (m, 2 H, CH_2CHNH), 2.29–2.37 (m, 2 H, CH_2NCH), 2.37 (s, 3 H, CH$_3$N), 2.52–2.62 (m, 2 H, NCH$_2$CH$_2$CH_2NCH$_3$), 2.67–2.74 (m, 2 H, NCH$_2$CH_2NCH$_3$), 2.78 (h, *J* = 6.6 Hz, 1 H, CH$_3$C*H*), 2.89–2.99 (m, 2 H, CH_2NCH), 3.88 (t, *J* = 6.4 Hz, 2 H, NCH_2CH$_2$CH$_2$NCH$_3$), 3.92 (s, 3 H, CH_3OCCHCCN), 3.94 (s, 3 H, CH_3OCCHCN), 3.96–4.00 (m, 2 H, NCH_2CH$_2$NCH$_3$), 4.02–4.13 (m, 1 H, C*H*NH), 5.02 (d, *J* = 7.2 Hz, 1 H, NH), 6.71 (s, 1 H, C*H*CCN), 6.90 (s, 1 H, CHCN). ^{13}C NMR (126 MHz, $CDCl_3$): δ = 18.70 (*C*H$_3$CH), 27.93 (NCH$_2$*C*H$_2$CH$_2$NCH$_3$), 32.61 (*C*H$_2$CHNH), 45.93 (NCN*C*H$_2$), 46.02 (NCN*C*H$_2$), 46.84 (CH$_3$N), 47.93 (*C*H$_2$NCH), 48.72 (CHNH), 54.80 (CH$_3$*C*H), 56.11 (*C*H$_3$OCCHCN), 56.51 (*C*H$_3$OCCHCCN), 57.50 (NCH$_2$CH$_2$*C*H$_2$NCH$_3$), 59.07 (NCH$_2$*C*H$_2$NCH$_3$), 100.91 (*C*HCCN), 102.88 (*C*CNH), 106.14 (*C*HCN), 145.16 (CH$_3$O*C*CHCCN), 149.57 (*C*CCNH), 154.46 (CH$_3$O*C*CHCN), 158.16 (CNH), 158.67 (*C*NCNH). HRMS-ESI m/z $[M+H]^+$ calcd. for $C_{24}H_{39}N_6O_2$: 443.3134, found: 443.3127.

4-Chloro-6,7-dimethoxy-2-(piperidin-1-yl)quinazoline (29)

According to GP7 with **24** (793 mg, 3.00 mmol, 1.0 equiv) and 1-methylpiperidine (733 µL, 601 mg, 6.00 mmol, 2.0 equiv) in 1,4-dioxane (7.5 mL). **29** was isolated by flash chromatography (CH_2Cl_2) as yellow solid (744 mg, 81% yield, 95% purity). mp.: 126 °C.

R_f = 0.34 (CH_2Cl_2). IR (film): $\tilde{\nu}$ = 2935, 2852, 1585, 1495, 1238, 754 cm^{-1}. ^1H NMR (500 MHz, CD_2Cl_2): δ = 1.57–1.65 (m, 4 H, CH_2CH_2N), 1.65–1.72 (m, 2 H, CH_2CH_2CH_2N), 3.77–3.86 (m, 4 H, CH_2N), 3.92 (s, 3 H, CH_3OCCHCCCl), 3.95 (s, 3 H, CH_3OCCHCCCCl), 6.88 (s, 1 H, CHCCCCl), 7.16 (s, 1 H, CHCCCl). ^{13}C NMR (126 MHz, CD_2Cl_2): δ = 25.27 (*C*H_2CH_2CH_2N), 26.23 (*C*H_2CH_2N), 45.49 (CH_2N), 56.36 (*C*H_3OCCHCCCl), 56.55 (*C*H_3OCCHCCCCl), 103.99 (*C*HCCCl), 105.11 (*C*HCCCCl), 112.31 (*C*CCl), 147.73 (*C*CHCCCl), 151.97 (*C*CCCl), 157.41 (*C*CHCCCCl), 158.10 (*C*NCCl), 159.85 (CCl). HRMS-ESI m/z $[M+H]^+$ calcd. for $C_{15}H_{19}ClN_3O_2$: 308.1166, found: 308.1161.

6,7-Dimethoxy-2-(piperidin-1-yl)-*N*-[5-(pyrrolidin-1-yl)pentyl]quinazolin-4-amine (30a)
(Ma et al., 2014)

According to GP4 with **29** (123 mg, 0.400 mmol, 1.0 equiv), 5-pyrrolidin-1-ylpentan-1-amine (125 mg, 0.800 mmol, 2.0 equiv) and DIEA (213 µL, 158 mg, 1.20 mmol, 3.0 equiv) in *i*-PrOH (2.0 mL) for 15 min. **30a** (144 mg, 84% yield, 95% purity) was isolated by flash chromatography [5% to 7% 3 M NH_3 (in MeOH) in CH_2Cl_2] as pale yellow, hygroscopic solid. mp.: 58 °C. R_f = 0.15 [5% 3 M NH_3 (in MeOH) in CH_2Cl_2]. IR (film): $\tilde{\nu}$ = 2933, 1583, 1215, 756 cm^{-1}. ^1H NMR (500 MHz, CD_2Cl_2): δ = 1.40–1.50 (m, 2 H, CH_2CH_2CH_2NH), 1.51–1.62 [m, 6 H, CH_2CH_2CH_2NC, CH_2(CH_2)$_3$NH], 1.62–1.69 (m, 2 H, CH_2CH_2CH_2NC), 1.69–1.78 [m, 6 H, CH_2CH_2N(CH_2)$_3$CH_2], 2.35–2.49 (m, 6 H, CH_2NCH_2), 3.51–3.61 (m, 2 H, CH_2NH), 3.74–3.83 (m, 4 H, CH_2CH_2CH_2NC), 3.87 (s, 3 H, CH_3OCCHCCNH), 3.90 (s, 3 H, CH_3OCCHCCCNH), 5.29 (t, *J* = 6.5 Hz, 1 H, NH), 6.77 (s, 1 H, C*H*CCNH), 6.80 (s, 1 H, C*H*CCCNH). ^{13}C NMR (126 MHz, CD_2Cl_2): δ = 23.86 (*C*H_2CH_2N(CH_2)$_5$NH), 25.56 (*C*H_2CH_2CH_2NH)*, 25.59 (*C*H_2CH_2CH_2NC)*, 26.42 (CH_2*C*H_2CH_2NC), 29.23 [*C*H_2(CH_2)$_3$NH], 29.85 (*C*H_2CH_2NH), 41.61 (CH_2NH), 45.31 (CH_2CH_2*C*H_2NC), 54.50 (*C*H_2N(CH_2)$_5$NH), 56.14 (*C*H_3OCCHCCCNH), 56.60 (*C*H_3OCCHCCNH), 56.69 (*C*H_2(CH_2)$_4$NH), 101.48 (*C*HCCNH), 103.22 (*C*CNH), 106.27 (*C*HCCCNH), 145.63 (*C*CHCCNH), 149.79 (*C*CCNH), 154.88 (*C*CHCCCNH), 159.29 (*C*NCNH)**, 159.38 (CNH)**. HRMS-EI m/z $[M]^+$ calcd. for $C_{24}H_{37}N_5O_2$: 427.2947, found: 427.2940.

***N*-(1-Isopropylpiperidin-4-yl)-6,7-dimethoxy-2-(piperidin-1-yl)quinazolin-4-amine (30b)**
(Sundriyal et al., 2017)

According to GP4 with **29** (123 mg, 0.400 mmol, 1.0 equiv), 1-propan-2-ylpiperidin-4-amine (126 µL, 114 mg, 0.800 mmol, 2.0 equiv) and DIEA (213 µL, 158 mg, 1.20 mmol, 3.0 equiv) in *i*-PrOH (2.0 mL) for 15 min. **30b** (106 mg, 64% yield, 97% purity) was isolated by flash chromatography [5% to 7% 3 M NH_3 (in MeOH) in CH_2Cl_2] as colorless solid. mp.: 87 °C. R_f = 0.15 [5% 3 M NH_3 (in MeOH) in CH_2Cl_2]. IR (film): $\tilde{\nu}$ = 2935, 1579, 1493, 1246, 754 cm^{-1}. ^1H NMR (500 MHz, CD_2Cl_2): δ = 1.04 (d, *J* = 6.6 Hz, 6 H, CH_3CH), 1.39–1.76 (m, 8 H, CH_2CH_2CH_2NC, CH_2CHNH), 2.08–2.21 (m, 2 H, CH_2CHNH), 2.28–2.39 (m, 2 H, C$H_2$$CH_2$CHNH), 2.76 (hept, *J* = 6.6 Hz, 1 H, CH_3C*H*), 2.83–2.94 (m, 2 H, C$H_2$$CH_2$CHNH), 3.73–3.81 (m, 4 H, CH_2NC), 3.88 (s, 3 H, CH_3OCCHCCNH), 3.90 (s, 3 H, CH_3OCCHCCCNH), 4.02–4.16 (m, 1 H, C*H*NH), 5.03 (d, *J* = 7.2 Hz, 1 H, NH), 6.73 (s, 1 H, C*H*CCNH), 6.80 (s, 1 H, C*H*CCCNH). ^{13}C NMR (126 MHz, CD_2Cl_2): δ = 18.49 (CH_3CH), 25.59 (CH_2CH_2*C*H_2NC), 26.40 (CH_2*C*H_2NC), 33.12 (*C*H_2CHNH), 45.35 (*C*H_2NC), 48.07 (CH_2*C*H_2CHNH), 49.12 (CHNH), 54.88 (CH_3*C*H), 56.15 (*C*H_3OCCHCCCNH), 56.68 (*C*H_3OCCHCCNH), 101.44 (*C*HCCNH), 103.13 (*C*CNH), 106.29 (*C*HCCCNH), 145.66 (CH_3O*C*CHCCNH), 149.89 (*C*CCNH), 154.95

(*C*CHCCCNH), 158.60 (CNH), 159.25 (*C*NCNH). HRMS-EI m/z [M]$^+$ calcd. for $C_{23}H_{35}N_5O_2$: 413.2791, found: 413.2781.

_N_-(1-Cyclohexylpiperidin-4-yl)-2-(4-isopropyl-1,4-diazepan-1-yl)-6,7-dimethoxyquinazolin-4-amine (31)

According to GP2 with **26** (40.5 mg, 0.100 mmol, 1.0 equiv) and 1-propan-2-yl-1,4-diazepane (81.1 µL, 72.6 mg, 0.500 mmol, 5.0 equiv) in toluene (0.5 mL). **31** was isolated by flash chromatography [5% 3 M NH_3 (in MeOH) in CH_2Cl_2] as red solid (52.6 mg, > 99% yield, 95% purity). mp.: 86 °C. R_f = 0.17 [5% 4 M NH_3 (in MeOH) in CH_2Cl_2]. IR (film): $\tilde{\nu}$ = 2929, 1579, 1496, 1248 cm^{-1}. ^{1}H NMR (500 MHz, $CDCl_3$): δ = 1.01 (d, *J* = 6.5 Hz, 6 H, C*H*$_3$CH), 1.05–1.19 (m, 1 H, C*H*$_2$CH$_2$CH$_2$CHN), 1.19–1.34 (m, 4 H, C*H*$_2$C*H*$_2$CHN), 1.52–1.62 (m, 2 H, C*H*$_2$CHNH), 1.62–1.68 (m, 1 H, C*H*$_2$CH$_2$CH$_2$CHN), 1.75–1.86 (m, 2 H, C*H*$_2$CH$_2$CHN), 1.86–2.00 (m, 4 H, NCH$_2$C*H*$_2$CH$_2$NC, C*H*$_2$CHN), 2.14–2.22 (m, 2 H, C*H*$_2$CHNH), 2.29–2.37 (m, 1 H, CH$_2$C*H*N), 2.37–2.45 (m, 2 H, C*H*$_2$CH$_2$CHNH), 2.51–2.64 (m, 2 H, NC*H*$_2$CH$_2$CH$_2$NC), 2.72–2.82 (m, 2 H, NC*H*$_2$CH$_2$NC), 2.87–3.01 (m, 3 H, CH$_3$C*H*, C*H*$_2$CH$_2$CHNH), 3.84–3.90 (m, 2 H, NCH$_2$CH$_2$C*H*$_2$NC), 3.90–3.95 (m, 5 H, NCH$_2$C*H*$_2$NC, C*H*$_3$OCCHCCN), 3.95 (s, 3 H, C*H*$_3$OCCHCCCN), 4.02–4.12 (m, 1 H, C*H*NH), 4.90 (d, *J* = 7.1 Hz, 1 H, NH), 6.68 (s, 1 H, CHCCN), 6.88 (s, 1 H, CHCCCN). ^{13}C NMR (126 MHz, $CDCl_3$): δ = 18.68 (*C*H$_3$CH), 26.22 (CH$_2$*C*H$_2$CH$_2$CHN), 26.53 (*C*H$_2$CH$_2$CH$_2$CHN), 28.83 (NCH$_2$*C*H$_2$CH$_2$NC), 29.12 (CH$_2$CH$_2$*C*H$_2$CHN), 33.01 (CH$_2$*C*H$_2$CHNH), 45.84 (NCH$_2$CH$_2$*C*H$_2$NC), 47.81 (NCH$_2$*C*H$_2$NC), 48.34 (*C*H$_2$CH$_2$CHNH), 48.89 (CHNH), 50.77 (N*C*H$_2$CH$_2$CH$_2$NC), 52.33 (N*C*H$_2$CH$_2$NC), 55.30 (CH$_3$*C*H), 56.13 (*C*H$_3$OCCHCCCN), 56.55 (*C*H$_3$OCCHCCN), 63.97 (CH$_2$*C*HN), 100.89 (*C*HCCN), 102.87 (*C*CN), 106.28 (*C*HCCCN), 145.04 (CH$_3$O*C*CHCCN), 149.89 (*C*CCNH), 154.43 (CH$_3$O*C*CHCCCN), 158.19 (CNH), 158.86 (*C*NCNH). HRMS-ESI m/z [M+H]$^+$ calcd. for $C_{29}H_{47}N_6O_2$: 511.3760, found: 511.3755.

2-[(1,4'-Bipiperidin)-1'-yl]-_N_-(1-isopropylpiperidin-4-yl)-6,7-dimethoxyquinazolin-4-amine (32a)

According to GP2 with **27** (109 mg, 0.300 mmol, 1.0 equiv) and 1-piperidin-4-ylpiperidine (260 mg, 1.50 mmol, 5.0 equiv) in toluene (1.5 mL). **32a** was isolated by flash chromatography [5% to 10% 3 M NH_3 (in MeOH) in CH_2Cl_2] as pale yellow solid (135 mg, 91% yield, 95% purity). mp.: 107 °C. R_f = 0.36 [10% 3 M NH_3 (in MeOH) in CH_2Cl_2]. IR (film): $\tilde{\nu}$ = 2929, 2360, 1579, 1246, 754 cm^{-1}. ^{1}H NMR (500 MHz, CD_2Cl_2): δ = 1.04 (d, *J* = 6.6 Hz, 6 H, C*H*$_3$CH), 1.38–1.50 (m, 4 H, C*H*$_2$CH$_2$CH$_2$NCHC*H*$_2$CH$_2$NC), 1.50–1.57 (m, 6 H, CH$_2$C*H*$_2$CH$_2$NCH, C*H*$_2$CHNH), 1.78–1.87 (m, 2 H, CHC*H*$_2$CH$_2$NC), 2.10–2.20 (m, 2 H, C*H*$_2$CHNH), 2.26–2.39 (m, 2 H, C*H*$_2$CH$_2$CHNH), 2.41–2.56 (m, 5 H, CH$_2$CH$_2$C*H*$_2$NC*H*), 2.68–2.82 (m, 3 H, CH$_2$NC, CH$_3$C*H*), 2.83–2.96 (m, 2 H, C*H*$_2$CH$_2$CHNH), 3.88 (s, 3 H, C*H*$_3$OCCHCCNH), 3.90 (s, 3 H, C*H*$_3$OCCHCN), 4.08 (dtd, *J* = 11.2, 7.0, 3.8 Hz, 1 H, C*H*NH), 4.80–4.93 (m, 2 H, CH$_2$NC), 5.05 (d, *J* = 7.2 Hz, 1 H, NH), 6.73 (s, 1 H, C*H*CCNH), 6.80 (s, 1 H, C*H*CCCNH). ^{13}C NMR (126 MHz, CD_2Cl_2): δ = 18.51 (*C*H$_3$CH), 25.38 (*C*H$_2$CH$_2$CH$_2$NCH), 26.99 (CH$_2$*C*H$_2$CH$_2$NCH), 28.45 (CH*C*H$_2$CH$_2$NC), 33.13 (*C*H$_2$CHNH), 44.29 (CHCH$_2$*C*H$_2$NC), 48.07 (*C*H$_2$CH$_2$CHNH), 49.16 (CHNH), 50.62 (CH$_2$CH$_2$*C*H$_2$NCH), 54.83 (CH$_3$*C*H), 56.15 (*C*H$_3$OCCHCCCNH), 56.67 (*C*H$_3$OCCHCCNH), 63.72 (*C*HCH$_2$CH$_2$NC), 101.41 (*C*HCCNH), 103.20 (*C*CNH), 106.30 (*C*HCCCNH), 145.76 (*C*H$_3$O*C*CHCCNH), 149.83 (*C*CCNH), 154.96 (CH$_3$O*C*CHCCCNH),

158.64 (CNH), 159.08 (NCNCNH). HRMS-EI m/z [M]$^+$ calcd. for $C_{28}H_{44}N_6O_2$: 496.3526, found: 496.3518.

***N*-(1-Isopropylpiperidin-4-yl)-6,7-dimethoxy-2-[4-(3-methylpyridin-4-yl)-1,4-diazepan-1-yl]quinazolin-4-amine (32b)**

According to GP2 with **27** (182 mg, 0.500 mmol, 1.0 equiv) and 1-(3-methylpyridin-4-yl)-1,4-diazepane (503 mg, 2.50 mmol, 5.0 equiv) in toluene (2.5 mL). **32b** was isolated by flash chromatography [5% 3 M NH_3 (in MeOH) in CH_2Cl_2] as pale yellow solid (174 mg, 67% yield, 98% purity). mp.: 76 °C. R_f = 0.44 [10% 3 M NH_3 (in MeOH) in CH_2Cl_2]. IR (film): $\tilde{\nu}$ = 2096, 1581, 1497, 1246, 754 cm^{-1}. ^{1}H NMR (500 MHz, CD_2Cl_2): δ = 1.04 (d, *J* = 6.6 Hz, 6 H, C*H*$_3$CH), 1.48–1.59 (m, 2 H, C*H*$_2$CHNH), 2.03–2.10 (m, 2 H, NCH$_2$C*H*$_2$CH$_2$NCH), 2.10–2.18 (m, 2 H, C*H*$_2$CHNH), 2.27 (s, 3 H, CH$_3$C), 2.30–2.35 (m, 2 H, C*H*$_2$CH$_2$CHNH), 2.75 (hept, *J* = 6.6 Hz, 1 H, CH$_3$C*H*), 2.85–2.91 (m, 2 H, C*H*$_2$CH$_2$CHNH), 3.24–3.29 (m, 2 H, NC*H*$_2$CH$_2$CH$_2$NCH), 3.43–3.48 (m, 2 H, NC*H*$_2$CH$_2$NC), 3.88 (s, 3 H, C*H*$_3$OCCHCCNH), 3.89–3.96 (m, 5 H, NCH$_2$CH$_2$C*H*$_2$NCH, C*H*$_3$OCCHCN), 4.01–4.12 (m, 3 H, NCH$_2$C*H*$_2$NC, C*H*NH), 5.09 (d, *J* = 7.2 Hz, 1 H, NH), 6.75 (s, 1 H, C*H*CCNH), 6.77 (d, *J* = 5.6 Hz, 1 H, C*H*CCCH$_3$), 6.81 (s, 1 H, C*H*CCCNH), 8.10–8.15 (m, 2 H, C*H*NC*H*CCH$_3$). ^{13}C NMR (126 MHz, CD_2Cl_2): δ = 18.05 (*C*H$_3$C), 18.50 (*C*H$_3$CH), 28.54 (NCH$_2$*C*H$_2$CH$_2$NCH), 33.19 (*C*H$_2$CHNH), 46.21 (NCH$_2$CH$_2$*C*H$_2$NCH), 48.09 (NCH$_2$*C*H$_2$NC, *C*H$_2$CH$_2$CHNH), 49.33 (CHNH), 52.74 (NCH$_2$CH$_2$CH$_2$NCH), 53.90 (NCH$_2$CH$_2$NC), 54.85 (CH$_3$*C*H), 56.16 (*C*H$_3$OCCHCN), 56.69 (*C*H$_3$OCCHCCNH), 101.47 (*C*HCCNH), 103.21 (*C*CNH), 106.29 (*C*HCCCNH), 112.87 (*C*HCCCH$_3$), 124.19 (CH$_3$*C*), 145.66 (CH$_3$O*C*CHCCNH), 148.43 (*C*HNCHCCH$_3$), 149.99 (*C*CCNH), 152.58 (*C*HCCH$_3$), 154.99 (CH$_3$O*C*CHCN), 158.60 (CNH), 158.70 (*C*NCH$_2$CH$_2$N*C*). HRMS-EI m/z [M]$^+$ calcd. for $C_{29}H_{41}N_7O_2$: 519.3322, found: 519.3317.

***N*-(1-Isopropylpiperidin-4-yl)-6,7-dimethoxy-2-[4-(4-methylpiperazin-1-yl)piperidin-1-yl]quinazolin-4-amine (32c)**

According to GP2 with **27** (182 mg, 0.500 mmol, 1.0 equiv) and 1-methyl-4-piperidin-4-ylpiperazine (482 mg, 2.50 mmol, 5.0 equiv) in toluene (2.5 mL). **32c** was isolated by flash chromatography [7% to 10% 3 M NH_3 (in MeOH) in CH_2Cl_2] as pale yellow solid (214 mg, 84% yield, 98% purity). mp.: 111 °C. R_f = 0.22 [10% 3 M NH_3 (in MeOH) in CH_2Cl_2]. IR (film): $\tilde{\nu}$ = 2939, 2810, 1579, 1248, 752 cm^{-1}. ^{1}H NMR (500 MHz, CD_2Cl_2): δ = 1.10 (d, *J* = 6.6 Hz, 6 H, C*H*$_3$CH), 1.37–1.50 (m, 2 H, C*H*$_2$CH$_2$NC), 1.60–1.74 (m, 2 H, C*H*$_2$CHNH), 1.82–1.90 (m, 2 H, C*H*$_2$CH$_2$NC), 2.13–2.21 (m, 2 H, C*H*$_2$CHNH), 2.22 (s, 3 H, CH$_3$N), 2.27–2.51 (m, 7 H, C*H*NC*H*$_2$CH$_2$NCH$_3$, C*H*$_2$CH$_2$CHNH), 2.58 (s, 4 H, C*H*$_2$NCH$_3$), 2.74–2.84 (m, 2 H, C*H*$_2$NC), 2.84–2.91 (m, 1 H, CH$_3$C*H*), 2.91–3.02 (m, 2 H, C*H*$_2$CH$_2$CHNH), 3.88 (s, 3 H, C*H*$_3$OCCHCCNH), 3.90 (s, 3 H, C*H*$_3$OCCHCCCNH), 4.13 (dtd, *J* = 11.1, 7.0, 3.7 Hz, 1 H, C*H*NH), 4.78–4.88 (m, 2 H, C*H*$_2$NC), 5.15 (d, *J* = 7.3 Hz, 1 H, NH), 6.76 (s, 1 H, C*H*CCNH), 6.82 (s, 1 H, C*H*CCCNH). ^{13}C NMR (126 MHz, CD_2Cl_2): δ = 18.27 (*C*H$_3$CH), 28.78 (*C*H$_2$CH$_2$NC), 32.49 (*C*H$_2$CHNH), 44.05 (*C*H$_2$NC), 46.17 (CH$_3$N), 48.08 (*C*H$_2$CH$_2$CHNH), 48.75 (CHNH), 49.38 (*C*H$_2$NCH$_3$), 55.35 (CH$_3$*C*H), 55.98 (*C*H$_2$CH$_2$NCH$_3$), 56.17 (*C*H$_3$OCCHCCCNH), 56.68 (*C*H$_3$OCCHCCNH), 62.82 (*C*HNCH$_2$CH$_2$NCH$_3$), 101.41 (*C*HCCNH), 103.21 (*C*CNH), 106.23 (*C*HCCCNH), 145.86 (CH$_3$O*C*CHCCNH), 149.67 (*C*CCNH), 155.01 (CH$_3$O*C*CHCCCNH), 158.65 (CNH), 158.96 (*C*NCNH). HRMS-EI m/z [M]$^+$ calcd. for $C_{28}H_{45}N_7O_2$: 511.3635, found: 511.3628.

2-(4,4-Difluoropiperidin-1-yl)-*N*-(1-isopropylpiperidin-4-yl)-6,7-dimethoxyquinazolin-4-amine (32d) (Cui et al., 2020)

According to GP2 with **27** (182 mg, 0.500 mmol, 1.0 equiv) and 4,4-difluoropiperidine (319 mg, 2.50 mmol, 5.0 equiv) in toluene (2.5 mL). **32d** was isolated by flash chromatography [5% 3 M NH_3 (in MeOH) in CH_2Cl_2] as colorless solid (218 mg, 97% yield, 98% purity). mp.: 88 °C. R_f = 0.23 [5% 3 M NH_3 (in MeOH) in CH_2Cl_2]. IR (film): $\tilde{\nu}$ = 2968, 1581, 1495, 1211, 756 cm^{-1}. ^1H NMR (500 MHz, CD_2Cl_2): δ = 1.04 (d, J = 6.6 Hz, 6 H, CH_3CH), 1.51–1.59 (m, 2 H, CH_2CHNH), 1.90–2.06 (m, 4 H, CH_2CF_2), 2.09–2.19 (m, 2 H, CH_2CHNH), 2.27–2.41 (m, 2 H, CH_2CH$_2$CHNH), 2.76 (hept, J = 6.6 Hz, 1 H, CH$_3$CH), 2.83–2.92 (m, 2 H, CH_2CH$_2$CHNH), 3.89 (s, 3 H, CH_3OCCHCCNH), 3.91 (s, 3 H, CH_3OCCHCCCNH), 3.94–4.00 (m, 4 H, CH_2CH$_2$CF$_2$), 4.01–4.13 (m, 1 H, CHNH), 5.11 (d, J = 7.3 Hz, 1 H, NH), 6.75 (s, 1 H, CHCCNH), 6.83 (s, 1 H, CHCCCNH). ^{13}C NMR (126 MHz, CD_2Cl_2): δ = 18.49 (*C*H$_3$CH), 33.12 (*C*H$_2$CHNH), 34.19 (t, J = 22.3 Hz, *C*H$_2$CF$_2$), 41.49 (t, J = 5.0 Hz, *C*H$_2$CH$_2$CF$_2$), 48.04 (*C*H$_2$CH$_2$CHNH), 49.29 (CHNH), 54.84 (CH$_3$*C*H), 56.19 (*C*H$_3$OCCHCCCNH), 56.67 (*C*H$_3$OCCHCCNH), 101.24 (*C*HCCNH), 103.49 (*C*CNH), 106.43 (*C*HCCCNH), 123.51 (t, J = 241.2 Hz, *C*F$_2$), 146.23 (*C*CHCCNH), 149.58 (*C*CCNH), 155.09 (*C*CHCCCNH), 158.57 (*C*NCNH), 158.85 (CNH). HRMS-EI m/z $[M]^+$ calcd. for $C_{23}H_{33}F_2N_5O_2$: 449.2602, found: 449.2597.

***N*^{4}-(1-Isopropylpiperidin-4-yl)-6,7-dimethoxyquinazoline-2,4-diamine (32e) and *N*-(1-isopropylpiperidin-4-yl)-6,7-dimethoxyquinazolin-4-amine (32f)**

According to GP3, with **27** (146 mg, 0.400 mmol, 1.0 equiv) and NaN_3 (28.6 mg, 0.440 mmol, 1.1 equiv) in EtOH/AcOH (4:1) (2.68 mL) and afterwards 10% Pd/C (47.4 mg, 40.0 µmol, 0.10 equiv) and hydrazine hydrate (30.0 µL, 30.0 mg, 0.600 mmol, 1.5 equiv). **32e** (108 mg, 78% yield, 96% purity) and **32f** (6.20 mg, 5% yield, 95% purity) were isolated by flash chromatography [5% to 10% (7 M NH_3 (in MeOH) in CH_2Cl_2] as colorless solids. **32e**: mp.: 113 °C. R_f = 0.27 [10% (7 M NH_3 (in MeOH) in CH_2Cl_2]. IR (film): $\tilde{\nu}$ = 1624, 1585, 1429, 1248, 754 cm^{-1}. ^1H NMR (500 MHz, CD_2Cl_2): δ = 1.03 (d, J = 6.6 Hz, 6 H, CH_3CH), 1.44–1.59 (m, 2 H, CH_2CH), 2.05–2.18 (m, 2 H, CH_2CH), 2.26–2.40 (m, 2 H, CH_2N), 2.75 (hept, J = 6.6 Hz, 1 H, CH$_3$CH), 2.82–2.94 (m, 2 H, CH_2N), 3.88 (s, 3 H, CH_3OCCHCCNH), 3.89 (s, 3 H, CH_3OCCHCCCNH), 4.12 (tdt, J = 10.6, 7.3, 3.9 Hz, 1 H, CHNH), 4.61 (s, 2 H, NH_2), 4.98–5.23 (m, 1 H, NH), 6.76 (s, 1 H, CHCCNH), 6.79 (s, 1 H, CHCCCNH). ^{13}C NMR (126 MHz, CD_2Cl_2): δ = 18.48 (*C*H$_3$CH), 33.28 (*C*H$_2$CH), 48.04 (CH_2N), 48.82 (CHNH), 54.79 (CH$_3$*C*H), 56.18 (CH$_3$OCCHCCCNH), 56.67 (*C*H$_3$OCCHCCNH), 101.34 (*C*HCCNH), 104.07 (*C*CNH), 106.14 (*C*HCCCNH), 146.29 (*C*CHCCNH), 149.31 (*C*CCNH), 155.07 (*C*CHCCCNH), 159.37 (CNH), 160.07 (CNH_2). HRMS-ESI m/z $[M+H]^+$ calcd. for $C_{18}H_{28}N_5O_2$: 346.2243, found: 346.2236. **32f**: mp.: 241 °C (decomposition). R_f = 0.39 [10% (7 M NH_3 (in MeOH) in CH_2Cl_2]. IR (film): $\tilde{\nu}$ = 1626, 1506, 1473, 1252 cm^{-1}. ^1H NMR (500 MHz, CD_2Cl_2): δ = 1.03 (d, J = 6.6 Hz, 6 H, CH_3CH), 1.51–1.65 (m, 2 H, CH_2CHNH), 2.04–2.20 (m, 2 H, CH_2CHNH), 2.27–2.42 (m, 2 H, CH_2CH$_2$CHNH), 2.75 (hept, J = 6.6 Hz, 1 H, CH$_3$CH), 2.80–2.95 (m, 2 H, CH_2CH$_2$CHNH), 3.94 (s, 3 H, CH_3OCCHCCNH), 3.95 (s, 3 H, CH_3OCCHCCCNH), 4.12–4.27 (m, 1 H, CHNH), 5.36 (d, J = 7.6 Hz, 1 H, NH), 6.89 (s, 1 H, CHCCNH), 7.14 (s, 1 H, CHCCCNH), 8.44 (s, 1 H, CHNCNH). ^{13}C NMR (126 MHz, CD_2Cl_2): δ = 18.45 (*C*H$_3$CH), 33.19 (*C*H$_2$CHNH), 48.02 (*C*H$_2$CH$_2$CHNH), 49.08 (*C*HNH), 54.81 (CH$_3$*C*H), 56.38 (CH$_3$O)*, 56.58 (CH$_3$O)*, 100.02

(*C*HCCNH), 108.12 (*C*HCCCNH), 108.86 (*C*CNH), 147.11 (*C*CCNH), 149.41 (*C*CHCCNH), 154.33 (*C*HNCNH), 154.81 (*C*CHCCCNH), 158.03 (CNH). HRMS-ESI m/z $[M+H]^+$ calcd. for $C_{18}H_{27}N_4O_2$: 331.2134, found: 331.2128.

7-(Benzyloxy)-4-chloro-6-methoxy-2-(piperidin-1-yl)quinazoline (33)

According to GP7 with **4** (138 mg, 0.400 mmol, 1.0 equiv) and 1-methylpiperidine (58.6 mL, 48.1 mg, 0.480 mmol, 1.2 equiv) in 1,4-dioxane (1.0 mL). **33** was isolated by flash chromatography (CH_2Cl_2) as yellow solid (132 mg, 86% yield, 100% purity). mp.: 162 °C. R_f = 0.84 (CH_2Cl_2). IR (film): $\tilde{\nu}$ = 2929, 1626, 1583, 1491, 1240 cm^{-1}. ^1H NMR (500 MHz, CD_2Cl_2): δ = 1.57–1.65 (m, 4 H, CH_2CH$_2$N), 1.65–1.73 (m, 2 H, CH_2CH$_2$CH$_2$N), 3.76–3.85 (m, 4 H, CH$_2$N), 3.93 (s, 3 H, CH$_3$O), 5.20 (s, 2 H, CH$_2$O), 6.95 (s, 1 H, C*H*COCH$_2$), 7.19 (s, 1 H, C*H*COCH$_3$), 7.34–7.40 (m, 1 H, C*H*CHCHCC), 7.40–7.45 (m, 2 H, C*H*CHC), 7.45–7.51 (m, 2 H, C*H*CCH$_2$O). ^{13}C NMR (126 MHz, CD_2Cl_2): δ = 25.27 (*C*H$_2$CH$_2$CH$_2$N), 26.24 (*C*H$_2$CH$_2$N), 45.48 (CH$_2$N), 56.45 (CH$_3$O), 71.22 (CH$_2$O), 104.25 (*C*HCOCH$_3$), 106.28 (*C*HCOCH$_2$), 112.45 (*C*CCl), 128.26 (*C*HCCH$_2$O), 128.76 (*C*HCHCHC), 129.08 (*C*HCHC), 136.37 (*C*CH$_2$O), 147.90 (*C*OCH$_3$), 151.83 (*C*CCCl), 156.43 (*C*OCH$_2$), 158.09 (*C*NCCl), 159.88 (CCl). HRMS-ESI m/z $[M+H]^+$ calcd. for $C_{21}H_{23}ClN_3O_2$: 384.1479, found: 384.1474.

7-(Benzyloxy)-6-methoxy-2-(piperidin-1-yl)-*N*-[5-(pyrrolidin-1-yl)pentyl]quinazolin-4-amine (34a)

According to GP4 with **33** (154 mg, 0.400 mmol, 1.0 equiv), 5-pyrrolidin-1-ylpentan-1-amine (125 mg, 0.800 mmol, 2.0 equiv) and DIEA (213 µL, 158 mg, 1.20 mmol, 3.0 equiv) in *i*-PrOH (2.0 mL) for 15 min. **34a** (173 mg, 86% yield, 99% purity) was isolated by flash chromatography [5% 3 M NH_3 (in MeOH) in CH_2Cl_2] as pale yellow, hygroscopic solid. mp.: 66 °C. R_f = 0.17 [5% 3 M NH_3 (in MeOH) in CH_2Cl_2]. IR (film): $\tilde{\nu}$ = 2933, 1579, 1491, 1244, 756 cm^{-1}. ^1H NMR (500 MHz, CD_2Cl_2): δ = 1.39–1.51 (m, 2 H, CH_2CH$_2$CH$_2$NH), 1.52–1.68 [m, 8 H, CH_2CH_2CH$_2$NC,CH_2(CH$_2$)$_3$NH], 1.68–1.78 [m, 6 H, CH_2CH$_2$N(CH$_2$)$_3$CH_2], 2.31–2.52 [m, 6 H, CH$_2$CH_2NCH_2(CH$_2$)$_4$NH], 3.53–3.61 (m, 2 H, CH_2NH), 3.74–3.82 (m, 4 H, CH$_2$CH$_2$CH_2NC), 3.89 (s, 3 H, CH$_3$O), 5.15 (s, 2 H, CH$_2$O), 5.37 (t, *J* = 5.5 Hz, 1 H, NH), 6.82 (s, 1 H, C*H*COCH$_3$), 6.86 (s, 1 H, C*H*COCH$_2$), 7.31–7.38 (m, 1 H, C*H*CHCHC), 7.38–7.44 (m, 2 H, C*H*CHC), 7.44–7.49 (m, 2 H, C*H*CCH$_2$O). ^{13}C NMR (126 MHz, CD_2Cl_2): δ = 23.83 [*C*H$_2$CH$_2$N(CH$_2$)$_5$NH], 25.52 (*C*H$_2$CH$_2$CH$_2$NH)*, 25.58 (*C*H$_2$CH$_2$CH$_2$NC)*, 26.42 (*C*H$_2$CH$_2$NC), 29.15 [*C*H$_2$(CH$_2$)$_3$NH], 29.76 (*C*H$_2$CH$_2$NH), 41.60 (*C*H$_2$NH), 45.31 (*C*H$_2$NC), 54.47 [*C*H$_2$N(CH$_2$)$_5$NH], 56.63 [*C*H$_2$(CH$_2$)$_4$NH], 56.75 (CH$_3$O), 70.83 (CH$_2$O), 101.94 (*C*HCOCH$_3$), 103.50 (*C*CNH), 107.51 (*C*HCOCH$_2$), 128.19 (*C*HCCH$_2$O), 128.51 (*C*HCHCHC), 128.98 (*C*HCHC), 137.03 (*C*CH$_2$O), 145.80 (*C*OCH$_3$), 149.64 (*C*CCNH), 153.95 (*C*OCH$_2$), 159.29 (*C*NCNH)*, 159.38 (CNH)*. HRMS m/z $[M]^+$ calcd. for $C_{30}H_{41}N_5O_2$: 503.3260, found: 503.2079.

7-(Benzyloxy)-*N*-(1-cyclohexylpiperidin-4-yl)-6-methoxy-2-(piperidin-1-yl)quinazolin-4-amine (34b)

According to GP4 with **33** (154 mg, 0.400 mmol, 1.0 equiv), 1-cyclohexylpiperidin-4-amine (146 mg, 0.800 mmol, 2.0 equiv) and DIEA (213 µL, 158 mg, 1.20 mmol, 3.0 equiv) in *i*-PrOH (2.0 mL) for 15 min. **34b** (145 mg, 68% yield, 99% purity) was isolated by flash

chromatography [5% 3 M NH_3 (in MeOH) in CH_2Cl_2] as colorless solid. mp.: 192 °C. R_f = 0.32 [5% 3 M NH_3 (in MeOH) in CH_2Cl_2]. IR (film): $\tilde{\nu}$ = 2931, 2852, 1579, 1491, 1246, 754 cm^{-1}. ^1H NMR (500 MHz, CD_2Cl_2): δ = 1.03–1.18 (m, 1 H, CH_2CH$_2$CH$_2$CH), 1.19–1.32 (m, 4 H, CH$_2$CH_2CH_2CH), 1.45–1.72 (m, 9 H, CH_2CH_2CH$_2$N, CH_2CHNH, CH_2CH$_2$CH$_2$CH), 1.74–1.90 (m, 4 H, CH$_2$CH_2CH_2CH), 2.09–2.20 (m, 2 H, CH_2CHNH), 2.27–2.36 (m, 1 H, CH$_2$CH$_2$CH$_2$CH), 2.38–2.46 (m, 2 H, CH_2NCH), 2.83–2.96 (m, 2 H, CH_2NCH), 3.71–3.82 (m, 4 H, CH$_2$CH$_2$CH_2N), 3.89 (s, 3 H, CH_3O), 3.99–4.15 (m, 1 H, CHNH), 5.05 (d, J = 7.2 Hz, 1 H, NH), 5.15 (s, 2 H, CH_2O), 6.77 (s, 1 H, CHCOCH$_3$), 6.86 (s, 1 H, CHCOCH$_2$), 7.32–7.38 (m, 1 H, CHCHCHC), 7.38–7.44 (m, 2 H, CHCHCHC), 7.44–7.50 (m, 2 H, CHCHCHC). ^{13}C NMR (126 MHz, CD_2Cl_2): δ = 25.58 (CH_2CH$_2$CH$_2$N), 26.41 (CH$_2$CH_2CH$_2$N)*, 26.51 (CH$_2$CH$_2$CH$_2$CH)*, 26.87 (CH$_2$CH$_2$CH$_2$CH), 29.29 (CH$_2$CH$_2$CH$_2$CH), 33.26 (CH$_2$CHNH), 45.33 (CH$_2$CH$_2$CH$_2$N), 48.54 (CH$_2$NCH), 49.18 (CHNH), 56.83 (CH_3O), 64.15 (CH$_2$CH$_2$CH$_2$CH), 70.83 (CH_2O), 101.86 (CHCOCH$_3$), 103.39 (CCNH), 107.56 (CHCOCH$_2$), 128.18 (CHCHCHC), 128.51 (CHCHCHC), 128.98 (CHCHCHC), 137.01 (CCH$_2$O), 145.83 (COCH$_3$), 149.77 (CCCNH), 154.02 (COCH$_2$), 158.58 (CNH), 159.26 (CNCNH). HRMS-ESI m/z $[M+H^+]^+$ calcd. for $C_{32}H_{44}N_5O_2$: 530.3495; found: 530.3499.

7-(Benzyloxy)-*N*-[1-(cyclohexylmethyl)piperidin-4-yl]-6-methoxy-2-(piperidin-1-yl)quinazolin-4-amine (34c)

According to GP4 with **33** (154 mg, 0.400 mmol, 1.0 equiv), 1-(cyclohexylmethyl)piperidin-4-amine (157 mg, 0.800 mmol, 2.0 equiv) and DIEA (213 µL, 158 mg, 1.20 mmol, 3.0 equiv) in *i*-PrOH (2.0 mL) for 15 min. **34c** (158 mg, 73% yield, 97% purity) was isolated by flash chromatography [5% to 10% 3 M NH_3 (in MeOH) in CH_2Cl_2] as colorless solid. mp.: 181 °C. R_f = 0.35 [5% 3 M NH_3 (in MeOH) in CH_2Cl_2]. IR (film): $\tilde{\nu}$ = 2924, 2360, 1576, 1491, 1246, 754 cm^{-1}. ^1H NMR (500 MHz, CD_2Cl_2): δ = 0.75–0.99 (m, 2 H, CH_2CHCH$_2$N), 1.12–1.34 (m, 3 H, CH_2CH_2CH$_2$CH), 1.41–1.53 (m, 1 H, CHCH$_2$N), 1.53–1.74 (m, 11 H, CH_2CH_2CH$_2$N, CH_2CHNH, CH_2CH_2CH$_2$CH), 1.75–1.81 (m, 2 H, CH_2CHCH$_2$N), 1.97–2.27 (m, 6 H, CH_2NCH_2CH_2CHNH), 2.68–2.98 (m, 2 H, CH_2CH$_2$CHNH), 3.71–3.83 (m, 4 H, CH$_2$NC), 3.89 (s, 3 H, CH_3O), 4.04–4.17 (m, 1 H, CHNH), 5.06 (d, J = 7.1 Hz, 1 H, NH), 5.15 (s, 2 H, CH_2O), 6.77 (s, 1 H, CHCOCH$_3$), 6.87 (s, 1 H, CHCOCH$_2$), 7.27–7.38 (m, 1 H, CHCHCHC), 7.38–7.43 (m, 2 H, CHCHCHC), 7.44–7.53 (m, 2 H, CHCHCHC). ^{13}C NMR (126 MHz, CD_2Cl_2): δ = 25.57 (CH_2CH$_2$CH$_2$N), 26.40 (CH$_2$CH_2CH$_2$N)*, 26.62 (CH$_2$CH_2CH$_2$CH)*, 27.30 (CH_2CH$_2$CH$_2$CH), 32.28 (CH$_2$CH$_2$CH_2CH), 32.72 (CH_2CHNH), 35.78 (CH$_2$CH$_2$CH$_2$CH), 45.35 (CH$_2$CH$_2$CH_2N), 48.88 (CHNH), 53.55 (CH_2CH$_2$CHNH), 56.82 (CH_3O), 66.06 (CHCH_2N), 70.84 (CH_2O), 101.83 (CHCOCH$_3$), 103.38 (CCNH), 107.52 (CHCOCH$_2$), 128.19 (CHCHCHC), 128.52 (CHCHCHC), 128.98 (CHCHCHC), 137.00 (CHCHCHC), 145.85 (COCH$_3$), 149.70 (CCCNH), 154.03 (COCH$_2$), 158.60 (CNH), 159.20 (CNCNH). HRMS-ESI m/z $[M+H^+]^+$ calcd. for $C_{33}H_{46}N_5O_2$: 544.3652; found: 544.3657.

Supplemental References

Cui, R., Yin, C., Deng, X., Zhang, T., 2020. STK19 inhibitors for treatment of cancer. Trustees of Boston University, Xiamen University.

Davis, I., Jin, J., Janzen, W.P., Pattenden, S., Jayakody, C., 2016. A novel compound for the treatment of ewing sarcoma and high-throughput assays for identifying small molecules that modulate aberrant chromatin accessibility. Google Patents.

Doig, P., Boriack-Sjodin, P.A., Dumas, J., Hu, J., Itoh, K., Johnson, K., Kazmirski, S., Kinoshita, T., Kuroda, S., Sato, T.-o., Sugimoto, K., Tohyama, K., Aoi, H., Wakamatsu, K., Wang, H., 2014. Rational design of inhibitors of the bacterial cell wall synthetic enzyme GlmU using virtual screening and lead-hopping. Bioorganic & Medicinal Chemistry 22, 6256-6269.

Jiang, Y.-H., Kim, Y., Lee, H.-M., Jin, J., Roth, B.L., 2017. Preparation of quinazolin-4-amine derivatives as histone methyltransferase G9a inhibitors and methods for the treatment of Prader-willi syndrome. Duke University, The University of North Carolina at Chapel Hill.

Kaiser, J., Gertzen, C.G.W., Bernauer, T., Nitsche, V., Höfner, G., Niessen, K.V., Seeger, T., Paintner, F.F., Wanner, K.T., Steinritz, D., Worek, F., Gohlke, H., 2024. Identification of ligands binding to MB327-PAM-1, a binding pocket relevant for resensitization of nAChRs. bioRxiv, p. 2023.2012.2021.572862.

Liu, F., Barsyte-Lovejoy, D., Allali-Hassani, A., He, Y., Herold, J.M., Chen, X., Yates, C.M., Frye, S.V., Brown, P.J., Huang, J., Vedadi, M., Arrowsmith, C.H., Jin, J., 2011. Optimization of Cellular Activity of G9a Inhibitors 7-Aminoalkoxy-quinazolines. Journal of Medicinal Chemistry 54, 6139-6150.

Ma, A., Yu, W., Li, F., Bleich, R.M., Herold, J.M., Butler, K.V., Norris, J.L., Korboukh, V., Tripathy, A., Janzen, W.P., 2014. Discovery of a selective, substrate-competitive inhibitor of the lysine methyltransferase SETD8. Journal of medicinal chemistry 57, 6822-6833.

Somnarin, T., Pobsuk, N., Chantakul, R., Panklai, T., Temkitthawon, P., Hannongbua, S., Chootip, K., Ingkaninan, K., Boonyarattanakalin, K., Gleeson, D., Paul Gleeson, M., 2022. Computational design, synthesis and biological evaluation of PDE5 inhibitors based on N2,N4-diaminoquinazoline and N2,N6-diaminopurine scaffolds. Bioorganic & Medicinal Chemistry 76, 117092.

Sundriyal, S., Chen, P.B., Lubin, A.S., Lueg, G.A., Li, F., White, A.J.P., Malmquist, N.A., Vedadi, M., Scherf, A., Fuchter, M.J., 2017. Histone lysine methyltransferase structure activity relationships that allow for segregation of G9a inhibition and anti-Plasmodium activity. MedChemComm 8, 1069-1092.

Vital, T., Wali, A., Butler, K.V., Xiong, Y., Foster, J.P., Marcel, S.S., McFadden, A.W., Nguyen, V.U., Bailey, B.M., Lamb, K.N., 2023. MS0621, a novel small-molecule modulator of Ewing sarcoma chromatin accessibility, interacts with an RNA-associated macromolecular complex and influences RNA splicing. Frontiers in Oncology 13.

Wang, P.G., Kondengaden, M.S., Zhang, Q., Zang, L., 2019. Histone deacetylase and histone methyltransferase inhibitors and methods of making and use of the same. Google Patents.

4 Nicht veröffentlichte Experimente

Ergebnisse, die im Laufe dieser Arbeit erzielt, jedoch in keiner der vorherigen Publikationen vorgestellt wurden, werden im folgenden Kapitel beschrieben. Es handelt sich dabei um die Synthesen sowie biologischen Untersuchungen von A366-Analoga.

4.1 A366-Analoga als potenzielle Resensitizer desensitisierter nikotinischer Acetylcholinrezeptoren

Von den beim Library-Screening identifizierten Hit-Substanzen (Sichler et al., 2024) wurde insbesondere A366 aufgrund seiner hohen *ligand efficiency* als ein besonders vielversprechender Ansatzpunkt für die Entwicklung neuer Resensitizer für desensitisierte neuromuskuläre nikotinische Acetylcholinrezeptoren erachtet. Entsprechend wurde eine Reihe davon abgeleiteter Analoga synthetisiert und auf ihre biologische Wirkung untersucht. Da sich im Laufe des Projekts herausstellte, dass das A366-Analogon **59b** (siehe Schema 10), welches in 3-Position des 3*H*-Indol-Grundgerüsts anstelle des Cyclobutanrings von A366 zwei synthetisch einfacher einzuführende Methylgruppen aufweist, keine wesentlich geringere Affinität zur MB327-PAM-1-Bindungsstelle des nAChR als A366 zeigt, wurde das Augenmerk auf die Untersuchung entsprechender 3,3-Dimethyl-substituierter A366-Analoga gelegt. Dabei wurde zum einen die Kettenlänge und zum anderen die Ringgröße des Heterocyclus der ω-Aminoalkoxyseitenkette variiert. Darüber hinaus wurde ein Analogon von Verbindung **59b** hergestellt, bei dem die beiden Substituenten an der 5- und 6-Position des 2-Amino-3*H*-indol-Grundgerüsts vertauscht sind.

4.1.1 Synthesen von A366-Analoga mit abgewandelten ω-Aminoalkoxyseitenketten

Um das Potential der von A366 abgeleiteten Substanzklasse für die Entwicklung potenter Resensitizer auszuloten, war es erforderlich, einen effizienten und flexiblen Zugang zu entsprechenden Analoga zu entwickeln. Das Synthesekonzept orientierte sich dabei an den Arbeiten von Sweis *et al.* und Fagan *et al.* (Fagan et al., 2019; Sweis et al., 2014), welche in den Schlüsselschritten auf einer Dialkylierung von Phenylacetonitrilbausteinen in α-Position zur Nitrilgruppe, einer regioselektiven Nitrierung des Phenylrings, dem Aufbau einer ω-Aminoalkoxyseitenkette in 4-Position des Phenylrings sowie dem abschließenden Ringschluss zu dem für die Substanzklasse charakteristischen 2-Amino-3*H*-indol-Ringsystem beruhen. Um eine Vielzahl von A366-Analoga mit möglichst hoher struktureller Diversität auf effiziente Weise zugänglich zu machen, sollten die literaturbekannten Syntheserouten in zwei

wesentlichen Schritten optimiert werden. Zum einen sollte der Alkylierungsschritt und die Nitrierung in ihrer Abfolge vertauscht werden. Diese Vorgehensweise hätte den Vorteil, dass sich die Anzahl der linearen Syntheseschritte zu den A366-Analoga ab dem ersten Variationspunkt, der Dialkylierung des *o*-Nitro-substituierten Phenylacetonitrilbausteins, um einen Schritt verkürzen ließe. Zum anderen sollte der Aufbau der ω-Aminoalkoxyseitenkette über eine *Mitsunobu*-Reaktion mit entsprechenden Aminoalkoholbausteinen erfolgen, um sich die breite kommerzielle Verfügbarkeit dieser Bausteine zu Nutze zu machen. In den literaturbekannten Synthesen von A366-Analoga erfolgte der Aufbau der Seitenketten mit einer begrenzten Auswahl entsprechender kommerziell verfügbarer Alkylhalogenidbausteine. Die Synthese der Zielverbindungen **59a**-**d** ist in Schema 10 dargestellt.

Die regioselektive Einführung einer Nitrogruppe in die 6-Position des kommerziell erhältlichen 4-Benzyloxy-3-Methoxy-substituierten Phenylacetonitrilbausteins **51** erfolgte mit Hilfe von Acetylnitrat, welches durch Mischung von 70%iger Salpetersäure, Essigsäureanhydrid und Essigsäure bei 0 °C *in situ* erzeugt wurde und häufig für die Nitrierung von für elektrophile Substitutionen aktivierte Aromaten eingesetzt wird. Nach einer Reaktionszeit von 30 Minuten wurde das Reaktionsgemisch auf Eis gegossen und der dabei gebildete Niederschlag abfiltriert. Das Produkt **54** konnte auf diese Weise ohne weitere Aufreinigung in sehr guten Ausbeuten (90%) und in einer für die weitere Umsetzung ausreichenden Reinheit erhalten werden. Die Dimethylierung des *o*-Nitro-substituierten Phenylacetonitrilbausteins **54** in der α-Position gelang durch Umsetzung mit einem Überschuss von Methyliodid (4.0 Äq.) in Gegenwart von Natriumhydroxid (50%ige wässrige Lösung, 4.0 Äq.) in DMSO. Das gewünschte Dialkylierungsprodukt **55** konnte dabei nach zweistündigem Rühren bei Raumtemperatur und Extraktion der mit Wasser verdünnten alkalischen Reaktionslösung mit Toluol in einer Ausbeute von 95% und hoher Reinheit (95%) gewonnen werden. Um den Aufbau der ω-Aminoalkoxyseitenketten in 6-Position zu ermöglichen, musste im nächsten Schritt zunächst die Benzylschutzgruppe selektiv abgespalten werden. Dies gelang hydrogenolytisch mittels Wasserstoff (2.5 bar) und Palladium auf Aktivkohle in einem Gemisch aus Essigsäureethylester und Ethanol (9:1) bei Raumtemperatur (5.5 h). Das gewünschte Phenol **56** konnte nach Filtration der Reaktionslösung über Celite und anschließender säulenchromatographischer Aufreinigung in einer Ausbeute von 60% gewonnen werden.

Die beiden Cyclisierungsvorstufen **58a** und **58b** wurden unter *Mitsunobu*-Bedingungen (Kim and Han, 2015) in einem Schritt aus dem Phenol **56** und den Aminoalkoholen 3-Pyrrolidin-1-ylpropan-1-ol bzw. 2-Pyrrolidin-1-ylethanol in Gegenwart von jeweils 1.3 Äquivalenten Triphenylphosphin und DIAD (THF, 0 °C → RT, 24 h bzw. 1.5 h) erhalten. Nach Aufreinigung des Rohproduktes mittels Säulenchromatographie konnten die Verbindungen in guten bis sehr guten Ausbeuten (**58a**: 63% und **58b**: 81%) gewonnen werden.

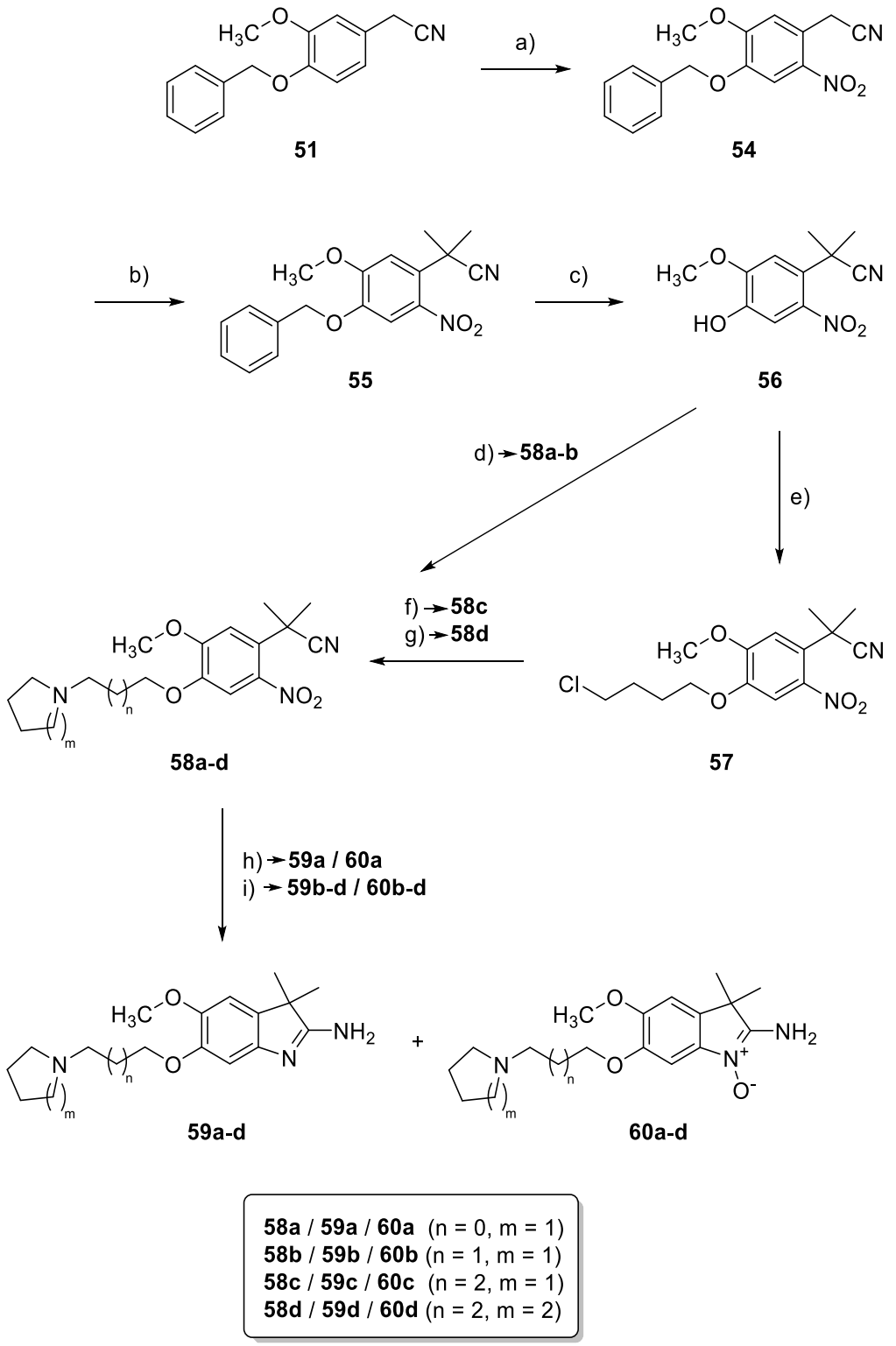

Schema 10: Reaktionsbedingungen: (a) HNO_3, Ac_2O, AcOH, 0 °C, 30 min, 90%; (b) NaOH (4.0 Äq.), MeI (4.0 Äq.), DMSO, RT, 2 h, 95%; (c) Pd/C (10%), H_2 (2.5 bar), EtOAc : EtOH (9:1), RT, 5.5 h, 60%; (d) 2-Pyrrolidin-1-ylethanol oder 3-Pyrrolidin-1-ylpropan-1-ol (1.3 Äq.), PPh_3 (1.3 Äq.), DIAD (1.3 Äq.), THF, 0 °C bis RT, 24 h oder 1.5 h; **58a**: 63%; **58b**: 81%; (e) 4-Chlorbutan-1-ol (1.3 Äq.), PPh_3 (1.3 Äq.), DIAD (1.3 Äq.), THF, 0 °C bis RT, 24 h, 96%; (f) Pyrrolidin (1.5 Äq.), KI (2.0 Äq.), K_2CO_3 (3.0 Äq.), Acetonitril, 50 °C, 72 h, 65%; (g) KI (2.0 Äq.), Piperidin, 50 °C, 20 h, 96%; (h) Pd/C (10%), H_2 (10 bar), AcOH, RT, 160 h, **59a**: 47%; **60a**: 15%; (i) Pd/C (10%), H_2 (1 bar), AcOH, RT, 24 h, **59b**: 16%; **59c**: 26%, **59d**: 41%; **60b**: 57%; **60c**: 49%; **60d**: 36%.

Für die Zielverbindungen **58c** und **58d** mit einem C4-Spacer in der ω-Aminoalkoxyseitenkette musste eine neue Strategie entwickelt werden, da die Verwendung von 4-(Pyrrolidin-1-yl)-butan-1-ol als Alkoholkomponente bei der *Mitsunobu*-Reaktion nicht zum Erfolg führte. Bei den entsprechenden Versuchen wurde das Phenol **56** quantitativ zurückerhalten. Vermutlich kommt es durch Cyclisierung des von 4-(Pyrrolidin-1-yl)butan-1-ol abgeleiteten, intermediär auftretenden Alkoxyphosphoniumions zur Bildung eines 5-Azaspiro[4.4]nonan-5-ium-Ions (Gmeiner et al., 1994), welches mit dem von **56** abgeleiteten Phenolat nicht weiterreagiert. Deshalb wurde eine zweistufige Syntheseroute über eine *Mitsunobu*-Reaktion mit einem 4-Halogenbutan-1-ol-Baustein und anschließender Alkylierung eines cyclischen Amins mit dem bei der *Mitsunobu*-Reaktion erhaltenen Baustein ins Auge gefasst. Entsprechend wurde zunächst der Schlüsselbaustein **56** mit jeweils 1.3 Äquivalenten 4-Chlorbutan-1-ol, Triphenylphosphin und DIAD (THF, RT, 24h) umgesetzt. Das gewünschte Produkt **57** wurde nach säulenchromatographischer Aufreinigung des Rohproduktes nahezu quantitativ (96% Ausbeute) erhalten. Die Substitution des Chloratoms in der Seitenkette des Bausteins **57** erfolgte dann mit Piperidin bzw. Pyrrolidin. Zur Darstellung von Verbindung **58d** wurde das Alkylchlorid **57** in Gegenwart von 2.0 Äquivalenten Kaliumiodid in Piperidin als Lösungsmittel für 20 Stunden auf 50 °C erhitzt. Das gewünschte Produkt **58d** konnte dabei nach säulenchromatographischer Aufreinigung des Rohproduktes in nahezu quantitativer Ausbeute (96%) gewonnen werden. Unter gleichen Reaktionsbedingungen wurde der Baustein **57** dann auch mit Pyrrolidin umgesetzt. Dabei wurde aber überraschenderweise nicht **58c**, sondern ein zweifach Pyrrolidin-substituiertes Produkt erhalten (89% Ausbeute). Im Unterschied zu Piperidin substituierte das nukleophilere Pyrrolidin zusätzlich zum Chloratom der Seitenkette von **57** auch den Methoxyrest des Phenylrings, der durch seine *para*-Stellung zur Nitrogruppe für eine S_NAr-Reaktion aktiviert ist. Eine deutlich höhere Reaktivität von Pyrrolidin gegenüber Piperidin bei S_NAr-Reaktionen an vergleichbaren Arylethern wurde bereits von Bunnett *et al.* beobachtet (Bunnett and Cartano, 1981). Um eine selektive Substitution an der gewünschten Position des Bausteins **57** zu erzielen, wurden in einem weiteren Versuch die Reaktionsbedingungen modifiziert und der Überschuss an Pyrrolidin deutlich verringert. Statt es als Lösemittel zu verwenden, wurden nur 1.5 Äquivalente eingesetzt. Die Reaktion wurde unter klassischen S_N2-Bedingungen unter Verwendung von Acetonitril als Lösemittel und in Gegenwart von 2.0 Äquivalenten Kaliumiodid und 3.0 Äquivalenten Kaliumcarbonat als Hilfsreagenzien durchgeführt. Das gewünschte Produkt **58c** konnte so nach Rühren des Reaktionsgemisches bei 50 °C für 72 Stunden und säulenchromatographischer Reinigung des Rohproduktes in einer Ausbeute von 65% gewonnen werden. Das Edukt **57** wurde in einer Ausbeute von 21% zurückerhalten. Das zweifach substituierte Produkt wurde unter diesen Reaktionsbedingungen nicht beobachtet.

Der abschließende Syntheseschritt, die reduktive Cyclisierung der α,α-Dimethyl-substituierten 2-Nitrophenylacetonitrilbausteine zu den entsprechenden 2-Amino-3*H*-indolen, erschien herausfordernd. So wurden sowohl von Sweis *et al.* (Sweis et al., 2014) als auch von Fagan *et al.* (Fagan et al., 2019) für die Cyclisierung von vergleichbaren Verbindungen sehr stark variierende Ausbeuten im Bereich von 8-97% bzw. 5-83% erhalten. Als vielversprechendste Methode erschien dabei die reduktive Cyclisierung mit Wasserstoff (1 bar) in Gegenwart von 10% Palladium auf Aktivkohle in Essigsäure bei Raumtemperatur. Unter diesen Reaktionsbedingungen konnten die gewünschten 3,3-Dimethyl-substituierten A366-Analoga **59a-d** ausgehend von den Vorstufen **58a-d** tatsächlich erhalten werden, wenngleich die Ausbeuten bestenfalls zufriedenstellend waren. Die literaturbekannte Verbindung **59b** (Luise et al., 2021; Sweis et al., 2014) wurde, ausgehend von **58b**, nach säulenchromatographischer Aufreinigung des Rohproduktes nur in einer Ausbeute von 16% erhalten. Zusätzlich zum gewünschten Produkt **59b** wurde als Hauptprodukt der Reaktion das Amidin-*N*-Oxid **60b** in einer Ausbeute von 57% erhalten. Es konnte u.a. mit Hilfe der Massenspektrometrie identifiziert werden. So wurden sowohl die Masse des *N*-Oxids **60b**, als auch die charakteristische Masse von M-16, die sich aus der Abspaltung von Sauerstoff ergibt, gefunden. Entsprechende Amidin-*N*-Oxide wurden bereits bei der Cyclisierung verwandter 2-Nitrophenylacetonitrilbausteine beobachtet (Jawdosiuk and Makosza, 1976). Sie entstehen vermutlich durch Cyclisierung der als Zwischenprodukte bei der Reduktion auftretenden *N*-Phenylhydroxylamine. Die Reaktionen der Seitenketten-Analoga **58c** und **58d** mit einem C4-Spacer lieferten etwas bessere Ausbeuten der entsprechenden 2-Amino-3*H*-indole **59c** und **59d** (26% bzw. 41%). Auch hier wurden in deutlichem Umfang die entsprechenden Amidin-*N*-Oxide erhalten (**60c**: 49% und **60d**: 36%). Die Cyclisierung des Seitenketten-Analogons **58a** mit einem C2-Spacer wurde, abweichend von den oben beschriebenen Versuchen, bei höherem Druck (10 bar) und deutlich längerer Reaktionsdauer (160 h) durchgeführt. Das gewünschte Produkt **59a** konnte so in etwas besseren Ausbeuten (47%) gewonnen werden. Der Anteil des Amidin-*N*-Oxids **60a** lag hier bei nur 15%.

4.1.2 Synthese der zu Verbindung 59b regioisomeren Verbindung 64

Das Regioisomer **64** des 3,3-Dimethyl-substituierten A366-Analogons **59b**, welches die ω-Aminoalkoxyseitenkette in der 5- statt in der 6-Position des 2-Amino-3*H*-indol-Grundgerüsts trägt, wurde ausgehend von dem 3,4-Dimethoxyphenylacetonitrilbaustein **53** dargestellt. Dieser kommerziell erhältliche Synthesebaustein trägt bereits die für die Cyclisierung erforderliche Nitrofunktion, so dass der Syntheseweg, verglichen mit der Darstellung der regioisomeren Verbindung **59b**, um einen Schritt verkürzt wird (siehe Schema 11).

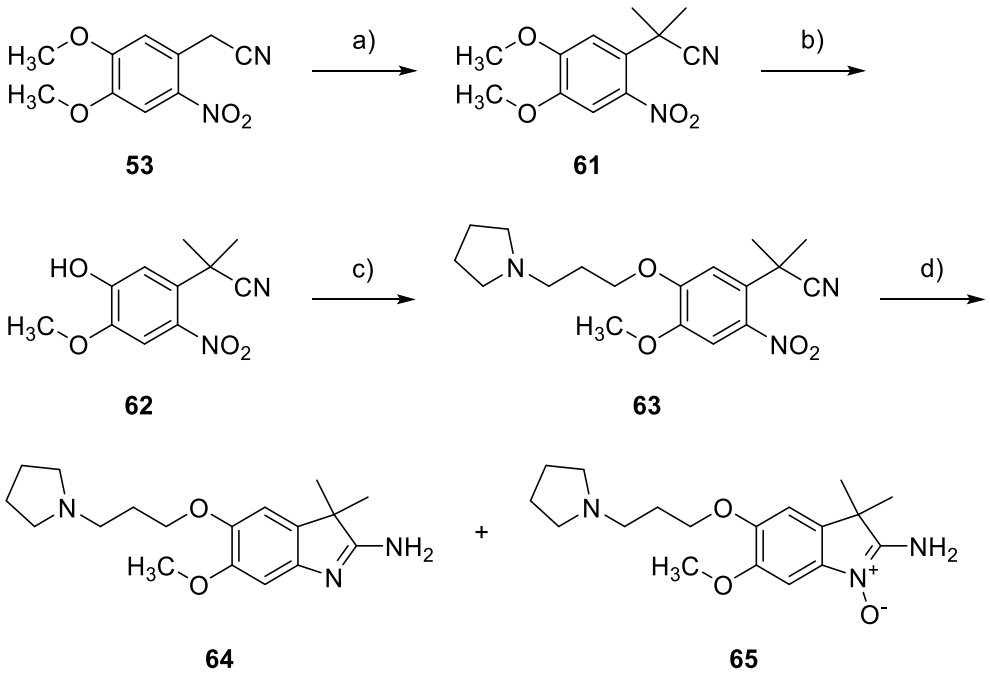

Schema 11: Reaktionsbedingungen: (a) NaOH (4.0 Äq.), MeI (4.0 Äq.), DMSO, RT, 2 h, 96%; (b) Dodecan-1-thiol (2.3 Äq.), Kalium *tert*-Butoxid (2.37 Äq.), DMF, 0 °C bis RT, 24 h → 50 °C, 45 min, 76%; (c) 3-Pyrrolidin-1-ylpropan-1-ol (1.3 Äq.), PPh_3 (1.3 Äq.), DIAD (1.3 Äq.), THF, 0 °C bis RT, 2 h, 65%; (d) Pd/C (10%), H_2 (1 bar), AcOH, RT, 24 h, **64**: 55%; **65**: 8%.

Die Synthese des α,α-dimethylierten Phenylacetonitrilbausteins **61** erfolgte ausgehend von Verbindung **53** analog zur Darstellung von Verbindung **55** durch Alkylierung mit 4.0 Äquivalenten Methyliodid in Gegenwart von NaOH (50%ige wässrige Lösung, 4.0 Äq.) in DMSO (RT, 2 h). Dabei konnte das gewünschte Produkt **61** nach Extraktion der mit Wasser verdünnten alkalischen Reaktionslösung mit Toluol ohne weitere Aufreinigung in nahezu quantitativer Ausbeute (96%) und hoher Reinheit (99%) erhalten werden. Die regioselektive Spaltung des Methylethers in *para*-Position zur Nitrogruppe des Bausteins **61** gelang durch nukleophilen Angriff eines Thiolats. Angelehnt an eine Vorschrift von Fagan *et al.*, die auf Arbeiten von Chae und Magano *et al.* basiert (Chae, 2008; Fagan et al., 2019; Magano et al., 2006), wurde ein *in sito* erzeugtes Dodecanthiolat genutzt, um selektiv den reaktiveren Aryl-methylether zu spalten. Dazu wurde die 3,4-Dimethoxyverbindung **61** unter Eiskühlung zu einem Gemisch aus Dodecan-1-thiol und Kalium-*tert*-butanolat in DMF gegeben und zunächst

für 24 Stunden bei Raumtemperatur und anschließend noch für 45 Minuten bei 50 °C gerührt. Das Phenol **62** konnte so in guter Ausbeute (76%) gewonnen werden. Neben der Verbindung **62** wurde auch das regioisomere Produkt, welches die freie OH-Funktion in *meta*-Position zur Nitrogruppe trägt, in einer Ausbeute von 9% erhalten. Die Veretherung der Hydroxylgruppe in *para*-Position zur Nitrogruppe des Bausteins **62** mit 3-Pyrrolidin-1-ylpropan-1-ol erfolgte analog zu den oben beschriebenen Synthesen unter *Mitsunobu*-Bedingungen und lieferte das gewünschte Produkt **63** mit einer Ausbeute von 65%. Der abschließende Syntheseschritt, die reduktive Cyclisierung der *o*-Nitrophenylacetonitril-Teilstruktur zum 2-Amino-3*H*-indol-Ringsystem, gelang, ausgehend von der Cyclisierungsvorstufe **63**, wie oben beschrieben unter einer Wasserstoff-Atmosphäre (1 bar) in Anwesenheit von 10% Pd/C-Katalysator in Essigsäure bei Raumtemperatur (24 h). Nach säulenchromatographischer Aufarbeitung des Rohprodukts konnten das gewünschte 2-Amino-3*H*-indol **64** als Hauptprodukt in vergleichsweiser guter Ausbeute (55%) gewonnen werden. Daneben wurde aber auch hier in geringer Menge das entsprechende Amidin-*N*-Oxid **65** (Ausbeute 8%) erhalten.

Die Reinheiten der 2-Amino-3*H*-indole **59a-d** und **64** wurden mittels ^{1}H q-NMR mit dem internen Standard Ethyl-4-(dimethylamino)benzoat auf ≥ 98% bestimmt. Das Ziel, eine Reihe 3,3-Dimethyl-substituierter Analoga von A366 mit unterschiedlichen ω-Aminoalkoxyseitenketten zu synthetisieren, wurde, trotz der nicht in allen Fällen zufriedenstellenden Ausbeuten, erreicht.

4.1.3 Biologische Untersuchungen von A366 und davon abgeleiteter Analoga

Um Erkenntnisse über die Struktur-Wirkungs-Beziehungen von A366 sowie davon abgeleiteter Analoga zu gewinnen, wurden der Screening-Hit A366 sowie die von mir synthetisierten Analoga **59a-d** und **64** zusammen mit dem Amidin-*N*-Oxid-Nebenprodukt **60b** hinsichtlich ihrer Affinität zur MB327-PAM-1-Bindungsstelle im UNC0642-MS-Bindungsassay sowie hinsichtlich ihrer intrinsischen Aktivität in *ex vivo*-Untersuchungen an Soman-vergifteten Ratten-Diaphragmen charakterisiert.

UNC0642-MS-Bindungsassay

Zunächst wurden die Bindungsaffinitäten zur MB327-PAM-1-Bindungsstelle des *Torpedo*-nAChR untersucht. Hierfür wurden für die oben genannten Verbindungen mit Hilfe des von V. Nitsche entwickelten kompetitiven UNC0642-MS-Bindungsassays (Nitsche et al., 2024) die pK_i-Werte bestimmt. Aufgrund der nur begrenzt verfügbaren Substanzmengen erfolgte die Ermittlung der pK_i-Werte nicht durch Mehrfachbestimmungen, wie sonst üblich, sondern in Einzelexperimenten (n = 1). Die Experimente wurden von Valentin Nitsche im Arbeitskreis von Prof. Dr. F. F. Paintner / Prof. Dr. K. T. Wanner an der Ludwig-Maximilians-Universität München durchgeführt und erlauben eine erste Einschätzung der Bindungsaffinität. Zur einheitlichen Benennung wurden die synthetisierten Verbindungen mit einer PTMD-Nr. (Pharmazie und Toxikologie München Düsseldorf) versehen. Die Ergebnisse sind in Tabelle 1 dargestellt.

Tabelle 1: pK_i-Werte von A366 und davon abgeleiteten Analoga, bestimmt durch Kompetitionsexperimente im UNC0642-MS-Bindungsassay (n = 1).

#	Nr.	PTMD02-000x	Strukturformel	pK_i
1	**A366**	-	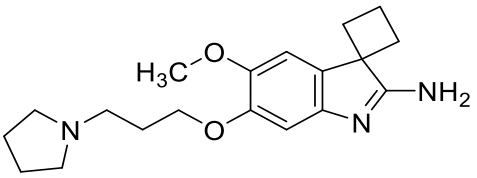	4.42
2	**59a**	2	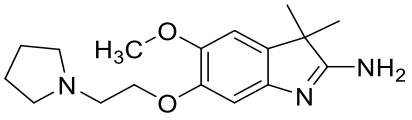	4.18
3	**59b**	1L*	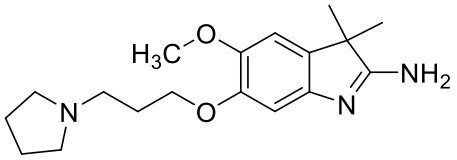	4.15
4	**59c**	5	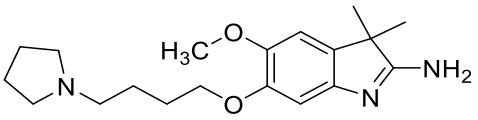	4.28
5	**59d**	4	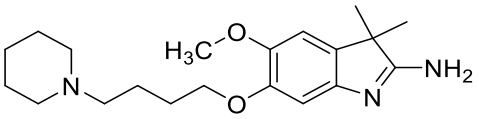	4.32
6	**64**	6	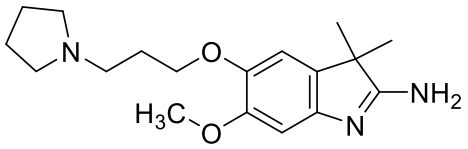	3.78
7	**60b**	7	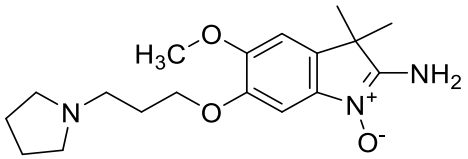	3.23

* PTMD02-0001L ist eine literaturbekannte Verbindung (Luise et al., 2021; Sweis et al., 2014).

Für den Screening-Hit A366 wurde im UNC0642-MS-Bindungsassay ein pK_i-Wert von 4.42 ermittelt (Tabelle 1, Eintrag 1). Wie oben bereits angedeutet, zeigte das 3,3-Dimethyl-substitutierte Analogon **59b** (PTMD02-0001L, Tabelle 1, Eintrag 3) mit einem pK_i-Wert von 4.15 eine, im Vergleich zu A366, etwas geringere Affinität zur MB327-PAM-1-Bindungsstelle. Der Ersatz der spirocyclischen Cyclobutyl-Teilstruktur in 3-Position des 2-Amino-3*H*-indol-Grundgerüsts durch zwei Methylgruppen führt damit zu einer Abnahme der Bindungsaffinität.

Eine Verkürzung der ω-Aminoalkoxyseitenkette um eine CH_2-Einheit hat keinen signifikanten Einfluss auf die Bindungsaffinität. So wurde für Verbindung **59a** (PTMD02-0002, Tabelle 1, Eintrag 2), welche einen C2-Spacer aufweist, ein pK_i-Wert von 4.18 bestimmt, welcher dem des Analogons mit einem C3-Spacer **59b** (pK_i = 4.15) gleicht. Eine Verlängerung der ω-Aminoalkoxyseitenkette um eine CH_2-Einheit führt dagegen zu einer nominell geringfügig höheren Affinität. So wurde für Verbindung **59c** mit einem C4-Spacer ein pK_i-Wert von 4.28 ermittelt (PTMD02-0005, Tabelle 1, Eintrag 4). Die Ringgröße des Heterocyclus scheint dagegen keinen wesentlichen Einfluss auf die Bindungsaffinität zu haben. Für Verbindung **59d** (PTMD02-0004, Tabelle 1, Eintrag 5), welche einen über einen C4-Spacer gebundenen Piperidinring anstelle des in Verbindung **59c** vorhandenen Pyrrolidinrings aufweist, wurde eine vergleichbare Affinität (pK_i = 4.32) wie für **59c** (pK_i = 4.28) ermittelt. Interessanterweise bindet Verbindung **64** (PTMD02-0006, pK_i = 3.78, Tabelle 1, Eintrag 6), das **59b**-Analogon, bei dem die Reste in 5- und 6-Position vertauscht sind, mit einer um etwa 0.4 log Einheiten geringeren Affinität als die Vergleichsverbindung **59b** (pK_i = 4.15) an die untersuchte Bindungsstelle. Das Amidin-*N*-Oxid **60b** (PTMD02-0007, pK_i = 3.23, Tabelle 1, Eintrag 7), welches als Nebenprodukt bei der Synthese von **59b** isoliert wurde, zeigte unter den untersuchten A366-Analoga die geringste Bindungsaffinität. Sie lag nominell um ca. 0.9 log Einheiten unter der des entsprechenden stärker basischen Amidin-Analogons **59b**.

Zusammenfassend lässt sich feststellen, dass die Affinitäten der Analoga **59a**-**d** nominell nur etwas geringer sind als die Affinität von A366. Die einzigen Verbindungen, deren Affinitäten deutlicher von den oben genannten abweichen, sind das Regioisomer **64** sowie insbesondere das Amidin-*N*-Oxid **60b**. Für beide Verbindungen wurden im Vergleich zu der sehr nahe verwandten Verbindung **59b** deutlich niedrigere pK_i-Werte gefunden. Es scheint, dass sowohl die Anknüpfungsstelle der basischen ω-Aminoalkoxyseitenkette am 2-Amino-3*H*-indol-Grundgerüst, als auch eine basische Amidin-Teilstruktur für eine hohe Bindungsaffinität zur MB327-PAM-1-Bindungsstelle von Bedeutung sind.

Um gezielt weitere A366-Analoga mit höherer Bindungsaffinität zu entwickeln, sollte auf der Basis der vorhandenen Ergebnisse zunächst der Bindemodus dieser Verbindungen in der MB327-PAM-1-Bindungstasche in *in silico*-Studien untersucht werden, um Molekülbereiche zu identifizieren, an denen sich durch Strukturvariationen die Wechselwirkungen mit der Bindungstasche möglicherweise verbessern lassen.

Ex vivo-Untersuchungen an Ratten-Diaphragma-Präparationen

Zusätzlich zu den Bindungsaffinitäten an der MB327-PAM-1-Bindungsstelle des *Torpedo*-nAChR wurden A366 und die davon abgeleiteten Analoga **59a-d**, **60b** und **64** in *ex vivo*-Untersuchungen an Ratten-Diaphragma-Präparationen auch hinsichtlich ihrer intrinsischen Aktivitäten charakterisiert. Dabei wurde mit Hilfe von myographischen Assays zunächst das Vermögen bestimmt, die Muskelkraft Soman-vergifteter Ratten-Diaphragmen wiederherzustellen (Seeger et al., 2012).

Bei diesen Untersuchungen werden präparierte Ratten-Diaphragma-Hemisphären zunächst mit einer Lösung behandelt, die 3 µM Soman enthält. Während bei einer indirekten elektrischen Feldstimulation, die üblicherweise bei Frequenzen von 20 Hz, 50 Hz und 100 Hz durchgeführt wird, bei nicht vergifteten Ratten-Diaphragma-Präparationen Muskelkontraktionen auftreten, sind bei den vergifteten Proben keine oder nur sehr schwache Kontraktionen messbar. Diese Hemmung verschwindet auch nicht, wenn die vergifteten Proben durch Waschen vom Toxin befreit werden, was üblicherweise als Kontrolle durchgeführt wird, da dies keinen Einfluss auf die irreversible Hemmung der AChE durch das Nervengift hat. Eine positive intrinsische Aktivität von Testverbindungen liegt dann vor, wenn ihre Zugabe zu den vergifteten Muskelpräparationen, die üblicherweise in ansteigenden Konzentrationen von 0.1 bis 100 µM erfolgt, eine zumindest teilweise Wiederherstellung der Muskelkraft der Soman-vergifteten Ratten-Diaphragmen bewirkt. Die Hemmung der Muskelkraft tritt wieder auf, wenn die Proben nach Erreichen der jeweils höchsten Testkonzentrationen einem abschließenden Waschschritt unterzogen werden. Dies ist auf die irreversible Inaktivierung der AChE zurückzuführen und weist auf die Reversibilität der rezeptorvermittelten resensitierenden Wirkung der Prüfsubstanzen hin. Da bekannt ist, dass die größte Wirksamkeit bei niedrigen Stimulationsfrequenzen beobachtet wird (Seeger et al., 2012), werden im Folgenden nur die Ergebnisse der Experimente bei 20 Hz dargestellt (siehe Abbildung 22) und diskutiert. Die Ergebnisse sind als %-Werte der maximalen Muskelkraft in Balkendiagrammen dargestellt (Mittelwerte mit Standardabweichungen, n = 3-17). Da für die Messungen in den Organbädern relativ hohe Substanzmengen erforderlich sind, konnten nicht bei allen untersuchten Verbindungen alle angegebenen Konzentrationen gemessen werden.

Die myographischen Untersuchungen wurden von Dr. Thomas Seeger und seiner Arbeitsgruppe am Institut für Pharmakologie und Toxikologie der Bundeswehr in München durchgeführt.

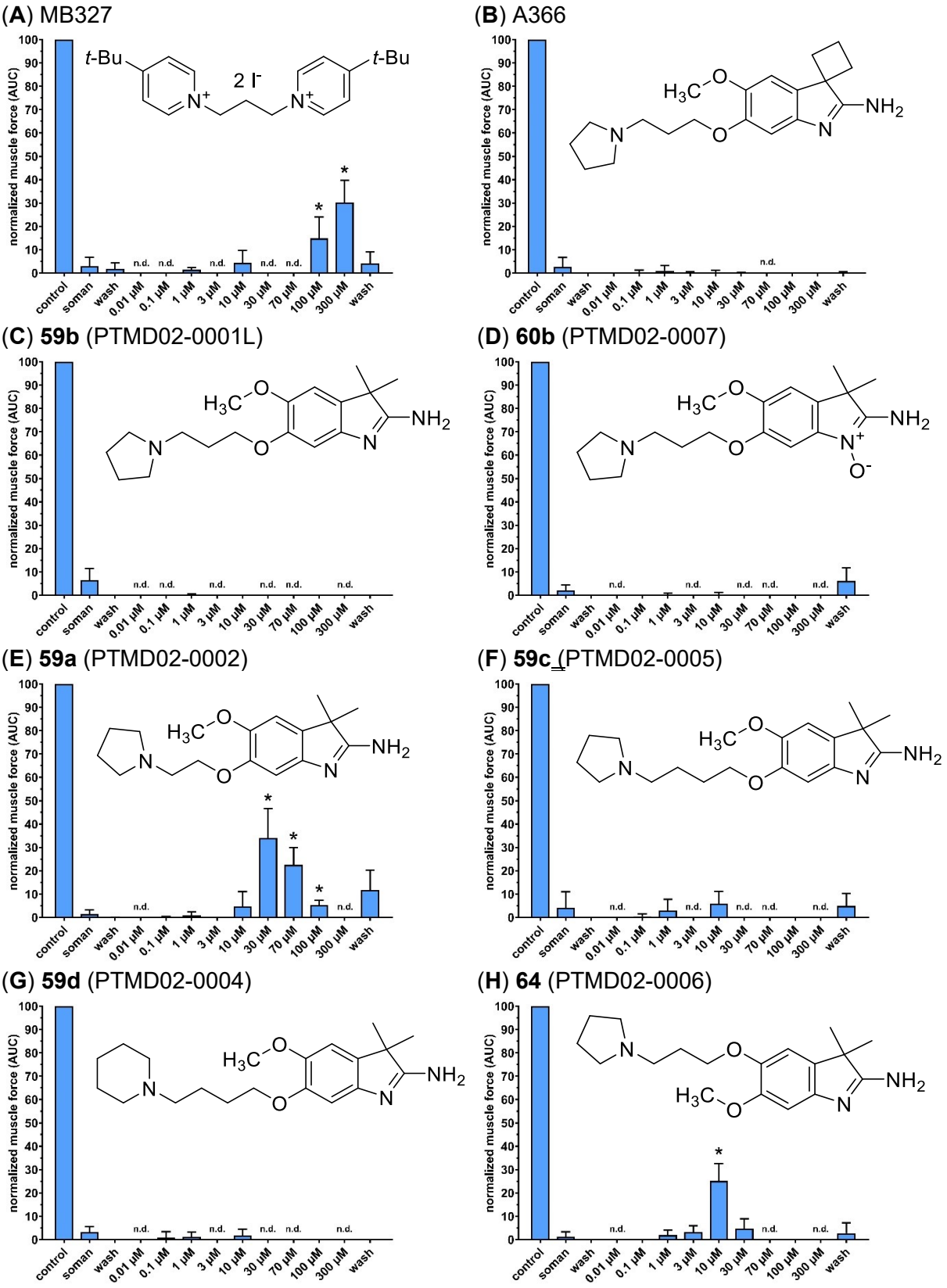

Abbildung 22: Konzentrationsabhängige Wiederherstellung der Muskelkraft durch (**A**) MB327 (Niessen et al., 2018), (**B**) A366, (**C**) **59b** (PTMD02-0001L), (**D**) **60b** (PTMD02-0007), (**E**) **59a** (PTMD02-0002), (**F**) **59c** (PTMD02-0005), (**G**) **59d** (PTMD02-0004) und (**H**) **64** (PTMD02-0006) an Soman-vergifteten (3 µM) Ratten-Diaphragmen bei einer Anregungsfrequenz von 20 Hz. Asterisken (*) zeigen die statistisch signifikanten Unterschiede zwischen der jeweiligen Substanz und der Soman-Applikation an ($p < 0.01$).

Der Screening-Hit A366, das 3,3-Dimethyl-substituierte Analogon **59b** (PTMD02-0001L) sowie das entsprechende Amidin-*N*-Oxid **60b** (PTMD02-0007), die alle einen C3-Spacer in der ω-Aminoalkoxyseitenkette aufweisen, führten in den gemessenen Konzentrationsbereichen zu keinerlei Muskelkraft-wiederherstellendem Effekt (siehe Abbildung 22, **B**, **C** und **D**). Ebenso zeigten auch das kettenlängere Analogon **59c** (PTMD02-0005), mit einer zusätzlichen CH_2-Gruppe in der Seitenkette, sowie die davon abgeleitete Verbindung **59d** (PTMD02-0004), mit einem Piperidin-Rest anstelle des Pyrrolidin-Restes in der Seitenkette, keinen statistisch signifikanten Effekt (siehe Abbildung 22 **F** und **G**). Im Unterschied dazu konnte für das kettenkürzere Analogon **59a**, mit einem C2-Spacer in der Seitenkette, sowie für Verbindung **64**, bei der im Vergleich zu Verbindung **59b** die Substituenten in 5- und 6-Position vertauscht sind, in einem engen Konzentrationsbereich ein deutlicher Muskelkraft-wiederherstellender Effekt beobachtet werden (siehe Abbildung 22, **E** und **H**). So zeigte Verbindung **59a** (PTMD02-0002) nach Anregung bei 20 Hz bei einer Testsubstanzkonzentration von 30 µM eine Wiederherstellung der Muskelkraft auf 34% ± 13% des Maximalwertes. Dies entspricht etwa dem maximalen Effekt, der mit der prototypischen Verbindung MB327 - allerdings erst bei einer Konzentration von 300 µM - unter gleichen Versuchsbedingungen – erreicht wird (siehe Abbildung 22, **A**) (Niessen et al., 2018). Bei einer Konzentration von 70 µM nahm der Effekt von Verbindung **59a** zwar wieder leicht ab, war aber mit 22% ± 8% immer noch signifikant. Bei einer weiteren Erhöhung der Substanzkonzentration auf 100 µM sank der %-Wert für die Wiederherstellung der Muskelkraft dann aber deutlich ab (5% ± 2%). Für das zu **59b** regioisomere Analogon **64** (PTMD02-0006) wurde nach Anregung bei 20 Hz schon bei einer Konzentration von 10 µM eine signifikante Wiederherstellung der Muskelkraft von 25% ± 7% beobachtet. Allerdings nahm auch hier der Effekt bei einer Erhöhung der Konzentration wieder deutlich ab und war bereits bei 30 µM statistisch nicht mehr signifikant.

Nach dem abschließenden Waschschritt waren in keinem Fall mehr statistisch signifikante Werte für die Muskelkraft zu beobachten, was auf eine weitgehend vollständige Inhibition der AChE in den untersuchten Muskelpräparationen hindeutet. Deshalb weist die teilweise Wiederherstellung der Muskelkraft im Falle der A366-Analoga **59a** und **64** auf einen Rezeptor-vermittelten Effekt der beiden Substanzen hin (Niessen et al., 2018).

Bei der Betrachtung der Ergebnisse ist zum einen bemerkenswert, dass die beiden A366-Analoga **59a** und **64** im Vergleich zu MB327 einen, in seiner Größenordnung vergleichbaren, Muskelkraft-wiederherstellenden Effekt bereits bei deutlich geringeren Konzentrationen (30 µM und 10 µM bei **59a** bzw. **64** im Vergleich zu 300 µM bei MB327) erreichen. Zum anderen fällt auf, dass auch im Falle von **59a** und **64** – wie bei MB327, Cycloguanil und den meisten der bereits von uns untersuchten MB327- und UNC0646-Analoga (Bernauer et al., 2024; Kaiser et al., 2024; Nitsche et al., 2024) – ein biphasischer Verlauf der Konzentrations-Wirkungs-Beziehungen vorliegt. Nach Erreichen eines Maximums für die wiederhergestellte

Muskelkraft nimmt diese bei höheren Konzentrationen der Testverbindungen wieder deutlich ab oder verschwindet gänzlich. Es wird vermutet, dass der positive intrinsische Effekt von einem sekundären, inhibitorischen Effekt überlagert wird, der möglicherweise durch Bindung an die orthosterische Bindungsstelle des nAChR hervorgerufen wird (Bernauer et al., 2024; Kaiser et al., 2023; Niessen et al., 2018).

Um eine mögliche inhibitorische Wirkung von A366 und seinen Analoga auf den Rattenmuskel zu untersuchen, wurden entsprechende myographische Untersuchungen auch an nicht Soman-vergifteten Muskelpräparationen durchgeführt.

Dafür wurden, analog zu den Versuchen mit Soman-vergifteten Ratten-Diaphragmen, nicht vergiftete Muskelpräparationen mit steigenden Konzentrationen von A366 (1-300 µM) bzw. der Analoga **59a-d** und **64** (0.1-100 µM oder 1-100 µM) versetzt und anschließend indirekt bei 20 Hz stimuliert. Um mögliche Muskelermüdungen zu berücksichtigen, wurden, außer im Fall von Verbindung **59b**, Kontrollversuche durchgeführt, bei welchen nur die Puffer in den Organbädern von stimulierten unbehandelten Muskelpräparationen ausgetauscht wurden. Im Verlauf der Versuche lässt sich ein unausweichlicher Abfall der Muskelkraft beobachten, wie aus den stetig leicht sinkenden %-Werte in den Kontrollkurven ersichtlich ist. Um den Einfluss der Testsubstanzen auf die Muskelkraft bewerten zu können, wurden die gemessenen Aktivitäten mit den zugehörigen Kontrollwerten ohne Substanz verglichen. Die Ergebnisse der Untersuchungen sind als %-Werte der maximalen Muskelkraft (Mittelwerte mit Standardabweichungen, n = 4-17) in Abbildung 23 dargestellt.

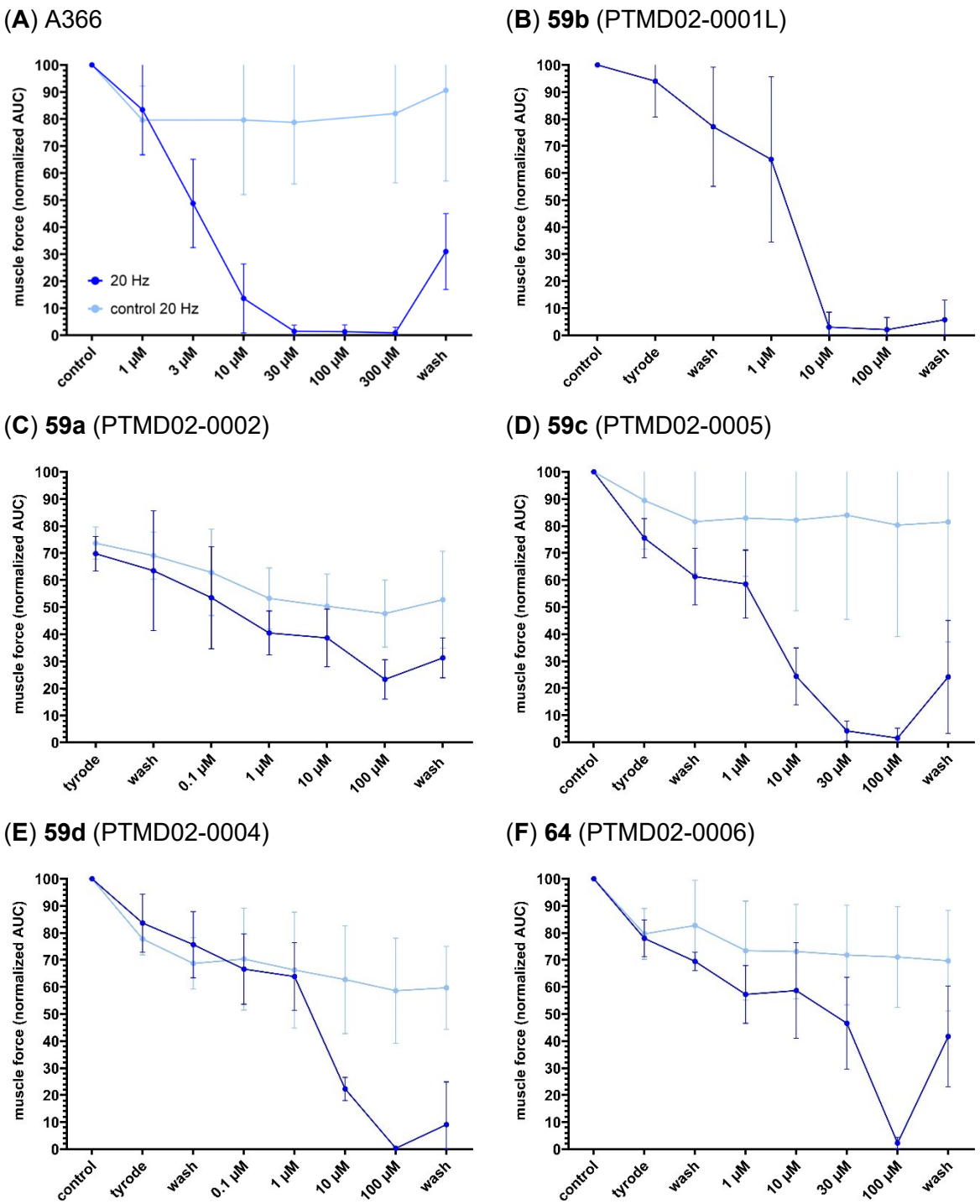

Abbildung 23: Muskelkraft unvergifteter Ratten-Diaphragmen nach Behandlung mit (**A**) A366, (**B**) **59b** (PTMD02-0001L), (**C**) **59a** (PTMD02-0002), (**D**) **59c** (PTMD02-0005), (**E**) **59d** (PTMD02-0004) und (**F**) **64** (PTMD02-0006) bei einer Anregungsfrequenz von 20 Hz. Die erzeugte Muskelkraft wird als Fläche unter der Kurve (AUC) dargestellt, die auf die Muskelkraft unter Kontrollbedingungen zu Beginn der Messung normiert wurde.

Alle untersuchten Testverbindungen führten bei steigenden Konzentrationen zu einer teilweisen oder vollständigen Abnahme der Muskelkraft. Im Falle des Screening-Hits A366 kommt es bereits bei einer Konzentration von 3 µM zu einem deutlichen Abfall der Muskelkraft. Ab einer Konzentration von 30 µM ist der Muskel dann vollständig gehemmt. Diese Hemmung

scheint aber prinzipiell reversibel zu sein, da nach einem abschließenden Waschschritt die Muskelkraft teilweise wiederhergestellt wurde (siehe Abbildung 23, **A**). Ähnliche Kurvenverläufe finden sich auch für das zu A366 nahe verwandte Analogon **59b** (PTMD02-0001L) sowie für die Analoga mit C4-Spacer in der Seitenkette **59c** (PTMD02-0005) und **59d** (PTMD02-0004) (siehe Abbildung 23, **B**, **D** und **E**). So sind bei einer Konzentration von 10 µM jeweils eine deutliche, und bei 100 µM eine vollständige Hemmung der Muskelkraft zu beobachten. Auch in diesen Fällen war – wenn zum Teil auch nur wenig ausgeprägt – nach dem abschließenden Waschschritt eine teilweise Wiederherstellung der Muskelkraft festzustellen. Die beiden A366-Analoga **59a** (PTMD02-0002) und **64** (PTMD02-0006), die in den Versuchen mit den Soman-vergifteten Ratten-Diaphragmen zu einer Wiederherstellung der Muskelkraft führten, zeigten eine geringere Hemmung des nicht Soman-vergifteten Muskels (siehe Abbildung 23, **C** und **F**). So wurde für das Analogon **64** erst ab einer Konzentration von 30 µM ein etwas deutlicherer Abfall der Muskelkraft festgestellt. Erst bei einer Konzentration von 100 µM war der Muskel dann, wie im Falle der oben genannten Analoga, vollständig gehemmt. Nach dem abschließenden Waschschritt war die Muskelkraft etwa zur Hälfte wiederhergestellt. Bei dem Analogon **59a** mit C2-Spacer in der ω-Aminoalkoxyseitenkette zeigte sich eine statistisch signifikante Abnahme der Muskelkraft erst bei einer Konzentration von 100 µM. Dabei ist die Hemmung des Muskels aber nicht vollständig und noch eine deutliche Restaktivität messbar.

Bei den beiden in den myographischen Assays mit Soman-vergifteten Ratten-Diaphragmen wirksamen Verbindungen **59a** und **64** tritt im Unterschied zu A366 und den anderen Analoga eine deutliche Hemmung des nicht vergifteten Muskels erst bei höheren Konzentrationen ab ca. 100 µM bzw. 30 µM auf. Das sind genau die Konzentrationsbereiche, in denen es in den jeweiligen myographischen Assays mit Soman-vergifteten Muskeln nach einem maximalen Wert zu einem deutlichen Rückgang der Muskelkraft kam. Dies spricht dafür, dass hier möglicherweise ein, auf der Bindung an die MB327-PAM-1-Bindungsstelle des nAChR beruhender, positiver intrinsischer Effekt, ab den oben genannten Konzentrationen von einem stärkeren inhibierenden Effekt überlagert wird, was den biphasischen Verlauf der Konzentrations-Wirkungskurven erklären würde. Die Tatsache, dass im Falle von A366 und der Analoga **59b**-**d** trotz angenommener Bindung an die MB327-PAM-1-Bindungsstelle keine Muskelkraft-wiederherstellende Aktivität an den Soman-vergifteten Ratten-Diaphragmen beobachtet wurde, liegt vermutlich daran, dass die Muskel-inhibierenden Effekte im Unterschied zu den Analoga **59a** und **64** bereits bei deutlich geringeren Konzentrationen auftreten.

Eine große Herausforderung für die Entwicklung von Resensitizern auf Basis des Screening-Hits A366 ist demnach, dass A366 genauso wie alle untersuchten Analoga neben einem positiv allosterischen Effekt, vermittelt über die MB327-PAM-1-Bindungsstelle des nAChR,

auch einen inhibitorischen Effekt ausübt, der vermutlich über die orthosterische Bindungstasche des nAChR erfolgt. Eine Bindung von A366 an die orthosterische Bindungstasche konnte mit Hilfe von *in silico*-Untersuchungen in der Arbeitsgruppe von Prof. Dr. H. Gohlke an der Heinrich-Heine-Universität Düsseldorf in der Tat vorhergesagt werden (Kaiser et al., 2023). Entsprechende Bindungsstudien stehen jedoch noch aus.

Parallel zu einer Optimierung der Liganden hinsichtlich einer möglichst hohen Affinität zur allosterischen Bindungstasche ist es deshalb in Zukunft notwendig, die Affinität zur orthosterischen Bindungstasche zu minimieren.

Die Ergebnisse der Untersuchungen von A366 und seinen Analoga hinsichtlich ihrer Affinität zur allosterischen MB327-PAM-1-Bindungsstelle am *Torpedo*-nAChR und hinsichtlich ihrer intrinsischen Aktivität in den *ex vivo*-Untersuchungen zeigen erneut die Komplexität des biologischen Systems und unterstreichen die Notwendigkeit weiterer Forschung, um ein besseres Verständniss für die komplexen Mechanismen der Muskelreaktivierung durch Resensitizer desensitisierter nAChR zu erlangen.

4.2 Experimental Part

4.2.1 Synthesis of A366-Analoga

All chemicals were used as purchased from commercial sources. Solvents used for purification were distilled before use. Anhydrous reactions were performed under an argon atmosphere in vacuum-dried glassware. For TLC, plates purchased from Merck (silica gel 60F_{254} on aluminum sheet) were used. Flash chromatography (FC) was carried out using silica gel 60 (40-63 mm mesh size) purchased from Merck as stationary phase. All synthesized compounds were dried under high vacuum. ^{1}H and ^{13}C NMR spectra were recorded on a Bruker BioSpin Avance III HD 400 and 500 MHz at 25 °C. For data processing, MestReNova (Version 14.1.0) from Mestrelab Research S.L. 2019 and for calibration, the solvent signal ($CDCl_3$, CD_2Cl_2 or CD_3OD) was used. The purity of the test compounds was unless otherwise noted ≥ 95%, determined by means of quantitative NMR spectroscopy using TraceCERTS® ethyl 4-(dimethylamino)benzoate from *Sigma Aldrich* as internal calibrant (Cushman et al., 2014; Pauli et al., 2014). High resolution mass spectrometry was performed on a Finnigan MAT 95 (EI) or a Finnigan LTQ FT (ESI). Melting points were determined with a Büchi 510 melting point apparatus and are uncorrected. For IR spectroscopy, an FT-IR Spectrometer 1600 from *PerkinElmer* was used.

General Procedures

Mitsunobu-reaction on phenols 56 and 62 (GP1):

To a slurry of the respective phenols **56** or **62** (1.0 equiv), the corresponding alcohol (1.3 equiv) and PPh_3 (1.3 equiv) in dry THF (2.0-2.4 mL/mmol), DIAD (1.3 equiv) was added at 0 °C in portions. The resulting solution was stirred at rt for 1.5-24 h, quenched with water (2 mL/mmol) and extracted with EtOAc (4 mL/mmol) or CH_2Cl_2 (2-4 mL/mmol). The organic phase was separated, washed with brine (2 mL/mmol), dried over $MgSO_4$, filtrated and the solvent was removed in vacuo. The crude product was purified via FC [0% to 20% MeOH in CH_2Cl_2 or 5% 4 M NH_3 (in MeOH) in CH_2Cl_2].

Formation of 2-amino-3*H*-indoles by intramolecular cyclisation (GP2):

A suspension of the respective 2-amino-3*H*-indoles precursor molecules **58a-d** or **63** (1.0 equiv) and Pd/C (10%, 0.18 equiv) in AcOH (5.8-6 mL/mmol) was stirred under hydrogen atmosphere (1 bar) at rt for 24 h. The reaction mixture was filtrated over celite, washed with EtOH (30 mL/mmol) and the solvent was evaporated. The residue was solved in CH_2Cl_2

(8 mL/mmol) and stirred with K_2CO_3 (10 equiv) until gas formation stopped (30 min). After anew filtration and evaporation of the solvent, the crude product was purified via FC [10% to 20% 3 M NH_3 (in MeOH) in CH_2Cl_2]. The product fractions were dissolved in CH_2Cl_2, filtered through a syringe filter (PTFE, 0.2 µm), concentrated and then lyophilized (4 mL/mmol, H_2O bidist.) to obtain the hygroscopic products as solids.

2-[4-(Benzyloxy)-5-methoxy-2-nitrophenyl]acetonitrile (54)

A solution of **51** (1.06 g, 4.20 mmol, 1.0 equiv) in AcOH and Ac_2O (3.0 mL, 1:1) was added dropwise to a mixture of AcOH, Ac_2O and HNO_3 (9.0 mL, 1:1:1) at 0 °C and stirred for 30 min. The reaction mixture was poured over ice and stirred for 10 min. **54** (1.13 g, 90%) was isolated without further purification as beige precipitate after filtration, wash with cold water (10 mL) and drying in vacuo.

m.p. 137 °C; ^{1}H NMR (500 MHz, $CDCl_3$): δ = 4.02 (s, 3 H, CH_3O), 4.21 (s, 2 H, CH_2CN), 5.21 (s, 2 H, CH_2O), 7.10 (s, 1 H, C*H*COCH$_3$), 7.32-7.50 (m, 5 H, C*H*C*H*C*H*CCH$_2$O), 7.83 (s, 1 H, CHCNO$_2$); ^{13}C NMR (126 MHz, $CDCl_3$): δ = 23.18 (*C*CN), 56.80 (CH_3O), 71.53 (CH_2O), 110.91 (*C*HCNO$_2$), 112.48 (*C*HCOCH$_3$), 116.91 (CN), 120.60 (*C*CNO$_2$), 127.73 (*C*HCCH$_2$O), 128.68 (*C*HCHCHCCH$_2$O), 128.97 (*C*HCHCCH$_2$O), 135.42 (*C*CH$_2$O), 139.89 (CNO$_2$), 147.88 (*C*OCH$_2$), 154.58 (*C*OCH$_3$); IR (KBr): $\tilde{\nu}$ = 1585, 1511, 1366, 1281, 741 cm^{-1}; HRMS (EI): *m*/*z* calcd for $C_{16}H_{14}N_2O_4$: 298.0954 [*M*]$^+$; found: 298.0948.

2-[4-(Benzyloxy)-5-methoxy-2-nitrophenyl]-2-methylpropanenitrile (55) (Fagan et al., 2019; Luise et al., 2021)

To a solution of **54** (597 mg, 2.00 mmol, 1.0 equiv) and NaOH (aq. 50 wt%, 320 mg, 8.00 mmol, 4.0 equiv) in DMSO (3.4 mL) at 0 °C, iodomethane (500 µL, 1.15 g, 8.00 mmol, 4.0 equiv) was added dropwise over 30 min. After stirring for 2 h, H_2O (34 mL) was added and the mixture was extracted with toluene (3 × 10 mL). The organic phase was dried over Na_2SO_4, filtered and the solvent was removed in vacuo, to afford **55** (618 mg, 95%) without further purification as brown solid.

m.p. 139 °C; ^{1}H NMR (500 MHz, $CDCl_3$): δ = 1.89 (s, 6 H, CCH_3), 3.98 (s, 3 H, CH_3O), 5.17 (s, 2 H, CH_2O), 7.06 (s, 1 H, C*H*COCH$_3$), 7.31-7.45 (m, 6 H, C*H*C*H*C*H*CCH$_2$OCC*H*); ^{13}C NMR (126 MHz, $CDCl_3$): δ = 28.51 (C*C*H$_3$), 36.53 (*C*CH$_3$), 56.60 (CH_3O), 71.51 (CH_2O), 110.28 (*C*HCOCH$_3$), 111.20 (*C*HCNO$_2$), 123.13 (CN), 127.66 (*C*HCCH$_2$O), 127.91 (*C*CNO$_2$), 128.65 (*C*HCHCHCCH$_2$O), 128.96 (*C*HCHCCH$_2$O), 135.50 (*C*CH$_2$O), 142.36 (CNO$_2$), 147.53

(*C*OCH$_2$), 152.69 (*C*OCH$_3$); IR (KBr): $\tilde{\nu}$ = 1521, 1275, 1217, 1045, 750 cm^{-1}; HRMS (EI): *m/z* calcd for $C_{18}H_{18}N_2O_4$: 326.1267 [*M*]$^+$; found: 326.1263.

2-(4-Hydroxy-5-methoxy-2-nitrophenyl)-2-methylpropanenitrile (56) (Luise et al., 2021)

A suspension of **55** (392 mg, 1.13 mmol, 1.0 equiv) and Pd/C (10%, 253 mg, 0.237 mmol, 0.21 equiv) in EtOAc and EtOH (30 mL, 9:1) was stirred for 5.5 h under H_2-Amosphere (2.5 bar) at rt. After filtration over celite, wash with MeOH (35 mL) and evaporating of the solvent, the crude product was purified via FC (CH_2Cl_2), to afford **56** as yellow solid (159 mg, 60%).

R_f = 0.25 (CH_2Cl_2); m.p. 147 °C; ^{1}H NMR (400 MHz, CD_3OD): δ = 1.88 (s, 6 H, CH_3C), 3.97 (s, 3 H, CH_3O), 7.08 (s, 1 H, C*H*COH), 7.29 (s, 1 H, $CHCNO_2$); ^{13}C NMR (101 MHz, CD_3OD): δ = 29.29 (*C*H$_3$C), 36.45 (CH$_3$*C*), 56.90 (CH_3O), 110.77 (*C*HCOH), 113.70 (*C*HCNO$_2$), 124.02 (CN), 127.10 (*C*CCN), 144.00 (CNO_2), 147.79 (COH), 152.50 (*C*OCH$_3$); IR (KBr): $\tilde{\nu}$ = 2938, 2249, 1530, 1224, 1048 cm^{-1}; HRMS (EI): *m*/*z* calcd for $C_{11}H_{12}N_2O_4$: 236.0797 [*M*]$^+$; found: 236.0791.

2-{5-Methoxy-2-nitro-4-[2-(pyrrolidin-1-yl)ethoxy]phenyl}-2-methylpropanenitrile (58a)

According to GP1 from **56** (236 mg, 1.00 mmol, 1.0 equiv), 2-pyrrolidin-1-ylethanol (157 µl, 154 mg, 1.30 mmol, 1.3 equiv), PPh_3 (344 mg, 1.30 mmol, 1.3 equiv) and DIAD (269 µL, 277 mg, 1.30 mmol, 1.3 equiv) in THF (2.0 mL). Reaction time: 24 h. Reaction was quenched with H_2O (2.0 mL) and extracted with EtOAc (4.0 mL). **58a** (210 mg, 63%) was isolated as yellow oil via FC (0% to 5% MeOH in CH_2Cl_2).

R_f = 0.21 (5% MeOH in CH_2Cl_2); ^{1}H NMR (500 MHz, CD_3OD): δ = 1.81-1.86 (m, 4 H, C*H*$_2$CH$_2$NCH$_2$CH$_2$O), 1.90 (s, 6 H, CH_3CCN), 2.67-2.74 (m, 4 H, C*H*$_2$NCH$_2$CH$_2$O), 2.98 (t, *J* = 5.5 Hz, 2 H, NC*H*$_2$CH$_2$O), 3.96 (s, 3 H, CH_3O), 4.21 (t, *J* = 5.5 Hz, 2 H, CH_2O), 7.13 (s, 1 H, C*H*COCH$_3$), 7.50 (s, 1 H, $CHCNO_2$); ^{13}C NMR (126 MHz, CD_3OD): δ = 24.25 (*C*H$_2$CH$_2$NCH$_2$CH$_2$O), 29.22 (*C*H$_3$CCN), 36.57 (*C*CN), 55.61 (*C*H$_2$CH$_2$O), 55.69 (*C*H$_2$NCH$_2$CH$_2$O), 56.93 (CH_3O), 69.41 (CH_2O), 110.95 (*C*HCOCH$_3$), 111.66 (*C*HCNO$_2$), 123.82 (CN), 128.95 (*C*CNO$_2$), 143.75 (CNO_2), 149.00 (*C*OCH$_2$), 154.15 (*C*OCH$_3$); IR (KBr): $\tilde{\nu}$ = 2935, 1530, 1347, 1276 cm^{-1}; HRMS (ESI): *m*/*z* calcd for $C_{17}H_{23}N_3O_4$+H$^+$: 334.1767 [*M*+H]$^+$; found: 334.1763.

2-{5-Methoxy-2-nitro-4-[3-(pyrrolidin-1-yl)propoxy]phenyl}-2-methylpropanenitrile (58b) (Luise et al., 2021; Sweis et al., 2014)

According to GP1 from **56** (118 mg, 0.500 mmol, 1.0 equiv), 3-pyrrolidin-1-ylpropan-1-ol (92.2 µL, 88.4 mg, 0.650 mmol, 1.3 equiv), PPh_3 (172 mg, 0.650 mmol, 1.3 equiv) and DIAD (134 µL, 138 mg, 0.650 mmol, 1.3 equiv) in THF (1.0 mL). Reaction time: 1.5 h. Reaction was quenched with H_2O (1.0 mL) and extracted with CH_2Cl_2 (2.0 mL). **58b** (140 mg, 81%) was isolated as yellow oil via FC (5% to 10% MeOH in CH_2Cl_2).

R_f = 0.14 (10% MeOH in CH_2Cl_2); ^{1}H NMR (500 MHz, CD_3OD): δ = 1.89 (s, 6 H, CH_3C), 1.95-2.06 (m, 4 H, C*H*$_2$CH$_2$NCH$_2$CH$_2$CH$_2$O), 2.14-2.26 (m, 2 H, C*H*$_2$CH$_2$O), 3.07-3.13 (m, 4 H, C*H*$_2$NCH$_2$CH$_2$CH$_2$O), 3.11-3.17 (m, 3 H, C*H*$_2$CH$_2$CH$_2$O), 3.97 (s, 3 H, CH_3O), 4.18 (t, *J* = 5.9 Hz, 2 H, CH_2O), 7.12 (s, 1 H, C*H*COCH$_3$), 7.48 (s, 1 H, $CHCNO_2$). ^{13}C NMR (126 MHz, CD_3OD): δ = 24.06 (*C*H$_2$CH$_2$NCH$_2$CH$_2$CH$_2$O), 27.76 (*C*H$_2$CH$_2$O), 29.27 (*C*H$_3$C), 36.45 (CH$_3$*C*), 54.07 (*C*H$_2$CH$_2$CH$_2$O), 55.22 (*C*H$_2$NCH$_2$CH$_2$CH$_2$O), 57.06 (CH_3O), 68.41 (CH_2O), 110.81 (*C*HCOCH$_3$), 111.42 (*C*HCNO$_2$), 123.82 (CN), 129.05 (*C*CCN), 143.64 (CNO_2), 148.79 (*C*CHCNO$_2$), 153.99 (*C*OCH$_3$); IR (KBr): ṽ = 2939, 2236, 1524, 1349 cm^{-1}; HRMS (ESI): *m*/*z* calcd for $C_{18}H_{25}N_3O_4$+H$^+$: 348.1923 [*M*+H]$^+$; found: 348.1920.

2-[4-(4-Chlorobutoxy)-5-methoxy-2-nitrophenyl]-2-methylpropanenitrile (57)

According to GP1 from **56** (472 mg, 2.00 mmol, 1.0 equiv), 4-chlorobutan-1-ol (305 µL, 332 mg, 2.60 mmol, 1.3 equiv), PPh_3 (696 mg, 2.60 mmol, 1.3 equiv) and DIAD (537 µL, 553 mg, 2.60 mmol, 1.3 equiv) in THF (4.0 mL). Reaction time: 24 h. Reaction was quenched with H_2O (4.0 mL) and extracted with CH_2Cl_2 (4.0 mL). **57** (628 mg, 96%) was isolated as yellow oil via FC (CH_2Cl_2). (CH_2Cl_2/MeOH 19:1 → 9:1).

R_f = 0.78 (CH_2Cl_2); ^{1}H NMR (500 MHz, CD_2Cl_2): δ = 1.88 (s, 6 H, CH_3C), 1.93-2.01 (m, 4 H, C*H*$_2$C*H*$_2$CH$_2$Cl), 3.62-3.68 (m, 2 H, CH_2Cl), 3.94 (s, 3 H, CH_3O), 4.02-4.10 (m, 2 H, CH_2O), 6.97 (s, 1 H, CHCCCN), 7.35 (s, 1 H, $CHCNO_2$); ^{13}C NMR (126 MHz, CD_2Cl_2): δ = 26.79 (*C*H$_2$CH$_2$O), 29.03 (*C*H$_3$C), 29.62 (*C*H$_2$CH$_2$Cl), 35.99 (CH$_3$*C*), 45.18 (CH_2Cl), 56.81 (CH_3O), 69.16 (CH_2O), 110.13 (*C*HCCCN), 110.66 (*C*HCNO$_2$), 123.10 (CN), 128.07 (*C*CCN), 142.74 (CNO_2), 148.16 (*C*OCH$_2$), 153.00 (*C*OCH$_3$); IR (KBr): ṽ = 2943, 1527, 1275, 1225, 1043 cm^{-1}; HRMS (EI): *m*/*z* calcd for $C_{15}H_{19}N_2O_4Cl$: 326.1033 [*M*]$^+$; found: 326.1028.

2-{5-Methoxy-2-nitro-4-[4-(pyrrolidin-1-yl)butoxy]phenyl}-2-methylpropanenitrile (58c)

A mixture of **57** (261 mg, 0.800 mmol, 1.0 equiv), KI (266 mg, 1.60 mmol, 2.0 equiv) and K_2CO_3 (332 mg, 2.40 mmol, 3.0 equiv) in pyrrolidine (98.5 µL, 85.3 mg, 1.20 mmol, 1.5 equiv) was stirred for 72 h at 50 °C. After cooling down, the solvent was removed in vacuo and the crude product purified via FC [10% 3 M NH_3 (in MeOH) in CH_2Cl_2] to isolate **58c** (188 mg, 65%) as yellow oil.

R_f = 0.51 [10% 4 M NH_3 (in MeOH) in CH_2Cl_2]; ^{1}H NMR (400 MHz, CD_2Cl_2): δ = 1.57-1.70 (m, 2 H, C*H*$_2$CH$_2$CH$_2$O), 1.70-1.79 (m, 4 H, C*H*$_2$CH$_2$NCH$_2$CH$_2$CH$_2$CH$_2$O), 1.87 (s, 8 H, C*H*$_2$CH$_2$O, CH$_3$C), 2.31-2.58 (m, 6 H, C*H*$_2$NC*H*$_2$CH$_2$CH$_2$CH$_2$O), 3.93 (s, 3 H, CH$_3$O), 4.06 (t, *J* = 6.6 Hz, 2 H, CH$_2$O), 6.96 (s, 1 H, CHCCCN), 7.35 (s, 1 H, CHCNO$_2$); ^{13}C NMR (101 MHz, CD_2Cl_2): δ = 23.88 (*C*H$_2$CH$_2$NCH$_2$CH$_2$CH$_2$CH$_2$O), 25.63 (*C*H$_2$CH$_2$CH$_2$O), 27.31 (*C*H$_2$CH$_2$O), 29.05 (CH$_3$*C*), 35.98 (CH$_3$*C*), 54.44 (C*H*$_2$NCH$_2$CH$_2$CH$_2$CH$_2$O), 56.12 (*C*H$_2$CH$_2$CH$_2$CH$_2$O), 56.82 (CH$_3$O), 69.82 (CH$_2$O), 110.10 (*C*HCCCN), 110.49 (*C*HCNO$_2$), 123.16 (CN), 127.71 (*C*CCN), 142.81 (CNO$_2$), 148.40 (CH$_2$O*C*), 152.94 (CH$_3$O*C*); IR (film): ṽ = 2924, 1639, 1527, 1275 cm^{-1}; HRMS (ESI): *m*/*z* calcd for $C_{19}H_{27}N_3O_4$+H$^+$: 362.2080 [*M*+H]$^+$; found: 362.2077.

2-{5-Methoxy-2-nitro-4-[4-(piperidin-1-yl)butoxy]phenyl}-2-methylpropanenitrile (58d)

A mixture of **57** (20.3 mg, 62.0 µmol, 1.0 equiv), KI (20.6 mg, 0.124 mmol, 2.0 equiv) and piperidine (612 µL, 528 mg, 6.20 mmol, 100 equiv) was stirred for 20 h at 50 °C. After cooling down, the solvent was removed in vacuo and the crude product purified via FC [10% 3 M NH_3 (in MeOH) in CH_2Cl_2] to isolate **58d** (22.3 mg, 96%) as yellow oil.

R_f = 0.50 [10% 4 M NH_3 (in MeOH) in CH_2Cl_2]; ^{1}H NMR (500 MHz, CD_2Cl_2): δ = 1.37-1.45 (m, 2 H, C*H*$_2$CH$_2$CH$_2$NCH$_2$CH$_2$CH$_2$CH$_2$O), 1.50-1.57 (m, 4 H, C*H*$_2$CH$_2$NCH$_2$CH$_2$CH$_2$CH$_2$O), 1.57-1.66 (m, 2 H, C*H*$_2$CH$_2$CH$_2$O), 1.78-1.92 (m, 8 H, C*H*$_2$CH$_2$O, C*H*$_3$C), 2.13-2.55 (m, 6 H, C*H*$_2$NC*H*$_2$CH$_2$CH$_2$CH$_2$O), 3.94 (s, 3 H, CH$_3$O), 4.05 (t, *J* = 6.7 Hz, 2 H, CH$_2$O), 6.96 (s, 1 H, CHCCCN), 7.35 (s, 1 H, CHCNO$_2$); ^{13}C NMR (126 MHz, CD_2Cl_2): δ = 23.79 (*C*H$_2$CH$_2$CH$_2$O), 25.14 (*C*H$_2$CH$_2$CH$_2$NCH$_2$CH$_2$CH$_2$CH$_2$O), 26.66 (*C*H$_2$CH$_2$NCH$_2$CH$_2$CH$_2$CH$_2$O), 27.49 (*C*H$_2$CH$_2$O, 29.20 (*C*H$_3$C), 36.12 (CH$_3$*C*), 55.14 (*C*H$_2$NCH$_2$CH$_2$CH$_2$CH$_2$O), 56.96 (CH$_3$O), 59.21 (*C*H$_2$CH$_2$CH$_2$CH$_2$O), 69.99 (CH$_2$O), 110.21 (*C*HCCCN4), 110.61 (*C*HCNO$_2$), 123.30 (CN), 127.85 (*C*CCN), 142.94 (CNO$_2$), 148.54 (*C*OCH$_2$), 153.08 (*C*OCH$_3$); IR (film): ṽ = 2935, 1527, 1275, 1043 cm^{-1}; HRMS (ESI): *m*/*z* calcd for $C_{20}H_{29}N_3O_4$+H$^+$: 376.2236 [*M*+H]$^+$; found: 376.2231.

5-Methoxy-3,3-dimethyl-6-[2-(pyrrolidin-1-yl)ethoxy]-3*H*-indol-2-amine (59a) and 2-amino-5-methoxy-3,3-dimethyl-6-[2-(pyrrolidin-1-yl)ethoxy]-3*H*-indol 1-oxide (60a)

A suspension of **8a** (167 mg, 0.500 mmol, 1.0 equiv) and Pd/C (10%, 160 mg, 0.150 mmol, 0.30 equiv) in AcOH (3.0 mL) was stirred under H_2-atmosphere (10 bar) for 160 h at rt. After filtration and wash with MeOH (10 mL), the solvent was removed in vacuo. The residue was resolved in CH_2Cl_2 (2 mL) and stirred with K_2CO_3 (1.38 g, 10.0 mmol, 20 equiv) until gas formation stopped (2 h). The mixture was filtrated and the solvent evaporated. Purification via FC [15% 1 M NH_3 (in MeOH) in CH_2Cl_2] afforded **59a** (71.4 mg, 47%) as yellow and **60a** (24.4 mg, 15%) as brown solid.

59a: Purity: 99%; R_f = 0.41 [20% 1 M NH_3 (in MeOH) in CH_2Cl_2]; m.p. 66 °C; ^{1}H NMR (500 MHz, CD_3OD): δ = 1.38 (s, 6 H, CH_3C), 1.94-2.01 (m, 4 H, C*H*$_2$CH$_2$NCH$_2$CH$_2$O), 3.05-3.15 (m, 4 H, C*H*$_2$NCH$_2$CH$_2$O), 3.27 (t, *J* = 5.4 Hz, 2 H, C*H*$_2$CH$_2$O), 3.84 (s, 3 H, CH_3O), 4.21 (t, *J* = 5.4 Hz, 2 H, CH_2O), 6.78 (s, 1 H, CHCN), 6.97 (s, 1 H, CHCCN); ^{13}C NMR (126 MHz, CD_3OD): δ = 24.08 (*C*H$_2$CH$_2$NCH$_2$CH$_2$O), 25.12 (*C*H$_3$C), 49.93 (CH$_3$*C*), 55.62 (*C*H$_2$NCH$_2$CH$_2$O), 55.73 (*C*H$_2$CH$_2$O), 57.55 (CH_3O), 68.25 (CH_2O), 104.30 (*C*HCN), 108.65 (*C*HCCN), 135.20 (*C*CCNH$_2$), 146.01 (*C*NCNH$_2$), 147.22 (*C*OCH$_3$), 149.15 (*C*OCH$_2$), 182.11 (CNH_2); IR (KBr): $\tilde{\nu}$ = 2964, 1649, 1558, 1489, 1165 cm^{-1}; HRMS (ESI): *m*/*z* calcd for $C_{17}H_{25}N_3O_2$+H$^+$: 304.2025 [*M*+H]$^+$; found: 304.2021.

60a: Purity: 85%; R_f = 0.18 [20% 1 M NH_3 (in MeOH) in CH_2Cl_2]; m.p. 146 °C; ^{1}H NMR (500 MHz, CD_3OD): δ = 1.48 (s, 6 H, CH_3C), 2.06-2.19 (m, 4 H, C*H*$_2$CH$_2$NCH$_2$CH$_2$O), 3.41-3.58 (m, 4 H, C*H*$_2$NCH$_2$CH$_2$O), 3.63-3.69 (m, 2 H, C*H*$_2$CH$_2$O), 3.91 (s, 3 H, CH_3O), 4.30-4.41 (m, 2 H, CH_2O), 7.06 (s, 1 H, CHCN), 7.22 (s, 1 H, CHCCN); ^{13}C NMR (126 MHz, CD_3OD): δ = 23.93 (*C*H$_2$CH$_2$NCH$_2$CH$_2$O), 24.29 (*C*H$_3$C), 45.42 (CH$_3$*C*), 55.27 (*C*H$_2$CH$_2$O), 55.77 (*C*H$_2$NCH$_2$CH$_2$O), 57.34 (CH_3O), 66.87 (CH_2O), 100.63 (*C*HCN), 108.31 (*C*HCCN), 130.58 (*C*CCNH$_2$), 138.25 (*C*HCNH$_2$), 148.84 (*C*OCH$_2$), 149.47 (*C*OCH$_3$), 163.39 (CNH_2); IR (KBr): $\tilde{\nu}$ = 2972, 1662, 1496, 1173 cm^{-1}; HRMS (ESI): *m*/*z* calcd for $C_{17}H_{25}N_3O_3$+H$^+$: 320.1974 [*M*+H]$^+$; found: 320.1970.

5-Methoxy-3,3-dimethyl-6-[3-(pyrrolidin-1-yl)propoxy]-3*H*-indol-2-amine (59b) (Luise et al., 2021; Sweis et al., 2014) **and 2-amino-5-methoxy-3,3-dimethyl-6-[3-(pyrrolidin-1-yl)-propoxy]-3*H*-indol 1-oxide (60b)**

According to **GP2** from **58b** (278 mg, 0.800 mmol, 1.0 equiv) and Pd/C (10%, 153 mg, 0.144 mmol, 0.18 equiv) in AcOH (4.6 mL) under H_2-atmosphere (1 bar). **59b** (40.4 mg, 16%) and **60b** (154 mg, 57%) were isolated as beige solids.

59b: Purity: 99%; R_f = 0.50 [15% 3 M NH_3 (in MeOH) in CH_2Cl_2]; m.p. 51 °C; ^{1}H NMR (500 MHz, CD_2Cl_2): δ = 1.31 (s, 6 H, CH_3C), 1.73-1.84 (m, 4 H, C*H*$_2$CH$_2$NCH$_2$CH$_2$CH$_2$O), 1.94-2.07 (m, 2 H, C*H*$_2$CH$_2$O), 2.48-2.62 (m, 4 H, C*H*$_2$NCH$_2$CH$_2$CH$_2$O), 2.67 (t, *J* = 7.4 Hz, 2 H, C*H*$_2$CH$_2$CH$_2$O), 3.80 (s, 3 H, CH_3O), 4.03 (t, *J* = 6.5 Hz, 2 H, CH_2O), 6.75 (s, 1 H, CHCCN), 6.78 (s, 1 H, CHCN); ^{13}C NMR (126 MHz, CD_2Cl_2): δ = 23.90 (*C*H$_2$CH$_2$NCH$_2$CH$_2$CH$_2$O), 25.22 (*C*H$_3$C), 29.00 (*C*H$_2$CH$_2$O), 49.23 (*C*CH$_3$), 53.28 (*C*H$_2$CH$_2$CH$_2$O), 54.46 (*C*H$_2$NCH$_2$CH$_2$CH$_2$O), 57.57 (CH_3O), 67.97 (CH_2O), 103.75 (*C*HCN), 107.76 (*C*HCCN), 133.87 (*C*CCNH$_2$), 145.52 (*C*OCH$_3$), 148.22 (*C*NCNH$_2$), 149.20 (*C*CHCN), 179.51 (CNH_2); IR (KBr): $\tilde{\nu}$ = 2926, 1651, 1560, 1489, 1165 cm^{-1}; HRMS (ESI): *m*/*z* calcd for $C_{18}H_{27}N_3O_2$+H$^+$: 318.2182 [*M*+H]$^+$; found: 318.2176

60b: Purity: 98%; R_f = 0.35 [15% 3 M NH_3 (in MeOH) in CH_2Cl_2]; m.p. 186 °C; ^{1}H NMR (500 MHz, CD_2Cl_2): δ = 1.39 (s, 6 H, CH_3C), 1.67-1.81 (m, 4 H, C*H*$_2$CH$_2$NCH$_2$CH$_2$CH$_2$O), 1.91-2.04 (m, 2 H, C*H*$_2$CH$_2$O), 2.42-2.54 (m, 4 H, C*H*$_2$NCH$_2$CH$_2$CH$_2$O), 2.59 (t, *J* = 7.2 Hz, 2 H, C*H*$_2$CH$_2$CH$_2$O), 3.83 (s, 3 H, CH_3O), 4.09 (t, *J* = 6.6 Hz, 2 H, CH_2O), 6.82 (s, 1 H, CHCCN), 7.08 (s, 1 H, CHCN); ^{13}C NMR (126 MHz, CD_2Cl_2): δ = 23.88 (*C*H$_2$CH$_2$NCH$_2$CH$_2$CH$_2$O), 24.59 (*C*H$_3$C), 28.83 (*C*H$_2$CH$_2$O), 44.13 (CH$_3$*C*), 53.07 (*C*H$_2$CH$_2$CH$_2$O), 54.43 (*C*H$_2$NCH$_2$CH$_2$CH$_2$O), 57.37 (CH_3O), 68.06 (CH_2O), 97.99 (*C*HCN), 107.12 (*C*HCCN), 127.16 (*C*CCNH$_2$), 138.11 (*C*NCNH$_2$), 147.70 (*C*OCH$_3$), 149.71 (*C*CHCN), 160.14 (CNH_2); IR (KBr): $\tilde{\nu}$ = 2927, 1668, 1495, 1198 cm^{-1}; HRMS (ESI): *m*/*z* calcd for $C_{18}H_{27}N_3O_3$+H$^+$: 334.2131[*M*+H]$^+$; found: 334.2126.

5-Methoxy-3,3-dimethyl-6-[4-(pyrrolidin-1-yl)butoxy]-3*H*-indol-2-amine (59c) and 2-amino-5-methoxy-3,3-dimethyl-6-[4-(pyrrolidin-1-yl)butoxy]-3*H*-indol 1-oxide (60c)

According to **GP2** from **58c** (181 mg, 0.500 mmol, 1.0 equiv) and Pd/C (10%, 95.8 mg, 0.0900 mmol, 0.18 equiv) in AcOH (3.0 mL) under H_2-atmosphere (1 bar). **59c** (43.2 mg, 26%) and **60c** (85.3 mg, 49%) were isolated as beige solids.

59c: Purity: 98%; R_f = 0.38 [15% 3 M NH_3 (in MeOH) in CH_2Cl_2]; m.p. 42 °C (Hygroscopic); ^{1}H NMR (500 MHz, CD_2Cl_2): δ = 1.39 (s, 6 H, CH_3C), 1.61-1.71 (m, 2 H, C*H*$_2$CH$_2$CH$_2$O), 1.71-1.79 (m, 4 H, C*H*$_2$CH$_2$NCH$_2$CH$_2$CH$_2$CH$_2$O), 1.79-1.89 (m, 2 H, C*H*$_2$CH$_2$O), 2.40-2.59 (m, 6 H, C*H*$_2$NC*H*$_2$CH$_2$CH$_2$CH$_2$O), 3.83 (s, 3 H, CH_3O), 4.05 (t, *J* = 6.6 Hz, 2 H, CH_2O), 6.83 (s, 1 H, C*H*CCCNH$_2$), 7.06 (s, 1 H, CHCN); ^{13}C NMR (126 MHz, CD_2Cl_2): δ = 23.82 (*C*H$_2$CH$_2$NCH$_2$CH$_2$CH$_2$CH$_2$O), 24.58 (*C*H$_3$C), 25.37 (*C*H$_2$CH$_2$CH$_2$O), 27.49 (*C*H$_2$CH$_2$O), 44.07 (CH$_3$*C*), 54.32 (*C*H$_2$NCH$_2$CH$_2$CH$_2$CH$_2$O), 56.14 (*C*H$_2$CH$_2$CH$_2$CH$_2$O), 57.37 (CH_3O), 69.60 (CH_2O), 98.04 (*C*HCN), 107.10 (*C*HCCCNH$_2$), 127.22 (*C*CCNH$_2$), 138.23 (*C*NCNH$_2$), 147.68

(CH_3OC), 149.69 (CH_2OC), 159.62 (CNH_2); IR (KBr): $\tilde{\nu}$ = 2927, 1643, 1560, 1489, 1215 cm^{-1}; HRMS (ESI): *m*/*z* calcd for $C_{19}H_{29}N_3O_2+H^+$: 332.2338 [*M*+H]$^+$; found: 332.2333.

60c: Purity: 90%. R_f = 0.27 [15% 3 M NH_3 (in MeOH) in CH_2Cl_2]; m.p. 192 °C; ^{1}H NMR (500 MHz, CD_2Cl_2): δ = 1.31 (s, 6 H, CH_3C), 1.68-1.78 (m, 2 H, $CH_2CH_2CH_2O$), 1.78-1.87 (m, 6 H, $CH_2CH_2NCH_2CH_2CH_2CH_2O$), 2.59-2.70 (m, 6 H, $CH_2NCH_2CH_2CH_2CH_2O$), 3.80 (s, 3 H, CH_3O), 3.99 (t, *J* = 6.4 Hz, 2 H, CH_2O), 6.76 (s, 1 H, $CHCCCNH_2$), 6.77 (s, 1 H, CHCNO); ^{13}C NMR (126 MHz, CD_2Cl_2): δ = 23.84 ($CH_2CH_2NCH_2CH_2CH_2CH_2O$), 25.21 ($CH_3C$), 25.35 ($CH_2CH_2CH_2O$), 27.64 ($CH_2CH_2O$), 49.21 ($CH_3C$), 54.32 ($CH_2NCH_2CH_2CH_2CH_2O$), 56.22 ($CH_2CH_2CH_2CH_2O$), 57.56 ($CH_3O$), 69.45 ($CH_2O$), 103.58 ($CHCNO$), 107.76 ($CHCCNO$), 133.66 ($CCCNH_2$), 145.55 ($CH_3OC$), 147.86 ($CNCNH_2$), 149.21 ($CH_2OC$), 179.59 ($CNH_2$); IR (KBr): $\tilde{\nu}$ = 2926, 1660, 1495, 1198 cm^{-1}; HRMS (ESI): *m*/*z* calcd for $C_{19}H_{29}N_3O_3+H^+$: 348.2287 [*M*+H]$^+$; found: 348.2283.

5-Methoxy-3,3-dimethyl-6-[4-(piperidin-1-yl)butoxy]-3*H*-indol-2-amine (59d) and 2-amino-5-methoxy-3,3-dimethyl-6-[4-(piperidin-1-yl)butoxy]-3*H*-indol 1-oxide (60d)

According to **GP2** from **58d** (203 mg, 0.540 mmol, 1.0 equiv) and Pd/C (10%, 103 mg, 0.0972 mmol, 0.18 equiv) in AcOH (3.2 mL) under H_2-atmosphere (1 bar). **59d** (76.7 mg, 41%) and **60d** (69.6 mg, 36%) were isolated as beige solids.

59d: Purity: 98%; R_f = 0.62 [15% 3 M NH_3 (in MeOH) in CH_2Cl_2]; m.p. 102 °C; ^{1}H NMR (500 MHz, CD_2Cl_2): δ = 1.31 (s, 6 H, CH_3C), 1.37-1.45 (m, 2 H, $CH_2CH_2CH_2NCH_2CH_2CH_2CH_2O$), 1.47-1.59 (m, 4 H, $CH_2CH_2NCH_2CH_2CH_2CH_2O$), 1.59-1.67 (m, 2 H, $CH_2CH_2CH_2O$), 1.73-1.83 (m, 2 H, CH_2CH_2O), 2.15-2.60 (m, 6 H, $CH_2NCH_2CH_2CH_2CH_2O$), 3.80 (s, 3 H, CH_3O), 3.98 (t, *J* = 6.6 Hz, 2 H, CH_2O), 6.75 (s, 1 H, CHCCN), 6.77 (s, 1 H, CHCN); ^{13}C NMR (126 MHz, CD_2Cl_2): δ = 23.80 ($CH_2CH_2CH_2O$), 24.94 ($CH_2CH_2CH_2NCH_2CH_2CH_2CH_2O$), 25.22 ($CH_3C$), 26.41 ($CH_2CH_2NCH_2CH_2CH_2CH_2O$), 27.83 ($CH_2CH_2O$), 49.24 ($CH_3C$), 54.95 ($CH_2NCH_2CH_2CH_2CH_2O$), 57.58 ($CH_3O$), 59.27 ($CH_2CH_2CH_2CH_2O$), 69.50 ($CH_2O$), 103.62 ($CHCN$), 107.77 ($CHCCN$), 133.75 ($CCCNH_2$), 145.46 ($CH_3OC$), 148.41 ($CNCNH_2$), 149.30 ($CH_2OC$), 179.52 ($CNH_2$); IR (KBr): $\tilde{\nu}$ = 2926, 1643, 1489, 1215, 756 cm^{-1}; HRMS (ESI): *m*/*z* calcd for $C_{20}H_{31}N_3O_2+H^+$: 346.2495 [*M*+H]$^+$; found: 346.2489.

60d: Purity: 99%; R_f = 0.35 [15% 3 M NH_3 (in MeOH) in CH_2Cl_2]; m.p. 178 °C; ^{1}H NMR (500 MHz, CD_2Cl_2): δ = 1.31-1.49 (m, 8 H, CH_3C, $CH_2CH_2CH_2NCH_2CH_2CH_2CH_2O$), 1.49-1.62 (m, 4 H, $CH_2CH_2NCH_2CH_2CH_2CH_2O$), 1.62-1.70 (m, 2 H, $CH_2CH_2CH_2O$), 1.73-1.84 (m, 2 H, CH_2CH_2O), 2.24-2.63 (m, 6 H, $CH_2NCH_2CH_2CH_2CH_2O$), 3.83 (s, 3 H, CH_3O), 4.04 (t, *J* = 6.6 Hz, 2 H, CH_2O), 6.83 (s, 1 H, CHCCNO), 7.05 (s, 1 H, CHCNO); ^{13}C NMR (126 MHz,

CD_2Cl_2): δ = 23.35 (*C*$H_2CH_2CH_2O$), 24.56 (*C*H_3C, *C*$H_2CH_2CH_2NCH_2CH_2CH_2CH_2O$), 25.90 (*C*$H_2CH_2NCH_2CH_2CH_2CH_2O$), 27.51 (*C*$H_2CH_2O$), 44.06 ($CH_3$*C*), 54.70 (*C*$H_2NCH_2CH_2CH_2CH_2O$), 57.35 ($CH_3O$), 58.89 (*C*$H_2CH_2CH_2CH_2O$), 69.61 ($CH_2O$), 98.05 (*C*HCNO), 107.01 (*C*HCCNO), 127.20 (*C*$CCNH_2$), 138.14 (*C*$NCNH_2$), 147.78 (CH_3O*C*), 149.71 (CH_2O*C*), 159.22 (CNH_2); IR (KBr): ṽ = 2926, 1659, 1495, 1198 cm^{-1}; HRMS (ESI): *m*/*z* calcd for $C_{20}H_{31}N_3O_3$+H^+: 362.2444 [*M*+H]$^+$; found: 362.2439.

2-(4,5-Dimethoxy-2-nitrophenyl)-2-methylpropanenitrile (61)

Synthesis from **53** (11.1 g, 50.0 mmol, 1.0 equiv), NaOH (aq. 50 wt%, 8.00 g, 200 mmol, 4.0 equiv) and iodomethane (12.6 mL, 28.7 g, 200 mmol, 4.0 equiv) in DMSO (90 mL) in analogy to **55**. After stirring for 2 h, H_2O (900 mL) was added and the mixture was extracted with toluene (3 × 270 mL). **61** (12.0 g, 96%) was isolated without further purification as brown solid.

m.p. 136 °C; ^{1}H NMR (500 MHz, $CDCl_3$): δ = 1.89 (s, 6 H, CCH_3), 3.93 (s, 3 H, C*H*$_3$OCCHCNO_2), 3.98 (s, 3 H, C*H*$_3$OCCCHCNO_2), 7.04 (s, 1 H, CHCCNO_2), 7.33 (s, 1 H, CHCNO_2); ^{13}C NMR (126 MHz, $CDCl_3$): δ = 28.52 (C*C*H_3), 36.48 (*C*CH_3), 56.56 (*C*H_3OCCHCNO_2), 56.58 (*C*H_3OCCCHCNO_2), 109.16 (*C*HCNO_2), 109.87 (*C*HCCNO_2), 123.10 (CN), 127.57 (*C*CNO_2), 142.55 (CNO_2), 148.48 (*C*CHCNO_2), 152.11 (*C*CCHCNO_2); IR (KBr): ṽ = 2943, 2233, 1530, 1345, 1227 cm^{-1}; HRMS (EI): *m*/*z* calcd for $C_{12}H_{14}N_2O_4$, 250.0954 [*M*]$^+$; found: 250.0958.

2-(5-Hydroxy-4-methoxy-2-nitrophenyl)-2-methylpropanenitrile (62)

Dodecane-1-thiol (1.10 mL, 0.931 g, 4.60 mmol, 2.3 equiv) was added under argon atmosphere to a solution of potassium *tert*-butoxide (0.548 mg, 4.74 mmol, 2.37 equiv) in dry DMF (16 mL) by forming a colorless precipitate. The mixture was cooled to 0 °C and **61** (0.501 mg, 2.00 mmol, 1.0 equiv), dissolved in dry DMF (8 mL), was added dropwise. After stirring for 24 h at rt, the reaction mixture was heated for 45 min to 50 °C and again cooled to rt. NaH_3SO_5 (1.11 g, 8.00 mmol, 4.0 equiv) was added and the mixture was stirred until color change from dark orange to light yellow. The solvent was removed in vacuo and **62** (357 mg, 76%) was isolated via FC [10% 1 M NH_3 (in MeOH) in CH_2Cl_2] as yellow oil.

R_f = 0.51 [10% 1 M NH_3 (in MeOH) in CH_2Cl_2]; ^{1}H NMR (500 MHz, $CDCl_3$): δ = 1.87 (s, 6 H, CH_3C), 3.97 (s, 3 H, CH_3O), 7.10 (s, 1 H, C*H*COH), 7.42 (s, 1 H, CHCNO_2); ^{13}C NMR (126 MHz, $CDCl_3$): δ = 28.97 (*C*H_3C), 35.51 (CH_3*C*), 56.73 (CH_3O), 109.09 (*C*HCOH), 113.37 (*C*HCNO_2), 122.74 (CN), 129.07 (*C*CCN), 142.12 (CNO_2), 145.66 (COH), 149.50 (*C*OCH_3); IR

(KBr): $\tilde{\nu}$ = 2986, 2241, 1519, 1337, 1047 cm^{-1}; HRMS (ESI): *m*/*z* calcd for $C_{11}H_{12}N_2O_4$-H^+: 235.0719 [*M*-H]$^-$; found: 235.0724.

2-{4-Methoxy-2-nitro-5-[3-(pyrrolidin-1-yl)propoxy]phenyl}-2-methylpropanenitrile (63)

According to GP1 from **62** (520 mg, 2.20 mmol, 1.0 equiv), 3-pyrrolidin-1-ylpropan-1-ol (385 µL, 370 mg, 2.86 mmol, 1.3 equiv), PPh_3 (758 mg, 2.86 mmol, 1.3 equiv) and DIAD (591 µL, 609 mg, 2.86 mmol, 1.3 equiv) in THF (4.5 mL). Reaction time: 2 h. Reaction was quenched with H_2O (4.4 mL) and extracted with CH_2Cl_2 (8.8 mL). **63** (499 mg, 65%) was isolated as yellow solid via FC [5% 4 M NH_3 (in MeOH) in CH_2Cl_2].

R_f = 0.15 [5% 4 M NH_3 (in MeOH) in CH_2Cl_2]; m.p. 108 °C; ^{1}H NMR (400 MHz, CD_2Cl_2): δ = 1.68-1.82 (m, 4 H, C*H*$_2$CH$_2$NCH$_2$CH$_2$CH$_2$O), 1.87 (s, 6 H, CH$_3$C), 2.01 (p, *J* = 6.8 Hz, 2 H, C*H*$_2$CH$_2$O), 2.36-2.56 (m, 4 H, C*H*$_2$NCH$_2$CH$_2$CH$_2$O), 2.59 (t, *J* = 7.0 Hz, 2 H, C*H*$_2$CH$_2$CH$_2$O), 3.89 (s, 3 H, CH$_3$O), 4.16 (t, *J* = 6.6 Hz, 2 H, CH$_2$O), 7.00 (s, 1 H, C*H*COCH$_2$), 7.36 (s, 1 H, C*H*COCH$_3$); ^{13}C NMR (101 MHz, CD_2Cl_2): δ = 23.91 (*C*H$_2$CH$_2$NCH$_2$CH$_2$CH$_2$O), 28.95 (*C*H$_3$C), 29.07 (*C*H$_2$CH$_2$O), 35.95 (CH$_3$*C*), 52.84 (*C*H$_2$CH$_2$CH$_2$O), 54.51 (*C*H$_2$NCH$_2$CH$_2$CH$_2$O), 56.80 (CH$_3$O), 68.32 (CH$_2$O), 109.67 (*C*HCOCH$_2$), 111.10 (*C*HCOCH$_2$), 123.16 (CN), 127.99 (*C*CCN), 142.65 (CNO$_2$), 149.08 (*C*OCH$_3$), 152.40 (*C*OCH$_2$); IR (KBr): $\tilde{\nu}$ = 2924, 2236, 1525, 1227 cm^{-1}; HRMS (EI): *m*/*z* calcd for $C_{18}H_{25}N_3O_4$: 347.1845 [*M*]$^+$; found: 347.1838.

6-Methoxy-3,3-dimethyl-5-[3-(pyrrolidin-1-yl)propoxy]-3*H*-indol-2-amine (64) and 2-amino-6-methoxy-3,3-dimethyl-5-[3-(pyrrolidin-1-yl)propoxy]-3*H*-indol 1-oxide (65)

According to **GP2** from **63** (243 mg, 0.700 mmol, 1.0 equiv) and Pd/C (10%, 134 mg, 0.126 mmol, 0.18 equiv) in AcOH (4.0 mL) under H_2-atmosphere (1 bar). **64** (122 mg, 55%) and **65** (18.2 mg, 8%) were isolated as red solids.

64: Purity: 98%; R_f = 0.33 [10% 3 M NH_3 (in MeOH) in CH_2Cl_2]; m.p. 153 °C; ^{1}H NMR (500 MHz, CD_2Cl_2): δ = 1.30 (s, 6 H, CH$_3$C), 1.61-1.83 (m, 4 H, C*H*$_2$CH$_2$NCH$_2$CH$_2$CH$_2$O), 1.95 (p, *J* = 6.9 Hz, 2 H, C*H*$_2$CH$_2$O), 2.42-2.56 (m, 4 H, C*H*$_2$NCH$_2$CH$_2$CH$_2$O), 2.60 (t, *J* = 7.2 Hz, 2 H, C*H*$_2$CH$_2$CH$_2$O), 3.81 (s, 3 H, CH$_3$O), 4.00 (t, *J* = 6.6 Hz, 2 H, CH$_2$O), 6.77 (s, 1 H, CHCN), 6.78 (s, 1 H, CHCCN); ^{13}C NMR (126 MHz, CD_2Cl_2): δ = 23.90 (*C*H$_2$CH$_2$NCH$_2$CH$_2$CH$_2$O), 25.24 (*C*H$_3$C), 29.51 (*C*H$_2$CH$_2$O), 49.21 (CH$_3$*C*), 53.32 (*C*H$_2$CH$_2$CH$_2$O), 54.51 (*C*H$_2$NCH$_2$CH$_2$CH$_2$O), 56.54 (CH$_3$O), 69.20 (CH$_2$O), 102.38 (*C*HCN), 109.26 (*C*HCCN), 133.76 (CH*C*CN), 144.37 (CH$_3$O*C*), 148.74 (CHC*C*N), 150.26 (CH$_2$O*C*), 179.73 (CNH$_2$); IR (KBr): $\tilde{\nu}$ = 2962, 1649, 1487, 1194 cm^{-1}; HRMS (ESI): *m*/*z* calcd for $C_{18}H_{27}N_3O_2$+H^+: 318.2182 [*M*+H]$^+$; found: 318.2176.

65: R_f = 0.25 [30% 3 M NH_3 (in MeOH) in CH_2Cl_2]; mp: 203 °C; ^{1}H NMR (500 MHz, CD_2Cl_2): δ = 1.41 (s, 6 H, CH_3C), 1.86-2.00 (m, 4 H, C*H*$_2$CH$_2$NCH$_2$CH$_2$CH$_2$O), 2.08-2.19 (m, 2 H, C*H*$_2$CH$_2$O), 2.80-3.07 (m, 6 H, C*H*$_2$NC*H*$_2$CH$_2$CH$_2$O), 3.84 (s, 3 H, CH_3O), 4.04 (t, *J* = 6.2 Hz, 2 H, CH_2O), 6.88 (s, 1 H, C*H*CCCNH$_2$), 7.00 (s, 1 H, CHCNO); ^{13}C NMR (126 MHz, CD_2Cl_2): δ = 23.84 (*C*H$_2$CH$_2$NCH$_2$CH$_2$CH$_2$O), 24.61 (*C*H$_3$C), 27.87 (*C*H$_2$CH$_2$O), 44.42 (CH$_3$*C*), 53.21 (*C*H$_2$CH$_2$CH$_2$O), 54.32 (*C*H$_2$NCH$_2$CH$_2$CH$_2$O), 56.77 (CH_3O), 68.70 (CH_2O), 96.58 (*C*HCNO), 109.72 (*C*HCCCNH$_2$), 126.91 (*C*CCNH$_2$), 138.24 (*C*NCNH$_2$), 146.27 (*C*OCH$_2$), 151.03 (*C*OCH$_3$), 162.23 (CNH_2); IR (KBr): $\tilde{\nu}$ = 2926, 1666, 1495, 1454, 1169 cm^{-1}; HRMS (ESI): *m*/*z* calcd for $C_{18}H_{27}N_3O_3$+H$^+$: 334.2131 [M+*H*]$^+$; found: 334.2126.

4.2.2 Determination of Binding Affinities by Means of MS Binding Assay

Competition experiments applying the recently developed UNC0642-MS-Binding Assays were performed as described previously (n = 1) (Bernauer et al., 2024; Kaiser et al., 2024; Nitsche et al., 2024).

4.2.3 Determination of Intrinsic Activities by Means of Rat Diaphragm Myography

All procedures using animals followed animal care regulations. Preparation of rat diaphragm hemispheres from male Wistar rats (300 ± 50 g) and experimental protocol of myography was performed as previously described with slight modifications (Seeger et al., 2012). In short, for all procedures (including wash-out steps, preparation of soman and bispyridinium compound solutions) aerated Tyrode solution (125 mM NaCl, 24 mM $NaHCO_3$, 5.4 mM KCl, 1 mM $MgCl_2$, 1.8 mM $CaCl_2$, 10 mM glucose, 95% O_2, 5% CO_2; pH 7.4; 25 ± 0.5 °C) was used. After the recording of control muscle force, the muscle preparations were incubated in the Tyrode solution, containing 3 µM soman. Following a 20 min wash-out period, the test compounds were added in ascending concentrations (0.1 µM to 300 µM). The incubation time was 20 min for each concentration. The electric field stimulation was performed with 10 µs pulse width and 0.2 A amplitudes. The titanic trains of 20 Hz, 50 Hz, 100 Hz were applied for 1 s and in 10 min intervals. Muscle force was calculated as a time-force integral (area under the curve, AUC) and constrained to values obtained for maximal force generation (muscle force in the presence of Tyrode solution without any additives; 100%). All results were expressed in means ± SD (n = 3-17). For all data analysis, Prism 5.0 (GraphPad Software, San Diego, CA, USA) was used.

5 Zusammenfassung der Arbeit

Bei einer Vergiftung mit phosphororganischen Verbindungen wird das cholinerge System gestört. Die Substanzen, teilweise in Pflanzenschutzmitteln enthalten, aber auch missbräuchlich als Nervengifte eingesetzt, inhibieren irreversibel die Acetylcholinesterase, was zu einer unkontrollierten Akkumulation von Acetylcholin im synaptischen Spalt führt. Dies löst u.a. eine Überstimulation der nikotinischen Acetylcholinrezeptoren aus. Hält diese an, gehen die Rezeptoren in einen desensitisierten, inaktiven Zustand über, was bei unzureichender Behandlung schnell zu Atemlähmung und damit zum Tod führen kann. Standard-Therapieregime bei Organophosphatvergiftungen versuchen, die inhibierte Acetylcholinesterase durch Oxime zu reaktivieren. Gelingt dies, wie im Falle von Vergiftungen mit den Nervenkampfstoffe Tabun und Soman, nicht oder nur unzureichend, besteht eine therapeutische Lücke. Um diese zu schließen, sind dringend neue Wirkstoffe als Therapieoptionen erforderlich. Als vielversprechender Ansatzpunkt gilt die allosterische Modulation desensitisierter, nikotinischer Acetylcholinrezeptoren durch sogenannte Resensitizer. Die für diesen Behandlungsansatz prototypische Verbindung MB327, ein Bispyridiniumsalz, das sowohl in *ex vivo*- als auch in *in vivo*-Experimenten mit Organophosphaten eine vielversprechende Aktivität gezeigt hat, weist aufgrund seiner zu geringen Affinität zum nikotinischen Acetylcholinrezeptor eine für die Anwendung am Menschen zu geringe therapeutische Breite auf. Es war deshalb das Ziel der vorliegenden Arbeit, ausgehend von MB327 und davon abgeleiteter Bispyridiniumverbindungen, wie z.B. PTM0056, sowie ausgehend von den Hits eines im Vorfeld dieser Arbeit durchgeführten Screenings, UNC0646 und A366, neue allosterische Modulatoren als Resensitizer für desensitisierte nAChR zu entwickeln.

MB327-Analoga

In dieser Arbeit wurden zahlreiche von MB327 und PTM0056 abgeleitete Bispyridiniumverbindungen synthetisiert, die sich in der überwiegenden Mehrzahl von MB327 dadurch unterschieden, dass wie bei PTM0056 einer der beiden *tert*-Butyl-Reste in 4-Position der Pyridinium-Teilstrukturen durch Aminosubstituenten ersetzt wurde. Die erhaltenen nichtsymmetrischen Bispyridiniumverbindungen wurden hinsichtlich ihrer biologischen Aktivitäten untersucht. Dabei wurde neben der Affinität zur allosterischen Bindungsstelle MB327-PAM-1 des nAChR von *Torpedo californica* mit Hilfe des UNC0642-MS-Bindungsassays auch die intrinsische Aktivität an mit Soman-vergifteten Ratten-Diaphragmen bestimmt. Zusätzlich wurden *in silico*-Methoden, wie Blind-Docking-Experimente und Molekulardynamik-Simulationen, herangezogen, um das Bindeverhalten der Liganden am nAChR näher zu charakterisieren.

Dies führte zur Identifizierung der potenziellen allosterischen Bindungstasche MB327-PAM-1 und einem Vorschlag für den Bindemodus von MB327. Um in den polaren Bereichen der Bindungstasche stärkere Wechselwirkungen mit den Liganden zu ermöglichen, wurden nicht-symmetrische MB327-Analoga mit polareren Amin-Teilstrukturen anstelle einer der beiden *tert*-Butylgruppen synthetisiert. Ausgehend von 1,3-Diiodpropan und den entsprechenden Pyridinbausteinen wurden die Zielverbindungen in einer Mikrowellen-unterstützten Synthese in zwei Schritten erhalten. Sie wurden allgemein in hoher Ausbeute sowie hoher Reinheit gewonnen. Für die meisten dieser neuen MB327-Analoga konnten bei den Untersuchungen im UNC0642-MS-Bindungsassay, verglichen mit MB327, tatsächlich höhere Bindungs-affinitäten für die MB327-PAM-1-Bindungstasche gefunden werden. Darüber hinaus zeigten einzelne der neuen MB327-Analoga, wie z.B. PTM0069, auch eine stärkere Wiederherstellung der Muskelkraft von mit Soman-vergifteten Ratten-Diaphragmen als MB327. Bemerkens-werterweise waren auch die Konzentrationen, bei denen eine Wiederherstellung der Muskel-kraft festgestellt werden konnte, geringer als im Falle von MB327. Auffällig war jedoch auch ein, bereits für MB327 bekannter, biphasischer Verlauf der Konzentrations-Wirkungskurven. So war bei hohen Konzentrationen nach einem Maximum eine deutliche Abnahme der Muskel-kraft-wiederherstellenden Aktivität zu beobachten. Dies war in Einklang mit *ex vivo*-Versuchen an nicht vergifteten Ratten-Diaphragmen. Hier zeigten die meisten der untersuchten Verbindungen bei höheren Konzentrationen eine Muskelkraft-inhibierende Wirkung. Vermutet wird, dass hierfür ein antagonistischer Effekt an der orthosterischen Bindungsstelle verantwortlich ist. Eine gewisse Affinität von MB327 für die orthosterische Bindungsstelle wurde auch durch *in silico*-Studien vorhergesagt.

Ein weiterer Ansatzpunkt zur Erhöhung der Bindungsaffinität von Liganden in der MB327-PAM-1-Bindungstasche war die Verdrängung von ungünstigen Wasser-Clustern durch Hydroxylgruppen. Tatsächlich konnte für die Verbindung PTMD90-0012, die anstelle eines der beiden 4-*tert*-Butylpyridiniumringe über eine 7-Hydroxychinazolinium-Teilstruktur verfügt, verglichen mit MB327, eine höhere Bindungsaffinität festgestellt werden.

Neben den Bispyridiniumverbindungen wurden im Rahmen dieser Arbeit zahlreiche weitere potenzielle Resensitizer untersucht. Abgeleitet von UNC0646 und A366, zwei in einem Bibliotheks-Screening als hochaffine nAChR-Liganden identifizierte Verbindungen, wurden zahlreiche Chinazolin- und 2-Amino-3*H*-indol-Derivate synthetisiert und biologisch untersucht.

UNC0646-Analoga

Das Hauptaugenmerk lag dabei auf der Synthese von UNC0646-Analoga. Zu Beginn der vorliegenden Arbeit war UNC0646 als der Ligand mit der bislang höchsten bekannten Affinität zur MB327-PAM-1-Bindungstasche identifiziert worden und erschien deshalb als ein sehr vielversprechender Ansatzpunkt. Bei der Auswahl der Zielverbindungen wurden vor allem Modifikationen an den basische Reste enthaltenden Substituenten des Chinazolinrings in 2-, 4- und/oder 7-Position vorgenommen, da dort potenziell starke Wechselwirkungen mit der Bindungstasche erwartet wurden. Die Auswahl variierte von strukturverwandten Substituenten über kleinere Substituenten bis hin zu Wasserstoffatomen. Ergänzend zu der systematischen Variation der Substituenten wurden Zielverbindungen aus liganden- sowie strukturbasierten *in silico*-Screenings ausgewählt.

Ausgehend von 7-Benzyloxy-2,4-dichlor-6-methoxychinazolin und verwandten kommerziell verfügbaren Bausteinen konnten die Zielverbindungen in meist wenigen Schritten und in größtenteils hohen Ausbeuten sowie hohen Reinheiten synthetisiert werden. Eine der wiederkehrenden Reaktionssequenzen war dabei die schrittweise nukleophile Substitution der Chloratome in der 2- und 4-Position der Chinazolin-Grundstruktur durch Aminobausteine. Unter Verwendung von primären oder sekundären Aminen erfolgte zunächst eine nukleophile Substitution in der 4-Position des Ringsystems und bei anschließender erneuter Reaktion unter forcierteren Bedingungen in der 2-Position. Im Rahmen dieser Arbeit konnte eine sehr effiziente Mikrowellen-gestützte Methode zur gezielten Substitution der Chloratome in der 2-Position von 2,4-Dichlor-substituierten Chinazolinen entwickelt werden. Diese basiert auf dem Einsatz von tertiären *N*-Methyl-substituierten Aminen als Nukleophilen. Dies ermöglichte eine effiziente Syntheseplanung, nach der eine große Anzahl von Zielverbindungen sehr variabel in möglichst wenigen linearen Syntheseschritten erzeugt werden konnte. Für Zielverbindungen, die auf diesen Wegen nicht erreichbar waren, wurden eigene Synthesen mit entsprechenden speziellen Reaktionsschritten, wie beispielsweise der regioselektiven Reduktion der 4-Position von 2,4-Dichlorchinazolinen, entwickelt. Neben der Anbringung von Aminosubstituenten an die 2- und 4-Position der Chinazolinbausteine, war ein weiterer Schlüsselschritt die Anknüpfung von ω-Aminoalkoxyseitenketten an die 7-Position. Dies wurde in der Vielzahl der Fälle nach hydrogenolytischer Abspaltung der Benzylschutzgruppe von den entsprechenden 7-Benzyloxychinazolinbausteinen durch *Mitsunobu*-Reaktionen der gebildeten 7-Hydroxychinazoline mit entsprechenden Aminoalkoholbausteinen erreicht. Chinazolin-7-amine konnten hingegen ausgehend von einem 7-Fluor-substituierten Chinazolinbaustein durch Substitution mit primären oder sekundären Aminen erzeugt werden.

Bei den Untersuchungen der zahlreichen neuen UNC0646-Analoga in den UNC0642-MS-Bindungsassays konnten für viele Verbindungen deutlich höhere Affinitäten zur

MB327-PAM-1-Bindungsstelle als für die Bisypyridiniumverbindungen festgestellt werden. Es wurden jedoch im Rahmen dieser Arbeit nicht nur Chinazoline entwickelt, welche durch ihre geringere Molekülmasse eine bessere *ligand efficiency* als UNC0646 aufweisen, wie z.B. PTMD01-0070, auch konnte der Strukturraum der Chinazoline hinsichtlich ihrer Bindung an die MB327-PAM-1-Bindungstasche genauer beleuchtet werden. So wurden auch hochaffine Verbindungen, wie z.B. PTMD01-0062, identifiziert, welche anstelle einer basischen Seitenkette in der 7-Position über einen 7-Benzyloxy-Substituenten sowie über einen konformativ flexiblen basischen Substituenten in der 4-Position verfügen. Die hohe Bindungsaffinität hängt vermutlich mit einem veränderten Bindemodus dieser Substanzen in der Bindungstasche zusammen.

A366-Analoga

Wie bereits erwähnt, wurden in der vorliegenden Arbeit neben Chinazolinen auch 2-Amino-3*H*-indole, abgeleitet von A366, untersucht. Aufgrund der im Vergleich zu UNC0646 deutlich geringeren Molekülmasse und einer Bindungsaffinität an die MB327-PAM-1-Bindungsstelle, die in einer vergleichbaren Größenordnung lag, erschien A366 ebenfalls als vielversprechender Ausgangspunkt für eine Wirkstoffentwicklung. Die synthetisierten Zielverbindungen weisen im Unterschied zu A366 anstelle einer spirocyclischen Cyclobutanteilstruktur ein synthetisch leichter zugängliches Dimethyl-Strukturmotiv in der 3-Position auf und unterschieden sich voneinander entweder in der Struktur der ω-Aminoalkoxyseitenkette (Länge des Spacers oder Ringgröße der cyclischen Amine) oder deren Anknüpfungspunkt an das 2-Amino-3*H*-indol-Ringsystem. Ausgehend von kommerziell verfügbaren Bausteinen waren die A366-Analoga in vier bis sechs Syntheseschritten gut zugänglich. Allerdings stellte der letzte Syntheseschritt, die reduktive Cyclisierung der α,α-Dimethyl-substituierten 2-Nitrophenylacetonitrilbausteine, eine besondere Herausforderung dar. Die Zielverbindungen wurden, ähnlich wie bei vergleichbaren literaturbekannten Synthesen, zusammen mit entsprechenden Amidin-*N*-Oxid-Nebenprodukten in stark variierenden und bestenfalls zufriedenstellenden Ausbeuten erhalten.

Für die meisten synthetisierten A366-Analoga konnten bei Untersuchungen im UNC0642-MS-Bindungsassay keine Unterschiede in den Bindungsaffinitäten, verglichen mit A366, gemessen werden. Für das Regioisomer PTMD02-0006 sowie insbesondere für das Amidin-*N*-Oxid PTMD02-0007 wurden sogar deutlich niedrigere pK_i-Werte im Vergleich zu A366 gefunden. Versuche an Soman-vergifteten Ratten-Diaphragmen zur Untersuchung der intrinsischen Aktivität der 2-Amino-*3H*-indole lieferten jedoch bemerkenswerte Ergebnisse. Während A366 sowie PTMD02-0001L, PTMD02-0004, PTMD02-0005 und PTMD02-0007 die Muskelkraft nicht wiederherstellen konnten, wurde für PTMD02-0002 (C2-Spacer) und

PTMD02-0006 (Regioisomer) eine Wiederherstellung der Muskelkraft festgestellt. Die Reaktivierung durch diese beiden 2-Amino-*3H*-indole erfolgte, ähnlich wie bei den Bispyridiniumverbindungen, nicht nur in einem vergleichbaren Ausmaß wie bei MB327, sondern auch bei deutlich geringeren Substanzkonzentrationen verglichen mit MB327. Bei höheren Konzentrationen zeigte sich für PTMD02-0002 und PTMD02-0006 ein biphasischer Verlauf der Konzentrations-Wirkungskurve, wobei die Muskelaktivität in beiden Fällen wieder auf nahezu 0% zurückging. Die Untersuchung der A366-Analoga an nicht vergifteten Ratten-Diaphragmen zeigte schließlich ein stimmiges Bild. Wie bereits bei den Bispyridinium-verbindungen beschrieben, wurde für A366 sowie alle untersuchten PTMD02-Verbindungen (PTMD02-0001L, PTMD02-0002, PTMD02-0004, PTMD02-0005, PTMD02-0006, PTMD02-0007) eine reversible, muskelhemmende Wirkung beobachtet. Für die beiden Verbindungen PTMD02-0002 und PTMD02-0006 setzte dieser Effekt jedoch erst bei entsprechend höheren Konzentrationen ein. Vermutlich binden sowohl die Bispyridiniumverbindungen als auch die 2-Amino-3*H*-indole in hohen Substanzkonzentrationen auch an die orthosterische Bindungs-stelle des nAChRs, wodurch sie neben einem, durch Bindung an die allosterische MB327-PAM-1-Bindungsstelle vermittelten, positiv allosterischen Effekt auch einen inhibitorischen Effekt ausüben.

Zusammenfassend leistet die vorliegende Arbeit mit der Synthese einer Vielzahl strukturell diverser potenzieller Resensitizer auf der Basis von MB327, UNC0646 und A366 einen substanziellen Beitrag zur Entwicklung neuer Wirkstoffe gegen Vergiftungen mit phosphor-organischen Verbindungen. Zusammen mit den ermittelten biologischen Daten und den daraus geschlussfolgerten Struktur-Aktivitäts-Beziehungen zeigt die Arbeit aussichtsreiche Ansatzpunkte für zukünftige Forschungsarbeiten in diesem Bereich auf. Für eine Entwicklung von Resensitizern für die klinische Anwendung auf der Grundlage der in dieser Arbeit beschriebenen Verbindungen und künftig identifizierten Screening-Hits wird die Optimierung der Zielstrukturen insbesondere auf eine möglichst hohe Affinität zur allosterischen MB327-PAM-1-Bindungsstelle und gleichzeitig auf eine möglichst geringe Affinität zur orthosterischen Bindungsstelle abzielen müssen.

6 Verzeichnis der synthetisierten Substanzen

Alle im Laufe des Forschungsprojekts synthetisierten PTM/D-Verbindungen sind in den folgenden Tabellen aufgelistet (Tabelle 2-4). Die Reinheiten der Testverbindungen wurden mittels quantitativer ^{1}H-NMR-Spektroskopie mit Sigma-Aldrich TraceCERT® Ethyl 4-dimethylaminobenzoat als internem Standard wenn nicht anders vermerkt auf ≥ 95% bestimmt.

Tabelle 2: Strukturformeln der synthetisierten Bispyridiniumsalze mit zugehöriger PTM/D-Bezeichnung, Summenformel und Molekülmasse.

PTM-Code	Strukturformel	Summenformel	MW [g/mol]
0062	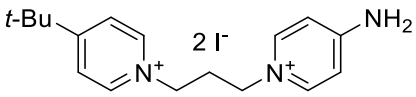	$C_{17}H_{25}I_2N_3$	525.21
0063	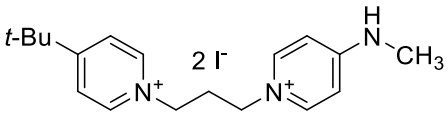	$C_{18}H_{27}I_2N_3$	539.24
0064	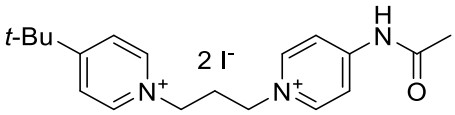	$C_{19}H_{27}I_2N_3O$	567.25
0065[1]	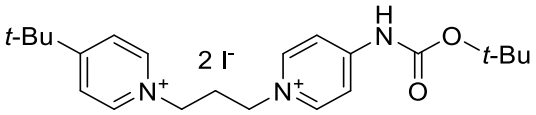	$C_{22}H_{33}I_2N_3O_2$	625.33
0066	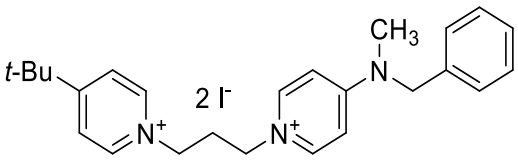	$C_{25}H_{33}I_2N_3$	629.37
0067	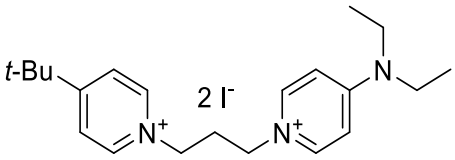	$C_{21}H_{33}I_2N_3$	581.32
0068	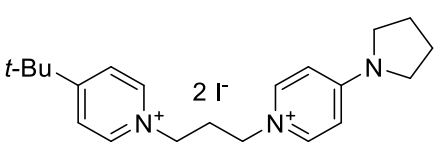	$C_{21}H_{31}I_2N_3$	579.31

[1]Reinheit: ≥ 94%

PTM-Code	Strukturformel	Summenformel	MW [g/mol]
0069	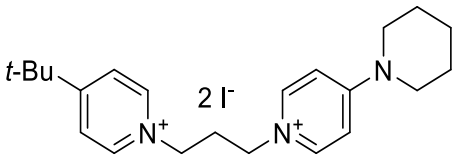	$C_{22}H_{33}I_2N_3$	593.33
0070	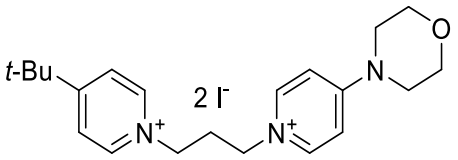	$C_{21}H_{31}I_2N_3O$	595.31
0071	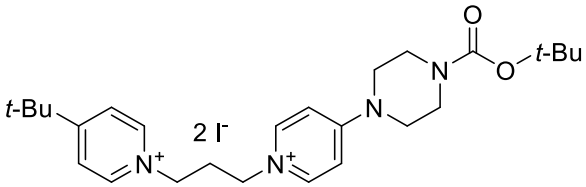	$C_{26}H_{40}I_2N_4O_2$	694.44
0072	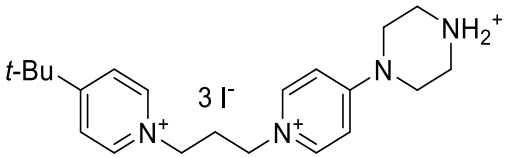	$C_{21}H_{33}I_3N_4$	722.23
D90-0012	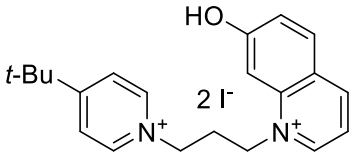	$C_{21}H_{26}I_2N_2O$	576.26
D90-0015	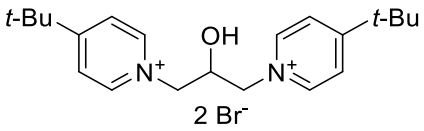	$C_{21}H_{32}Br_2N_2O$	488.31

Tabelle 3: Strukturformeln der synthetisierten UNC0646-Analoga mit zugehöriger PTMD-Bezeichnung, Summenformel und Molekülmasse.

PTMD-01-Code	Strukturformel	Summenformel	MW [g/mol]
0001	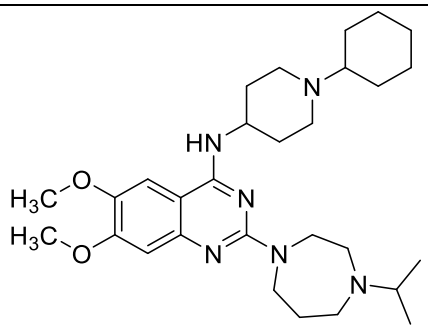	$C_{29}H_{46}N_6O_2$	510.72
0002[2]	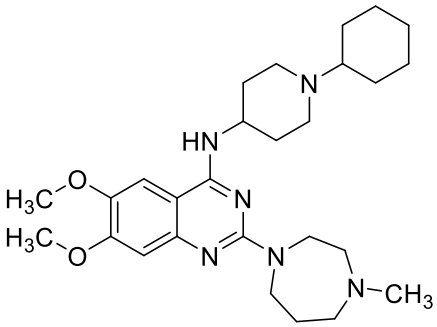	$C_{27}H_{42}N_6O_2$	482.67
0003[3]	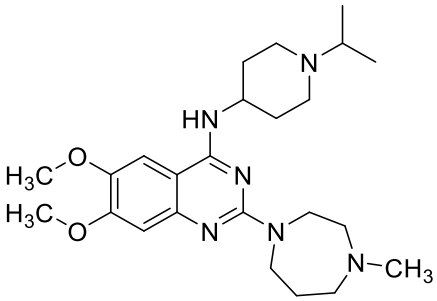	$C_{24}H_{38}N_6O_2$	442.61
0004	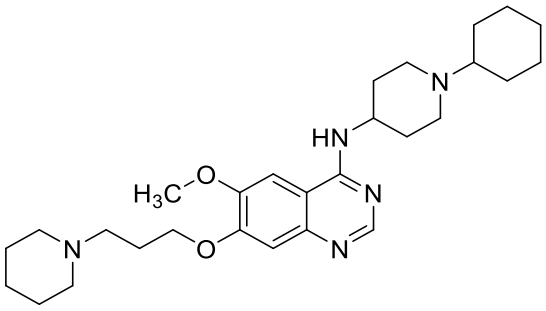	$C_{28}H_{43}N_5O_2$	481.68

[2,3] Literaturbekannte Substanz Sundriyal, S., Chen, P.B., Lubin, A.S., Lueg, G.A., Li, F., White, A.J.P., Malmquist, N.A., Vedadi, M., Scherf, A., Fuchter, M.J., 2017. Histone lysine methyltransferase structure activity relationships that allow for segregation of G9a inhibition and anti-Plasmodium activity. MedChemComm 8, 1069-1092.

PTMD-01-Code	Strukturformel	Summenformel	MW [g/mol]
0005	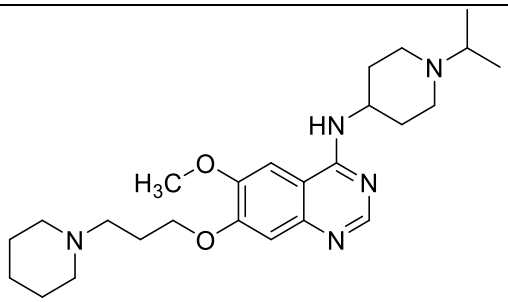	$C_{25}H_{39}N_5O_2$	441.62
0006	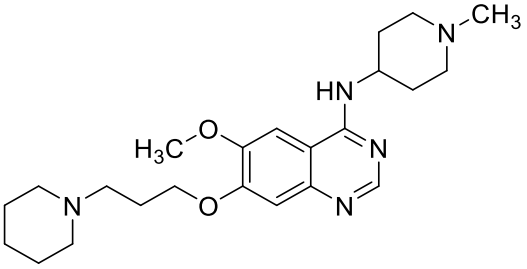	$C_{23}H_{35}N_5O_2$	413.56
0007	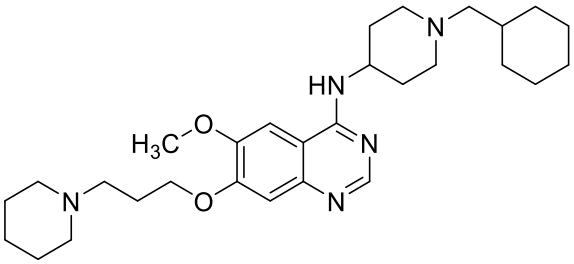	$C_{29}H_{45}N_5O_2$	495.71
0008	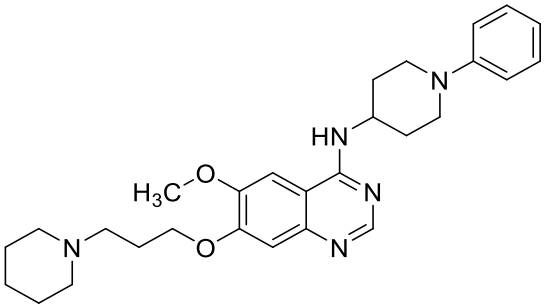	$C_{28}H_{37}N_5O_2$	475.63
0009	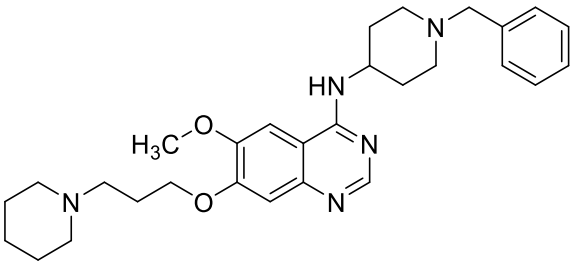	$C_{29}H_{39}N_5O_2$	489.66
0010	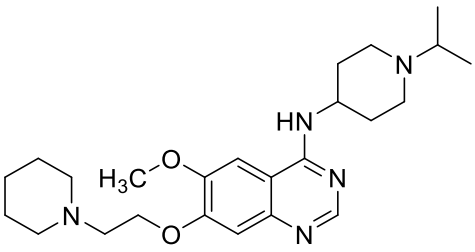	$C_{24}H_{37}N_5O_2$	427.59

PTMD-01-Code	Strukturformel	Summenformel	MW [g/mol]
0011	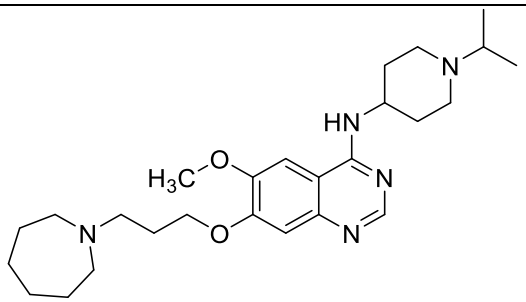	$C_{26}H_{41}N_5O_2$	455.64
0012	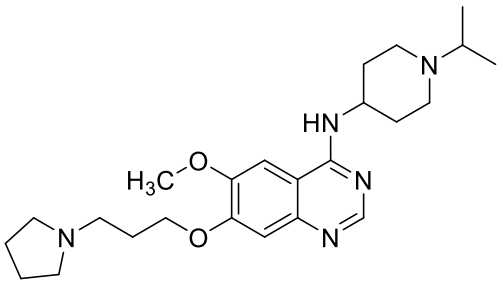	$C_{24}H_{37}N_5O_2$	427.59
0013	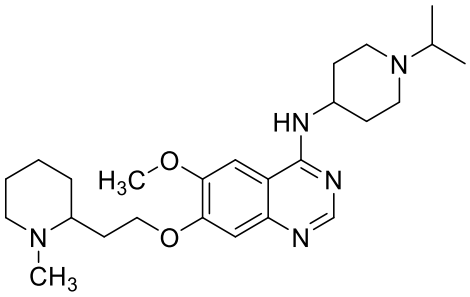	$C_{25}H_{39}N_5O_2$	441.62
0014	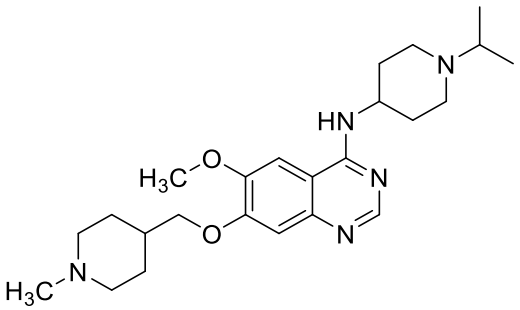	$C_{24}H_{37}N_5O_2$	427.59
0015	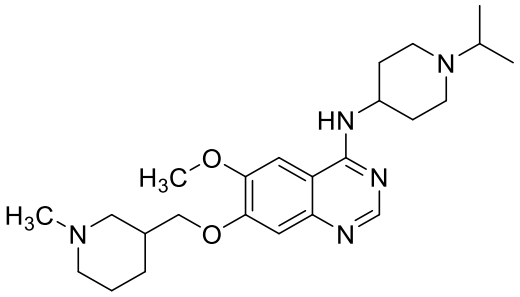	$C_{24}H_{37}N_5O_2$	427.59
0016	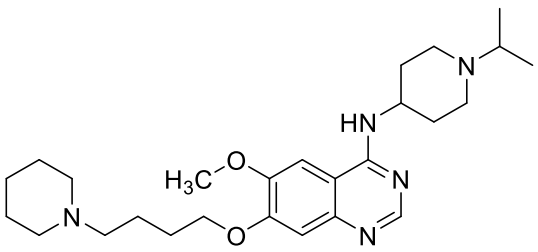	$C_{26}H_{41}N_5O_2$	455.64

PTMD-01-Code	Strukturformel	Summenformel	MW [g/mol]
0017	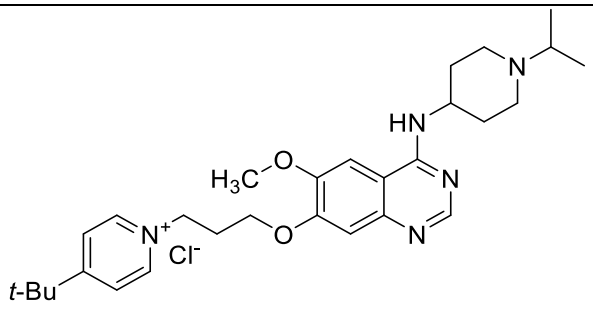	$C_{29}H_{42}ClN_5O_2$	528.14
0027	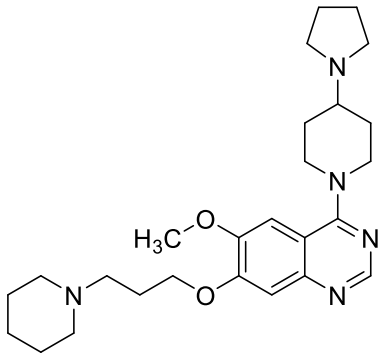	$C_{26}H_{39}N_5O_2$	453.63
0030	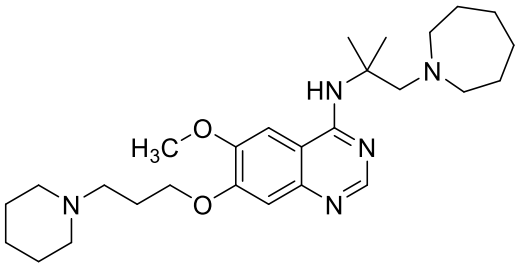	$C_{27}H_{43}N_5O_2$	469.67
0032	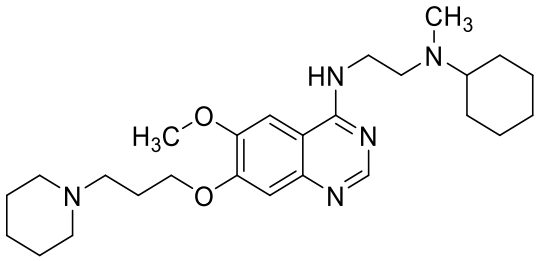	$C_{26}H_{41}N_5O_2$	455.65
0040	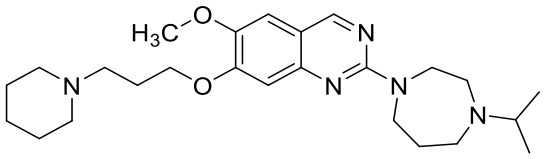	$C_{25}H_{39}N_5O_2$	441.62
0041	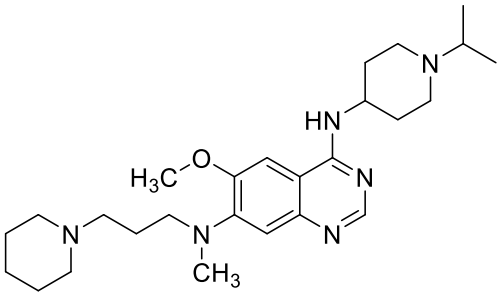	$C_{26}H_{42}N_6O$	454.66

PTMD-01-Code	Strukturformel	Summenformel	MW [g/mol]
0042	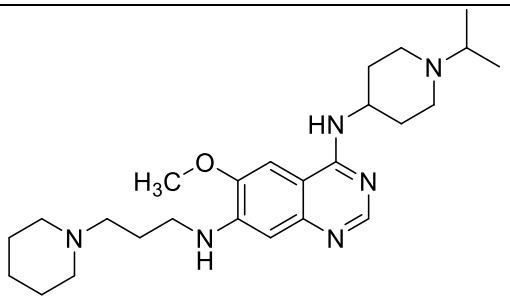	$C_{25}H_{40}N_6O$	440.64
0043	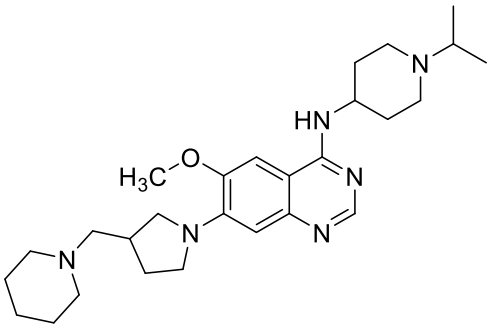	$C_{27}H_{42}N_6O$	466.67
0044L[4]	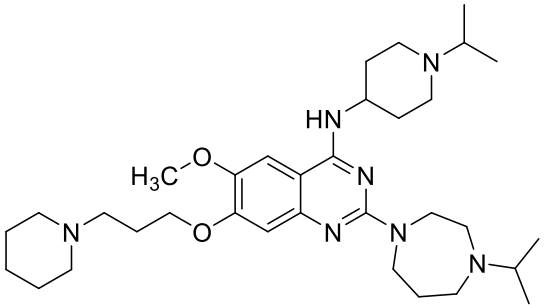	$C_{33}H_{55}N_7O_2$	581.85
0045	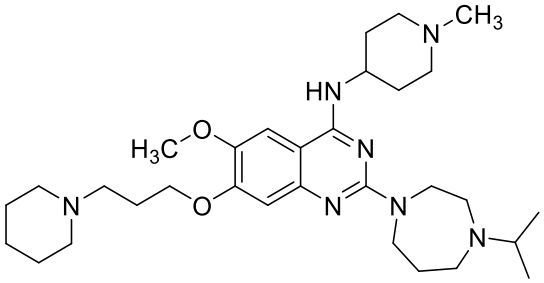	$C_{31}H_{51}N_7O_2$	553.80
0046	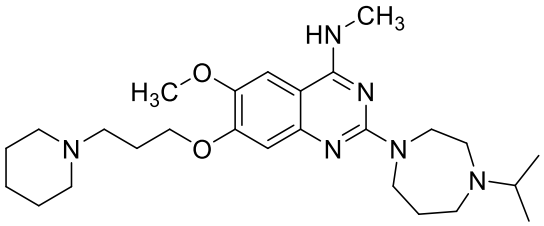	$C_{26}H_{42}N_6O_2$	470.66

[4] Literaturbekannte Substanz Jiang, Y.-H., Kim, Y., Lee, H.-M., Jin, J., Roth, B.L., 2017. Preparation of quinazolin-4-amine derivatives as histone methyltransferase G9a inhibitors and methods for the treatment of Prader-willi syndrome. Duke University, The University of North Carolina at Chapel Hill, Liu, F., Barsyte-Lovejoy, D., Allali-Hassani, A., He, Y., Herold, J.M., Chen, X., Yates, C.M., Frye, S.V., Brown, P.J., Huang, J., Vedadi, M., Arrowsmith, C.H., Jin, J., 2011. Optimization of Cellular Activity of G9a Inhibitors 7-Aminoalkoxy-quinazolines. Journal of Medicinal Chemistry 54, 6139-6150.

PTMD-01-Code	Strukturformel	Summenformel	MW [g/mol]
0047L[5]	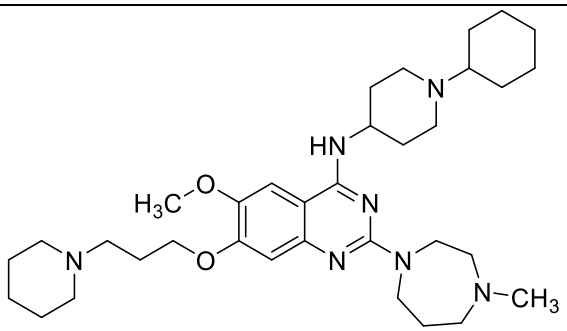	$C_{34}H_{55}N_7O_2$	593.86
0048	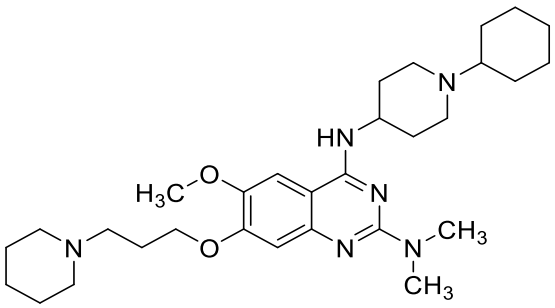	$C_{30}H_{48}N_6O_2$	524.75
0049	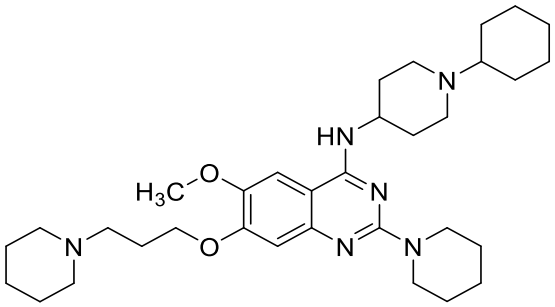	$C_{33}H_{52}N_6O_2$	564.82
0050	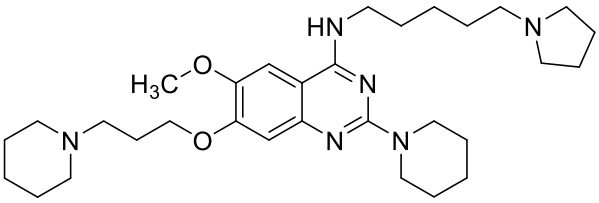	$C_{31}H_{50}N_6O_2$	538.78
0051	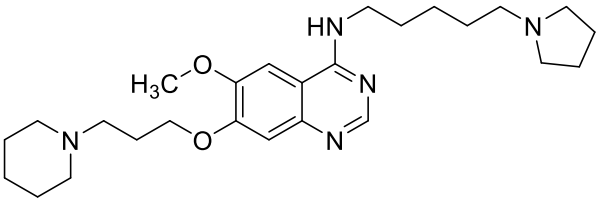	$C_{26}H_{41}N_5O_2$	455.65

[5] Literaturbekannte Substanz Liu, F., Barsyte-Lovejoy, D., Allali-Hassani, A., He, Y., Herold, J.M., Chen, X., Yates, C.M., Frye, S.V., Brown, P.J., Huang, J., Vedadi, M., Arrowsmith, C.H., Jin, J., 2011. Optimization of Cellular Activity of G9a Inhibitors 7-Aminoalkoxy-quinazolines. Journal of Medicinal Chemistry 54, 6139-6150.

PTMD-01-Code	Strukturformel	Summenformel	MW [g/mol]
0052	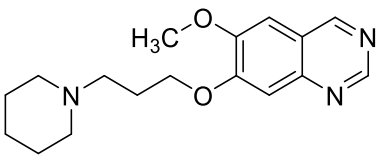	$C_{17}H_{23}N_3O_2$	301.39
0053	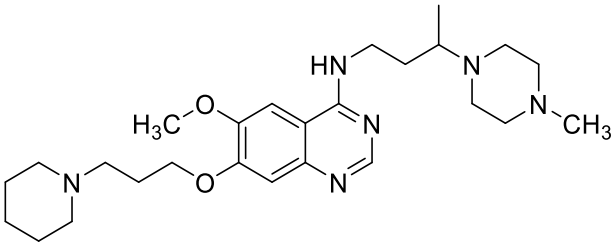	$C_{26}H_{42}N_6O_2$	470.66
0054	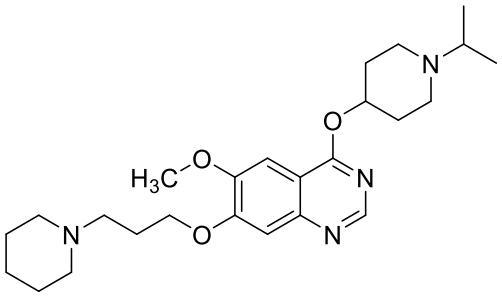	$C_{25}H_{38}N_4O_3$	442.60
0055	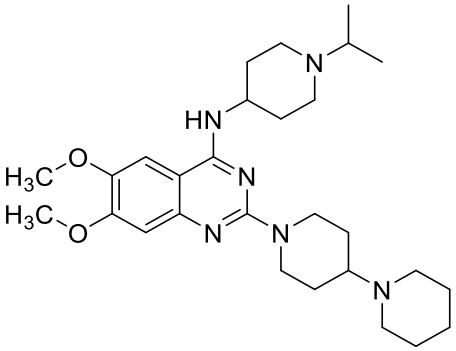	$C_{28}H_{44}N_6O_2$	496.70
0056	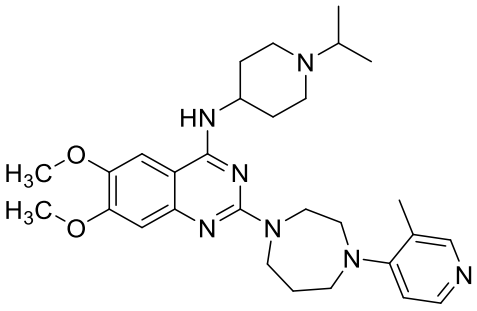	$C_{29}H_{41}N_7O_2$	519.69

PTMD-01-Code	Strukturformel	Summenformel	MW [g/mol]
0057	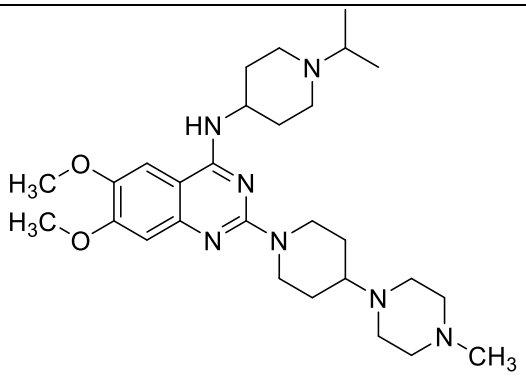	$C_{28}H_{45}N_7O_2$	511.72
0058L[6]	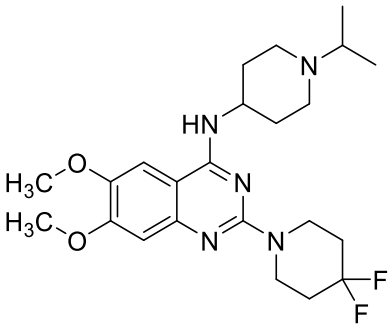	$C_{23}H_{33}F_2N_5O_2$	449.55
0059	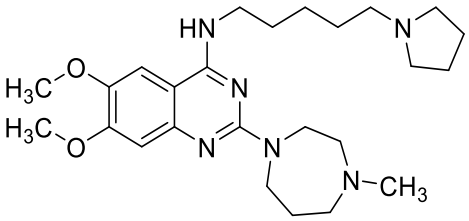	$C_{25}H_{40}N_6O_2$	456.64
0060L[7]	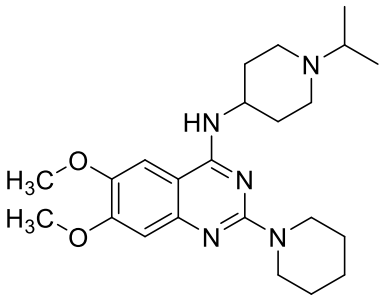	$C_{23}H_{35}N_5O_2$	413.57
0061L[8]	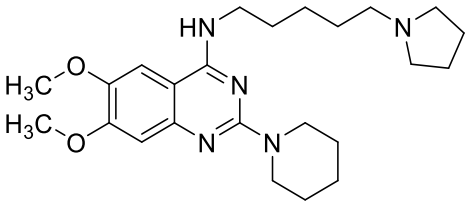	$C_{24}H_{37}N_5O_2$	427.59

[6] Literaturbekannte Substanz Cui, R., Yin, C., Deng, X., Zhang, T., 2020. STK19 inhibitors for treatment of cancer. Trustees of Boston University, Xiamen University.

[7] Literaturbekannte Substanz Sundriyal, S., Chen, P.B., Lubin, A.S., Lueg, G.A., Li, F., White, A.J.P., Malmquist, N.A., Vedadi, M., Scherf, A., Fuchter, M.J., 2017. Histone lysine methyltransferase structure activity relationships that allow for segregation of G9a inhibition and anti-Plasmodium activity. MedChemComm 8, 1069-1092.

[8] Literaturbekannte Substanz Ma, A., Yu, W., Li, F., Bleich, R.M., Herold, J.M., Butler, K.V., Norris, J.L., Korboukh, V., Tripathy, A., Janzen, W.P., 2014. Discovery of a selective, substrate-competitive inhibitor of the lysine methyltransferase SETD8. Journal of medicinal chemistry 57, 6822-6833.

PTMD-01-Code	Strukturformel	Summenformel	MW [g/mol]
0062	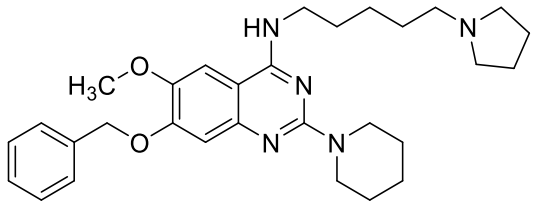	$C_{30}H_{41}N_5O_2$	503.69
0063	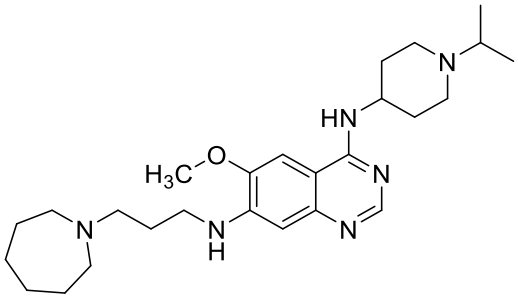	$C_{26}H_{42}N_6O$	454.66
0064	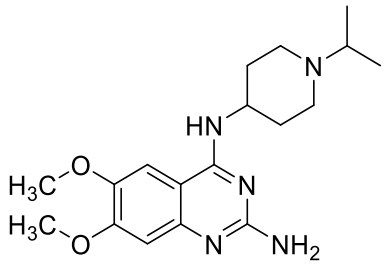	$C_{18}H_{27}N_5O_2$	345.45
0065	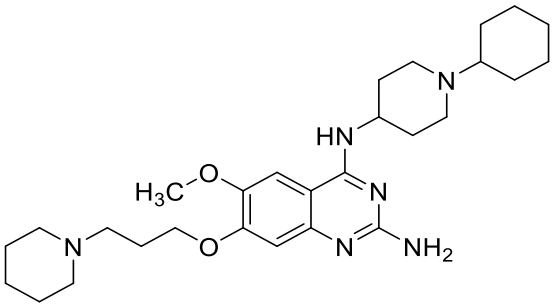	$C_{28}H_{44}N_6O_2$	496.70
0066	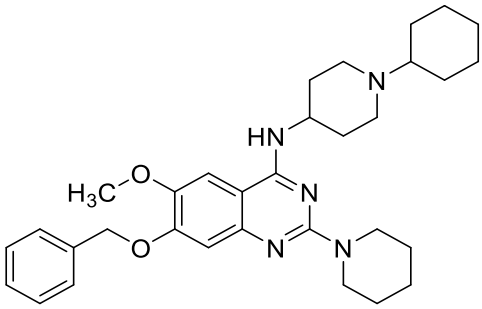	$C_{32}H_{43}N_5O_2$	529.73
0067	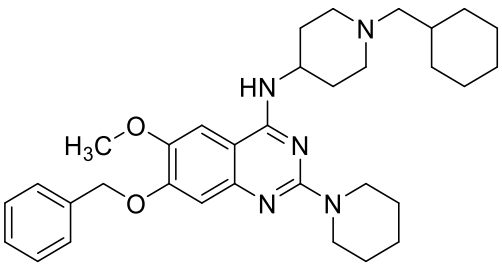	$C_{33}H_{45}N_5O_2$	543.76

PTMD-01-Code	Strukturformel	Summenformel	MW [g/mol]
0068	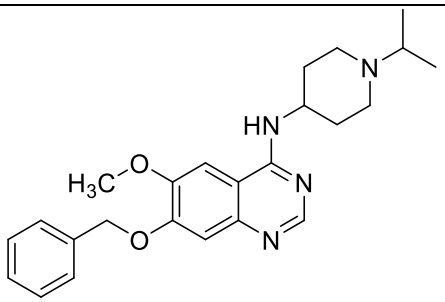	$C_{24}H_{30}N_4O_2$	406.53
0069	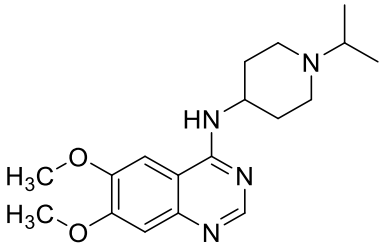	$C_{18}H_{26}N_4O_2$	330.43
0070	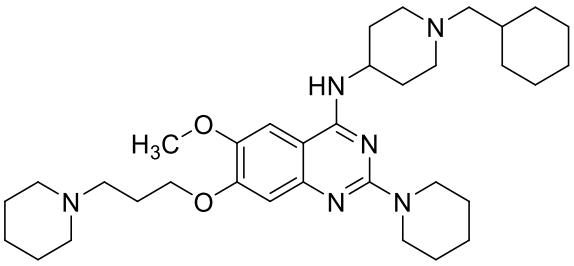	$C_{34}H_{54}N_6O_2$	578.85
0071	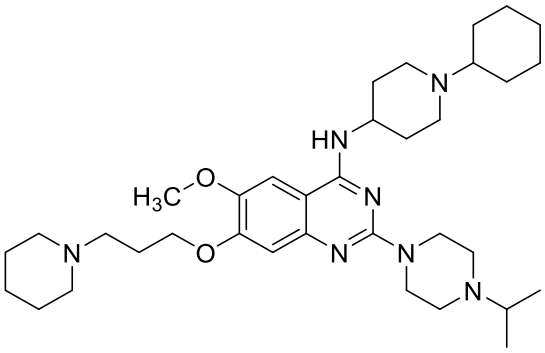	$C_{35}H_{57}N_7O_2$	607.89
0072	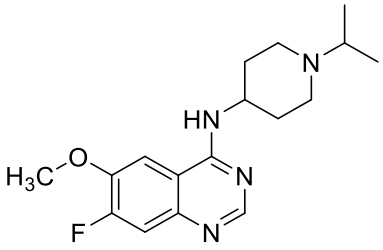	$C_{17}H_{23}FN_4O$	318.40

Tabelle 4: Strukturformeln der synthetisierten A366-Analoga mit zugehöriger Molekülnummer, PTMD-Bezeichnung, Summenformel und Molekülmasse.

PTMD-02-Code	Strukturformel	Summenformel	MW [g/mol]	Nr.
0001L[9]	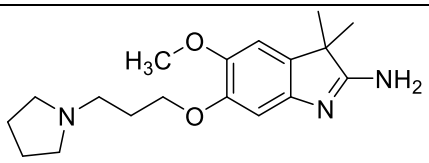	$C_{18}H_{27}N_3O_2$	317.43	**59b**
0002	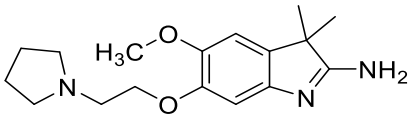	$C_{17}H_{25}N_3O_2$	303.41	**59a**
0004	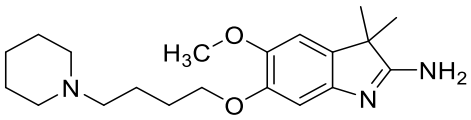	$C_{20}H_{31}N_3O_2$	354.49	**59d**
0005	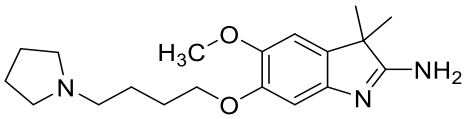	$C_{19}H_{29}N_3O_2$	331.46	**59c**
0006	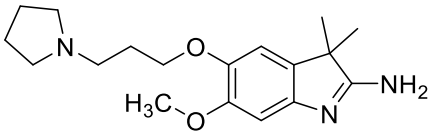	$C_{18}H_{27}N_3O_2$	317.43	**64**
0007	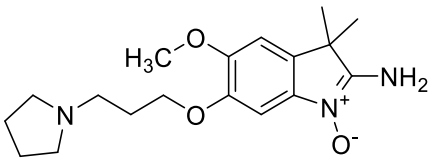	$C_{18}H_{27}N_3O_3$	333.43	**60b**
0008[10]	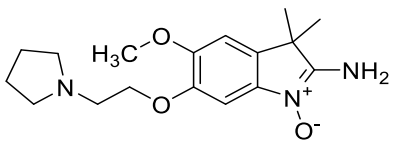	$C_{17}H_{25}N_3O_3$	319.41	**60a**
0010	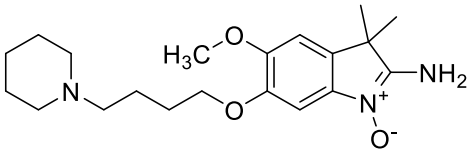	$C_{20}H_{31}N_3O_3$	361.49	**60d**
0011[11]	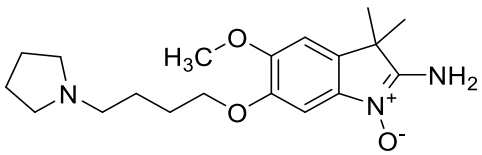	$C_{19}H_{29}N_3O_3$	347.46	**60c**
0012[12]	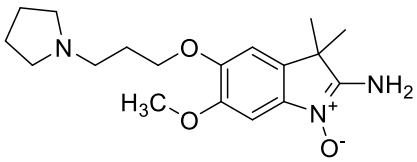	$C_{18}H_{27}N_3O_3$	333.43	**65**

[9] Literaturbekannte Substanz Luise, C., Robaa, D., Regenass, P., Maurer, D., Ostrovskyi, D., Seifert, L., Bacher, J., Burgahn, T., Wagner, T., Seitz, J., Greschik, H., Park, K.-S., Xiong, Y., Jin, J., Schüle, R., Breit, B., Jung, M., Sippl, W., 2021. Structure-Based Design, Docking and Binding Free Energy Calculations of A366 Derivatives as Spindlin1 Inhibitors. International Journal of Molecular Sciences 22, 5910, Sweis, R.F., Pliushchev, M., Brown, P.J., Guo, J., Li, F., Maag, D., Petros, A.M., Soni, N.B., Tse, C., Vedadi, M., Michaelides, M.R., Chiang, G.G., Pappano, W.N., 2014. Discovery and Development of Potent and Selective Inhibitors of Histone Methyltransferase G9a. ACS Medicinal Chemistry Letters 5, 205-209.

[10] Reinheit: ≥ 85%

[11] Reinheit: ≥ 90%

[12] Reinheit konnte aufgrund niedriger Substanzmenge nicht bestimmt werden

7 Abkürzungsverzeichnis

3D	Dreidimensional
Å	Ångström
°C	Grad Celsius
δ	Chemische Verschiebung
µM	Mikromolar
µs	Mikrosekunde
$\tilde{\nu}$	Wellenzahl
Ac-CoA	Acetyl-Coenzym-A
ACh	Acetylcholin
AChE	Acetylcholinesterase
AcOH	Essigsäure
Ac_2O	Essigsäureanhydrid
Äq.	Äquivalente
AUC	Engl.: *Area Under Curve*
BAAINBw	Bundesamt für Ausrüstung, Informationstechnik und Nutzung der Bundeswehr
Bn	Benzyl
CADD	engl.: *Computer Aided Drug Design*
calcd	engl.: *calculated*
ChAT	Cholinacetyltransferase
ChT	Choline Transporter

d	Dublett (NMR)
DBU	1,8-Diazabicyclo[5.4.0]undec-7-en
DIAD	Diisopropyl azodicarboxylat
DMF	*N*,*N*-Dimethylformamid
DMSO	Dimethylsulfoxid
EI	Elektronenionisation
equiv	engl.: *equivalents*
ESI	Elektronensprayionisation
Et	Ethyl
EtOAc	Ethylacetat
EtOH	Ethanol
FC	engl.: *Flash Chromatography*
FDA	engl.: *Food and Drug Administration*
g	Gramm
GABA	γ-Aminobuttersäure
GP	engl.: *General Procedure*
h	Stunde
HRMS	Hochauflösende Massenspektrometrie (engl.: *High Resolution Mass Spectrometry*)
Hz	Hertz

i-Pr	Isopropyl
InstPharmToxBw	Institut für Pharmakologie und Toxikologie der Bundeswehr
IVA	engl.: *Intermediate Volatility Agents*
K_i	Inhibitionskonstante
log	dekadischer Logarithmus
m	Multiplett (NMR)
M	Molar
$[M]^+$	Molekülionenpeak
m.p.	engl.: *melting point*
mAChR	muskarinischer Acetylcholinrezeptor
Me	Methyl
MeOH	Methanol
min	Minute
mg	Milligramm
mHz	Megahertz
mL	Milliliter
mM	Millimolar
mmHg	Millimeter-Quecksilbersäule
MS	Massenspektrometrie
MW	eng.: *Molecular Weight*
m/*z*	Verhältnis Masse zu Ladung

nAChR	nikotinischer Acetylcholinrezeptor
NMR	Kernmagnetresonanz (engl.: *Nucelar Magnetic Resonance*)
OP	Organophosphat/Organophosphonat
OPCW	engl.: *Organisation for the Prohibition of Chemical Weapons*
p	Signifikanzwert
PAM	Positiv allosterischer Modulator
PDB	engl.: *Protein Data Bank*
Ph	Phenyl
PTFE	Polytetrafluorethylen
PTM	engl.: *Pharmacy and Toxicology Munich* bzw. Pharmazie und Toxikologie München
PTMD	engl.: *Pharmacy and Toxicology Munich Düsseldorf* bzw. Pharmazie und Toxikologie München Düsseldorf
PyBOP	Benzotriazol-1-yloxy(tripyrrolidin-1-yl)phosphonium Hexafluorphosphat
R_f	Retardationsfaktor
rt	engl.: *room temperature*
RT	Raumtemperatur
s	Singulett (NMR)
s	Sekunde
Ser	Serin
SSM	engl.: *Solid Supported Membrane*
SURFE^{2}R	engl.: *Surface Electronic Event Reader*

T	Temperatur
t	Zeit
t	Triplett (NMR)
t-Bu	*tert*-Butyl
TFA	Trifluoressigsäure (engl.: *2,2,2-trifluoroacetic acid)*
THF	Tetrahydrofuran
TLC	engl.: *Thin Layer Chromatography*
UN	engl.: *United Nations*
VAChT	vesikulärer Acetylcholintransporter
ZNS	Zentrales Nervensystem

8 Literaturverzeichnis

Homepage der Organisation für das Verbot chemischer Waffen. (https://www.opcw.org/about-us/history) (online abgerufen am 02.03.2024).

Homepage der Organisation für das Verbot chemischer Waffen. https://www.opcw.org/about-us/member-states (online abgerufen am 02.03.2024).

Abreu-Villaça, Y., Filgueiras, C.C., Manhães, A.C., 2011. Developmental aspects of the cholinergic system. Behavioural Brain Research 221, 367-378.

Albuquerque, E.X., Pereira, E.F.R., Alkondon, M., Rogers, S.W., 2009. Mammalian Nicotinic Acetylcholine Receptors: From Structure to Function. Physiological Reviews 89, 73-120.

Ali, J., 2001. Chemical weapons and the Iran-Iraq war: A case study in noncompliance. The Nonproliferation Review 8, 43-58.

Alkondon, M., Albuquerque, E.X., 1989. The nonoxime bispyridinium compound SAD-128 alters the kinetic properties of the nicotinic acetylcholine receptor ion channel: a possible mechanism for antidotal effects. Journal of Pharmacology and Experimental Therapeutics 250, 842.

Alozi, M., Rawas-Qalaji, M., 2020. Treating organophosphates poisoning: management challenges and potential solutions. Critical Reviews in Toxicology 50, 764-779.

Amend, N., Niessen, K.V., Seeger, T., Wille, T., Worek, F., Thiermann, H., 2020. Diagnostics and treatment of nerve agent poisoning—current status and future developments. Annals of the New York Academy of Sciences 1479, 13-28.

Antonijevic, B., Stojiljkovic, M.P., 2007. Unequal efficacy of pyridinium oximes in acute organophosphate poisoning. Clinical medicine & research 5, 71-82.

Bajgar, J., Fusek, J., Kassa, J., Kuca, K., Jun, D., 2020. Chapter 64 - Pharmacological prophylaxis against nerve agent poisoning: experimental studies and practical implications. In: Gupta, R.C. (Ed.) Handbook of Toxicology of Chemical Warfare Agents (Third Edition). Academic Press, Boston, pp. 1091-1101.

Barak, D., Ordentlich, A., Kaplan, D., Barak, R., Mizrahi, D., Kronman, C., Segall, Y., Velan, B., Shafferman, A., 2000. Evidence for P−N Bond Scission in Phosphoroamidate Nerve Agent Adducts of Human Acetylcholinesterase. Biochemistry 39, 1156-1161.

Berman, H.M., Westbrook, J., Feng, Z., Gilliland, G., Bhat, T.N., Weissig, H., Shindyalov, I.N., Bourne, P.E., 2000. The Protein Data Bank. Nucleic Acids Research 28, 235-242.

Bernauer, T., Nitsche, V., Kaiser, J., Gertzen, C.G.W., Höfner, G., Niessen, K.V., Seeger, T., Steinritz, D., Worek, F., Gohlke, H., Wanner, K.T., Paintner, F.F., 2024. Synthesis and Biological Evaluation of Novel MB327 Analogs as Resensitizers for Desensitized Nicotinic Acetylcholine Receptors after Intoxication with Nerve Agents. bioRxiv, 2024.2002.2009.579646.

Bertrand, D., Gopalakrishnan, M., 2007. Allosteric modulation of nicotinic acetylcholine receptors. Biochemical pharmacology 74, 1155-1163.

Bhakhoa, H., Rhyman, L., Ramasami, P., 2019. Theoretical study of the molecular aspect of the suspected novichok agent A234 of the Skripal poisoning. Royal Society open science 6, 181831.

Black, R., 2016. Development, historical use and properties of chemical warfare agents. In: Worek, F., Jenner, J., Thiermann, H. (Eds.) Chemical Warfare Toxicology: Volume 1: Fundamental Aspects, vol. 1. Royal Society of Chemistry, London, pp. 1-18.

Böhm, S., 2016. Cholinerge Systeme. In: Freissmuth, M., Offermanns, S., Böhm, S. (Eds.) Pharmakologie und Toxikologie: Von den molekularen Grundlagen zur Pharmakotherapie. Springer Berlin Heidelberg, Berlin, Heidelberg, pp. 123-127.

Bolt, H.M., Hengstler, J.G., 2022. Recent research on Novichok. Archives of toxicology, 1-4.

Bunnett, J.F., Cartano, A.V., 1981. Differing behavior of pyrrolidine and piperidine as nucleophiles toward 2,4-dinitrophenyl and 2,4-dinitro-6-methylphenyl phenyl ethers. Journal of the American Chemical Society 103, 4861-4865.

Cannard, K., 2006. The acute treatment of nerve agent exposure. Journal of the Neurological Sciences 249, 86-94.

Chae, J., 2008. Practical demethylation of aryl methyl ethers using an odorless thiol reagent. Archives of Pharmacal Research 31, 305-309.

Chai, P.R., Hayes, B.D., Erickson, T.B., Boyer, E.W., 2018. Novichok agents: a historical, current, and toxicological perspective. Toxicology Communications 2, 45-48.

Changeux, J.-P., 2020. Discovery of the First Neurotransmitter Receptor: The Acetylcholine Nicotinic Receptor. Biomolecules, vol. 10.

Chatzidaki, A., Millar, N.S., 2015. Allosteric modulation of nicotinic acetylcholine receptors. Biochemical Pharmacology 97, 408-417.

Chauhan, S., Chauhan, S., D'Cruz, R., Faruqi, S., Singh, K.K., Varma, S., Singh, M., Karthik, V., 2008. Chemical warfare agents. Environmental Toxicology and Pharmacology 26, 113-122.

Corradi, J., Bouzat, C., 2016. Understanding the Bases of Function and Modulation of α7 Nicotinic Receptors: Implications for Drug Discovery. Molecular Pharmacology 90, 288.

Cui, R., Yin, C., Deng, X., Zhang, T., 2020. STK19 inhibitors for treatment of cancer. Trustees of Boston University, Xiamen University.

Cushman, M., Georg, G.I., Holzgrabe, U., Wang, S., 2014. Absolute Quantitative 1H NMR Spectroscopy for Compound Purity Determination. Journal of Medicinal Chemistry 57, 9219-9219.

Doig, P., Boriack-Sjodin, P.A., Dumas, J., Hu, J., Itoh, K., Johnson, K., Kazmirski, S., Kinoshita, T., Kuroda, S., Sato, T.-o., Sugimoto, K., Tohyama, K., Aoi, H., Wakamatsu, K., Wang, H., 2014. Rational design of inhibitors of the bacterial cell wall synthetic enzyme GlmU using virtual screening and lead-hopping. Bioorganic & Medicinal Chemistry 22, 6256-6269.

Eidgenössisches Departement für Verteidigung, B.u.S.d.S., 1925. Protokoll über das Verbot der Verwendung von erstickenden, giftigen oder ähnlichen Gasen sowie von bakteriologischen Mitteln im Kriege.

Fagan, V., Johansson, C., Gileadi, C., Monteiro, O., Dunford, J.E., Nibhani, R., Philpott, M., Malzahn, J., Wells, G., Faram, R., Cribbs, A.P., Halidi, N., Li, F., Chau, I., Greschik, H., Velupillai, S., Allali-Hassani, A., Bennett, J., Christott, T., Giroud, C., Lewis, A.M., Huber, K.V.M., Athanasou, N., Bountra, C., Jung, M., Schüle, R., Vedadi, M., Arrowsmith, C., Xiong, Y., Jin, J., Fedorov, O., Farnie, G., Brennan, P.E., Oppermann, U., 2019. A Chemical Probe for Tudor Domain Protein Spindlin1 to Investigate Chromatin Function. Journal of Medicinal Chemistry 62, 9008-9025.

Fitzgerald, G.J., 2008. Chemical Warfare and Medical Response During World War I. American Journal of Public Health 98, 611-625.

Franca, T.C.C., Kitagawa, D.A.S., Cavalcante, S.F.d.A., da Silva, J.A.V., Nepovimova, E., Kuca, K., 2019. Novichoks: The Dangerous Fourth Generation of Chemical Weapons. International Journal of Molecular Sciences 20, 1222.

Freire, C., Koifman, S., 2013. Pesticides, depression and suicide: a systematic review of the epidemiological evidence. International journal of hygiene and environmental health 216, 445-460.

Friedrich, B., Hoffmann, D., Renn, J., Schmaltz, F., Wolf, M., 2017. One hundred years of chemical warfare: Research, deployment, consequences. Springer Nature.

Gerecke, M., 1983. Chemical structure and properties of midazolam compared with other benzodiazepines. British Journal of Clinical Pharmacology 16, 11S-16S.

Giniatullin, R., Nistri, A., Yakel, J.L., 2005. Desensitization of nicotinic ACh receptors: shaping cholinergic signaling. Trends in Neurosciences 28, 371-378.

Gmeiner, P., Junge, D., Kaertner, A., 1994. Enantiomerically pure amino alcohols and diamino alcohols from L-aspartic acid. Application to the synthesis of epi-and diepislaframine. The Journal of Organic Chemistry 59, 6766-6776.

Grip, L., Hart, J., 2009. The use of chemical weapons in the 1935–36 Italo-Ethiopian War. SIPRI Arms Control and Non-proliferation Programmme 8.

Höfer, M., 2002. Chemische Kampfstoffe: Ein Überblick. Chemie in unserer Zeit 36, 148-155.

Hogg, R., Raggenbass, M., Bertrand, D., 2003. Nicotinic acetylcholine receptors: from structure to brain function. Reviews of physiology, biochemistry and pharmacology, 1-46.

Hurst, R., Rollema, H., Bertrand, D., 2013. Nicotinic acetylcholine receptors: From basic science to therapeutics. Pharmacology & Therapeutics 137, 22-54.

Hurst, R.S., Hajós, M., Raggenbass, M., Wall, T.M., Higdon, N.R., Lawson, J.A., Rutherford-Root, K.L., Berkenpas, M.B., Hoffmann, W.E., Piotrowski, D.W., Groppi, V.E., Allaman, G., Ogier, R., Bertrand, S., Bertrand, D., Arneric, S.P., 2005. A Novel Positive Allosteric Modulator of the α7 Neuronal Nicotinic Acetylcholine Receptor: In Vitro and In Vivo Characterization. The Journal of Neuroscience 25, 4396.

Jawdosiuk, M., Makosza, M., 1976. Synthesis of 2-Aminoindolenine Derivatives via Reductive Cyclization of 2-(o-Nitrophenyl)-2-phenylalkanenitriles. Roczniki Chem Ann Soc Chim Polonorum 50, 857-866.

Jeong, W.-H., Lee, J.-Y., Lim, K.-C., Kim, H.-S., 2021. Identification and Study of Biomarkers from Novichok-Inhibited Butyrylcholinesterase in Human Plasma. Molecules 26, 3810.

Jiang, Y.-H., Kim, Y., Lee, H.-M., Jin, J., Roth, B.L., 2017. Preparation of quinazolin-4-amine derivatives as histone methyltransferase G9a inhibitors and methods for the treatment of Prader-willi syndrome. Duke University, The University of North Carolina at Chapel Hill.

Joint Program Executive Office for Chemical, B., Radiological and Nuclear Defense, 2022. FDA Approves New Drug Application for the DoD's Advanced Anticonvulsant System Program.

Jones, M.V., Westbrook, G.L., 1996. The impact of receptor desensitization on fast synaptic transmission. Trends in Neurosciences 19, 96-101.

Joy, R.J., 1997. Historical aspects of medical defense against chemical warfare. Medical aspects of chemical and biological warfare 90.

Kaiser, J., Gertzen, C.G.W., Bernauer, T., Höfner, G., Niessen, K.V., Seeger, T., Paintner, F.F., Wanner, K.T., Worek, F., Thiermann, H., Gohlke, H., 2023. A novel binding site in the nicotinic acetylcholine receptor for MB327 can explain its allosteric modulation relevant for organophosphorus-poisoning treatment. Toxicology Letters 373, 160-171.

Kaiser, J., Gertzen, C.G.W., Bernauer, T., Nitsche, V., Höfner, G., Niessen, K.V., Seeger, T., Paintner, F.F., Wanner, K.T., Steinritz, D., Worek, F., Gohlke, H., 2024. Identification of ligands binding to MB327-PAM-1, a binding pocket relevant for resensitization of nAChRs. bioRxiv, p. 2023.2012.2021.572862.

Karlin, A., 2002. Emerging structure of the Nicotinic Acetylcholine receptors. Nature Reviews Neuroscience 3, 102-114.

Kim, S.-H., Han, Y.T., 2015. Design, synthesis, and biological evaluation of pyrimidine-2-carboxamide analogs: investigation for novel RAGE inhibitors with reduced hydrophobicity and toxicity. Archives of Pharmacal Research 38, 1952-1962.

Koelle, G.B., 1981. Organophosphate poisoning—An overview. Fundamental and Applied Toxicology 1, 129-134.

Lawler, H.C., 1961. Turnover time of acetylcholinesterase. Journal of Biological Chemistry 236, 2296-2301.

Layish, I., Krivoy, A., Rotman, E., Finkelstein, A., Tashma, Z., Yehezkelli, Y., 2005. Pharmacologic prophylaxis against nerve agent poisoning. Isr Med Assoc J 7, 182-187.

Lee, J.Y., Lim, K.C., Kim, H.S., 2021. Characterization and study on fragmentation pathways of a novel nerve agent,'Novichok (A234)', in aqueous solution by liquid chromatography–tandem mass spectrometry. Molecules 26, 1059.

Liu, F., Barsyte-Lovejoy, D., Allali-Hassani, A., He, Y., Herold, J.M., Chen, X., Yates, C.M., Frye, S.V., Brown, P.J., Huang, J., Vedadi, M., Arrowsmith, C.H., Jin, J., 2011. Optimization of Cellular Activity of G9a Inhibitors 7-Aminoalkoxy-quinazolines. Journal of Medicinal Chemistry 54, 6139-6150.

Liu, F., Chen, X., Allali-Hassani, A., Quinn, A.M., Wasney, G.A., Dong, A., Barsyte, D., Kozieradzki, I., Senisterra, G., Chau, I., 2009. Discovery of a 2, 4-diamino-7-aminoalkoxyquinazoline as a potent and selective inhibitor of histone lysine methyltransferase G9a. Journal of medicinal chemistry 52, 7950-7953.

Liu, F., Chen, X., Allali-Hassani, A., Quinn, A.M., Wigle, T.J., Wasney, G.A., Dong, A., Senisterra, G., Chau, I., Siarheyeva, A., Norris, J.L., Kireev, D.B., Jadhav, A., Herold, J.M., Janzen, W.P., Arrowsmith, C.H., Frye, S.V., Brown, P.J., Simeonov, A., Vedadi, M., Jin, J., 2010. Protein Lysine Methyltransferase G9a Inhibitors: Design, Synthesis, and Structure Activity Relationships of 2,4-Diamino-7-aminoalkoxy-quinazolines. Journal of Medicinal Chemistry 53, 5844-5857.

López-Muñoz, F., García-García, P., Alamo, C., 2009. The pharmaceutical industry and the German National Socialist Regime: I.G. Farben and pharmacological research. Journal of Clinical Pharmacy and Therapeutics 34, 67-77.

Luise, C., Robaa, D., Regenass, P., Maurer, D., Ostrovskyi, D., Seifert, L., Bacher, J., Burgahn, T., Wagner, T., Seitz, J., Greschik, H., Park, K.-S., Xiong, Y., Jin, J., Schüle, R., Breit, B., Jung, M., Sippl, W., 2021. Structure-Based Design, Docking and Binding Free Energy Calculations of A366 Derivatives as Spindlin1 Inhibitors. International Journal of Molecular Sciences 22, 5910.

Ma, A., Yu, W., Li, F., Bleich, R.M., Herold, J.M., Butler, K.V., Norris, J.L., Korboukh, V., Tripathy, A., Janzen, W.P., 2014. Discovery of a selective, substrate-competitive inhibitor of the lysine methyltransferase SETD8. Journal of medicinal chemistry 57, 6822-6833.

Magano, J., Chen, M.H., Clark, J.D., Nussbaumer, T., 2006. 2-(Diethylamino)ethanethiol, a New Reagent for the Odorless Deprotection of Aromatic Methyl Ethers. The Journal of Organic Chemistry 71, 7103-7105.

Marrs, T.C., 2004. The role of diazepam in the treatment of nerve agent poisoning in a civilian population. Toxicol Rev 23, 145-157.

Meier, O., 2016. Gefahren durch Chemiewaffen in Syrien. Berlin: SWP.

Mercey, G., Verdelet, T., Renou, J., Kliachyna, M., Baati, R., Nachon, F., Jean, L., Renard, P.-Y., 2012. Reactivators of acetylcholinesterase inhibited by organophosphorus nerve agents. Accounts of chemical research 45, 756-766.

Meselson, M., Robinson, J.P., 1980. Chemical Warfare and Chemical Disarmament. Scientific American 242, 38-47.

Millar, N., 2003. Assembly and subunit diversity of nicotinic acetylcholine receptors. Biochemical Society Transactions 31, 869-874.

Millar, N.S., Gotti, C., 2009. Diversity of vertebrate nicotinic acetylcholine receptors. Neuropharmacology 56, 237-246.

Mishina, M., Takai, T., Imoto, K., Noda, M., Takahashi, T., Numa, S., Methfessel, C., Sakmann, B., 1986. Molecular distinction between fetal and adult forms of muscle acetylcholine receptor. Nature 321, 406-411.

Miyazawa, A., Fujiyoshi, Y., Unwin, N., 2003. Structure and gating mechanism of the acetylcholine receptor pore. Nature 423, 949-955.

Monod, J., Wyman, J., Changeux, J.-P., 1965. On the nature of allosteric transitions: A plausible model. Journal of Molecular Biology 12, 88-118.

Nachon, F., Asojo, O.A., Borgstahl, G.E.O., Masson, P., Lockridge, O., 2005. Role of Water in Aging of Human Butyrylcholinesterase Inhibited by Echothiophate: The Crystal Structure Suggests Two Alternative Mechanisms of Aging. Biochemistry 44, 1154-1162.

Nakagawa, T., Tu, A.T., 2018. Murders with VX: Aum Shinrikyo in Japan and the assassination of Kim Jong-Nam in Malaysia. Forensic Toxicology 36, 542-544.

Nepovimova, E., Kuca, K., 2018. Chemical warfare agent NOVICHOK - mini-review of available data. Food and Chemical Toxicology 121, 343-350.

Newmark, J., 2007. Nerve Agents. The Neurologist 13, 20-32.

Newmark, J., 2019. Therapy for acute nerve agent poisoning. Neurology: Clinical Practice 9, 337.

Niessen, K.V., Muschik, S., Langguth, F., Rappenglück, S., Seeger, T., Thiermann, H., Worek, F., 2016. Functional analysis of Torpedo californica nicotinic acetylcholine receptors in multiple activation states by SSM-based electrophysiology. Toxicology Letters 247, 1-10.

Niessen, K.V., Seeger, T., Rappenglück, S., Wein, T., Höfner, G., Wanner, K.T., Thiermann, H., Worek, F., 2018. In vitro pharmacological characterization of the bispyridinium non-oxime compound MB327 and its 2- and 3-regioisomers. Toxicology Letters 293, 190-197.

Niessen, K.V., Seeger, T., Tattersall, J.E.H., Timperley, C.M., Bird, M., Green, C., Thiermann, H., Worek, F., 2013. Affinities of bispyridinium non-oxime compounds to [3H]epibatidine binding sites of Torpedo californica nicotinic acetylcholine receptors depend on linker length. Chemico-Biological Interactions 206, 545-554.

Niessen, K.V., Tattersall, J.E.H., Timperley, C.M., Bird, M., Green, C., Seeger, T., Thiermann, H., Worek, F., 2011. Interaction of bispyridinium compounds with the orthosteric binding site of human α7 and Torpedo californica nicotinic acetylcholine receptors (nAChRs). Toxicology Letters 206, 100-104.

Nitsche, V., Höfner, G., Kaiser, J., Gertzen, C.G.W., Seeger, T., Niessen, K.V., Steinritz, D., Worek, F., Gohlke, H., Paintner, F.F., Wanner, K.T., 2024. MS Binding Assays with UNC0642 as reporter ligand for the MB327 binding site of the nicotinic acetylcholine receptor. Toxicology Letters 392, 94-106.

Oldiges, H., Schoene, K., 1970. Pyridinium- und Imidazoliumsalze als Antidote gegenüber Soman- und Paraoxonvergiftungen bei Mäusen. Archiv für Toxikologie 26, 293-305.

Papke, R.L., 2014. Merging old and new perspectives on nicotinic acetylcholine receptors. Biochemical Pharmacology 89, 1-11.

Pauli, G.F., Chen, S.-N., Simmler, C., Lankin, D.C., Gödecke, T., Jaki, B.U., Friesen, J.B., McAlpine, J.B., Napolitano, J.G., 2014. Importance of Purity Evaluation and the Potential of Quantitative 1H NMR as a Purity Assay. Journal of Medicinal Chemistry 57, 9220-9231.

Pita, R., Domingo, J., 2014. The Use of Chemical Weapons in the Syrian Conflict. Toxics 2, 391-402.

Pitschmann, V., 2014. Overall View of Chemical and Biochemical Weapons. Toxins 6, 1761-1784.

Price, M.E., Docx, C.J., Rice, H., Fairhall, S.J., Poole, S.J.C., Bird, M., Whiley, L., Flint, D.P., Green, A.C., Timperley, C.M., Tattersall, J.E.H., 2016. Pharmacokinetic profile and quantitation of protection against soman poisoning by the antinicotinic compound MB327 in the guinea-pig. Toxicology Letters 244, 154-160.

Rappenglück, S., Sichler, S., Höfner, G., Wein, T., Niessen, K.V., Seeger, T., Paintner, F.F., Worek, F., Thiermann, H., Wanner, K.T., 2018a. Synthesis of a Series of Non-Symmetric Bispyridinium and Related Compounds and Their Affinity Characterization at the Nicotinic Acetylcholine Receptor. ChemMedChem 13, 2653-2663.

Rappenglück, S., Sichler, S., Höfner, G., Wein, T., Niessen, K.V., Seeger, T., Paintner, F.F., Worek, F., Thiermann, H., Wanner, K.T., 2018b. Synthesis of a Series of Structurally Diverse MB327 Derivatives and Their Affinity Characterization at the Nicotinic Acetylcholine Receptor. ChemMedChem 13, 1806-1816.

Rose, A.S., Hildebrand, P.W., 2015. NGL Viewer: a web application for molecular visualization. Nucleic Acids Research 43, W576-W579.

Rusyniak, D.E., Nañagas, K.A., 2004. Organophosphate poisoning. Seminars in neurology, vol. 24. Copyright© 2004 by Thieme Medical Publishers, Inc., 333 Seventh Avenue, New …, pp. 197-204.

Schecter, W.P., 2004. Cholinergic symptoms due to nerve agent attack: a strategy for management. Anesthesiology Clinics of North America 22, 579-590.

Seeger, T., Eichhorn, M., Lindner, M., Niessen, K.V., Tattersall, J.E.H., Timperley, C.M., Bird, M., Green, A.C., Thiermann, H., Worek, F., 2012. Restoration of soman-blocked neuromuscular transmission in human and rat muscle by the bispyridinium non-oxime MB327 in vitro. Toxicology 294, 80-84.

Seeger, T., Worek, F., Thiermann, H., 2013. Recovery of soman blocked neuromuscular function by non-oxime bispyridinium compounds in rat diaphragm. Naunyn-Schmiedeberg's Archives of Pharmacology, vol. 386. Deutsche Gesellschaft für Experimentelle und Klinische Pharmakologie und Toxikologie e.V, Halle/Saale, p. 77.

Segesser, D.M., Segesser, D.M., 2007. Die Haager Landkriegsordnung in der internationalen wissenschaftlichen Debatte über Kriegsverbrechen im Ersten und Zweiten Weltkrieg. Die Friedens-Warte, 65-82.

Sheridan, R.D., Smith, A.P., Turner, S.R., Tattersall, J.E.H., 2005. Nicotinic Antagonists in the Treatment of Nerve Agent Intoxication. Journal of the Royal Society of Medicine 98, 114-115.

Sichler, S., Höfner, G., Nitsche, V., Niessen, K.V., Seeger, T., Worek, F., Paintner, F.F., Wanner, K.T., 2024. Screening for new ligands of the MB327-PAM-1 binding site of the nicotinic acetylcholine receptor. Toxicology Letters 394, 23-31.

Sichler, S., Höfner, G., Rappenglück, S., Wein, T., Niessen, K.V., Seeger, T., Worek, F., Thiermann, H., Paintner, F.F., Wanner, K.T., 2018. Development of MS Binding Assays targeting the binding site of MB327 at the nicotinic acetylcholine receptor. Toxicology Letters 293, 172-183.

Sidell, F.R., Takafuji, E.T., Franz, D.R., 1997. Medical aspects of chemical and biological warfare. Office of the Surgeon General (ARMY) Falls Church VA.

Sine, S.M., Engel, A.G., 2006. Recent advances in Cys-loop receptor structure and function. Nature 440, 448-455.

Sirin, G.S., Zhang, Y., 2014. How is acetylcholinesterase phosphonylated by soman? An ab initio QM/MM molecular dynamics study. The journal of physical chemistry A 118, 9132-9139.

Sirin, G.S., Zhou, Y., Lior-Hoffmann, L., Wang, S., Zhang, Y., 2012. Aging mechanism of soman inhibited acetylcholinesterase. The journal of physical chemistry B 116, 12199-12207.

Soukup, O., Tobin, G., Kumar, U.K., Binder, J., Proska, J., Jun, D., Fusek, J., Kuca, K., 2010. Interaction of Nerve Agent Antidotes with Cholinergic Systems. Current Medicinal Chemistry 17, 1708-1718.

Spradling, K.D., Dillman, J.F., 2011. Chapter Three - The Molecular Toxicology of Chemical Warfare Nerve Agents. In: Fishbein, J.C. (Ed.) Advances in Molecular Toxicology, vol. 5. Elsevier, pp. 111-144.

Steindl, D., Boehmerle, W., Körner, R., Praeger, D., Haug, M., Nee, J., Schreiber, A., Scheibe, F., Demin, K., Jacoby, P., Tauber, R., Hartwig, S., Endres, M., Eckardt, K.-U., 2021. Novichok nerve agent poisoning. The Lancet 397, 249-252.

Sundriyal, S., Chen, P.B., Lubin, A.S., Lueg, G.A., Li, F., White, A.J.P., Malmquist, N.A., Vedadi, M., Scherf, A., Fuchter, M.J., 2017. Histone lysine methyltransferase structure activity relationships that allow for segregation of G9a inhibition and anti-Plasmodium activity. MedChemComm 8, 1069-1092.

Sweis, R.F., Pliushchev, M., Brown, P.J., Guo, J., Li, F., Maag, D., Petros, A.M., Soni, N.B., Tse, C., Vedadi, M., Michaelides, M.R., Chiang, G.G., Pappano, W.N., 2014. Discovery and Development of Potent and Selective Inhibitors of Histone Methyltransferase G9a. ACS Medicinal Chemistry Letters 5, 205-209.

Tattersall, J.E.H., 1993. Ion channel blockade by oximes and recovery of diaphragm muscle from soman poisoning in vitro. British Journal of Pharmacology 108, 1006-1015.

Thakur, R., Haru, E., 2007. The Chemical Weapons Convention: Implementation, Challenges, Opportunities.

Thiermann, H., Worek, F., Kehe, K., 2013. Limitations and challenges in treatment of acute chemical warfare agent poisoning. Chemico-Biological Interactions 206, 435-443.

Timperley, C.M., Bird, M., Green, C., Price, M.E., Chad, J.E., Turner, S.R., Tattersall, J.E., 2012. 1, 1′-(Propane-1, 3-diyl) bis (4-tert-butylpyridinium) di (methanesulfonate) protects guinea pigs from soman poisoning when used as part of a combined therapy. MedChemComm 3, 352-356.

Turner, S.R., Chad, J.E., Price, M., Timperley, C.M., Bird, M., Green, A.C., Tattersall, J.E.H., 2011. Protection against nerve agent poisoning by a noncompetitive nicotinic antagonist. Toxicology Letters 206, 105-111.

Unwin, N., 2005. Refined Structure of the Nicotinic Acetylcholine Receptor at 4Å Resolution. Journal of Molecular Biology 346, 967-989.

Unwin, N., Miyazawa, A., Li, J., Fujiyoshi, Y., 2002. Activation of the Nicotinic Acetylcholine Receptor Involves a Switch in Conformation of the α Subunits. Journal of Molecular Biology 319, 1165-1176.

Vale, A., Marrs, T.C., Rice, P., 2016. Chemical terrorism and nerve agents. Medicine 44, 106-108.

Vale, J.A., Marrs, T.C., Maynard, R.L., 2018. Novichok: a murderous nerve agent attack in the UK. Clinical Toxicology 56, 1093-1097.

van Courtland Moon, J.E., 1984. Chemical weapons and deterrence: The World War II experience. International Security 8, 3-35.

Vital, T., Wali, A., Butler, K.V., Xiong, Y., Foster, J.P., Marcel, S.S., McFadden, A.W., Nguyen, V.U., Bailey, B.M., Lamb, K.N., 2023. MS0621, a novel small-molecule modulator of Ewing sarcoma chromatin accessibility, interacts with an RNA-associated macromolecular complex and influences RNA splicing. Frontiers in Oncology 13.

Wein, T., Höfner, G., Rappenglück, S., Sichler, S., Niessen, K.V., Seeger, T., Worek, F., Thiermann, H., Wanner, K.T., 2018. Searching for putative binding sites of the bispyridinium compound MB327 in the nicotinic acetylcholine receptor. Toxicology Letters 293, 184-189.

Wiener, S.W., Hoffman, R.S., 2004. Nerve Agents: A Comprehensive Review. Journal of Intensive Care Medicine 19, 22-37.

Worek, F., Thiermann, H., 2013. The value of novel oximes for treatment of poisoning by organophosphorus compounds. Pharmacology & Therapeutics 139, 249-259.

Worek, F., Thiermann, H., Szinicz, L., Eyer, P., 2004. Kinetic analysis of interactions between human acetylcholinesterase, structurally different organophosphorus compounds and oximes. Biochemical Pharmacology 68, 2237-2248.

Worek, F., Thiermann, H., Wille, T., 2016. Oximes in organophosphate poisoning: 60 years of hope and despair. Chemico-Biological Interactions 259, 93-98.

Worek, F., Thiermann, H., Wille, T., 2020. Organophosphorus compounds and oximes: a critical review. Archives of Toxicology 94, 2275-2292.

Yoshida, K., Taguchi, M., 1992. Reaction of N-substituted cyclic amines with 2, 4-dichloroquinazoline, 2, 4-dichloropyrimidine, and its 5-methyl derivative. Journal of the Chemical Society, Perkin Transactions 1, 919-922.

Zimmerman, G., Soreq, H., 2006. Termination and beyond: acetylcholinesterase as a modulator of synaptic transmission. Cell and tissue research 326, 655-669.